THE JOURNAL
OF
CHEMICAL PHYSICS

VOLUME 32, NUMBER 1 JANUARY, 1960

Theory of Flame Propagation in Solid Nitrogen at Low Temperatures*

S. G. REED, *Office of Naval Research, Washington, D. C.*
AND
C. M. HERZFELD, *National Bureau of Standards, Washington, D. C.*

(Received June 25, 1959)

A theory for a flame in a solid whose speed is controlled by diffusion of radicals and heat is applied to slowly propagating flashes observed in solid nitrogen deposited at 4°K from a microwave discharge. Reasonable agreement is obtained with observed speeds.

WHEN nitrogen gas is passed through a high-frequency electric discharge and deposited at 4.2°K, bright flashes are observed in the deposit,[1] which originate from excited N atoms, N_2 molecules, etc.[2] These flashes have been filmed in color.[3] Two types of flashes are observed: (1) "Slow flashes," which begin at one spot and travel over an area of about one centimeter squared with a speed of approximately 2 cm/sec as measured from the film. (2) "Fast flashes," which cover a similar area in less time than it takes to change the frames of the film, and have a propagation speed of at least 10^3 cm/sec. Jackson[4] has shown in an elegant discussion that an excess of trapped radicals above a critical concentration n_c leads to chain reactions which consume the trapped radicals, and that branching of the chains occurs when $n>n_c$. It seems likely to us that two regimes of radical disappearance exist. First, when $n\approx n_c$, few or no branched chains occur, and the radicals are consumed in a slow flamelike process. Second, when $n>n_c$, branching of chains leads to an explosive disappearance of radicals. These two regimes resemble the two types of flashes which are observed.

We propose that the "slow flash" is a flame in the cold solid, which heats the solid only slightly, and whose speed is governed by the diffusions of radicals and of heat. It is possible to write down simple equations describing such a flame, and to estimate the propagation velocity of the flame. We assume that a heated region is generated by a radical recombination or by a thermal fluctuation. This heat travels through the solid at a rate governed by the thermal diffusivity of the solid. The heat liberates trapped radicals, which then diffuse through the solid at a rate governed by the radical diffusion speed, then react with each other, produce additional heat, and so on. This gives a chain made of two types of steps which must alternate. If enough radicals participate in this process, a flame can be formed, which will have a definite reaction zone in which the above processes take place. This zone moves through the solid at a definite speed which is governed by the speeds of the foregoing processes. To check our suggested mechanism of the process, we calculate the speed of propagation of the reaction zone. We treat the diffusion of heat macroscopically and use a measured value of the thermal diffusivity of bulk solid nitrogen. We estimate the diffusion rate of nitrogen atoms with the usual Eyring theory, and we make the important assumption that, in order to keep the flame front moving, the liberated radicals must diffuse rapidly enough so that the mean time for a liberated radical to meet another radical is of the same order of magnitude as the mean time for the reaction zone of the flame to move a distance equal to its own width.

Let the flame have a profile given by $T=T_\infty$ for $x<0$ and

$$T=T_\infty e^{-x/x_0} \text{ for } x\geq 0, \tag{1}$$

where T is the temperature at x, T_∞ the temperature well behind the flame, $x_0=K/v$, where K is the thermal

* This work was supported in part by the Free Radical Research Program at the National Bureau of Standards, under contract with the Department of the Army.

[1] H. P. Broida and J. R. Pellam, Phys. Rev. **95**, 845 (1954).

[2] C. M. Herzfeld, Phys. Rev. **107**, 1239 (1957); Peyron, Hörl, Brown, and Broida, J. Chem. Phys. **30**, 1304 (1959).

[3] These films were taken by W. Richardson of the National Bureau of Standards.

[4] J. L. Jackson, J. Chem. Phys. **31**, 154, 722 (1959).

Copyright © 1960 by the American Institute of Physics

diffusivity of the material, and v the velocity of the reaction zone. T_i is the temperature ahead of the flame, and is $\approx 4°K$, but is arbitrarily set equal to zero here. In the experiments[5] which we consider, $T_\infty \approx 35°K$ (it must be less than 64°K, the melting point of N_2, because the flame does not melt the solid). Assume that the temperature at which radicals begin to be released is $T_c = \frac{1}{2}T_\infty$. Then the effective width of the reaction zone of the flame, x_c, is given by

$$x_c = (K/v)\ln 2. \tag{2}$$

The mean time between encounters of radicals with radicals is approximately $t_R = t_M/n = \delta^2/(2nD)$, where n is the mole fraction of trapped radicals, δ^2 the mean squared free path of radicals diffusing through the solid, $t_M = \delta^2/2D$ the mean time between encounters of radicals and molecules, and D is the diffusion constant for the radicals. Let $t_c = x_c/v$ be the time for the reaction zone to advance its own width, then t_c must be equal to t_R to keep the flame from dying out. Thus

$$v^2 = (2KDn/\delta^2)\ln 2. \tag{3}$$

D is given approximately by[6] $D = \delta^2\nu \exp(-E/kT)$ where ν is a frequency factor related to the "jumping frequency" of radicals, E the activation energy for "jumping" of radicals ($E \approx kT_\infty = 2kT_c$), and k the Boltzman factor. It is reasonable to take D at T_c, hence $D = \delta^2\nu \exp(-2)$. Substituting this result in Eq. (3) we obtain for the speed of the reaction zone

$$v = (2e^{-2}\ln 2)^{\frac{1}{3}}(K\nu n)^{\frac{1}{3}} = 0.43(k\nu n)^{\frac{1}{3}}. \tag{4}$$

This speed is the geometric mean of K, the rate at which heat diffuses, and of νn, the rate at which radicals recombine. The concentration n is 10^{-2} or less.[4,5] The thermal conductivity of a disordered N_2 lattice at 10°K is approximately [7] 0.2 mw/cm deg, hence K is approximately 1.5×10^{-3} cm²/sec. A reasonable upper limit of ν may be obtained from the width of the *hf* lines in the paramagnetic resonance spectrum of trapped N atoms. The *hf* lines are roughly 1 gauss wide,[8] hence $\nu \approx 10^6$ sec^{-1}. These values of the parameters give a speed of the reaction zone of the order of 3 cm/sec, in good agreement with the observed value. The thickness of the reaction zone $x_c \approx 4\times10^{-4}$ cm. The flame has a front from several millimeters to a centimeter wide, hence the one-dimensional model of the reaction zone is appropriate.

In summary, we see that a simple theory for flames whose speed is controlled by diffusion of heat and radicals, using reasonable choices of parameters, explains in a qualitative way the slow flames observed in solid nitrogen deposited at 4°K from an electric discharge.

ACKNOWLEDGMENT

We acknowledge stimulating discussions with Dr. J. L. Jackson, Dr. K. E. Shuler, and Dr. H. P. Broida; thank Mr. A. L. Stober for help in measuring the flame velocities on the films and Mr. H. M. Roder for giving us his preliminary value of the thermal conductivity of solid nitrogen in advance of publication.

[5] B. J. Fontana, J. Chem. Phys. **30**, 148 (1959).

[6] Glasstone, Laidler, and Eyring, *The Theory of Rate Processes* (McGraw-Hill Book Company, Inc., New York, 1941), p. 538.

[7] H. M. Roder, National Bureau of Standards, Boulder, Colorado (private communication).

[8] Cole, Harding, Pellam, and Yost, J. Chem. Phys. **27**, 593 (1957).

THE JOURNAL OF CHEMICAL PHYSICS VOLUME 32, NUMBER 1 JANUARY, 1960

Molecular Orbital Studies of Diatomic Molecules. I. Method of Computation for Single Configurations of Heteronuclear Systems

FRANK E. HARRIS

Department of Chemistry, University of California, Berkeley, California

(Received May 7, 1959)

This paper describes a method of molecular orbital calculation for heteronuclear diatomic molecules, in the approximation of a single spatial configuration which is a product of one-electron functions. The method is applicable to systems in which the one-electron orbitals are not required to be either orthogonal or filled in pairs. A practical procedure is presented for treating permutational symmetry and spin for an arbitrary spatial wave function, and using this procedure we consider simultaneously all the spin configurations associated with the chosen spatial wave function. The wave functions used are parametric expressions in spheroidal coordinates, and include the usual Slater orbitals as special cases. All necessary integrals are evaluated in a manner suitable for machine computation. A computer program to implement this method of calculation has been prepared, and with it an approximate energy level for a 6-electron molecule can be obtained in about 8 min. Provision was made to program the computer to vary the parameters of the wave functions so as to find automatically the wave function of minimum energy of the parametric form chosen. Only a part of the calculation need be repeated after varying parameters, and the optimum retention of computed data for re-use is discussed.

I. INTRODUCTION

THE molecular orbital approach to the quantum mechanics of many-electron molecules has yielded much qualitative and semi-quantitative information about molecular structure. However, until relatively recently the formidable amount of calculation involved has deterred thorough quantitative study of all but a few of the simplest systems. In the last few years, the use of large-scale computing machines has finally made it possible to explore many somewhat larger problems. The greatest amount of study has been given to schemes using linear combinations of Slater type atomic orbitals, and both self-consistent field and configuration interaction methods have been extensively investigated.[1] Much fine work has been done to develop mathematical methods for implementing these schemes. Unfortunately, it has been found that the methods in use do not usually lead to quantitatively satisfactory results, and that even large computers are not adequate to solve molecular problems in this way.

The work to be described in this paper represents a somewhat different approach than that to which we have already referred. In fact, the present work is based on the view that the best chance of successful molecular computations may not lie with a more elaborate development of the existing framework. Taking this view, it becomes appropriate to ask to what extent the lack of complete success is due to the molecular orbital method itself, and to what extent the responsibility lies with approximations which have been made to implement it. Accordingly, this paper outlines a program of molecular orbital computation in which as many as possible of the usual approximations are removed or modified. It was decided to restrict consideration to diatomic molecules, since the mathematical difficulties would be less severe than for larger systems.

Examination of the existent studies of the simplest systems, such as H_2^+ and H_2,[2] and in particular the work of James and Coolidge,[3] suggested that a better molecular orbital system might well include the use of orbitals which are simple expressions in a natural coordinate system of their molecule. Hence, we adopted orbitals which were simple expressions in an ellipsoidal coordinate system with the nuclei as foci, and which had correct limiting behavior at infinity. Such orbitals correspond, for diatomic molecules, to the well-known Slater orbitals for atoms, and can be chosen to give considerably more flexibility to the electron distribution than can simple combinations of atomic orbitals. The orbitals chosen also had the advantage that they led to integrals similar to those involved in the Slater orbital LCAO method.

In choosing a set of one-electron orbitals for a molecular problem, it is desirable to recognize the effect of interelectron repulsions as well as the distribution of the electrons relative to the nuclei. In conventional molecular orbital calculations, the assignment of pairs of electrons to each spatial orbital, and the requirement that different spatial orbitals be orthogonal, both make difficult any consideration of interelectron effects. The orthogonality requirement is, of course, of no consequence if a sufficiently complete basis set is used for characterizing the wave functions, but in practice, computational limitations prevent the use of bases which are large enough. If the orthogonality requirement is removed, electrons whose orbitals are ordinarily paired into "closed shells" can be split into similar but distinct spatial orbitals, thus allowing for interelectron

[1] For a bibliography, see for example, M. Kotani, *Table of Molecular Integrals* (Maruzen Company, Ltd., Tokyo, Japan, 1955).

[2] See, for example, L. Pauling and E. B. Wilson, Jr., *Introduction to Quantum Mechanics* (McGraw-Hill Book Company, Inc., New York, 1935).

[3] H. M. James and A. S. Coolidge, J. Chem. Phys. **1**, 825 (1933).

repulsion without changing the charge distribution appreciably. Some such "open shell" calculations have already been performed with encouraging results.[4] As a result of the foregoing discussion, the orbital pairing and orthogonality assumptions were not used in this research.

The nature of the approach outlined in the foregoing is such as to materially increase the complexity of those aspects of the molecular problem which are ordinarily simplified by applying orthogonality relations either in ordinary or spin space. This increase in difficulty is to some extent offset by the simplification in the evaluation of the necessary integrals. This simplification results from the use of orbitals all of the same parametric form, so that, for example, there is but one generic two-electron integral in this study. For systems with not more than about six electrons, the gain in simplicity from one source is comparable with the loss from the other. However, further increases in system size cause factorial increases in the spin and permutational analysis, due to the nonorthogonality, and the method described here will become intractable for moderate increases beyond six electrons, at an exact point dependent on the computational equipment available.

The methods of this research are applicable, without change, for calculating all the 1- and 2-center, 1- and 2-electron integrals between Slater atomic orbitals. This is true because Slater orbitals result if certain relations are satisfied by the parameters defining the wave functions discussed here. However, if the usual closed shell or orthogonality assumptions are used, our methods for combining the one- and two-center integrals into matrix elements would have to be superceded by a suitable version of the standard procedures for such postulational systems.

Of equal importance with the removal of potentially damaging restrictions is the introduction of numerical methods which will tend to increase the efficiency of calculation. Accordingly, not only the evaluation of integrals, but all stages of the manipulations of them to yield final results, have been synthesized into a unified computational program. This program was written so as to include provision for automatically optimizing the parameters appearing in the descriptions of the various orbitals, so as to take full advantage of the functional form adopted for computation. Timewise, the over-all program has benefitted considerably by a unified approach. We have obtained average computing times of the order of one second for evaluating 2-electron integrals, and over-all running times of 2 to 10 minutes for a complete molecular calculation with given wave functions.

Some parts of this over-all program are useful independently of the rest of the scheme. In addition to the integral calculations, as already referred to, there is the possibility of taking integrals, as supplied by any source whatever, and using this molecular program to make matrix elements. Such an application, to the rotational barrier in ethane-like molecules, has already been reported.[5] Further such work will be described later.[6]

This paper is restricted to a method of single configuration calculation, for heteronuclear diatomic molecules. The extension of the method to many configurations has been made and will be the subject of a separate communication. Treatment of homonuclear systems introduces matters of symmetry which also will be discussed later. Further papers of the series will describe the results which have been obtained with the formulation to be described here.

II. METHOD OF COMPUTATION

The problem to be discussed here will be that of the motion of the electrons of a diatomic system in the presence of two fixed nuclei. We seek approximations to the solutions of the Schroedinger equation, using a Hamiltonian which has been simplified by omitting all magnetic terms, all contributions dependent upon spin, and all relativistic effects. We are thus concerned with the usual approximation to the electronic energy levels.

The electronic wave functions and energies will be determined by the variation method.[2] We therefore introduce wave functions depending upon parameters which are to be adjusted to obtain stationary values of the energy. The lowest stationary value will correspond to the ground state, other values to excited states. The wave functions used must satisfy the usual continuity and boundary conditions, must have appropriate spin dependence, and must satisfy the Pauli exclusion principle. We shall limit this paper to the study of wave functions whose spatial part can be derived from a simple product of 1-electron spatial orbitals. We refer to this product as a *primitive function*, and designate it by Φ.* Denoting the one-electron spatial orbitals by ϕ_i, $1 \leq i \leq N$, where N is the number of electrons in the problem, Φ is of the form

$$\Phi(\mathbf{r}) = \prod_{i=1}^{N} \phi_i(\mathbf{r}_i), \tag{1}$$

where $\mathbf{r}_i$ is the position vector of the ith electron and $\mathbf{r}$ symbolizes collectively the coordinates of all N electrons. A primitive function cannot be an acceptable

[4] See, for example, H. Shull and P-O. Lowdin, Phys. Rev. **101**, 1730 (1956); J. Chem. Phys. **23**, 1565 (1955); **25**, 1035 (1956).

[5] G. M. Harris and F. E. Harris, J. Chem. Phys. **31**, 1450 (1959).

[6] G. M. Harris and F. E. Harris (to be published).

* We use the following notational conventions. Vectors and matrices are represented by lower and upper case bold face characters, respectively. Elements of vectors and matrices are given by appropriately subscripted corresponding light face characters. Dynamical operators are in upper case script. One-electron and many-electron wave functions are lower and upper case Greek letters, respectively. Φ, ϕ refer to spatial wave functions, Θ, Ω to spin functions, and Ψ to wave functions involving both space and spin. The symbol φ, and never ϕ, is used to denote an angular coordinate.

wave function because it has no spin dependence and is not properly symmetrized. It does, however, satisfy the continuity and boundary conditions, due to the choice of the ϕ_i. By adding spin dependence and considering the functions obtained by permuting the electron coordinates in Φ, a function $\Psi(\mathbf{r}, \mathbf{s})$ can sometimes be formed which is antisymmetric in all the electrons and represents a definite spin state.[7] Here $\mathbf{s}$ represents the spin coordinates of all the electrons, and $\mathbf{s}_i$, when used, will indicate the spin coordinate of the ith electron. A function Ψ will exist when the primitive function Φ is consistent with the possibility of forming the desired spin state. Ψ will be a bilinear form, one factor of each term being proportional to a permutation of Φ, the other factor being a suitable spin function.

Frequently the assumption is made at this point that the ϕ_i are pairwise identical, resulting in closed shells in which the electron spins must be paired to satisfy the Pauli principle. In such a case there will be a single function Ψ which can be generated by assigning to each electron a spin function and forming the well-known Slater determinant.[2] We shall make no such pairing assumption in this paper. As a result, in general, there will, be more than one, say d, wave functions $\Psi^u(\mathbf{r}, \mathbf{s})$, $1 \leq u \leq d$, derivable from a given Φ, where d depends on the numbers of identical ϕ_i, on N, and on the spin state specified.[7] We shall seek to minimize the energy not only by varying the parameters determining the ϕ_i, and therefore also Φ, but also by taking linear combinations of all the Ψ^u.

When the variation method is to be applied to a linear combination of parametric wave functions with undetermined coefficients, the problem becomes that of adjusting the parameters to find stationary values of the eigenvalues, λ, of the matrix equation

$$(\mathbf{H}-\lambda\mathbf{S})\mathbf{a}=0, \tag{2}$$

where the matrices $\mathbf{H}$ and $\mathbf{S}$ are related to the wave functions Ψ^u, the Hamiltonian operator $\mathcal{H}$, and the identity operator, as follows:

$$H_{uv}=\int \Psi^{u*}\mathcal{H}\Psi^{v}d\tau, \tag{3}$$

$$S_{uv}=\int \Psi^{u*}\Psi^{v}d\tau. \tag{4}$$

The volume element $d\tau$ implies integration over all values of both spatial and spin coordinates of all electrons. The asterisk means complex conjugate. The vector $\mathbf{a}$ represents the coefficients of the Ψ^u in the wave function, so that

$$\Psi=\sum_{u=1}^{d} a_u\Psi^u. \tag{5}$$

Thus the eigenvector $\mathbf{a}$ corresponding to any λ defines a wave function according to Eq. (5).

The major task in carrying out a calculation as outlined above is the evaluation of the integrals of Eqs. (3) and (4). This evaluation naturally divides into two parts. First, the Ψ^u can be written in terms of Φ and its permutations, and the integrations over spin coordinates can be carried out, since $\mathcal{H}$ is spin independent. Our procedure for doing this is described in Sec. III of this paper. It then remains to evaluate the spatial integrals involving Φ, its permutations, and the Hamiltonian operator. Since $\mathcal{H}$ is a sum of 1- and 2-electron contributions, all the spatial integrations can be reduced to a set of 1- and 2-electron integrals. The evaluation of these integrals, and their collection into forms suitable for use in Sec. III, forms the second part of the computation of $\mathbf{H}$ and $\mathbf{S}$, and is detailed in Secs. IV through VII of the paper.

The steps outlined in Secs. III through VII provide, for any given values of the adjustable parameters, the information needed to solve Eq. (2) to obtain approximations to the energy levels. In this study the variation of parameters was carried out by an iterative numerical method which made direct use of the calculated energies for trial values of the parameters. This procedure seemed advisable because of the difficulty of setting up a more analytical method not involving excessive calculation at each step. The method used is outlined in Sec. VIII of this paper.

The entire set of calculations outlined in the preceding paragraphs was programed for an IBM Type 701 computer in a manner which permitted entirely automatic processing from input describing the identity of the problem and an initial set of parameters for the wave functions, to a final output giving the best wave functions and energies obtainable from the parametric forms used. Those aspects of the computer operations which may be of general scientific interest are collected in Sec. IX of this paper.

III. CONSTRUCTION OF MATRIX ELEMENTS FROM A PRIMITIVE FUNCTION

This section is concerned with the relationship connecting a primitive function Φ to total wave functions Ψ^u of the proper permutational and spin symmetry, and to the matrices corresponding to operators of interest. Although the application in this paper will be only to the matrices $\mathbf{H}$ and $\mathbf{S}$, the formalism applies to the matrix elements of any operator which is symmetric in all the electrons and which is independent of spin. As pointed out in the preceding section, we are concerned with matrices, rather than numbers, because in general there will be more than one Ψ^u resulting from a given primitive function Φ, and we seek a means of simultaneously studying the entire set of Ψ^u. The remainder of this section will be written in terms of a general operator $\mathcal{O}$, to be characterized by the matrix whose (u, v) element will be

$$O_{uv}=\int \Psi^{u*}(\mathbf{r}, \mathbf{s})\,\mathcal{O}\Psi^{v}(\mathbf{r}, \mathbf{s})d\tau. \tag{6}$$

Equation (6) will be simplified by substituting for the Ψ^u their equivalents in terms of $\Phi(\mathbf{r})$, its permutations $\Phi(P\mathbf{r})$, and a set of orthonormal spin functions $\Theta_j(\mathbf{s})$ which span the spin space for N electrons with the appropriate value of the total resultant electron spin and its component along one axis. In particular,

$$\Psi^u(\mathbf{r},\mathbf{s})=(N!)^{-\frac{1}{2}}\sum_{j=1}^{d}\sum_{P}U_{ju}(P)\Phi(P\mathbf{r})\Theta_j(\mathbf{s}) \quad 1\leq u\leq d. \tag{7}$$

P, Q, and R are used in this paper to denote permutations of the electron coordinates. Sums over these symbols span the permutation group of order N. It may be shown that the coefficients $\mathbf{U}(P)$ are elements of a unitary, irreducible representation of the Nth-order permutation group.

Substituting Eq. (7) into Eq. (6)

$$0_{uv}=(N!)^{-1}\sum_{j,k=1}^{d}\sum_{P,R}U_{ju}(P)U_{kv}(R)\cdot\int\Theta_j(\mathbf{s})\Theta_k(\mathbf{s})d\mathbf{s}\int\Phi^*(P\mathbf{r})\mathcal{O}\Phi(R\mathbf{r})d\mathbf{r} \tag{8}$$

which becomes, making use of the assumption that $\mathcal{O}$ is totally symmetric and that therefore $P^{-1}\mathcal{O}=\mathcal{O}$, invoking the unitary representation property of $\mathbf{U}(P)$, and noting that the $\Theta_j(\mathbf{s})$ are orthonormal

$$0_{uv}=(N!)^{-1}\sum_{P,R}U_{uv}(P^{-1}R)\int\Phi^*(\mathbf{r})\mathcal{O}\Phi(P^{-1}R\mathbf{r})d\mathbf{r}. \tag{9}$$

Substituting Q for $P^{-1}R$ and performing the summation over the then trivial index P,

$$0_{uv}=\sum_{Q}U_{uv}(Q)0(Q) \tag{10}$$

where

$$0(Q)=\int\Phi^*(\mathbf{r})\mathcal{O}\Phi(Q\mathbf{r})d\mathbf{r}. \tag{11}$$

Equations (10) and (11) show how to proceed from a knowledge of the spatial integrals involving an operator $\mathcal{O}$ to its matrix $\mathbf{0}$. To do so requires a knowledge of the matrix representation $\mathbf{U}(P)$. The explicit use of the spin functions is at no time required. The foregoing analysis is not new, but is reproduced here for reference in the remainder of the paper.[7,8]

For functions Φ with permutational symmetry the matrices $\mathbf{0}$ will be singular. The singularity arises from the properties of $\mathbf{U}(P)$, and is basically due to the exclusion principle. In this event there are not d independent wave functions Ψ^u and Eq. (2) cannot be solved until the dependent Ψ^u have been removed. This problem has been discussed.[7,8] The various matrix representations which it might be desired to use constitute an unwieldy body of numerical data. For example, the six-electron singlet state is represented by a collection of 720 five-by-five matrices, while the 6-electron triplet state requires 720 nine-by-nine matrices. It is apparent that a convenient means must be available for generating these matrices when needed.

The consideration determining the $\mathbf{U}(P)$ is basically that each Ψ^u transform properly into plus or minus itself upon permutation of the electron coordinates,

$$\Psi^u(\mathbf{r},\mathbf{s})=\epsilon_Q\Psi^u(Q\mathbf{r},Q\mathbf{s}) \tag{12}$$

$$=\epsilon_Q(N!)^{-\frac{1}{2}}\sum_{i=1}^{d}\sum_{P}U_{iu}(Q^{-1}P)\Phi(QQ^{-1}P\mathbf{r})\Theta_i(Q\mathbf{s}) \tag{13}$$

where ϵ_Q is plus or minus one according as Q is an even or odd permutation. The choice of dummy indices is designed to lead to simpler expressions later. The spin functions transform according to

$$\Theta_i(Q\mathbf{s})=\sum_{j=1}^{d}V_{ij}(Q)\Theta_j(\mathbf{s}) \qquad 1\leq i\leq d. \tag{14}$$

Thus, using Eq. (14), invoking the unitary representation property to replace $U_{iu}(Q^{-1}P)$ by

$$\sum_{k=1}^{d}U_{ki}(Q)U_{ku}(P),$$

and putting $QQ^{-1}P=P$, Eq. (13) becomes

$$\Psi^u(\mathbf{r},\mathbf{s})=(N!)^{-\frac{1}{2}}\sum_{j,k=1}^{d}\sum_{P}\Big[\sum_{i=1}^{d}U_{ki}(Q)\epsilon_QV_{ij}(Q)\Big]\cdot U_{ku}(P)\Phi(P\mathbf{r})\Theta_j(\mathbf{s}). \tag{15}$$

It may be seen that Eqs. (7) and (15) are consistent if the quantity in square brackets is $\delta(j,k)$, where $\delta(j,k)=$ unity if $j=k$, zero otherwise. This is true if

$$\epsilon_QV_{ij}(Q)=U_{ji}(Q). \tag{16}$$

Equation (16) permits expression of the $\mathbf{U}(P)$ in terms of the equally voluminous matrices $\mathbf{V}(P)$.[7] However, the $\mathbf{V}(P)$ depend upon the spin functions, which can be stated relatively compactly. Our contribution to this formalism is to generate all the $\mathbf{V}(P)$ from a single rectangular matrix whose rows correspond to the d functions $\Theta_j(\mathbf{s})$, and whose columns correspond to simple products of one-electron spin functions. The method is given in Appendix I. This rectangular matrix could in principle be generated when needed, but it did not seem to be worth the effect, as the amount of data involved is not large. For example, the matrix for the 6-electron singlet state is only five-by-twenty.

IV. REDUCTION OF THE SPATIAL INTEGRALS

This section, together with Secs. V through VII, deals with the evaluation of the spatial integrals defined in

[7] M. Kotani, reference 1, Chap. I.
[8] R. Serber, Phys. Rev. **45**, 461 (1934).

Eq. (11). The operators of interest at this time will be $\mathfrak{IC}$ and $\mathfrak{S}$, although the method is not restricted to these. The integral $S(Q)$ is immediately factorable into a product of one-electron integrals, namely overlap integrals. Using the notation

$$(i\,|\,j)=\int\phi_i^*(\mathbf{r}_1)\phi_j(\mathbf{r}_1)d\mathbf{r}_1 \tag{17}$$

we write

$$S(Q)=\prod_{i=1}^{N}(i\,|\,q_i) \tag{18}$$

where the notation q_i refers to the number of the electron put in the place of electron i by the permutation Q.

In order to handle the integral $H(Q)$ we require a more explicit form of the operator $\mathfrak{IC}$. In accord with the assumptions stated early in the paper,

$$\mathfrak{IC}=(Z_AZ_B/R)+\sum_{i=1}^{N}h_i+\sum_{i>j\geq 1}^{N}1/r_{ij}, \tag{19}$$

$$h_i=-\tfrac{1}{2}\nabla_i^2-(Z_A/r_{iA})-(Z_B/r_{iB}) \tag{20}$$

where Z_A and Z_B are the charges of nuclei A and B, which are separated by the distance R. The quantities r_{xy} are the distances between particles x and y, and ∇_i^2 is the Laplace operator for electron i. These equations are in atomic units, the unit of energy being twice the ionization energy of the H atom, or 27.21 ev, the unit of length being the first hydrogenic Bohr orbit for a nucleus of infinite mass, or 0.529 A, and the unit of charge being the absolute value of the electronic charge.

Since no term of $\mathfrak{IC}$ involves the coordinates of more than two electrons, $H(Q)$ is reducible to sums of products of one- and two-electron integrals. On making the definitions

$$(i\,|\,h\,|\,j)=\int\phi_i^*(\mathbf{r}_1)h_1\phi_j(\mathbf{r}_1)d\mathbf{r}_1 \tag{21}$$

$$(ij\,|\,1/r\,|\,kl)=\int\phi_i^*(\mathbf{r}_1)\phi_j^*(\mathbf{r}_2)(1/r_{12})\phi_k(\mathbf{r}_1)\phi_l(\mathbf{r}_2)d\mathbf{r}_1d\mathbf{r}_2, \tag{22}$$

one may write

$$H(Q)=(Z_AZ_B/R)\,S(Q)+\sum_{i=1}^{N}\Big[\prod_{j=1,j\neq i}^{N}(j\,|\,q_i)\Big](i\,|\,h\,|\,q_i)+\sum_{i>j\geq 1}^{N}\Big[\prod_{k=1;k\neq i,j}^{N}(k\,|\,q_k)\Big](ij\,|\,1/r\,|\,q_iq_j). \tag{23}$$

For computational purposes it is convenient to form all the 1- and 2-electron integrals first, and to then look up the values needed for each Q, since each integral is used more than once in a given calculation. We prepared tables of $(i\,|\,j)$, $(i\,|\,h\,|\,j)'\equiv(i\,|\,h\,|\,j)/(i\,|\,j)$ and $(ij\,|\,1/r\,|\,kl)'\equiv(ij\,|\,1/r\,|\,kl)/(i\,|\,k)(j\,|\,l)$, in the last two tables replacing zero factors in the denominators with unity. One may then, for each Q, compute $S(Q)$, or, if it is zero, $S'(q)$, the overlap product in which the zero factors have been replaced by ones. Counting the number of zero factors in $S(Q)$, four cases may be distinguished. If no factor $(i\,|\,q_i)$ is zero, Eq. (23) becomes

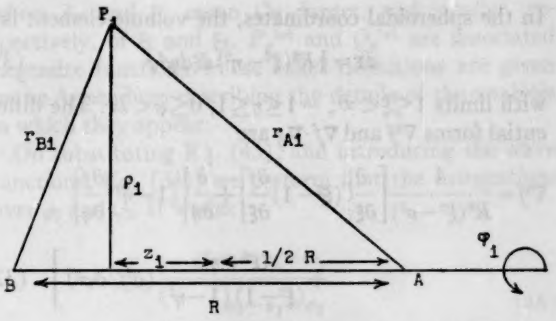

FIG. 1. Coordinate system

$$H(Q)=S(Q)\Big[(Z_AZ_B/R)+\sum_{i=1}^{N}(i\,|\,h\,|\,q_i)'+\sum_{i>j\geq 1}^{N}(ij\,|\,1/r\,|\,q_iq_j)'\Big]. \tag{24}$$

If one factor is zero, say $(i\,|\,q_i)$,

$$H(Q)=S'(Q)\Big[(i\,|\,h\,|\,q_i)'+\sum_{j=1,j\neq i}^{N}(ij\,|\,1/r\,|\,q_iq_j)'\Big]. \tag{25}$$

If two factors are zero, $(i\,|\,q_i)$ and $(j\,|\,q_j)$,

$$H(Q)=S'(Q)\,(ij\,|\,1/r\,|\,q_iq_j)'. \tag{26}$$

If more than two factors are zero, then $H(Q)$ is zero. The formulation of this paragraph has the advantage that the number of multiplications necessary to make a set of $H(Q)$ is reduced to a minimum.

V. WAVE FUNCTIONS AND COORDINATES

The computations of this paper will be based on a prolate spheroidal coordinate system whose foci are at the positions of nuclei A and B. Various relations involving this coordinate system will be described with reference to Fig. 1. The coordinates of the ith particle, at the point P_i, are the dimensionless quantities

$$\xi_i=(r_{Ai}+r_{Bi})/R, \tag{27}$$

$$\eta_i=(r_{Ai}-r_{Bi})\,R, \tag{28}$$

and the azimuthal angle φ_i about the internuclear axis. For some purposes one needs cylindrical coordinates $(z_i,\ \rho_i,\ \varphi_i)$, centered halfway between A and B, defined by

$$z_i=\tfrac{1}{2}R\xi_i\eta_i \tag{29}$$

$$\rho_i=\tfrac{1}{2}R[(\xi_i^2-1)(1-\eta_i^2)]^{\frac{1}{2}}. \tag{30}$$

In the spheroidal coordinates, the volume element is

$$d\mathbf{r}=\tfrac{1}{8}R^3(\xi^2-\eta^2)\,d\xi d\eta d\varphi \tag{31}$$

with limits $1\leq\xi<\infty$, $-1\leq\eta\leq 1$, $0\leq\varphi<2\pi$. The differential forms $\nabla^2 f$ and $\nabla f\cdot\nabla g$ are

$$\nabla^2 f=\frac{4}{R^2(\xi^2-\eta^2)}\left[\frac{\partial}{\partial\xi}\left\{(\xi^2-1)\frac{\partial f}{\partial\xi}\right\}+\frac{\partial}{\partial\eta}\left\{(1-\eta^2)\frac{\partial f}{\partial\eta}\right\}+\frac{(\xi^2-\eta^2)}{(\xi^2-1)(1-\eta^2)}(\partial^2 f/\partial\varphi^2)\right] \tag{32}$$

$$\nabla f\cdot\nabla g=\frac{4}{R^2(\xi^2-\eta^2)}\left[(\xi^2-1)(\partial f/\partial\xi)(\partial g/\partial\xi)+(1-\eta^2)(\partial f/\partial\eta)(\partial g/\partial\eta)+\frac{(\xi^2-\eta^2)}{(\xi^2-1)(1-\eta^2)}(\partial f/\partial\varphi)(\partial g/\partial\varphi)\right]. \tag{33}$$

The 1-electron wave functions chosen are all of a single parametric form as shown in Eq. (34):

$$\phi_i(\mathbf{r}_j)=\exp(-\delta_i\xi_j-\zeta_i\eta_j)\xi_j^{n_i}\eta_j^{m_i}\cdot\exp(i\nu_i\varphi_j)[(\xi_j^2-1)(1-\eta_j^2)]^{\frac{1}{2}|\nu_i|}. \tag{34}$$

The parameter δ_i must be positive to cause regularity at infinite distance from the molecule. The parameter ζ_i governs the axial distribution of charge, $\zeta_i=\delta_i$ corresponding to an atomic orbital on nucleus A, $\zeta_i=-\delta_i$ to an orbital about B, while $\zeta_i=0$ denotes a symmetric distribution. However, we do not restrict consideration to these particular values. The exponents n and m, which for simplicity we have restricted to positive integral values, are of use in forming higher orbitals. Nonzero values of m place a node in the plane midway between the two nuclei. The factor $\exp(i\nu\varphi)$ determines the orbital angular momentum about the internuclear axis, and the wave functions are eigenfunctions of this operator with eigenvalues $\hbar\nu_i$, where ν_i may be any positive or negative integer or zero. The factor

$$[(\xi_j^2-1)(1-\eta_j^2)]^{\frac{1}{2}|\nu_i|}=(2\rho_j/R)^{|\nu_i|}$$

is inserted with the dual objective of providing regularity on the internuclear axis and making the integrations as simple as possible. The form chosen is not unique.

VI. 1-ELECTRON INTEGRALS

The 1-electron integrals needed are $(i\,|\,j)$ and $(i\,|\,h\,|\,j)$. The latter can be expanded by using the definition Eq. (20) of h_i and the coordinates described in the last section. In particular, $(i\,|\,h\,|\,j)$ separates into a kinetic energy integral and two nuclear attraction integrals,

$$(i\,|\,h\,|\,j)=(i\,|\,-\tfrac{1}{2}\nabla^2\,|\,j)-(2/R)(Z_A+Z_B)[i\,|\,\xi/(\xi^2-\eta^2)\,|\,j]+(2/R)(Z_A-Z_B)[i\,|\,\eta/(\xi^2-\eta^2)\,|\,j]. \tag{35}$$

With the wave function (34), all these one-electron integrals may be expressed in closed form in terms of the well-known functions[9]

$$A_n(x)=\int_1^\infty t^n\exp(-xt)\,dt \tag{36}$$

$$B_n(x)=\int_{-1}^1 t^n\exp(-xt)\,dt. \tag{37}$$

The integrals for nonzero ν may be compactly handled if we extend the definitions of Eq. (36) and (37) to

$$A_n^{\nu}(x)=\sum_{k=0}^{|\nu|}\binom{|\nu|}{k}(-1)^{\nu-k}A_{n+2k}(x) \tag{38}$$

$$B_n^{\nu}(x)=\sum_{k=0}^{|\nu|}\binom{|\nu|}{k}(-1)^{k}B_{n+2k}(x). \tag{39}$$

Then, by direct substitution of the wave functions, followed by separation of the variables and integration over φ, it may be found that

$$(i\,|\,j)=(\pi R^3/4)\,\delta(\nu_i,\nu_j)[A_{n+2}^{\nu}(\delta)B_m^{\nu}(\zeta)-A_n^{\nu}(\delta)B_{m+2}^{\nu}(\zeta)] \tag{40}$$

$$(i\,|\,\xi/(\xi^2-\eta^2)\,|\,j)=(\pi R^3/4)\,\delta(\nu_i,\nu_j)A_{n+1}^{\nu}(\delta)B_m^{\nu}(\zeta) \tag{41}$$

$$(i\,|\,\eta/(\xi^2-\eta^2)\,|\,j)=(\pi R^3/4)\,\delta(\nu_i,\nu_j)A_n^{\nu}(\delta)B_{m+1}^{\nu}(\zeta) \tag{42}$$

where $n=n_i+n_j$, $m=m_i+m_j$, $\delta=\delta_i+\delta_j$, $\zeta=\zeta_i+\zeta_j$, but $\nu=\nu_i$ or ν_j.

The kinetic energy integral is more tedious. We found it simplest to apply Green's theorem and convert, in the integral, $\phi_i^*\nabla^2\phi_j$ to $\frac{1}{4}(\phi_i^*\nabla^2\phi_j+\phi_j\nabla^2\phi_i^*-2\nabla\phi_i^*\cdot\nabla\phi_j)$.[3] Now, let us write $\phi_i=\phi_i^0\phi_i'$, where

$$\phi_i^0=\exp(-\delta_i\xi-\zeta_i\eta)\xi^{n_i}\eta^{m_i},$$

$$\phi_i'=[(\xi^2-1)(1-\eta^2)]^{\frac{1}{2}|\nu|}\exp(i\nu\varphi)=[2\rho/R]^{|\nu|}\exp(i\nu\varphi).$$

The φ integration will cause the integral to vanish unless $\phi_i'=\phi_j'$. Using this fact, the vector identities

$$\nabla^2(fg)=f\nabla^2 g+g\nabla^2 f+2\nabla f\cdot\nabla g$$

$$\nabla(fg)=f\nabla g+g\nabla f,$$

the reality of $\phi_i^*\nabla^2\phi_j$, and the fact that $\nabla^2\phi_i'=0$, the quantity $\phi_i^*\nabla^2\phi_j$ in the integrand may be converted to the form

$$\tfrac{1}{4}|\phi_i'|^2(\phi_i^0\nabla^2\phi_j^0+\phi_j^0\nabla^2\phi_i^0-2\nabla\phi_i^0\cdot\nabla\phi_j^0)-\tfrac{1}{2}\phi_i^0\phi_j^0|\nabla\phi_i'|^2.$$

[9] M. Kotani, reference 1, Chap. II.

Since $|\nabla\phi_i'|^2=2\nu^2\rho^{-2}|\phi_i'|^2$, the kinetic energy integral may be expressed

$$(i|-\tfrac{1}{2}\nabla^2|j)=-[\delta(\nu_i,\nu_j)/8]\int d\tau[2\rho/R]^{2|\nu|}$$
$$\cdot(\phi_i^0\nabla^2\phi_j^0+\phi_j^0\nabla^2\phi_i^0-2\nabla\phi_i^0\cdot\nabla\phi_j^0-4\nu^2\rho^{-2}\phi_i^0\phi_j^0).$$

This equation shows that the integral for nonzero ν is related to that for $\nu=0$ by changing A_n and B_n to A_n^ν and B_n^ν, respectively, and adding a term in ν^2. The final result is

$$\begin{aligned}(i|-\tfrac{1}{2}\nabla^2|j)&=(\pi R^3/4)\delta(\nu_i,\nu_j)[-(1/2R^2)]\\
&\cdot[\{\delta'^2A_{n+2}^\nu(\delta)-2(\delta'n'+\delta)A_{n+1}^\nu(\delta)+2\delta'n'A_{n-1}^\nu(\delta)\\
&\quad+(n-n'^2)A_{n-2}^\nu(\delta)\}B_m^\nu(\zeta)\\
&-\{\zeta'^2B_{m+2}^\nu(\zeta)-2(\zeta'm'+\zeta)B_{m+1}^\nu(\zeta)+2\zeta'm'B_{m-1}^\nu(\zeta)\\
&\quad+(m-m'^2)B_{m-2}^\nu(\zeta)\}A_n^\nu(\delta)\\
&+\{n'^2+n-\delta'^2-m'^2-m+\zeta'^2\}A_n^\nu(\delta)B_m^\nu(\zeta)\\
&-4\nu^2\{A_{n+2}^{\nu-1}(\delta)B_m^{\nu-1}(\zeta)-A_n^{\nu-1}(\delta)B_{m+2}^{\nu-1}(\zeta)\}]\end{aligned}\tag{43}$$

where $n'=n_i-n_j$, $m'=m_i-m_j$, $\delta'=\delta_i-\delta_j$, and $\zeta'=\zeta_i-\zeta_j$. The coefficients of A_n^ν and B_n^ν vanish when negative indices would be required, and correct results are obtained when these undefined values of A_n^ν and B_n^ν are assumed to be zero. For computation, note that the last curly bracket of Eq. (43) is of the form of the overlap integral of Eq. (40), with ν replaced by $\nu-1$.

Actual evaluation of these one-electron integrals was by use of Eqs. (38)–(43). The $A_n(\zeta)$ were obtained by the well-known recursion formula

$$A_n(\delta)=A_0(\delta)+n\delta^{-1}A_{n-1}(\delta)\tag{44}$$

with $A_0(\delta)=\delta^{-1}e^{-\delta}$.[9] The $B_n(\zeta)$ were computed by Corbato's method[10] in conjunction with related functions needed for the 2-electron integrals. Further details may be found in Appendix II.

VII. 2-ELECTRON INTEGRALS

Because all the orbitals in this problem are of a single parametric form, there is but one type of 2-electron integral in our work, rather than the usual plethora of hybrid, coulomb, exchange, and one-center integrals. To evaluate the 2-electron integral $(ij|1/r|kl)$, we use Neumann's expansion[11] of $1/r_{12}$,

$$R/2r_{12}=\sum_{\mu=0}^{\infty}\sum_{\sigma=-\mu}^{\mu}(-1)^\sigma(2\mu+1)\left[\frac{(\mu-|\sigma|)!}{(\mu+|\sigma|)!}\right]^2$$
$$\cdot P_\mu^{|\sigma|}(\xi_-)Q_\mu^{|\sigma|}(\xi_+)P_\mu^{|\sigma|}(\eta_1)P_\mu^{|\sigma|}(\eta_2)\exp[i\sigma(\varphi_1-\varphi_2)],\tag{45}$$

where ξ_+ and ξ_- mean the larger, and smaller, respectively, of ξ_1 and ξ_2. $P_\mu^{|\sigma|}$ and $Q_\mu^{|\sigma|}$ are associated Legendre functions whose exact definitions are given in the Appendices describing the details of the analysis in which they appear.

On substituting Eq. (45), and introducing the wave functions, Eq. (34), we perform first the integrations over φ_1 and φ_2. If we let

$$\begin{aligned}\nu_k-\nu_i&=\sigma_1,\\ \nu_l-\nu_j&=\sigma_2\end{aligned}\tag{46}$$

the φ dependence of the integral is $\exp[i(\sigma_1+\sigma)\varphi_1+i(\sigma_2-\sigma)\varphi_2]$, so the integral vanishes unless

$$\sigma_1+\sigma_2=0,\tag{47a}$$

in that case the sum over σ collapses to the single value (or its negative)

$$\sigma=|\sigma_1|=|\sigma_2|.\tag{47b}$$

Henceforth we shall use σ to mean the value given by Eqs. (47a)–(47b). The φ integrations then cause the removal of the σ summation, and the change of the lower limit of the μ summation to σ, while contributing to $(ij|1/r|kl)$ a factor $4\pi^2\delta(\sigma_1,-\sigma_2)$.

We next consider the factors involving (ξ^2-1) and $(1-\eta^2)$. When the contributions from all four wave functions are collected, we have

$$[(\xi_1^2-1)(1-\eta_1^2)]^{\frac{1}{2}|\nu_i|+\frac{1}{2}|\nu_k|}[(\xi_2^2-1)(1-\eta_2^2)]^{\frac{1}{2}|\nu_j|+\frac{1}{2}|\nu_l|}.$$

When we do the ξ and η integrations, we will find it convenient to write this as

$$[(\xi_1^2-1)(1-\eta_1^2)]^{\frac{1}{2}\sigma+\tau_1}[(\xi_2^2-1)(1-\eta_2^2)]^{\frac{1}{2}\sigma+\tau_2},$$

since the $\frac{1}{2}\sigma$ power can be naturally associated with the Legendre functions. In general, the τ value to be associated with any two orbitals, say ϕ_u and ϕ_v, will be $\tau=\frac{1}{2}(|\nu_u|+|\nu_v|-|\nu_u-\nu_v|)$, and in particular

$$\begin{aligned}\tau_1&=\tfrac{1}{2}(|\nu_i|+|\nu_k|-\sigma)\\ \tau_2&=\tfrac{1}{2}(|\nu_j|+|\nu_l|-\sigma).\end{aligned}\tag{48}$$

Note that these definitions imply that τ is a positive integer or zero.

We are now prepared to consider the integrations over ξ_1 and ξ_2. It is evident that the integrand cannot be factored to separate the coordinates (ξ_1,η_1) from (ξ_2,η_2) because of the presence of the Legendre functions involving ξ_+ and ξ_-. This situation can be alleviated somewhat by using a slight generalization of a formula published by Ruedenberg.[12] The formula we

[10] F. J. Corbato, J. Chem. Phys. **24**, 452 (1956).

[11] F. E. Neumann, *Vorlesungen über die Theorie des Potentials und der Kugelfunktionen* (B. G. Teubner, Leipzig, Germany, 1878), Chap. 13.

[12] K. Ruedenberg, J. Chem. Phys. **19**, 1459 (1951).

need can be expressed as

$$(-1)^{\sigma}(2\mu+1)\int_1^{\infty}d\xi_1\int_1^{\infty}d\xi_2 P_\mu^{\sigma}(\xi_-)Q_\mu^{\sigma}(\xi_+)g_\mu^{1}(\xi_1)g_\mu^{2}(\xi_2)$$

$$=\int_1^{\infty}dx G_\mu^{1}(x)G_\mu^{2}(x) \quad (49)$$

where $g_\mu^{\gamma}(\xi)$ and $G_\mu^{\gamma}(x)$, $\gamma=1$ and 2, are related by

$$G_\mu^{\gamma}(x)=\{(2\mu+1)[(\mu+\sigma)!/(\mu-\sigma)!]\}^{\frac{1}{2}}$$

$$\cdot[P_\mu^{\sigma}(x)(x^2-1)^{\frac{1}{2}}]^{-1}\int_1^{x}d\xi P_\mu^{\sigma}(\xi)g_\mu^{\gamma}(\xi). \quad (50)$$

This transformation may be applied whenever all the operations indicated are meaningful. The exponential dependence of the wave functions is sufficient to guarantee the utility of Eqs. (49) and (50).

Summing both sides of Eq. (49) from $\mu=\sigma$ to ∞, we have, with suitable definition of $g_\mu^{\gamma}(\xi)$, an expression for $(ij\,|\,1/r\,|\,kl)$. Examining the result of the substitution of Eqs. (45) and (34) into $(ij\,|\,1/r\,|\,kl)$, it may be seen that

$$g_\mu^{\gamma}(\xi)=[(\mu-\sigma)!/(\mu+\sigma)!]\int_{-1}^{1}d\eta(\xi^2-\eta^2)\exp(-\delta_\gamma\xi-\zeta_\gamma\eta)$$

$$\cdot P_\mu^{\sigma}(\eta)(\xi^2-1)^{(\sigma/2)+\tau_\gamma}(1-\eta^2)^{(\sigma/2)+\tau_\gamma}\xi^{n_\gamma}\eta^{m_\gamma}. \quad (51)$$

Here, $\delta_1=\delta_i+\delta_k$, $\delta_2=\delta_j+\delta_l$, with corresponding definitions for ζ_γ, n_γ, and m_γ. The η integrations appearing in Eq. (51) are all of the same general form. Define

$$i_\mu^{\sigma}(m,\zeta,\tau)=\{(2\mu+1)[(\mu-\sigma)!/(\mu+\sigma)!]\}^{\frac{1}{2}}$$

$$\cdot\int_{-1}^{1}d\eta P_\mu^{\sigma}(\eta)\exp(-\zeta\eta)\eta^{m}(1-\eta^2)^{(\sigma/2)+\tau}, \quad (52)$$

and Eq. (51) may be rewritten

$$\{(2\mu+1)[(\mu+\sigma)!/(\mu+\sigma)!]\}^{\frac{1}{2}}g_\mu^{\gamma}(\xi)$$

$$=\exp(-\delta_\gamma\xi)\xi^{n_\gamma}(\xi^2-1)^{(\sigma/2)+\tau_\gamma}$$

$$\cdot[\xi^2 i_\mu^{\sigma}(m_\gamma,\zeta_\gamma,\tau_\gamma)-i_\mu^{\sigma}(m_\gamma+2,\zeta_\gamma,\tau_\gamma)]. \quad (53)$$

The integrals defined in Eq. (52) are related to spherical Bessel functions, and also to the $B_n(\zeta)$ used in Sec. IV. Their evaluation is discussed in Appendix II.

The next step is to substitute Eq. (53) into Eq. (50), and perform the ξ integration. When doing so, it is convenient to define another set of integrals

$$K_\mu^{\sigma}(n,\delta,\tau,x)=[P_\mu^{\sigma}(x)(x^2-1)^{\frac{1}{2}}]^{-1}$$

$$\cdot\int_1^{x}d\xi P_\mu^{\sigma}(\xi)\exp(-\delta\xi)\xi^{n}(\xi^2-1)^{(\sigma/2)+\tau} \quad (54)$$

in terms of which Eqs. (53) and (50) yield

$$G_\mu^{\gamma}(x)=K_\mu^{\sigma}(n_\gamma+2,\delta_\gamma,\tau_\gamma,x)i_\mu^{\sigma}(m_\gamma,\zeta_\gamma,\tau_\gamma)$$

$$-K_\mu^{\sigma}(n_\gamma,\delta_\gamma,\tau_\gamma,x)i_\mu^{\sigma}(m_\gamma+2,\zeta_\gamma,\tau_\gamma). \quad (55)$$

To show more clearly the role of the wave functions in $G_\mu^{\gamma}(x)$, we shall from now on use the notation $(u\,|\,G_\mu(x)\,|\,v)$ to mean a form like $G_\mu^{\gamma}(x)$, but with n_γ replaced by n_u+n_v, etc.

Recapitulating the earlier discussion in more explicit form, we obtain the result that the two-electron integral has been reduced to the form

$$(ij\,|\,1/r\,|\,kl)=(\pi R^3/4)^2(2/R)\delta(\sigma_1,-\sigma_2)$$

$$\cdot\int_1^{\infty}dx\sum_{\mu=\sigma}^{\infty}(i\,|\,G_\mu(x)\,|\,k)(j\,|\,G_\mu(x)\,|\,l). \quad (56)$$

The integral over x in Eq. (56) is now to be evaluated numerically. Using values of the integrand at points x_κ, the integral can be written

$$(ij\,|\,1/r\,|\,kl)=(\pi R^3/4)^2$$

$$\cdot(2/R)\delta(\sigma_1,-\sigma_2)\sum_\kappa w_\kappa\sum_{\mu=\sigma}^{\infty}(i\,|\,G_\mu(x_\kappa)\,|\,k)(j\,|\,G_\mu(x_\kappa)\,|\,l),$$

where w_κ is a weight factor. Defining

$$(w_\kappa)^{\frac{1}{2}}(i\,|\,G_\mu(x_\kappa)\,|\,j)=(i\,|\,G_{\mu\kappa}\,|\,j), \quad (57)$$

Eq. (56) becomes

$$(ij\,|\,1/r\,|\,kl)=(\pi R^3/4)^2$$

$$\cdot(2/R)\delta(\sigma_1,-\sigma_2)\sum_\kappa\sum_{\mu=\sigma}^{\infty}(i\,|\,G_{\mu\kappa}\,|\,k)(j\,|\,G_{\mu\kappa}\,|\,l). \quad (58)$$

The only remaining problems, besides evaluating Eq. (54), are the choice of points x_κ and weights w_κ, and the upper limit to which it is necessary to carry the sum over μ. A direct examination was made of the functions $(i\,|\,G_\mu(x)\,|\,j)$ for the range $0.25<\delta_i+\delta_j<20$ to determine suitable integration formulas. The annoyance of preparing test tables at irregular intervals caused us to restrict consideration to constant interval formulas, so that only the Newton-Cotes expressions of various degrees were explored.[13] We finally found that by taking points at equal intervals of $1/x$, the range $0\leq 1/x\leq 1$ could be spanned with 7 significant figure accuracy with 35 points, not including the point $x=1$ where $(i\,|\,G_\mu(x)\,|\,j)=0$ for all sets of parameters. The integration was done with four Newton-Cotes formulas, a 10 point formula for $0\leq 1/x\leq 0.36$, an 11 point formula for $0.36\leq 1/x\leq 0.76$, both at 0.04 interval, and nine point formulas, for $0.76\leq 1/x\leq 0.92$ at 0.02 interval, and for $0.92\leq 1/x\leq 1$, at intervals of 0.01. These formulas contribute to the weights w_κ.

Since we have used equal intervals of $1/x$, the weight factors w_κ will be x^2 times the customary Newton-Cotes weightings. This means that at the point $x=\infty$, quantities proportional to

$$\lim_{x\to\infty} x G_\mu^{\gamma}(x)$$

[13] W. E. Milne, *Numerical Calculus* (Princeton University Press, Princeton, New Jersey, 1949), Chap. 4.

must be evaluated for Eq. (58). These limits exist, and are in fact zero unless $\mu=0$. For this reason, among others, it is convenient to compute $(w_\kappa)^{\frac{1}{2}}K_\mu^\sigma(n, \delta, \tau, x_\kappa)$, and to multiply Eq. (55) through by $(w_\kappa)^{\frac{1}{2}}$ before evaluation. The integrals $(w_\kappa)^{\frac{1}{2}}K^\sigma(n, \delta, \tau, x_\kappa)$ are discussed in Appendix III.

The number of terms one must keep in the sum over μ may be estimated by studying the behavior of the K and i integrals, Eqs. (52) and (54). By far the most important quantities affecting the convergence of the sum are found to be $|\zeta_1|$ and $|\zeta_2|$, larger values of which correspond to slower convergence. In fact, for $\zeta=0$ the series reduces to a finite number of terms. Since the speed of computation depends on the number of terms, we actually compute a number chosen for each integral after examining its $|\zeta_1|$ and $|\zeta_2|$. As a rough indication, we use an average of 13 terms for $|\zeta|=10$, and 19 terms for the maximum value, $|\zeta|=19.9$. Since the κ sum is over 35 values, the maximum number of $G_\mu^\gamma(x_\kappa)$, for given γ, is 665.

The paramount advantage of the procedure using Eq. (58) is that $(i\,|\,G_{\mu\kappa}\,|\,j)$ depends upon the parameters of one electron only, so that if tables of $(i\,|\,G_{\mu\kappa}\,|\,j)$ are prepared for all the necessary combinations of one-electron parameters, these tables may be combined to form the much larger number of two-electron integrals. By testing to see that Eq. (47a) is satisfied, those two-electron integrals which vanish for symmetry reasons may readily be excluded.

With the computational procedure we are using, each $(i\,|\,G_{\mu\kappa}\,|\,j)$ is used an average of $(N-1)^2$ times while doing an N electron problem. Since the procedure outlined above has been found, for single integrals, to be comparable in computing speed with the previously published methods, the use of the present method for a group of integrals based on the same orbitals can reduce the computation time by an order of magnitude.

A second feature of the method using Eq. (58) is that the integrand of Eq. (56) is positive for all x, so that the numerical integration does not introduce large computational inaccuracies. This situation is in contrast with the completely analytical methods, which copiously shed significant figures through the taking of differences between numbers of approximately equal size.

A slight complication arises because some of the w_κ are negative, making the corresponding $(i\,|\,G_{\mu\kappa}\,|\,j)$ imaginary. We must then store $|(i\,|\,G_{\mu\kappa}\,|\,j)\,|$ in the computer, and change the signs of the products of imaginary $(i\,|\,G_{\mu\kappa}\,|\,j)$ appearing in Eq. (58).

VIII. ITERATION METHOD

The procedure of the preceding five sections enables the calculation of the energy levels associated with a given set of 1-electron orbitals ϕ_i. As outlined in Sec. II, it is desired to make the energy level calculation repeatedly for different values of the orbital parameters, adjusting them so as to reach stationary values of the energy levels. In particular, the minimum energy which can be reached in this way is an approximation to the ground state.

The method we used involved steps which change the parameters of but one ϕ_i at a time. From a practical viewpoint, this is advantageous because but a small fraction of the 1- and 2-electron integrals are then altered from the previous computation, and most of the altered 2-electron integrals use one previously calculated set of $(i\,|\,G_{\mu\kappa}\,|\,j)$. Accordingly, provision is made to retain from each calculation all the $(i\,|\,j)$, $(i\,|\,h\,|\,j)'$, $(ij\,|\,1/r\,|\,kl)'$, and $(i\,|\,G_{\mu\kappa}\,|\,j)$, and not to destroy any values until it has been determined that they pertain to a parameter set from which a step will not be made. This retention of material for possible re-use makes possible great savings in computation time. For a 4-electron problem, the time saved is about 50% per step; for a six-electron problem, the time is cut by a factor of 3.

In the iteration method used here, one parameter is moved by successive steps of some size, Δ, until a relative minimum is reached in the ground-state energy. The other parameters, in turn, are similarly treated, and the process is repeated until all the parameters are at optimum values with respect to steps of size Δ. The step size is then decreased, usually by a factor 4, and the searching is resumed. The program terminates when a sufficiently small step size has been reached. The parameters adjusted are usually the δ and ζ values for the various ϕ_i. We have kept the n, m, and ν parameters fixed.

Our experience has not yet been adequate to enable us to make strong and definitive remarks about the efficiencies of various searching techniques. We have found, however, that usually there is much more interaction between changes in the values of the δ and ζ referring to the same ϕ_i than between two parameters not so related, and that in most problems there are some ϕ_i which affect the energy much more sensitively than others. These observations suggest that a method whereby human intelligence can supplement the speed and reliability of the computer would be most valuable here. This is particularly true in view of the large amount of computer time required to solve molecular problems.

We have found that the method outlined here works equally well no matter what initial parameter values are chosen, except that a poor initial guess does not lead to convergence as soon. If a group of similar problems are done, as is the case when R is changed gradually for a given molecule, it is found that after one or two problems, very good starting parameters can be selected, and the searching time thus minimized. This point will be discussed at greater length in communications dealing with computed results.

The method used here is stable in the sense that it can not lead to oscillatory behavior, inasmuch as only steps which decrease the energy will be taken. However,

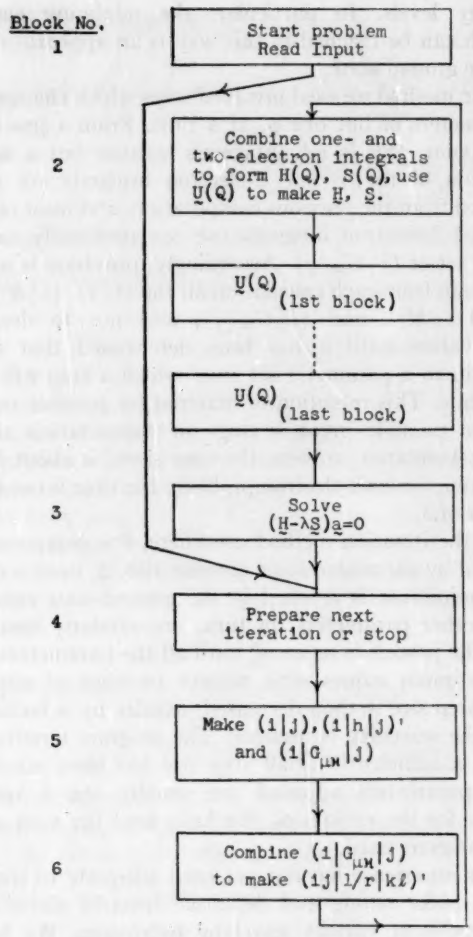

FIG. 2. Block diagram of program tape.

it is possible to find a minimum which is relative, but not absolute. Since such points are not usually good approximations to states of interest, it is desirable to avoid them. It is difficult to guarantee that this has been done, but by starting with physically reasonable parameter values, and taking large initial step sizes, it becomes improbable that one would get permanently trapped in a wrong well of the energy surface in the parameter space. Further assurance must come from an examination of the results.

The formalism used in this paper provides for another type of parameter adjustment, namely the variation of the internuclear distance R while keeping all the parameters of the ϕ_i invariant. Since our work is all in dimensionless variables, it is easy to see that all the potential energy terms have the dependence $1/R$, after dividing through by the R dependence of S, while the kinetic energies depend similarly on $1/R^2$. Minimizing the energy with respect to R may be seen to be equivalent to choosing that value of R which satisfies the virial theorem. This fact leads us to the conclusion that the virial theorem is automatically satisfied for the wave functions resulting from this study for a diatomic system at its equilibrium internuclear separation.

IX. COMPUTER OPERATIONS

A. General

The program of computation outlined in the previous sections of this paper was coded for the IBM Type 701 data processing machine. The equipment used, at the University of California Computer Center, Berkeley, consisted of a two frame, magnetic core main unit, 4 tape units, 4 drums, card reader, punch, and line printer. The fast storage capacity is 4096 10 decimal digit words. One program instruction occupies one half of one of these words. There are 8192 words of drum storage. The program was coded using a non-interpretive symbolic assembly routine similar to the "New York" Assembly program for the IBM 704.[14] The code we prepared consisted of some 10 000 instructions, and in addition required much data storage. Consequently, it was necessary to store the program on tape, and to call forth sections of it as needed. It was also necessary to use tape to retain computed matter for use later in the problem. Tape reading is only fast when the numbers to be read are near the reading station, so it was necessary to make careful plans for the retrieval of information placed upon the tapes. Since the amount of data we work with is larger than the fast storage capacity of any scientific computer now in operation, it seems appropriate to indicate how our coding is organized.

The over-all plan of the code can be described with the aid of Fig. 2. The blocks marked with numbers 1–6 are read into fast storage and the programing on them executed, one at a time. At the start of the problem, block No. 1 is executed, thereby causing the definition of the problem, and initial parameters, to be entered into memory. The program tape is then skipped to block No. 4, wasting some time only once. Here the parameters for the current calculation (this time the initial values) are selected, and block No. 5 is read in and begun. Here the integrals $(i\,|\,h\,|\,j)'$ and $(i\,|\,j)$ are computed and placed as a table in storage. The total number of such integrals is small enough (N^2 of each) that they could be permanently retained in fast storage. The integrals $(i\,|\,G_{\mu\kappa}\,|\,j)$ use some common information, as indicated in Appendix III. However, there are so many $(i\,|\,G_{\mu\kappa}\,|\,j)$, due to the many values of μ and κ, that each set must be placed into auxiliary storage to make room for the computation of the next.

Tables of $(i\,|\,G_{\mu\kappa}\,|\,j)$ are thus placed on tape, in the order $(i, j) = (1, 1), (1, 2), \cdots, (1, N), (2, 1), \cdots, (N, N-1), (N, N)$. Then the $(i\,|\,j)$ and $(i\,|\,h\,|\,j)'$ which have been accumulating in fast storage are placed

[14] A description can be obtained from IBM, 590 Madison Avenue, New York 22, New York.

behind the (N, N) tape record, and we pass to program block No. 6.

Block No. 6 computes the $(ij \mid 1/r \mid kl)$ according to Eq. (58). That equation requires the presence in fast storage of two sets of $G_{\mu\kappa}$ integrals, and the coding should take the $G_{\mu\kappa}$ off the tape and combine them in the most efficient manner. The tape units we use can be read in either direction, and hence make possible the following scheme, in which the tape is always positioned correctly for the next record to be read. Suppose that there is enough space in fast memory for j sets of $G_{\mu\kappa}$. Then starting from (N, N) (to which the tape is near at the conclusion of block No. 5), read backwards j sets of $G_{\mu\kappa}$, and make all 2-electron integrals possible by taking these sets pairwise. Then, replace the set of $G_{\mu\kappa}$ last read, with the next set of $G_{\mu\kappa}$, continuing to read backwards, and make all integrals possible using the new set. This process is continued until (1, 1) has been reached, at which point the entire process is repeated, this time reading forward, starting with (1, 1), and proceeding up to, but not including, the last $j-1$ sets of $G_{\mu\kappa}$. Alternatively going backward and forward, each time stopping $j-1$ sets of $G_{\mu\kappa}$ further from the end of the tape than the last time the tape was moved in that direction, one proceeds until all pairs of $G_{\mu\kappa}$ sets have been combined. The procedure that has been outlined causes the 2-electron integrals to be computed in a most peculiar order. Before going on, they are converted to $(ij \mid i/r \mid kl)'$ and rearranged according to their indices for ease of later use.

While the program of block No. 6 is being executed, there is time to reposition the program tape to block No. 2, which is used next. Here the tables of $(i \mid j)$, $(i \mid h \mid j)'$, and $(ij \mid 1/r \mid kl)'$ are combined according to Eqs. (18) and (24)–(26) to make $H(Q)$ and $S(Q)$, and these quantities are combined with $\mathbf{U}(Q)$, which are read off the program tape subsequent to block No. 2 as needed. This causes the program tape to be positioned at block No. 3, and the quantities $\mathbf{H}$ and $\mathbf{S}$ to be accumulated in the machine. Proceeding to block No. 3, the eigenvalue equation is solved, and the smallest eigenvalue retained for use in connection with the next iteration to which one now proceeds in block No. 4.

The program loops repeatedly through blocks No. 2 through No. 6, stopping when the best possible parameters have been found. The only differences between the first and subsequent passes arise because after the first pass there are existent sets of $(i \mid j)$, $(i \mid h \mid j)'$, $(i \mid G_{\mu\kappa} \mid j)$, and $(ij \mid 1/r \mid kl)'$ on tape or in storage. On the second pass, in block No. 5 only those integrals which are different are recomputed, and a new $G_{\mu\kappa}$ tape is made by transferring from the old tape all unchanged sets of $G_{\mu\kappa}$, writing newly computed values in place of the old ones for the sets which have been changed. The "old" tape is not destroyed. Then, in block No. 6, only the changed $(ij \mid 1/r \mid kl)$ are computed. For the third and subsequent passes, the $G_{\mu\kappa}$ tape which corresponds to the parameter set from which the current step is being taken is used as the "old" tape already referred to, and the "new" tape is written over the other existent tape, which is no longer needed. This means that the tape corresponding to the best parameter set found so far is the one which is retained.

B. Time

Practically all the programing described above is written to operate directly in the standard fixed-point binary arithmetic of the Type 701 Computer. Floating point routines were used only when the time involved was negligible, and no other interpretive routines were employed. The add time is 36 μsec, and the multiply or divide time is 456 μsec. Coupling times to tape and drum storage average somewhat over 1 msec per word transferred. These figures provide a basis for evaluating the computing times we have determined for the various parts of this program.

To make the integrals of block No. 5 for one pair of one-electron functions requires between 3 and 8 sec, depending upon how many values of μ are required. An average time is about 5 sec. Including all tape movement time, it requires an average of about 0.3 sec to compute, in block No. 6, one $(ij \mid 1/r \mid kl)$. These figures, taken together, imply average lower and upper limits of 0.3 and 10.3 sec per 2-electron integral, a time of about 1.3 sec per integral for doing all the two-electron integrals of a four-electron problem, or about 0.7 sec per integral for all those of a 6-electron problem.

The program of block No. 2, which works with the permutation matrices, requires about 8 sec for a 4-electron problem, about 3 min for a 6-electron problem. This section of the program is proportional to $N!$ in time. The time involved in matrix diagonalization is not large, but is quite dependent upon the matrices involved. For five by five matrices, the time averages 2 sec.

The over-all time, comprised mainly of the items already mentioned, but also including a few lines of printing, is, for a four-electron problem, about 2 minutes, and, for a six-electron problem, about 10 min. On iteration, these times improve because not all the time-consuming 2-electron integrals need be recomputed. A 4-electron problem has been found to take about 89 sec per iteration, and a six-electron problem about 8 min.

C. Special Programs

In the course of developing this program, it was necessary to develop codes to perform several simple processes which come up frequently in quantum-mechanical applications. We shall discuss two such codes.

First, there is the problem of solving the matrix equation

$$(\mathbf{H}-\lambda\mathbf{S})\mathbf{a}=0. \tag{2}$$

Our procedure is to start by finding a unitary matrix, **L**, which diagonalizes **S**, so that $\mathbf{LSL}^{-1}=\mathbf{D}$, where **D** is a diagonal matrix with positive elements. Letting $\mathbf{D}^{\pm\frac{1}{2}}$ be the diagonal matrix whose elements are in the $\pm\frac{1}{2}$ power of the corresponding elements of **D**, Eq. (2) can be transformed to

$$[\mathbf{D}^{-\frac{1}{2}}\mathbf{LHL}^{-1}\mathbf{D}^{-\frac{1}{2}}-\lambda\mathbf{I}]\mathbf{D}^{\frac{1}{2}}\mathbf{La}=0, \tag{59}$$

where **I** is the unit matrix. Diagonalizing the symmetric matrix $\mathbf{D}^{-\frac{1}{2}}\mathbf{LHL}^{-1}\mathbf{D}^{-\frac{1}{2}}$ with the unitary matrix **M**, we obtain the diagonal matrix of the eigenvalues, $\mathbf{MD}^{-\frac{1}{2}}\mathbf{LHL}^{-1}\mathbf{D}^{-\frac{1}{2}}\mathbf{M}^{-1}=\Lambda$, and the eigenvectors $\mathbf{a}_i=\mathbf{L}^{-1}\mathbf{D}^{-\frac{1}{2}}\mathbf{M}^{-1}\mathbf{e}_i$, where $\mathbf{e}_i$ is a column vector containing unity in the ith row and zero elsewhere. The eigenvalue corresponding to $\mathbf{a}_i$ is of course Λ_{ii}. The two diagonalizations required here were done by the method of successive 2-by-2 transformations. The procedure outlined above was found to be faster than the use of a Schmidt orthogonalization process followed by a single diagonalization.

The second problem is that of systematically generating permutations. In our method each permutation is made from the one preceding it by the application of a relatively simple algorithm. The advantage of the method is that it minimizes the difference between successive permutations, and thereby also the computation time. We are able to generate permutations at about 1 msec each, essentially regardless of the number of elements being permutated. The algorithm may be stated as follows: Consider the permutation P. To make the next permutation, Q, (1) Find the smallest i such that $p_i<p_{i+1}$, where p_i is the number of the object placed by P in the position originally occupied by the ith object. If no such i exists, P is the last permutation. (2) Find the smallest j such that $p_j<p_{i+1}$. (3) Set

$$\begin{aligned} q_k&=p_k, \qquad k\geq i+2,\\ q_{i+1}&=p_j,\\ q_{i-j+1}&=p_{i+1},\\ q_{i-k+1}&=p_k, \qquad k\neq j, \qquad 1\leq k\leq i. \end{aligned} \tag{60}$$

This process causes half the permutations to be generated from their predecessors by a single pairwise exchange, two-thirds of the remaining permutations to be generated by a triple exchange, etc.

X. ACKNOWLEDGMENTS

This work would not have been possible without the aid of the University of California Computer Center, in Berkeley. The Computer Center has been able to provide much computing time for this research through its grant from the National Science Foundation. In addition, the Director and staff of the Computer Center have been most helpful and cooperative in all phases of the work. Mr. Ferris T. Ross, of IBM, has contributed many valuable suggestions with regard to the use of his company's equipment. Mr. Harold Gillette and Mr. Walter Hutchinson assisted in the programing of the one-electron integrals. We wish to acknowledge the assistance of Mr. Howard Taylor, who made many valuable contributions to this project. The author has been aided in the support of this research by a grant from the Alfred P. Sloan Foundation.

APPENDIX I. SPIN MATRIX GENERATION

We shall now show how the spin transformation matrices $\mathbf{V}(P)$ can be generated, for arbitrary P, from a single rectangular matrix **C**. **C** relates the spin functions Θ_i to simple product spin functions we shall denote by Ω_j, according to

$$\Theta_i=\sum_j C_{ij}\Omega_j(\mathbf{s}), \quad 1\leq i\leq d, \quad 1\leq j\leq d'. \tag{61}$$

Each Ω_j consists of a succession of α and β spin functions for the individual electrons. All the Ω_j have the same number of α and β functions, so that they all are eigenfunctions of the z component, of the total spin with the same eigenvalue. The set of Ω_j, $1\leq j\leq d'$, consists of all possible permutations of the electrons among the α and β functions. For example, the six Ω_j for 4 electrons with zero z spin component are $\alpha(\mathbf{s}_1)\alpha(\mathbf{s}_2)\beta(\mathbf{s}_3)\beta(\mathbf{s}_4)$, $\alpha(\mathbf{s}_1)\beta(\mathbf{s}_2)\alpha(\mathbf{s}_3)\beta(\mathbf{s}_4)$, and (suppressing arguments) $\alpha\beta\beta\alpha$, $\beta\alpha\alpha\beta$, $\beta\alpha\beta\alpha$, and $\beta\beta\alpha\alpha$. The matrix C is chosen so the Θ_i will also be eigenfunctions of the total spin squared, with a given eigenvalue.

Now, consider the effect of applying a permutation P to both sides of Eq. (61). The Θ_i will transform according to the matrix $\mathbf{V}(P)$. The Ω_j will transform into one another, as is evident from the way in which they are constructed. Let Ω_{p_l} be the function into which Ω_l transforms under P. Eq. (61), when permuted, then becomes

$$\sum_l V_{kl}(P)\Theta_l(\mathbf{s})=\sum_l C_{kl}\Omega_{p_l}(\mathbf{s}) \tag{62}$$

where the indices have been changed. If we multiply the left and right sides of Eq. (62) by corresponding sides of Eq. (61), we get

$$\sum_l V_{kl}(P)\Theta_l(\mathbf{s})\Theta_i(\mathbf{s})=\sum_{j,l} C_{ij}C_{kl}\Omega_j(\mathbf{s})\Omega_{p_l}(\mathbf{s}). \tag{63}$$

On integrating over the spin coordinates, much simplification results from the orthonormality of both the Θ_i and the Ω_j. The result is

$$V_{ki}(P)=\sum_l C_{ip_l}C_{kl}. \tag{64}$$

This result is operationally useful, since the matrix **C** is known and it is possible to determine p_l from l.

Finding p_l consists of determining which Ω_j the function Ω_l transforms into under the permutation P. Since each Ω_i is an ordered product of α and β functions, it can be represented very conveniently in a binary computer as a series of zeros and ones. The

effect of the permutation P can be directly evaluated by permuting the zeros and ones, and then finding which such series is identical with the one resulting from the permutation.

APPENDIX II. INTEGRATIONS OVER η

The integrals B_n, introduced in Eq. (37) of Sec. VI, and the $i_\mu^\sigma(m, \zeta, \tau)$, appearing in Eq. (52) of Sec. VII, can be constructed together. Although it is possible to compute the B_n independently of the $i_\mu^\sigma(m, \zeta, \tau)$, either by direct integration or by a recursion formula, both these methods suffer from extreme numerical inaccuracy over large portions of the required range. The method used here, in which the B_n are expressed as linear combinations of the $i_\mu^0(0, \zeta, 0)$, is due to Corbato.[10] In this method the various contributions to each B_n are all of the same sign, and can be computed quite accurately.

For the discussion of this Appendix, we make the modified definition

$$I_\mu^\sigma(m, \zeta, \tau) = \frac{(\mu-\sigma)!}{(\mu+\sigma)!}\int_{-1}^{1} d\eta \cdot \exp(-\zeta\eta) P_\mu^\sigma(\eta) \eta^m (1-\eta^2)^{\frac{1}{2}\sigma+\tau}. \quad (65)$$

To simplify some of the following equations, we sometimes shall abbreviate by omitting the arguments of I_μ^σ, and suppressing the upper index σ when it is zero. The relation between I_μ^σ and i_μ^σ is

$$i_\mu^\sigma = \left[\frac{(\mu+\sigma)!}{(\mu-\sigma)!}(2\mu+1)\right]^{\frac{1}{2}} I_\mu^\sigma. \quad (66)$$

To complete the definition of I_μ^σ, we list here the expression we are using for the associated Legendre functions $P_\mu^\sigma(\eta)$. For $-1<\eta<1$,

$$P_\mu^\sigma(\eta) = [(-1)^\sigma/2^\mu\mu!](1-\eta^2)^{\sigma/2}(d/d\eta)^{\sigma+\mu}(\eta^2-1)^\mu. \quad (67)$$

For any given calculation, we shall require I_μ^σ for single values of σ, τ, and ζ, a series of up to 19 consecutive μ values proceeding upward from $\mu=\sigma$, and two values of m, namely m_i+m_j, and m_i+m_j+2, where i and j refer to the two one-electron orbitals involved in a set of B and i integrals. Note that the same pairs of orbitals are involved in both the B and i integrals.

Our first step is to generate the $I_\mu^\sigma(0, \zeta, 0)$. If $\sigma=0$, we then proceed to make the B_n by Corbato's method. If $\sigma\neq 0$, the B_n are not required, since the corresponding one-electron integrals vanish identically on account of the φ integrations. We are therefore free to generate the I_μ^σ, $\sigma\neq 0$, by means of a method not passing through the I_μ.

The I_μ are related by the well-known recursion formula

$$(2\mu+1)\zeta^{-1}I_\mu = I_{\mu+1} - I_{\mu-1}. \quad (68)$$

Eq. (68) should not be used in the ascending direction since $\zeta^{-1}I_\mu$ is of opposite sign to $I_{\mu\pm1}$. Following Corbato, one may introduce the ratios

$$x_\mu = I_{\mu+1}/I_\mu \quad (69)$$

in terms of which Eq. (68) becomes equivalent to

$$x_{\mu-1} = -\zeta/(2\mu+1-\zeta x_\mu). \quad (70)$$

Setting $x_M=0$, for some large M, one may work downwards to x_0, with increasing proportional accuracy in the x_μ at each step. Corbato has estimated the minimum values of M for various conditions. We used here the criterion $M=27+|\zeta/1.95|$. This M value is designed to yield 10 significant decimal digits in the first few I_μ, with the later I_μ, which decrease in magnitude, given to about the same absolute accuracy as the first I_μ.

To convert the ratios x_μ to the I_μ themselves, we start from Corbato's result,

$$I_0 = \frac{2e^{|\zeta|}}{1+|\zeta|-\zeta x_0}, \quad (71)$$

and work up to higher I_μ using Eq. (69). Note that Eq. (71) does not introduce inaccuracy through its denominator, since all three terms are actually of the same sign.

When $\sigma\neq 0$, there are two good alternative routes to the I_μ^σ. One is based on the recursion formula

$$(2\mu+1)I_\mu^\sigma(m, \zeta, \tau) - I_{\mu+1}^{\sigma-1}(m, \zeta, \tau) - I_{\mu-1}^{\sigma-1}(m, \zeta, \tau) \quad (72)$$

using the special case $m=\tau=0$, while the other is based on the apparently less widely known formula

$$I_\mu^\sigma(0, \zeta, 0) = \zeta^{-\sigma} I_\mu(0, \zeta, 0). \quad (73)$$

By virtue of Eq. (73), one may use the procedure involving Eqs. (69) and (70), along with the expression (71) for I_0, except that before generating the I_μ, one divides I_0 by ζ^σ, so as to produce the I_μ^σ. One thereby works through quantities I_μ^σ, $\sigma>\mu$, which are ordinarily thought of as undefined. In these cases Eq. (73) may be regarded as an extension of the definition. In any case, the numerical procedure is completely specified. The alternative route, through Eq. (72), obviously involves production of the I_μ, followed by stepwise increase of σ.

Which of Eqs. (72) and (73) to use depends upon the details of the computer programing and upon the value of $|\zeta|$. For large $|\zeta|$, the x_μ will be nearly unity, and the difference appearing in Eq. (72) will be between nearly equal quantities. This situation suggests the use of Eq. (73). For small $|\zeta|$, the quantities on the right side of Eq. (72) are widely different and it may be used to advantage. On the other hand, there may be computer scaling problems associated with the use of Eq. (73), since I_μ^σ may be much larger than I_μ. We actually used Eq. (72) for this reason.

In the case $\sigma=0$, the B_n are to be obtained from the I_μ. The formula for this conversion is[10]

$$B_n=\sum_{\mu=0,1}^{n}{}' D_{n\mu}I_\mu, \tag{74}$$

where

$$D_{n\mu}=n!(2\mu+1)/[(n-\mu)!!(n+\mu+1)!!], \tag{75}$$

with

$$n!!=n(n-2)(n-4)\cdots(2 \text{ or } 1), \quad \text{and} \quad \sum_{\mu=0,1}^{n}{}'$$

summed over even values of $n=\mu$ only. The sum of the coefficients of the I_μ contributing to any B_n is unity, and, as remarked earlier, all contributions have the same sign. This makes Eq. (74) very advantageous numerically.

Whether or not $\sigma=0$, there is still, in general, the necessity of considering the $I_\mu{}^\sigma(m, \zeta, \tau)$ for nonzero values of m and τ. Direct expansion of $(1-\eta^2)^\tau$ enables expression of the formulas for nonzero τ values in terms of values for which $\tau=0$, but with higher values of m. The basic problem, then, is to proceed from lower to higher m values. The simplest way of doing so is to use the formula

$$I_\mu{}^\sigma(m, \zeta, \tau)=[(\mu+\sigma+1)/(2\mu+1)]I_{\mu+1}{}^\sigma(m-1, \zeta, \tau) +[(\mu-\sigma)/(2\mu+1)]I_{\mu-1}{}^\sigma(m-1, \zeta, \tau). \tag{76}$$

Note that the sum of the two coefficients on the right side of Eq. (76) is unity. Since none of the coefficients in Eq. (76) depend upon m, observe that that equation also applies for $\tau\neq0$. Further, it can be seen that the order of application of Eqs. (72) and (76) can be chosen with reference to the convenience of the computer programing, since Eq. (72) does not require $m=0$.

The integrals with nonzero τ are given in terms of those for which $\tau=0$ by

$$I_\mu{}^\sigma(m, \zeta, \tau)=\sum_{k=0}^{\tau}(-1)^k\binom{\tau}{k}I_\mu{}^\sigma(m+2k, \zeta, 0). \tag{77}$$

Although we did not find it convenient to use them, there are a few additional formulas whose use might well simplify calculation of the B_n in certain cases. First, let us note that if $\sigma=0$, the necessarily equal values of ν from the two orbitals appearing in the B and i integrals are equal in absolute value to τ, according to the definitions of Sec. VII. Then, because the relations involved are linear, one may write

$$B_n{}^\nu(\zeta)=\sum_{\mu=0,1}^{n}{}' D_{n\mu}I_\mu{}^0(0, \zeta, \nu) \tag{78}$$

so that the binomial summation involved in going from B_n to $B_n{}^\nu$ can be avoided. The $I_\mu{}^0(0, \zeta, \nu)$ appearing on the right side of Eq. (78) will have to be made whether or not Eq. (78) is to be used. Generalizing still further,

$$B_{n+m}{}^\nu(\zeta)=\sum_{\mu=0,1}^{n}{}' D_{n\mu}I_\mu{}^0(m, \zeta, \nu). \tag{79}$$

Equation (79) contains as a special case an alternative formulation for B_n,

$$B_n(\zeta)=I_0{}^0(n, \zeta, 0). \tag{80}$$

APPENDIX III. INTEGRATIONS OVER ξ

The integrals $K_\mu{}^\sigma(n, \delta, \tau, x)$, defined in Eq. (54) of Sec. VII, are important in the evaluation of the ξ integrals as described there. These functions are interesting in that they possess a mixture of the properties characteristic of incomplete gamma functions, and generalized Bessel and Legendre functions, particularly in some limiting cases.

We start by defining the associated Legendre functions as used in this paper in the range $(1, \infty)$.

$$P_\mu{}^\sigma(x)=[(x^2-1)^{\frac{1}{2}\sigma}/2^\mu\mu!](d/dx)^{\sigma+\mu}(x^2-1)^\mu \tag{81}$$

$$Q_\mu{}^\sigma(x)=(x^2-1)^{\frac{1}{2}\sigma}(d/dx)^\sigma Q_\mu(x), \tag{82}$$

with

$$Q_\mu(x)=\tfrac{1}{2}P_\mu(x)\log[(x+1)/(x-1)] -\sum_{j=1}^{\leq\frac{1}{2}(\mu+1)}\frac{2\mu-4j+3}{(2j-1)(\mu-j+1)}P_{\mu-2j+1}(x). \tag{83}$$

The functions of the second kind appear only in the main text of Sec. VII.

For work in this Appendix, we shall find it convenient to use functions

$$f_\mu{}^\sigma(t)=\sum_{j=0}^{\mu}\frac{(\mu+j)!t^{\sigma+j}}{(\mu-j)!2^j j!(\sigma+j)!}, \qquad \sigma,\mu\geq0 \tag{84}$$

which are essentially a generalization of the $P_\mu{}^\sigma$.[15] For appropriate values of the indices, i.e., $0\leq\sigma\leq\mu$,

$$(x^2-1)^{\sigma/2}P_\mu{}^\sigma(x)=[(\mu+\sigma)!/(\mu-\sigma)!]f_\mu{}^\sigma(x-1). \tag{85}$$

However, the $f_\mu{}^\sigma$ formulation includes values of σ in the range $\sigma>\mu$.

In general, relations valid for $P_\mu{}^\sigma$ correspond to similar relations for $f_\mu{}^\sigma$ even when $\sigma>\mu$. In particular

$$(2\mu+1)f_\mu{}^{\sigma+1}(t)=f_{\mu+1}{}^\sigma(t)-f_{\mu-1}{}^\sigma(t) \tag{86}$$

$$(\mu+\sigma)f_\mu{}^\sigma(t)=(2\mu-1)(t+1)f_{\mu-1}{}^\sigma(t) -(\mu-\sigma-1)f_{\mu-2}{}^\sigma(t). \tag{87}$$

Equation (87) may be used to generate $f_\mu{}^\sigma(t)$, starting from the value

$$f_0{}^\sigma(t)=t^\sigma/\sigma! \tag{88}$$

[15] The possibility of using this series representation in conjunction with a formulation such as Eq. (49) was suggested by Dr. K. Ruedenberg during a meeting on molecular calculations at Wright Air Development Center, Dayton, Ohio, June, 1958.

and from the further extension of the definition

$$f_{-1}^{\sigma}(t)=f_0^{\sigma}(t). \tag{89}$$

If only values $\mu\geq\sigma$ are needed, one may start from

$$f_{\sigma}^{\sigma}(t)=t^{\sigma}(t+2)^{\sigma}/2^{\sigma}\sigma! \tag{90}$$

alone, since the coefficient of $f_{\sigma-1}^{\sigma}(t)$ is zero in the expression Eq. (87) for $f_{\sigma+1}^{\sigma}(t)$.

We shall sometimes need ratios of various f_{μ}^{σ}. Setting

$$f_{\mu+1}^{\sigma}(t)/f_{\mu}^{\sigma}(t)=[(2\mu+1)/(\mu+\sigma+1)]X_{\mu}^{\sigma}(t) \tag{91}$$

it is possible to show that

$$t+1-X_{\mu+1}^{\sigma}(t)=[(\mu+\sigma+1)/(2\mu+1)]\cdot[(\mu-\sigma+1)/(2\mu+3)]1/X_{\mu}^{\sigma}(t). \tag{92}$$

Starting with

$$X_0^{\sigma}(t)=\sigma+t+1 \tag{93}$$

or

$$X_{\sigma}^{\sigma}(t)=t+1 \tag{94}$$

one may use Eq. (92) to generate $X_{\mu}^{\sigma}(t)$. In terms of $X_{\mu}^{\sigma}(t)$,

$$f_{\mu-2}^{\sigma}/f_{\mu}^{\sigma}=[(\mu+\sigma)/(\mu-\sigma-1)]\cdot\{[t+1-X_{\mu-1}^{\sigma}(t)]/X_{\mu-1}^{\sigma}(t)\}. \tag{95}$$

Note that Eq. (95) is indeterminate for $\mu=\sigma+1$.

We shall proceed toward the functions $K_{\mu}^{\sigma}(n,\delta,\tau,x)$ of Eq. (54) by defining the simpler functions

$$k_{\mu}^{\sigma}(\delta,x)=\int_1^x d\xi\exp(-\delta\xi)P_{\mu}^{\sigma}(\xi)(\xi^2-1)^{\frac{1}{2}\sigma}. \tag{96}$$

Introducing f_{μ}^{σ} through Eq. (85), one may write

$$k_{\mu}^{\sigma}(\delta,x)=[(\mu+\sigma)!/(\mu-\sigma)!]\exp(-\delta)\int_0^y dt\exp(-\delta t)f_{\mu}^{\sigma}(t) \tag{97}$$

where

$$y=x-1. \tag{98}$$

It can be shown that

$$df_{\mu}^{\sigma+1}(t)/dt=f_{\mu}^{\sigma}(t) \tag{99}$$

so that an integration by parts applied to Eq. (97) leads to

$$k_{\mu}^{\sigma}(\delta,x)=[(\mu+\sigma)!/(\mu-\sigma)!]\cdot e^{-\delta}\left[e^{-\delta y}f_{\mu}^{\sigma+1}(y)+\delta\int_0^y dte^{-\delta t}f_{\mu}^{\sigma+1}(t)\right] \tag{100}$$

since $f_{\mu}^{\sigma+1}(0)=0$ for all $\sigma\geq 0$. Repeated integrations by parts yield

$$k_{\mu}^{\sigma}(\delta,x)=[(\mu+\sigma)!/(\mu-\sigma)!]e^{-\delta x}\sum_{j=0}^{\infty}\delta^j f_{\mu}^{\sigma+j+1}(y). \tag{101}$$

A comparison of Eq. (101) as applied to k_{μ}^{σ} and k_{μ}^{0} shows that

$$k_{\mu}^{\sigma}(\delta,x)=[(\mu+\sigma)!/(\mu-\sigma)!][\delta^{-\sigma}k_{\mu}^{0}(\delta,x)-e^{-\delta x}\sum_{j=0}^{\sigma-1}\delta^{j-\sigma}f_{\mu}^{j+1}(y)]. \tag{102}$$

The ratio $f_{\mu}^{\sigma+1}(y)/f_{\mu}^{\sigma}(y)$ is less than y, so that successive terms in the summations of Eqs. (101) and (102) decrease by a factor smaller than $y\delta$. It may thus be seen that if it is possible to obtain k_{μ}^{0} independently of Eq. (101), Eq. (102) would provide a good route to k_{μ}^{σ} for large values of $y\delta$, while Eq. (101) would be the preferred form for small $y\delta$.

Generation of k_{μ}^{0} independently of Eq. (101) may be accomplished by using the relationship,

$$(2\mu-1)P_{\mu-1}(x)=(d/dx)[P_{\mu}(x)-P_{\mu-2}(x)], \tag{103}$$

and integrating Eq. (96) by parts.

$$k_{\mu}^{0}(\delta,x)=k_{\mu-2}^{0}(\delta,x)+(2\mu-1)\delta^{-1}k_{\mu-1}^{0}(\delta,x)-\delta^{-1}e^{-\delta x}[P_{\mu}(x)-P_{\mu-2}(x)]. \tag{104}$$

Equation (104), together with directly computed values of k_0^0 and k_1^0, could be used to generate the higher k_{μ}^{0}. We have found Eq. (104) to be numerically poor for small $y\delta$, and it is therefore not only convenient, but necessary to use Eqs. (104) and (102) for large $y\delta$, and Eq. (101) for small $y\delta$.

We are now prepared to consider the main problem of this Appendix. We consider first the special case $n=\tau=0$. We thus need

$$w_x^{\frac{1}{2}}K_{\mu}^{\sigma}(0,\delta,0,x_x)=\frac{w_x^{\frac{1}{2}}k_{\mu}^{\sigma}(\delta,x_x)}{(x_x^2-1)^{\frac{1}{2}}P_{\mu}^{\sigma}(x_x)}, \tag{105}$$

In Sec. VII, it was pointed out that w_x will be a Newton-Cotes weight, multiplied by x_x^2. This fact causes the quotient $w_x/(x_x^2-1)$ to remain bounded at $x_x=\infty$. Defining

$$R_x(\delta)=\frac{w_x^{\frac{1}{2}}e^{-\delta x_x}}{\delta(x_x^2-1)^{\frac{1}{2}}}, \tag{106}$$

Eqs. (101) and (102) become equivalent to the following formulas, which we used for actual computation for small, and large $\delta(x_x-1)$, respectively:

$$w_x^{\frac{1}{2}}K_{\mu}^{\sigma}(0,\delta,0,x_x)=\frac{(x_x^2-1)^{\frac{1}{2}\sigma}R_x(\delta)}{\delta^{\sigma}f_{\mu}^{\sigma}(x_x-1)}\sum_{j=\sigma+1}^{\infty}\delta^j f_{\mu}^{j}(x_x-1) \tag{107}$$

$$=\frac{(x_x^2-1)^{\frac{1}{2}\sigma}}{\delta^{\sigma}f_{\mu}^{\sigma}(x_x-1)}[w_x^{\frac{1}{2}}K_{\mu}^{\sigma}(0,\delta,0,x_x)f_{\mu}^{0}(x_x-1)-R_x(\delta)\sum_{j=1}^{\sigma}\delta^j f_{\mu}^{j}(x_x-1)]. \tag{108}$$

Our working formula equivalent to Eq. (104) is

$$w_\kappa^{\frac{1}{2}}K_\mu^0(0,\delta,0,x_\kappa)$$
$$=[X_{\mu-1}(x_\kappa)]^{-1}[w_\kappa^{\frac{1}{2}}K_{\mu-2}^0(0,\delta,0,x_\kappa)+R_\kappa(\delta)]$$
$$\cdot[\mu/(\mu-1)][x_\kappa-X_{\mu-1}(x_\kappa)]+\mu\delta^{-1}w_\kappa^{\frac{1}{2}}K_{\mu-1}^0(0,\delta,0,w_\kappa), \quad (109)$$

where the $X_\mu(x_\kappa)$ are defined in Eq. (91) and computed using Eqs. (92) and (93). The initial values used in conjunction with Eq. (109) are

$$w_\kappa^{\frac{1}{2}}K_0^0(0,\delta,0,x_\kappa)=R_\kappa(\delta)\{\exp[\delta(x_\kappa-1)]-1\}, \quad (110a)$$
$$w_\kappa^{\frac{1}{2}}K_1^0(0,\delta,0,x_\kappa)=(x\delta)^{-1}K_0^0(0,\delta,0,x_\kappa)$$
$$+R_\kappa(\delta)\{x_\kappa^{-1}\exp[\delta(x_\kappa-1)]-1\}. \quad (110b)$$

The f_μ^σ values appearing in Eqs. (107) and (108) were computed by means of Eqs. (87)–(89). Since a series of μ values is always needed, nearly all the f_μ^σ which are generated are used. Since f_μ^σ always appears in combination with δ^σ, we found it convenient to multiply Eq. (87) through by δ^σ, and to generate the product directly. Finally, since the f_μ^σ always appear in both numerator and denominator of any term in which they appear at all, they may be at arbitrary scaling, provided only that all f_μ^σ with the same μ value have the same scaling. This fact was quite useful in programing for fixed-point arithmetic.

Numerical studies led us to the conclusion that the optimum point for us to switch between formulas for small and large $\delta(x_\kappa-1)$ was at about $\delta(x_\kappa-1)=1$. Six-figure accuracy was then obtainable, carrying f_μ^σ up to $\sigma=9$.

The integrals for nonzero n and τ are obtained by operating with recursion formulas on the $K_\mu^\sigma(0,\delta,0,x_\kappa)$. Using Eq. (87), and comparing with the definition, Eq. (54),

$$K_\mu^\sigma(n,\delta,0,x_\kappa)=[(\mu-\sigma+1)/(2\mu+1)]$$
$$\cdot[P_{\mu+1}^\sigma(x_\kappa)/P_\mu^\sigma(x_\kappa)]K_{\mu+1}^\sigma(n-1,\delta,0,x_\kappa)$$
$$+[(\mu+\sigma)/(2\mu+1)][P_{\mu-1}^\sigma(x_\kappa)/P_\mu^\sigma(x_\kappa)]$$
$$\cdot K_{\mu-1}^\sigma(n-1,\delta,0,x_\kappa). \quad (111)$$

On introducing $X_\mu^\sigma(x_\kappa)$, using Eqs. (91) and (92), Eq. (111) is transformed into our working formula

$$w_\kappa^{\frac{1}{2}}K_\mu^\sigma(n,\delta,\tau,x_\kappa)=X_\mu^\sigma(x_\kappa)w_\kappa^{\frac{1}{2}}K_{\mu+1}^\sigma(n-1,\delta,\tau,x_\kappa)$$
$$+[x_\kappa-X_\mu^\sigma(x_\kappa)]w_\kappa^{\frac{1}{2}}K_{\mu-1}^\sigma(n-1,\delta,\tau,x_\kappa). \quad (112)$$

The above analysis only proves Eq. (112) for $\tau=0$.

Advancement to nonzero τ values is achieved by expanding in terms of $K_\mu^\sigma(n,\delta,0,x_\kappa)$.

$$w_\kappa^{\frac{1}{2}}K_\mu^\sigma(n,\delta,\tau,x_\kappa)$$
$$=\sum_{i=0}^{\tau}\binom{\tau}{i}(-1)^{\tau-i}w_\kappa^{\frac{1}{2}}K_\mu^\sigma(n+2i,\delta,0,x_\kappa). \quad (113)$$

Since the coefficients in the formulas of Eqs. (112) and (113) do not depend upon n, one may use Eq. (113) to extend Eq. (112) to nonzero τ, as was shown there without immediate proof. The computation procedure requiring the least temporary storage is to use Eq. (112) for 2τ steps, then to apply Eq. (113), followed by $n+2$ additional steps with Eq. (112).

For $x=\infty$, many of the formulas already given are inapplicable. Since the integrals $k_\mu^\sigma(\delta,\infty)$ are convergent, the P_μ^σ factor in the denominator of Eq. (54) causes $K_\mu^\sigma(n,\delta,\tau,\infty)$ to vanish unless both σ and μ are zero. Taking the limit, we write

$$w_\infty^{\frac{1}{2}}K_0^0(n,\delta,\tau,\infty)=v_\infty^{\frac{1}{2}}\int_1^\infty d\xi e^{-\delta\xi}\xi^n(\xi^2-1)^\tau, \quad (114)$$

where the subscript ∞ refers to the κ such that $x_\kappa=\infty$, and v_∞ is the limit of $w_\kappa/(x_\kappa^2-1)$ at $x_\kappa=\infty$. Equation (114) for $\tau=0$ is just

$$w_\infty^{\frac{1}{2}}K_0^0(n,\delta,0,\infty)=v_\infty^{\frac{1}{2}}A_n(\delta). \quad (115)$$

Eq. (113) is still applicable for $x=\infty$, and completes the procedure for making $K_0^0(n,\delta,\tau,\infty)$.

The equations given in this Appendix have been checked by comparing results of their use with integrals calculated by the methods outlined in Kotani.[9] Complete agreement was achieved to within the numerical accuracy of the various procedures.

Self-Diffusion in Liquid Argon

G. CINI-CASTAGNOLI, *Istituto di Fisica Università, Roma, Istituto Nazionale di Fisica Nucleare-Sezione di Roma, Italy*

AND

F. P. RICCI, *Comitato Nazionale Ricerche Nucleari, Roma, Italy*

(Received July 13, 1959)

The self-diffusion coefficient of liquid argon has been measured by the capillary technique at 84.56±0.04 °K and at about 70 cm Hg. The average value of $D(A^{37}-A^{40})$ is $(1.53\pm0.03)10^{-5}$ cm²/sec.

INTRODUCTION

EXPERIMENTAL data on the self-diffusion coefficient of liquid argon are very important, since recent theories have reached the stage where numerical calculations for transport processes of simple liquids can be made. As a matter of fact, the intermolecular potential of argon can be accurately described by the Lennard-Jones model, and the radial distribution function has been well investigated by means of x-rays,[1] and by neutron diffraction.[2] For this reason we have investigated the diffusion of A^{37} in A^{40}, though another measurement of self-diffusion of argon has been reported by other authors[3] at nearly the same temperature and pressure; their results will be discussed later.

EXPERIMENTAL METHOD

The self-diffusion coefficient has been measured at a temperature of 84.56°K and at a pressure of about 70 cm Hg. The capillary method of Anderson and Saddington has been adapted to low-temperature work, and the apparatus is described fully in earlier papers.[4-6] The experimental procedure is as follows: The capillary filled with pure argon, closed at the upper end and open at the other end, is placed in a bath of argon tagged with A^{37} (A^{37} concentration c_s is about 10^{-7}%). The diffusion of the tracer into the capillary is allowed to proceed for a certain length of time, t. After the diffusion, the liquid at concentration c_{dlu} is removed from the capillary with a Töpler pump, and analyzed in gas form. Two samples from the liquid of the bath are taken before and after the diffusion, to be sure that c_s is constant during the experiment. Before the diffusion a sample of the pure argon is condensed in the capillary and analyzed to check that there are no leaks through the sealings, and that the initial concentration c_i is zero.

The temperature regulation for this experiment is provided by controlling the pressure over a bath of liquid oxygen and is kept constant within less than a tenth of a degree Kelvin.

The concentrations of A^{37}, radioactive for electron capture with a half-life of 35 days, are reported all on the same day, owing to the short half-life. The samples were analyzed with internal gas G.M. counters, in this our technique differs from that of Corbett and Wang, who used a mass spectrometer to analyze the stable isotope A^{36}. However, we have found[6] in the diffusion of argon in liquid nitrogen (performed with A^{40} and A^{37}), the perfect agreement between results obtained with both methods of analysis.

Our method of investigation of self-diffusion differs from the method of previous authors essentially in the dimensions of the diffusion capillaries. We have been using a length L of 1.39 and 2.51 cm and a diameter d of 0.04 and 0.050 cm against a length of 0.762 and 0.508 cm and a diameter of 0.080 cm of the Corbett and Wang capillaries.

EXPERIMENTAL RESULTS

The one-dimensional self-diffusion coefficient D is defined by the well-known Fick law,

$$\partial c/\partial t = D(\partial^2 c/\partial x^2). \quad (1)$$

The solution of this equation, with boundary conditions of zero flux at $t=0$, $c=c_s$ for $x \geq L$ and $t \geq 0$, and initial tracer distribution in the capillary $c_i=0$, is

$$\frac{c_s-c_{dlu}}{c_s}=f(\tau D)$$

$$=\frac{8}{\pi^2}\sum_{n=0}^{\infty}\left\{\frac{1}{(2n+1)^2}\exp\left[-\frac{(2n+1)^2\pi^2 Dl}{4L^2}\right]\right\} \quad (2)$$

where $\tau=t/L^2$. The function $f(\tau D)$ numerically calculated with $n=10$ is shown in Fig. 1.

The results of $D(A^{37}-A^{40})$ are listed in Table I. The errors in D are determined primarily by the un-

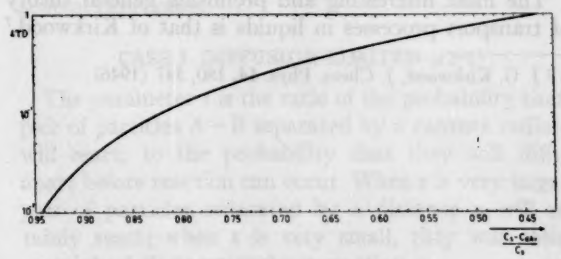

FIG. 1. $4\tau D$ vs $(c_s-c_{dlu})/c_s$.

[1] A. Eisenstein and N. S. Gingrich, Phys. Rev. **62**, 216 (1942).
[2] D. G. Henshaw, Phys. Rev. **105**, 976 (1957).
[3] T. W. Corbett and J. H. Wang, J. Chem. Phys. **25**, 422 (1956).
[4] Cini-Castagnoli, Pizzella and Ricci, Nuovo cimento **10**, 300 (1958).
[5] Cini-Castagnoli, Giardini, and Ricci, Nuovo cimento **13**, 916 (1959).
[6] Cini-Castagnoli, Dupré, and Ricci, Nuovo cimento **13**, 464 (1959).

TABLE I. Experimental results: Self-diffusion in liquid argon.

Run n°	Diameter d (cm)	Length L (cm)	Time t (sec)	$\tau=t/L^2$	Temperature (°K)	$D\times10^5$ cm²/sec
1	0.04	1.39±0.02	4980	2580	84.56±0.04	1.50±0.04
2	0.04	1.39±0.02	11 400	5906	84.56±0.08	1.60±0.05
3	0.04	1.39±0.02	600	311	84.60±0.04	1.30±0.20
4	0.05	2.51±0.04	7800	1238	84.52±0.04	1.55±0.05
5	0.05	2.51±0.04	3900	619	84.52±0.04	1.49±0.05
					$\bar{T}=84.56$	$\bar{D}=(1.53\pm0.03)10^{-5}$

certainty of L, and secondarily by the errors of the concentration measurements. Therefore we have taken the weighted mean of the obtained values,

$$D_{exp}(A^{37}-A^{40})=(1.53\pm0.03)\ 10^{-5}\ \text{cm}^2/\text{sec}.$$

The value, $D(A^{36}-A^{40})=(2.07\pm0.06)\ 10^{-5}$ cm²/sec, previously reported, differs significantly from our result outside the experimental errors.

The discrepancy is due probably to the different approaches used in the two experiments. In this regard we want to emphasize some aspects of our experimental procedure.

1. Our technique avoids initial turbulence, since the value of D is not dependent on the time of diffusion, although t varies by a factor ~ 20.

2. Our chosen ratio between L and d is very low $(d/L\leq0.03)$, and allows us to consider, with good approximation, the diffusion process as one-dimensional for the over-all length of the capillary; the effects of the deformations at the lower end of the capillary during the sealing operations are negligible for this ratio. It is reasonable to believe that these deformations involve, in addition to the corrections already considered by Corbett and Wang, a modification of the boundary conditions of the Fick equation (1); that is, $c=c_s$ for $x\geq L\pm\delta$, where δ is a length of the order of magnitude of the capillary radius $d/2$. Now Eq. (2) of Fick's law becomes

$$(c_s-c_{dlv})/c_s=f(\tau' D), \qquad (3)$$

where $\tau'=t/(L\pm\delta)^2$, with values of δ, $0\leq\delta\leq d/2$. This correction on the capillary length gives in our case a maximum variation on D of 3%.

DISCUSSION

The most interesting and promising general theory of transport processes in liquids is that of Kirkwood,[7] and co-workers. The provisional value of the frictional constant given by Kirkwood and Hammerle[8] for argon at 89°K and 1.2 atmos is $\zeta=8.8\cdot10^{-10}$ g/sec. From the expression $\zeta=KT/D$, we find $\zeta_{exp}=7.6\cdot10^{-10}$ g/sec. With this experimental value of ζ, we may compute the shear viscosity η by means of the expression given by Kirkwood, Buff, and Green,[9] $\eta_{calc}=2.04\cdot10^{-3}$ poise, to be compared with the experimental value of $\eta=2.74\cdot10^{-3}$ poise.

Our result for the self-diffusion coefficient, though giving better agreement with Kirkwood's theory than the previous result,[3] still leaves a large discrepancy.

The Longuet-Higgins and Pople theory of transport properties in a hard sphere fluid gives the expression

$$D=\tfrac{2}{5}(a^2/\eta)(NkT/V), \qquad (4)$$

where a is the radius of the spheres, N is the number of spheres in the volume V, and η is the viscosity. If we substitute in Eq. (4) the experimental values of η, and N/V (from the density), and for a the value 1.5 A, which represents the nearest half distance of approach of two atoms in the liquid argon[2] at about 84°K, we find $D_{calc}=0.9\cdot10^{-5}$ cm²/sec. Better agreement with our experimental data is found with the Stokes-Einstein relationship $D=kT/6\pi a\eta$; with the same radius, $D_{calc}=1.51\cdot10^{-5}$ cm²/sec.

Our experimental result is in excellent agreement with the value expected by calculations based on a phenomenological expression given by us[4] from the available data of previous investigations. This value is $D_{calc}=1.6\cdot10^{-5}$ cm²/sec. Another value for self-diffusion of liquid argon given by E. McLaughlin,[10] following a modified rate theory, is $1.69\cdot10^{-5}$ cm²/sec.

Measurements of the self-diffusion coefficient of liquid argon in a wide temperature range are in progress.

[7] J. G. Kirkwood, J. Chem. Phys. **14**, 180, 347 (1946).

[8] J. K. Kirkwood and W. G. Hammerle (to be published).

[9] Kirkwood, Buff, and Green, J. Chem. Phys. **17**, 988 (1949).

[10] E. McLaughlin, Trans. Faraday Soc. No. 433, **55**, 128 (1959).

THE JOURNAL OF CHEMICAL PHYSICS VOLUME 32, NUMBER 1 JANUARY, 1960

Bimolecular Reaction Rates in Solids and Liquids

THOMAS R. WAITE*

Physics Department, California Institute of Technology, Pasadena, California

(Received July 14, 1959)

The purposes of this article are: (1) to call attention to the fact that bimolecular reactions (A+B→AB) in solids and liquids do not, in general, follow simple second-order kinetics and, (2) to discuss some of the complications arising when deviations occur. In a previous paper a general expression for the rate of bimolecular reactions in liquids and solids was derived. The general reaction rate is second-order in the concentrations but the "rate constant" is time dependent. That expression is simplified and presented here in terms of three physically significant parameters, D, the sum of the diffusion coefficients of species A and B, r_0, the A—B capture radius, and s, the ratio of the probability that a pair of particles A—B separated by a capture radius r_0 will react, to the probability that they will diffuse apart before reaction can occur. The dependence of the "rate constants" on these parameters and on the time is illustrated graphically. The physical significance of the limiting cases is discussed. A simple, accurate, physically meaningful approximation to the rather abstract general rate expression is presented. An experimental method of distinguishing bimolecular reactions when they do not follow simple second-order kinetics is discussed. Reactions involving particles with long-range forces are considered briefly.

BIMOLECULAR reactions (A+B→AB) in solids and liquids do not, in general, follow simple second-order kinetics. Although the rate expressions are second order in the concentrations, the "rate constants" are time dependent in a manner determined by the molecular parameters of the system. The general rate equations have been derived in previous publications.[1,2] The assumptions necessary for their validity may be summarized:

(1) A and B particles are randomly distributed initially.

(2) The particles undergo random motions described by diffusion constants D_A and D_B characteristic of the system.

(3) Whenever an A and a B approach to within a capture radius, r_0, they have a definite probability of reaction determined by reasonable microscopic collision parameters.

(4) Although the correlation of the probability distribution of each A with that of each B as a result of the possibility for reaction is fully considered, the correlation of one A with another A which may result from their direct interaction or mutual interaction with the B's is neglected (similar assumption for the B's).

Assumptions 1 and 2 may be generalized to include nonrandom initial distributions,[2] and to random motion modified by long-range A−B forces.[1]

The general rate equations derived in references 1 and 2 may be simplified to

$$dC_A/d\tau = dC_B/d\tau = -k(r_0, s, \tau)C_AC_B, \tag{1}$$

$$k(r_0, s, \tau) = 4\pi r_0^3[s/(s+1)]\left(1-2\exp[(s+1)^2\tau]\int_{(s+1)\tau^{\frac{1}{2}}}^{\infty}\frac{\exp(-\alpha^2)}{\pi^{\frac{1}{2}}}d\alpha\right), \tag{2}$$

$$s = \frac{r_0\Delta r_0 \nu p \exp[-(E^*/RT)]}{D} \approx \exp\left(\frac{E_D - E^*}{RT}\right), \tag{3}$$

and

$$\tau = Dt/r_0^2, \tag{4}$$

where

C_A = concentration of A's (cm^{-3}).
C_B = concentration of B's (cm^{-3}).
t = time (sec).
r_0 = AB capture radius (cm).
Δr_0 = thickness of nearest neighbor shell (cm).
D = sum of diffusion coefficients of A particles and B particles (cm^2/sec).
E_D = activation energy for diffusion of more rapid of A and B (cal/mole).
E^* = activation energy for reaction of A and B upon collision (cal/mole).
R = gas constant (calories/mole-deg).
T = temperature (deg abs).
ν = average frequency with which nearest neighbor A and B are driven together (sec^{-1}).
p = probability that colliding A and B are oriented properly for reaction.

The significance of the form of $k(r_0, s, \tau)$ is not immediately clear. This may be remedied by considering physically significant limiting cases which will suggest a meaningful and accurate approximation to the general expression.

CASE I. DIFFUSION LIMITED ($s \gg 1$)

The parameter s is the ratio of the probability that a pair of particles A−B separated by a capture radius r_0 will react, to the probability that they will diffuse apart before reaction can occur. When s is very large, a pair of particles separated by a distance r_0 will certainly react; when s is very small, they will almost certainly drift apart without reacting.

* National Science Foundation Postdoctoral Fellow on leave of absence from Bell Telephone Laboratories.

[1] T. R. Waite, J. Chem. Phys. **28**, 103, (1958).

[2] T. R. Waite, Phys. Rev. **107**, 463, (1957).

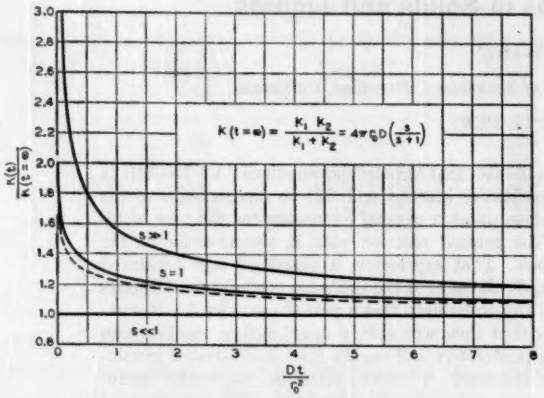

FIG. 1. Variation of second-order rate constant with time during bimolecular reaction in a solid or liquid. $dC_A/dt=-k(t)C_AC_B$. Solid curve: Eqs. (1) and (2). Dotted curve: Eqs. (11) and (12).

When $s\gg1$, the reaction rate is determined solely by the probability of encounter of an A and a B in their random diffusive motion. Any A is assumed to react with any B when they approach to within a capture radius r_0. The reaction rate is given by

$$dC_A/dt=-\left(1+\frac{1}{(\pi\tau)^{\frac{1}{2}}}\right)k_1C_AC_B, \tag{5}$$

$$k_1=4\pi r_0D. \tag{6}$$

Equation (5) was derived by Smoluchowski[3] in 1917 under more restrictive assumptions. As one might imagine, the chemical problem is similar to the diffusion of the A's in a medium in which each of the B's present acts as a spherical sink (or *vice versa*). The rate constant, Eqs. (5) and (6), is characteristic of a spherical sink in a three dimensional diffusion problem. However, the expression for the rate of reaction, Eq. (5), incorporates the effects of competition between the B's for each of the A's (and *vice versa*) and the effects of eliminating "sinks" upon reaction. The time dependent factor shows that a very rapid initial transient occurs. The reason for this transient, and its relation to assumptions 1 and 2, are discussed in reference 2.

CASE II. BARRIER TO REACTION ($s\ll1$)

When $s\ll1$, the reaction rate is determined solely by the probability that an A and a B will react upon collision. Due to a large activation energy for combination, an A and a B separated by a collision radius, r_0, have a high probability of diffusing apart without reacting. Diffusion is rapid enough to maintain a random distribution in spite of the slow reaction of the nearest neighbor A—B pairs. Consequently the number of nearest neighbor pairs present at any time is essentially the equilibrium number for nonreacting particles at concentrations $C_A(t)$ and $C_B(t)$. The rate may be expressed simply as the product of four expressions.

(1) The density of A's.

(2) The probability that a B is in the nearest neighbor shell of a particular A assuming random distributions (volume of shell times the density of B's).

(3) The average vibration frequency with which nearest neighbors A and B are driven together.

(4) The probability that an A and a B will react when driven together.

The resulting reaction rate is given by

$$dC_A/dt=-k_2C_AC_B, \tag{7}$$

and

$$k_2=(4\pi r_0^2\Delta r_0)\nu p\exp[-(E^*/RT)]. \tag{8}$$

CASE III. STEADY STATE ($\tau\gg1$)

The steady-state rate is given by

$$dC_A/dt=-[k_1k_2/(k_1+k_2)]C_AC_B, \tag{9}$$

and

$$k_1k_2/(k_1+k_2)=4\pi r_0D[s/(s+1)]. \tag{10}$$

The steady state applies after prolonged times for all values of the parameter s. This limiting rate is easily derived in a number of special cases, and these have had a rather wide application. The rate at which the steady state is approached, and the subsequent validity of the steady-state approximation for several values of s have been illustrated in Fig. 1.

GENERAL CASE

The general reaction rate, Eq. (1), reduces to Case I when $s\gg1$, to Case II when $s\ll1$, and to Case III when $\tau\gg1$. The general time-dependent rate constant, Eqs. (1) and (2), is shown graphically in Fig. 1 for three values of s. It is apparent that the bimolecular reaction follows simple second-order kinetics only when there is a large barrier to reaction upon collision (Case II above), or only after very long times (Case III above). For a system with initial concentrations of A's and B's each equal to 5 mole percent, the half-life on the scale of Fig. 1 is about 5 (for s of the order of 1 or greater). The rate constant after half the material has reacted may still exceed its steady-state value by 20%.

In reference 1, it was mentioned that the general steady-state expression, Eq. (9), could be related to the steady-state cases when the reaction rate is determined entirely by diffusion or entirely by a barrier to reaction. The reciprocals of the rate constants $[k_1]^{-1}$ and $[k_2]^{-1}$ may be interpreted respectively as the resistances of the two consecutive steps: (1) diffusion together, and (2) reaction upon collision. Addition of these series resistances leads directly to the reciprocal of the general steady-state rate constant in Eq. (9). Since this reasoning gives the correct answer for the steady state, we might attempt to extend it to earlier times by interpreting $\{k_1[1+(1/(\pi\tau)^{\frac{1}{2}})]\}^{-1}$, the re-

[3] M. V. Smoluchowski, Z. physik. Chem. **92**, 192 (1917).

ciprocal of the entire time-dependent "rate constant" of Eq. (5), as the diffusion resistance. This leads to

$$dC_A/dt = -\frac{k_2 k_1[1+(1/(\pi\tau)^{\frac{1}{2}})]}{k_2+k_1[1+(1/(\pi\tau^{\frac{1}{2}})]} C_A C_B \qquad (11)$$

$$= -4\pi r_0 D \frac{s(1+(\pi\tau)^{\frac{1}{2}})}{1+(s+1)(\pi\tau)^{\frac{1}{2}}} C_A C_B. \qquad (12)$$

This solution gives the correct limiting cases for $s \gg 1$ and for $s \ll 1$. It agrees with the general solution, Eq. (1), for $\tau = 0$ as well as for $\tau \gg 1$. Its validity for intermediate values of s and τ may be seen by comparing the solid and dotted curves for $s=1$ in Fig. 1. The dotted curve corresponds to the approximate Eq. (11). The error in approximation is only a few percent. The approximate equation agrees exactly with the other two curves in Fig. 1. Comparing Eq. (1) with Eq. (11) and noting the small numerical differences permits a physical understanding of the general time-dependent rate constant.

EXPERIMENTAL TEST FOR BIMOLECULAR KINETICS

It should be noted that the most general rate constant $k(r_0, s, \tau)$ is a function of the reaction parameters of the reacting particles and the time only [see Eqs. (1) and (2)]. It is independent of concentration (if the diffusion parameters are independent of concentration) and in this sense the reaction is second-order in the concentrations. One can take advantage of this fact to distinguish a second-order reaction with time-dependent rate constant from reactions of other orders. Consider the dependence of the amount reacting in a specified time L on the initial concentrations C_A^0 and C_B^0. For the case $C_A^0 = C_B^0$ one has

$$\frac{1}{C(\tau=L)} = \frac{1}{C^0} + \int_0^L k(r_0, s, \tau)\, d\tau. \qquad (13)$$

The integration may be performed if the approximate rate "constant" of Eq. 11 is used. The usual graph of the reciprocal of the initial concentration *vs* reciprocal concentration at time $\tau = L$ will be linear, irrespective of the time dependence of the "rate constant." The additive constant [the integral in Eq. (13)] is L times the average value of $k(r_0, s, \tau)$ in the time interval $(0, L)$. This average value is sensitive to the choice of zero time so that this zero must be the same for all values of the initial concentrations considered. It should be emphasized that the usual tests for simple second-order kinetics are not adequate to distinguish a bimolecular reaction in a solid or liquid phase.

LONG-RANGE FORCES

When long-range forces, such as Coulomb interactions, exist between the reacting particles a more general treatment is necessary. Differential equations describing the rate when assumptions 1 to 4 above are valid have been presented in reference 1. The neglect of the correlation between nonreacting particles (assumption 4) may not be reasonable if long-range forces also exist between two A's (or between two B's). Furthermore, the differential equations can not be solved in general. Only the steady-state case ($\tau \gg 0$) has been solved exactly. This solution suggests that, for an attractive A—B force, a solution approximately valid for all times might be obtained by ignoring the long range force and introducing the effective capture radius,[1]

$$r_{0\,\mathrm{eff}} = \frac{1}{\int_{r_0}^{\infty} \exp(V/kT)\,(dr/r^2)}, \qquad (14)$$

where $V(r)$ is the A—B interaction potential. This capture radius corresponds to an A—B separation for which the A—B attractive potential is of the order of kT. It may be quite large leading to very severe deviations from second-order kinetics during the early transients.

Reiss[4] has pointed out that if the capture radius is comparable in magnitude to the average distance between reacting particles, many of the particles are already "captured" initially ($t=0$). For long-range forces, this "just captured" state ($r_{AB} \sim 50$ A) may be significantly different from the reacted state ($r_{AB} \sim 2$ A). If the experiment being considered distinguishes between these states, and if diffusion is slow even when aided by the AB force, the decay from the "just captured" to the "reacted" configuration may dominate the kinetics. Reiss has given physical arguments to show that under some circumstances the combined effects of the transients and the decay of the just captured state may lead to kinetics which are very nearly first order. This follows from the assumption that the forces acting on any A (or B) are dominated by the nearest B (or A). It seems that the precise manner in which one deals theoretically with the problem of long-range forces should be determined by the conditions of each specific experiment. Several authors have dealt successfully with specific cases.[4,5,6]

ACKNOWLEDGMENTS

The author would like to thank H. Reiss, J. Dewald, and C. Heller for very helpful discussions and suggestions.

[4] Reiss, Fuller, and Morin, Bell System Tech. J. **35**, 535–636 (1956), especially p. 586.
[5] A. Weller, Z. physik. Chem. **13**, 335 (1957).
[6] E. J. W. Verwey and J. T. G. Overbeek, *Theory of the Stability of Lyophobic Colloids* (Elsevier Publishing Company, Inc., Amsterdam, 1948), p. 165.

On Chemical Reactions in Free Molecule Flow*

PAUL L. CHAMBRÉ

University of California, Berkeley, California

(Received September 8, 1958)

This paper deals with heterogeneous chemical reactions within systems in which the relevant geometric dimensions are small compared with the mean free path of gas molecules. A typical example can be found in a surface reaction occurring at moderate pressures inside the pore of a catalyst with a radius of several angstroms.

Specific problems of this type have in the past been formulated, subject to the well-known limitations of ordinary diffusion theory, in terms of differential equations for the species concentrations. This in turn supposes that the reaction pattern is dependent on local conditions. A more general and exact formulation given in the following shows that the concentration of a molecular species at a point is determined by the concentration distributions of all species stemming from the entire system. Thus one is led to a formulation in terms of integral equations. In an application of the theory the validity of the conventional differential equation approach is investigated and is found to yield satisfactory results only under certain limiting conditions.

INTRODUCTION

FREE molecule conditions in a system are characterized by the fact that the molecular mean free path is many times greater than a characteristic geometric dimension of the system. Such a state can occur under two widely different circumstances. In one instance one may deal with a gas at very low pressure in an apparatus of cm dimensions. The gas under these conditions does not behave as a continuous fluid but rather exhibits some characteristics of its coarse molecular structure. Molecules will collide on the average much more frequently with the internal surfaces of the system than with each other. On the other hand one may concern oneself with a gas at ordinary pressures in an extremely fine capillary. This case exhibits again the preponderance of gas-wall collisions over intermolecular collisions.

The problem of free molecule conditions in internal flow systems (interior Knudsen flows) in absence of chemical interaction was exactly formulated originally by Clausing.[1] Exterior Knudsen flows, i.e., flows about submerged bodies, have been discussed by the writer in a summary article on rarefied gas dynamics.[2] In the following, we will be concerned with internal free molecule flows with chemical surface interactions.

It will be assumed that isothermal adsorption equilibrium exists at all points of the system. Under this condition the fraction of the surface covered, i.e., θ, is dependent on all molecular collision densities. The forward chemical reaction act is schematized as follows: A certain fraction α of reactant molecules colliding with the surface is chemisorbed and undergoes a reaction; the remainder returns unreacted to the gas phase. Chemisorption theory shows that the forward reaction coefficient α is given by[3]

$$\alpha = Cf(\theta), \tag{1}$$

where C is a quantity which describes the reaction act on successful occupancy of a vacant site. For later use the form of α for a three-component mixture occupying single sites (mobile or immobile layers alike) based on Langmuir's model is

$$\alpha = \frac{C}{1+(1/\nu_0)(n_r\tau_r+n_p\tau_p+n_i\tau_i)}. \tag{2}$$

Here ν_0 is the number of molecules which would fill a unit area completely with a unimolecular layer. The τ's are the average times the species molecules remain on the surface while the n's represent their collision densities. The ratio of reactant molecules to product molecules generated by collision of the latter with the surface will be denoted by β. Finally it is postulated that for all types of interactions the surface emission is purely random and without memory of the past history of the molecule before collision. This condition is probably quite closely satisfied in practice.

THE INTEGRAL EQUATIONS

Consider an isothermal system of length L connected at both ends to reservoirs which contain reactant, product, and inert molecules. These may enter the system where reactant and product molecules can undergo a reversible chemical reaction while being adsorbed on internal surfaces. It will be assumed that a steady state prevails and that all pertinent quantities which describe the reaction pattern can be expressed by a single distance variable x which is measured along an axis from one of the entrances, see Fig. 1. Typical examples of such one-dimensional systems are, a tube of constant or slightly varying cross section, two parallel plates the widths of which are large compared

* This research was supported in part by the Office of Naval Research under Contract Nonr-222(04).

[1] P. Clausing, "Over den verblijtijd van moleculen en de strooming van zeer verdunde gassen" (thesis, Leyden, 1929).

[2] S. Schaaf and P. L. Chambré, *Flow of rarefied gases, High Speed Aerodynamics and Jet Propulsion* (Princeton University Press, Princeton, New Jersey, 1958), Vol. III.

[3] B. M. W. Trapnell, *Chemisorption* (Academic Press, Inc., New York, 1955).

to the spacing between the plates, and a homogeneous isotropic porous medium with a large void fraction.

The number of collisions of each molecular class (such as the reactant r) at any point in the system is determined by the following number balance. The total number of reactant molecules colliding per unit axial length of surface per unit time is due to (a) reactant molecules directly incident from the reservoirs, (b) reactant molecules originating from chemically unsuccessful collisions which are incident from all parts of the system, and (c) incident reactant molecules produced in the reverse reaction.

Let the number of reactant molecules which enter the system per unit time at $x=0$ and collide without intervening collision for the first time in the interval between x and $(x+dx)$ (hereafter referred to as: in dx at x) be denoted by $n_{r,0}(x)dx$. Similarly let the number of reactant molecules which enter the system per unit time at $x=L$ and subsequently suffer their first collision in dx at x be $n_{r,L}(x)dx$. Then the total number of direct collisions of reactant molecules per unit interval length per unit time at x is $n_{r,0}(x)+n_{r,L}(x)$. Let the probability that a molecule issuing from the point x' will hit dx at x without intervening collision depend only on the distance between x and x'. If this is denoted by $K(|x-x'|)dx$, then the total number of reactant molecules colliding per unit length per unit time at x is, according to the above balance,

$$n_r(x)=n_{r,0}(x)+n_{r,L}(x)+\int_0^L K(|x-x'|)[1-\alpha(n_r, n_p, n_i, x')]n_r(x')dx'+\int_0^L K(|x-x'|)\beta(n_r, n_p, n_i, x')n_p(x')dx', \quad (3)$$

where $n_p(x)$ and $n_i(x)$ are the collision densities of product and inert particles, respectively, which are incident on x.

By an identical conservation of number argument one can derive an analogous integral equation for the collision density of product molecules. With an obvious change in subscripts and comparable physical implication

$$n_p(x)=n_{p,0}(x)+n_{p,L}(x)+\int_0^L K(|x-x'|)\alpha(n_r, n_p, n_i, x')n_r(x')dx'+\int_0^L K(|x-x'|)[1-\beta(n_r, n_p, n_i, x')]n_p(x')dx'. \quad (4)$$

In Eqs. (3) and (4) α and β depend on the local collision density of all species at the point x' and possibly on x' itself if the surface of the system is heterogeneous, causing a variation of adsorptive properties from site to site. For the inert molecules one obtains

$$n_i(x)=n_{i,0}(x)+n_{i,L}(x)+\int_0^L K(|x-x'|)n_i(x')dx'. \quad (5)$$

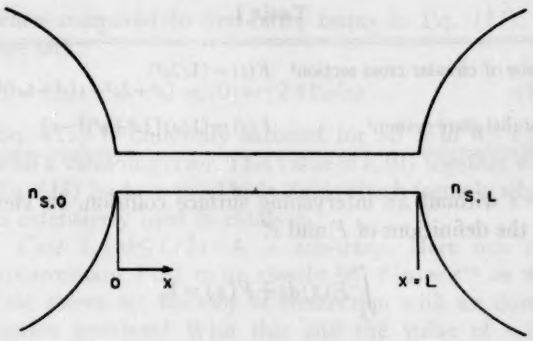

FIG. 1. The coordinate system.

Once the interrelated set of integral equations (3–5) has been solved and $n_r(x)$, $n_p(x)$ are known one can readily determine the rate at which product molecules are generated or reactant molecules are consumed in the system.

We consider next the mathematical relations which exist between the geometric scattering probability $K(|x-x'|)dx$, and the entrance flows such as $n_{r,0}(x)$, $n_{r,L}(x)$. The relationships between these functions are reduced essentially to relations between geometric probabilities which apply to any molecular species. Clausing[1] has shown that if any one of these probabilities is known all other probabilities can be calculated in terms of it.

The number of reactant molecules which enter the system from the reservoir end $x=0$ and collide for the first time in dx at x can be expressed in terms of the number of molecules crossing the entrance area per unit time, and the probability that a molecule entering the flow system at $x=0$ makes its first collision between x and $x+dx$, i.e., $E(x)dx$.
Hence

$$n_{r,0}(x)dx=A_0\Gamma_{r,0}E(x)dx,$$

and similarly

$$n_{r,L}(x)dx=A_L\Gamma_{r,L}E(L-x)dx. \quad (6)$$

Here A_0, A_L are the effective areas which communicate with the reservoirs at $x=0$, $x=L$; $\Gamma_{r,0}$, $\Gamma_{r,L}$ denote, respectively, the number of molecules crossing unit entrance area at $x=0$ and $x=L$ per unit time. Analogous expressions to Eq. (6) hold for the product and inert species. It should be noted that the entrance probability is assumed to be a function of the distance from the entrance to the point x only.

To establish the desired expressions for E and K consider the auxiliary function $F(s)$ which describes the probability that a molecule entering the system at $x=0$ will pass through the cross section located at

TABLE I.

Tube of circular cross section[1]	$F(s)=(1/2a^2)[s^2+2a^2-s(s^2+4a^2)^{\frac{1}{2}}]$
Parallel plate system[1]	$F(s)=(1/a)[(s^2+a^2)^{\frac{1}{2}}-s]$

$x=s$ without an intervening surface collision. In view of the definitions of F and E

$$\int_0^x E(s)ds+F(x)=1,$$

so that on differentiation

$$E(x)=-(dF/ds)_{s=x};$$

similarly one obtains

$$E(L-x)=-(dF/ds)_{s=L-x}. \tag{7}$$

An elementary argument shows that K and E are related by

$$\int_0^L K(|x-x'|)dx'+(a/2)[E(x)+E(L-x)]=1. \tag{8}$$

Here $a/2$ is defined as the ratio of flow channel volume to the surface area of the flow channel walls. Subdividing the range of integration into two parts one obtains with Eq. (7)

$$\int_0^x K(s)ds+\int_0^{L-x} K(s)ds-(a/2)[(dF/ds)_{s=x}+(dF/ds)_{s=L-x}]=1,$$

which yields on differentiation with respect to x

$$K(x)-K(L-x)=(a/2)[(d^2F/ds^2)_{s=x}-(d^2F/ds^2)_{s=L-x}].$$

This equation in turn implies that

$$K(|x-x'|)=(a/2)(d^2F/ds^2)_{s=|x-x'|}. \tag{9}$$

Equations (7) and (9) define the various entrance functions and probabilities in terms of the basic function $F(s)$. Analytical expressions for $F(s)$ which apply to a variety of geometric situations can be found in the literature.[1] The forms of F for a tube of circular cross section and a parallel plate system the width of which is large compared to its spacing are given in Table I.

COMPARISON BETWEEN INTEGRAL AND DIFFERENTIAL EQUATION FORMULATIONS

Consider the problem of chemical surface reaction in a tube of constant radius a and length L under free molecule flow conditions. The addition of Eqs. (3–5) yields, together with Eq. (6),

$$[n_r(x)+n_p(x)+n_i(x)]=A(\Gamma_{r,0}+\Gamma_{p,0}+\Gamma_{i,0})E(x)+A(\Gamma_{r,L}+\Gamma_{p,L}+\Gamma_{i,L})E(L-x)+\int_0^L K(|x-x'|)[n_r(x')+n_p(x')+n_i(x')]dx'. \tag{10}$$

If the total rate of molecules incident per unit area at $x=0$ and $x=L$ are equal, a solution to this integral equation is in view of Eq. (8),

$$n_r(x)+n_p(x)+n_i(x)=(2A/a)(\Gamma_{r,0}+\Gamma_{p,0}+\Gamma_{i,0}). \tag{11}$$

The result shows that the total collision density of all species is constant along the entire channel.

The problem is now specialized. Let the backward reaction be negligible ($\beta=0$), the inert collision density be zero ($n_i=0$), the surface residence times be equal ($\tau_r=\tau_p$), and the Γ's for an individual species be such that $\Gamma_{r,0}=\Gamma_{r,L}\equiv\Gamma_r$ etc. Equations (2) and (11) show that α is then independent of the collision rates of the individual species and furthermore if α is constant with respect to x' Eq. (3) reduces to

$$n_r(x)=A\Gamma_r[E(x)+E(L-x)]+(1-\alpha)\int_0^L K(|x-x'|)n_r(x')dx'. \tag{12}$$

The principal aim in the following is to ascertain under what conditions conventional diffusion theory, which is based on the differential equation

$$d^2C_r/dx^2=(2k/aD)C_r, \tag{13}$$

yields a mathematically exact solution to the integral equation (12). Here C_r denotes the reactant concentration, k is the first-order reaction rate constant, and D is the Knudsen diffusion coefficient which is obtained in principle from the solution of an integral equation such as (5), i.e., in absence of chemical reaction. D can be represented by an empirical equation which has the functional form $D=\bar{v}ah(L/a)$ where $\bar{v}$ is the mean molecular speed of the species. On the assumption that $C_r=(\text{constant})n_r$, and with $k=\alpha(\bar{v}/4)$, Eq. (13) reduces to

$$d^2n_r/dx^2=(\lambda/a)^2n_r,$$

where

$$\lambda^2=\alpha/[2h(L/a)]. \tag{14}$$

Making use of the fact that the $n_r(x)$ distribution is symmetric about $x=L/2$ (the solution to Eq. (12) possesses the same property) the solution to the differential equation reads

$$n_r(x)=n_r(0)\left[\frac{\exp[-\lambda(x/a)]+\exp[-\lambda(L-x)/a]}{1+\exp(-\lambda L/a)}\right]. \tag{15}$$

An attempt to verify this as a solution of Eq. (12) leads to unmanageable integrals. Instead one can employ the differential equation (14) directly. Differentiate Eq. (12) twice with respect to x and transform the integral by integration by parts. There results

$$d^2n_r/dx^2 = A\Gamma_r(d^2/dx^2)[E(x)+E(L-x)] + (1-\alpha)\{n_r(0)(d/dx)[K(x)-K(L-x)] + (dn_r/dx)_{x=0}[K(x)+K(L-x)]\} + (1-\alpha)\int_0^L K(|x-x'|)[d^2n_r/d(x')^2]dx'$$

where use has been made of the fact that $n_r(0) = n_r(L)$ and $(dn_r/dx)_{x=0} = -(dn_r/dx)_{x=L}$. In this equation the second derivatives of n_r are replaced by $(\lambda/a)^2 n_r$ and the integral is subsequently eliminated with help of Eq. (12). This yields

$$A\Gamma_r\{(d^2/dx^2)[E(x)+E(L-x)] - (\lambda/a)^2[E(x)+E(L-x)]\} + (1-\alpha)\{n_r(0)(d/dx)[K(x)-K(L-x)] + (dn_r/dx)_{x=0}[K(x)+K(L-x)]\} = (A\Gamma_r/a^3)\epsilon(x, \cdots). \quad (16)$$

If $n_r(x)$ as a solution of the differential equation (14) is also a solution of the integral equation (12) then ϵ as defined by Eq. (16) must vanish uniformly for all x in $0 \leq x \leq L$. In order to discuss this problem we express the functions E and K in terms of $F(\eta)$ where $\eta = s/a$. Furthermore since Eq. (15) has the property that

$$(dn_r/dx)_{x=0} = -(\lambda/a)n_r(0)\tanh(\lambda L/2a),$$

Eq. (16) reduces with help of Eqs. (7) and (9) to

$$f(x)+[an_r(0)/2A\Gamma_r]g(x) = \epsilon[x, n_r(0)] \quad (17)$$

where

$$f(x) = \{-(d^3F/d\eta^3)_{\eta=x/a} - (d^3F/d\eta^3)_{\eta=(L-x)/a} + \lambda^2[(dF/d\eta)_{\eta=x/a} + (dF/d\eta)_{\eta=(L-x)/a}]\},$$

and

$$g(x) = (1-\alpha)\{(d^3F/d\eta^3)_{\eta=x/a} + (d^3F/d\eta^3)_{\eta=(L-x)/a} - \lambda\tanh(\lambda L/2a)[(d^2F/d\eta^2)_{\eta=x/a} + (d^2F/d\eta^2)_{\eta=(L-x)/a}]\}.$$

A detailed investigation shows that in general $\epsilon \not\equiv 0$ and hence that the solution to Eq. (14) is in general not an exact mathematical solution to the integral equation. However under certain special conditions it may serve as a useful approximation. This is illustrated for a tube of cylindrical cross section.

Case 1.—$\alpha \ll 1$, $\alpha^3(L/2a) \gg 1$. In this case $h(L/a) = \frac{2}{3}$ and the terms involving α, λ^2, and λ can be neglected when compared to first-order terms in Eq. (17). If one sets

$$n_r(0) = (2A\Gamma_r/a) \quad (18)$$

Eq. (17) is uniformly satisfied for all x in $0 \leq x \leq L$ with a vanishing error. This value of $n_r(0)$ together with Eq. (15) leads to the Thiele-Zeldowitsch formula which is extensively used in catalysis.[4]

Case 2.—$0 \leq L/2a < 4$, α arbitrary. Here one can approximate $F(\eta)$ quite closely by $F(\eta) = e^{-\eta}$ as was first shown by Buckley in connection with an illumination problem.[5] With this and the value of $n_r(0)$ given by

$$n_r(0) = (2A\Gamma_r/a)\frac{1-\lambda^2}{(1-\alpha)[1+\lambda\tanh(\lambda L/2a)]}, \quad (19)$$

Eq. (17) is again uniformly satisfied for all x in $0 \leq x \leq L$ with a vanishing error.

Case 3.—Arbitrary α and L/a values. In this case one can resort to the following approximation technique. $n_r(0)$ is determined so that ϵ is small throughout $0 \leq x \leq L$. In this way one can establish an approximate solution which is likely to come closer to the exact solution the smaller the average absolute value of ϵ. In order to attain this let

$$\int_0^L \epsilon^2[x, n_r(0)]dx = M[n_r(0)]$$

be a minimum. The necessary condition to achieve this is, that $\partial M/\partial n_r(0) = 0$ which with Eq. (17) results in

$$n_r(0) = -(2A\Gamma_r/a)\left[\int_0^L f(x)g(x)dx \Big/ \int_0^L [g(x)]^2 dx\right]. \quad (20)$$

Due to lack of space the final result is not detailed here. With $n_r(0)$ determined the error can subsequently be assessed.

It should be noted in conclusion that the determination of $n_r(0)$ in the integral equation approach requires in essence the knowledge of the entire $n_r(x)$ distribution in the channel. In contrast to this the differential equation approach prescribes this quantity *a priori* through the explicit assumption that the state of the gas at the reservoir ends alone determines $n_r(0)$. The preceeding discussion has centered around a comparison of the integral equation formulation and the approximate diffusion equation approach in order to establish a justification of the latter within the exact framework. The solution of the integral equation system proper (for certain specific problems) will be discussed elsewhere.

[4] A. Wheeler, "Reaction rates and selectivity in catalyst pores," *Advances in Catalysis* (Academic Press, Inc., New York, 1951), Vol. III.

[5] H. Buckley, Phil. Mag. **4**, 753 (1927).

Annihilation of Positrons in Organic Liquids*

C. R. HATCHER,† T. W. FALCONER,‡ AND W. E. MILLETT

The University of Texas, Austin, Texas

(Received October 24, 1958)

The mean life τ_2 and fraction I_2 of positrons which form ^3S positronium have been measured for annihilation in 20 organic liquids—alcohols, glycols, acids, benzene derivatives, and others. By using the measured value of τ_2, it is possible to calculate $\langle\sigma v\rangle_{Av}$ where σ is the molecular cross section for annihilating ^3S positronium on collision and v is the velocity of the positronium atom. The results show that in general $\langle\sigma v\rangle_{Av}$ is related to the "size" of the molecule although there are some consistent exceptions to this rule. There is also a rough correlation between τ_2 and density, τ_2 being shortest for the most dense liquids and longest for the least dense ones.

1. INTRODUCTION

UPON entering a liquid or a solid (metals and gases are excluded in this discussion)[1] a high energy positron will lose most of its energy in inelastic collisions. The probability of annihilating or forming positronium at high energies is small, therefore in this energy region a positron acts much like an ordinary free electron. When the energy of the positron drops below a certain definite value, depending on the surrounding matter, the formation of positronium is not possible and hence either scattering or "free" annihilation will occur. There is therefore a fairly narrow energy band considerably above thermal energies where positronium formation is most likely.[2]

The chances of forming positronium in an excited state are thought to be small[3]; therefore, of the positronium formed, three-fourths should be ^3S and one-fourth ^1S. The lifetime of ^1S positronium, as well as the lifetime of free positrons in most condensed media, is of the order of 10^{-10} sec. If ^3S positronium is isolated, decay will occur by the emission of three photons with a lifetime of roughly 10^{-7} sec. Although this is observed in some gases, in solids the interactions between the positronium atom and its surrounding molecules are so numerous that the measured lifetime of the "long" τ_2 component is about 10^{-9} sec and decay occurs primarily by two instead of three photons. To explain this it was initially postulated that the τ_2 component in solids is due to the formation of ^3S positronium which is converted to the ^1S state by spin-exchange.[4] Later work gives evidence that in most cases spin-exchange is less likely than "pickoff" annihilation.[5] "Pickoff" is said to occur when ^3S positronium is formed but the positron annihilates with an electron bound to a neighboring molecule rather than with the electron of the positronium.

In a previous paper[6] values of τ_2 and I_2 were reported for a number of organic compounds, mostly derivatives of benzene. The present investigation merely extends these measurements to other compounds; therefore, a sketch of some of the earlier results will be given here in order to make disussion of the present measurements more meaningful.

It was found that I_2 goes in decreasing order for fluoro-, chlor-, bromo-, and iodobenzene and for *para-*, *meta-*, and *ortho*-xylene. To explain these and other results two models were suggested. According to one picture positronium formation and rupture of the molecules are looked upon as competitive processes. In an environment of molecules which possess strong interatomic bonds, the rupture of a molecule on collision with a positron is less likely and hence there is a better chance that positronium will be formed. More positronium is formed in fluorobenzene than in chlorobenzene because fluorine is more tightly bound to the ring than chlorine. Similarly, it could be argued on the basis of this picture that the CH_3 groups are harder to remove from the ring in *para*-xylene than they are in *ortho*-xylene.

The second model assumes that positronium formation and positron capture are competing processes. It is possible that an iodine attached to a benzene ring will find it easier to capture a positron than a fluorine would under the same circumstances. Once the positron is captured it annihilates very quickly because it is in a region of high electron density. It then seems likely that the reason a smaller I_2 was measured in *ortho*-xylene than in *para*-xylene is because the distribution of charge in *ortho*-xylene is more conducive to positron capture. There is no reason why positronium formation cannot compete with both capture and rupture, in which case a combination of the two models would be needed to describe the situation.

* This research was supported in part by the U. S. Air Force Office of Scientific Research of the Air Research and Development Command and in part by The University of Texas Research Institute.

† Now at the Lawrence Radiation Laboratory, Livermore, California.

‡ Now with Texas Instruments, Inc., Dallas 9, Texas.

[1] Background and references as well as a summary of the work done on metals and gases will be found in the following review articles: S. Berko and F. L. Hereford, Revs. Modern Phys. **28**, 299 (1956); Richard A. Ferrell, Revs. Modern Phys. **28**, 308 (1956); M. Deutsch, Progr. Nuclear Phys. **3**, 131 (1953).

[2] Positronium formation in solids has been discussed by Ferrell, reference 1, p. 309.

[3] P. R. Wallace, Phys. Rev. **100**, 738 (1955).

[4] R. E. Bell and R. L. Graham, Phys. Rev. **90**, 644 (1953).

[5] R. E. Green and R. E. Bell, Can. J. Phys. **35**, 398 (1957). Robert de Zafra, Bull. Am. Phys. Soc. **3**, 229 (1958).

[6] Hatcher, Millett, Brown, Phys. Rev. **111**, 12 (1958).

TABLE I. Results obtained for positrons annihilating in organic liquids.

Compound		I_2(%)	τ_2 (10^{-9}) sec	σv (10^{-14} cm^3 sec^{-1})	Source holder[a]
$F(C_6H_4)CH_3$	*o*-fluorotoluene	33±2	2.3±.1	7.9±.3	A
$F(C_6H_4)CH_3$	*m*-fluorotoluene	27±2	2.5±.1	7.3±.3	A
$F(C_6H_4)CH_3$	*p*-fluorotoluene	27±2	2.4±.1	7.6±.3	A
CH_3OH	methyl alcohol	18±3	2.6±.1	2.6±.1	B
CH_3CH_2OH	ethyl alcohol	12±2	3.1±.2	3.1±.2	B
$CH_3CH_2CH_2OH$	*n*-propyl alcohol	19±3	2.5±.1	5.0±.3	B
$CH_3CHOHCH_3$	*iso*-propyl alcohol	14±2	3.1±.2	4.1±.3	B
$CH_3(CH_2)_3OH$	*n*-butyl alcohol	15±2	2.7±.2	5.6±.3	B
$(CH_3)_2CHCH_2OH$	*iso*-butyl alcohol	16±2	3.2±.2	4.8±.3	B
$(CH_3)_3COH$	*tert*-butyl alcohol	26±3	3.1±.2	5.0±.3	C
$CH_3CHOHCH_2CH_3$	*sec*-butyl alcohol	22±2	3.3±.2	4.6±.3	C
CH_2OHCH_2OH	ethylene glycol	14±2	2.7±.1	3.4±.2	B
$CH_3CHOHCH_2OH$	propylene glycol	17±2	2.9±.2	4.2±.3	B
$CH_2OHCHOHCH_2OH$	glycerol	21±4	2.0±.1	6.1±.3	B
$CH_3(CH_2)_2COOH$	*n*-butyric acid	25±4	2.5±.2	6.1±.4	D
$(CH_3)_2CHCOOH$	*iso*-butyric acid	25±4	2.8±.2	5.5±.4	D
$CH_3CH_2OCH_2CH_3$	ethyl ether	28±5	3.1±.3	5.6±.5	A
$CH_3COCH_2CH_3$	butanone	16±3	2.7±.2	5.5±.5	A
C_6H_6	benzene	41±3	2.5±.1	5.9±.2	A
$(C_6H_5)CH_3$	toluene	45±3	2.3±.1	7.8±.4	A

[a] Source holder A was made of aluminum foil, the other three were made of mica as described in Section 2. The fraction of annihilations occurring in the source holder was measured as A 18±5, B 7±3, C 20±5, and D 8±3.

2. EXPERIMENTAL TECHNIQUE

The source of positrons in most lifetime measurements is the positive beta emitter Na^{22}. Na^{22} decays to an excited state of Ne^{22} which in turn decays to the ground state by emitting a 1.3-Mev gamma ray. The lifetime of the excited state is so short that the 1.3-Mev gamma can be used as a signal for the creation of the positron. When the positron annihilates a short time later, there will most likely be produced two 0.51-Mev gammas.

A Na^{22} source of a few microcuries and the sample to be studied are arranged with the source in the middle and the sample on both sides so that essentially all of the positrons will be stopped in the sample. The sample holder is placed between two diphenyl acetylene scintillating crystals mounted on 931-A photomultipliers. The coincidence counting rate between a 1.3-Mev "creation" gamma and one of the 0.51-Mev annihilation quanta is then measured as a function of the artificial time delay inserted in the "creation" channel. It is necessary to use separate channels for energy selection in order to distinguish the 1.3-Mev from the 0.51-Mev radiation. Delayed coincidence arrangements of this sort have been used for a number of years and the design has become fairly standardized.[7]

Two types of sample holders have been used for the liquids studied in this work. In one type, the liquid is contained in two aluminum tanks which have 0.0002 in. aluminum foil windows through which the positrons enter the sample. The source is supported between the two tanks by a very thin collodion film. Another type of sample holder that has been found to be more versatile has the source mounted between thin mica films which are sealed at the edges and mounted between aluminum rings for support. This source holder is then emersed in the liquid which is contained in a single aluminum tank. If one coats the rings on which the source was mounted and the inside of the aluminum tank with some substance which does not interact with the sample, the same source holder can be used for a large number of samples.

In order to calculate the intensity I_2 of the long component, it is necessary to know the prompt curve $P(x)$, or the curve that would be obtained for zero lifetime. A close approximation to the true prompt curve can be obtained by using the two gamma rays from a Co^{60} source, leaving the energy selection channels the same as they are for Na^{22}.

The fraction of annihilations occurring in the source holders given in Table I was determined in each case by studying a Teflon sample with the source holder used to study liquids and again with Na^{22} deposited directly on the Teflon sample. In taking all data, the procedure followed was to take two complete delayed coincidence curves, i.e., coincidence counting rate as a function of time delay, for each sample studied.

3. DATA REDUCTION

The delayed coincidence curves are corrected for annihilations which occur in the source holder and for

[7] Bell, Graham, and Petch, Can. J. Phys. **30**, 35 (1952).

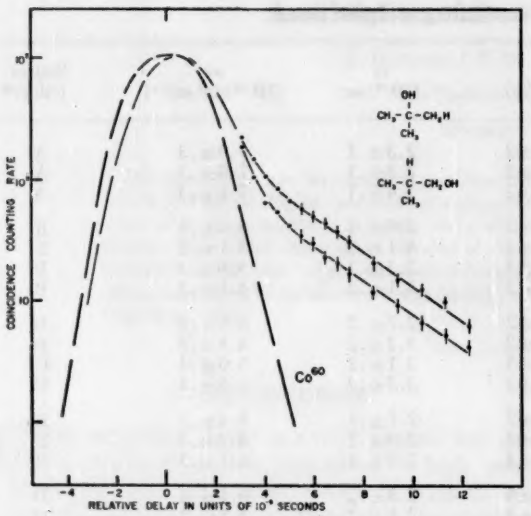

FIG. 1. The compounds *tert* butyl alcohol and *iso* butyl alcohol show a wide variation in the intensity of the long component. The prompt curve $P(x)$ taken with Co^{60} is used in the data analysis.

accidentals and normalized to a convenient unit area to give $f(x)$ which is the function plotted in Figs. 1 and 2. It has been shown that for $f(x)>>P(x)$ a plot of ln $f(x)$ *vs* x is a straight line with slope $-\lambda=-1/\tau_2$.[8] The method used to find the slope of an exponential tail was to give the points on the tail a least squares fit to a straight line. The mean life and the fraction of the long component are then calculated by

$$\tau_2=\Sigma(x_n-x_b)^2/\Sigma[\ln f(x_n)\,(x_n-x_b)]\text{ and }I_2=e^b/f_2(x_b),$$

where

$$f_2(x)=\lambda\exp(-\lambda x)\int_{-\infty}^{x}\exp(\lambda t)\,P(t)\,dt,$$

$$b=(1/N)\Sigma\ln f(x_n),$$

$$x_b=(1/N)\Sigma x_n,$$

and the summations are carried out over the N points on the exponential tail.

If it is assumed that the quenching of the ^3S positronium lifetime is due to collisions between the positronium atom and molecules of the liquid, that the lifetime of any intermediate state is short, and that the three-photon rate can be neglected, then the annihilation rate of the ^3S component is given by $\lambda_2=1/\tau_2=N\langle\sigma v\rangle_{Av}$. Here N is the number of molecules per unit volume, σ the molecular cross section for quenching interactions, and v the velocity of the positronium atom. The symbol $\langle\sigma v\rangle_{Av}$ is used to denote a mean value obtained by averaging over the velocity distribution of the positronium atoms relative to the molecules of the liquid. Since N and τ_2 are known for the liquids studied it is possible to calculate $\langle\sigma v\rangle_{Av}$.

[8] T. D. Newton, Phys. Rev. **78**, 490 (1950).

4. RESULTS

The results obtained for positrons annihilating in organic liquids are shown in Table I. Two sets of delayed coincidence curves, Figs. 1 and 2, are presented to illustrate the types of variations in the long components that are observed.

The purpose of studying the fluorotoluenes was to try to obtain an explanation of the results reported previously for the xylene family.[6] It was suggested that I_2 was a minimum for *o*-xylene either because the CH_3 groups are less tightly bound in this configuration or because the maximum charge asymmetry makes positron capture more likely. In order to help weigh one explanation against the other, a family of compounds was studied which has minimum asymmetry of charge in the *ortho*-arrangement. The fact that I_2 was greatest for *ortho*-fluorotoluene and least for *ortho*-xylene stresses the importance of the charge distribution in the molecule; however, it is possible that the results could also be explained in terms of molecular rupture.

The first group of alcohols seem uninteresting if only I_2 and τ_2 are considered; however, the values of $\langle\sigma v\rangle_{Av}$ show the general trend for larger molecules to have bigger cross sections. An exception to this trend was found for all of the normal and isomolecules studied. The propyl alcohols, butyl alcohols, and butyric acids give a larger $\langle\sigma v\rangle_{Av}$ in the *n* configuration than in the *iso* arrangement. This may mean that the positronium atom finds more electrons with which it can interact in the former case than it does in the latter, or it could be that the forces between the molecule and the positronium atom are greater for the normal arrangement.

All of the butyl alcohols except normal butyl gave a $\langle\sigma v\rangle_{Av}$ within one probable error of 4.8×10^{-14} cm^3 sec^{-1}. I_2 on the other hand was observed to vary over a fairly

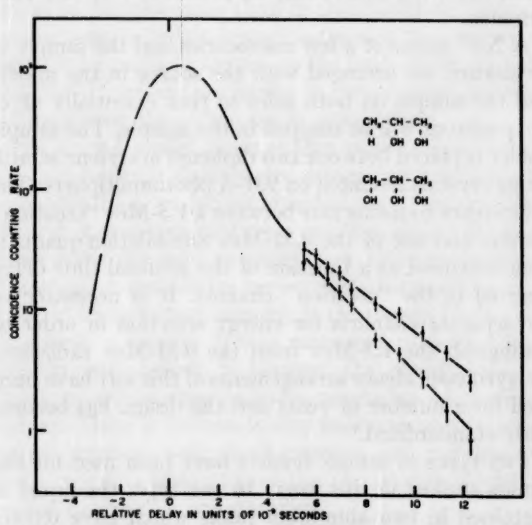

FIG. 2. Delayed coincidence curves for propylene glycol and glycerol, an example of two very similar compounds in which the mean life of ^3S positronium is noticeably different.

wide range of values, Fig. 1. With the exception of *sec* butyl, I_2 is larger for molecules which are more compact, or less chain-like. This can probably be attributed to stronger bonds in the more compact molecules.

The increase in $\langle\sigma v\rangle_{Av}$ with an increase in molecular weight can be seen very clearly for the group of compounds consisting of ethylene glycol, propylene glycol, and glycerol, Fig. 2. It is also worth noting that essentially the same $\langle\sigma v\rangle_{Av}$ was found for ethyl ether, butanone, and iso-butyric acid.

To a very crude approximation $\langle\sigma v\rangle_{Av}$ seems to be proportional to the molecular weight—at least for the compounds studied thus far. If it is assumed that this is true, and that $1/\tau_2=\langle N\sigma v\rangle_{Av}$, then τ_2 should be inversely proportional to the density of the liquid. While an approach of this sort could be expected to express only the roughest dependence of τ_2 upon ρ, it will be seen that for the results presented in Table I as well as those reported earlier,[6] τ_2 is generally larger in the less dense liquids and smaller for the more dense ones. As pointed out earlier, there are certain interesting exceptions such as normal and *iso* propyl alcohol. These deviations may be due to more complex interactions between the molecule and the positronium atom.

5. ERRORS

The errors quoted in Table I were computed by standard techniques and are thought to be a good estimate of the probable error of our measurement relative to another; however, absolute values of τ_2 and I_2 may be off by more than these errors indicate.

Some of the earlier lifetime measurements carried out in this laboratory gave results which are consistently lower than more recent values. To illustrate this, in Table I mean lives of 2.5 and 2.3×10^{-9} sec are quoted for benzene and toluene as compared with previously reported values of 2.1 and 1.9×10^{-9} sec.

The apparatus used in all measurements was the same except for scintillators. The original *p*-terphenyl in toluene liquid scintillators were replaced with crystals of diphenyl acetylene. Efforts to show that the differences in the measured values of τ_2 could be attributed to energy selection, fast-coincidence resolving time, or scintillators were fruitless.

It is now thought that most of the discrepancies in measurements of τ_2 not accountable for in terms of drift in the electronic equipment are the result of an inaccurate determination of the accidental counting rate. The larger the ratio of peak counting rate to accidental counting rate, the less effect on τ_2 an error in accidental counting rate will have, and for this reason, the more recent quotations should be the more accurate, or the values of τ_2 quoted earlier are probably unrealistically low.

TABLE II. Fluorotoluene data.

Compound	Run	I_2(%)	$\tau_2(10^{-9}$ sec)
o-fluorotoluene	1	33.1	2.36
	2	33.7	2.22
m-fluorotoluene	1	26.2	2.43
	2	26.9	2.49
p-fluorotoluene	1	24.8	2.49
	2	28.4	2.28

On the other hand, the values of I_2 published earlier should be more nearly internally consistent than the present ones. This is due to the fact that a separate determination of the fraction of annihilations occurring in the mica, r, had to be made for each mica source holder used in this work, whereas previously the same source holder was used for all liquids studied. The error introduced by the source holder correction is not as serious as it might appear since τ_2 is hardly affected by an error in r and since if no correction was made, the resulting error in I_2 would be $rI_2/(1-r)$, or in most cases $<3\%$.

Table II is included to give some indication of the degree of reproducibility that can be obtained with the present apparatus. The curves for the fluorotoluenes were so similar that it was decided to measure each compound twice. The results seem reasonable in terms of the computed probable errors quoted in Table I.

In conclusion, it might be said that the present techniques are not good enough to make possible a precise determination of τ_2 and I_2. However, variations of these quantities are sufficiently wide to permit the establishing of certain trends. The interpretation of these trends given here is largely speculative, and more work will be necessary before a definite picture can be formulated.

Vibration-Rotation Bands of Ammonia.* IV. The Stretching Fundamentals and Associated Bands near 3 μ

W. S. BENEDICT, *Laboratory of Astrophysics and Physical Meteorology, The Johns Hopkins University, Baltimore, Maryland*

AND

EARLE K. PLYLER AND E. D. TIDWELL, *National Bureau of Standards, Washington 25, D. C.*

(Received June 5, 1959)

High-resolution spectra of NH_3, yielding 1800 lines between 3060–3580 cm^{-1}, are presented. Analysis of the ν_3 fundamental is complete through $J'=9$ and presents no unexpected features. Resolution of the K substructure in the ν_1 fundamental shows that several perturbations are present. The most important of these, involving a Fermi resonance with the parallel component of $2\nu_4$, and a Coriolis resonance with its perpendicular component, are clarified. Lines in both components of $2\nu_4$ are identified through $J'=6$, and a strong Coriolis interaction between the $l=0$ and $l=2$ states is observed and discussed.

INTRODUCTION

THE first band of NH_3 to be resolved and analyzed[1] was ν_1, the symmetrical stretching fundamental at 3μ. The doublet structure of the "lines" in the P and R branches was recognized as being caused by the low potential barrier to inversion in the plane of the hydrogens, and remains the classical example of this effect in molecular spectra. The asymmetrical stretching fundamental ν_3 proved less easy to locate, but the studies of Cumming and Welsh[2] and Cumming[3] have demonstrated conclusively that its band origin lies near 3442 cm^{-1}, 108 cm^{-1} higher than ν_1. The first overtone of the asymmetrical bending vibration $\nu_4=$ 1626.8 cm^{-1} should also lie in the 3-μ region, but, except for an attribution of a weak Raman shift at 3215 cm^{-1} to the A component of this overtone, no identifications of these levels have been made.

We have studied the region 2.75–3.2μ under high resolution as part of a comprehensive reinvestigation of the infrared spectra of the ammonias. In previous papers[4–6] we have described our general aims and methods and have given detailed results in the regions flanking the fundamentals. We have chosen to defer presentation of our results in the fundamental region because the findings are quite complex, and very high resolution is required in order to clarify the situation resulting from the mutual interactions of ν_3, ν_1, and $2\nu_4$. Approximately 1500 lines have been resolved and measured between 3080–3580 cm^{-1}. Most of these have been assigned to the three expected bands, whose relative intensities are roughly 6:5:2. The structure of ν_3 is that of a normal perpendicular band; that of ν_1 is a parallel band with normal structure at low J, K, but with abnormalities at the higher rotational quantum numbers; and $2\nu_4$ has both parallel ($l=0$, vibrational symmetry A_1) and perpendicular ($l=2$, vibrational symmetry E) components. These show interactions with each other and with ν_1 that are not considered in standard band descriptions (as for example in our first paper).[4] Accordingly, before presenting the experimental results we shall review briefly the principal features expected theoretically for the $2\nu_4-\nu_1$ situation.

Properties of the ν_4 vibration have been obtained from measurements of the fundamental[7] and its combination with ν_2.[6] These show a number of features which are the result of unusually large interaction terms. (1) The component of internal angular momentum ζ_4 has the calculated value -0.2491, and is observed to be -0.2535 in ν_4 and -0.235 in $\nu_4+\nu_2$. (2) As a result principally of the strong first-order Coriolis interaction between ν_4 and ν_3 (the calculated value of $\zeta_{24}^{(x)}$ being 0.6114), there is a large second-order interaction term connecting the pairs of levels in ν_4 with $[l_4, K \mid l_4\pm2, K\pm2]$. This is made manifest both by the (A_1, A_2) splitting of the $K=1^+$ levels, by the values $\pm0.171\ J(J+1)$ in ν_4 and $\pm0.135\ J(J+1)$ in $\nu_4+\nu_2$, and by the displacement of K^-, $(K+2)^+$ levels (where the $^-$ index refers to the states of lower energy in the P branch, and the $^+$ to the higher energy states observed in the R branch). (3) As a further result of the large value of $\zeta_{24}^{(x)}$, the rotational constant B_0 undergoes a large increase, $B_4-B_0=+0.2462$ cm^{-1} in ν_4. (4) One quantum of ν_4 vibration increases the inversion splitting; for the nonrotating molecule the increase is 31% in ν_4 and 27% in $\nu_4+\nu_2$. (5) In both ν_4 and $\nu_4+\nu_2$ there are abnormal variations of the inversion with J and K, the splitting increasing at $K=0$, with increasing J, and being much greater for K^+ than for K^-. These may be correlated by postulating (a) a specific second-order Coriolis interaction of ν_4 with $2\nu_2$ (the origin of $2\nu_2^e$ lies only 29.8 cm^{-1} below ν_4^a, so that although the force between the states is one order less than ζ_{24}, it would have an appreciable per-

* This research was supported in part by the U. S. Air Force and in part by the U. S. Atomic Energy Commission.

[1] D. M. Dennison and J. D. Hardy, Phys. Rev. **39**, 938 (1932).
[2] C. Cumming and H. C. Welsh, J. Chem. Phys. **21**, 1119 (1953).
[3] C. Cumming, Can. J. Phys. **33**, 635 (1955).
[4] Benedict, Plyler, and Tidwell, J. Research Natl. Bur. Standards **61**, 123 (1958).
[5] Benedict, Plyler, and Tidwell, Can. J. Phys. **35**, 1235 (1957).
[6] Benedict, Plyler, and Tidwell, J. Chem. Phys. **29**, 829 (1958).
[7] Garing, Nielsen, and Rao, J. Mol. Spectroscopy **3**, 496 (1959).

turbing effect); (b) a different effective ζ_4 for the inversion pairs, and (c) a different effective ζ_{24} for the inversion pairs.

In the overtone $2\nu_4$, all the above effects should be present, and would be roughly doubled in magnitude. In the E state ($l=\pm 2$), the effective ζ for the K splitting would be $\sim -2\zeta_4 \sim 0.5$. The second-order effect of the $\zeta_{24}^{(x)}$ will be to set up interactions among the three levels $(l_4, K)=(-2, K-2)$; $(0, K)$; and $(+2, K+2)$. The origin of the $l=0$ state will be displaced from that of $l=2$ by $4g_{44}$. The latter constant includes a term k_{144} connecting nearly resonant levels $2\nu_4$ and ν_1, so that g_{44} must be positive ($2\nu_4^2$ above $2\nu_4^0$). When k_{144} is of the same order of magnitude as $\nu_1-2\nu_4$, it is necessary to divide g_{44} into two portions, grouping the nonresonant terms as g_{44}' and treating the remainder as a case of Fermi resonance. Here the Coriolis interaction must also be considered, so that the energies have to be obtained as the roots of the 4×4 secular determinant of the form

$$\begin{vmatrix} \nu_1, K & E_1(J,K)-\lambda & 0 & k_{144} & 0 \\ \nu_4=2, l_4=-2, K-2 & 0 & E_4^-(J,K)-\lambda & \alpha_1(J,K) & 0 \\ \nu_4=2, l_4=0, K & k_{144} & \alpha_1(J,K) & E_4^0(J,K)-\lambda & \alpha_2(J,K) \\ \nu_4=2, l_4=2, K+2 & 0 & 0 & \alpha_2(J,K) & E_4^+(J,K)-\lambda \end{vmatrix}, \quad (1)$$

where (ignoring inversion effects and centrifugal stretching terms)

$$E_1=\nu_1+B_1J(J+1)+(C_1-B_1)K^2, \quad (1a)$$

$$E_4^0=2\nu_4+2x_{44}-2g_{44}'+B_4'J(J+1)+(C_4'-B_4')K^2, \quad (1b)$$

$$E_4^-=2\nu_4+2x_{44}+2g_{44}'+B_4'J(J+1)+(C_4'-B_4')(K-2)^2-4C_4'\zeta_4(K-2), \quad (1c)$$

$$E_4^+=2\nu_4+2x_{44}+2g_{44}'+B_4'J(J+1)+(C_4'-B_4')(K+2)^2+4C_4'\zeta_4(K+2), \quad (1d)$$

$$\alpha_1=2\sqrt{2}q_4[J(J+1)-(K-2)(K-1)]^{\frac{1}{2}}\cdot[J(J+1)-(K-1)K]^{\frac{1}{2}}, \quad (1e)$$

$$\alpha_2=2\sqrt{2}q_4[J(J+1)-K(K+1)]^{\frac{1}{2}}\cdot[J(J+1)-(K+1)(K+2)]^{\frac{1}{2}}. \quad (1f)$$

The B', C' constants are the effective rotational constants for $2\nu_4$, approximately $B_4'=B_0+2(B_4-B_0)$, etc.

Consideration of the selection rules for transitions to the levels subject to the $(Kl \mid K\pm 2, l\pm 2)$ interaction shows that the triple interaction is between sets $({}^P1, {}^Q1, {}^P3)$, $({}^P0, {}^Q2, {}^P4)$, $({}^R1, {}^Q3, {}^P5)$, etc. where the superscript is the ΔK, and the number is the K of the $2\nu_4$ state. ${}^RJ$ and ${}^R(J-1)$ do not interact; ${}^R(J-2)$ and ${}^QJ$ form a doublet; and the triplet $({}^P2, {}^Q0, {}^P2)$ factors into a singlet ${}^P2$ and a $({}^P2, {}^Q0)$ doublet, resulting in the first-order (A_1, A_2) splitting of ${}^P2$, analogous to the splitting of ${}^R1$ when $l=1$.

Consideration of the approximate values of the constants in Eq. (1) and the solution of the resulting equations, shows that the perturbations of the energies caused by the off-diagonal elements will be as follows. The k_{144} interaction is essentially between E_4^0 and E_1. If $E_4^- - E_4^0 \ll E_4 - E_4^0$, the E_1 root may be factored off, as in the familiar case of Fermi resonance, so that $\lambda_1=E_1+\delta$ and $\lambda_4^0=E_4^0-\delta$, where $\delta^2=k_{144}^2+(E_1-E_4^0)^2$. Since $E_1-E_4^0$ is strongly J-dependent ($B_1-B_4' \cong 0.68$ cm^{-1}), δ will not be a simple function of $J(J+1)$. Moreover, for high values of J, E_4^0 approaches E_1 and, at high values of K, E_4^- may become greater than E_1. For such levels the factoring procedure is no longer valid and strong perturbations may appear. The α_1, α_2 (Coriolis) interactions are greatest when $J \gg K$, and will have the strongest perturbing effects when the unperturbed energies are nearly equal. It may be shown that this will occur between $E_4^0-\delta$ and E_4^+ at a relatively low value of K. If the K_{144} factorization is valid, we have

$$E_4^+ - E_4^0 = 4g_{44}'+\delta+(C_4'-B_4')(4K+4)+4C_4'\zeta_4(K+2) \cong 4g_{44}'+\delta-5.4-11.4K \text{ (cm}^{-1}\text{)}. \quad (2)$$

The most strongly perturbed lines in $2\nu_4$ will accordingly be ${}^Q1-{}^Q3$, ${}^P2-{}^P4$; but all the lines, except for ${}^RJ$ and ${}^R(J-1)$, will show effects of the Coriolis interaction.

The foregoing description summarizes the situation anticipated from the Fermi and Coriolis interactions. Inversion may be expected to produce additional complications.

EXPERIMENTAL METHODS AND RESULTS

The methods are those described in previous papers from this laboratory. The absorption in this region is moderately strong, so that with an absorption cell 600 cm in length, pressures as low as 1 mm Hg were used for the regions of highest intensity, namely, in the Q branch of ν_1, in some of the P and R branch groups of lines of that band, and in the central region of ν_3,

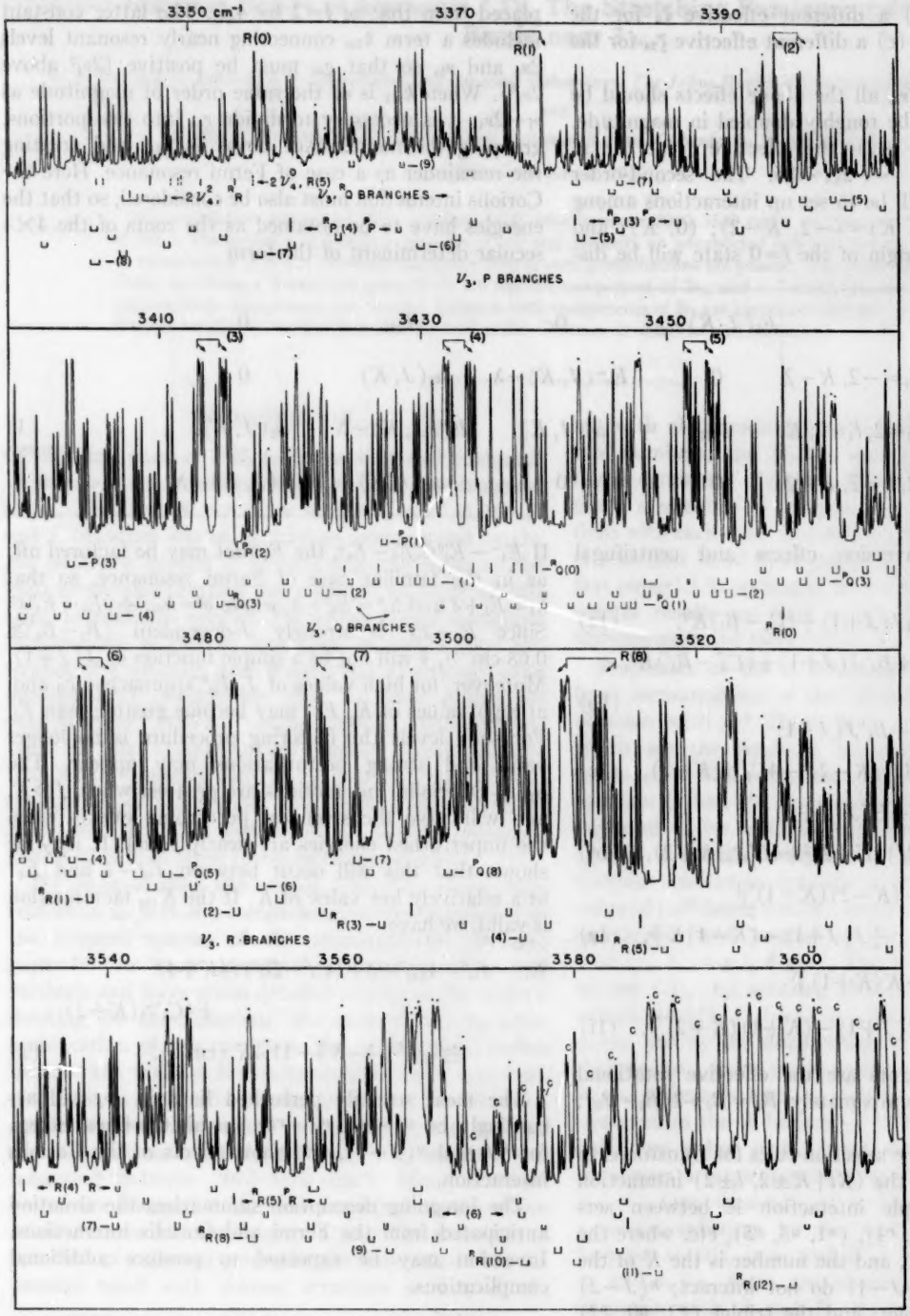

FIG. 1. NH_3 spectra 3337–3605 cm^{-1}. Cell length, 600 cm; pressure, top panel, 3.8 mm; second panel, 10 mm; two bottom panels, 15 mm. H_2O lines are marked with dots, and (above 3570 cm^{-1}) CO_2 lines with C. Most of the NH_3 lines belong to ν_3, and are identified below the spectra. They occur in doublets (except for $K''=0$); the identifying marks are arranged so that doublets with common J (in R and P branches) or common K'' (in Q branches) are at the same level. The R branches of ν_1 are indicated above the spectrum. In the top panel, a few lines of $2\nu_4$ are identified.

from 3400–3470 cm^{-1}. Pressures up to 20 cm Hg were used to develop the weaker lines which occur between the strong groups and which extend to longer wavelength, merging below 3080 cm^{-1} with the band $3\nu_2{}^a-0^s$, which was discussed in the preceding paper. The spectra selected for measurement were at appropriate pressures, generally at about 2 cm Hg. Some interference with the NH_3 spectrum is caused by atmospheric H_2O absorption, which is present throughout the region 3080–3500 cm^{-1}, and which increases in intensity at higher frequencies so that the upper limit of our accurate measurements was 3552 cm^{-1}. A single trace taken on an unusually dry day revealed additional lines in the 3500–3600 cm^{-1} region. Approximate measurements for these were obtained by interpolation between the measured NH_3 lines and H_2O standards.

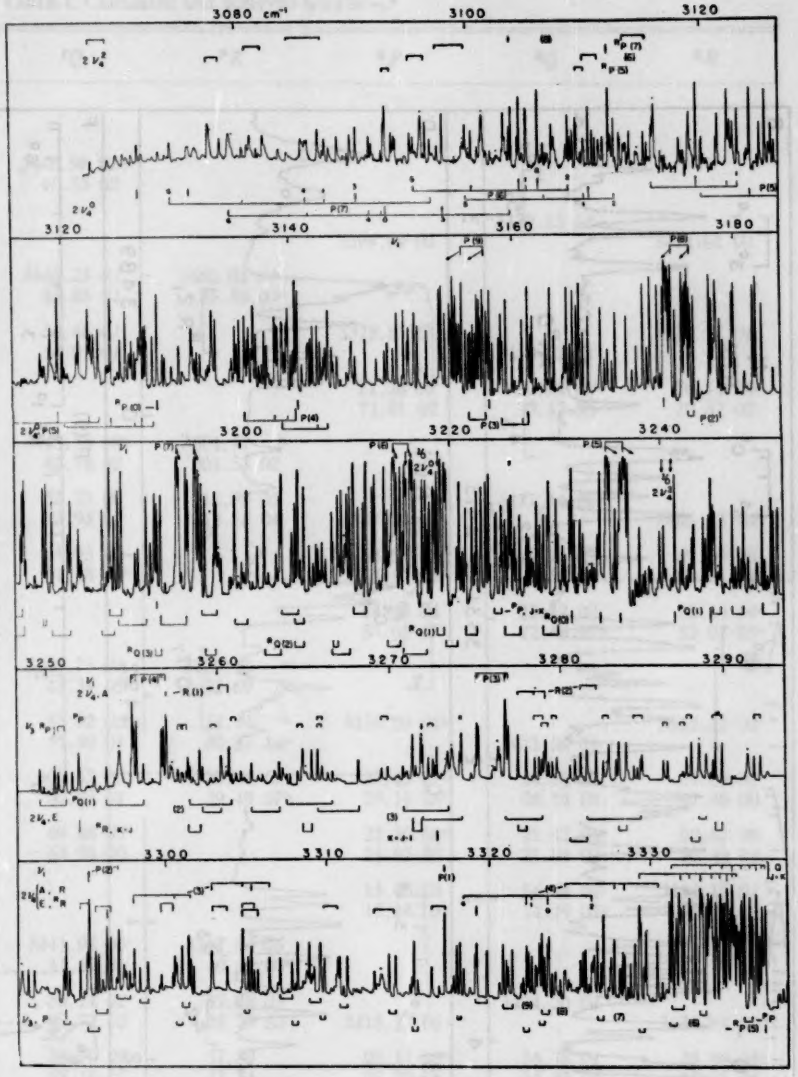

FIG. 2. NH_3 spectra, 3068–3340 cm^{-1}. Cell length, 600 cm; pressure, 3 upper panels, 20 mm; 2 lower panels, 2.5 mm. Atmospheric H_2O lines are identified by dots. Various NH_3 regularities in four overlapping bands are identified. Top panel; above spectrum, doublets in the ${}^RP$ and ${}^PP$ branches of $2\nu_4{}^3$, $J''=5$–8; below spectrum, P branches of $2\nu_4{}^0$. Second panel; above spectrum, $P(8)$ and $P(9)$ of ν_1; below spectrum $P(2)$–$P(5)$ of $2\nu_4{}^0$ and the $K=0$, ${}^RP$ series of $2\nu_4{}^3$. Third panel; above spectrum, $P(5)$–$P(7)$ of ν_1; below spectrum, $2\nu_4{}^3$. The origins of $2\nu_4$ are indicated, and the Q branch of $2\nu_4{}^0$ accounts for much of the strong absorption between 3210–3230 cm^{-1}. Fourth panel; above spectrum, $P(3)$ and $P(4)$ of ν_1, $R(1)$ and $R(2)$ of $2\nu_4{}^0$, and numerous ${}^PP$ and ${}^RP$ doublets of ν_3; below spectrum, ${}^PQ$ and ${}^RR$ of $2\nu_4{}^3$. Bottom panel; above spectrum, $P(2)$, $P(1)$ and Q of ν_1; $R(3)$ and $R(4)$ of $2\nu_4{}^0$ and ${}^RR$ doublets of $2\nu_4{}^3$; below spectrum, ${}^PP$ and ${}^RP$ of ν_3.

The results are presented by illustrative spectra in Figs. 1–3. It is apparent that the combination of the high-resolution spectrometer and the low pressure has resulted in a spectrum of much more complex appearance than is seen at lower resolution. It has been possible, however, to account for all of the prominent features by assuming that they arise from the three bands ν_3, ν_1, and $2\nu_4$, whose general characteristics have been described in the introduction. Each shows inversion doubling, ranging from 0.2–6 cm^{-1}. The wave numbers of identified lines are given in Tables I–III. The several bands will now be discussed briefly.

The Band ν_3

The pattern of this band is quite regular, and the assignments can be made without difficulty. As noted by Cumming,[3] the lines occur in pairs of equal intensity, with spacings of from 0.2 cm^{-1} to 0.75 cm^{-1}. This is the result of the inversion doubling. The combination differences and the location of the $K''=0$ lines (which are unpaired) prove unambiguously that the higher-frequency lines belong to the $s-s$ transitions, so that the inversion splitting of ν_3 is less than in the ground state. This conforms with the situation in $\nu_3+\nu_2$.

The ν_3 doublets are indicated in Figs. 1 and 2 by U-shaped brackets beneath the spectra. They account for most of the absorption above 3340 cm^{-1}, except for the narrow groups in the R branch of ν_1. The higher-J members of the ${}^RR$ and ${}^PR$ branches are obscured by water-vapor absorption. In the ${}^PP$ and ${}^RP$ branches, some pairs of ν_3 have been observed down to 3220 cm^{-1}, but they are with few exceptions weaker than lines in $2\nu_4$ below 3300 cm^{-1}. The highest complete set of observed levels is thus $J'=9$. Molecular constants were derived by standard methods for all levels up to $J'=8$, and the line positions resulting are compared with

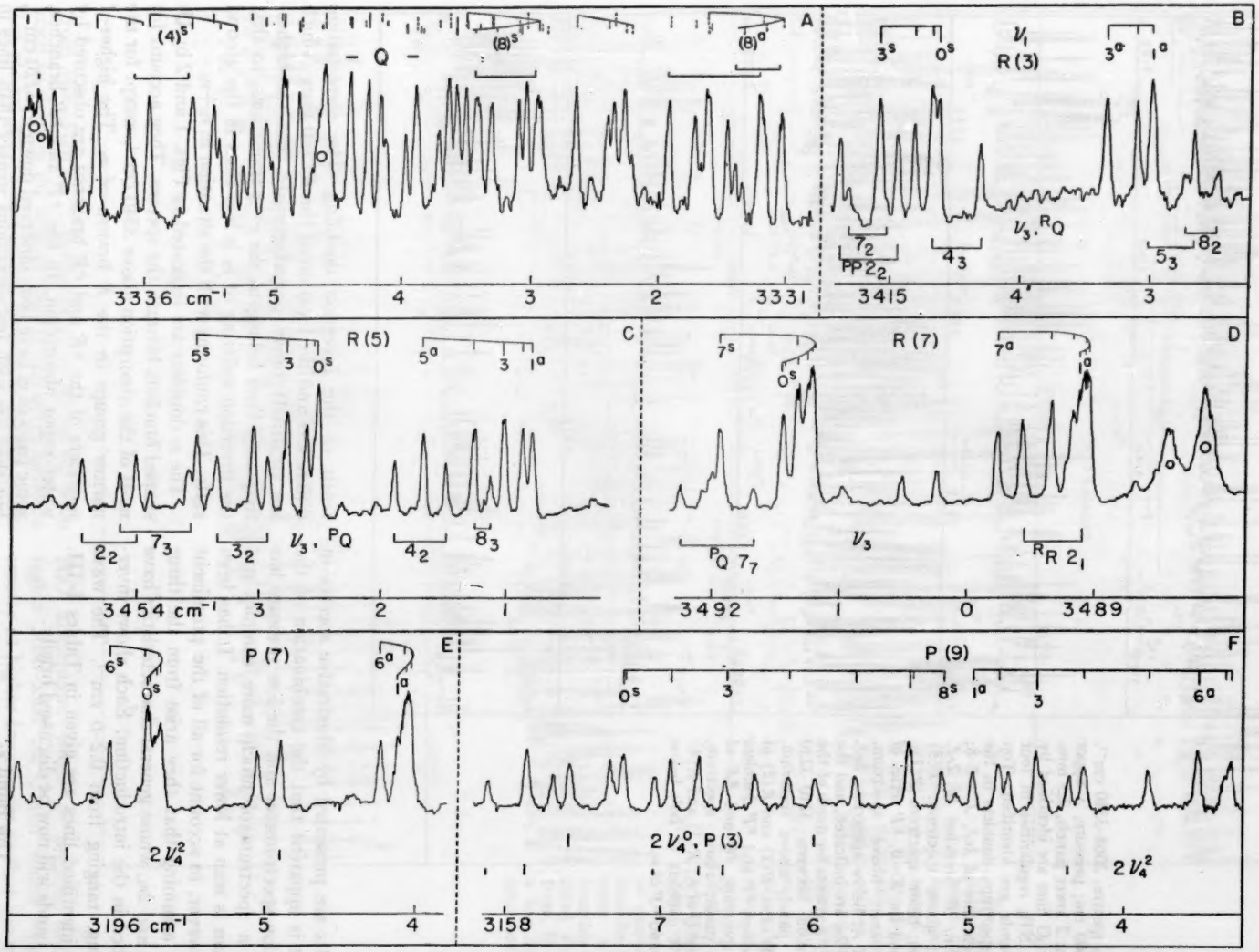

FIG. 3. High dispersion NH_3 spectra in various regions. Cell length, 600 cm; pressure, Panels A–C, 1 mm; D and E, 2.5 mm; F, 5 mm. H_2O lines at atmospheric pressure, with enclosed circles, are noticeably broader than NH_3 lines. The K structure in ν_1 is indicated at the top. Lines of other bands are identified below. Panel A, Q branch: The a-s (higher frequency lines) are denoted by solid markers, s-a are dashed. Markers for the strongest lines, with $K=J$, are on highest level, for $K=J-1$ on next lower level, etc. A few of the sets with common J are linked and numbered. Lines in ν_3 are identified immediately above spectrum; cf. Fig. 2, bottom panel. Note that at low J, in Q and R branches (panel B), the lines of higher K are at higher frequency; but that with increasing J, (panels D, E, F) low-K lines are displaced to higher frequency.

TABLE I. Calculated and observed lines in ν_3.[a]

J_K'	ψ''	^PP	^PQ	^PR	^RP	^RQ	^RR
0	s	3427.46 *01*					
	a	27.04 *01*					
1_0	s	3407.21 03	3446.98 02[b]				
	a	06.80 01	46.55 02				
1_1	s	15.41 *02*				3439.15 *02*	
	a	14.99 *01*			3398.99 02		3458.61 00
2_0	s	3386.66 02	3446.25 *01*	3486.02 *04*			
	a	86.26 01	45.83 *01*	85.58 03[c]			
2_1	s	94.84 01	54.46 *01*		3378.85 04[c]		3478.17 01
	a	94.42 00	54.01 *01*			3438.02 *01*	
2_2	s	3403.40 00			71.38 *02*	30.98 06[b]	70.74 *00*[c]
	a	02.95 *01*			71.01 02	30.57 00	70.32 *02*
3_0	s	3365.80 *05*[b]	3445.18 08[b]	3504.77 [b]			
	a	65.41 04	44.76 *02*	04.33 02			
3_1	s	73.95 00	53.37 00	12.99 03		3437.36 02	
	a	73.55 03	52.93 02	12.52 04	3357.63 03		3496.52 *10*[b]
3_2	s	82.47 *01*	61.95 00		50.53 03	29.91 03	89.50 00
	a	82.04 02	61.48 *08*[b]		50.17 03	29.52 03	89.09 01[b]
3_3	s	91.39 *01*			53.40 04	22.82 02	82.44 *04*[c]
	a	90.90 *01*			53.05 *07*	22.43 *07*[b]	82.02 05[b]
4_0	s	3344.68 01	3443.75 *01*	3523.13 [b]			
	a	44.31 06[c]	43.34 *05*[c]	22.69 [b]			
4_1	s	52.80 00	51.92 *02*	31.34 [b]	3336.89 *01*[c]		3515.32 *02*
	a	52.41 03	51.49 01	30.87 14[c]		3435.56 01	
4_2	s	61.38 01	60.47 *01*	39.95 *03*	29.43 07[b]	28.51 02	07.89 *01*
	a	60.99 00	60.05 *01*	39.49 *07*[b]	29.11 08[b]	28.14 01	07.49 00
4_3	s	70.16 00	69.46 *03*		22.30 04[c]	21.42 04	00.83 00
	a	69.71 00	68.96 00		21.97 05	21.04 02	00.42 *01*
4_4	s	79.43 00			15.48 03	14.68 01[b]	3494.15 *01*
	a	78.92 *03*[c]			15.14 *08*[c]	14.29 01[b]	93.73 00
5_0	s	3323.31 *01*	3441.98 00	3541.06 *05*			
	a	22.97 03	41.59 03	40.62 00[c]			
5_1	s	31.41 04	50.14 *02*	49.26 *05*		3434.20 *01*	
	a	31.04 01[c]	49.72 *03*	48.79 *03*	3315.22 06		3532.84 00
5_2	s	39.88 *02*	58.70 *09*	57.89	08.11 02[b]	26.78 *01*	25.86 *05*[c]
	a	39.43 03	58.19 02	57.34	07.79 *01*	26.42 *06*	25.45 *06*
5_3	s	48.68 *02*	67.62 *03*	66.92	00.98 07[b]	19.71 02	18.83 04
	a	48.25 01	67.13 *01*	66.38	00.67 03	19.35 08[c]	18.42 00
5_4	s	57.89 *01*	76.99 *03*		3294.16 03[c]	12.98 [b]	12.17 *02*[c]
	a	57.41 00	76.45 00		93.84 06	12.61 04	11.75 *05*[c]
5_5	s	67.50 00			87.61 [b]	06.55 04	05.85 00[c]
	a	66.96 *02*			87.29 06	06.17 01	05.42 02
6_0	s	3301.74 *01*	3439.90 *04*				
	a	01.41 04[c]	39.53 01				
6_1	s	09.81 *03*	48.03 *04*		3294.00 *10*[c]		3550.79 *09*
	a	09.47 05	47.63 00			3431.78 06	
6_2	s	18.14 *01*	56.46 *02*		86.58 01	24.73 *01*	43.40 [b]
	a	17.91 00	56.17 00[c]		86.29 07[c]	24.39 04[c]	43.01 *02*[b]
6_3	s	26.98 00	65.45 *07*		79.45 06[c]	17.67 01	36.40 [b]
	a	26.57 01	64.98 *01*		79.17 *04*[c]	17.33 *07*[c]	36.01 *09*
6_4	s	36.13 *01*[c]	74.78 *02*[b]		72.62 05	10.95 02	29.77 *05*
	a	35.67 *03*[b]	74.26 *02*		72.36 03	10.60 05[c]	29.36 [b]
6_5	s	45.66 *03*	84.54 *04*		66.06 [b]	04.53 *02*[c]	23.47 *08*
	a	45.15 00	83.96 01		65.77 [b]	04.18 03	23.06 [b]

TABLE I.—*Continued.*

$J_{K'}$	p''	^{P}P	^{P}Q	^{P}R	^{R}P	^{R}Q	^{R}R
6_6	*s*	3355.61 *02*			3259.79 01	3398.44 03	3517.54 *01*
	a	55.04 *04*[c]			59.46 07[c]	98.05 01	17.09 03
7_0	*s*	3280.01 *02*	3437.51 *06*[b]				
	a	79.71 04	37.16 01				
7_1	*s*	88.03 *01*	45.61 *05*			3429.78 *02*	
	a	87.71 03	45.23 *13*[b]		3272.01 02		3567.53
7_2	*s*	96.52 *02*	54.21 *07*		64.89 08	22.39 *03*[b]	60.55
	a	95.90 *10*	53.54 *04*[b]		64.62 05	22.07 01	60.17
7_3	*s*	3305.09 *01*	62.95 12[c]		57.79 04	15.35 [b]	53.57
	a	04.71 04	62.51 05[b]		57.51 08	15.03 [b]	53.19
7_4	*s*	14.16 *01*	72.23 *13*[b]		50.94 06	08.63 *01*	46.95 *05*[b]
	a	13.70 06	71.74 *04*[b]		50.67 *07*	08.31 *13*	46.57 *14*
7_5	*s*	23.62 *06*	81.95 *05*[b]		44.37 05	02.23 00	40.70 *08*[c]
	a	23.14 02	81.40 *02*		44.10 02[b]	01.90 02	40.31 01
7_6	*s*	3333.47 *02*	3492.11 12[c]		3238.06 08[c]	3396.13 04[b]	3534.78 02
	a	32.94 03	91.49 18[c]		37.77 05[c]	95.77 *02*[c]	34.36 00
7_7	*s*	43.75 *03*			32.01	90.34 00	29.22 [b]
	a	43.14 06			31.67	89.93 05	28.74 06
8_0	*s*	3258.15 05[c]	3434.84 *06*				
	a	57.87 *04*	34.51 *04*				
8_1	*s*	66.13 *04*	42.90 *04*		3250.47 *06*		
	a	65.84 00	42.55 [b]			3426.82 *05*[c]	
8_2	*s*	74.18 21[c]	51.09 [b]		43.09 *11*	19.78 *05*[b]	
	a	74.32 07[c]	51.15 [b]		42.84 *01*	19.48 *05*[b]	
8_3	*s*	83.12 *06*[c]	60.21 *17*[b]		35.93 *07*[b]	12.70 *05*[b]	
	a	82.76 03	59.79 *01*		35.70 11[c]	12.41 07	
8_4	*s*	92.06 04	69.39 04[b]		29.15 *04*	06.06 *05*	
	a	91.66 06	68.92 04[b]		28.93 06	05.76 05	
8_5	*s*	3301.42 03[c]	79.04 *01*		22.56 07[c]	3399.65 *02*	
	a	00.98 07[c]	78.52 07		22.31 *09*[c]	99.34 *14*	
8_6	*s*	11.19 *01*	89.15 [b]		16.22 [b]	93.55 10	3551.62
	a	10.70 00	88.56 01		15.96 [b]	93.22 *05*	51.22 00
8_7	*s*	21.35 *03*	99.71 02[b]		10.14 06	87.76 05	46.09 00
	a	20.77 *01*	99.04 03		09.84 06	87.39 08	45.65 05[b]
8_8	*s*	31.94 *02*[c]			04.28	82.24 *03*[c]	40.88 00
	a	31.28 *08*[c]			03.96	81.82 08	40.38 02
9_0	*s*	3236.20 07	3431.91 [b]				
	a	35.96 04	31.61 [b]				
9_1	*s*	44.14 *02*[c]	39.93 [b]			3424.24 *11*	
	a	43.86 02	39.60 [b]				
9_2	*s*	52.75 *05*	48.67 *10*			16.90 00	
	a	51.71 09[c]	47.44 20[c]			16.63	
9_3	*s*	60.93 *04*	57.08 *11*			09.89 *04*	
	a	60.61 12	56.70 12			09.64 *06*	
9_4	*s*	69.86 10	66.27 15			03.21 [b]	
	a	69.49 12	65.83 14			02.94 [b]	
9_5	*s*	79.12 01	75.85 *02*			3396.82	
	a	78.70 01	75.36 14			96.55 07	
9_6	*s*	89.77 06	86.88 *08*			90.73 17[b]	
	a	89.30 02	86.33 [b]			90.44 *10*[b]	
9_7	*s*	98.81 16	96.37 13[b]			84.92 *06*	
	a	98.28 13[c]	95.75 17			84.60 *02*	
9_8	*s*	3309.26 25[c]	3507.34 *05*[c]			79.40 03[b]	
	a	08.68 34[b]	06.63 11[c]			79.03 03	
9_9	*s*	20.19 *39*				74.16 01	
	a	19.48 *37*[c]				73.72 01	

[a] The first entry for each upper rotational state ($J_{K'}$), lower inversion state (*s* or *a*), and branch is the calculated wave number (cm^{-1}). The second entry is the deviation, observed-calculated (10^{-2} cm^{-1}). Italic numbers signify a negative deviation.

[b] Observed lines with heavy blending.

[c] Observed lines with moderate blending.

TABLE II. Observed lines (cm^{-1}) in ν_1.

J_K'	p''	P	Q	R
0	s	3317.21		
1_0	a	3295.40[a]		3355.00[a]
1_1	s	97.19	3336.96	
	a	95.40[a]	35.19	
2_0	s	3276.94		3376.29
2_1	s	76.97	3336.58	76.32
	a	75.24	34.82[a]	74.54
2_2	s	77.10	36.73	
	a	75.34	34.91	
3_0	a	3254.93[a]		3393.81
3_1	s	56.66	3335.98[b]	95.60
	a	54.93[a]	34.27[a]	93.84
3_2	s	56.76	36.12	95.75
	a	55.03	34.40	93.97
3_3	s	56.94	36.42	
	a	55.17	34.61	
4_0	s	3236.20[a]		3414.63
4_1	s	36.23	3335.30[a]	14.68
	a	34.62	33.65[b]	12.98
4_2	s	36.31	35.42	14.82
	a	34.66	33.73	13.09
4_3	s	36.47	35.64	15.09
	a	34.76	33.91	13.33
4_4	s	36.67	35.98	
	a	34.94	34.16	
5_0	a	3214.32[a]		3431.89[a]
5_1	s	15.94[a]		33.65
	a	14.28[a]		31.89[a]
5_2	s	15.94[a]	3334.61[b]	33.75
	a	14.28[a]	32.95[a]	32.02
5_3	s	16.01	34.82[a]	33.97
	a	14.32[a]	33.10[a]	32.22
5_4	s	16.14	35.04	34.35
	a	14.42	33.32[a]	32.54
5_5	s	16.39	35.47	
	a	14.61	33.65	
6_0	s	3195.73[a]		3452.52
6_1	s	95.73[a]		52.56
	a	94.14		50.80
6_2	s	95.69[a]	3333.88	52.63
	a	94.05[a]	32.21	50.87
6_3	s	95.69[a]	33.98	52.76
	a	94.05[a]	32.26	51.02
6_4	s	95.69[a]	34.14	53.04
	a	94.05[a]	32.38	51.27
6_5	s	95.81	34.40	53.50
	a	94.05[a]	32.64	51.67
6_6	s	96.06	34.91	
	a	94.25	33.04	
7_0	a	3174.31		3469.71[a]
7_1	s	3176.07		3471.64[a]
	a	74.28		69.71[a]
7_2	s	75.96		71.64[a]
	a	74.17		69.71[a]
7_3	s	75.79	3333.43[a]	71.70
	a	74.03	31.63[a]	69.83
7_4	s	75.61	33.40	71.84
	a	73.88	31.63[a]	69.98
7_5	s	75.50	33.52[a]	72.14
	a	73.73[a]	31.75[a]	70.29[a]
7_6	s	75.31	33.59	72.45
	a	73.73[a]	31.93[a]	70.74[a]
7_7	s	75.67	34.27	
	a	73.77	32.33	
8_0	s	3157.28[a]		3491.42[a]
8_1	s	57.28[a]		91.42[a]
	a	54.99		89.10
8_2	s	56.95		91.31[a]
	a	54.82		89.04[a]
8_3	s	56.59	3333.43[a]	91.22
	a	54.57	31.41[a]	89.04[a]
8_4	s	56.16	33.27	91.20[a]
	a	54.28	31.35	89.04[a]
8_5	s	55.75	33.10[a]	91.20[a]
	a	53.87	31.13	89.14
8_6	s	55.39	32.95[a]	91.31[a]
	a	53.56	31.05[a]	89.30
8_7	s	55.36	33.31[a]	91.92
	a	53.35	31.22	89.72
8_8	s	55.19	33.52[a]	
	a	53.39	31.63	
9_0	a	3136.75		3509.03[a]
9_1	s	42.73		15.04
	a	36.71		09.03[a]
9_2	s	41.60	3337.31	14.02
	a	36.55		09.03[a]
9_3	s	39.76		12.64
	a	36.31		09.03[a]
9_4	s	38.91		12.15[a]
	a	36.04		09.07
9_5	s	37.94		11.74[a]
	a	35.51[a]		09.15
9_6	s	37.73	34.40[a]	11.98
	a	35.10	31.75[a]	09.28
9_7	s	35.51[a]	33.52[a]	10.63
	a	33.36[a]	31.05[a]	08.17
9_8	s	34.65	32.26[a]	10.54
	a	33.36[a]	30.85	09.07
9_9	s	33.05	31.05[a]	
	a	31.26	29.16[a]	
10_9	s	3112.15	3329.26	
	a	10.60	27.63[a]	
10_{10}	s	11.51	29.16[a]	
	a	09.81	27.39	

[a] Observed lines with moderate blending.
[b] Observed lines with heavy blending.

TABLE III. Observed lines (cm^{-1}) in $2\nu_4$.

		$l=0$			$l=2$					
$J_{K'}$	p''	P	Q	R	^{P}P	^{P}Q	^{P}R	^{R}P	^{R}Q	^{R}R
0	s	3197.75			3224.00					
	a				24.63					
1_0	s				3205.06	3244.78				
	a	3176.35		3235.96	05.87	45.61				
1_1	s	78.72	3218.45[a]		17.36				3231.30	
	a	75.79	15.54		18.20			3192.22		3251.80
2_0	s	3161.31		3260.61	3187.13	3246.72	3286.48			
	a				88.24	47.77	87.52			
2_1	s	60.79	3220.38[a]	60.15[a]	99.43	59.04[a]		3173.60		3272.90
	a	57.59	17.12	56.89	3200.59	60.15[a]			3234.00	
2_2	s	58.88	18.45[a]		10.53			58.88[a]	18.45[a]	58.17
	a	56.01	15.54		11.69			59.60	19.13	58.88
3_0	s				3170.22	3249.56	3309.15			
	a	3140.51		3279.36	71.78	51.08	10.57			
3_1	s	43.39	3222.75[a]	82.36	82.55	61.92	21.49			
	a	39.83	19.17[a]	78.71	84.24	63.57	23.15[a]	3157.68		3296.50[a]
3_2	s	42.46	21.87	81.44	92.57	72.06		41.87	21.24	80.78
	a	38.69	18.10	77.70	94.92	74.32		42.95	22.22	81.79[a]
3_3	s	39.35	17.80		3203.75			25.90	05.31[a]	64.97
	a	35.95	15.37		05.31			26.52	05.87[a]	65.49
4_0	s	3126.87		3305.28	3154.37	3253.42				
	a				56.59	55.55				
4_1	s	26.25	3225.33[a]	04.72	66.76	65.84		3140.71		3319.16
	a	22.25	21.24	00.62	69.26	68.26	3347.63		3241.18	
4_2	s	3127.88	3227.00	3306.41	3177.77	3276.96[a]		3126.47	3225.52	3304.81
	a	23.12	22.22[a]	01.56	79.96	79.13[a]		27.32	26.35	05.66
4_3	s	24.18	23.37	02.83	88.59	87.88		09.40	08.60	3288.02
	a	19.56	18.72	3298.14	91.21	90.43		10.85	09.90	89.32
4_4	s	20.02	19.26		95.08			3092.83	3192.02	71.46
	a	15.74	14.97		96.35			93.38	92.53	71.96
5_0	s				3139.51	3258.28	3357.41[a]			
	a	3105.91		3323.52	42.06	60.73				
5_1	s	09.86		27.62	52.21	70.90	70.04		3244.63	
	a	04.90		22.55	54.82	73.49	72.57	3128.27		3345.86
5_2	s	12.42	3231.14	30.28[a]	62.93	81.79	80.95	09.86	28.53	27.63
	a	08.53	27.24	26.33	63.69	82.36	81.44	11.19	29.83	28.91
5_3	s	10.28	29.11	28.24	72.42	91.37[a]		3095.00	13.73	12.85[a]
	a	04.32	23.11	22.24[a]	74.68	93.60		96.30	14.97[a]	14.08
5_4	s	06.37	25.33	24.58[a]	78.33	97.52[a]		77.83	3196.66	3295.80[a]
	a	00.22	19.13[a]	18.35	81.97	3301.50[a]		78.77	97.61	96.70[a]
5_5	s	3099.70	18.80		87.85			59.37	78.33	77.70
	a	95.27	14.32[a]		88.93			59.91	78.97	78.18
6_0	s	3092.83		3349.63	3125.83	3263.99				
	a				28.74	66.71	3385.48			
6_1	s	92.52		49.35	38.80	76.96[b]	95.75[b]	3112.02		3368.79
	a	87.70		44.36[a]	41.87	80.01[a]	98.80		3251.44	
6_2	s	3103.47	3241.66	60.40	49.58	87.88	3406.59[b]	3097.31	35.47	54.12
	a	3096.69	34.85[a]	53.51	54.53	92.82	11.48	99.70	37.82	56.41[a]
6_3	s	97.74	36.04	54.90	57.86	96.22	15.39[b]	81.08	19.26[a]	38.01
	a	90.33	28.59	47.36	61.55	99.99	18.87	82.44	20.60[a]	39.45[a]

TABLE III.—*Continued*

		$l=0$			$l=2$					
J_K'	p''	P	Q	R	^PP	^PQ	^PR	^RP	^RQ	^RR
6_4	s	3091.48	3230.00	3348.83[a]	3162.93	3301.56	3420.76	3063.85	3202.18	3321.07
	a	86.04	24.46	43.43[a]	63.69	02.24	21.27	65.35	03.62	22.35
6_5	s	86.18	24.93	43.96	73.09	12.05		45.48	3184.00	02.88
	a	80.65	19.26[a]	38.28	73.97	12.85[a]		46.51	84.96	03.81
6_6	s	79.60[a]	18.45		79.84				64.63	3283.70
	a	74.60[a]	13.45		81.74				65.12	84.15
7_4	s							3050.81	3208.51	3346.81
	a							52.96[a]	10.20[a]	48.48
7_5	s								3190.17	28.64
	a								91.21[a]	29.59
7_6	s								71.14	09.78
	a								72.11	10.68
7_7	s							2992.21	50.59	3289.46
	a								51.11	89.83
8_7	s							2980.38[a]	3158.11	3316.37
	a								59.34	17.67
8_8	s								36.22	3294.86
	a								36.55	95.12
9_7	s							2971.03	3167.82	3345.35
	a								68.94	46.43
9_8	s								45.06	22.91
	a								45.83	23.78
9_9	s								21.42	3299.79
	a								22.25[a]	3300.50
10_{10}	s								3106.76	3304.72
	a								07.40	05.45

[a] Observed lines with moderate blending.
[b] Observed lines with heavy blending.

observations in Table I. The agreement between these is satisfactory. The constants have been listed previously.[6] The energy levels as derived from the fundamental are completely consistent with those found in $\nu_3-\nu_2$.

A preliminary study of intensities also was made. At pressures of 2 mm Hg and below, used for optimum resolution, the line shapes result from combined Doppler and collision broadening, so that the intensities are a complicated function of the line strengths, and it is difficult to obtain a quantitative measure of either the strength or the collision width. At higher pressures (and shorter paths) where such measurements might be made, overlap problems would appear insuperable in this closely spaced spectrum. Hence we have not obtained more than a qualitative indication of the relative intensities. These appear consistent with the rigid-rotator line strengths, with perhaps some enhancement of the lines of high-K and high-J in the ^RP branch over the corresponding lines in the ^PP branch. Comparison of ν_3 lines with resolved lines in both P and R branches of ν_1, shows that the two bands are of comparable strength, with ν_3 perhaps slightly stronger, in the ratio 6:5. This is not in agreement with the impression obtained from low-resolution spectra. In their quantitative study of band strengths, McKean and Schatz[8] assigned 60% of the total intensity in the region to ν_1. Our high resolution shows clearly, however, that few of the closely spaced ν_1 groups, including the Q branch, are free from overlap by the other more widely spaced bands, so that the contribution of ν_1 would naturally be overestimated in low-resolution studies, in which moreover all the absorption on the low-frequency side of the ν_1 Q branch was assigned to ν_1, whereas we shall show that $2\nu_4$ makes a considerable contribution in that region.

The Band ν_1

Our measurements have successfully resolved most of the K structure in the R and P branches of ν_1, although it is quite narrow, and have, moreover, shown several perturbations caused by the interactions with $2\nu_4$. These perturbations are least for the levels of lowest J.

[8] D. C. McKean and P. N. Schatz, J. Chem. Phys. **24**, 316 (1956).

In these the lines of high K fall at higher frequencies than those of low K, in both the P and R branches. The coefficient of the K^2 term in the Q branch, i.e., the effective constant $(C'-C''-B'+B'')$, from these lines of low J, is ~ 0.05 cm^{-1}. For higher J and low K the effective constant decreases, so that the P branch cannot be resolved at $J'=5$ and 6. At higher J, the constant changes sign, so that the higher K lines are at lower frequencies in the P branch, while in the R branch there is a low-frequency head at intermediate K. The cause of the sign reversal is the upward perturbation of the low-K levels by the k_{144} interaction.

The behavior just sketched is illustrated in Fig. 3 which shows the spectra at highest resolution for several of the J' groups. Figure 3 shows, also, the intrusion of ν_3 lines in the R branch and of $2\nu_4$ lines in the P branch. The doublet structure, as may be seen from the spectra and the line frequencies as listed in Table II, is fairly constant at 1.80 ± 0.05 for the lines with $K\sim J$ up to $J\sim 6$, decreases at low K for the lower J's, but increases rapidly at low K for $J'>7$. The $J'=9$ levels appear quite strongly perturbed, with inversion doubling up to 6 cm^{-1} for the lines of low K. The identification of $J'=10$ and higher is uncertain, because the perturbations become very large at the same time as the lines become weaker than those of the other bands. However, a few of the high K, $J'=10$ levels are sufficiently well established to be included in Table II, and are marked in the figures. For the $K=J$ levels, which form the strongest series in the Q-branch, an irregularity appears between $J=8$ and 9. This is the result of the second perturbation of ν_1 by the $2\nu_4^-$ levels.

The Band $2\nu_4$

The perturbations of ν_1 indicate that the Fermi resonance parameter $k_{144}/2(E_1-E_4^0)$ is moderately large at low J, and increases with increasing J; $2\nu_4^0$ should accordingly be moderately strong, even if the transition moment of the overtone is low. Its Q-branch is obviously in the neighborhood of 3220 cm^{-1}, where Fig. 1 shows a considerable concentration of lines. Analysis of the band has presented some difficulties, however, attributable to the combination of the Coriolis interaction with $2\nu_4^2$, the Fermi interaction with ν_1, and an irregular inversion pattern such as was encountered in ν_4 and $\nu_4+\nu_2$. A highly probable analysis of the lines up to $J'=6$ is given in Table III, and is shown in the figures. The $2\nu_4^0$ structure may be seen to best advantage in the upper panel of Fig. 1, covering the lowest frequencies considered in this paper, where other bands make the least relative contribution. It will be noted that the K structure is irregular, $K=0$ and 1 lying 5–10 cm^{-1} below $K=2$, that is, between $K=3$ and 4. It will be recalled that Eq. (2) predicted a maximum displacement of the E_4^0 levels at $K=(4g_{44}'+\delta-5.4/11.4)$; it thus appears that $4g_{44}'+\delta-5.4\sim 16$ cm^{-1}.

The origin of $2\nu_4^2$ should accordingly lie near 3240 cm^{-1}, and the most prominent lines of the band have been located. These are also given in Table III and are marked in the figures. The series of ${}^RR$ doublets with $J'=K$ is quite regular and strong; other levels are more or less perturbed, and show irregular inversions, but are believed to be established through the combination relations. Moreover, the course of the perturbations is roughly in agreement with the discussion in the introduction. The inversion doubling in $2\nu_4^2$ is also irregular, being least, in general, in the least-perturbed$^-$ levels; moreover, the average inversion of the $\pm$ levels at a given J, K is less than at the same J, K in $2\nu_4^0$.

In Fig. 4 the perturbation situation caused by the $(K, l \mid K+2, l+2)$ interactions is illustrated, for the $J=6$ levels. For simplicity, the E_1 levels are not considered. The energy levels are plotted as a function of K. The three dashed lines are parabolas giving calculated positions for the average of the inversion doublets, for $l=0$ and $l=\pm 2$. Higher-order terms in the rotational energy are ignored, and the rotational constants in the three states are taken as equal. The solid line segments pair the interacting levels, and are drawn with lengths roughly proportional to the matrix elements, $[42-K(K-1)][42-(K-1)(K-2)]$. The horizontal extension of the segments is thus a measure of the perturbation; the observed levels are seen to deviate from the curves in the expected direction and by roughly the expected amounts. The strong perturbation is between $l=0$ and $l=+2$ (E^0 and E^+) and the levels are so located that the perturbation on $l=0$ changes sign between $K=2$ and $K=3$. The levels of high-K are least perturbed, and those with $K=5$ and 6 for the R branch ($l=-2$) are totally unperturbed.

Molecular Constants for ν_1 and $2\nu_4$

Because of the described irregularities it has not been possible to derive a set of molecular constants for ν_1 and $2\nu_4$ that will reproduce all the observed levels. Numerous attempts have been made by using the average positions of the sets of four interacting states E_1, E_4^-, E_4^0, and E_4^+ to establish the average rotational constants, and then solving the resulting sets of Eqs. (1) with various trial values of k_{144} and q_4 in an effort to find the pair of values that would best fit all the data. The approximate magnitude of q_4 is established by the closest perturbations in which it is operative, those involving the pairs ${}^QQ({}^1J)$ and ${}^PQ({}^3J)$; ${}^QQ({}^2J)$ and ${}^PQ({}^4J)$; and ν_1 ${}^QQ({}^9J)$ and ${}^RQ({}^7J)$, where the superscript number is the upper-state K. The approximate magnitude of k_{144} is obtained by noting that the intersection of the $K=1$ states of ν_1 and $2\nu_4^0$ must be near $J=10$ or 11. However, within these rough limits, namely $2\sqrt{2}q_4=0.22\pm 0.05$ cm^{-1} and $k_{144}=38\pm 8$ cm^{-1}, there appears to be no set of constants that is successful

in reproducing the observed levels to within ± 1 cm^{-1}, even if fairly large terms $D_4{}^J - D_0{}^J$, etc., are introduced.

A representative situation, that involving the $J=6$ levels of $2\nu_4$, is illustrated by Fig. 5. The ordinates are energy differences between the observed levels and those calculated by a formula using only quadratic terms in the rotational energy, with the same constants for both inversion states and for $l=0$ and $l=\pm 2$. The abscissa is the K for $l=0$; the interacting levels for $l=\pm 2$ are slightly offset to the left and the right of unit K. The circles indicate the observed perturbed levels; the crosses denote the fictitious unperturbed levels that would yield the observed levels, by assuming a value for the interaction constant $2\sqrt{2}q_4=(0.05)^4$ cm^{-1}. It will be seen that the observed perturbations, which range up to 10 cm^{-1}, are reduced considerably with this value of the interaction constant, but there still remains a scatter about the symmetrical solid lines which might represent the unperturbed positions if the rotational constants were equal for the upper and lower levels, and for the $l=0$ and $l=2$ states, and if the inversion were a simple linear function of K decreasing at higher K.

Similar results were obtained at other values of J, and when the influence of ν_1 on the rotational constants of $\nu_4{}^0$ was considered. It appears, therefore, that although we have demonstrated the source and approximate magnitude of the principal interaction, namely, the second-order Coriolis effect between (K, l) and $(K+2, l+2)$, additional interactions have been neglected. Of these, probably the most important is that with $2\nu_2+\nu_4$. The lower inversion level of this state should fall about 45 cm^{-1} below $2\nu_4{}^0$, 70 cm^{-1} below $2\nu_4{}^2$, and would accordingly affect the upper inversion levels of $2\nu_4$, resulting both in an increased splitting at

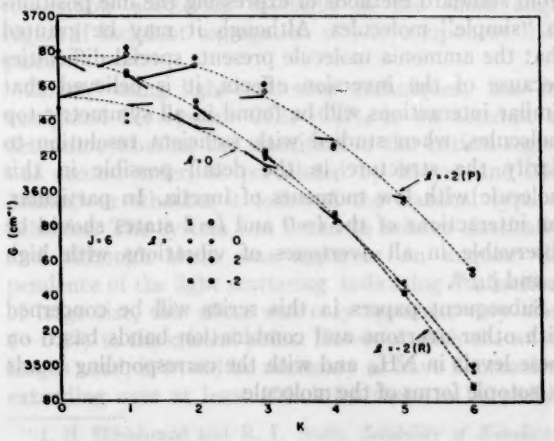

FIG. 4. $(K, l \mid K\pm 2, l\pm 2)$ perturbations affecting the $J=6$ energy levels of $2\nu_4$. Dashed lines are calculated energies with the perturbation and the inversion splitting ignored; solid line segments point to interacting pairs of levels and are of length proportional to the interaction; points are the resulting observed energy levels, displaced by the interaction and split by inversion.

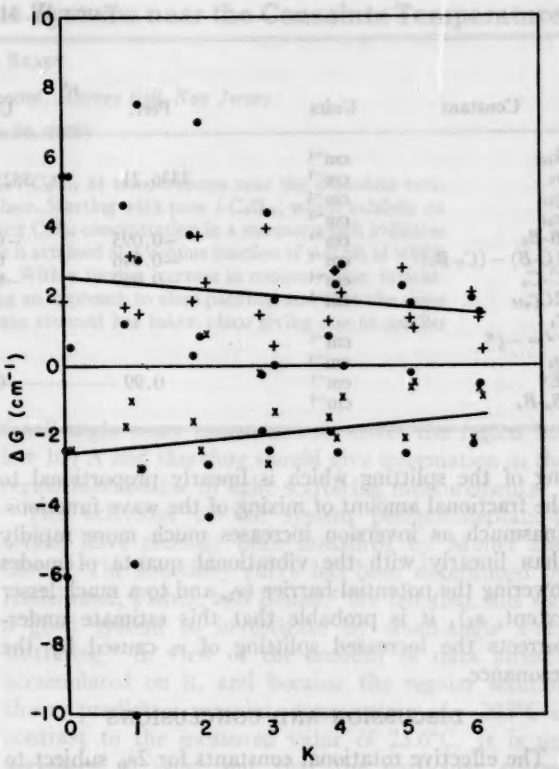

FIG. 5. Deviations of the $J=6$ energy levels of $2\nu_4$ from the calculated energies before (circles) and after (crosses) taking into account the $(K, l \mid K\pm 2, l\pm 2)$ perturbation.

higher (J, K), and in a larger effective B for $2\nu_4{}^0$ than for $2\nu_4{}^2$.

One of the many possible sets of constants that give a fair representation of the data is presented in Table IV. Its adequacy is limited by the simplifying assumptions made in its derivation, namely, that all the D's had their ground-state values, and that B_4' and C_4' had the same effective value in $2\nu_4{}^0$ and $2\nu_4{}^2$. However, this set does reproduce the principal trends in the data, and, in particular, yields the correct behavior for the principal perturbation, namely, the reversal of sign in the coefficient of K^2 for ν_1, and the displacement between $K=1$ and $K=2$ for $2\nu_4{}^0$. Two sets of constants are given, the unperturbed set being the one used in Eqs. (1), the perturbed set referring to the actual levels. The perturbed set cannot of course be used without large correction terms quartic in J and K, while the unperturbed set is uncertain because of the uncertainty in k_{144}.

The values of the inversion constants E and B_e-B_v are also uncertain, except in perturbed ν_1, because of the incompletely understood interaction of inversion with the vibration and rotation in $2\nu_4$. The numbers given for the unperturbed states were estimated on the assumption that the Fermi resonance produces a shar-

TABLE IV. Molecular constants.

Constant	Units	State ν^1 Pert.	ν^1 Unp.	$2\nu_4^0$ Pert.	$2\nu_4^0$ Unp.	$2\nu_4^2$
k_{144}	cm^{-1}		37.4			
ν_0	cm^{-1}	3336.21	3323.06	3216.71	3229.86	3240.45
g_{44}	cm^{-1}			5.93	2.65	
x_{44}	cm^{-1}			−12.08	−8.80	
$B-B_0$	cm^{-1}	−0.095	−0.177	0.423	0.505	
$(C-B)-(C_0-B_0)$	cm^{-1}	−0.046	0.140	−0.546	−0.640	
$C-C_0$	cm^{-1}	−0.049	−0.037	−0.123	−0.135	
$2C\zeta_{eff}$	cm^{-1}					5.46
ζ_4						−0.225
$\zeta^J=-\zeta^K$	cm^{-1}					−0.006
q_4	cm^{-1}					0.079
E^i	cm^{-1}	0.99	0.84	2.24	2.39	1.42
B_a-B_s	cm^{-1}				0.07	

ing of the splitting which is linearly proportional to the fractional amount of mixing of the wave functions. Inasmuch as inversion increases much more rapidly than linearly with the vibrational quanta of modes lowering the potential barrier (ν_2, and to a much lesser extent, ν_4), it is probable that this estimate undercorrects the increased splitting of ν_1 caused by the resonance.

DISCUSSION AND CONCLUSIONS

The effective rotational constants for $2\nu_4$, subject to the limitations of their derivation, are close to the values expected from the fundamental. The interaction constant q_4 is also not greatly different from that found in ν_4 and $\nu_4+\nu_2$. However, ζ_4 shows a considerable variation from its fundamental value, which again emphasizes that caution must be used in deriving the C constant by the ζ sum rule.

The normal behavior of ν_3 is in contrast to the perturbed behavior of ν_1 and ν_4. The reason for this lies in the low value of the Coriolis interaction parameter with its nearest neighbor $\zeta_{13}^{(x)}$. From the constants of the harmonic potential function derived in Eq. (2), we calculate $\zeta_{13}^{(x)}=0.0127$. It will be recalled that $\nu_1+\nu_2$ and $\nu_3+\nu_2$ showed evidence of this interaction, with $\zeta_{13}=0.017$, in the levels with $K(\nu_3)\geq 13$. The energy difference $\nu_1-\nu_3=107.2$ cm^{-1}, as compared with the 96.9 cm^{-1} in the combination with ν_2, so that the close perturbing effects of the interaction would not be apparent until $K\sim 16$. Moreover, the effective ζ_{13} in the fundamental is less than in the combination with ν_2, as evidenced by the absence of any observable (A_1, A_2) doubling ($q_3<10^{-4}$ cm^{-1}); whereas in the combination we observed $q_3=0.0049$ cm^{-1}.

The analysis just presented accounts for practically all the strong absorption lines at wave numbers greater than 3200 cm^{-1}. In addition, many of the weak lines can be accounted for as transitions in the difference bands, $(\nu_1+\nu_2)-\nu_2$ and $(\nu_3+\nu_2)-\nu_2$. The levels in these states are known,[4,6] and the present measurements agree to within 0.05 cm^{-1} of the predicted positions. The analysis is, however, unsatisfactory, for the reasons stated above, for ν_1 at $J'\geq 10$, and for most of the $2\nu_4$ levels with $J\geq 7$, so that a few lines above 3200 cm^{-1}, and a sizable proportion of the lines below 3180 cm^{-1} have not been assigned. Presumably some of the weaker lines in the low-frequency region may also belong to $2\nu_2+\nu_4$. It is hoped that further study may clarify the nature of the perturbations so that the remaining lines may be assigned.

In its present status, however, the results of this research again emphasize the omnipresent effect of rotation-vibration interactions in causing deviations from standard methods of expressing the line positions in "simple" molecules. Although it may be granted that the ammonia molecule presents special difficulties because of the inversion effects, it is believed that similar interactions will be found in all symmetric-top molecules, when studied with sufficient resolution to clarify the structure in the detail possible in this molecule with low moments of inertia. In particular, the interactions of the $l=0$ and $l=2$ states should be observable in all overtones of vibrations with high ζ_i and $\zeta_{ij}^{(x)}$.

Subsequent papers in this series will be concerned with other overtone and combination bands based on these levels in NH_3, and with the corresponding bands in isotopic forms of the molecule.

Cluster Formation in Perfluoroheptane-*i*-Octane Systems near the Consolute Temperature

GEORGE W. BRADY

Bell Telephone Laboratories, Incorporated, Murray Hill, New Jersey

(Received June 26, 1959)

Small-angle x-ray measurements on the system C_7F_{16}-*i*-C_8H_{18} at temperatures near the consolute temperature show that a large degree of clustering takes place. Starting with pure *i*-C_8H_{18}, which exhibits no scattering, the scattered intensity increases with increasing C_7F_{16} concentration in a manner which indicates that the clusters are increasing in size. The maximum size is attained at a volume fraction of ~0.50, at which point the clusters are made up of ~140 C_7F_{16} molecules. With a further increase in concentration, interaction peaks first appear in the intensity curves, indicating an approach to close packing, and then the slope of the curves begins to decrease, indicating that a phase reversal has taken place giving rise to smaller clusters of hydrocarbon in perfluorocarbon.

THE success of the regular solution theory[1] in describing the properties of nonpolar nonelectrolytes has stimulated a great amount of research in this field. As the work proceeded it became evident that some systems did not conform, even qualitatively, to the theory. This was particularly true in the case of mixtures of fluorocarbons and hydrocarbons.[2,3] A basic tenet of the theory is that the excess free energy of a regular solution depends primarily on the difference between the cohesive energy densities of the two components. In the fluorocarbon-hydrocarbon systems this difference is very small, yet the measured departures from ideality are very great.

Our attention was engaged by these systems, because we were interested in studying solutions near the critical point, and we suspected that the anomalies present in these solutions were caused by clustering. From an x-ray viewpoint, these systems are appealing because of the difference in electron density of the two components and the reasonably low absorption coefficients, both of which it was hoped would promote a measurable scattering intensity in the small angle region if incipient segregation of one component took place.

Zimm,[4] using light-scattering techniques, has investigated the system CCl_4—C_7F_{14} in an attempt to determine whether the transition in the critical region was second order, as postulated by Mayer and McMillan,[5] or whether it followed the classical type of behavior. The system was found to behave classically, and although there was apparent an angular dependence of the light scattering, indicating fluctuations of large size, this effect was only apparent very close (~0.1°) to the critical point. However, with the wavelength used, it would be necessary to have fluctuations extending over at least 100 A for them to be visible. Small-angle x-ray measurements cover the region below 100 A and therefore should give information in the region inaccessible to light scattering measurements.

The activities of the system perfluoroheptane-*i*-octane have recently been measured by Muller and Lewis.[6] The solubility curve has been determined by Hildebrand, Fisher, and Benesi.[2] We felt that this was a good system to investigate by small-angle x-ray scattering,* in view of the amount of data already accumulated on it, and because the regular solution theory predicts a consolute temperature of −203°C in contrast to the measured value of 23.6°C. It is unnecessary to point out that the particular system chosen is not the important thing; what is important is to learn more about the critical region and to gain a more complete understanding of the nucleation process.

EXPERIMENTAL

The experiments were made in a Phillips Electronics Diffractometer, modified for small angle work. The modifications consisted first of replacing the standard 20-mil spacers in the Soller slit by 2-mil spacers. To avoid buckling of the 1-mil metal foils defining the slits, the spacers were made to such a height that only an opening of $\frac{1}{8}$ in. was left for the x-ray beam. The Soller slits at the detector were also modified. It was found necessary, however, to increase the width of each slit to 6 mils to obtain sufficient intensity. A beveled screw fitted with a knurled knob was mounted in the detector arm to allow some slight horizontal adjustment of the detecting slit system.

Secondly, a mounting was designed and positioned on the goniometer base, to allow for insertion of a second slit just before the sample, the latter being positioned at the axis of the goniometer. The mounting for the second slit was equipped with screw adjustments to allow translational movement of the slit in the vertical and horizontal directions, and rotation

[1] J. H. Hildebrand and R. L. Scott, *Solubility of Nonelectrolytes* (Reinhold Publishing Corporation, New York, 1950), third edition.
[2] Hildebrand, Fisher, and Benesi, J. Am. Chem. Soc. **72**, 4348 (1950).
[3] R. L. Scott, J. Phys. Chem. **62**, 136 (1958).
[4] B. H. Zimm, J. Phys. Chem. **54**, 1306 (1950).
[5] W. G. McMillan and J. E. Mayer, J. Chem. Phys. **13**, 276 (1945).
[6] C. R. Muller and J. E. Lewis, J. Chem. Phys. **26**, 286 (1957).
* It was subsequently brought to our attention that small-angle scattering had been observed by Brackett, Dunlap, and Biscoe, Bull. Am. Phys. Soc. **98**, 1210 (1955). The work was never published.

around the horizontal axis to permit lineup with the take-off angle of the first slit.

To insure an air-free path between sample and detector a 1-in. diam aluminum pipe was positioned between them. Slits $\frac{1}{2}$ by $\frac{1}{8}$ in. were machined in the discs which closed the ends of the pipe. Then (0.3-mil) polystyrene windows were cemented over the slits. A petcock was soldered onto the pipe, and to this was attached vacuum tubing which connected with a Hyvac pump.

The sample holders were made by machining out rectangular holes ($\frac{1}{8}\times\frac{1}{2}$ in.) in flat 1-in. square metal plates of varying thicknesses. The windows were made of the same material as the windows in the vacuum system. The windows were attached to the metal plate with Goodyear Pliobond cement and the whole baked overnight at 100°C.

Background corrections were determined by measuring the scattering from pure liquids with different absorption coefficients (H_2O, C_7F_{16}, C_8H_{18}) and with cells of different thicknesses. In this way backgrounds were determined for different values of μ, the absorption coefficient, and x, the cell thickness. From this a series of backgrounds for values of μx were determined. Since pure liquids do not scatter in the small angle region, the background is due essentially to scattering from the slits and any other parasitic type of scattering. The advantage of determining background corrections in this way is that it is then only necessary to measure μx for the solution under study, and then apply the appropriate correction for this value.

The experiments were done at 28.3°C. Readings were taken by scaling at intervals of 0.02° of arc. Each point was scaled for approximately 200″, and each scattering curve was determined from the mean of at least three measurements. Monochromatisation of the Cu radiation was achieved by using a scintillation counter in series with a Ni filter and a pulse height analyzer.

Slit corrections were calculated by modifying the procedure of Yudowitch[7] to make it applicable to the geometry described above. Essentially, the calculation involves the evaluation of

$$I=\int_{\epsilon_1}^{\epsilon_2}[\Phi^2(sR)/\Delta\epsilon]d\epsilon,$$

where ϵ_1 and ϵ_2 are the minimum and maximum angles of divergence of the incident beam, $\Delta\epsilon=\epsilon_2-\epsilon_1$, and $\Phi^2(sR)$ is the scattering function for the particle shape being investigated. The minimum angle ϵ_1 can be calculated from the expression $\epsilon_1=r-\alpha/L$; here L is the distance between sample and detector, $r=L\times(2\theta)$ where 2θ is the scattering angle, and $\alpha=(2L+l/2L)a$. In this expression l is the distance between the first and second slits, and $a=a_1=a_2$ is the width of the slits. In our geometry, we have the following dimensions:

$$a_1=a_2=0.20 \text{ mm}$$

$$l=100 \text{ mm}$$

$$L=200 \text{ mm}.$$

The evaluation of ϵ_2 is slightly more complicated because the virtual height b_2 of the second slit is defined by the divergence of the Soller slits. In addition, account has to be taken of the divergence of the receiving Soller slits. An easy way to do this is to calculate the height b_2 from the divergence of the primary Soller slit, determine the direction cosines of the line defining the maximum angle of scattering, then move this line upwards to a point determined by the divergence of the receiving slit, keeping the direction cosines constant. It is necessary to do this because the separation of the Soller slits in the detecting system, 0.15 mm (6 mils), is greater than the 0.05-mm (2 mils) separation of the divergence slit; also, the distance l is not the same as L. The calculations are fairly straightforward and lead to the following dimensions for the slits:

$$a_1=a_2=0.20$$

$$b_1=0.05$$

$$b_2=0.86.$$

When we take into account the receiving slit divergence, we find that the height b_2 must be increased to 3.8 mm. It is easily shown that a line passing through the point defined by this height and the width 0.20 mm, and parallel to the first defines a virtual slit system of the following dimensions:

$$a_1'=1.59 \text{ mm}$$

$$a_2=0.20 \text{ mm}$$

$$b_1=0.05 \text{ mm}$$

$$b_2'=3.8 \text{ mm}$$

$$l'=442 \text{ mm}$$

$$L=200 \text{ mm}.$$

The angle ϵ_2 may then be determined by substituting these values into the formula

$$\epsilon_2=[(r+\beta_a)^2+(\beta_b)^2]^{\frac{1}{2}}/L,$$

where

$$\beta_a=(a_2/2)+(a_1'+a_2)(L/2l')$$

[7] K. L. Yudowitch, J. Appl. Phys. **22**, 214 (1951).

and

$$\beta_b=(b_2'/2)+(b_1+b_2')(L/2l').$$

Figure 1 shows the effect of these corrections on some typical small angle scattering curves.

CALCULATIONS

For a system exhibiting inhomogeneity, such as a system of particles or clusters, the small angle scattering may be written as[8]

$$I=I_e\bar{N}F^2(s)[1-(v/v_0)] \quad (1)$$

if the particles exhibit spherical symmetry. In this expression I_e is the scattering due to one electron, $\bar{N}$ is the average number of particles in the irradiated volume V, F^2 is the structure factor for the inhomogeneity, $v_0=V/N$ is the average volume available to a particle, and v is defined by the expression

$$v=\int_0^\infty[1-P(r)](\sin sr/sr)4\pi r^2dr.$$

In this expression $s=[4\pi/\lambda]\sin\theta$, where θ is one-half the scattering angle. P may be defined from the condition that the probability of finding particles i and j in volumes dv_i and dv_j is

$$P(dv_idv_j/V^2).$$

The quantities v and P, which characterize the interactions between particles, are of primary importance thermodynamically. The volume v, the correlation volume, is a function of concentration, and for dilute systems is very small compared to v_0, in which case the scattered intensity is given by the first term in expression (1). The probability parameter P can be used to characterize the effects of impenetrability of particles, or to evaluate their intermolecular potential.

In the case where the particles are widely enough dispersed so that they may be considered as randomly distributed, that is when v/v_0 is very small, the scattering function F^2 determines the shape of the scattering curve. It can be written explicitly as

$$F^2=v'\rho^2\int_0^\infty\gamma_0(r)(\sin sr/sr)4\pi r^2dr, \quad (2)$$

where v' is the volume of the particle, ρ is the electron density, and $\gamma_0(r)$ is a characteristic correlation length for the particle.[9] The latter can be defined simply as the probability that two points at a distance r will both be in the particle, or alternatively may be defined as the average electron density at a distance r from points averaged over the entire volume.[10] We can use this expression to calculate the intensity patterns of different shapes of particles. For example, the sphere of radius R exhibits scattering defined by

$$F^2=v'^2\rho^2(9\pi/2)[J_{\frac{3}{2}}(sR)/(sR)^{\frac{3}{2}}]^2, \quad (3)$$

where J is the Bessel function. A cylinder of radius R and height $2H$ has the scattering function

$$F^2=n^2\int_0^{\pi/2}\frac{\sin^2(sH\cos\theta)}{s^2H^2\cos^2\theta}\times\frac{4J_1^2(sR\sin\theta)}{s^2R^2\sin^2\theta}\sin\theta d\theta, \quad (4)$$

where $n=v'\rho$ is the number of electrons per particle. Other shape functions have been calculated but these two will be the ones used in the discussions and are sufficient to show the general approach taken in studies of this sort. The spherical scattering function [Eq. (3)] has been tabulated.[8] The cylindrical scattering function [Eq. (4)] was programmed for the IBM 704 and calculated for values of R from 0 to 20 and axial ratios H/R of 1 to 10.

In general a system exhibiting small angle scattering will not consist of a uniform distribution of particle sizes or of a uniform fluctuation in electron density. The intensity pattern will thus be an average of the scattering from the assembly, suitably weighted to account for the R^6 dependence on particle radius. In principle it is possible to obtain this distribution from the measured intensity by using various transformation techniques.[10,11] In practice, however, the problem is complicated by the fact that slit errors introduce deviations into the analytic functions characteristic of

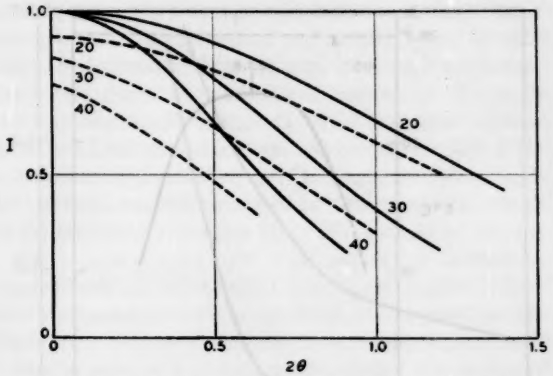

FIG. 1. Effect of slit correction on scattering curves. The full lines are the uncorrected ones. The Bragg angle 2θ is given in degrees of arc.

[8] A. Guinier and G. Fournet, *Small Angle Scattering of X-Rays* (John Wiley & Sons, Inc., New York, 1955). Translation by C. B. Walker.

[9] G. H. Vineyard, Phys. Rev. **74**, 1076 (1948).

[10] S. H. Bauer, J. Chem. Phys. **13**, 450, (1945).

[11] C. G. Shull and L. C. Roess, J. Appl. Phys. **18**, 295, 308 (1947).

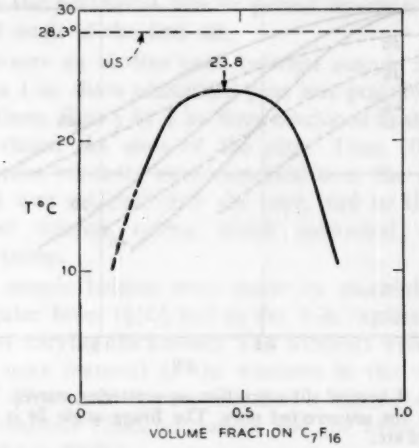

FIG. 2. Phase diagram of the C_7F_{16}-*i*-C_8H_{18} system.[2]

the particle shape. These can be corrected for, although the methods are involved, but in many cases it is questionable whether the procedure is worthwhile. A more general approach has been suggested by Debye and Bueche.[12] They define a correlation function γ, characteristic of the system, which is a measure of the extent of inhomogeneity. It may be calculated from the scattered intensity by a Fourier transformation. From γ one obtains a distance of heterogeneity L_c given by

$$L_c/2=\int_0^\infty \gamma(r)\,dr. \tag{5}$$

This relation is useful when there is no supplementary information which allows one to determine the cause of inhomogeneity. The correlation function measures all long-range fluctuations in electron density caused by strains, particles, clusters, etc., and also mirrors the interaction of these regions. We shall not use the correlation function in the interpretation of our results, but we discuss it here to give a better understanding of the origins of small angle scattering.

RESULTS AND DISCUSSION

The phase diagram for C_7F_{16}-*i*-C_8H_{18} is shown in Fig. 2. The dotted curve shows the region in which our experiments were made. In Fig. 3 the small angle scattering data is presented. In all the curves, the intensity has been divided by $xe^{-\mu x}$, to correct for absorption effects.

We will discuss first the qualitative aspects of the curves in Fig. 3. At a volume fraction of 0.122 perfluoroheptane, there is already evident a faint scattering, which decreases only slightly with increasing angle. At the next volume fraction 0.360, there is a large increase in both slope and intensity indicating an increase in size and number of particles. The next curve 0.460 shows an increase in intensity without any significant change in slope.

We first see the appearance of interference peaks at a volume function of 0.57 perfluoroheptane. There is a pronounced maximum at $2\theta=0.30°$. Although at this angle the correction for background is considerable, because of interference from the main beam, there is no question that the peak is present, although its shape and position may be somewhat uncertain. At the next concentration, however, we observe the peak clearly, since it has moved out from the main beam and now has its maximum at $2\theta=0.55°$. At the same time there appears to be a general decrease in slope in passing through this region.

Finally, as the fraction of perfluoroheptane is increased further to 0.748, the interference effects disappear, and a smooth curve is again obtained, with a decrease in slope. Beyond this concentration the absorption is so high that the scattering approaches background level.

We can interpret the behavior of these curves qualitatively, but rigorously, to mean that, starting at a low concentration, the perfluoroheptane molecules tend to segregate from the solution, producing clusters. These clusters increase in size and number as the concentration is increased. At the equimolar point in the phase diagram, Fig. 2, the number of clusters has increased to a point where their distribution can no longer be considered as random. In this region the correlation volume v of Eq. (1) is a significant fraction of the available volume v_0 and as we shall see, we can explain the peaks and the shift in peak position on this basis, that is, as an excluded volume effect. The decrease in slope of the curve beyond this region, indicating a decrease in size of clusters, leads to the obvious explanation that a phase reversal has taken place and that we are now measuring clusters of hydrocarbons in a continuous fluorocarbon phase. [From an x-ray

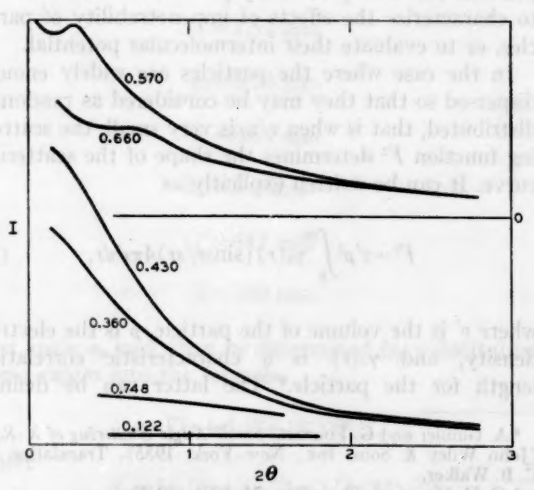

FIG. 3. The experimental scattering curves measured at various values of ϕ_2, the volume fraction of C_7F_{16}. 2θ is in degrees of arc.

[12] P. Debye and A. M. Bueche, J. Appl. Phys. **20**, 518 (1949).

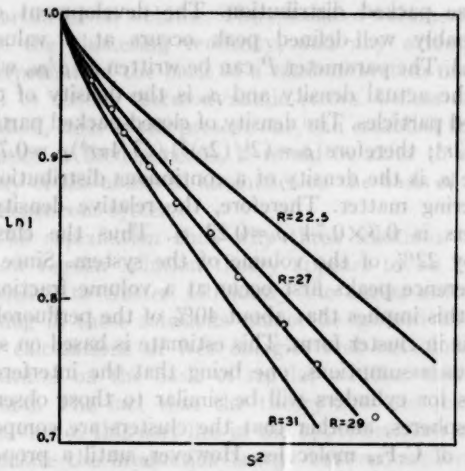

FIG. 4. Log I *vs* s^2 for various values of R, the radius of gyration. The circles are the experimental values for $\Phi_2=0.460$.

viewpoint it is the absolute value of $(\rho-\rho_0)$ which determines the scattering, so that an excess or a deficit in electron density produces the same scattering.] To determine quantitative values for the cluster sizes, we use Guinier's method. All small angle scattering curves can be represented, in the absence of interference effects, and at limiting small angle, by

$$F^2=n^2I=n^2\exp(-s^2R^2/3), \qquad (6)$$

where R is the radius of gyration. This simple relation, independent of particle shape, permits an easy determination of R from the slope of a plot of $\ln I$ against s^2. Logarithms of Eq. (6), calculated for various values of R and corrected for slit errors are shown in Fig. 4. The circles are the points of the 0.46 volume fraction curve. It is seen that a good fit is obtained over a considerable range for a value of $R=29$ A. At the larger s values the points begin to diverge upwards from the curve indicating that the Guinier approximation is invalid beyond this point, either because of the individual shape characteristics affecting the curve, or because of size distribution. The other concentrations also exhibit good $\ln I$ *vs* s^2 plots, except of course, the two curves which show interference peaks. The results are shown in Table I, where the R values are listed for each value of ϕ_2, the volume fraction of perfluoroheptane. Listed also are the corresponding values of

TABLE I.

ϕ_2	$T-T_c$	R
0.12	19	7.2
0.36	5	28.7
0.40	4	28.7
0.57	5	...
0.66	7	...
0.75	13	12.2

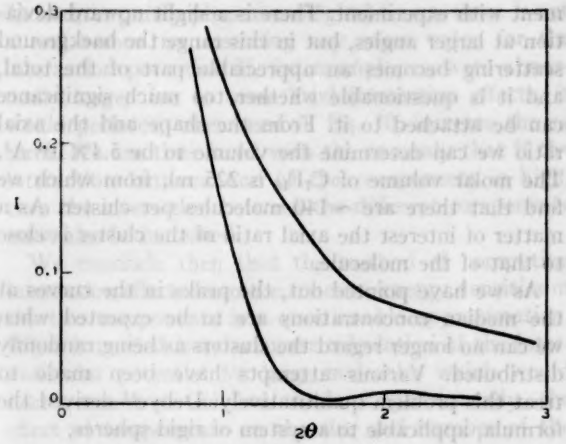

FIG. 5. A plot of experimental scattering *vs* sR, for a sphere, showing divergence of experimental curve from the scattering curve for this slope. The lower curve is the calculated one. 2θ is in degrees of arc.

$T-T_c$, the temperature above the consolute curve. The value of R for $\phi_2=0.12$ is of the same order as that calculated from dimensions of the molecule. Worthy of comment are the large temperature intervals at which the phenomenon is observed, indicating that the "transition" region is quite large.

The determination of the shape of the clusters involves a comparison of the complete scattering curves, Eq. (3) and (4), with experiment. Figure 5 shows such a comparison with the scattering curve of a sphere of radius of gyration of 29 A. (Slit corrections have been applied.) The upper curve is the experimental one. It is evident that there is no agreement between the curves, nor would a size distribution of spheres be of any help to the data, because the deviation between the curves becomes greater at larger angles.

Figure 6 shows the calculated scattering curve for a uniform cylinder of axial ratio 3.5 and radius of 13.5 A. The circles are the experimental points. It is seen that this scattering function is in excellent agree-

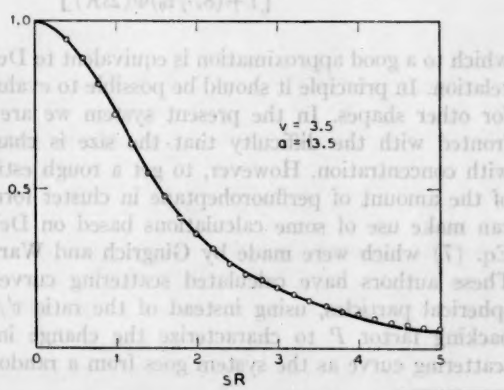

FIG. 6. A plot of experiment scattering *vs* sR for a cylinder, showing agreement of experimental curve with the calculated scattering curve. The points are the experimental values.

ment with experiment. There is a slight upward deviation at larger angles, but in this range the background scattering becomes an appreciable part of the total, and it is questionable whether too much significance can be attached to it. From the shape and the axial ratio we can determine the volume to be 5.4×10^4 A^3. The molar volume of C_7F_{16} is 225 ml, from which we find that there are $\sim$140 molecules per cluster. As a matter of interest the axial ratio of the cluster is close to that of the molecule.

As we have pointed out, the peaks in the curves at the median concentrations are to be expected when we can no longer regard the clusters as being randomly distributed. Various attempts have been made to treat this problem quantitatively. Debye[13] derived the formula, applicable to a system of rigid spheres;

$$I=I_eN\Phi^2(sR)[1-8(v'/v_0)\Phi(2sR)], \qquad (7)$$

where the $\Phi(sR)$ is the amplitude scattered by a sphere of radius R, v' is the volume of a particle and v_0 is the volume available to the particle. This equation considers no other interaction but that of impenetrability. A more general equation has been derived by Fournet,[14] valid for all shapes

$$I=I_eN\left[\langle F^2(s)\rangle+\langle F(s)^2\rangle\frac{\epsilon\beta(s)}{v_0(2\pi)^{-1}-\epsilon\beta(s)}\right], \qquad (8)$$

where $\epsilon\sim1$, F is the structure factor, and $\beta(s)$ is given by

$$s\beta(s)=[2/\sqrt{2}(\pi)^{\frac{1}{2}}]\int_0^\infty\left\{\exp\left[-\frac{\phi(r)}{kT}\right]-1\right\}r\sin srdr.$$

For spherical symmetry $\langle F^2\rangle=\bar{F}^2=\Phi^2$, and using a Lennard-Jones potential for $\phi(r)$, Fournet has shown that Eq. (8) reduces to

$$I=I_eN\Phi^2(sR)\left[\frac{1}{1+(8v'/v_0)\Phi(2sR)}\right], \qquad (9)$$

which to a good approximation is equivalent to Debye's relation. In principle it should be possible to evaluate β for other shapes. In the present system we are confronted with the difficulty that the size is changing with concentration. However, to get a rough estimate of the amount of perfluoroheptane in cluster form we can make use of some calculations based on Debye's Eq. (7) which were made by Gingrich and Warren.[15] These authors have calculated scattering curves for spherical particles, using instead of the ratio v'/v_0, a packing factor P to characterize the change in the scattering curve as the system goes from a random to a close packed distribution. The development of a reasonably well-defined peak occurs at a value of $P\sim0.3$. The parameter P can be written as ρ/ρ_0, where ρ is the actual density and ρ_0 is the density of close packed particles. The density of closed-packed particles is $2^{\frac{1}{2}}/2r^3$; therefore $\rho_0=(2^{\frac{1}{2}}/(2r)^3)/(3/4\pi r^3)\rho_c=0.74\ \rho_c$ where ρ_c is the density of a continuous distribution of scattering matter. Therefore, the relative density of clusters is $0.3\times0.74\ \rho_c=0.22\ \rho_c$. Thus the clusters occupy 22% of the volume of the system. Since the interference peaks first occur at a volume fraction of 0.57, this implies that about 40% of the perfluoroheptane is in cluster form. This estimate is based on some tenuous assumptions, one being that the interference effects for cylinders will be similar to those observed with spheres, another that the clusters are composed solely of C_7F_{16} molecules. However, until a proper β for this particle shape is worked out, we can accept it tentatively as a reasonable value for the cluster concentration.

The cylindrical shape of the clusters allows some speculation as to the mechanics of the phenomenon. If the attraction between perfluorocarbon molecules were greater than that between perfluorocarbon and hydrocarbon, then we would expect that the shape would tend to form a flattened cylinder (or ellipsoid) because this shape would make the interaction between fluorocarbon chains a maximum. But there is no *a priori* reason to expect an overwhelming attraction between the fluorocarbons. Indeed, as has been discussed by Scott,[3] we would actually expect a repulsive contribution to the intermolecular potential from the electronegative fluorine atoms in the chains. The assumption that this repulsive effect may well be important is supported by the tendency of the molecules to line up in such a way as to form long cylinders, where the sidewise interaction of the molecules is minimized. This leads to the conjecture that perhaps it is the greater attraction of the hydrocarbons for each other that causes the segregation. This idea was proposed by Simons and Dunlap[16] to explain the wide discrepancy between calculated and measured critical solution temperatures. Dunlap proposed that because of the small size of the H atoms in the hydrocarbon chain the packing would be much greater and therefore the attraction much stronger than for either the fluorocarbon-fluorocarbon or fluorocarbon-hydrocarbon interactions. Scott has criticized this theory mainly because the anomalies seem independent of shape of the components, but when we look at the problem from a local point of view, rather than at the molecule as a whole, there is still a large possibility that interpenetration effects may be present. It is obvious that many of the usual techniques when applied to these systems will not give a satisfactory picture of the actual state of affairs. As an example, we can cite attempts to measure

[13] P. Debye, J. Math. and Phys. **4**, 133 (1927).
[14] G. Fournet, Compt. rend. **228**, 1801 (1949).
[15] N. S. Gingrich and B. E. Warren, Phys. Rev. **46**, 248 (1934).
[16] J. H. Simons and R. D. Dunlap, J. Chem. Phys. **18**, 335 (1950).

a partial molar volume. The measured volume will reflect the clustering tendency, and any attempts to interpret it on the basis of a random system may well lead to serious thermodynamic errors. Unless another method, such as the present one, can establish that the solution is homogeneous, it would be safer to explain many of the observed anomalies on the basis of a nonhomogeneous system.

The explanation then why these solutions do not follow regular solution theory appears to lie in their tendency to cluster. Obviously the excess entropy of mixing in these solutions cannot be ignored and thus the calculations of free energies and consolute temperatures on the basis of regular solution theory are invalid. The fact that the theory does not predict a behavior of this sort lies in the approximation used to calculate the interaction energy between unlike molecules in the system. The assumption is made that the cohesive energy of unlike molecules is given by

$$c_{12}=(c_{11}c_{22})^{\frac{1}{2}}. \tag{10}$$

Scott[3] has discussed the factors entering into this assumption and has attempted to take account of polarity effects, ionization potential difference, and noncentral force fields. This discussion, although it does not offer any method for improving the approximation, does indicate the complexity of the situation. Indeed, in purely phenomenological terms, there is not a real reason for assuming any mean value for the interaction potential. If, for example, c_{11} were abnormally large, due to some local interaction effects, it would perforce, when used in Eq. 10, increase the c_{12} term. We are thus faced with the anomaly that if the interaction between one of the components is high, then the interaction between the different components must also be increased.

We conclude then that the method of computing interaction effects from the cohesive energy densities of the two components is a questionable approximation. What is needed is an accurate calculation of the intermolecular potential for large molecules which would take account of the local fields. Experimentally, the effect of temperature on the size and number of the clusters must be measured.

ACKNOWLEDGMENTS

We would like to acknowledge the assistance of Miss M. Hellmann, who prepared the solutions, and W. J. Romanow, who programmed the cylindrical scattering function for the IBM 704. The modification of the Phillips Diffractometer for small-angle work owes much to the mechanical work of O. Schaeffer and J. E. Carley. The work benefited by discussion with J. L. Lundberg.

Isotropic Proton Hyperfine Interaction in the Methyl Radical

JIRO HIGUCHI, *Laboratory of Physical Chemistry, Tokyo Institute of Technology, Ookayama, Meguro-ku, Tokyo, Japan*

AND

SHIGEYUKI AONO, *Chiba 1st High School, Chiba, Japan*

(Received June 22, 1959)

The isotropic hyperfine interactions of radicals or ions have been discussed from the viewpoint of the self-consistent field (SCF) molecular orbital theory. In these phenomena, the most important electron configurations concerned are those arising due to the one electron excitations from the double occupied orbital to the vacant orbital together with the lowest energy configuration. The proton hyperfine splitting of the methyl radical was calculated nonempirically by using the SCF-LCAO-MOs in adopting the first order perturbation. The agreement with the observed value is quite good when one uses MOs that include the 3*s* AO of carbon atom, while it is not so satisfactory in the case of the MOs without the 3*s* AO, because of the improvement of the form of the totally symmetric antibonding vacant orbital which gives the main contribution to the phenomena.

RECENTLY, isotropic proton hyperfine splitting (hfs) in the electron spin resonance (ESR) absorption spectra has theoretically been investigated by many authors,[1–4] and the many semiempirical calculations have been carried out with fruitful results.[3,5–9] Nevertheless nonempirical works are very few,[10,11] because of the difficulties in obtaining the energy integrals of the radical in question. Especially from the viewpoint of the molecular orbital (MO), such an investigation is of great importance in connection with the various mechanisms which are the origin of these phenomena. In the present paper, therefore, such a calculation is taken up for the methyl radical by adopting the MO treatment.

METHOD

For a strong magnetic field, the dipole-dipole interaction becomes zero on the average and only the Fermi contact interaction[12] contributes to the hfs, on the assumption of the rapid rotation of the free radical.[1] If the ground state electronic wave function (WF) Ψ_G is expanded by the WF's of configurations with the same symmetry as follows,

$$\Psi_G=\sum_\lambda a_\lambda \Psi_\lambda, \tag{1}$$

the proton hfs coupling constant is expressed as

$$a_N=(8\pi g\,|\,\beta\,|/3h)\,(\mu_N/I)\sum_\lambda\sum_\mu a_\lambda a_\mu \delta_{N\lambda\mu}, \tag{2}$$

where β is the Bohr magneton, μ_N is the nuclear magnetic moment, I is the nuclear spin angular momentum in units of $\hbar$, and

$$\delta_{N\lambda\mu}=\langle\Psi_\lambda\,|\,\sum_k \delta(\mathbf{r}_{kN})\,S_{kz}\,|\,\Psi_\mu\rangle/S_z. \tag{3}$$

Here, $\delta(\mathbf{r}_{kN})$ is the Dirac delta function of distance $\mathbf{r}_{kN}$ between electron k and nucleus N, and S_z is the total z component of the electron spin angular momentum. In the MO treatment, the expansion of the ground state WF in Eq. (1) corresponds to the procedure of the configuration interaction (CI), which is one of the most difficult processes in the calculation of the isotropic hfs of the free radical. In fact, this is the important problem in the calculation of electronic energy and can become very complicated according to the choice of the MO's. Accordingly, the self-consistent field (SCF) procedure has often been used, since the MOs so obtained are the best MO's and the energy of the state in question can, in general, be well approximated without CI. Furthermore, in this case the CI calculation is somewhat simplified because of the SCF–MO's being the solutions of the Hartree-Fock equation. In the present paper, therefore, the discussion will be carried out along this line.

Hereafter, the doubly occupied, singly occupied, and vacant orbitals are represented by $\phi_i(i<0)$, ϕ_0 and $\phi_j(j>0)$, respectively. The eigenfunction of radicals with one singly occupied orbital in the lowest energy configuration is expressed as

$$\Psi_0=\mathfrak{A}\phi_{-n}\phi_{-n}\cdots\phi_{i-1}\phi_{i-1}\phi_i\phi_i\phi_{i+1}\phi_{i+1}\cdots\phi_{-1}\phi_{-1}\phi_0 \times\alpha\beta\cdots\alpha\beta\alpha\beta\alpha\beta\cdots\alpha\beta\alpha, \tag{4}$$

where $\mathfrak{A}$ is the projection operator for antisymmetrization and renormalization, and the electronic energy is

$$E=2\sum_{i=-n}^{-1}(H:ii)+\sum_{i,k=-n}^{-1}[2(ii:kk)-(ik:ki)] +(H:00)+\sum_{i=-n}^{-1}[2(ii:00)-(i0:0i)], \tag{5}$$

where H is the electronic Hamiltonian for the core field.

[1] S. I. Weissman, J. Chem. Phys. **22,** 1378 (1954).
[2] B. Venkataraman and G. K. Fraenkel, J. Chem. Phys. **24,** 737 (1956).
[3] H. M. McConnell, J. Chem. Phys. **24,** 764 (1956).
[4] S. I. Weissman, J. Chem. Phys. **25,** 890 (1956).
[5] H. S. Jarrett, J. Chem. Phys. **25,** 1289 (1956).
[6] H. M. McConnell and D. B. Chesnut, J. Chem. Phys. **28,** 107 (1958).
[7] D. B. Chesnut, J. Chem. Phys. **29,** 43 (1958).
[8] A. D. McLachlan, Molecular Phys. **1,** 233 (1958).
[9] M. Karplus, J. Chem. Phys. **30,** 15 (1959).
[10] R. Bersohn, J. Chem. Phys. **24,** 1066 (1956).
[11] M. Krauss and J. F. Wehner, J. Chem. Phys. **29,** 1287 (1958).
[12] E. Fermi, Z. Physik **60,** 320 (1930).

As the SCF-MO's are satisfied by the condition of $\delta E=0$, subject to the orthonormality condition, so the following relations are also obtained:

$$(H:fi)+\sum_{k=-n}^{-1}[2(kk:fi)-(fk:ki)]$$
$$+\tfrac{1}{2}[2(00:fi)-(f0:0i)]=\epsilon_{ii}S_{fi}+\tfrac{1}{2}\epsilon_{i0}S_{f0}, \quad (6)$$

$$(H:f0)+\sum_{k=-n}^{-1}[2(kk:f0)-(fk:k0)]$$
$$=\sum_{k=-n}^{-1}\epsilon_{k0}S_{fk}+\epsilon_{00}S_{f0}, \quad (7)$$

and

$$(H:i0)+\sum_{k=-n}^{-1}[2(kk:i0)-(ik:k0)]+(i0:00)=0.^{13} \quad (8)$$

For the discussion of the CI and of the hfs coupling constant, it is convenient to classify the excited configurations as follows:

(1) configurations arising from excitation of one electron,

(2) configurations arising from excitation of two electrons, and

(3) configurations arising from excitation of more than two electrons.

In these, some WF's arising from these configurations do not mix strongly with that of the ground state by using the SCF-MO's. The contributions of these WF's can be estimated approximately by the first order perturbation coefficients

$$\lambda_i=H_{i0}/(H_{00}-H_{ii}), \quad (9)$$

where

$$H_{ij}=\langle\Psi_i\,|\,\mathfrak{H}\,|\,\Psi_j\rangle, \quad (10)$$

$\mathfrak{H}$ is the electronic Hamiltonian of the system.

The configurations (1) are generally of low energy, so it is of great importance to take care in dealing with them. Furthermore, they are divided into three classes arising from following excitations:

(1a) $\phi_i\rightarrow\phi_0$
(1b) $\phi_0\rightarrow\phi_j$
: configurations with one singly occupied MO

(1c) $\phi_i\rightarrow\phi_j$: configurations with three singly occupied MO's, and the corresponding WF's are as follows:

$$\Psi_{1a}=\mathfrak{A}\phi_{-n}\phi_{-n}\cdots\phi_{i-1}\phi_{i-1}\phi_{i+1}\phi_{i+1}\cdots\phi_{-1}\phi_{-1}\phi_0\phi_0\phi_i$$
$$\times\alpha\beta\cdots\alpha\beta\alpha\beta\cdots\alpha\beta\alpha\beta\cdots\alpha\beta\alpha\alpha, \quad (11)$$

$$\Psi_{1b}=\mathfrak{A}\phi_{-n}\phi_{-n}\cdots\phi_{i-1}\phi_{i-1}\phi_i\phi_i\phi_{i+1}\phi_{i+1}\cdots\phi_{-1}\phi_{-1}\phi_j$$
$$\times\alpha\beta\cdots\alpha\beta\alpha\beta\alpha\beta\cdots\alpha\beta\alpha\alpha, \quad (12)$$

$$\Psi_{1c}=(1/\sqrt{2})\mathfrak{A}\phi_{-n}\phi_{-n}\cdots\phi_{i-1}\phi_{i-1}\phi_{i+1}\phi_{i+1}\cdots\phi_{-1}\phi_{-1}\phi_i\phi_j\phi_0$$
$$\times\alpha\beta\cdots\alpha\beta\alpha\beta\cdots\alpha\beta(\alpha\beta\alpha-\beta\alpha\alpha), \quad (13)$$

and

$$\Psi_{1c'}=(1/6^{\frac{1}{2}})\mathfrak{A}\phi_{-n}\phi_{-n}\cdots\phi_{i-1}\phi_{i-1}\phi_{i+1}\phi_{i+1}\cdots\phi_{-1}\phi_{-1}\phi_i\phi_j\phi_0$$
$$\times\alpha\beta\cdots\alpha\beta\alpha\beta\cdots\alpha\beta(2\alpha\alpha\beta-\alpha\beta\alpha-\beta\alpha\alpha). \quad (14)$$

On referring to Eqs. (8), (7), and (6), one obtains the matrix elements of Eq. (10) as follows:

$$H_{1a0}=(H:i0)+\sum_{k=-n}^{-1}[2(i0:kk)-(ik:k0)]$$
$$+(i0:00)=0, \quad (15)$$

$$H_{1b0}=(H:0j)+\sum_{k=-n}^{-1}[2(0j:kk)-(0k:kj)]=0, \quad (16)$$

$$H_{1c0}=(H:ij)+\sum_{k=-n}^{-1}[2(ij:kk)-(ik:kj)]$$
$$+\tfrac{1}{2}[2(ij:00)-(i0:0j)]=0, \quad (17)$$

and

$$H_{1c'0}=(i0:0j). \quad (18)$$

It can be noted that the WF's arising from configurations (1) with the nonzero contributions to the ground state only $\Psi_{1c'}$'s, while, excluding the symmetry relation, they have appreciable values of δ_{N1i0} as follows:

$$\delta_{N1a0}=\phi_i(r_N)\phi_0(r_N), \quad (19)$$

$$\delta_{N1b0}=\phi_0(r_N)\phi_j(r_N), \quad (20)$$

$$\delta_{N1c0}=0, \quad (21)$$

and

$$\delta_{N1c'0}=(2/6^{\frac{1}{2}})\phi_i(r_N)\phi_j(r_N). \quad (22)$$

Configurations (2) are, in general, rather high in energy as compared with configurations (1). The considerable mixings with the ground state are generally given by Ψ_{2a}'s which arise from the excitation $(\phi_i,\phi_i)\rightarrow(\phi_j,\phi_j)$, because of the fairly large values of

$$H_{2a0}=(ij:ji). \quad (23)$$

For this hfs coupling constant, however, Ψ_{2a}'s give almost no contribution because

$$\delta_{N2a0}=0, \quad (24)$$

as in the case of the other WF's with configurations (2). On the other hand, it is possible to have some appreciable values of δ_{N2i2i} in the configurations (2), and so the contributions to the hfs should not be absolutely

[13] J. Higuchi, J. Chem. Phys. 26, 151 (1957).

TABLE I. SCF-LCAO-MOs for the ground state of the methyl radical.[a]

(Case I)

$1a_1' = (a_1'1s)$

$2a_1' = 0.56_2(a_1'2s) - 0.05_4(a_1'3s) + 0.41_2(a_1'h)$

$3a_1' = -0.31_7(a_1'2s) + 0.91_4(a_1'3s) + 0.19_1(a_1'h)$

$4a_1' = 1.73_3(a_1'2s) + 0.71_4(a_1'3s) - 1.53_8(a_1'h)$

$1e' = 0.60_1(e'2p) + 0.56_8(e'h)$

$2e' = 1.17_7(e'2p) - 1.39_7(e'h)$

$1a_2'' = (a_2''2p)$

(Case II)

$1a_1' = (a_1'1s)$

$2a_1' = 0.58_8(a_1'2s) + 0.38_5(a_1'h)$

$3a_1' = 1.56_8(a_1'2s) - 1.32_7(a_1'h)$

$1e' = 0.60_7(e'2p) + 0.56_1(e'h)$

$2e' = 1.17_3(e'2p) - 1.40_0(e'h)$

$1a_2'' = (a_2''2p)$

where

$a_1'h = 3^{-\frac{1}{2}}(h_1+h_2+h_3)$

$e_\pm'h = 3^{-\frac{1}{2}}[h_1+h_2\exp(\pm 2\pi i/3)+h_3\exp(\pm 4\pi i/3)]$

[a] $1s$, $2s$, $2p$, $3s$ and h_i are $1s$, $2s$, $2p$, $3s$ AO's of carbon and $1s$ of hydrogen i, respectively.

zero. In general, however, they are of high energy and some of them become $\delta_{N2i2i}=0$ by taking the symmetry of the radical into consideration. Accordingly, they are not discussed in detail in the present case.

For all the configurations (3), one can easily obtain the relations

$$H_{3i0}=0 \tag{25}$$

and

$$\delta_{N3i0}=0. \tag{26}$$

This indicates that their contributions to the ground state in general may be disregarded for the hfs as well as for the electronic energy, and they are excluded from the present discussion.

In view of these facts, one can deduce the fact that the most important configurations for the isotropic hyperfine interaction arise from one electron excitations ($1c'$) together with the lowest energy configuration (0). One obtains the following facts concerning the hfs in ESR spectra in regard to the electronic orbitals of radicals or ions. In the case of the singly occupied orbital ϕ_0 having an appreciable value at a magnetic nucleus, the coupling constant of this mechanism is mainly determined by the charge distribution of the unpaired orbital ϕ_0 only. This is certainly true when the symmetry of the ϕ_0 orbital is different from that of the vacant orbitals. Such an example can be seen in the hyperconjugation mechanism of the ethyl radical.[14] Even in the case of $\phi_0=0$ at a magnetic nucleus, it is possible to obtain the spectra which can be explained by the CI when some doubly occupied orbital ϕ_i and the vacant orbital ϕ_j with the same symmetry as that of ϕ_i give appreciable values at the nucleus. If the symmetry of the ϕ_i and the ϕ_j is different from that of the ϕ_0, one can generally obtain a somewhat small hfs coupling constant, and typical examples arising from the so-called $\sigma-\pi$ interaction have been well known in the methyl radical, the ethyl radical and many aromatic hydrocarbon radicals or ions. In the following section, the validity of the foregoing discussion will be illustrated practically from the result of the methyl radical.

RESULTS

The methyl radical is a most fundamental hydrocarbon radical and the ESR spectrum has been observed by Gordy and McCormick[15] and by Smaller and Matheson[14] as the hfs of 23–27 gauss. On the other hand, the electronic structures were carefully investigated by one of the authors[16] by using the SCF–LCAO–MO method[17] even to the effect on the $3s$ AO of carbon atom. Accordingly, this radical is one of the most suitable examples for investigating the isotropic hyperfine interaction of free radicals or ions from the MO consideration.

In the calculation, the spatial configuration was assumed as a regular triangle, which belongs to the symmetry group D_{3h}, and the internuclear distances between the carbon and the hydrogen were taken as 1.124 A as in the previous paper.[16] The carbon AO's used were the approximate SCF–AO's as follows[16]:

$$1s=(1s)_{5.7}$$

$$2s=-0.2260(1s)_{5.7}+1.0252(2s)_{1.625}$$

$$2p=0.5143(2p)_{2.00}+0.5561(2p)_{1.00}$$

$$3s=0.0677(1s)_{5.7}-0.3338(2s)_{1.625}+1.0517(3s)_{0.6374} \tag{27}$$

where (nl) is the nl simple Slater AO with orbital exponent δ, while the $1s$ AO of hydrogen used was

$$h=(1s)_{1.00}. \tag{28}$$

The SCF–LCAO–MO's of the methyl radical used were those obtained by one of the authors[16] and are given in Table I, in which the MO's with and without $3s$ AO are referred to as case I and case II, respectively. Thus, the calculation was carried out along the line of the previous section.

[14] B. Smaller and M. S. Matheson, J. Chem. Phys. **28**, 1169 (1958).
[15] W. Gordy and C. G. McCormick, J. Am. Chem. Soc. **78**, 3243 (1956).
[16] J. Higuchi, J. Chem. Phys. **28**, 527 (1958).
[17] C. C. J. Roothaan, Revs. Modern Phys. **23**, 69 (1951).

For simplicity, the configurations taken into account are the following ones, arising from one electron excitations together with the lowest energy configuration:

(0) $(1a_1')^2(2a_1')^2(1e')^4(1a_2'')$

(I) $(1a_1')^2(2a_1')^2(1e')^3(1a_2'')(2e')$

(II) $(1a_1')^2(2a_1')(1e')^4(1a_2'')(3a_1')$

(III) $(1a_1')^2(2a_1')(1e')^4(1a_2'')(4a_1'')$ (case I only).

By adopting the first-order perturbation, one obtains ground state WF as follows:

$$\Psi_G=\Psi_0+0.0087\Psi_{1e'(I)}-0.0218\Psi_{1e'(II)}+0.0933\Psi_{1e'(III)} \quad \text{(case I)}$$

and

$$\Psi_G=\Psi_0+0.0089\Psi_{1e'(I)}+0.0925\Psi_{1e'(II)} \quad \text{(case II)}$$

By using these WF's, the corresponding proton hfs coupling constants are calculated as -20.4 gauss for case I and -16.8 gauss for case II on the assumption of $\lambda_i^2 \ll 1$. The result obtained in case I is in good agreement with the observed value of 23–27 gauss but case II is not as satisfactory as the result discussed by Krauss and Wehner.[11] The contribution of the $\Psi_{1e'(I)}$ is fairly small, i.e., -2.5 gauss for case I and -2.6 gauss for case II; the small difference of 0.1 gauss is due to the slight change in form of $1e'$ MO between these cases. The contribution of the $\Psi_{1e'(II)}$ in case I is only -0.5 gauss and does not take an important role in the hfs, since the $3a_1'$ MO is $3s$-like and the LCAO–MO coefficient of the $1s$ AO's of hydrogen is very small. On the other hand, the repulsive excited configuration ($1c'$(III) for case I and $1c'$(II) for case II) has a substantial effect on the hfs; i.e., the contribution is -17.4 gauss for case I and -14.2 gauss for case II. Accordingly, one can recognize the better result in case I being due mainly to the improvement of the form of the antibonding a_1' MO by including the $3s$ AO of carbon. A similar example can be seen in the excited state $^1B_{1u}$ of the ethylene molecule in which the influence of the $3p\pi$ AO is fairly large.[18] In case I, the residual discrepancy from the observed value is still about 3–7 gauss and can be explained as being due mainly to the adoption of the first-order perturbation.* At any rate, it is interesting to note that the main contribution to the hfs is due to the configuration excited to the totally symmetric antibonding orbital in the methyl radical.

By varing the apex angle of the methyl radical, some change of the hfs is expected.[9] However, the structure of the methyl radical is nearly planar[19,20] and even if it were not the difference would be very small,[21] so the present result would not be changed greatly, although the radical is low pyramidal. In the present calculation, the CH bond distance used was 1.124 A of the CH radical; the distance of the methyl radical CH bond may be considered close to the 1.094 A of the methane molecule.[22] It is noted, however, that if the calculation is carried out at the CH bond distance of 1.094 A, using the SCF–LCAO–MO's used of the present work, the result is not changed more than 1%.

The first-order perturbation calculation has some uncertainty but may be acceptable for the simple aliphatic hydrocarbon radicals in consideration of the result of the CH radical by one of the authors,[23] since in that case the contribution of the excited configurations are fairly small. In the semiempirical treatment in π-electron radicals by McConnell and Chesnut,[6] the energy differences between the ground state and the excited states were taken as 5-15 ev on the average, but the average value assumed is rather smaller than the value of 20–30 ev which is expected from the present result.† Similarly, disregarding the contribution of the proton hfs from the AO's, other than the $1s$ AO of the corresponding hydrogen, the approximation is not so good since the contributions from the $2s$ and $2p\sigma$ AO of the carbon atom are 13.4% and 23.0%, respectively, of the $1s$ AO of the hydrogen. Accordingly, the success of their treatment may be due to the cancellation of these points, although the values treated are fairly small.

[18] J. Jacobs, Proc. Phys. Soc. (London) **A68**, 72 (1955).

* The calculation by Krauss and Wehner[11] showed the contribution of the one electron excitation configurations being about 50% of the hfs which may be due to the non-inclusion of the $3s$ AO.

[19] G. Herzberg and J. Shoosmith, Can. J. Phys. **34**, 523 (1956).

[20] Cole, Pritchard, Davidson, and McConnell, Molecular Phys. **1**, 406 (1958).

[21] Itoh, Ohno and Kotani, J. Phys. Soc. Japan **8**, 41 (1953).

[22] G. Herzberg, *Infrared and Raman Spectra of Polyatomic Molecules* (D. Van Nostrand Company, Inc., Princeton, New Jersey, 1945), p. 439.

[23] J. Higuchi, J. Chem. Phys. **22**, 1339 (1954). In the first order perturbation calculation of the CH radical, for example, the WF of the ground state $^2\Pi$ is as follows:

$$\Psi_2=\Psi(1^22^2\pi)$$
$$-0.0030\Psi(1^22^13\pi)-0.0372\Psi(1^22^13\pi)+0.0690\Psi(1^23^1\pi)$$
$$+0.0321\Psi(2^13^1\pi)-0.1589\Psi(1^2\pi^3)-0.0785\Psi(2^1\pi^3)$$
$$-0.0303\Psi(123^1\pi)-0.0380\Psi(12\pi^3)+0.0703\Psi'(12\pi^3),$$

where $\Psi(1^22^2\pi)$ means the WF with configuration of

$$K(\sigma)1\sigma^22\sigma^21\pi.$$

† For these radicals, such excitation energies have not yet been observed.

Paramagnetic Resonance Absorption in Neptunium Hexafluoride*

CLYDE A. HUTCHISON, JR., AND BERNARD WEINSTOCK

Enrico Fermi Institute for Nuclear Studies and Department of Chemistry, University of Chicago, Chicago, Illinois and Argonne National Laboratory, Lemont, Illinois

(Received May 26, 1959)

The paramagnetic resonance absorption of crystalline NpF_6 has been studied at 3 cm wavelength and at the boiling point of liquid He. The data were fitted to the spin Hamiltonian, $\mathcal{H}=\beta\mathbf{H}\cdot g\cdot\mathbf{S}+\mathbf{I}\cdot A\cdot\mathbf{S}$. The parameters are isotropic within the errors of the measurements, with $g=-0.604$ and $|A/hc|=0.1100$ cm^{-1}. These results are interpreted in terms of the configuration f^1 perturbed by spin-orbit coupling and an octahedral molecular potential. The relationships of the present results to optical data and measurements of magnetic susceptibility for the same substance are discussed. Hyperfine structure due to F is observed and is anisotropic.

INTRODUCTION

THE molecules UF_6, NpF_6, and PuF_6 have a structure in the gas phase in which the metal atom is at the body center of a regular octahedral arrangement of six F atoms. This fact has been deduced from investigations of infrared and Raman spectra[1–4] and from electron diffraction.[5,6] The metal to F distances in the molecules are found to be 1.996 A for UF_6, 1.981 A for NpF_6, and 1.971 A for PuF_6 from the electron diffraction data.[6] Crystalline UF_6, NpF_6, and PuF_6 have all been shown by x-ray diffraction[7–9] to be isostructural, to possess orthorhombic holohedry, and to crystallize in the space group $Pnma(D_{2h}^{16})$. The lattice dimensions are the same for all three within the estimated experimental errors of about 0.003 A. The positions of the fluorines in the crystals have not been precisely determined. The crystal structure is approximately a close packed arrangement of fluorines with heavy metal atoms in the interstices but there may be a slight distortion of the octahedra. The crystals may therefore be regarded simply as close packed arrangements of hexafluoride octahedra bound together by van der Waals forces. The crystals of all three compounds have relatively high vapor pressures,[10] consistent with this view.

The similarity of the magnitudes of the vibrational frequencies and the "lanthanide-like" contraction of the bond lengths of UF_6, NpF_6, and PuF_6 indicate that the extra electrons (one in NpF_6 and two in PuF_6) play a minor role in the bonding and are $5f$ electrons.

The one nonbonding electron in NpF_6 gives rise to a paramagnetic ground state as shown by measurements of the magnetic susceptibility in static fields.[11] This paper describes an investigation of paramagnetic resonance of the ground electronic state of crystalline NpF_6.

EXPERIMENTS

The samples of NpF_6 (Np^{237}) were contained in sealed quartz capsules. Two samples were used for the measurements of peak positions, one of which contained 488 mg of a 2.1 mole % solution of NpF_6 in UF_6 and the other 207 mg of 4 mole % NpF_6. Both capsules were placed in a He atmosphere for several hours before measurements were made during which time sufficient He diffused into the capsules to provide thermal contact at the liquid He boiling point. The 4% sample originally consisted of a single crystal that was prepared by distillation from a reservoir to the resonance bulb under a small temperature gradient and at a rate of about 14 mg per hour. This crystal, when cooled to the boiling point of nitrogen preparatory to sealing it off without attendant decomposition, cracked into 3 or 4 pieces. The resonance measurements were made upon these fragments which from visual inspection did not appear to subdivide further in the concomitant thermal cycling. The 2.1% sample was more finely divided. A third sample containing approximately 400 mg of 5.6% NpF_6 in UF_6 in a spherical bulb was used for the determination of the sign of g.

Many experiments at 1, 3, and 8 cm wavelength were made in an attempt to observe paramagnetic resonance in the gas phase at room temperature. A wide range of power levels was employed and pressures from 4 mm to 72 mm Hg were used. The same apparatus proved quite satisfactory with O_2 gas but none of these experiments gave a detectable paramagnetic resonance for NpF_6.

Recorder charts of the spectra obtained at the boiling point of liquid He from a finely divided crystalline solution of 3.0 mole percent NpF_6 in 1.83 g UF_6 are

* This work was supported by the U. S. Atomic Energy Commission.

[1] Bigeleisen, Mayer, Stevenson, and Turkevich, J. Chem. Phys. **16**, 442 (1948).

[2] Malm, Weinstock, and Claassen, J. Chem. Phys. **23**, 2192 (1955).

[3] Claassen, Weinstock, and Malm, J. Chem. Phys. **25**, 426 (1956).

[4] J. Gaunt, Trans. Faraday Soc. **49**, 1122 (1953).

[5] R. Glauber and V. Schomaker, Phys. Rev. **89**, 667 (1953).

[6] Schomaker, Kimura, Smith, and Weinstock (to be published).

[7] J. L. Hoard and J. D. Stroupe, quoted by J. J. Katz and E. Rabinowitch, *The Chemistry of Uranium*, (McGraw-Hill Book Company, Inc., New York, 1951), Part I, p. 439.

[8] W. H. Zachariasen, Paper 20.5, *The Transuranium Elements*, IV-14B, p. 1465, p. 1470, (McGraw-Hill Book Company, Inc., New York, 1949).

[9] Florin, Tannenbaum, and Lemons, J. Inorg. & Nuclear Chem. **2**, 368 (1956).

[10] Weinstock, Weaver, and Malm (to be published).

[11] B. Weinstock and J. G. Malm, J. Chem. Phys. **27**, 594 (1957).

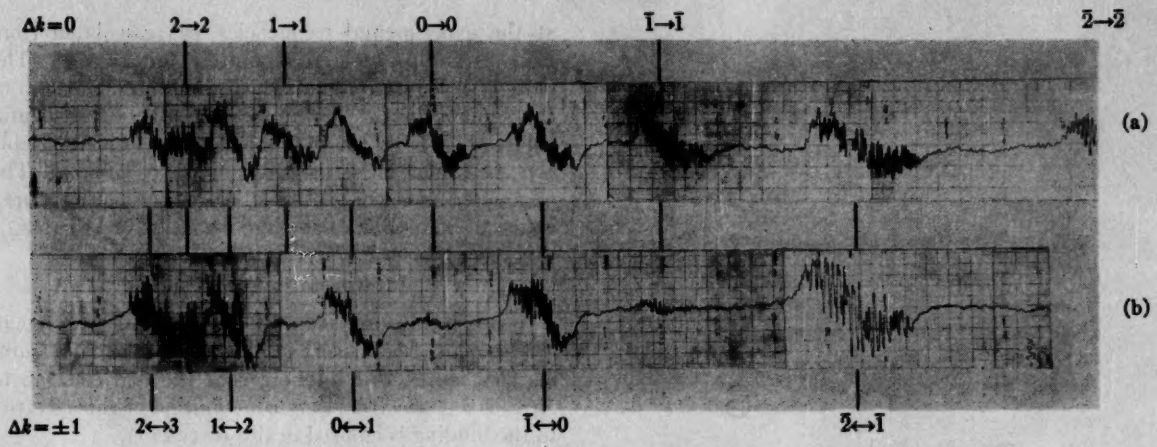

FIG. 1. Paramagnetic resonance spectrum of NpF_6.

shown in Fig. 1. A resonant cavity in the form of a section of rectangular waveguide operated in the TE_{101} mode was used. The chart (a) was obtained with H_{DC} parallel to the short edge of the guide. Thus H_{RF} was everywhere perpendicular to H_{DC}. Chart (b) was obtained with H_{DC} parallel to the longer dimension of the guide and therefore, since the sample occupied an appreciable fraction of the cavity volume, H_{RF} was in some places in the sample parallel to, and in others perpendicular to H_{DC}.

Two sets of measurements of peak positions were made, one on each of the two samples, at the boiling point of liquid He. The frequencies used were 8964 Mc sec^{-1} for the 4% sample and 9488 Mc sec^{-1} for the 2.1% sample. Field strengths were measured by superposing a proton resonance signal on the electron resonance signal at a point as near to the center of each Np^{237} hyperfine component as permitted by the very complicated F hyperfine structure.

The measurements on the 4% sample were made with H_{RF} parallel to H_{DC}. The measurements on the 2.1% sample were made with H_{RF} perpendicular to H_{DC} for the $\Delta k=\pm 1$ transitions and with H_{RF} parallel to H_{DC} for the $\Delta k=0$ transitions.

Additional measurements not used in fitting the spin Hamiltonian were made with the magnet in a variety of positions with respect to the sample and no anisotropies of the center positions of the Np^{237} hyperfine components could be observed. The F hyperfine structure was highly anisotropic.

The measured fields and frequencies for the various Np^{237} hyperfine lines are listed in Table I.

The sign of g for the paramagnetic resonance of NpF_6 was determined using the apparatus shown schematically in Fig. 2 which is similar to that employed by Galt *et al.*[12] The coupling iris, I, was centered at a point along the broad face of the wave guide at which the TE_{10} traveling wave is circularly polarized. The absorbers reduced the intensities of any reflections to small values. The cavity, C, was a right circular cylinder operated in the circularly polarized TE_{111} mode. The sample S was mounted on the base of the cavity where H_{RF} is most intense. Resonance was detected by means of the probe, P. Due to asymmetries of the sample the tuning screws, T, were required to secure equal intensities of the two $\pi/2$ out of phase components of H_{RF}. This apparatus was quite compact and well suited for immersion in the liquid He Dewar.

Knowledge of the direction of H_{DC} sufficed for a determination of the sign of g. Observations were made using an oscilloscope. H_{DC} was along the axis of the cylindrical cavity. The resonance signal from a sample of 1,1-diphenyl-2-picrylhydrazyl with H_{DC} directed from the cavity toward the guide was about 1000

TABLE I. Field strengths and frequencies of observed Np^{237} hyperfine lines.

Concentration	$k_1 \rightarrow k_2$[a]	ν Mc sec^{-1}	H gauss
4.%	2→2	8963.7	4376
	1→1		5801
	0→0		7833
	Ī→Ī		10 544
4.%	2→3		3904
	1→2		5076
	0→1		6775
	Ī→0		9138
	2̄→Ī		12 180
2.1%	2→2	9488.2	5192
	1→1		6676
	0→0		8734
	Ī→Ī		11 379
2.1%	2→3		4812
	1→2		6052
	0→1		7806
	Ī→0		10 208

[12] Galt, Yager, Merritt, Cetlin, and Dail, Phys. Rev. **100**, 748 (1955).

[a] The signs of the k values are chosen so as to make A and g in the spin Hamiltonian (1) have the same sign.

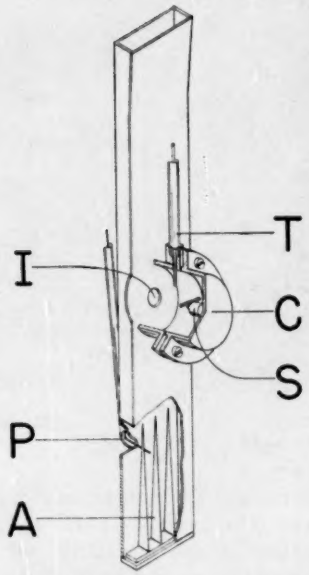

FIG. 2. Apparatus for the determination of the sign of g.

times as intense as when $\mathbf{H}_{DC}$ was directed from the guide toward the cavity. In an experiment in which both the hydrazyl and NpF_6 were placed in the cavity the intensity of the hydrazyl signal was altered by a factor of about 10 during the same reversal. The sign of g for NpF_6 was found to be negative. In the direction of $\mathbf{H}_{DC}$ in which the hydrazyl showed the more intense signal the NpF_6 signal was not observable at the H_2 boiling point and was approximately equal to noise at the He boiling point. In the direction in which hydrazyl showed the weaker signal the NpF_6 signal was 2 to 3 times noise at the H_2 boiling point and about 10 times noise at the He boiling point. At the boiling point of liquid He the NpF_6 signal increased with decreasing microwave power over the range which was studied.

DISCUSSION OF RESULTS

Fitting of the Spin Hamiltonian

The data were fitted to the spin Hamiltonian

$$\mathcal{H}=\beta\mathbf{H}\cdot g\cdot\mathbf{S}+\mathbf{I}\cdot A\cdot\mathbf{S} \qquad (1)$$

with g and A isotropic, $S=\frac{1}{2}$, and $I=\frac{5}{2}$.

The eigenvalues of this Hamiltonian are[13]

$$W=-(A/4)\pm\tfrac{1}{2}\{[kA+G]^2+A^2[(I+\tfrac{1}{2})^2-k^2]\}^{\frac{1}{2}}, \qquad (2)$$

where $G=g\beta H$ and $k=m_I+m_S$ takes values $I+\frac{1}{2}$, $I-\frac{1}{2}$, $\cdots$, $-(I+\frac{1}{2})$. It is understood that in this expression only the $+$ is used before $\{\ \}^{\frac{1}{2}}$ when $k=+(I+\frac{1}{2})$ and only the $-$ when $k=-(I+\frac{1}{2})$; otherwise eigenvalues exist for both the $+$ and the $-$.

For various assumed pairs of values of g and A/hc the set of values of $\mathbf{H}_{DC}$ at which resonance should be seen at the experimental frequencies was calculated from Eq. (2) for $\Delta k=0$ and separately for $\Delta k=\pm 1$. The pairs g, A/hc were found which minimized the sum of the squares of the deviations from the experimental values of $|\mathbf{H}|$ given in Table I, for specified sample and Δk value. These pairs are listed in Table II. The parameters given in Table II reproduce the measured values of $|\mathbf{H}|$ with an average deviation of 11 gauss.

[13] B. Bleaney, Phil. Mag. 7, xlii, 441 (1951).

Interpretation of Results

A simple interpretation of these results is given in this section. It is assumed, in view of the facts summarized in the introduction, that the odd electron in NpF_6 is a $5f$ electron. Any contribution of this electron to the binding is ignored in this discussion.

An f electron without spin when placed in an octahedral potential undergoes the splitting

$$f(7)\rightarrow\Gamma_2(1)+\Gamma_4(3)+\Gamma_5(3).$$

The degeneracies are listed in parentheses. The addition of spin gives the additional splittings

$$\Gamma_2\rightarrow\Gamma_7(2),$$

$$\Gamma_4\rightarrow\Gamma_6(2)+\Gamma_8'(4),$$

$$\Gamma_5\rightarrow\Gamma_7'(2)+\Gamma_8(4).$$

The relations given above show that the diagonalization of the energy of the octahedral potential plus the spin-orbit coupling requires only the solution of quadratic secular equations. We take as the two arbitrary parameters of our model (a) the ratio,

$$\xi=[E(\Gamma_4)-E(\Gamma_5)]/[E(\Gamma_5)-E(\Gamma_2)]$$

of the two molecular splittings in the absence of spin-orbit coupling and (b) the ratio,

$$\alpha=\zeta/[E(\Gamma_5)-E(\Gamma_2)]$$

of the spin-orbit coupling energy to the splitting produced by the octahedral potential.

In the case of f electrons both 4th and 6th degree terms in the octahedral potential must be considered.

TABLE II. Parameters in the spin Hamiltonian.

Sample	Δk	g	$\lvert A\rvert/hc$ cm^{-1}	$\lvert A\rvert/ghc$ cm^{-1}
4.%	0	−0.605	0.0672	0.1111
	±1	−0.609	0.0667	0.1095
2.1%	0	−0.605	0.0664	0.1098
	±1	−0.598	0.0655	0.1095
Average		−0.604	0.0665	0.1100
Average deviation from mean		±0.003	±0.0005	±0.0006

The energies in the absence of spin-orbit coupling are found to be

$$E(\Gamma_2) = -18a+4b,$$

$$E(\Gamma_5) = -8(a+b),$$

$$E(\Gamma_4) = 0,$$

where a and b are positive numbers representing the contributions to the energy of 4th and 6th degree terms respectively. We assume that Γ_4 orbitals are involved in the binding of the F's to the Np and that as a result $E(\Gamma_4)$ of our f electron is promoted to high values and will always be the highest of the three energies. On the other hand, $E(\Gamma_5)-E(\Gamma_2)$ may be either $+$ or $-$ depending on the relative magnitudes of a and b. We therefore let ξ range over $+$ and $-$ values. α is $+$ or $-$ according to whether ξ is $+$ or $-$.

Solution of the quadratic secular equations provides energy eigenvalues and eigenfunctions for all values of ξ and α. In Fig. 3 the results for the eigenvalues are summarized. In the left half of the figure, $E(\Gamma_5) > E(\Gamma_2)$, α is $+$, ξ is $+$; on the right half of the figure, $E(\Gamma_5) < E(\Gamma_2)$, α is $-$, ξ is $-$. On either side a Γ_7 state is lowest. Each curve of energy versus α is labeled with (a) a Γ denoting the transformation properties of the associated eigenstates and (b) a number (except for the cases of Γ_7 and Γ_7' levels) denoting the value of ξ, i.e., the relative spacings of the three molecular energy levels in the absence of spin-orbit coupling. The energy is given in units, $E(\Gamma_5)-E(\Gamma_2)$ in the extreme left one fourth and in units, $E(\Gamma_2)-E(\Gamma_5)$ in the extreme right one fourth of the figure. In the central one half of the figure the energy is given in units ζ. The Γ_7 and Γ_7' energies are, on this diagram, not influenced by the value of ξ. Since

(a) Γ_4 gives no Γ_7 state when it is decomposed under spin-orbit coupling,

(b) $E(\Gamma_7)$ or $E(\Gamma_7')$ is taken as zero, and

(c) $E(\Gamma_5)-E(\Gamma_2)$ is taken as the unit,

the height of $E(\Gamma_4)$ is of no consequence for $E(\Gamma_7)$ and $E(\Gamma_7')$.

By using the eigenstates found as described above, we may calculate the magnetic splittings of the ground state. When $E(\Gamma_5) > E(\Gamma_2)$ we have

$$g = 2\langle \Gamma_{7+} \mid L_z+2S_z \mid \Gamma_{7+} \rangle = 2\{A_n^2+4(\tfrac{1}{3})^{\frac{1}{2}}A_nB_n\}$$

where

$$\mid \Gamma_{7+} \rangle = \{(\tfrac{1}{2})^{\frac{1}{2}}A_n+(\tfrac{1}{6})^{\frac{1}{2}}B_n\} \mid 2+\rangle+\{-(\tfrac{1}{2})^{\frac{1}{2}}A_n + (\tfrac{1}{6})^{\frac{1}{2}}B_n\} \mid \bar{2}+\rangle+B_n\{\tfrac{1}{2} \mid 3-\rangle-(\tfrac{5}{12})^{\frac{1}{2}} \mid \bar{1}-\rangle\}$$

in terms of basic states described by

$$l_z = 3, 2, \cdots, \bar{3}; \; s_z = +, -,$$

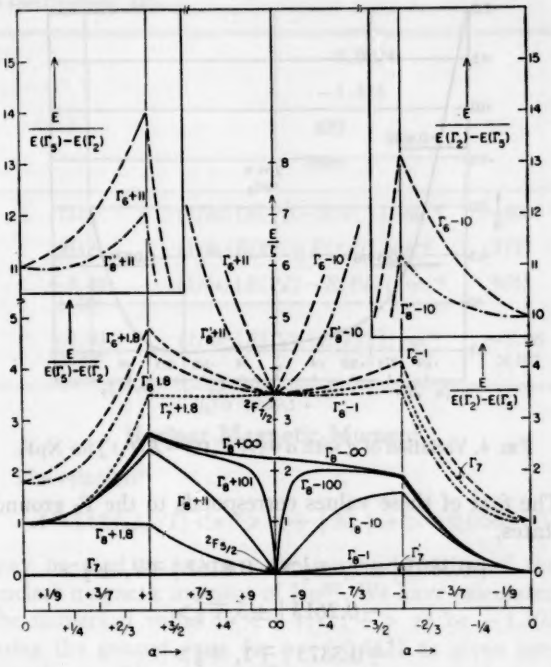

FIG. 3. Energy level diagram for NpF_6.

In this equation

$$A_n = A/\{A^2+B^2\}^{\frac{1}{2}};$$

$$B_n = B/\{A^2+B^2\}^{\frac{1}{2}};$$

$$A = 1-\tfrac{1}{2}\alpha+\{1-\alpha+\tfrac{49}{4}\alpha^2\}^{\frac{1}{2}};$$

$$B = -2\sqrt{3}\alpha.$$

When $E(\Gamma_2) > E(\Gamma_5)$ we have

$$g = 2\langle \Gamma_{7+}' \mid L_z+2S_z \mid \Gamma_{7+}' \rangle = 2\{B_n^2-4(\tfrac{1}{3})^{\frac{1}{2}}A_nB_n\}$$

where

$$\mid \Gamma_{7+}' \rangle = \{(\tfrac{1}{6})^{\frac{1}{2}}A_n-(\tfrac{1}{2})^{\frac{1}{2}}B_n\} \mid 2+\rangle+\{(\tfrac{1}{6})^{\frac{1}{2}}A_n + (\tfrac{1}{2})^{\frac{1}{2}}B_n\} \mid \bar{2}+\rangle+A_n\{\tfrac{1}{2} \mid 3-\rangle-(\tfrac{5}{12})^{\frac{1}{2}} \mid \bar{1}-\rangle\}.$$

The variation of g with α is shown in Fig. 4. In the left half of the figure, $E(\Gamma_5) > E(\Gamma_2)$ and α is $+$. In the right half of the figure, $E(\Gamma_5) < E(\Gamma_2)$ and α is $-$. The g which is given in this figure is that for the ground doublet Γ_7 or Γ_7' only, assuming no mixing with higher states by the magnetic field.

For $|g| = 0.604$ we find three possible values for α, the ratio of the spin-orbit coupling to the molecular splitting, namely,

$$\alpha = +0.1682, \quad +0.4416 \quad \text{or} \quad -0.0874.$$

For $g = -0.604$ as found in our measurements we have only the two possibilities.

$$\alpha = +0.4416 \quad \text{or} \quad -0.0874.$$

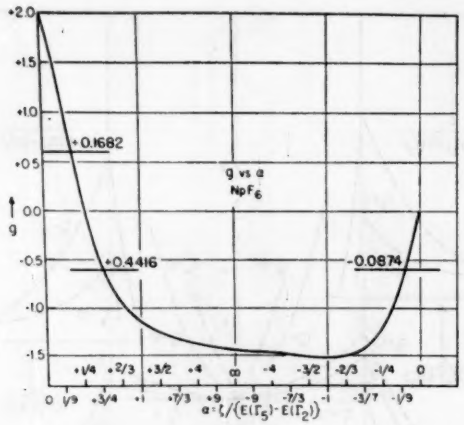

FIG. 4. Variation of g with $\alpha=\zeta/[E(\Gamma_6)-E(\Gamma_2)]$ for NpF_6.

The first of these values corresponds to the Γ_7 ground states,

$$+0.3895\,|\,\pm 2,\pm\tfrac{1}{2}\rangle-0.8162\,|\,\mp 2,\pm\tfrac{1}{2}\rangle$$
$$-0.2613\,|\,\pm 3,\mp\tfrac{1}{2}\rangle$$
$$+0.3373\,|\,\mp 1,\mp\tfrac{1}{2}\rangle.$$

Optical Absorptions

The optical electronic absorptions have been investigated by Fred.[14] His interpretation of the observed transitions using the observed vibrational frequencies as given by Malm, Weinstock, and Claassen,[2] leads to the assumption of two electronic transitions, one at 7711 cm^{-1} and one at 9515 cm^{-1}. He observes no absorption at smaller wave number values.

We consider first the case in which we take $\alpha=+0.4416$. We then assume

$$9515\ \text{cm}^{-1}=(1/hc)\{E(\Gamma_7')-E(\Gamma_7)\}.$$

This energy level spacing is independent of the value of ξ. If we now set

$$\xi=3.173=[E(\Gamma_4)-E(\Gamma_5)]/[E(\Gamma_5)-E(\Gamma_2)]$$

we find that

$$(1/hc)\{E(\Gamma_8)-E(\Gamma_7)\}=7711\ \text{cm}^{-1}.$$

We thus fit these two observed absorptions to the transitions from the ground state to the first and second excited states at $\xi=+3.173$. Two other absorptions should also be found corresponding to transitions to the Γ_8' and Γ_6 states. For the value of ξ required to obtain the fit described above we get

$$(1/hc)\{E(\Gamma_8')-E(\Gamma_7)\}\cong 2.49\times 10^4\ \text{cm}^{-1},$$
$$(1/hc)\{E(\Gamma_6)-E(\Gamma_7)\}\cong 2.93\times 10^4\ \text{cm}^{-1}.$$

Other fits using the value $+0.4416$ for α are impossible.

[14] M. Fred (personal communication); G. L. Goodman and M. Fred, J. Chem. Phys. **30**, 849 (1959).

If we fit the number 7711 to the transition $\Gamma_7'\rightarrow\Gamma_7$ then both $E(\Gamma_8')-E(\Gamma_7)$ and $E(\Gamma_6)-E(\Gamma_7)$ are considerably greater than 9515 for all $\xi>0.5$. Also one cannot fit the numbers 7711 and 9515 to the transitions $\Gamma_8'\rightarrow\Gamma_7$ and $\Gamma_6\rightarrow\Gamma_7$. This exhausts the possibilities.

With $\alpha=+0.4416$ and

$$(1/hc)\{E(\Gamma_7')-E(\Gamma_7)\}=9515\ \text{cm}^{-1}$$

we find from the ratios

$$[E(\Gamma_7')-E(\Gamma_7)]/[E(\Gamma_6)-E(\Gamma_2)]$$

plotted in Fig. 3 that $(1/hc)\{E(\Gamma_5)-E(\Gamma_2)\}=5542$ cm^{-1} and hence $(1/hc)\zeta=2447$ cm^{-1}.

Turning to the other possible value of α, namely, $\alpha=-0.0874$ we find, in a similar manner to that described just above, that the only possible fit to the spectroscopic data with the Γ_4 state highest in energy is one in which the experimental value 7711 cm^{-1} is associated with the $\Gamma_7'\rightarrow\Gamma_7$ transition and 9515 cm^{-1} with the $\Gamma_7'\rightarrow\Gamma_8'$ transition. The latter fit is accomplished by making

$$\xi=-1.324.$$

We then find for the two additional transitions the values

$$(1/hc)\{E(\Gamma_8)-E(\Gamma_7')\}\cong 500\ \text{cm}^{-1},$$
$$(1/hc)\{E(\Gamma_6)-E(\Gamma_7')\}\cong 10\,790\ \text{cm}^{-1}.$$

With $\alpha=-0.0876$ and $(1/hc)\{E(\Gamma_7)-E(\Gamma_7')\}=7711$ cm^{-1} we find from the ratios,

$$[E(\Gamma_7)-E(\Gamma_7')]/[E(\Gamma_5)-E(\Gamma_2)]$$

plotted in Fig. 3 that $(1/hc)\{E(\Gamma_2)-E(\Gamma_5)]=7096$ cm^{-1} and $(1/hc)\zeta=620$ cm^{-1}. These two fits of the spectroscopic data are summarized in Table III.

The fit using $\alpha=+0.4416$ leads to $\zeta/hc\cong 2450$ cm^{-1}. This is relatively high compared with the value 1300 cm^{-1} for ζ published by Eisenstein and Pryce[15] but is a much more reasonable value than that required by $\alpha=-0.0876$. Experimental information on the values of ζ for U and Pu has been given in previous papers.[16-17]

Magnetic Susceptibilities

The magnetic susceptibility of pure NpF_6, undiluted by UF_6, has been measured by Weinstock and Malm[11] and is given by the expression,

$$\chi_M=\text{molar susceptibility}=(0.0362/T)+321\times 10^{-6}$$
$$\text{cm}^3\ \text{mole}^{-1}.$$

[15] J. C. Eisenstein and M. H. L. Pryce, Proc. Roy. Soc. (London) **A229**, 29 (1955).

[16] C. A. Hutchison, Jr., and G. A. Candela, J. Chem. Phys. **27**, 707 (1957).

[17] Candela, Hutchison, and Lewis, J. Chem. Phys. **30**, 246 (1959).

TABLE III. Adjustment to spectroscopic data.

$\alpha=\zeta/[E(\Gamma_5)-E(\Gamma_2)]$	$+0.4416$		-0.0874
$\xi=[E(\Gamma_4)-E(\Gamma_5)]/[E(\Gamma_5)-E(\Gamma_2)]$	$+3.173$		-1.324
ζ/hc, cm^{-1}	2447		620
$(1/hc)\{E(\Gamma_5)-E(\Gamma_2)\}$, cm^{-1}	5542		7096
$(1/hc)\{E(\Gamma_5)-E(\Gamma_7)\}$, cm^{-1}	7711	$(1/hc)\{E(\Gamma_5)-E(\Gamma_7')\}$, cm^{-1}	~ 500
$(1/hc)\{E(\Gamma_7')-E(\Gamma_7)\}$, cm^{-1}	9515	$(1/hc\{E(\Gamma_7)-E(\Gamma_7')\}$, cm^{-1}	7711
$(1/hc)\{E(\Gamma_8')-E(\Gamma_7)\}$, cm^{-1}	$\sim 2.49\times 10^4$	$(1/hc)\{E(\Gamma_8')-E(\Gamma_7')\}$, cm^{-1}	9515
$(1/hc)\{E(\Gamma_6)-E(\Gamma_7)\}$, cm^{-1}	$\sim 2.93\times 10^4$	$(1/hc)\{E(\Gamma_6)-E(\Gamma_7')\}$, cm^{-1}	$\sim 1.08\times 10^4$

Using the relationship

$$0.0362/T=N\beta^2[g^2S(S+1)/3kT]; \qquad S=\tfrac{1}{2},$$

we obtain $g=0.621$. The measured value of $|g|$ for the present experiments is 0.604.

We may calculate for a set of values of ξ the values of

$$\Sigma=2(N\beta^2/hc)\sum_i |\langle\Gamma_i|L_z+2S_z|\Gamma_7\rangle|^2 \cdot\{[E(\Gamma_5)-E(\Gamma_2)]/[E(\Gamma_i)-E(\Gamma_7)]\}$$

from the states and energy levels, obtained as described previously, for the cases $\alpha=+0.4416$ and $\alpha=-0.0874$. Having done this we may interpolate the values of Σ for $\alpha=+0.4416$, $\xi=+3.173$ and for $\alpha=-0.0874$, $\xi=-1.324$. We find $\Sigma=0.286$ in the first case and $\Sigma=0.615$ in the second case. From the relation

$$\chi_M=\Sigma/[E(\Gamma_5)-E(\Gamma_2)]$$

and the values of $E(\Gamma_5)-E(\Gamma_2)$ given previously, we find for the temperature independent susceptibility the value 154.7×10^{-6} cm^3 mole^{-1} when $\alpha=+0.4416$ and 260×10^{-6} cm^3 mole^{-1} when $\alpha=-0.0874$. The experimental value, 321×10^{-6} cm^3 mole^{-1}, is in better agreement with the second of these values than with the first. However, the value of α which is required, namely -0.0874, seems unreasonable for reasons described in the foregoing. The magnetic susceptibility of NpF_6 in UF_6 is presently being investigated in these laboratories over a wide range of concentrations and temperatures.

Nuclear Magnetic Moment

The relation[18]

$$A=(4\beta\beta_N\mu_N/I)\langle r^{-3}\rangle\langle+|N_z|+\rangle=0.0665$$

may be used to estimate the numerical value of the nuclear magnetic moment of Np^{237}. We have calculated the numerical value of $\langle+|N_z|+\rangle$ to be -1.303 using the ground state for $\alpha=+0.4421$ as given previously in this paper. (The operator equivalent of Abragam and Pryce[18] was used with $\frac{2}{4.5}$ as the equivalent factor for the dipole-dipole term.) This leads to $\mu_N=2.70$ nuclear magneton, if we assume $\langle r^{-3}\rangle=50\times10^{24}$ cm^{-3}.[19,20] This is a much smaller value than that determined from the data for NpO_2^{++}.[21]

ACKNOWLEDGMENT

We thank Professor M. H. L. Pryce for his invaluable assistance to our theoretical understanding of our work and for suggesting that we determine the sign of g, Professor Julian C. Eisenstein for many helpful discussions, Dr. Eugene Y. Wong and Dr. Paul B. Dorain for their help with the experiments on gaseous NpF_6, Dr. Peter M. Llewellyn for his assistance in the development and construction of apparatus and assistance with some of the measurements, John G. Malm for his help with the preparation of samples, and Edward Bartal and J. S. D. Danielson for assistance in the design and development of equipment.

[18] A. Abragam and M. H. L. Pryce, Proc. Roy. Soc. (London) **A205**, 135 (1951).
[19] Hutchison, Llewellyn, Wong, and Dorain, Phys. Rev. **102**, 292 (1956).
[20] Bleaney, Hutchison, Llewellyn, and Pope, Proc. Phys. Soc. (London) **B69**, 1167 (1956).
[21] Bleaney, Llewellyn, Pryce, and Hall, Phil. Mag. **45**, 992 (1954).

Study of the Wurtzite-Type Binary Compounds. IV. Theory of Double Refraction*

FREDERIC KEFFER

University of Pittsburgh, Pittsburgh, Pennsylvania

(Received June 29, 1959)

The Ewald-Born theory of double refraction is applied to wurtzite-type compounds. Except for the small distortion and polarization, these compounds have identical near-neighbor symmetry to zinc blende (cubic) structures, and hence the double refraction is caused primarily by the distant-neighbor interactions. The effects of anisotropy of the Lorentz-Lorenz force and of the Coulomb force are calculated. In the (ionic) approximation of zero cation polarizability the theory predicts a double refraction larger than the measured one by a factor ~ 2 for all six compounds that have been measured. In the (covalent) approximation of zero effective ionic charge the theory underestimates the double refraction of AlN, but may be made to agree with the measured values of the other compounds by a suitable choice of atomic polarizabilities. In both approximations the theory predicts $n_0 < n_e$, in agreement with long-wavelength observations. Anisotropic interaction of polarized light with the solid as a whole, as in exciton transitions, seems to account for the inversion to $n_0 > n_e$ near the absorption edge of CdS.

I. INTRODUCTION

THE first two papers of this series[1,2] were concerned with the distortion and polarization of the wurtzite-type binary compounds away from the ideal wurtzite lattice structure. It was shown that the nonideal structures can be understood in terms of an interplay between ionic and covalent tendencies. The third paper of the series[3] demonstrated the profound effect of overlap of "ions" on the valence band structure of the wurtzite-type compound BeO. In this paper we study the effects of ionic *vs* covalent interactions on the optical double refraction of AlN, BeO, ZnO, ZnS, CdS, and AgI.

The theory of double refraction in crystals has been developed by Ewald,[4] Bragg,[5] Hylleraas,[6] Born,[7] Mueller,[8] and others. Causes of double refraction are generally considered to be:

(1) Anisotropy of the Lorentz-Lorenz force, or of what Born calls the electrodynamic coupling. The dipole lattice sum within the Lorentz sphere, which is zero for crystals with tetrahedral symmetry,[9] may for other symmetries have different values for polarization along and perpendicular to the extraordinary, or crystal axis.

(2) Anisotropy of the Coulomb force, or of what Born calls the electrostatic coupling. If we think of the electronic polarization as coming from an oscillating charge, this charge will be subjected to a field gradient from the ions of an ionic crystal; and in general this field gradient will have different values along and perpendicular to the crystal axis.

(3) Anisotropy of the electronic polarizabilities of the ions. As emphasized by Mueller,[8] this depends primarily on the arrangement of nearest-neighbor atoms.

These three causes become interrelated once one allows for overlap between adjacent ions. We discuss this further at the end of Sec. IV. In addition, overlap effects give rise to another cause which is important only for wavelengths near an absorption edge, namely:

(4) Anisotropic interaction of polarized light with the solid as a whole. This may be related to band-to-band transitions, as studied by Dresselhaus,[10] or to exciton transitions, as emphasized by Dutton.[11] In either case the absorption of light is anisotropic in the polarization (dichroism), and the accompanying dispersion should also in general be anisotropic in the polarization (double refraction). This cause will be inoperative in the long-wavelength limit.

In the second paper of this series[2] an attempt was made to explain the observed distortion and polarization of wurtzite structures in terms of anisotropic local fields and effective stresses. It was argued that so far as two-body, near-neighbor interactions are concerned, there can be no difference between ideal wurtzite structures and zinc blende (cubic) structures; and therefore long-range distant-neighbor interactions are of paramount importance in determining anisotropic behavior.

In this paper we use similar arguments in an attempt to account for the observed double refraction of binary wurtzite compounds. That is, we assume that the local electronic polarizabilities of the cations and anions are determined by near-neighbor arrangements, and hence are isotropic in the ideal wurtzite structure, just as they must be in the zinc-blende structure. This assumption eliminates cause (3) in the foregoing. However, there will be a small anisotropy in the polarizabilities coming

* Work was done in the Sarah Mellon Scaife Radiation Laboratory and was supported by the United States Air Force through the Air Force Office of Scientific Research of the Air Research and Development Command under Contract No. AF49(638)-323.

[1] Jeffrey, Parry, and Mozzi, J. Chem. Phys. **25**, 1024 (1956).
[2] F. Keffer and A. M. Portis, J. Chem. Phys. **27**, 675 (1957).
[3] W. O'Sullivan, J. Chem. Phys. **30**, 379 (1959).
[4] P. P. Ewald, Ann. Physik **49**, 1, 117 (1916).
[5] W. L. Bragg, Proc. Roy. Soc. (London) **A105**, 307 (1924); **A106**, 346 (1924).
[6] E. Hylleraas, Z. Physik **36**, 859 (1926); Z. Krist. **65**, 469 (1927).
[7] M. Born and M. Goeppert-Mayer, *Handbuch der Physik* (Verlag Julius Springer, Berlin, 1933), Vol. 24, part 2.
[8] H. Mueller, Phys. Rev. **47**, 947 (1935).
[9] M. Born and K. Huang, *Dynamical Theory of Crystal Lattices* (Oxford University Press, New York, 1954), Appendix VI.
[10] G. Dresselhaus, Phys. Rev. **105**, 135 (1957).
[11] See D. L. Dexter, J. Phys. Chem. Solids **8**, 473 (1959).

from the distortion away from the ideal structure, and therefore our simplified theory can be expected to fit best those compounds with smallest observed distortion.

II. THE ANISOTROPY OF THE LOCAL FIELD

The wurtzite unit cell contains two cations and two anions, and therefore a complete description of the fields and polarization can be made in terms of four sublattices. However, the lattice may be thought of as composed of two interpenetrating *hcp* lattices, one of cations and the other of anions; and the symmetry is such that monopole and dipole fields are the same at all sites on a given *hcp* sublattice. The problem of fields and polarizations is reduced from four to two sublattices, which we shall call 1 and 2.

The local field[12] in the jth direction at sites on sublattice 1 is given by

$$E_1^j = E_0^j + E_{c1}^j + L_{11}^j P_1^j + L_{12} P_2^j, \tag{1}$$

where E_0^j is the applied (optical frequency) external field, E_{c1}^j is the Coulomb field of the ions, to be discussed subsequently, P_1^j and P_2^j are the polarization densities of the two sublattices, and L_{11}^j and L_{12}^j are the appropriate Lorentz factors. Since the wurtzite lattice contains reflection planes, there can be no cross terms coupling E_1^j with P_1^k or P_2^k. The Lorentz factors are given by

$$L_{11}^j = N^{-1}\Sigma_t'[3(r_t^j)^2 - (r_t)^2]/r_t^5 + (4\pi/3). \tag{2}$$

Here r_t is the distance from a given site on sublattice 1 to the tth site on the same sublattice, which has N sites per unit volume. The sum is to be taken within a Lorentz sphere, and the prime on the summation sign indicates, as usual, the omission of the term with vanishing denominator.

The factor L_{12}^j is given by a similar sum with r_t as the distance to the tth site on the other sublattice.

The local field at sites on sublattice 2 is given by an expression similar to Eq. (1) with subscripts 1 and 2 interchanged.

The Coulomb field is given by

$$E_{c1} = E_{11}^j + u_1^j(\partial E_{11}^j/\partial r^j), \tag{3}$$

where E_{11}^j is the field in the jth direction at a lattice point on sublattice 1 produced by ionic charges at all other lattice points, and u_1^j is the periodic displacement of the equivalent oscillating charge[7] with which we can replace the electronic polarization:

$$P_1^j/N = -g_1 e u_1^j. \tag{4}$$

Here e is the (positive) electron charge and g_1 is the so-called oscillator strength representing the effective number of vibrating electrons. Most authors use the symbol f for the oscillator strength, but in the second paper of this series[2] we have used $\pm fe$ to represent a very different quantity, namely, the effective ionic charge at a lattice site. We will maintain our somewhat unfortunate notation. If sublattice 1 is taken to contain positive ions, we then have

$$E_{11}^j = -fe\Sigma'_{t(1)} r_t^j/r_t^3 + fe\Sigma_{t(2)} r_t^j/r_t^3, \tag{5}$$

where the first sum is over sublattice 1, the second over sublattice 2. The field derivative is given by

$$\partial E_{11}^j/\partial r^j = -feN(L_{11}^j - L_{12}^j). \tag{6}$$

The constant term E_{11}^j, which we have shown[2] is not zero along the c axis of wurtzite, will tend to shift the electronic cloud slightly away from the ideal position. This will give rise to opposing electric fields coming from the ion itself or from nearest neighbors, such that the total Coulomb field at the new lattice site is zero. We shall neglect both the small anisotropy in the polarizability which is introduced by this shift and any difference between the Lorentz factors at the actual site and at the ideal site. As mentioned in Sec. I, this limits our theory to those wurtzite-type compounds with small observed distortion.

The local fields are now

$$E_1^j = E_0^j + [L_{11} + (f/g_1)(L_{11}^j - L_{12}^j)]P_1^j + L_{12}^j P_2^j;$$
$$E_2^j = E_0^j + L_{21}^j P_1^j + [L_{22} - (f/g_2)(L_{22}^j - L_{21}^j)]P_2^j. \tag{7}$$

The Lorentz factors have been evaluated by an extension of the lattice-sum methods outlined in the second paper of this series.[2] The results are

$$L_{11}^x = L_{11}^y = L_{22}^x = L_{22}^y = 4.1863$$
$$L_{11}^z = L_{22}^z = 4.1938$$
$$L_{12}^x = L_{12}^y = L_{21}^x = L_{21}^y = 4.0872$$
$$L_{12}^z = L_{21}^z = 4.3902. \tag{8}$$

Here the z direction is taken along the c axis, and x and y are any orthogonal pair in the hexagonal plane. We note that L_{11} is the Lorentz factor at a lattice point for a *hcp* lattice, which has already been given by McKeehan.[13] Our results are in excellent agreement. As a further check, the factors were evaluated separately for x and z directions and subsequently found to satisfy the condition

$$2L^x + L^z = 4\pi. \tag{9}$$

III. ANISOTROPY OF THE SUSCEPTIBILITY

We now proceed to solve the susceptibility problem. We have

$$P_1^j = N\alpha_1 E_1^j; \quad P_2^j = N\alpha_2 E_2^j, \tag{10}$$

where α_1 is the electronic polarizability of the ions on sublattice 1 (taken as the positive ions), α_2 corre-

[12] For an elementary discussion of the Lorentz-Lorenz local field problem see, for example, C. Kittel, *Introduction to Solid State Physics* (John Wiley & Sons, Inc., New York, 1956), Chap. 7. For a discussion of the Coulomb field see reference 7, Sec. 59.

[13] L. W. McKeehan, Phys. Rev. **43**, 1025 (1933).

spondingly for negative ions. The macroscopic susceptibility is given by

$$\chi^i=(P_1{}^i+P_2{}^i)/E_0{}^i. \tag{11}$$

From simultaneous solution of the two linear equations (7), with the aid of Eqs. (8), (10), and (11), we obtain

$$\chi^i=\frac{N(\alpha_1+\alpha_2)-N^2\alpha_1\alpha_2(L_a{}^i+L_b{}^i-2L_{12}{}^i)}{1-L_a{}^iN\alpha_1-L_b{}^iN\alpha_2+N^2\alpha_1\alpha_2[L_a{}^iL_b{}^i-(L_{12}{}^i)^2]} \tag{12}$$

where

$$L_a{}^i=L_{11}{}^i+(f/g_1)(L_{11}{}^i-L_{12}{}^i);$$
$$L_b{}^i=L_{11}{}^i-(f/g_2)(L_{11}{}^i-L_{12}{}^i). \tag{13}$$

The extraordinary index of refraction is given by

$$(n_e{}^2-1)/4\pi=\chi_e=\chi^z, \tag{14a}$$

and the ordinary index by

$$(n_0{}^2-1)/4\pi=\chi_0=\chi^x=\chi^y. \tag{14b}$$

Thus Eq. (12) is in effect two independent equations, one for χ_e and one for χ_0. If we note that $N\alpha$ is ~ 0.1 and that all the Lorentz factors are near $4\pi/3$ and satisfy Eq. (9), we find that the following relation holds to within about 1%:

$$N(\alpha_1+\alpha_2)\approx[(4\pi/3+(1/\chi)]^{-1}, \tag{15}$$

where

$$1/\chi=\tfrac{1}{3}[(1/\chi_e)+(2/\chi_0)]. \tag{16}$$

Equation (15) is the usual Lorentz-Lorenz relation for isotropic χ. In addition to this usual relation we may obtain an equation in the difference between ordinary and extraordinary susceptibilities:

$$(\chi_0)^{-1}-(\chi_e)^{-1}\approx[3/(2\eta+2)]$$
$$\times\{D_a{}^z\eta+D_b{}^z-[(D_a{}^z+D_b{}^z-2D_{12}{}^z)\eta/(\eta+1)]\}$$
$$+[3\eta N\alpha_2/(4\eta+4)][(D_{12}{}^z)^2-D_a{}^zD_b{}^z]. \tag{17}$$

Here we have replaced each Lorentz factor by its corresponding dipole-field factor

$$L^i=D^i+(4\pi/3), \tag{18}$$

we have used relation (9), and we have introduced

$$\eta=\alpha_1/\alpha_2; \tag{19}$$

also we have made the following approximation in the right-hand side of Eq. (17):

$$(\chi_e)^{-1}+(2\chi_0)^{-1}\approx\tfrac{3}{2}\chi^{-1}\approx\tfrac{3}{2}[N\alpha_2(\eta+1)]^{-1}-2\pi. \tag{20}$$

We note that Eq. (17) yields isotropic susceptibility, as it must, in the limit all $D^i\to 0$, i.e., tetrahedral symmetry.

Most numerical evaluations of electronic polarizabilities from measured indices of refraction, such as the least-squares fit of Tessman, Kahn, and Shockley (TKS),[14] are based on the single Lorentz-Lorenz relation (15), which contains two unknowns, α_1 and α_2. To find both unknowns requires using the relation for a series of crystals, such as NaF, NaCl, NaBr, NaI, and assuming that the polarizability of the Na ion remains the same throughout the series. As TKS have shown from their results, this is not a bad assumption for the alkali halides; however, as TKS have also shown, the assumption breaks down for oxides and sulfides. We would expect the assumption to be worthless for our wurtzite compounds, which, as has been argued in the other papers in this series,[1-3] are neither covalent nor ionic and probably have quite anomalous polarizabilities.

On the other hand, because of the double refraction, we have here the extra Eq. (17) which we may use in attempting to evaluate α_1 and α_2. The equation is a mixed blessing, however, since it contains in $D_a{}^z$ and $D_b{}^z$ the extra unknowns (f/g_1) and (f/g_2). Nevertheless, with the aid of reasonable approximations we may use the equation for a study of the polarizabilities and in addition as a test of the theory of double refraction.

IV. APPROXIMATION OF ZERO CATION POLARIZABILITIES

Up to this point we have limited our analysis to causes (1) and (2) of double refraction, as outlined in Sec. I. Dispersion effects may be thought of as included in the polarizabilities and the oscillator strengths, i.e., these parameters are frequency dependent. The parameters are, however, to be considered as isotropic. We have neglected causes (3) and (4), Sec. I.

The comparison with experiment, therefore, should be made in the infinite-wavelength limit. However, good data are available only for the sodium D line (5893 A). We assume this is far enough from an absorption edge in the crystals considered (all of which are near insulators) to eliminate the effects of cause (4). In Sec. VI we discuss the double refraction of CdS near its absorption edge (4874 A).

Since often the polarizability of the positive ions (our sublattice 1) is very much smaller than that of the negative, many authors, e.g., Hylleraas in his study of rutile and anatase,[6] make the approximation $\eta\to 0$. In this limit Eq. (17) yields

$$(\chi_0)^{-1}-(\chi_e)^{-1}\to(3/2)D_b{}^z=0.0075+0.2973(f/g_2). \tag{21}$$

In Table I we list the wurtzite compounds for which double refraction has been measured. In evaluating (21) we have taken g_2 equal to the oscillator strength of the corresponding inert gas, an approximation found to be fairly reliable by Hylleraas[6] and Mueller.[8] The values of f are for a completely ionic lattice. We make the following observations:

(1) This simple approximation fits both the sign and the order of magnitude of the observed double refraction.

[14] Tessman, Kahn, and Shockley, Phys. Rev. **92**, 890 (1953).

(2) Both observed and calculated values decrease in going down the table.

(3) The polarizability of Zn should be much larger than that of Be; thus this approximation should give a poorer fit to ZnO than to BeO. It does. Similarly we expect, and find, a poorer fit to CdS than to ZnS.

(4) Our calculated values suggest that the Kohn, Cotter, and Potter numbers for AlN are probably more accurate than those of Lagrenaudie. Indeed, Lagrenaudie gives n_e as 2.18 ± 0.06, whereas the former authors quote both their numbers to ±0.02. Both sets of AlN measurements are for synthetic crystals, whereas the indices quoted for all other compounds are for natural crystals. Measured values of double refraction are known to vary from sample to sample, probably due to changes in stoichiometry and impurity content, and this variation introduces considerable uncertainty into our tabulated data.

(5) If we accept the Kohn, Cotter, and Potter numbers, we see that for all compounds the calculated values are too large by about a factor of 2. This is probably caused by an overestimate of f. In previous papers in this series[1,2] it has been argued that the partially covalent nature of wurtzite compounds will greatly reduce the size of the ionic charge. O'Sullivan[3] has shown that the wave functions of the electrons of an O^{--} configuration in BeO have tremendous overlap with the neighbor Be^{++} and even extend well into next-neighbor oxygens. Thus our model of point ions on a lattice can only retain meaning if we reduce the ionic charge, and Table I indicates that the proper reduction factor is ~2.

Once, however, we allow for overlap of charge, we introduce a number of difficulties. As far as near-neighbor fields are concerned, the whole Lorentz-Lorenz model breaks down. Mott and Gurney[15] believe this to be true even for alkali halides, and they claim that best theoretical fits to a number of experiments can be obtained with L_{12} taken as ~0. On the other hand, TKS[14] get definitely the best least-squares fit to the polarizabilities with L_{12} equal to the Lorentz value $4\pi/3$. Yamashita[16] has resolved this discrepancy by making a detailed quantum-mechanical calculation of overlap effects. He shows that, roughly speaking, one may account for the overlap energy by either (a) incorporating it into a different Lorentz factor and retaining approximately the isolated-ion polarizabilities (Mott and Gurney); or (b) keeping the point-ion Lorentz factor and allowing the polarizabilities to change (TKS). Neither (a) nor (b) is a completely correct procedure, yet both may be considered as reasonable approximations. For simplicity, we prefer to use (b).

We may take account of overlap by reducing f, that is, by transferring in effect some electronic charge from the anions to the cations. But this will increase the value of η, and the approximation of this section will break down. In the next section we try an approximation nearer the covalent extreme.

TABLE I. Comparison of observed and calculated double refraction in the approximation of zero cation polarizability. Refractive data, except as noted for AlN, are from Palache, Berman, and Frondel, *Dana's System of Mineralogy*, seventh edition. (John Wiley & Sons, Inc., New York, Vols. 1 and 2, 1944, 1951). All values are for the sodium D line (5893 A). It is assumed this is far from an absorption edge (see text).

	n_0	n_e	f	g_2	$[(\chi_0)^{-1}-(\chi_e)^{-1}]$ From data	From Eq. (21)
AlN	2.13[a]	2.20[a]	3	2.37	0.280	0.384
	2.00[b]	2.18[b]	3	2.37	0.840	0.384
BeO	1.719	1.733	2	2.37	0.155	0.258
ZnO	2.013	2.029	2	2.37	0.086	0.258
ZnS	2.356	2.378	2	4.58	0.062	0.137
CdS	2.506	2.529	2	4.58	0.051	0.137
AgI	2.21	2.22	1	5.61	0.036	0.061

[a] Kohn, Cotter, and Potter, Am. Mineralogist **41**, 355 (1956).
[b] J. Lagrenaudie, J. Chim. Phys. **53**, 222 (1956).

TABLE II. Calculated polarizabilities (for 5893 A) in the approximation of zero effective charge, Eq. (23). The first column gives the ratio of the Pauling ionic radii of cation to anion, as tabulated, e.g., in reference 12. The second column is taken from a table in reference 1.

	(R_c/R_a)	(c/a)	η	α_1	α_2
AlN	0.29	1.600	...	...	...
BeO	0.23	1.623	0.89	0.62	0.69
ZnO	0.53	1.602	0.18	0.45	2.45
ZnS	0.40	1.635	0.11	0.58	5.14
CdS	0.53	1.623	0.087	0.61	6.99
AgI	0.58	1.635	0.054	0.47	8.72

V. APPROXIMATION OF ZERO EFFECTIVE CHARGE

An approximation which probably overestimates the covalent tendencies is: zero effective charge, equal polarizabilities, i.e., $f=0$, $\eta=1$. Except for a negligible term in $N\alpha_2$, this approximation reduces Eq. (17) to

$$(\chi_0)^{-1}-(\chi_e)^{-1}\approx0.1564. \qquad (22)$$

It is seen from Table I that this is an underestimate for AlN, indicating, as seems reasonable, that in this compound $f>0$. For the remainder of the tabulated compounds Eq. (22) gives too large a double refraction, although it is very close for BeO.

[15] N. F. Mott and R. W. Gurney, *Electronic Processes in Ionic Crystals* (Oxford University Press, New York, 1948).
[16] J. Yamashita, Progr. Theoret. Phys. **8**, 280 (1952); **12**, 454 (1954); J. Yamashita and T. Kurosawa, J. Phys. Soc. Japan **10**, 610 (1955).

TABLE III. The insensitivity of double refraction to c/a ratio. Data from Czyzak, Crane, and Bieniewski.[17] All at 5500 A.

Crystal	c/a	n_0	n_e	$[(\chi_0)^{-1}-(\chi_e)^{-1}]$
CdS	1.624	2.580	2.593	0.0261
CdS: (1% O)	1.614	2.569	2.582	0.0265
CdS: (0.1% In)	1.630	2.559	2.573	0.0290

We shall now assume that, except for AlN with its large valence, the value of f for all compounds is close to zero, but we shall allow different values for η. In effect, this approximation eliminates the Coulomb force. Except for a negligible term in $N\alpha_2$, Eq. (17) becomes

$$(\chi_0)^{-1}-(\chi_e)^{-1}\approx 0.0075+0.5946[\eta/(\eta+1)^2]. \quad (23)$$

We may insert into this equation the measured values of the double refraction and solve for η. The results are listed in Table II, together with values of α_1 and α_2 obtained with the further aid of Eq. (15). We do not ascribe very much significance to these numbers except as they illustrate general trends. In Table II we also list the ratios of the Pauling ionic radii and the x-ray c/a lattice ratios. Ideal wurtzite has $c/a=1.633$.

A comparison of BeO with ZnO illuminating. The values of c/a suggest that (if the distortion is produced by the ionic forces)[2] f is more nearly zero in BeO than ZnO. The smaller ratio of the ionic radii in BeO gives rise to greater electronic overlap; and this together with the smaller electronegativity difference causes BeO to be more covalent than ZnO and hence have a larger value of η. (Allowing f to vary in calculating η does not change these qualitative conclusions.)

Similarly, a comparison of ZnS with CdS indicates that the former behaves in a consistent way as the more covalent of the two.

The value of c/a for AgI suggests that this compound has f very near to zero. Thus Eq. (23) should apply, and our computed value of η should have some meaning. On the other hand, TKS give polarizabilities for Ag^+ and I^- as obtained from cubic structures which lead to $\eta\approx 0.35$. Our value is very much smaller, whereas one would suppose that the covalent tendencies in the wurtzite structure would lead to a larger value. We offer no explanation except the repeated caution that the numerical values of Table II must not be taken too seriously.

It should be noted that with $f=0$ all distinction in our theory between the anion and the cation disappears, and we cannot tell which of the calculated polarizabilities in Table II belongs to which atom. In the above discussion we have assumed that the smaller of the two values of α belongs to the metallic atom, although it is possible that this is incorrect.

In all the above calculations we have used the Lorentz factors for the ideal lattice, whereas the distortion will produce a considerable change. We estimate, for example, that a reduction in c/a to 1.600, as in AlN, changes $L_{11}{}^s$ to 4.2394. The value of $L_{12}{}^s$ is also modified and furthermore is sensitive to a change in the u parameter (relative displacement of the two sublattices). Most of this latter change, however, comes from near-neighbor contributions, and it is impossible to estimate their net effect. Once we depart from tetrahedral near-neighbor symmetry our whole simple point-ion picture breaks down. Furthermore, the polarizability itself becomes anisotropic. Thus we prefer to neglect distortion effects and take comfort from the fact that experimental values of the double refraction show no correlation with c/a ratios.

The negligible effect of c/a ratio on double refraction is demonstrated by the data of Czyzak, Crane, and Bieniewski,[17] Table III.

VI. DOUBLE REFRACTION NEAR AN ABSORPTION EDGE

A comparison of the double refraction of CdS at 5893 A (Table I) and at 5500 A (Table III) indicates a rapid decrease in this region with decreasing wave length. By observations on a very pure crystal of CdS Czyzak *et al.*[17] were recently able to locate a crossover point at 5245 A. Below this wavelength they observed $n_0>n_e$. Accompanying this effect was a much larger absorption of the ordinary than of the extraordinary polarization (dichroism).

The absorption edge in CdS, according to measurements of Dutton,[11] occurs (at 90°K) at 4844 A for both polarizations, with an additional and stronger absorption at 4874 A for the ordinary polarization.

We suggest the following correlation of these observations on CdS: At long wavelengths the theory of Sec. III, in either the approximation of Sec. IV or of Sec. V, quite definitely predicts $n_0<n_e$. As the wavelength approaches the absorption edge, the anisotropy in crystalline exciton transitions (with respect to the polarization of the optical wave) produces stronger absorption of the ordinary than of the extraordinary polarization. This same anisotropy has a similar effect on the real part of the complex index of refraction, causing n_0 to become larger than n_e.

[17] Czyzak, Crane, and Bieniewski, J. Opt. Soc. Am. **49**, 485 (1959).

THE JOURNAL OF CHEMICAL PHYSICS VOLUME 32, NUMBER 1 JANUARY, 1960

Proton Magnetic Resonance Spectrum of Propane*

DONALD R. WHITMAN, *Chemistry Department, Case Institute of Technology, Cleveland, Ohio*

AND

LARS ONSAGER, MARTIN SAUNDERS, AND HUBERT E. DUBB, *Sterling Chemistry Laboratory, Yale University, New Haven, Connecticut*

(Received July 9, 1959)

Exact proton magnetic resonance eigenspectra of the spin Hamiltonian are calculated for a system containing one group of six identical protons and one group of two identical protons. The method of calculation considers each group of identical protons as a composite "particle" with fixed total spin, and does not require determination of the explicit form of the zero-order eigenfunctions. The calculated spectra are compared with experimental high-resolution spectra of propane at both 40 Mc and 60 Mc. Thevalues of ρ, the ratio of the spin coupling constant to the chemical shift, are found to be 0.415 and 0.277, respectively, at the two frequencies. The frequency-independent spin coupling constant is 7.26 cps.

A relatively simple spin Hamiltonian similar to Eq. (1) has been accepted as explaining, at least in principle, the high-resolution nuclear magnetic resonance spectra of most molecules. However, relatively few solutions for the eigenspectra of this type of Hamiltonian have been carried out because of the awkwardness of solution of the secular equation when many nuclei are involved. They become especially complex when chemical shifts and spin-spin couplings are of comparable magnitude. Therefore propane presents an interesting case since exact solution for the eigenspectra of its spin Hamiltonian is possible without a formidable amount of labor, even though the chemical shift and spin-spin coupling are comparable in magnitude and the number of nuclear moments is relatively large.

Aside from the computational complexity in calculating theoretical spectra, the major difficulty when many nuclei are involved is the large number of chemical shifts and spin-spin coupling constants which must be determined as parameters in fitting the observed spectrum. For example, the most general case with eight protons involves seven chemical shifts and twenty-eight spin-spin coupling constants. Even after obtaining a calculated spectrum to approximate an observed spectrum, in many cases because of the number of parameters it is difficult to say whether the solution is unique.

Because of its symmetry the case of propane involves only two different resonant frequencies and four different spin-spin coupling constants. Furthermore, three of the coupling constants, those between identical protons, can contribute nothing to the spectrum and can be omitted. The position and scale of the spectrum are arbitrary, so there remains only one real parameter. This is ρ, the ratio of the coupling constant J to the chemical shift δ.

The moment method of Anderson and McConnell[1] provides a means of estimating this ratio from the second and fourth moments of an experimental spectrum. The method is extremely valuable because it quickly yields an approximate value for ρ and eliminates the need for a trial-and-error search. However, the value found is not precise because of the sensitivity to small errors in moment determinations.

The value $\rho=0.37$ was calculated by the moment method for a propane spectrum obtained at 40 Mc. This value was used in the propane Hamiltonian and an exact solution for the eigenvalues and relative transition probabilities was carried out as discussed below. This gave a calculated spectrum which approximated the experimental spectrum and permitted identification of corresponding peaks. Then the numerical distances between peaks of the experimental spectrum were set equal to the analytical expressions for the separations between the corresponding peaks of the theoretical spectrum. From these equations, values of J and δ were calculated which are limited in accuracy only by the uncertainties in the peak-to-peak distances. Since it was necessary to use a very slow sweep rate to obtain a sufficiently resolved experimental spectrum, the variation of the rate of drift was appreciable and it was found that successive spectra varied from each other considerably in the exact positioning of peaks. For this reason the final best value of ρ was obtained by averaging data from eleven spectral traces at 40 Mc. The spacings between eighteen lines in each trace were measured and a value of ρ selected for which the differences between the theoretical spacings and the measured ones were a minimum. This corresponded to the value $\rho=0.415\pm0.006$. A theoretical spectrum calculated for $\rho=0.415$ is compared with an experimental 40-Mc spectrum in Fig. 1. The agreement is good even though the calculated spectrum corresponds even more closely with the average of eleven spectral traces than with any single trace (Table I).

The values of J and δ for propane at 40 Mc are $J=7.26$ cps., and $\delta=17.5$ cps. The value of δ was measured directly from the experimental spectrum. A spectrum was calculated also for the value $\rho=0.277$,

* Contribution No. 1555 from the Department of Chemistry of Yale University.

[1] W. Anderson and H. M. McConnell, J. Chem. Phys. **26**, 1496 (1957).

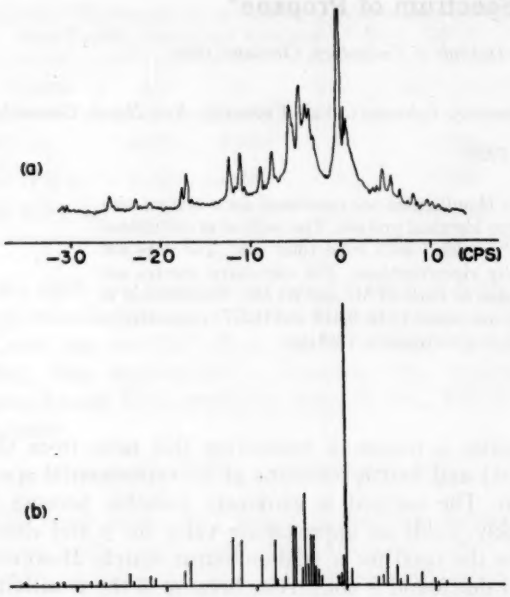

FIG. 1. High-resolution proton magnetic resonance spectrum of propane at 40 Mc. (a) Experiment spectrum. (b) Calculated spectrum with the value 0.415 for the ratio of the spin-coupling constant to the chemical shift.

two-thirds of the 40-Mc value. This calculated spectrum was compared with an experimental 60-Mc trace (see Fig. 2). The excellent fit reconfirmed the correctness of the values found for J and δ.

Narasimhan, Laine, and Rogers[2] have compared an experimental spectrum of propane with one calculated by perturbation methods, and reported a somewhat different value for J/δ. They were handicapped, however, by the lack of detail in their experimental spectrum, and the inadequacy of perturbation techniques for this case.

SOLUTION FOR THE EIGENSPECTRA

The effective spin Hamiltonian for the eight protons in propane can be written

$$\mathcal{H}=-\omega_A I_{Az}-\omega_B I_{Bz}-J\mathbf{I}_A\cdot\mathbf{I}_B. \quad (1)$$

The subscript A denotes the group of two equivalent methylene protons and B represents the group of six equivalent methyl protons. $\mathbf{I}_A$ and $\mathbf{I}_B$ are the total vector spin operators of the two groups and I_{Az} and I_{Bz} are the components of these operators along the direction of the magnetic field. ω_A and ω_B $(=\omega_A+\delta)$ are the resonant frequencies the two groups would exhibit in the absence of spin coupling. J is the spin-spin coupling between a proton of group A and one of group B. All energies are measured here in units of $\hbar$.

The square of the total spin angular momentum operator of a group of equivalent protons commutes with the x component of the total nuclear magnetic moment operator.[3] For this reason each set of terms in the total spin Hamiltonian involving couplings between protons within a single group of equivalent protons commutes with I_z. Transitions involving changes in the eigenvalues of these terms have zero relative transition probabilities and contribute nothing to the NMR spectrum. Therefore, such terms were omitted from the effective spin Hamiltonian, Eq. (1).

The fact that $\mathbf{I}_A^2$ and $\mathbf{I}_B^2$ commute with I_z means that the total spin of each group of equivalent protons is a good quantum number. Each group of equivalent protons can then be considered as a single composite "particle," with fixed total spin.[4] By using the notations $S, D, T, Q, Qt, Sx, Sp., \cdots$ for states with eigenvalues $\frac{1}{2}, 1, \frac{3}{2}, \cdots$ of the total spin, the two equivalent methylene protons in propane form an S or T particle with spin 0 or 1. The six equivalent methyl protons constitute an S, T, Qt, or Sp particle, with spin 0, 1, 2, or 3.

The eigenvalues of the spin Hamiltonian Eq. (1) are found by solution of the secular equation,

$$|\mathcal{H}_{mn}-\delta_{mn}E|=0, \quad (2)$$

where $\mathcal{H}_{mn}$ is the matrix element of $\mathcal{H}$ between the zero-order spin functions ϕ_m and ϕ_n. Three operators, I_z, $\mathbf{I}_A^2$ and $\mathbf{I}_B^2$ commute with $\mathcal{H}$ and, therefore, maximum factoring of the secular determinant is obtained by choosing zero-order spin functions which are

TABLE I. Comparison of calculated eigenspectrum for $\rho=0.415$ with averaged experimental 40-Mc spectrum of propane; only twenty of the more prominent lines are compared.

Average observed spectrum at 40 Mc (shift in cps from methyl)	$J=7.26$ cps $\delta=17.5$ cps $(\rho=0.415)$	Source (triplet, quintet, septet)	Relative transition probability
−35.79	−35.73	Qt	21
−31.54	−31.58	Qt	30
−27.50	−27.38	T	64
−24.50	−24.22	T	91
−22.30	−22.11	T	83
−21.30	−21.20	Qt	52
−18.10	−18.13	T	147
−17.50[a]	−17.50[a]		195
−12.81	−12.86	T	288
	−12.74	Qt	121
−11.67	−11.68	T	380
−9.42	−9.33	Qt	248
−8.01	−7.93	Qt	404
0.00[b]	0.00[b]	Qt	2563
4.56	4.62	$T+Qt$	210
	4.66	Sp	71
5.57	5.70	Qt	163
6.60	6.72	T	91
8.26	8.37	Qt	117
9.74	9.88	$T+Qt$	64
10.22	10.21	Sp	40
13.29	13.62	Qt	45

[a] Unshifted CH_2 peak.
[b] Unshifted CH_3 peak.

[2] Narasimhan, Laine, and Rogers, J. Chem. Phys. **28**, 1257 (1958); **29**, 1184 (1958).

[3] E. L. Hahn and D. E. Maxwell, Phys. Rev. **88**, 1070 (1952).
[4] D. R. Whitman, thesis, Yale University, 1957.

simultaneous eigenfunctions of these operators. Products of the spin functions, α and β, of individual protons are automatically eigenfunctions of I_z, and these may be combined to obtain eigenfunctions of $\mathbf{I}_A^2$ and $\mathbf{I}_B^2$. The eigenfunctions of $\mathbf{I}_A^2$ are

$$T_A^1=\alpha\alpha$$

$$T_A^0=(\alpha\beta+\beta\alpha)/\sqrt{2} \quad S_A^0=(\alpha\beta-\beta\alpha)/\sqrt{2}$$

$$T_A^{-1}=\beta\beta.$$

Here S_A and T_A indicate the eigenvalues 0 and 1 of $\mathbf{I}_A^2$, and the superscripts indicate the eigenvalues of I_z.

There are $2^6=64$ eigenfunctions of $\mathbf{I}_B^2$, consisting of one set of septet functions, five sets of quintet functions, nine sets of triplet functions, and five sets of singlet functions. Since the triplet functions are ninefold degenerate, it suffices to consider only one set of such functions, and later to weight the contribution of this set by the factor nine. Similarly, representative singlet and quintet functions may be chosen, with later weighting by the factor five.

Although it is possible to evaluate the explicit form of the representative sets of eigenfunctions of $\mathbf{I}_B^2$, as was done for $\mathbf{I}_A^2$, this is tedious and unnecessary. Let us merely represent these by the nomenclature given above. Thus, the representative sets are shown in Table II.

The zero-order spin functions to be used in the calculation of the secular determinant are then taken

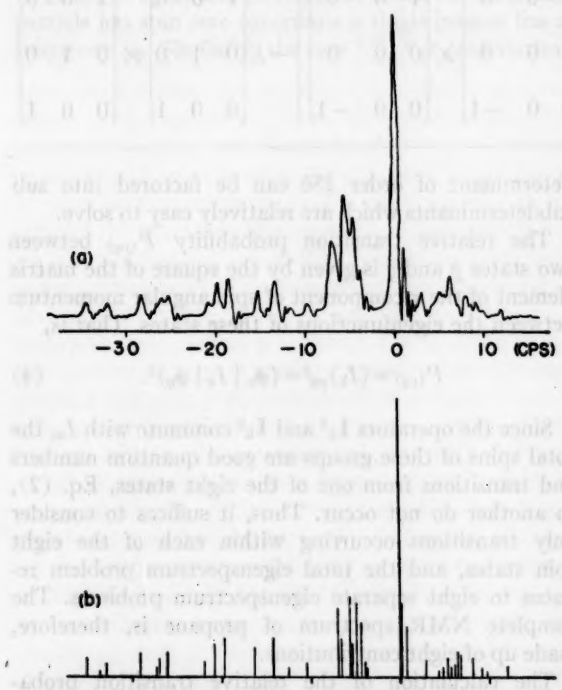

FIG. 2. High-resolution proton magnetic resonance spectrum of propane at 60 Mc. (a) Experimental spectrum. (b) Calculated spectrum with the value 0.277 for the ratio of the spin-coupling constant to the chemical shift.

TABLE II. Representative spin functions of a set of six identical protons.

Spin	3	2	1	0
	Sp_B^3			
	Sp_B^2	Qt_B^2		
	Sp_B^1	Qt_B^1	T_B^1	
	Sp_B^0	Qt_B^0	T_B^0	S_B^0
	Sp_B^{-1}	Qt_B^{-1}	T_B^{-1}	
	Sp_B^{-2}	Qt_B^{-2}		
	Sp_B^{-3}			
Degeneracy	1	5	9	5

as products of the eigenfunctions of $\mathbf{I}_A^2$ and the eigenfunctions of $\mathbf{I}_B^2$. There are eight types of these products:

$$S_AS_B \quad (1) \quad T_AS_B \quad (3)$$

$$S_AT_B \quad (3) \quad T_AT_B \quad (9)$$

$$S_AQt_B \quad (5) \quad T_AQt_B \quad (15)$$

$$S_ASp_B \quad (7) \quad T_ASp_B \quad (21).$$

The numbers in parentheses are the numbers of each type of product functions, and represent the orders of the corresponding subdeterminants into which the secular determinant factors. Each of these eight subdeterminants factors further according to eigenvalues of the operator I_z. Ultimately, the secular equation reduces to a product of sub-subdeterminants of order no larger than three. The solution for the eigenvalues and eigenvectors of these sub-subdeterminants is relatively easy, once the individual matrix elements $\mathcal{H}_{mn}$ are known.

Expressions have been developed,[5,6] which are useful in determination of the individual matrix elements $\mathcal{H}_{mn}$. However, these require a considerable amount of labor, and explicit knowledge of the form of the zero-order spin functions in terms of the simple product spin functions. This can be avoided by finding the entire set of matrix elements $\{\mathcal{H}_{mn}\}$ for given eigenvalues of $\mathbf{I}_A^2$ and $\mathbf{I}_B^2$, directly from the general angular momentum matrices corresponding to these eigenvalues.[4]

Let $\{\phi_A\}$ be the set of eigenfunctions of the operator $\mathbf{I}_A^2$ corresponding to the eigenvalue J_A, and similarly for $\{\phi_B\}$. Then, the secular subdeterminant for the states $\{\phi_A\phi_B\}$ is

$$\begin{aligned}|\mathcal{H}_{mn}-\delta_{mn}E| &= |(\phi_A\phi_B)_m(\mathcal{H}-E)(\phi_A\phi_B)_n| \\ &= |(\phi_A\phi_B)_m(-\omega_AI_{Az})(\phi_A\phi_B)_n| \\ &+ |(\phi_A\phi_B)_m(-\omega_BI_{Bz})(\phi_A\phi_B)_n| \\ &+ |(\phi_A\phi_B)_m(-J\mathbf{I}_A\cdot\mathbf{I}_B)(\phi_A\phi_B)_n| \\ &+ |(\phi_A\phi_B)_m(-E)(\phi_A\phi_B)_n| \\ &= |\omega_AI_z^A\times\mathbf{I}^B-\omega_B\mathbf{I}^A\times I_z^B \\ &-J(I_z^A\times I_z^B+I_y^A\times I_y^B+I_z^A\times I_z^B)-E\mathbf{I}^A\times\mathbf{I}^B|. \quad (3)\end{aligned}$$

[5] McConnell, McLean, and Reilly, J. Chem. Phys. **23**, 1152 (1955).

[6] P. L. Corio, J. Chem. Phys. **29**, 682 (1958)

In this expression $\mathbf{I}_x^A$, $\mathbf{I}_y^A$, and $\mathbf{I}_z^A$ are the matrices of the z component of angular momentum corresponding to the eigenvalue J_A for $\mathbf{I}_A^2$, and $\mathbf{I}^A$ is the unit matrix of order $(2J_A+1)$. The superscript B denotes the corresponding matrices for the eigenvalue J_B.

As an example, the determinant for the states (T_AT_B) is found by use of the angular momentum matrices[7] for $J=1$,

$$\mathbf{M}_x=1/\sqrt{2}\begin{pmatrix}0&1&0\\1&0&1\\0&1&0\end{pmatrix} \qquad \mathbf{M}_y=\tfrac{1}{2}\begin{pmatrix}0&-i&0\\i&0&-i\\0&i&0\end{pmatrix}$$

$$\mathbf{M}_z=\begin{pmatrix}1&0&0\\0&0&0\\0&0&-1\end{pmatrix} \qquad \mathbf{I}=\begin{pmatrix}1&0&0\\0&1&0\\0&0&1\end{pmatrix}$$

$$|\,\mathfrak{IC}_{mn}-\delta_{mn}E\,| = -\omega_A\begin{pmatrix}1&0&0\\0&0&0\\0&0&-1\end{pmatrix}\times\begin{pmatrix}1&0&0\\0&1&0\\0&0&1\end{pmatrix}-\omega_B\begin{pmatrix}1&0&0\\0&1&0\\0&0&1\end{pmatrix}\times\begin{pmatrix}1&0&0\\0&0&0\\0&0&-1\end{pmatrix}$$

$$-J\left\{\tfrac{1}{2}\begin{pmatrix}0&1&0\\1&0&1\\0&1&0\end{pmatrix}\times\begin{pmatrix}0&1&0\\1&0&1\\0&1&0\end{pmatrix}+\tfrac{1}{2}\begin{pmatrix}0&-i&0\\i&0&-i\\0&i&0\end{pmatrix}\times\begin{pmatrix}0&-i&0\\i&0&-i\\0&i&0\end{pmatrix}\right.$$

$$\left.+\begin{pmatrix}1&0&0\\0&0&0\\0&0&-1\end{pmatrix}\times\begin{pmatrix}1&0&0\\0&0&0\\0&0&-1\end{pmatrix}\right\}-E\begin{pmatrix}1&0&0\\0&1&0\\0&0&1\end{pmatrix}\times\begin{pmatrix}1&0&0\\0&1&0\\0&0&1\end{pmatrix}$$

Expanding and rearranging, the secular subdeterminant corresponding to the indicated arrangement of zero-order spin functions is shown in Table III.

The five sub-subdeterminants into which this subdeterminant factors, correspond to the eigenvalues 2, 1, 0, -1, and -2 of the operator I_z. If values are known, (or estimated) for J and δ, it is relatively easy to solve this secular subdeterminant for the nine eigenvalues and the corresponding eigenvectors of the spin Hamiltonian for the states (T_AT_B). Observe that, since Eq. (3) involves direct products of matrices, the matrices need not be of the same orders. That is, the total spin angular momenta of groups A and B need not be equal. Therefore, the seven other subdeterminants corresponding to different spin angular momentum eigenvalues can be evaluated similarly. None of the sub-subdeterminants obtained is of an order larger than three. Thus, the original secular determinant of order 256 can be factored into sub subdeterminants which are relatively easy to solve.

The relative transition probability $P_{(pq)}$ between two states p and q is given by the square of the matrix element of the x component of spin angular momentum between the eigenfunctions of these states. That is,

$$P_{(pq)}=(I_x)_{pq}^2=(\phi_p\,|\,I_x\,|\,\phi_q)^2. \tag{4}$$

Since the operators $\mathbf{I}_A^2$ and $\mathbf{I}_B^2$ commute with I_z, the total spins of these groups are good quantum numbers and transitions from one of the eight states, Eq. (2), to another do not occur. Thus, it suffices to consider only transitions occurring within each of the eight spin states, and the total eigenspectrum problem reduces to eight separate eigenspectrum problems. The complete NMR spectrum of propane is, therefore, made up of eight contributions.

The calculation of the relative transition probabilities from Eq. (4) can be made easier by direct use of angular momentum matrices. Let ϕ_p and ϕ_q be the

[7] See, for example, L. I. Shiff *Quantum Mechanics* (McGraw-Hill Book Company, Inc., New York, 1955).

eigenfunctions of the states p and q, with $P_{(pq)}$ the relative transition probability between these states. Then, in general,

$$\phi_p = \sum_i C_{pi}(\phi_{Ai}\phi_{Bi}),$$

$$\phi_q = \sum_i C_{qj}(\phi_{Aj}\phi_{Bj}),$$

where the set of $\{\phi_{Ai}\phi_{Bi}\}$ is some one of the eight sets of zero-order functions in Eq. (2). Then,

$$P_{(pq)} = \{\sum_i C_{pi}(\phi_{Ai}\phi_{Bi}) \mid I_{Ax}+I_{Bx} \mid \sum_j C_{qj}(\phi_{Aj}\phi_{Bj})\}^2$$

$$= \{\sum_{i,j} C_{pi}C_{qj}[(I_{Ax})_{ij}\delta_{ij}{}^{B}+\delta_{ij}{}^{A}(I_{Bx})_{ij}]\}^2.$$

Here $\delta_{ij}{}^{B}$ equals one if ϕ_{Bi} corresponds to the same eigenvalue of I_z as does ϕ_{Bj}, and $\delta_{ij}{}^{B}$ is zero otherwise. The same is true for $\delta_{ij}{}^{A}$.

The solution for the partial eigenspectra due to each of the eight spin states in Eq. (2) is relatively easy. The factored subdeterminant is solved for the energy levels of the spin system, and used to find the coefficients of the corresponding eigenfunctions. These coefficients are used in Eq. (5) to find relative transition probabilities between the various energy levels of the spin system. The contributions of each of the eight spin states are combined to give the total calculated spectrum.

The contribution of the singlet-singlet (S_AS_B) state is zero, since no transitions can occur. The three states (S_AT_B), (S_AQl_B) and ($S_AS\rho_B$) in which the methylene particle has spin zero contribute a single intense line at frequency ω_B. Similarly, the case (T_AS_B) contributes a single line with frequency ω_A. The remaining three cases, with $I_A=1$ and $I_B=1$, 2, and 3, make more complex contributions with a total of 102 spectral lines. The total spectra for two values of ρ are shown in Figs. 1(b) and 2(b). Not all lines are plotted, since some are too closely spaced to be drawn separately, and others are too weak to appear.

TABLE III. The factored secular subdeterminant for the triplet-triplet state of propane.

$\lvert -\omega_A-\omega_B-J \quad -E \rvert$	$T_A{}^1T_B{}^1$
$\begin{vmatrix} -\omega_B-E & -J \\ -J & -\omega_A-E \end{vmatrix}$	$T_A{}^1T_B{}^0$
$\begin{vmatrix} \omega_A-\omega_B+J-E & -J \\ -J & -E \end{vmatrix}$	$T_A{}^1T_B{}^{-1}$
$\begin{vmatrix} -E & -J \\ -J & -\omega_A+\omega_B+J-E \end{vmatrix}$	$T_A{}^0T_B{}^0$
$\begin{vmatrix} \omega_A-E & -J \\ -J & \omega_B-E \end{vmatrix}$	$T_A{}^{-1}T_B{}^1$
$\lvert \omega_A+\omega_B-J \quad -E \rvert$	$T_A{}^0T_B{}^{-1}$
	$T_A{}^{-1}T_B{}^0$
	$T_A{}^{-1}T_B{}^{-1}$

The calculation of the eigenspectrum of propane for a given value of ρ was done on an IBM 650 computer, which carries out the entire solution in about forty minutes including calculation of moments as checks.

The experimental spectra were obtained from liquid propane sealed in a standard glass sample tube. The spectra were examined with a 40-Mc Varian V-4300 high-resolution spectrometer equipped with a super stabilizer and conversion equipment for 60-Mc determinations.

THE JOURNAL OF CHEMICAL PHYSICS VOLUME 32, NUMBER 1 JANUARY, 1960

Theory of Ortho-Para Hydrogen Separation by Adsorption at Low Temperatures, Isotope Separation*

DAVID WHITE AND EDWIN N. LASSETTRE

Department of Chemistry, The Ohio State University, Columbus, Ohio

(Received July 7, 1959)

A theory of separation of ortho and para hydrogen, by adsorption at low temperatures, is developed by considering the energy levels of a three-dimensional hindered rotator. The Schroedinger equation and boundary conditions are identical with those for prolate spheroidal wave functions and tables of the latter have been employed in calculating the energies as functions of the barrier height. Separation factors, at low surface coverage, have also been computed as a function of barrier height and these pass continuously from unity at zero barrier height over into the limiting separation factor for a two-dimensional rotator (in the adsorbed state) which was used by Sandler in the approximate calculation of separation factors. The theory predicts that ortho hydrogen is more strongly adsorbed than para hydrogen at all barrier heights and that para deuterium is more strongly adsorbed than ortho deuterium. Moreover, the ortho-para hydrogen separation factor is larger at all barrier heights than the para-ortho separation factor for deuterium. These results agree with the experiments of Cunningham, Chapin, and Johnston. Calculated and observed separation factors for hydrogen and deuterium (at low surface coverages) are not in accurate quantitative agreement, however this may be due to the fact that experimental separation factors for both isotopes were not determined under comparable conditions. Calculations have been made first by assuming that rotation and (center of mass) vibration are separable. This model is then refined to take into account the interaction of rotation and vibration.

The separation of the hydrogen-deuterium isotopes is also considered. Although the inclusion of interaction between vibration and rotation does not greatly change the ortho-para separation factors, this effect has a marked influence on the calculated isotope separation factors. It is of considerable interest that isotope separation factors are strongly dependent on the ortho-para composition of the isotope mixture, at least at low surface coverages, in the theory developed here.

I. INTRODUCTION

FOR many years after the discovery of the catalyzed conversion of ortho to para hydrogen, it was believed that because the potential fields of ortho and para hydrogen were nearly identical, the species could not be readily separated. The first indication to the contrary was obtained by Sandler[1] who showed that the adsorption of the ortho and para species on activated charcoal and TiO_2 at 90°K took place to different extents. More recently, a much more exaggerated example of this effect was demonstrated by Cunningham and Johnston[2] in the investigation of the rate of ortho-para hydrogen conversion at liquid hydrogen temperatures, using as a catalyst a paramagnetic salt impregnated in a finely divided alumina support. The conversion rate was nearly independent of the composition of the liquid phase for a substantial fraction of the conversion, which suggested that ortho hydrogen was more strongly adsorbed than para hydrogen at liquid-hydrogen temperatures (20.4°K). This view was conclusively confirmed by Cunningham, Chapin, and Johnston,[3] who were able by successive adsorptions and desorptions to prepare essentially pure ortho hydrogen. It was also demonstrated that ortho-para deuterium could be separated by the same method and, as in the case of hydrogen, the molecules in the rotational state $J=1$ were more strongly adsorbed (para deuterium).

In his initial discussion of this subject, Sandler proposed a theory of separation factors, based essentially on the idea that rotation is hindered for adsorbed molecules. He considered two limiting cases: (one), extreme hindrance, in which the adsorbed molecule behaves as a two-dimensional rotator, and (two), a more extreme hindrance of rotation which leads to a loss of two rotational degrees of freedom (vibrator). The calculated separation factor for ortho-para hydrogen at 90°K, assuming the first limiting case, led to good agreement between theory and experiment,[1] particularly with TiO_2 as the adsorbent. The second limiting case led to a somewhat higher theoretical separation.[1] Since, on such a model, the magnitude of the separation factor is determined primarily by a Boltzmann factor, a more stringent test of the applicability of either limiting case can be made by comparison of theory and experiment at lower temperatures. Such a test can be made using the data of Cunningham *et al.*,[2] where it is found that the calculated separation factor is higher than the observed one by a factor greater than two, when the first limiting case is assumed, and greater by a factor of ten when the second is assumed. It seems evident, in the case of adsorption by alumina, that if the preferential adsorption is due to hindering of rotation, the hindrance is certainly not sufficiently great to lead to loss of two degrees of freedom, and probably not even one.

In an effort to resolve this problem in hydrogen as well as to account for the observed separation factor of deuterium, we have further investigated the theory of ortho-para separation factors of the hydrogen isotopes. The rotational energies are calculated (in fields which involve hindering potentials) as a function

* This work was supported in part by the Division of Research of The U. S. Atomic Energy Commission.

[1] Y. L. Sandler, J. Phys. Chem. **58**, 58 (1954).

[2] C. M. Cunningham and H. L. Johnston, J. Am. Chem. Soc. **80**, 2377 (1958).

[3] Cunningham, Chapin, and Johnston, J. Am. Chem. Soc. **80**, 2382 (1958).

of barrier height. Although the Schroedinger equation for a hindered three-dimensional rotator is not of the Mathieu type, it can nevertheless be reduced to a form which has been studied by others, and hence the separation factor can be calculated as a function of barrier height. In this way, as is shown in the following sections, the trend of the separation factor can be traced through from the extreme of no separation on one hand, to the extremes suggested by Sandler. This is done in a first approximation in which rotation and vibration (relative to the surface) are separable, and also to a higher degree of accuracy in which the interaction of rotation and vibration is taken into account, at least approximately.

It is interesting to note that the ortho-para separation factors for hydrogen and deuterium at the same temperature are quite different. This suggests that the separation of isotopes by preferential adsorption should be influenced by the concentration of the spin species of each of the isotopes. Any theory accounting for the magnitude of the ortho-para separation factors in the hydrogen isotopes should also predict the variation in the magnitude of the isotope separation factor as a function of the ortho-para concentration in each of the isotopes. A theory of this effect is also developed here, although there are, as yet, no precise data at low-surface coverages with which the theory can be compared.

II. ROTATIONAL ENERGY LEVELS FOR AN ADSORBED DIATOMIC MOLECULE

Let us adopt a model for the adsorbed homonuclear diatomic molecule similar to that proposed by Hill.[4] If the surface of the adsorbent is parallel to the $x-y$ plane, z, the distance of the center of mass of the molecule from the surface, and θ $(0\leq\theta\leq\pi)$, the angle the axis of the molecule makes with the z axis, then we assume that the interaction of molecule with the adsorbent is a function only of z and θ. A mobile adsorbed layer is therefore assumed. It is not fully established that this assumption is adequate at temperatures as low as 20°K. We have nevertheless employed this potential for purposes of exploratory calculations with the understanding that further refinements may ultimately be needed. At much lower temperatures it seems certain that some account must be taken of the dependence of potential on x and y.

In order to obtain the energy levels for an adsorbed molecule it is necessary to solve the Schroedinger equation for the Hamiltonian[4]

$$H=(p_x^2/2M)+(p_y^2/2M)+(p_z^2/2M)+(p_\theta^2/2I)+(p_\phi^2/2I\sin^2\theta)+V(z,\theta), \quad (1)$$

where M is the mass of the molecule, I the moment of inertia, and $V(z,\theta)$ the potential energy of interaction of the molecule with the surface. To separate the variables in the Schroedinger equation, one can write for the eigenfunction

$$\psi=F(x,y)G(\phi)R(z,\theta).$$

From the F equation one obtains the energy levels for a particle of mass M in a two-dimensional box

$$G(\phi)=[(2\pi)^{\frac{1}{2}}]^{-1}\exp(im\phi); \quad m=0,\pm1,\pm2,\cdots$$

and the R equation is

$$-(h^2/8\pi^2M)(\partial^2R/\partial z^2)-(h^2/8\pi^2I)\cdot\{(1/\sin\theta)(\partial/\partial\theta)[\sin\theta(\partial R/\partial\theta)]-(m^2/\sin^2\theta)R\}+V(z,\theta)R=WR. \quad (2)$$

From symmetry considerations it can be shown that V is a function of $\cos^2\theta$, $V(z,\cos^2\theta)$, regardless of the exact form of the potential function. By setting $\cos^2\theta=\eta^2$, and expanding $V(z,\eta^2)$ in a Taylor series about $z=z_0$ (the distance from the surface at equilibrium) and $\eta^2=0$ one obtains

$$V(z,\eta^2)=V(z_0,0)+\eta^2(\partial V/\partial\eta^2)+(z-z_0)^2(\partial^2V/\partial z^2)+\cdots$$
$$=V_0+C\eta^2+K(z-z_0)^2+\cdots, \quad (3)$$

where V_0, C, and K are constants. As a first approximation let us neglect the higher terms in the series so that the variables become separable. By setting

$$R(z,\theta)=H(z)\Theta(\theta),$$

and substituting Eq. (3) into Eq. (2) we obtain in the usual way

$$(d^2H/dz^2)+(8\pi^2M/h^2)(E_z-Kz^2)H=0\cdots \quad (4)$$

and

$$(d/d\eta)[(1-\eta^2)(d\Theta/d\eta)]+(8\pi^2I/h^2)\cdot\left(E_{\theta\phi}-C\eta^2-\frac{m^2h^2}{(1-\eta^2)8\pi^2I}\right)\Theta=0, \quad (5)$$

where

$$W+V_0=E_z+E_{\theta\phi}.$$

Equation (4) is simply the equation for an harmonic oscillator, the energy levels being

$$E_z=(n+1/2)h\nu, \quad n=0,1,2,\cdots,$$

where ν is the frequency for the oscillation of the molecule normal to the surface. This frequency can be evaluated provided the potential function is specified. This has been done by Hill[4] for a Lennard-Jones type potential function.

The form of the differential equation (5) is fortunately identical to one obtained in the treatment of the hydrogen molecule ion and also in separating variables in the Helmholtz wave equation (for sound or light) in spheroidal coordinates. The boundary conditions for

[4] T. L. Hill, J. Chem. Phys. **16**, 181 (1948).

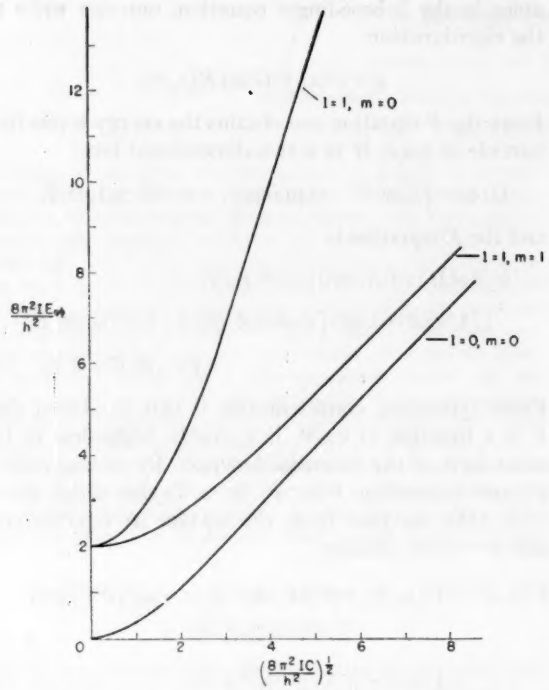

FIG. 1. Rotational energy as a function of barrier height, C.

Eq. (5) are that Θ shall be bounded and single valued at $\eta = \pm 1$. Eigenvalues, obtained by applying the same boundary conditions, have been calculated by others. Employing the table of Stratton *et al.*,[5] $E_{\theta\phi}$ for the ground state and two excited states have been calculated and are shown in Fig. 1. Each state of the hindered rotator correlates, in the limit of zero barrier height, with some state of the free rotator and hence the states have been identified with the rotational quantum numbers l, m, of the correlating state of the free rotator whose energy is $l(l+1)h^2/8\pi^2 I$. The center of mass coordinate z is equal to $\frac{1}{2}(z_1+z_2)$ where z_1, z_2 are the distances of the hydrogen atom from the surface. It follows that z is invariant under the operation of exchanging the nuclei, hence the function H of Eq. (4) is invariant. Exchange of nuclei replaces the rotational variables θ, ϕ by $\pi-\theta, \phi+\pi$. It is easy to verify from the expansions of reference 5 (in series of associated Legendre functions) that the functions $\Theta(\theta)e^{im\phi}$ behave under this transformation in the same way as the free rotator functions with which these correlate (these are associated Legendre functions P_l^m), i.e., the function changes sign if l is odd and remains invariant if l is even. Thus the nuclear spin function must be symmetric when l is odd (ortho states) and antisymmetric when l is even (para states) for hydrogen, in order to satisfy the requirements of the Fermi-Dirac statistics. In the case of deuterium, to which the Bose-Einstein statistics apply the spin function must be antisymmetric with l odd (para states) and symmetric with l even (ortho states).

Of the three states shown in Fig. 1, the two of highest energy are ortho states for hydrogen while that of lowest energy is a para state. It is to be noted that the energy difference between the lowest two states decreases as C increases, and approaches at large C to $h^2/8\pi^2 I$. This is just the energy difference for the two lowest states of a plane rotator and hence should lead to the separation factor computed by Sandler. As explained below, the energy difference between these two states is the primary factor in dealing with the separation of ortho and para hydrogen (or deuterium) since this determines the difference in adsorption energies of the two species. When, however, we consider the separation of hydrogen and deuterium isotopes the variation of energy of the state $l=0$, $m=0$ with barrier height is also important as will become evident in section V where isotope separation factors are discussed.

We have been treating the adsorbed molecule as moving in a static potential field [Eq. (3)] arising from the adsorbing solid. A straightforward application of statistical mechanics to the population of ortho and para states of the gas and adsorbed phases leads to the following expression for the separation factor:

$$S^{H_2} = (Q_p/Q_0)\ \text{gas}/(Q_0/Q_p)\ \text{ads.},$$
$$S^{D_2} = (Q_0/Q_p)\ \text{gas}/(Q_0/Q_p)\ \text{ads.} \qquad (6)$$

Here Q_0, Q_p are partition functions for the ortho and para hydrogen or deuterium as the case may be. These are complete partition functions in the sense that total molecular energies (translation, vibration, rotation) are involved. When translation, vibration, and rotation are separable, these relations can be simplified considerably and, in fact, only the ratios of rotational partition functions fail to cancel. Because of the extremely low temperatures involved only the three states shown in Fig. 1 need be considered in the treatment of separation factors at liquid hydrogen temperatures. Under these conditions the equation

$$S = \tfrac{2}{3}\exp\{[l(l+1)h^2/8\pi^2 kT] - (E_1^1 - E_0^0)/kT\}$$
$$+\tfrac{1}{3}\exp\{[l(l+1)/8\pi^2 kT] - (E_0^1 - E_0^0)/kT\} \qquad (7)$$

gives the separation factor for either hydrogen or deuterium if appropriate values of I and the energies are employed. Here the symbol E_m^l is used to designate the energy of that state which correlates with the state l, m of the free rotator. With the energies of Fig. 1, together with Eq. (7), separation factors have been calculated for both hydrogen and deuterium at 20.4°K and the results are given as a function of barrier height, C(kcal), in Fig. 2. We note that these separation factors approach, as C becomes large, to the limits

[5] Stratton, Morse, Chu, Chittle, and Corbato, *Spheroidal Wave Functions* (The Technology Press of Massachusetts Institute of Technology and John Wiley & Sons, Inc., New York, 1956).

obtained by Sandler for the two-dimensional rotator. The trends shown in the figure are in qualitative agreement with experiment in two important respects. First, ortho hydrogen is more strongly adsorbed than para hydrogen not only in the Sandler limit but at all intermediate stages and, moreover, para deuterium is more strongly adsorbed than is ortho deuterium. Second, the separation factor for deuterium is consistently smaller than that for hydrogen. Before attempting a quantitative comparison between theory and experiment it is necessary to briefly describe the low-temperature experimental results to which the theory is applicable.

Separation factors have been determined in two ways at 20.4°K. First, the rate studies of Cunningham and Johnston were interpreted in terms of preferential adsorption of ortho hydrogen, and separation factors are calculated from the rate data. In this way an ortho-para hydrogen separation factor of 16.±3 was obtained.[2] The separation here is between liquid hydrogen and an adsorbed film. The adsorbent was alumina impregnated with a paramagnetic salt. The mechanism of conversion is one in which spin reversal is caused by action of a magnetic ion on the hydrogen nucleus and this occurs only when the ion and the hydrogen molecule are in close proximity. It seems reasonable to assume therefore that ortho-para conversion is occurring in the first physically adsorbed monolayer and that the separation refers to this layer relative to the remainder of the mixture. If the present theory is to be applied to this case† then from Fig. 2 it is clear that a separation factor of 16 is attained with a barrier of $C=2.35$ kcal. If comparable experiments were carried out for deuterium then the same barrier height is to be expected, according to this theory at least, and a separation factor of 4.1 is predicted. Since no similar rate experiments were carried out with deuterium we have no experimental value with which to make a comparison. However, the separation of ortho-para hydrogen and para-ortho deuterium was studied using a second method by Cunningham, Chapin, and Johnston.[3] In these experiments gas was adsorbed to the extent of approximately a monolayer and the percentage of ortho hydrogen or para deuterium was determined at various states of desorption. If a separation factor is calculated from the composition of the last desorbed gas and the feed gas, a value of 2.4 is obtained for the para-ortho deuterium separation factor. This is substantially less than the predicted value of 4.1. However, the predicted value of 4.1 refers to adsorption, from the liquid, on alumina impregnated with a paramagnetic salt while the observed value, 2.4, refers to adsorption from the gas phase on alumina without any added salt. Moreover, we are

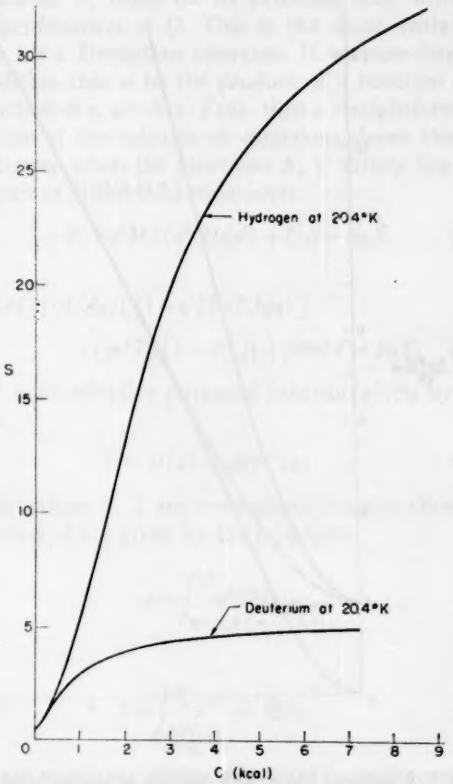

FIG. 2. Ortho-para separation factor for hydrogen as a function of barrier height. Para-ortho separation factor of deuterium as a function of barrier height.

comparing a separation factor calculated from a formula, Eq. (7), which assumes equilibrium between gas and adsorbed phase. Since the adsorbent had to be heated on desorption it is not certain that the desorbed sample has the composition of the adsorbed layer which was initially in equilibrium with the feed. Consideration of the experiments on hydrogen is complicated by the fact that a slow but nonnegligible conversion of ortho to para hydrogen accompanied the desorption. If, however, we calculate a separation factor from the gas analysis corresponding to maximum percent ortho hydrogen (see Fig. 1 of reference 3) and correct for conversion, a value of 16 is obtained. This agrees well with that obtained from the rate data. If we also calculate separation factors from corrected analytical data obtained beyond the maximum, then lower separation factors are obtained, the grand average being approximately 8. The uncertainty here is obviously large. If we tentatively accept the average (8) then the deuterium separation factor calculated from the theory is 3.3 which agrees better with the observed separation factor of 2.4.

In view of the situation discussed above, it is not clear how accurately the theoretical and experimental separation factors can be expected to agree. Neverthe-

† The small effect, arising from differences in ortho-para composition between the liquid and gas phases in equilibrium is neglected. That this effect is small is evident from the vapor pressure data of ortho and para hydrogen. See Wooley, Scott, and Brickwedde, J. Research, Natl. Bur. Standards **41**, 379 (1948).

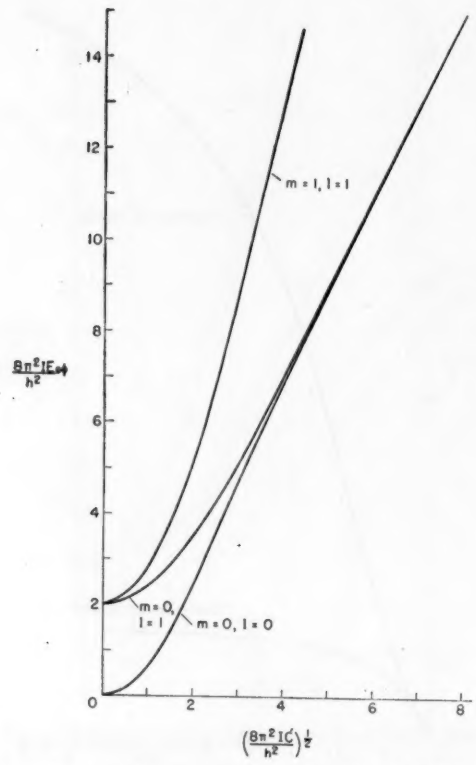

FIG. 3. Rotational energy as a function of barrier height, C'.

less, the possibility remains that the crude potential function of Eq. (3) may be inadequate, and hence several refinements have been considered. The first of these is described in the following.

III. ROTATIONAL ENERGIES FOR ADSORBED DIATOMIC MOLECULE IN WHICH EQUILIBRIUM POSITION OF MOLECULAR AXIS IS PERPENDICULAR TO PLANE OF SURFACE

In the potential function of Eq. (3) it has been tacitly assumed that $C>0$. Minimum energy is thus attained when the molecule is oriented parallel to the surface. If, however, $C<0$, then the equilibrium orientation is perpendicular to the surface. It is more convenient to expand in powers of $\sin^2\theta$. In this case the term $C\eta^2$ of Eq. (3) is replaced by $C'\sin^2\theta$. If $C'>0$ then the equilibrium orientation is perpendicular to the surface. Equation (5) is then replaced by one containing $C'(1-\eta^2)$ instead of $C\eta^2$. Solutions to this equation, bounded at $\eta=\pm1$, have also been tabulated by Stratton *et al.* (their oblate spheroidal wave function). When energies are calculated from these tables the results of Fig. 3 are obtained for the three states of lowest energy. This figure differs from Fig. 1 in two important ways. First, the two levels $l=1$, $m=1$ and $l=1$, $m=0$ are reversed in energy, and second, the energies of the two lowest energy states approach each other as C' increases. Hence the limiting separation factor approached is not that obtained assuming a two-dimensional rotator for the adsorbed molecule but a vibrator. Separation factors computed using Eq. (7) are given in Fig. 4. An ortho-para hydrogen separation factor of 16 is obtained when $C'=0.69$ kcal, and the para-ortho deuterium separation factor calculated for the same C' is 7.5. If a value of 8 is taken for hydrogen then the separation factor for deuterium calculated from the same C' is 4.5. Both calculated separation factors for deuterium disagree with the observed value of 2.4 by an even greater percentage than found in the last section. In view of the experimental uncertainty in the relative separation factors for hydrogen and deuterium it would be premature to conclude that this model has been *decisively* eliminated. However, the present experimental data certainly do not favor this model and we have not considered it further.

IV. HIGHER APPROXIMATIONS IN TREATMENT OF HINDERED SURFACE ROTATOR

By using the first three terms of a power series expansion [Eq. (3)] the potential becomes separable in the variables η, z. Where complete rotations are involved, however, this is apparently a poor approximation. Hill[4] has shown, using a plausible potential function, that the potential barrier calculated by assuming rotation around the equilibrium position ($z=z_0$) may be greater, by more than a factor of ten, than that calculated by permitting the molecular center of mass

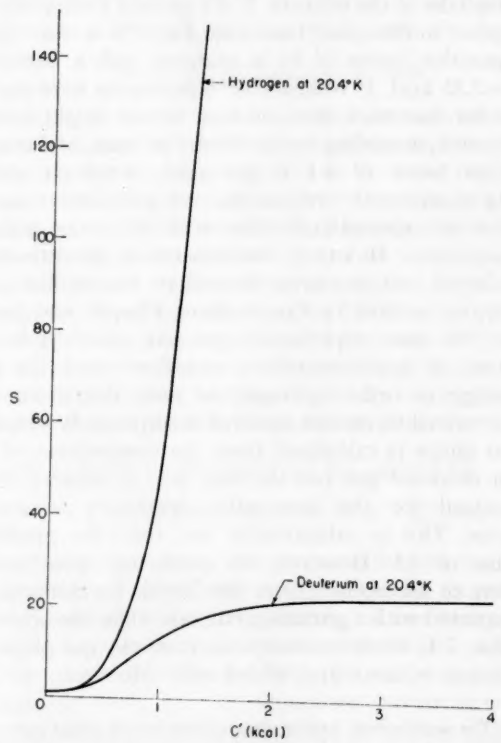

FIG. 4. Ortho-para separation factor for hydrogen as a function of barrier height. Para-ortho separation factor of deuterium as a function of barrier height.

to change position during rotation so that minimum energy is maintained at each angle. Although this extreme variation is obtained for diatomic molecules with internuclear distances much greater than for hydrogen, nevertheless, even for hydrogen this effect is not negligible. Thus the potential is not expressible as a sum of functions of z and η and the variables are not separable. If, in fact, the surface potential function be expanded in a power series in η, then the coefficient of η^2 is not a constant but is instead a rather rapidly varying function of z. It may still be possible to employ an approximation equivalent to the assumption that the potential is separable in the form $V(z)+C\eta^2$ but C must be some sort of average of the coefficient of η^2 that has been mentioned. This average may well differ for hydrogen and deuterium, i.e., may be mass dependent. Thus the adoption of a separable form of potential function as an approximation to the actual potential field carries with it the implication that C, the barrier height, will differ for hydrogen and deuterium. In order to quantitatively assess the importance of this factor some means must be found for accurate definition of the average involved in C. This problem is discussed in the remainder of this section which contains as well the results of numerical calculations using a special potential function.

We consider a molecule under the influence of a surface field. For simplicity we assume that each atom of the (diatomic) molecule interacts with the surface in accordance with the potential function $f(z_i)$ where z_i is the distance of the ith atom from the surface measured normal to the surface. Then the potential energy of the molecule is

$$V=f(z+b\cos\theta)+f(z-b\cos\theta), \tag{8}$$

where z, θ are the same variables previously used, and b is one-half the internuclear distance. If we expand in a power series in $\eta=\cos\theta$ we obtain

$$V=2f(z)+f''(z)b^2\eta^2+\cdots, \tag{9}$$

where f'' is the second derivative. When f is a typical potential function, with one minimum and a dissociation limit, the potential of Eq. (9) takes on its minimum (with respect to both z and θ) when the molecule is oriented with axis parallel to the surface.

When the potential of Eq. (9) is used the variables in Eq. (2) are not separable in any exact sense. Nevertheless, the condition for separability can be imposed arbitrarily by means of an application of the variation theorem in the following manner. Let the operator on the left of Eq. (2) be designated by Q so that Eq. (2) becomes $QR=WR$. Then, since Q is Hermitian, the quantity

$$E=\int uQu\,d\tau \Big/ \int u^2 d\tau \tag{10}$$

where u is a function obeying the same boundary conditions as R, takes on its extremes only when u is an eigenfunction of Q. This is the usual variation theorem for a Hermitian operator. If we now impose the condition that u be the product of a function of z by a function of η, $u=S(z)\,T(\eta)$, then a straightforward application of the calculus of variations shows that E is an extreme when the functions S, T satisfy the following pair of differential equations:

$$(-h^2/8\pi^2M)\,(d^2S/dz^2)+US=E_1S \tag{11}$$

and

$$(-h^2/8\pi I)\,\{(d/d\eta)[(1-\eta^2)\,(dT/d\eta)] -[m^2T/(1-\eta^2)]\}+\beta b^2\eta^2T=E_2T. \tag{12}$$

Here U is an effective potential function given by the formula

$$U=2f(z)+\alpha b^2 f''(z). \tag{13}$$

If the functions S, T are normalized to unity then the constants α, β are given by the equations

$$\alpha=\int_{-1}^{+1}\eta^2T^2d\eta \tag{14}$$

and

$$\beta=\int_{-\infty}^{\infty}f''(z)\,S^2dz. \tag{15}$$

E_1, E_2 are constants whose values are to be determined by imposing the usual boundary conditions on S, T. It is notable that Eq. (12) has precisely the same form as Eq. (5) with C replaced by βb^2. This, in conjunction with Eq. (15), defines the average value referred to in the foregoing. Since the eigenfunction T depends on β, and S depends on α, it follows that Eqs. (14) and (15) constitute a pair of simultaneous equations in the quantities α, β. Numerical values of α, β are obtained by solving this pair of equations.

In order to apply Eqs. (11–15) to the present problem some specific form for the function f must be employed. We have used a Morse type function for f:

$$f=(D/2)\,\{e^{-2az}-2e^{-az}\}, \tag{16}$$

where D and a are constants. This function has qualitatively the correct form but no doubt represents the potential at large z less accurately than that of Hill. Nevertheless, Morse type functions have been used by others[6] to represent the potential interaction of a molecule with a surface and this representation seems adequate for the present application. This function is especially convenient in the present application since Eq. (11) can be solved in general terms. With this assumption the potential function U of Eq. (13) becomes

$$U=(1+2\alpha y)\,De^{-2az}-(2+\alpha y)\,De^{-az}, \tag{17}$$

[6] J. E. Lennard-Jones and C. Strachan, Proc. Roy. Soc. (London) **A150**, 442 (1935).

with $y=(ab)^2$. With this function for U Eq. (11) can be transformed by the following changes of both dependent and independent variables:

$$x=e^{-az}\gamma, \tag{18}$$

$$S=G/(x)^{\frac{1}{2}}, \tag{19}$$

and

$$\gamma=(4\pi/ah)[2MD(1+2\alpha y)]^{\frac{1}{2}}. \tag{20}$$

The resulting equation is

$$(d^2G/dx^2)+\{[(1-\mu^2)/4x^2]+(B/x)-(\tfrac{1}{4})\}G=0, \tag{21}$$

where

$$\mu=(4\pi/ah)(-2ME_1)^{\frac{1}{2}}, \tag{22}$$

and

$$B=(\pi/ah)(2MD)^{\frac{1}{2}}[(2+\alpha y)/(1+2\alpha y)^{\frac{1}{2}}]. \tag{23}$$

Equation (21) is the differential equation for confluent hypergeometric functions and has solutions which vanish at both $x=0$ and $x=\infty$ if, and only if,

$$B=\tfrac{1}{2}(\mu+1)+n \tag{24}$$

where n is an integer. The function G then has the form $G=e^{-x/2}x^{(\mu+1)/2}L_n^{(\mu)}(x)$ where $L_n^{(\mu)}$ is an associated Laguerre polynomial. The notation employed is that of Szego.[7] The function S is then necessarily given by formula

$$S=Ne^{-x/2}x^{\mu/2}L_n^{(\mu)}, \tag{25}$$

where N is a normalizing constant. With the recursion formulas of reference 7, the following results are obtained for N^2 and β:

$$N^{-2}=(1/a)\int_0^\infty e^{-x}x^{\mu-1}(L_n^{(\mu)})^2dx$$

$$=(1/a)\sum_{m=0}^{n}[\Gamma(n-m+\mu)/(n-m)!] \tag{25a}$$

and

$$\beta=(Da/\gamma N^{-2})\int_0^\infty e^{-x}x^{\mu}(L_n^{(\mu)})^2[(2x/\gamma)-1]dx$$

$$=\frac{Da^2}{\gamma}\,\frac{\Gamma(n+\mu+1)}{n!}\,\frac{\{[2(2n+\mu+1)/\gamma]-1\}}{\sum_{m=0}^{n}[\Gamma(n-m+\mu)/(n-m)!]}. \tag{26}$$

In order that the normalizing integral be convergent it is essential that μ be positive. Using Eqs. (21) and (22) for μ, A, it is obvious that Eq. (24) determines the eigenvalues of E_1. It is clear from Eq. (21) that μ is real only when E_1 is negative, and the solution (25) applies only in this case. When E_1 is positive solutions also exist which are bounded (but nonvanishing) at $z=\infty$ corresponding to a dissociation continuum. These solutions are not of interest at low temperatures.

At sufficiently low temperatures only the lowest vibrational state is occupied and hence the state with $n=0$ is of greatest interest in the present research. In this special case we find from Eqs. (20), (23), (24), and (26) that

$$\gamma=2\lambda(1+2\alpha y)^{\frac{1}{2}}, \tag{27}$$

$$\beta=(Dy/b^2)(\mu/\gamma)\{[2(\mu+1)/\gamma]-1\}, \tag{28}$$

and

$$\mu+1=\frac{2\lambda[1+(\alpha y/2)]}{(1+2\alpha y)^{\frac{1}{2}}}. \tag{29}$$

Here $\lambda=(2\pi/ah)(2MD)^{\frac{1}{2}}$. Equation (28), together with (27), (29), and definitions of λ, y provides the relation between β and α arising from Eq. (15) when f is the Morse type function of Eq. (16). We now need a second relation between α and β as given by Eq. (14). Since the solutions T to Eq. (12) are known only through numerical tables such as those of Stratton *et al.*[5] it follows that no simple, and general, functional form is available and this second relation must be exhibited as a numerical table or graph. On comparing Eq. (12) with the standard form of Stratton *et al.* it is clear that the quantity h^2 used by these authors is equal to the quantity $(8\pi^2I/h^2)\beta b^2$. The notation can be simplified by the definition of a new quantity $Z=\beta b^2/Dy$. Then from Eqs. (27–29)

$$Z=\left[\frac{1+(\alpha y/2)}{1+2\alpha y}-\frac{1}{2\lambda(1+2\alpha y)^{\frac{1}{2}}}\right]\left(\frac{1-\alpha y}{1+2\alpha y}\right). \tag{30}$$

Since the moment of inertia $I=Mb^2$ it follows that $\lambda=(8\pi^2ID/yh^2)^{\frac{1}{2}}$ and

$$(8\pi^2I/h^2)\beta b^2=\lambda^2y^2Z. \tag{31}$$

Equation (12) can now be rewritten in the following form:

$$(d/d\eta)[1-\eta^2)(dT/d\eta)]-[m^2T/(1-\eta^2)]$$

$$-h_1^2\eta^2T+AT=0, \tag{32}$$

where

$$h_1^2=\lambda^2y^2Z, \tag{33}$$

and

$$A=(8\pi^2I/h^2)E_2. \tag{34}$$

If a solution to Eq. (32) is available in the form of a series expansion in terms of associated Legendre functions as follows:

$$T=\sum_{l=|m|}d_lP_l^m(\eta), \tag{35}$$

then a convenient expression for α can be found if we

[7] G. Szego, *Orthogonal Polynomials* (Am. Math. Soc. Publications, New York, 1939).

multiply (32) by T and integrate. Then

$$\alpha=\int_{-1}^{+1}T^2\eta^2d\eta=(1/h_1^2)\left[A+\int_{-1}^{+1}T\left\{\left(\frac{d}{d\eta}\right)(1+\eta^2)\frac{dT}{d\eta}\right]\right.$$
$$\left.-(m^2T/(1-\eta^2))\right\}d\eta\Bigg]$$
$$=(1/h_1^2)\left[A-\sum_{l=|m|}^{\infty}d_l^2l(l+1)\int_{-}^{+1}(P_l^{|m|})^2d\eta\right]$$
$$=(1/h_1^2)\left[A-\sum_{l=|m|}^{\infty}d_l^2l(l+1)[2/(2l+1)]\frac{(l+|m|)!}{(l-|m|)!}\right]. \quad (36)$$

In the last two steps Eq. (35) has been used, together with the differential equation for associated Legendre functions, to express the average value of η^2 as an infinite series. Equation (36) is quite convenient for numerical calculation and has been used in the calculation of α. In obtaining Eq. (36) it has been assumed that the function T is normalized to unity. Although the tables of Stratton *et al.* give the coefficients of series similar to Eq. (35) the functions tabulated are not normalized to unity. It is necessary therefore to multiply the function employed in compiling these tables by a normalizing factor in order to utilize Eq. (36) This is easily done and the values of α calculated in this way for three states are shown in Table I. Since h_1 is expressed in terms of Z, by Eq. (33) it follows that for particular values of λ, y α is known as a function of Z. Moreover, a second relation between α and Z is given by Eq. (30). Thus we have two relations between α and Z, one given by Eq. (30) and the other implied by a numerical table (Table I). If a graph of α *vs* Z be prepared using Eq. (30) and particular values of λ, y and another curve of α *vs* Z be plotted on the same graph using Table I and Eq. (33) then the intersection of the two curves provides a pair of values for α, Z which are simultaneously compatible with both relations. An example is shown in Fig. 5 which contains one curve computed from Eq. (30) and three curves showing α as a function of Z for the three states of Table I. Since the three intersection points are all different it is clear from Eq. (33) that the values of

TABLE I.

h_1^2	$l=0$ $m=0$ α	$l=1$ $m=0$ α	$l=1$ $m=1$ α
0	0.3333	0.6000	0.2000
0.25	0.3261	0.5971	0.1985
1.0	0.3052	0.5859	0.1913
4.0	0.2383	0.5430	0.1689
9.0	0.1726	0.4713	0.1414
16.0	0.1287	0.3856	0.1163
25.0	0.1017	0.3106	0.0966
36.0	0.0842	0.2559	0.0818

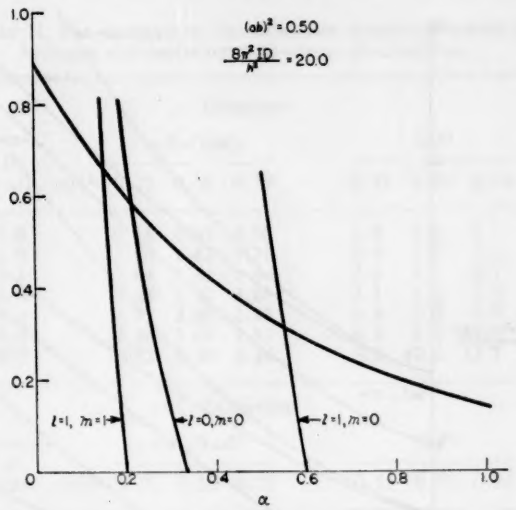

FIG. 5. Illustration of simultaneous solution of Eqs. (14) and (15).

h_1, and hence of the effective barrier heights, are different for the three states. Such calculations have been carried out for a whole range of values of λ and for $y=(ab)^2=1/4,\ 1/2,\ 3/4$. The intersection points were determined graphically in all cases. Since Z is proportional to β the determination of each intersection point is equivalent to the simultaneous solution of Eqs. (14) and (15) discussed previously. These graphical calculations have been checked for a few values of h_1 by a numerical method described in the Appendix.

Once the values of α, Z appropriate to each state have been computed then the total energy (E_T) can be calculated. For this purpose we use Eq. (10) with potential given by Eq. (9) and f from Eq. (16). For u we use $u=ST$ with S given by Eq. (25) with $n=0$. After evaluating the integrals over z this gives

$$(8\pi^2I/h^2)E_T=(8\pi^2I/h^2)E_1+(8\pi^2I/h^2)E_2-\alpha h_1^2. \quad (37)$$

The quantity E_1 can be calculated from Eqs. (22) and (29). We have made such calculations only for $n=0$. The quantity $(8\pi^2I/h^2)E_2=A$ [see Eqs. (32) and (34)] can be obtained from the tables of Stratton *et al.* To assist in comparing with the results of Sec. II, the quantity $(8\pi^2I/h^2)(E_T+D)$ has been calculated as a function of $[(8\pi^2I/h^2)D]^{\frac{1}{2}}$. E_T+D is the energy relative to the minimum possible potential energy. These calculated energies are shown in Fig. 6. Ordinates of the curves with $y=\frac{1}{2}$ and $\frac{3}{4}$ have been shifted up by 4 and 8 units, respectively. Each set of curves is somewhat similar in form to Fig. 1. The values for the parameter y, used in the calculation, were chosen such that the resulting potential functions, between the two extremes, are applicable to the adsorption of the hydrogen isotopes on alumina. The range in fact is probably sufficiently large to account for the adsorp-

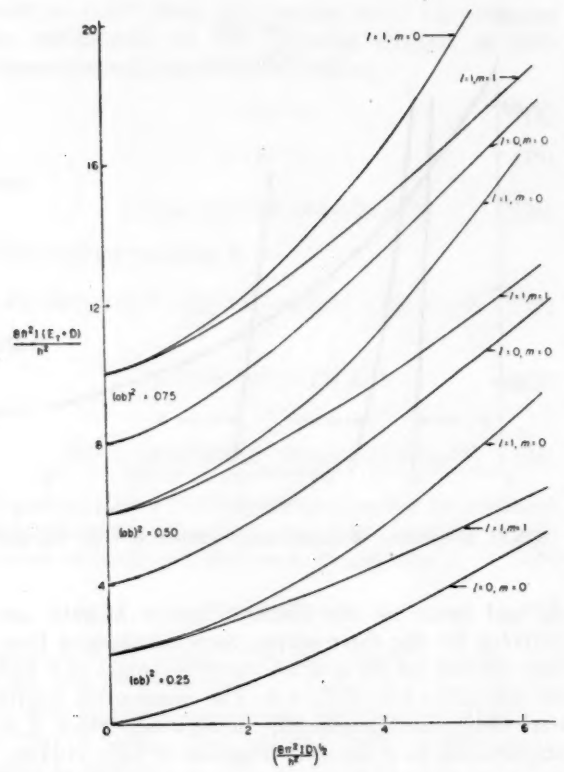

FIG. 6. Total energy (rotation and vibration) as a function of D for three values of $(ab)^2$.

tion of the hydrogen isotopes on most common adsorbents. The range of y was established by expansion of the Hill potential[4] in a Taylor series about the minimum, and comparing with the expanded form of the Morse function [Eq. (9)]. If it is required that the two expansions agree up to and including the square terms, then it is found that

$$a \approx 4.8/r_0,$$

where r_0 is the equilibrium distance of separation of an hydrogen atom, in the molecule, from an adsorbate atom. For an alumina adsorbate a value of $r_0 \approx 2.6$ A can be estimated from the van der Waals radii[8] of hydrogen and oxygen. Since b for all the hydrogen isotopes is the same and equal to 0.371 A, then $(ab)^2 = y \approx \frac{1}{2}$. Recognizing the approximations involved in arriving at this value a range of y was chosen, within which this value falls, which was sufficiently large to reasonably account for the physical situation. The ortho-para separation factors for hydrogen, $S_{0p}^{H_2}$, and para-ortho separation factors for deuterium, $S_{p0}^{D_2}$, calculated from the energy levels are shown in Figs. 7 and 8, respectively. These curves are similar to the ones in Fig. 2, except that the Sandler limit (two-dimensional rotator) is not reached for any of the values of y even when D is as high as 6 kcal.

The absolute value of the quantity E_T gives the energy change accompanying the removal of molecules from the quantum state considered to the gas phase with zero kinetic energy. If the lowest energy state is considered ($l=0$, $m=0$)‡ then this quantity will be approximately the adsorption energy of para hydrogen or ortho deuterium at such low temperatures that only the ground states are occupied. This quantity, together with separation factors, is given in Table II. For heterogeneous surfaces the calculated energies of adsorption should be identified with differential energies of adsorption on nearly bare surfaces. There are no experimentally determined differential energies of adsorption of hydrogen (or deuterium) on alumina which can be used to establish the range of expected separation factors, however it would not be reasonable to assume values greater than a few kcal for physical adsorption. The data of Van Dingenen and Von Itterbeck,[9] for the adsorption of hydrogen on charcoal, suggest values in the range 0.5 to 2.5 kcal.

It is evident from the table that the separation factor for hydrogen of 16 reported by Cunningham *et al.*[2] is

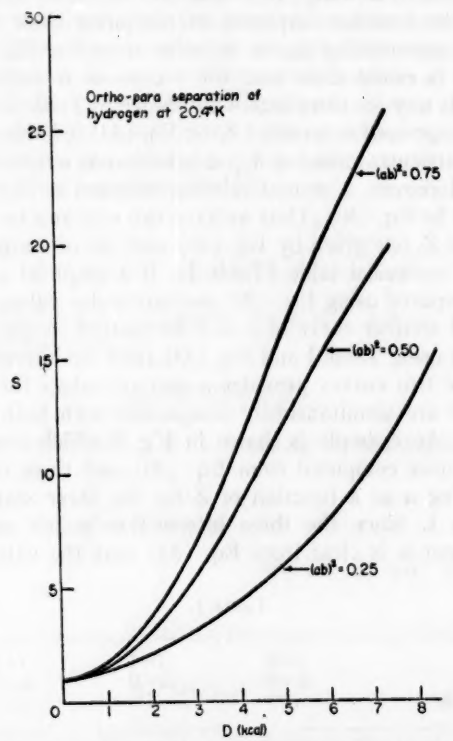

FIG. 7. Ortho-para separation factor for hydrogen as a function of D at three values of $(ab)^2$.

[8] L. Pauling, *Nature of the Chemical Bond*, (Cornell University Press, Ithaca, New York, 1940), second edition.

†† In a mixture containing both ortho and para species, the energy of adsorption would be only a few calories different from those given in Table II.

[9] W. Van Dingenen and A. Von Itterbeck, Physica **6**, 49 (1939).

obtained for $y=\frac{3}{4}$ with an energy of adsorption of approximately 3.5 kcal. Furthermore the para-ortho separation factor for deuterium computed for the same y and D gives a value somewhat larger than 4. This is still considerably larger than the 2.4 discussed in Sec. II; however, a careful inspection of the theory strongly suggests that $S_{p0}^{D_2}$ will not be as small as 2.4 on the same surface as that for which $S_{0p}^{H_2}=16$. For if one assumes a given value for the ortho-para separation factor of hydrogen and determines the D corresponding to this value for all values of y given, it is found that the predicted para-ortho separation factor for deuterium changes but little (less than 10%) with change in y. The theory therefore suggests that regardless of the magnitude of a for the potential function the ratio of ortho-para separation factor for hydrogen to para-ortho separation factor of deuterium is fixed. In view of this situation it seems clear that the separation factors should be further studied experimentally.

V. ISOTOPE SEPARATION

Although the separation of ortho-para hydrogen and ortho-para deuterium is primarily dependent on rotational energy, the separation of hydrogen and deuterium isotopes, without regard to spin state, depends on *total* energy. Thus both isotope separation factors and ortho-para hydrogen or deuterium separation factors are important in characterizing the interaction potential between hydrogen and a solid. Moreover, the isotope separation factor is strongly dependent on the ortho-para composition of the isotope mixture. Considerable information concerning this dependence can be obtained from the present theory and is described below.

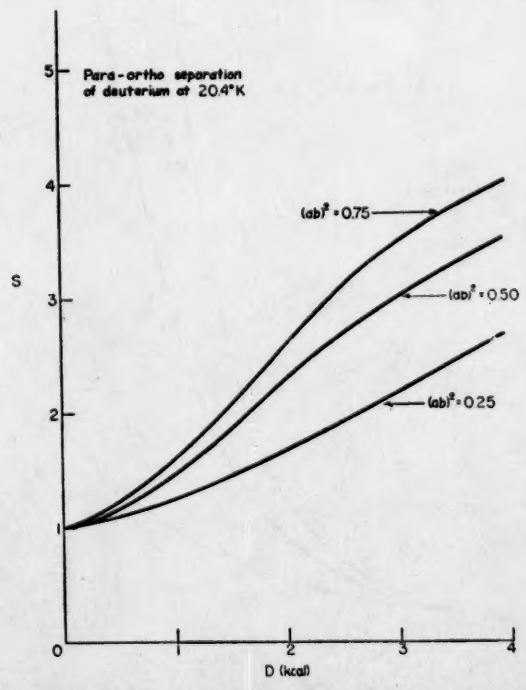

FIG. 8. Para-ortho separation factor for deuterium as a function of D at three values of $(ab)^2$.

TABLE II. The variation of the ortho-para separation factors of hydrogen and deuterium with energy of adsorption.

	Hydrogen					
		$-E_T$(kcal)			$S_{0p}^{H_2}$	
D (kcal)	$(ab)^2$—0.25	0.50	0.75	0.25	0.50	0.75
1.0	0.73	0.63	0.56	1.4	1.6	1.7
2.0	1.60	1.42	1.27	2.2	3.1	3.6
2.5	2.03	1.81	1.66	2.6	4.1	5.1
3.0	2.48	2.23	2.05	3.1	5.5	7.0
3.5	2.92	2.65	2.45	3.8	7.0	8.9
4.0	3.38	3.07	2.85	4.5	8.7	11.1
4.5	3.82	3.49	3.26	5.3	10.5	13.7
	Deuterium					
		$-E_T$(kcal)			$S_{p0}^{D_2}$	
D (kcal)	$(ab)^2$—0.25	0.50	0.75	0.25	0.50	0.75
1.0	0.80	0.71	0.63	1.2	1.5	1.6
2.0	1.68	1.53	1.42	1.7	2.3	2.5
2.5	2.13	1.96	1.84	1.9	2.7	3.1
3.0	2.59	2.39	2.26	2.2	3.0	3.5
3.5	3.04	2.84	2.69	2.4	3.3	3.8
4.0	3.51	3.28	3.12	2.7	3.5	4.0
4.5	3.97	3.74	3.57	3.0	3.7	4.1

Assume that the adsorbed layer is mobile, i.e., energy is independent of displacement parallel to the surface, as in the theory of preceding sections. Then by an application of statistical mechanics it follows that the separation factor for two isotopes, hydrogen and deuterium, between gas and adsorbed phase when hydrogen and deuterium are in para and ortho states, respectively, is given by

$$S_i^0=(M_{H_2}/M_{D_2})^{\frac{1}{2}}(Q_0^{D_2}/Q_p^{H_2})_{Ads}(Q_p^{H_2}/Q_0^{D_2})_{gas}, \quad (38)$$

where the M's are masses and Q_0, Q_p are partition functions for ortho and para species, respectively. This formula is obtained by a minor extension of a previous result.[10] It is easy to extend this equation to isotope separation factors in a system for which the ortho-para composition is arbitrary. The final result is

$$S_i=S_i^0\left[\frac{(R_{0p}^{H_2}+1)(S_{p0}^{D_2}R_{p0}^{D_2}+1)}{(S_{0p}^{H_2}R_{0p}^{H_2}+1)(R_{p0}^{D_2}+1)}\right]. \quad (39)$$

Here $R_{0p}^{H_2}$ and $R_{p0}^{D_2}$ are the ratios of ortho to para hydrogen and para to ortho deuterium, respectively, in the gas phase and $S_{0p}^{H_2}$, $S_{p0}^{D_2}$ are the ortho-para and para-ortho separation factors for hydrogen and deuterium, respectively. The isotope separation factor S_i is so defined as to exceed unity when deuterium is enriched on adsorption. The special case of this for-

[10] D. White and W. J. Haubach, J. Chem. Phys. **30**, 1368 (1959).

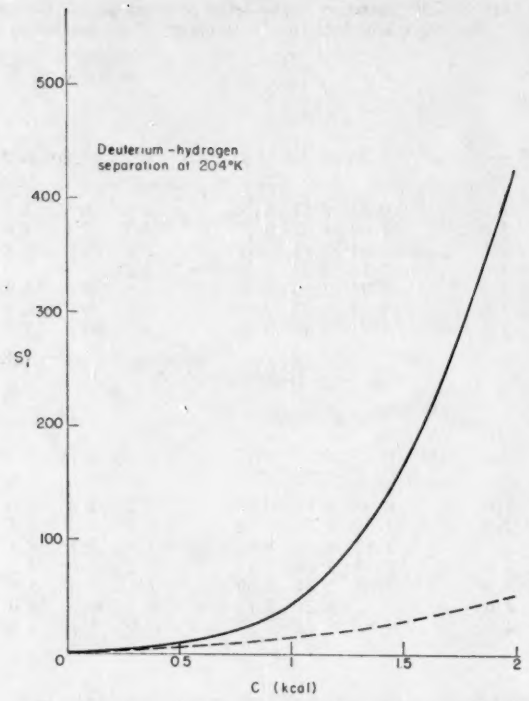

FIG. 9. Isotope separation factor as a function of barrier height assuming rotation and vibration to be independent (solid line). Dotted line gives separation factor when only vibration is considered.

mula obtained as $R_{0p}^{H_2}$ and $R_{p0}^{D_2}$ approach infinity is of interest. This limit is

$$S_i = S_i^0(S_{p0}^{D_2}/S_{0p}^{H_2}). \tag{40}$$

The theory of preceding section shows that invariably $S_{p0}^{D_2} < S_{0p}^{H_2}$ and hence the isotope separation factor when all molecules are in the rotational level with $l=1$ is substantially less than when all are in the level with $l=0$. Another limiting case of some interest arises as $R_{0p}^{H_2}$ decreases to zero and $R_{p0}^{D_2}$ increases to infinity. The limit is

$$S_i = S_i^0 S_{p0}^{D_2}. \tag{41}$$

This represents the maximum separation factor attainable and the gain over S_i^0 is sizable. The preceding theory suggests that S_i exceeds S_i^0 by a factor between 2.4 and 4. In fact Eq. (41) is the maximum separation factor attainable and in a practical isotope separation experiment it should be the goal to begin with the maximum amount of deuterium in the $l=1$ state and the maximum amount of hydrogen in the $l=0$ state. Since ortho-para conversion rate for hydrogen is much greater than the para-ortho conversion rate for deuterium it should be possible in practice to approach closely to the ratios $R_{0p}^{H_2}=0$ and $R_{p0}^{D_2}=\frac{1}{2}$. Under these conditions S_i should exceed S_i^0 by from one and a half to twofold in adsorbents such as alumina. If this separation factor is compared to the separation factor for normal mixtures of ortho-para hydrogen and ortho-para deuterium the ratio is $(3S_{0p}^{H_2}+1)/4$. In the two cases $S_{0p}^{H_2}=8$ and 16 the ratio is 6.25 and 12.25, respectively. There is obviously a big advantage to be gained by passing the original gas mixture over a catalyst at 20.4°K which rapidly converts the hydrogen to the para state and leaves deuterium as near as possible to the normal mixture.

The magnitude of the quantity S_i^0 is of obvious interest and the results of numerical calculations will now be presented. It is also of interest at this point to compare the approximations of Sec. II and IV. If the expansion of Eq. (3) be applied to the Morse function of Sec. IV we obtain

$$V = -D + (yDZ^2/b^2) + yD\eta^2 + \cdots. \tag{42}$$

If the higher powers in this series be discarded as before, then the theory of Sec. II applies. The calculated isotope separation factor can then be calculated from Eq. (38) and is shown in Fig. 9 (solid line) as a function of $yD=C$. (The dotted line gives the separation factor when the rotation is completely neglected.) If $y=\frac{3}{4}$ and $D=2.6$ kcal then S_i^0 exceeds 500, far too large to agree with the data of reference 10 and with further experimental results obtained since by White and Haubach (separation factor 40–60). If, on the other hand, the results of Sec. IV are used, the separation

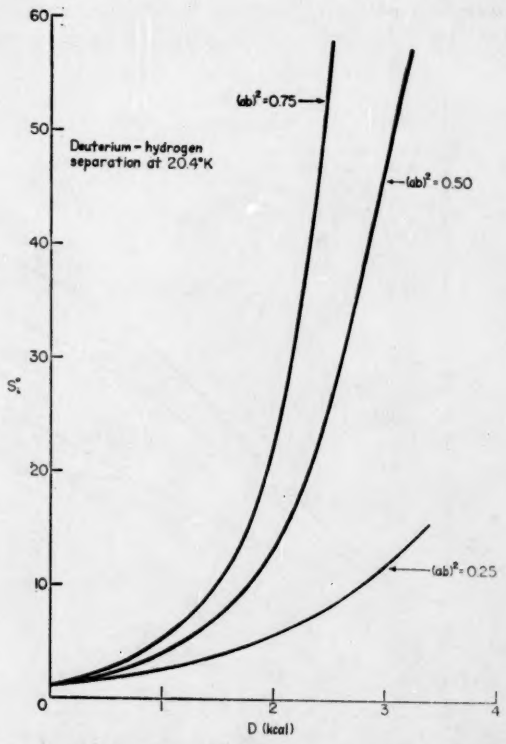

FIG. 10. Isotope separation factors as functions of D at three values of $(ab)^2$. Interaction between rotation and vibration taken into account.

TABLE III.

h_1	$(ab)^2=0.25$ $(8\pi^2ID/h^2)^{\frac{1}{2}}$	$(8\pi^2I/h^2)(E_T+D)$	$(ab)^2=0.50$ $(8\pi^2ID/h^2)^{\frac{1}{2}}$	$(8\pi^2I/h^2)(E_T+D)$	$(ab)^2=0.75$ $(8\pi^2ID/h^2)^{\frac{1}{2}}$	$(8\pi^2I/h^2)(E_T+D)$
			$m=0$ $l=0$			
1	2.487	1.56	2.135	1.83	2.066	2.11
2	4.679	3.54	3.816	3.98	3.554	4.45
3	6.728	5.60	5.283	6.07	4.785	6.61
4	8.714	7.63	6.682	8.08	5.893	8.58
5	10.705	9.63	8.076	10.08	7.023	10.55
6	12.700	11.64	9.484	12.08	8.162	12.53
			$m=1$ $l=1$			
1	2.351	3.33	1.955	3.51	1.797	3.63
2	4.516	5.00	3.573	5.27	3.241	5.57
3	6.612	6.85	5.123	7.22	4.560	7.60
4	8.657	8.80	6.598	9.19	5.788	9.61
5	10.676	10.76	8.037	11.19	6.970	11.61
6	12.683	12.74	9.462	13.18	8.133	13.59
			$m=0$ $l=1$			
1	2.830	4.14	2.693	4.86	2.878	5.76
2	5.428	7.66	4.995	9.31	5.210	11.43
3	7.803	11.87	6.948	14.26	7.015	17.15
4	9.936	16.14	8.519	18.73	8.324	21.80
5	11.932	20.23	9.903	22.79	9.382	25.62
6	13.901	24.27	11.252	26.70	10.423	29.35

factors of Fig. 10 are obtained. These differ markedly from the results of Fig. 9 and, moreover, provide a predicted separation factor with $y=\frac{3}{4}$ and $D=2.6$ kcal which agrees much better with experiment. This is in marked contrast with the ortho-para hydrogen separation factors where the discrepancy between theory and experiment is much smaller. A prime difference between Eq. (42) and the potential of Sec. IV lies in the fact that an harmonic oscillator potential (for vibration along the surface normal) is assumed for the former but an anharmonic potential for the latter case. This no doubt accounts for much of the difference, although the interaction between rotation and vibration, which is taken into account in Sec. IV, no doubt enters as well, although the relative importance of this factor to the anharmonic potential cannot be readily assessed.

More searching tests of this theory must await the collection of self-consistent data on both isotope and ortho-para separation factors. The theory is sufficient to show, however, that comparatively large ortho-para hydrogen and ortho-para deuterium separation factors are not only plausible but are to be expected when hydrogen or deuterium are adsorbed strongly on any solid adsorbent.

APPENDIX. MORE ACCURATE CALCULATION OF ENERGIES

Termination of Series Error

There are four primary sources of error in the theory of Secs. IV and V. These are (i) the assumption that the atoms of a molecule are independently attracted by a surface and the further assumption that the interaction of each atom with the surface is represented by a Morse type function which depends only on the normal distance from the surface; (ii) the use of a product type variation function; (iii) the use of a graphical method of solution of a pair of simultaneous equations; (iv) neglect of all except the first two terms of a power series expansion [(Eq. (9)]. Until the accuracy of the experimental data has been improved, further, there seems to be no need for further consideration of (i) and (ii) above. It is possible, however, to eliminate the graphical method of item (iii) in a manner which deserves comment and the error due to termination of series can be estimated and, if necessary, corrected at least approximately. Both these items are briefly discussed in the following.

In Sec. IV the energies were calculated by choosing values of the quantities y and D and then calculating the energies of three quantum states corresponding to the preassigned values of y, D. This is physically sensible since the complete potential function is obviously the same for each quantum state. If, however, the preassigned parameters are taken as y and h [of Eqs. (32) and (33)], the numerical calculations are greatly simplified. When this procedure is adopted, however, it is necessary to calculate the values of D which are required to produce the preassigned values of y, h_1. These values of D will differ from one quantum state to another and the energies of the quantum states at equal values of y, D (needed for separation factor calculations) must be obtained by interpolation. The calculations can best be done as follows.

TABLE IV.

h_1	$\langle\bar{\eta}^4\rangle$	$(8\pi^2 I\Delta E)/h^2$
$m=0$ $l=0$ $(ab)^2=0.75$		
3	0.0722	0.34_2
4	0.0431	0.34_3
5	0.0279	0.33_7
6	0.0194	0.33_3
$m=1$ $l=1$ $(ab)^2=0.75$		
3	0.0622	0.28_2
4	0.0348	0.27_8
5	0.0249	0.30_0
6	0.0183	0.31_2

If the quantity z be eliminated between Eqs. (30) and (33) then, on rearranging, we find

$$\lambda^2=a_1\lambda-a_0=0, \tag{43}$$

where

$$a_1=(1+2\alpha y)^{\frac{1}{2}}/(2+\alpha y), \tag{44}$$

and

$$a_0=\frac{h_1^2(1+2\alpha y)^2}{y^2[1+(\alpha y/2)](1-\alpha y)}. \tag{45}$$

Once h_1 has been chosen then a numerical value of α is known, e.g., from Table I. Then, when y is assigned, both a_1 and a_0 can be calculated from Eqs. (44) and (45). The coefficients of Eq. (43) are then determined and the roots of this equation give the values of λ. The negative root must be discarded since we have previously shown that μ must be positive. From Eq. (29) it follows that this condition is violated if $\lambda<0$. Moreover, since $\lambda^2 y=(8\pi^2 I/h^2)D$ the numerical values of D can be calculated. All graphical methods are thereby avoided. The results of such calculations, shown in Table III, have been used principally to check the graphical calculations of Sec. IV. The energies agree to within 0.01 (in units of $h^2/8\pi^2 I$).

We have now to consider the effect of terminating the series expansion of Eq. (9) after the first two terms. If we substitute in Eq. (8) the Morse type function of Eq. (16) we find

$$V=D[e^{-2az}\cosh(2ab\eta)-2e^{-az}\cosh(ab\eta)]\cdots. \tag{46}$$

Expansion in powers of η involves the two hyperbolic cosines. These expansions are

$$\cosh(2ab\eta)=1+2y\eta^2+\tfrac{2}{3}y^2\eta^4+\cdots, \tag{47}$$

and

$$\cosh(an\eta)=1+\tfrac{1}{2}y\eta^2+\tfrac{1}{24}y^2\eta^4+\cdots,$$

where $y=(ab)^2$. Only the first two terms of each of these expansions were used in Sec. IV. When y is large, however, the third and even higher terms may become important. An estimate of the error introduced by neglecting the third terms in these series can be made by employing the variation integral Eq. (10). Using for the trial function that $u=ST$ obtained in Sec. IV (or by the numerical method above), but retaining in the operator Q the third terms of Eq. (47), we obtain a correction to the energy of the form

$$\Delta E=(\tfrac{2}{3}\beta_2-\tfrac{1}{12}\beta_1)\langle\eta^4\rangle y^2. \tag{48}$$

Here β_1, β_2 are the average values of e^{-az} and e^{-2az}, respectively, while $\langle\eta^4\rangle$ is the average value of η^4. In the notation of Sec. IV $\beta_1=\mu/\gamma$, $\beta_2=\mu(\mu+1)/\gamma^2$. It is obvious that this correction is largest for large values of y. The calculated values of $\langle\eta^4\rangle$ and of $(8\pi^2 I/h^2)\Delta E$ at $y=\frac{3}{4}$ are shown in Table IV for $h_1=3, 4, 5, 6$. The quantity $\langle\eta^4\rangle_{Av}$ was calculated from the tables of Stratton *et al.* in a manner similar to the calculation of α previously described. These calculations have been made only for the two states $l=0$, $m=0$ and $l=1$, $m=1$ since only these two are important in separation factor calculations when $h_1\geq 3$. The correction amounts to less than two percent of the energy obtained by neglecting the term in η^4. Moreover, the correction is positive in each case so that both energy levels are raised. The difference between energies (at the same D and y) is, however, the significant quantity in ortho-para separation factor calculations and these correction terms tend to nearly cancel on subtraction. The maximum correction to the difference is 0.06 (units of $h^2/8\pi^2 I$). At 20.4°K this introduces an error of approximately 30% into the calculation of ortho-para hydrogen separation factors. Although this seems substantial at first sight, when we consider the uncertainty in the measured separation factors and the entremely crude assumptions made in obtaining the potential function, it hardly seems worthwhile to introduce the correction and we have not done so. A more refined treatment can only be justified when a more accurate approximation to the potential energy is employed.

Note added in proof: After this paper was accepted for publication a note by Evett appeared [J. Chem. Phys. **31**, 565 (1959)] which is equivalent to part of Sec. II.

Field Gradients at the Deuteron in Molecules*

R. BERSOHN

Department of Chemistry, Columbia University, New York, New York

(Received July 27, 1959)

A survey of the observed quadrupole coupling constants of the deuteron is presented. It is concluded on the basis of calculations that the field gradients at hydrogen nuclei will be positive in almost all molecules. The simple wave functions greatly underestimate the field gradients of the bonding electrons. A good part, but not all, of the discrepancy, previously noted by White, can be removed with the use of a contracted charge distribution and ionic character. The wave function of Ellison and Shull gives a very bad description of the field gradients at the deuterons in D_2O but the experimental data indicate the direction for future improvement. The field gradients at deuterons remain attractive quantities for characterizing the charge density in bonds involving hydrogen atoms.

THE first deuteron quadrupole coupling constant was observed in HD and D_2 by Kellogg, Rabi, Ramsey, and Zacharias.[1] Because sufficiently accurate wave functions are available for H_2, the quadrupole moment Q of the deuteron has been calculated as $2.77\pm 0.03\times10^{-27}$ cm.[2] One can, therefore, extract from the measured deuteron quadrupole coupling constant in other molecules the field gradient itself; the latter serves as a valuable indication of the nature of the bond involving the hydrogen atom.

The present article is divided into three sections. The first two present calculations of the field gradient at the deuteron of the neutral molecular fragment D—C≡, and D_2O, respectively. The final section attempts some generalizations on the basis of the preceding calculations.

I. MOLECULAR FRAGMENT D—C≡

White[3] made a calculation of the field gradient to be expected at the deuteron in the neutral molecular fragment D—C≡. His calculated† field gradient of 19.17×10^{14} statcoulombs/cm² was about twice the experimental field gradient of $8.85\pm0.90\times10^{14}$ in D—C≡C—Cl. Inasmuch as the field gradient originating from the carbon nucleus is 48.66×10^{14} esu, one can restate the problem as follows. Experimentally, the electrons are observed to cancel 82% of the carbon nucleus' field gradient but the wave mechanical calculation states that the electrons cancel only 61%.

To investigate this discrepancy, his calculation was repeated and the fundamental integrals of the field gradient are given in Table I. These integrals are matrix elements of the field gradient between all possible pairs of the following functions, hydrogen $1s$, carbon $2s$, $2p_z$, $2p_y$, and $2p_x$. For the present purposes, the carbon $1s$ density is treated as a delta function. In what follows the field gradients (f.g.) are expressed in the natural units of $ea_0^{-3}=32.41\times10^{14}$ statcoulombs cm$^3\cong$ a deuteron coupling constant of 651 kc sec.

The seven electrons of this neutral fragment are to be distributed as follows. One each is placed in the carbon atom $2p_z$, $2p_y$, and sp_x hybrid directed away from the deuteron. Two electrons are placed in the carbon K shell and two in the molecular orbital

$$(1+\lambda^2+2\lambda S)^{-\frac{1}{2}}\{\psi(1sH)+(\lambda/\sqrt{2})\,(\psi(2sC)+\psi(2pZC)\},$$

where for the present λ is taken to be one. The f.g. contributions may be evaluated immediately once the various integrals of the f.g. operator have been evaluated.

The all important choice of atomic wave functions must now be made. White[3] chose Slater functions with effective nuclear charges 3.20 for carbon $2s$ and $2p$ functions and 1 for the hydrogen $1s$ function. We used the Coulson-Duncanson[4] function in which the $2s$ function is orthogonal to the $1s$.

The operator whose matrix elements are to be determined is $r_a^{-3}(3\cos^2\Theta_a-1)$ where r_a is the vector from the deuteron to the electron and Θ_a is the angle between r_a and the bond axis. The necessary integrals, given in the first column of Table I, were evaluated using the Barnett-Coulson[5] zeta function technique. They were calculated for a bond distance of 1.052 A appropriate to D—C≡C—Cl. The result for the total field gradient is 0.5835 $ea_0^{-3}=18.91$ esu, negligibly different from White's result. One may verify readily that the use of a valence bond function to describe the pair of bonding electrons gives almost the identical result.

The ionicity of the C—H bond needs to be taken into account. While there is little polarity in the C—H bond involving an sp^3 hybridized carbon atom, an sp hybrid is considerably more electronegative. Its electronegativity will presumably be enhanced in the molecules DCCCl and DCN because of the electron-withdrawing atom

* This research was supported by the U. S. Atomic Energy Commission, Contract AT (30-1) 1662 with Cornell University where this work was performed.

[1] Kellogg, Rabi, Ramsey, and Zacharias, Phys. Rev. **55**, 318 (1939).

[2] G. F. Newell, Phys. Rev. **78**, 711 (1950).

[3] R. L. White, J. Chem. Phys. **23**, 253 (1954).

† A minor error in White's calculation has been corrected.

[4] W. E. Duncanson and C. A. Coulson, Proc. Roy. Soc. (Edinburgh) **62**, 37 (1944); Nature **164**, 1003 (1949); cf., also A. Tubis, Phys. Rev. **102**, 1049 (1956).

[5] M. P. Barnett and C. A. Coulson, Phil. Trans. Roy. Soc. London **A243**, 221 (1951).

TABLE I. Field gradient integrals for ≡C—H (R=1.052 A), (units of ea_0^{-3}).

	Coulson-Duncanson fns.	Contracted C atom	Contracted C atom and Z_H=1.2
$\langle 1s_H \mid q \mid 2p_{zC}\rangle$	0.0780	0.1005	0.1150
$\langle 1s_H \mid q \mid 2s_C\rangle$	0.0631	0.0714	0.0727
$\langle 2p_{zC} \mid q \mid 2p_{zC}\rangle$	0.2096	0.2641	0.2641
$\langle 2p\pm c \mid q \mid 2p\pm c\rangle$	0.0799	0.1026	0.1026
$\langle 2p_{zC} \mid q \mid 2s_C\rangle$	0.1078	0.1164	0.1164
$\langle 2s_C \mid q \mid 2s_C\rangle$	0.0556	0.0610	0.0610
$\langle 2p_H \mid q \mid 2p_{zC}\rangle$	0.0206	...	...
$\langle 2p_H \mid q \mid 2s_C\rangle$	0.0315	...	...
$2/R^3$	0.2545	0.2545	0.2545

at the other end. It would not be unreasonable therefore to associate a charge of +0.1 e with the hydrogen atom (using the Milliken population analysis); choosing $\lambda=\sqrt{2}$ accomplishes this redistribution. The total f.g. now becomes 0.5613 ea_0^{-3}=18.19 esu.

The electronic f.g. has increased in magnitude because charge has been removed from the hydrogen atom where it contributed nothing to the carbon atom where it makes a substantial contribution. This is perhaps as far as we can go if we adhere to the convention that the atomic wave functions should be chosen as the best analytic functions appropriate to the isolated atom. There is, however, little theoretical justification for the convention. In the hydrogen molecule, for example, the minimum energy is obtained with either a valence bond or molecular orbital 1s engienfunction with $Z\sim1.2$. In the hydrogen fluoride molecule[6] an effective nuclear charge of 1.322 for the hydrogen atom has been shown to minimize the total energy.

The second column of Table I exhibits the field gradient integrals computed using for carbon atom wave functions those appropriate to C^+.‡ The contracted charge distribution contributes actually more to the electronic field gradient. The average value of the factor r_a^{-3} has diminished but the average value of the factor $3\cos^2\Theta_a-1$ has increased relatively more. Comparing the various integrals with each other and with $2R^{-3}$ shows vividly the effect of increasing the effective nuclear charge. The net f.g. becomes 14.91 esu. Then, if as before, one assumes a 10% ionic character in the sense that a charge of +0.1e is associated with the hydrogen atom, the net f.g. becomes 14.01 esu.

In analogy with the results found for the hydrogen molecule, one ought also to increase the effective nuclear charge of the hydrogen atom wave function. If one chooses Z=1.2 for the 1s wave function, the total field gradient becomes 13.31 and 14.44 esu with and without the use of 10% ionic character. The use of a contracted charge distribution and a small amount of ionic character has, therefore, removed more than half of the original discrepancy between theory and experiment.

[6] R. A. Ballinger, Mol. Phys. **2**, 139 (1959).

‡ The C^+ functions were chosen as a convenient example of a contracted charge distribution and their use is not meant to imply anything about the net charge on the carbon atom.

II. THE WATER MOLECULE

The first complete valence treatment of the water molecule was that of F. O. Ellison and H. Shull[7] who calculated self-consistent molecular orbitals for all ten electrons of the molecule. No integrals were neglected although some were approximated. The starting atomic wave functions were the hydrogen atom 1s functions $h_1(1s)$ and $h_2(1s)$ and the oxygen atom functions 1s, 2s, 2 pX, 2 pY, and 2 pZ. The effective nuclear charges for oxygen were chosen according to the Slater rules so that $Z_{1s}=7.7$, $Z_{2s}=Z_{2p}=4.55$. The five molecular orbitals can be written as follows:

$$1a_1' = 1.000\phi_{1s}+0.016\phi_{2s}+0.005479\phi_{2pZ} +0.007141\phi_{2pY},$$

$$2a_1' = -0.013\phi_{1s}+0.962\phi_{2s}-0.1638\phi_{2pZ} -0.2134\phi_{2pY},$$

$$3a_1' = 0.269h_1(1s)+0.269h_2(1s)-0.046\phi_{1s}-0.012\phi_{2s} +0.4828\phi_{2pZ}+0.6292\phi_{2pY},$$

$$1b_2 = 0.548h_1(1s)-0.548h_2(1s)-0.4308\phi_{2pZ} +0.3306\phi_{2pY},$$

$$1b_1 = \phi_{2p\mu}.$$

The Z axis is the OH_1 axis and the X axis is normal to the H_1OH_2 plane. The coefficients of these molecular orbitals were chosen to minimize the total energy at a bond distance of 0.9581 A, and a bond angle of 105°. Later on the principal axes x, y, z of the field gradient

TABLE II. Matrix elements of field gradient operators for D_2O.

Wave function product	q_{ZZ}	q_{YY}	q_{YZ}
$h_2(1s)^2$	0.0216	0.0027	0.0352
ϕ_{1s}^2	0.3370	−0.1685	0
ϕ_{2s}^2	0.1309	−0.0655	0
ϕ_{2pZ}^2	0.4311	−0.2156	0
ϕ_{2pY}^2	0.1770	−0.0253	0
$h_1(1s)h_2(1s)$	0.0155	0.0020	0.0253
$h_1(1s)\phi_1(1s)$	0.0114	−0.0057	0
$\phi_{2s}h_1(1s)$	0.1227	−0.0614	0
$h_1(1s)\phi_{2pZ}$	0.1555	−0.0778	0
$h_1(1s)\phi_{2pY}$	0	0	0.2689
$h_2(1s)\phi_{1s}$	0.0191	−0.0096	−0.0010
$h_2(1s)\phi_{2s}$	0.1291	−0.0408	−0.1016
$h_2(1s)\phi_{2pZ}$	0.0433	−0.0134	−0.0378
$h_2(1s)\phi_{2pY}$	0	0	0
$\phi_{1s}\phi_{2s}$	0	0	0
$\phi_{1s}\phi_{2pZ}$	0.0302	−0.0151	0
$\phi_{1s}\phi_{2pY}$	0	0	0.0302
$\phi_{2s}\phi_{2pZ}$	0.1064	−0.0532	0
$\phi_{2s}\phi_{2pY}$	0	0	0.1474
$\phi_{2pY}\phi_{2pZ}$	0	0	0.1224

[7] F. O. Ellison and H. Shull, J. Chem. Phys. **23**, 2348, 2358 (1955).

tensor will be used, x being identical with X because of the plane of symmetry.

The task of computing the field gradient was lengthy but straightforward. The molecular symmetry plane reduced the number of field gradient components to three which were chosen to be

$$q_{ZZ}=(3\cos^2\Theta a-1)/r_a^3,$$

$$q_{YY}=(3\sin^2\Theta a\sin^2\phi a-1)/r_a^3,$$

$$q_{YZ}=3\cos\Theta_a\sin\Theta_a\sin\phi_a/r_a^3.$$

The required matrix elements of these operators are given in Table II.§ The q_{zz} integrals are about twice their counterparts for the ≡C—H fragment. Two related effects explain the difference. The oxygen atom functions have a larger effective nuclear charge (are "contracted") and hence contribute more to the field gradient; for the same reason the O—H bond is shorter than the C—H bond which also augments the field gradients.

The last step in the calculation is to combine the various matrix elements and obtain the expectation values of the field gradient operators for each of the five molecular states. The final result is given in Table III which can be compared with the experimental results given in Table IV. The maximum theoretical field gradient is about twice the experimental value. In addition, the experimental principal axis is almost identical (1°7′±47′) with the OD axis whereas the molecular orbital wave function predicts a rotation of about 10°.

One may perhaps derive a bit of comfort from the fact that $q_{yy}-q_{xx}=59$ kc is not in violent disagreement with the experimental result of 36±12 kc. Of all the possible combinations of field gradient components $q_{yy}-q_{xx}$ is the only one which is independent of the nature of the charge distribution near the hydrogen nucleus. It must come largely from the charge in the other O—H bond which is relatively remote. $q_{yy}-q_{xx}$ ought, therefore, to be much less sensitive to the exact function than q_{zz}.

TABLE III. Contributions to field gradient components (units e/a_0^3) in the water molecule.

	q_{ZZ}	q_{YY}	q_{ZY}
O^{16} nucleus	2.6963	−1.3482	0
H nucleus	0.0350	0.0044	0.0571
two electrons in			
$1a_1'$ (inner shell)	−0.6746	0.3374	−0.0008
$2a_1'$ (one pair)	−0.2148	0.1016	0.1036
$3a_1'$ (bonding)	−0.4436	0.1630	−0.3170
$1b_1$ (one pair)	−0.3540	0.3034	0
$1b_2$ (bonding)	−0.0871	0.0254	−0.0800
TOTALS	0.9572	−0.4130	−0.2371

Z axis is the OD bond to the deuteron under discussion
X axis is the normal to the plane of the molecule
Y axis is perpendicular to X and Z

$q_{XX}=q_{zz}=-(q_{ZZ}+q_{YY})=-0.5442\cong-354$ kc

$q_{yy}=-0.4528\cong-295$ kc

$q_{zz}=0.9970\cong 649$ kc

$|\eta|=0.092$

z is rotated 9.5° from the Z direction away from the bisector of the DOD angle.

TABLE IV. Deuteron quadrupole coupling constants.

Compound		eqQ/h (kc)	η	Reference
H—H	HD	227±4	0	N. F. Ramsey, *Molecular Beams* (Oxford University Press, New York, 1956).
	D_2	224.99±0.10	0	
H—C	DCN	±290±120	0	R. L. White, J. Chem. Phys. **23**, 253 (1954).
	DCCCl	175±20	0	
H—N	ND_3	200±20	0 assumed	G. Herrmann, J. Chem. Phys. **29**, 875 (1958).
H—O	HDO	305	0.115±0.041	D. W. Posener, Australian J. Phys., **10**, 276 (1957) and (private communication).
	$Li_2SO_4\cdot D_2O$	±237±10	0.14±0.04	Ketudat and Pound, J. Chem. Phys. **26**, 708 (1957).
	KD_2PO_4	±119	0.049	Bjorkstam and Uehling, Phys. Rev. **114**, (1959).

III. GENERAL DISCUSSION AND CONCLUSIONS

A. Comparison with Wave Mechanical Models

It appears that, at least for C—H and O—H bonds, the field gradients calculated from simple wave functions (valence bond or molecular orbital) with screening parameters appropriate to the isolated atom are far too large. In other words, the electronic contribution is grossly underestimated. A partial cure for this difficulty lies in the use of a contracted charge distribution in which the effective nuclear charges are distinctly larger than for the free atom presumably as a result of molecule formation. For the hydrogen molecule it has been shown[8] that whereas a poor field gradient is obtained with a simple VB or MO function, the use of an effective nuclear charge is sufficient to give a reasonably accurate field gradient. The vast improvement in the H—C≡ field gradient produced by using a larger effective nuclear charge supports the conclusion.

Without reflection on the able and useful efforts of Ellison and Shull, it seems clear that their wave function gives a rather poor description of the charge density in the OH bond. With the help of fast calculators, one may hope that future SCF LCAO treatments of molecules will be carried out with some atten-

§ There are a number of three-center integrals involved in the calculation which were crudely approximated using methods suggested by Ellison.[7] The final result was so poor that no attempt was made to improve the accuracy of these integrals.

[8] T. P. Das and R. Bersohn, Phys. Rev. **115**, 897 (1959).

tion to the variation of effective nuclear charge. The failure to give adequate field gradients emphasizes the necessity to modify the original atomic orbitals used in the calculation.|| Recent proton shielding calculations on the water molecule[9] also indicate the necessity of using an effective nuclear charge greater than one for the hydrogen atom 1*s* function.

B. Survey of Deuteron Field Gradients

The deuteron quadrupole coupling constants so far reported are collected in Table IV. The first observation is that the quadrupole coupling constants whose signs have been measured are positive; the deuteron quadrupole moment being positive, all the field gradients were positive. We believe this to be true in general and the argument is as follows. A deuteron will see in its environment a net charge of $-e$. However, one electron charge will be associated mainly with the hydrogen atom 1*s* state where it will contribute little or nothing to the field gradient. The rest of the charge distribution will be neutral and the electrons, because of their diffuse distribution, will tend to contribute less to the field gradient than the nuclei. The only exception to the rule of positive field gradients might be a negative ion in which the extra electron(s) compensated for the inadequacy of the others.

The coupling constants of $Li_2SO_4 \cdot D_2O$ and KD_2PO_4 deserve special mention. One expects—from considerations of lattice energies and the observed change of eqQ for other nuclei in going from the gas to the solid phase—an increase in ionic character of a molecule in the solid state. The previous analysis has shown that as charge is removed from the hydrogen atom and transferred to the atom to which it is bonded, the electronic field gradient will rise and the total field gradient will fall. Most of the discrepancy between the coupling constant of gaseous HDO (305 kc) and of crystalline $Li_2SO_4 \cdot D_2O$ (237 kc) is assigned to this increase of ionic character. A part is due to the molecular motion in the solid which tends to decrease the observed coupling constant.

The vibrational frequencies of water are evidently a much less sensitive indicator of the deformation of its charge distribution than the field gradient at the deuteron. Infrared[10] and Raman[11] studies of $Li_2SO_4 \cdot H_2O$ have shown differences in vibration frequencies between gas and solid of only a few percent.

The deuteron in KD_2PO_4 has a coupling constant which is still assumed to be positive but which is small because of the increased electron density in the OD bond of the negative ion. In this connection, we would predict a rather small coupling constant for OD^- (or ND_2^-) and a rather large one compared to D_2O (or ND_3) for D_3O^+ (or ND_4^+).

A gradual increase in coupling constant is observed as one goes across the first row of the periodic table. Basically this is due to the increase in number of electrons whose field gradients are ineffective in cancelling the increasing nuclear field gradients; the net field gradient also rises because the bond distances are shorter. In going down the columns of the periodic table the two effects oppose each other. The experimental finding[12] that the deuteron coupling is substantially less in HDS than in HDO indicates that the bond-lengthening effect is dominant. Analogous results are expected for PD_3 as compared to ND_3.

In a fashion which is qualitative but based on the results of numerical calculations, we have seen how the deuteron eqQ's will vary with ionic character, atomic radius of bonding partner, molecular charge, and position in the periodic table. Recently there has been great interest in correlating the magnetic resonance frequency shifts of protons with charge distribution in molecules. Only partial success has been achieved probably because the chemical shifts depend not only on the charge distribution of the ground state but on how the ground state function is deformed in the presence of an external magnetic field. The deuteron quadrupole coupling constants have theoretical simplicity in that they depend *only* on the ground state charge density.

|| A possibility strongly suggested by the necessity of introducing wave functions with stronger field gradients is to form sp hybrids in which the p function has a large effective nuclear charge. This solution is put forth tentatively until it can be tested on H_2. Hybridization with a p function whose nuclear charge is only one is ineffective in increasing the electronic field gradient as may be seen from the integrals at the bottom of Table I.

[9] T. P. Das, J. Chem. Phys. **31**, 42 (1959).

[10] Vassas-Dubuisson, J. Chim. Phys. **50**, 98 (1953).

[11] E. Drouard, Compt. Rend. **240**, 1700 (1955).

[12] P. Thaddeus (private communication).

Burning Rates of Solid Propellants*

GERALD ROSEN†

Guggenheim Jet Propulsion Center, Princeton, New Jersey

(Received July 13, 1959)

The burning mechanism of a solid propellant is described in terms of a pyrolysis law, a premixed laminar flame, and nothing more. A quantitatively accurate burning rate formula is derived from the theory. The predicted burning rate pressure dependence agrees with the experimental results for ammonium perchlorate propellants.

INTRODUCTION

THE laminar flame theory of a premixed gas predicts an iron-clad burning rate pressure dependence (a burning rate directly proportional to the pressure for a second-order chemical reaction). In attempts to explain the more complicated burning rates of homogeneous and composite solid propellants, authors have postulated various forms of *rate-controlling inhomogeneity* for the gas near the solid.[1–5] With noteworthy success, Summerfield's concept of *unmixedness*[5] has interpreted many burning rate experiments at Princeton. However, the existing theories[1–5] share a common defect: *ad hoc* postulates are necessary to describe the rate-controlling inhomogeneity in the gas.

Now it is reasonably well established that an Arrhenius-type pyrolysis law governs the surface decomposition of a solid propellant. A premixed laminar flame in combination with a pyrolysis law is a rich theory, without the addition of any questionable postulates. What are the precise quantitative predictions of such a flame theory? Are many burning rate *vs* pressure curves explicable in terms of a pyrolysis law, a premixed laminar flame, and nothing more?

Answers to these questions logically precede the consideration of more imaginative models. This paper studies the theory of a solid propellant which decomposes into a premixed laminar flame. A quantitatively accurate burning rate formula is derived, discussed, and finally compared with the experimental measurements for ammonium perchlorate propellants.

FUNDAMENTAL EQUATIONS

Let the x axis be established normal to the decomposing surface $[x=0]$ of a steadily burning solid propellant (see Fig. 1). Then, since negligible chemical reaction occurs within the solid $[x<0]$, the equation of heat conduction is

$$c_s r\rho_s(dT/dx)=(d/dx)[k_s(dT/dx)], \qquad [x<0]. \tag{1}$$

On integrating, we find

$$T=T_u+(T_s-T_u)\exp\left[c_s r\rho_s\int_0^x (dx/k_s)\right], \quad [x<0] \tag{2}$$

in which the average surface temperature, T_s, is related to the burning rate by an Arrhenius-type pyrolysis law[3]

$$r=a\exp(-Hn_s/c_sT_s). \tag{3}$$

The prefactor, a, depends on the composition of the propellant, but not on the pressure of the gas. The quantity n_s, which we call the *index* for the surface decomposition, ranges between 3 and 7 for the common solid propellants.

Next, we set up governing equations for the burning gas. A number of semiempirical approximations usually apply to the gaseous region $[x>0]$:

(a) Pressure is constant.
(b) Viscosity is negligible.
(c) Mach number is small.
(d) A rate-controlling second-order chemical reaction proceeds, α_1 grams of fuel gas unite with α_2 grams of oxidizer gas to produce 1 gram of products $[\alpha_1+\alpha_2=1]$.
(e) The mixture behaves like a perfect gas.
(f) Specific heat of the mixture is constant.
(g) Lewis numbers for the diffusional processes equal unity, that is, the mass diffusivity of the fuel or oxidizer equals the thermal diffusivity of the mixture.

Under these assumptions, the governing equations take the form:

Continuity:

$$\rho V=r\rho_s. \tag{4}$$

* This work was sponsored by Project SQUID which is supported by the Office of Naval Research, Department of the Navy, under contract Nonr 1858(25) NR-098-038. Reproduction in full or in part is permitted for any use of the United States Government.

† Research Associate, Department of Aeronautical Engineering, Princeton University.

[1] R. D. Geckler, *Selected Combustion Problems, AGARD* (Butterworths Scientific Publications, Ltd., London, 1954), p. 289.
[2] R. W. Lawrence and A. O. Dekker, Jet Propulsion **25**, 81 (1955).
[3] R. Schultz, L. Green, and S. S. Penner, *AGARD Combustion Reviews* (Butterworths Scientific Publications, Ltd., London, 1958).
[4] B. L. Crawford *et al.* J. Anal. Chem. **19**, 630 (1947).
[5] M. Summerfield *et al.*, "Burning mechanism of ammonium perchlorate propellants," presented at the 13th Annual Meeting of the American Rocket Society, 1958.

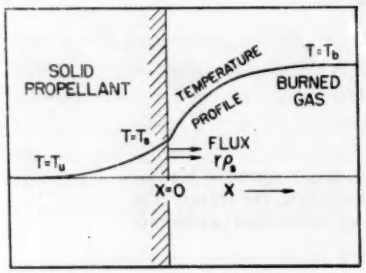

FIG. 1. The region near the surface of a burning propellant.

Heat transport:

$$c_p r\rho_s(dT/dx)=(d/dx)[k(dT/dx)]+H\omega_1\omega_2 P^2 f(T). \quad (5)$$

Reactant Transport:

$$r\rho_s(d\omega_i/dx)=(d/dx)[(k/c_p)(d\omega_i/dx)] -\alpha_i\omega_1\omega_2 P^2 f(T), \quad [i=1,2]. \quad (6)$$

Obvious linear combinations of Eqs. (5) and (6) produce

$$d/dx\{(k/c_p)(d/dx)[\omega_i+\alpha_i(c_p/H)T] +r\rho_s[\omega_i+\alpha_i(c_p/H)T]\}=0, \quad [i=1,2,]. \quad (7)$$

The only solutions to Eq. (7) which remain bounded as $x\to\infty$ are

$$\omega_i+\alpha_i(c_p/H)T=(\text{const})_i, \quad [i=1,2]. \quad (8)$$

Hence, if the ω_i approach zero as $x\to\infty$, the composition dependence is found to be

$$\omega_i=\alpha_i(c_p/H)(T_b-T), \quad [i=1,2]. \quad (9)$$

By substituting Eqs. (9) into Eq. (5), we obtain

$$c_p r\rho_s(dT/dx)=(d/dx)[k(dT/dx)] +(\alpha_1\alpha_2 c_p^2 P^2/H)(T_b-T)^2 f(T). \quad (10)$$

This final equation must be supplemented with the boundary conditions

$$x=0:\begin{cases}T=T_s & (11a)\\ k(dT/dx)=[k_s(dT/dx)]_{x=0-}-r\rho_s H_s, & (11b)\end{cases}$$

and

$$x=\infty:\begin{cases}T=T_b & (12a)\\ (dT/dx)=0, & (12b)\end{cases}$$

where H_s is positive (negative) for exothermic (endothermic) gasification of the propellant. Recalling the solution of Eq. (2) for the temperature within the solid, the gradient condition in Eq. (11b) becomes

$$x=0: \qquad k(dT/dx)=r\rho_s[c_s(T_s-T_u)-H_s]. \quad (13)$$

THE EIGENVALUE PROBLEM

We introduce the dimensionless distance variable,

$$\xi=\exp\left[c_p r\rho_s\int_0^x (dx/k)\right], \quad (14)$$

and the dimensionless temperature rise,

$$\tau=(1/H)[c_p(T-T_s)+c_s(T_s-T_u)-H_s]. \quad (15)$$

In terms of this new notation, Eq. (10) is

$$d^2\tau/d\xi^2+[(a/r)(P/b)]^2(1/\xi^2)(1-\tau)^2\tau^n=0, \quad (16)$$

in which a parameter with the dimensions of pressure has appeared,

$$b\equiv a\rho_s[(\alpha_1\alpha_2/c_p)(kf(T))_{T=T_b}]^{-\frac{1}{2}}. \quad (17)$$

The index n in Eq. (16) efficiently estimates the temperature sensitivity of the quantity $kf(T)$; n ranges between 8 and 14 for practical activation energies.[6]

The transformed boundary conditions, Eqs. (11a) (12), and (13), are found to be

$$\xi=1:\begin{cases}\tau=\tau_s\{\equiv(1/H)[c_s(T_s-T_u)-H_s]\} & (18a)\\ d\tau/d\xi=\tau_s, & (18b)\end{cases}$$

$$\xi=\infty:\begin{cases}\tau=1 & (19a)\\ d\tau/d\xi=0, & (19b)\end{cases}$$

where the dimensionless temperature rise at $\xi=\infty$ follows from simple energy considerations. Finally, the definition part of Eq. (18a) can be rewritten to embody the pyrolysis law of Eq. (3),

$$\tau_s=\frac{n_s}{\ln(a/r)}-\frac{(c_s T_u+H_s)}{H}. \quad (20)$$

This completes our formulation of the burning rate eigenvalue problem. Equation (16) with the boundary conditions [Eqs. (18) and (19)] provides $[(a/r)(P/b)]$

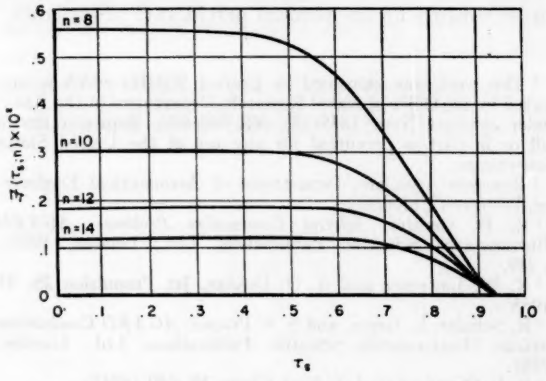

FIG. 2. Eq. (28) for typical values of the index n.

[6] G. Rosen, Jet Propulsion **28**, 839 (1958).

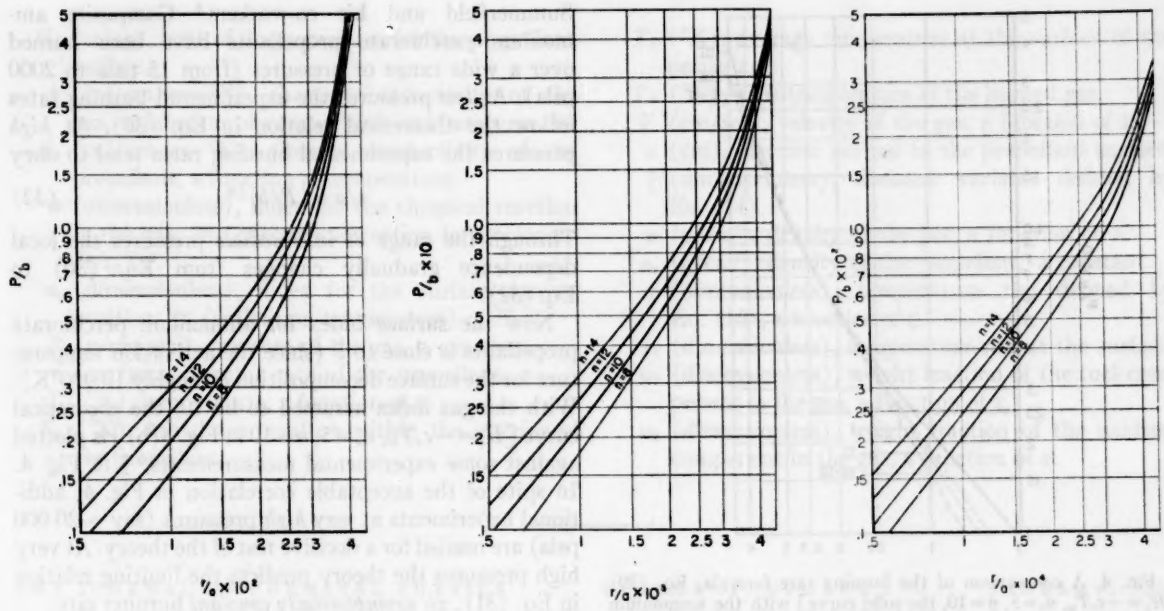

FIG. 3. (a) The burning rate formula, Eq. (29) with $H_s=-c_sT_u$, $n_s=3$. (b) The burning rate formula, Eq. (29) with $H_s=-c_sT_u$, $n_s=5$. (c) The burning rate formula, Eq. (29) with $H_s=-c_sT_u$, $n_s=7$.

as a function of τ_s; the latter quantity can then be expressed physically with the help of Eq. (20). In this way an implicit equation for (r/a) is obtained.

Solving Eq. (16) with Eqs. (18) and (19) is very easy, since the eigenvalue problem is formally equivalent to an ordinary laminar flame with a *truncated* rate expression. To see this, consider the ordinary laminar flame system‡

$$d^2\tau/d\xi^2+[(a/r)(P/b)]^2(\epsilon/\xi^2)(1-\tau)^2\tau^n=0, \quad (21)$$

where

$$\xi=0:\begin{cases}\tau=0 & (22a)\\ d\tau/d\xi\equiv\tau_s, & (22b)\end{cases}$$

$$\xi=\infty:\begin{cases}\tau=1 & (23a)\\ d\tau/d\xi=0. & (23b)\end{cases}$$

In Eq. (21), ϵ is zero for $\tau<\tau_s$ and unity for $\tau>\tau_s$. Thus Eq. (21) can be integrated for $\tau<\tau_s$; with Eqs. (22) this gives $\tau=\tau_s\xi$ for $0\leq\xi\leq1$, and therefore conditions Eqs. (18) at $\xi=1$. Hence, the eigenvalue problems for $[(a/r)(P/b)]$, expressed in the domain $1\leq\xi<\infty$, are identical.

The solution of the eigenvalue problem Eqs. (21)–(23) has been obtained by setting up an action principle.[7,8] A Rayleigh-Ritz procedure then gives the result

$$[(r/a)(b/P)]^2=\frac{\int_{\tau_s}^1(1-\tau)^2\tau^n d\tau}{\frac{1}{6}+\frac{1}{3}[(1-q+q^2)^{\frac{1}{2}}-q]}, \quad (24)$$

in which

$$q\equiv\frac{\int_{\tau_s}^1(1-\tau)^2\tau^{n-1}d\tau}{\int_{\tau_s}^1(1-\tau)^2\tau^n d\tau}-1. \quad (25)$$

Since we can expect $\frac{1}{4}\lesssim\tau_s<1$, q, defined by Eq. (25) is much less than unity. Thus Eq. (24) becomes

$$[(r/a)(b/P)]^2\cong2(1+q)\int_{\tau_s}^1(1-\tau)^2\tau^n d\tau$$
$$=2\int_{\tau_s}^1(1-\tau)^2\tau^{n-1}d\tau, \quad (26)$$

so

$$r/a=(P/b)[\mathfrak{F}(\tau_s;n)]^{\frac{1}{2}} \quad (27)$$

with the abbreviation

$$\mathfrak{F}(\tau_s;n)=[4/n(n+1)(n+2)]-(2/n)\tau_s^n$$
$$+[4/(n+1)]\tau_s^{n+1}-[2/(n+2)]\tau_s^{n+2}. \quad (28)$$

‡ Replacing ξ with $c\xi$ (c an arbitrary positive constant) does not alter the physical content of an ordinary laminar flame solution.[8] Hence, Eq. (22b) is at our disposal as an unobservable *scale condition*.

[7] G. Rosen, *Seventh International Combustion Symposium* (Butterworths Scientific Publications, Ltd., London, 1958), pp. 339, 412.

[8] G. Rosen, J. Chem. Phys. **31**, 311 (1959).

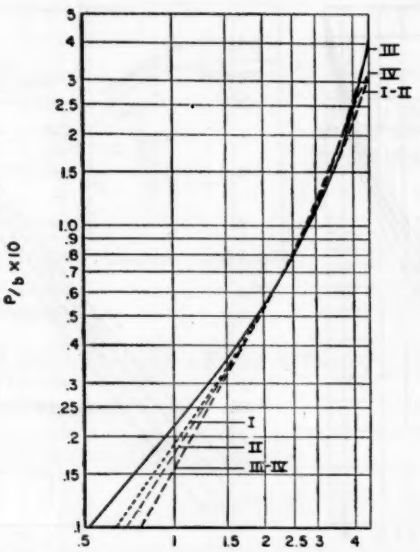

FIG. 4. A comparison of the burning rate formula, Eq. (29) [$H_s = -c_s T_u$, $n_s = 5$, $n = 10$, the solid curve] with the ammonium perchlorate experiments[5] § [dashed curves]: I 75:25 fine. II 80:20 fine. III 80:20 coarse. IV 75:25 coarse.

The latter function is plotted in Fig. 2 for typical values of n. An implicit equation for the burning rate is obtained from Eq. (27) by recalling Eq. (20), so that

$$(r/a) = (P/b)\left[\mathfrak{F}\left(\frac{n_s}{\ln(a/r)} - \frac{(c_s T_u + H_s)}{H}; n\right)\right]^{\frac{1}{2}}. \quad (29)$$

BURNING RATES

For most cases of practical interest, $|c_s T_u + H_s|$ is small compared to H. Thus, we shall concentrate attention on the simplifying condition $H_s = -c_s T_u$. With this assignment for H_s and for typical values of n and n_s, the burning rate formula [see Eq. (29)] has been plotted in Figs. 3(a), 3(b), and 3(c).

All these curves are qualitatively similar. At sufficiently *low* pressures, Eq. (29) gives

$$r/a \propto P/b. \quad (30)$$

This *linear* relation characterizes a simple laminar flame and shows that the pyrolysis law is ineffectual at low pressures. On the other hand, at *very high* pressures Eq. (29) predicts

$$r/a \to \exp(-n_s) = \text{const.} \quad (31)$$

This *limiting* relation asserts that the burning rate is *asymptotically constant* and shows that the pyrolysis law, evaluated with T_s equal to the adiabatic flame temperature, provides the maximum burning rate. Through the range of *intermediate* pressures the local dependence of r/a on P/b gradually changes from Eq. (30) to Eq. (31), as shown in Figs. 3(a-c).

In order to compare these theoretical results with experiment, we turn to the recent investigations of Summerfield and his co-workers.[5] Composite ammonium perchlorate propellants have been burned over a wide range of pressures (from 15 psia to 2000 psia). At *low* pressures the experimental burning rates follow the theoretical relation in Eq. (30). At *high* pressures the experimental burning rates tend to obey

$$r/a \propto (P/b)^{1/3}. \quad (32)$$

Through the range of *intermediate* pressures the local dependence gradually changes from Eq. (30) to Eq. (32).

Now the surface index for ammonium perchlorate propellants is close to 5 (since the activation temperature for the surface decomposition is roughly 10 000°K). With the gas index assumed to be 10, the theoretical curve [$H_s = -c_s T_u$, $n_s = 5$, $n = 10$ in Fig. 3(b)] is plotted against some experimental measurements,[5] § in Fig. 4. In spite of the acceptable correlation in Fig. 4, additional experiments at *very high* pressures (say ~20 000 psia) are needed for a decisive test of the theory. At very high pressures the theory predicts the limiting relation in Eq. (31), an *asymptotically constant* burning rate.

It must be remarked that an asymptotically constant burning rate does not follow from Summerfield's concept of *unmixedness*. According to the latter, the functional dependence in Eq. (32) is supposed to become increasingly accurate at very high pressures. Hence, new experiments will determine the burning mechanism of ammonium perchlorate propellants in an unambiguous fashion.

Unlike the ammonium perchlorate mixtures, some solid propellants exhibit more complicated burning rates. Experiments have shown anomalous behavior at low pressures and so-called "pressure plateaus" at higher pressures. Can the theory of a pyrolysis law and a premixed laminar flame (without the addition of *ad hoc* postulates) elucidate these facts? Qualitatively the answer is "yes," for a more general representation of the combustion chemistry (say reactions of various orders in competition) will produce anomalous behavior at low pressures and "pressure plateaus" at higher pressures. The quantitative answer requires an appropriate theoretical analysis.

NOMENCLATURE

a (cm/sec), prefactor of the pyrolysis law, a constant related to the propellant composition.
b (g/cm-sec^2), parameter defined by Eq. (17).
c_p (cal/g °K), specific heat of the gas, a constant.
c_s (cal/g °K), specific heat of the propellant, a constant.
$f(T)$ (sec^3/g-gm), temperature dependent part of the reaction rate expression.
H (cal/g), heat of reaction in the gas.

§ Taken from Fig. 15. In reducing these experimental data to dimensionless form, we have systematically chosen $b = 5000$ psia and a such that the theoretical and experimental values agree at 400 psia. Less systematic assignments for a, b, and n ($\equiv 10$ here) would naturally improve the over-all correlation.

H_s (cal/g), heat of decomposition for the propellant surface.
k (cal/cm-sec °K), thermal conductivity of the gas, a function of composition and temperature.
k_s (cal/cm-sec °K), thermal conductivity of the propellant, a function of temperature.
n (dimensionless), index for the chemical reaction in the gas, $\cong$ (effective activation temperature) $H/c_pT_b^2$.
n_s (dimensionless), index for the surface decomposition, $\cong$ (activation temperature) c_s/H.
P (g/cm-sec^2), pressure of the gas, a constant.
r (cm/sec), burning rate of the propellant.
T (°K), temperature, a function of x.
T_u (°K), initial temperature within the interior of the propellant.
T_s (°K), average temperature at the surface of the propellant.
T_b (°K), final temperature of the burned gas.
V (cm/sec), velocity of the gas, a function of x.
x (cm), distance normal to the propellant surface.
ξ (dimensionless), distance variable defined by Eq. (14).
ρ (g/cm^3), density of the gas, a function of x.
ρ_s (g/cm^3), density of the propellant, a constant.
τ (dimensionless), temperature rise defined by Eq. (15), a function of ξ.
τ_s (dimensionless), temperature rise at the surface.
ω_1 (dimensionless), weight fraction of the fuel component in the gas, a function of x.
ω_2 (dimensionless), weight fraction of the oxidizer component in the gas, a function of x.

THE JOURNAL OF CHEMICAL PHYSICS VOLUME 32, NUMBER 1 JANUARY, 1960

Nucleation of Alumina at High Supersaturations and Subsequent Recrystallization

G. W. SEARS AND R. C. DEVRIES
General Electric Research Laboratory, Schenectady, New York

(Received July 30, 1959)

Previous studies of the growth of alumina crystals have demonstrated the validity of current crystal growth theory for a high-temperature system involving a chemical reaction. The nucleation of alumina on a perfect alumina surface has been studied in the present report at very high supersaturations. The nucleation event is not consistent with the classical theory of nucleation, but rather is described by the Cahn-Hilliard theory of nucleation based on their treatment of the thermodynamics of nonuniform systems. In addition, the recrystallization of polycrystalline deposits to give near perfect crystal was observed.

IT has been reported in previous studies[1] that the growth of alumina crystals by a vapor phase reaction at high temperatures furnishes an ideal system for testing the applicability of current crystal growth theories to high temperature systems. The present report describes unique observations on the nucleation event involved in crystal growth as well as a subsequent recrystallization process which transforms a polycrystalline mass into a perfect crystal region. The nucleation behavior will be described in the framework of Cahn and Hilliard's[2] treatment of nucleation from a two component incompressible fluid.

EXPERIMENTAL

A detailed description of the crystal growth apparatus[1] has been given in an earlier report. An alumina rod was heated to 1800°C–2000°C by a coaxial helical coil of tungsten wire. The assembly was contained in a vessel through which a flow of hydrogen was maintained. In the hottest region Al_2O_3 was reduced to a lower volatile oxide. The crystal growth occurred in the cooler region by the reversal of the reduction reaction. Observation ports allowed the growth process to be followed at binocular magnifications up to 80×.

Sapphire has a crystal structure in which the oxide ions are hexagonally close packed and the aluminum ions are located in the octahedral interstices of the oxygen framework.[3,4] Whiskers can be grown as c whiskers having a [0001] orientation and also as a whiskers having a [1$\bar{1}$00] type axial direction, i.e., the whisker axis is parallel to the hexagonal plane of the crystal. These whiskers widen into blades at their free end to the shape shown in Fig. 1. When a blade was first formed, it was too thin to exhibit interference colors. The lateral surfaces of the blades were perfect {0001} type surfaces in that they were free of emergent screw dislocations. The absence of screw dislocations was

[1] R. C. DeVries and G. W. Sears, J. Chem. Phys. **31**, 1256 (1959).
[2] J. W. Cahn and J. E. Hilliard, J. Chem. Phys. **31**, 688 (1959).
[3] L. Pauling and S. Hendricks, J. Am. Chem. Soc. **47**, 781 (1925).
[4] W. L. Bragg, *Atomic Structure of Minerals* (Cornell University Press, Ithaca, New York, 1939).

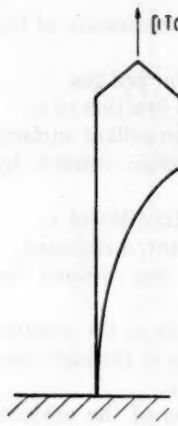

FIG. 1. Widened *a* whisker viewed along *c* axis.

deduced from the growth behavior.[2] It was also surmised that the surface was free of edge dislocations, but empirical evidence was lacking.

Experimental crystals were grown at a constant coil current such that the alumina source rod was maintained at a constant high temperature. When a crystal showing a perfect {0001} face as large as 100 $\mu \times 100$ μ was grown, this face served as an experimental region for investigating self-nucleation on a perfect surface. Perfect surfaces as large at 100 $\mu \times 500$ μ were occasionally obtained.

The heating current in the tungsten coil was reduced as rapidly as possible by turning down a Variac to a predetermined value. After thirty seconds the coil current was raised back to the value used during the growth process. The temperature of the crystal and its vapor environment dropped much more rapidly than the vapor and solid phases could come to thermodynamic equilibrium. Thus the perfect surface was maintained temporarily in contact with a limited volume of heavily supersaturated vapor phase.

When a crystal after exposure to a high supersaturation was again observed at the high temperature (the heating coil served as a light source), no immediate change could be seen in the crystal surface at 80× magnification. After two or three minutes at the high temperature growth occurred on some of the nuclei that were formed during the quench. This growth only occurred after the quenching procedure. The growth behavior depended on the quenching temperature.

If the system was quenched to a coil current corresponding to 1000°C and then was heated to the original growth temperature, interference colored hexagons grew in apparent coherence with the parent platelet surface. The various colored hexagons expanded about their appearance sites until eventually the crystal assumed the interference color and thickness corresponding to the thickest original hexagonal patch. Each hexagonal patch maintained constant interference color until overgrown by a thicker patch. The final colored crystal maintained its uniform shade of color for the times involved in the experiment (~30 min).

If the system was quenched to zero coil current before reheating, the surface nucleation and growth process followed a different pattern. When the temperature was raised back to the growth value again, no evidence for nucleation could be immediately observed. After about two minutes, a few white dots had appeared on the perfect surface. In another two or three minutes, the white dots had transformed to apparently coherent interference colored hexagonal patches as in the 1000°C quench. The subsequent growth behavior was the same as observed with the 1000°C quench.

DISCUSSION

Nucleation at High Supersaturations

The classical analysis of phase stability was formulated by Gibbs.[5] Although he recognized that a critical nucleus of a stable phase might be so small that it was completely inhomogeneous, he developed an artificial model which allowed the application of the thermodynamic treatment apropos of homogeneous phases. Gibbs formulated a self-consistent method of describing the critical nucleus as though it were homogeneous up to a sharp interface with the parent phase. The total free energy of forming a nucleus was split into a positive interfacial free energy term and a negative volume free energy term.

In the classical theory of nucleation which has been developed from Gibbs theory of phase stability, the specific interfacial free energy is equated to the specific free energy of a flat interface and the volume free energy is equated to the volume free energy of transformation for bulk phases.

Recently Cahn and Hilliard[6] have presented a thermodynamic treatment of a nonuniform system. They have found that the free energy of a small volume of such a system can be represented as the sum of two terms—one characteristic of the free energy at the local composition and a second that is nearly proportional to the square of the local composition gradient. Hart[7] later confirmed the validity of Cahn and Hilliard's[6] results by a classical thermodynamic formulation involving undetermined multipliers and redundant variables. Cahn[8] established the equivalence of the two treatments.

Since the knowledge of the free energy of nonuniform systems allows an analysis of the nucleation event without the use of an artificially defined nucleus, Cahn and Hilliard[2] have recently treated nucleation in a two-component incompressible fluid. The results of their treatment of pertinence to the present observations are concerned with the nature of the critical nucleus at high supersaturations. Although the nucleation of a

[5] J. W. Gibbs, *Collected Works* (Yale University Press, New Haven, Connecticut, 1948), Vol. 1, pp. 105–115, 252–258.
[6] J. W. Cahn and J. E. Hilliard, J. Chem. Phys. **28**, 258 (1958).
[7] E. W. Hart, Phys. Rev. **113**, 412 (1959).
[8] J. W. Cahn, J. Chem. Phys. **30**, 1121 (1959).

solid phase on the perfect surface of its own phase appears to be a much different system than described by Cahn and Hilliard,[2] it has a common critical characteristic—the lack of an energy term involving elastic strains, at least to a first approximation.

In resume, the Cahn-Hilliard theory predicts that the free energy of formation at increasing supersaturations should be less than calculated by classical nucleation theory, the composition at the center of a nucleus should deviate from that of a classical nucleus, and the radius should be at first less than but finally larger than the radius of a classical nucleus. At still higher supersaturations, the radius should become large, the free energy of nucleation should approach zero and no part of the nucleus should be homogeneous.

At the lowest supersaturations nucleation did not occur[1] on perfect sapphire surfaces. At somewhat higher supersaturations thickening occurred by a nucleation mechanism. The qualitative behavior was consistent[1] with a two-dimensional nucleation process.

When the alumina crystals and the parent vapor phase were quenched by cooling the tungsten heating coil, the temperature of the system dropped so rapidly that equilibrium could not be maintained between solid and vapor phase. Thus the perfect sapphire surfaces were temporarily exposed to a limited volume of highly supersaturated vapor phase.

The nature of the nuclei forming at high supersaturation was deduced from their subsequent growth behavior. The dots that originally grew at some sites on the crystal surface must have contained many interfaces to account for their white appearance. Qualitatively the parent nuclei might equally well be described as inhomogeneous in structure or as polycrystalline. Classical nucleation theory would predict a very small nucleus at high supersaturations, but small nuclei could not contain sufficient structural inhomogeneities to yield the white masses of a few microns diameter after further growth at lower supersaturations. It is deduced in agreement with the Cahn-Hilliard[2] theory of nucleation that the radius is larger than that of a classical nucleus at high supersaturations, and that substantial portions of the nucleus must be structurally inhomogeneous.

The nucleation event occurring at a given site on a perfect surface must represent a single event since the local supersaturation must diminish following the formation of a stable nucleus. Thus consecutive fluctuations leading to a polycrystalline or inhomogeneous nucleus cannot furnish a possible path of formation.

The intermediate quench to 1000°C in which white dots were not observed as an intermediate growth form must be interpreted as following the same steps as the lower quench, the recrystallization of the polycrystalline mass occurring before the growing nucleus reached a visible size.

RECRYSTALLIZATION

The white polycrystalline regions recrystallized to hexagonal regions which were apparently coherent with the parent platelet. No screw dislocations emerged from the {0001} surfaces of either the parent platelet or from the recrystallized hexagonal patches, since no thickening occurred during the lateral growth at low supersaturations. Growth sites were not generated at the intersections of the growing hexagons. It follows that the hexagons were in exact coherence with the parent platelet with respect to tilt, i.e., the {0001} planes of the hexagons and of the parent platelet were exactly parallel. It is not possible to demonstrate the absence of a very small twist of the hexagons with respect to the parent platelet about the [0001] axis by the growth behavior. Lateral growth in the {0001} plane occurred by two-dimensional nucleation, so the presence of screw dislocations defining the possible twist boundary could not be established or denied.

The recrystallization of the polycrystalline material on the perfect platelet is consistent with the theory[9] that the mechanisms of crystalline growth that are appropriate for vapor phase deposition are generally valid for crystal growth from any parent phase, be it solid, liquid, or vapor.

[9] J. W. Cahn and G. W. Sears (unpublished results).

Quantum Mechanical Cell Model of the Liquid State. I*

J. M. H. LEVELT† AND R. P. HURST‡

The University of Wisconsin Theoretical Chemistry Laboratory, Madison, Wisconsin

(Received June 26, 1959)

In this paper the cell model for the liquid state, as proposed by Lennard-Jones and Devonshire, is recast in terms of quantum statistical mechanics. A method is developed by which the energy levels and wave functions in the liquid cell can be determined to any prescribed accuracy. Thus, in the present work, no additional approximations are introduced which are not inherent in the cell model. When a sufficient number of energy levels is obtained, the partition function and thus the thermodynamic properties are derived.

A method is devised by which from a knowledge of the wave function, the derivative of the corresponding energy with respect to the volume may be obtained. This derivative is required for the evaluation of the pressure.

The theory is applied to H_2 and D_2 at a density near that of the crystals at 0°K. The corresponding classical Lennard-Jones and Devonshire thermodynamic functions are obtained and compared with the results of the present theory. The calculations involved were performed on a Bendix G–15D computer.

The quantized cell theory predicts that for hydrogen and deuterium experimentally detectable differences in energy, entropy, and specific heat must persist at temperatures as high as −150°C.

I. INTRODUCTION

THE cell theory of Lennard-Jones and Devonshire[1] is a fruitful attempt to obtain an understanding of the liquid state. Many modifications and elaborations of the original theory have been proposed.[2] However, it is only for the model in almost its simplest form, that extensive numerical results have as yet been obtained.[3]

Due to the assumptions involved, the cell theory can be expected to give reasonable results only at high densities. Apart from the statistical short-comings, however, there are other reasons for failure of the simple theory.

Since the cell theory of Lennard-Jones and Devonshire is based on the assumptions of additivity, Lennard-Jones 6–12 interaction, and classical statistics, a law of corresponding states follows from this theory.[4]

Experiments show, however, that a law of corresponding states is not strictly valid, even for gases consisting of simple molecules. At low temperatures, for instance, the compressibility factor PV/NkT for the light gases helium, hydrogen, and deuterium is appreciably higher than for the heavy noble gases (Fig. 1).

Recent measurements of the compressibility of hydrogen and deuterium reveal a difference in behavior of these gases, which even persists to room temperatures[5] (Table I).

Large deviations from corresponding states are also observed for coexisting gas and liquid densities of light and heavy noble gases.[6]

To account for the experimental differences, several attempts have been made to introduce quantum corrections into the classical cell theory. One method is to make an estimate of the zeropoint energy in the liquid cell by replacing the actual potential somewhat arbitrarily by a square potential well.[7] A second approach[8] is based on the expansion of the quantum-statistical Slater sum in powers of the quantum parameter.[9] Although the latter method is to be preferred above the first, because no further approximations have to be introduced in the cell model itself, it has the disadvantage that at low temperatures it fails for quantum parameters larger than 1, that is, for He, H_2, and D_2.

The object of this paper is to present an exact quantum-mechanical treatment of the cell theory. It is exact in that no approximations are introduced other than those inherent in the cell model. The theory is presented in two parts, as will be explained in Sec. II. The first part (Sec. III) involves the solution of the Schroedinger equation for the motion of a particle in the sphericalized potential field of the theory of Lennard-Jones and Devonshire. In the second part the macroscopic thermodynamic properties are derived from a knowledge of the energy levels in the cells (Sec. IV).

* This work is being reported under Contract DA–11–022–ORD–2526.

† Present Address: Van der Waals Laboratorium, Gemeente-Universiteit, Amsterdam, Holland.

‡ Noyes Chemical Laboratory, University of Illinois, Urbana, Illinois.

[1] J. E. Lennard-Jones and A. F. Devonshire, Proc. Roy. Soc. (London) **A163**, 53 (1937).

[2] J. G. Kirkwood, J. Chem. Phys. **18**, 380 (1950); P. Janssens and I. Prigogine, Physica **XVI**, 895 (1950); J. S. Rowlinson and C. F. Curtiss, J. Chem. Phys. **19**, 1519 (1951); J. de Boer, Proc. Roy. Soc. (London) **A215**, 4 (1952); J. de Boer, Physica **XX**, 655 (1954); Cohen, de Boer, and Salsburg, Physica **XXI**, 137 (1955).

[3] Wentorff, Buehler, Hirschfelder, and Curtiss, J. Chem. Phys. **18**, 1484 (1950); Hirschfelder, Curtiss, and Bird, *Molecular Theory of Gases and Liquids* (John Wiley & Sons, New York, 1954), p. 293 ff.

[4] E. A. Guggenheim, J. Chem. Phys. **13**, 253 (1945); K. S. Pitzer, *ibid.* **7**, 583 (1939); J. de Boer, Physica **XV**, 139 (1948).

[5] Michels, de Graaff, Wassenaar, Levelt, and Louwerse, Physica **XXV**, 123 (1959).

[6] J. de Boer and R. J. Lunbeck, Physica **XIV**, 520 (1948).

[7] I. Prigogine and J. Philippot, Physica **XVIII**, 729 (1952); S. D. Hamann, Trans. Faraday Soc. **48**, 303 (1952); H. G. David and S. D. Hamann, *ibid.* **49**, 711 (1953).

[8] R. J. Lunbeck, Thesis, Amsterdam (1951).

[9] J. G. Kirkwood, Phys. Rev. **44**, 31 (1933); R. W. Zwanzig, *ibid.* **106**, 13 (1957).

In Sec. V an application of the theory has been made to the gases hydrogen and deuterium, at a density close to that of the crystal, and for a fairly wide temperature range. The corresponding classical computations have been made for the same density and temperatures.

II. THE MODEL

Since a survey of the classical theory of Lennard-Jones and Devonshire may be found elsewhere,[1-3] only those aspects relevant to the present treatment will be considered here.

The classical partition function for a system of molecules without internal degrees of freedom is given by

$$Z_{cl}=(1/N!)\,(2\pi mkT/h^2)^{3N/2}\int\cdots\int \exp(-\phi(r)/kT)\,d\tau_1\cdots d\tau_N$$
$$=(2\pi mkT/h^2)^{3N/2}Q_{cl}, \tag{1}$$

where Q_{cl} is the so-called configurational integral and $\phi(r)$ the total potential energy of the system of interacting molecules. In the L.J-D. cell theory, the integration is not performed over all possible configurations of the molecules. The assumption is made that at liquid densities the main contribution to the configurational integral comes from situations in which each molecule is restricted in its motion to a cell formed by its neighbors; consequently, the configurational integral Q_{cl} is simplified to a product of one particle integrals

$$Q_{cl}=(1/N!)\left\{\int \exp\{-[V(r)-V(0)]/kT\}d\tau\right\}^N \times \exp(-\tfrac{1}{2}NV(0)/kT), \tag{2}$$

where

$$\int \exp\{-[V(r)-V(0)]/kT\}d\tau \tag{3}$$

is called the free volume v_f. The quantity $V(r)-V(0)$ is approximated by a function $\bar{V}(r)$ in the following way. First, the assumption is made that the molecules interact according to a spherically symmetric Lennard-Jones (6-12) potential

$$\varphi(r')=4\epsilon[(\sigma/r')^{12}-(\sigma/r')^6], \tag{4}$$

where r' is the distance between the centers of two particles, and ϵ and σ are two parameters characteristic of the substance under consideration.

For the computation of the potential in the cell, the particles are assumed to be distributed over a close-packed lattice, so that each particle has 12 nearest neighbors at distance a. In the simple cell theory the potential distribution in the cell is determined by averaging the contributions from the twelve nearest neighbors over all angles. The result of this spherically is

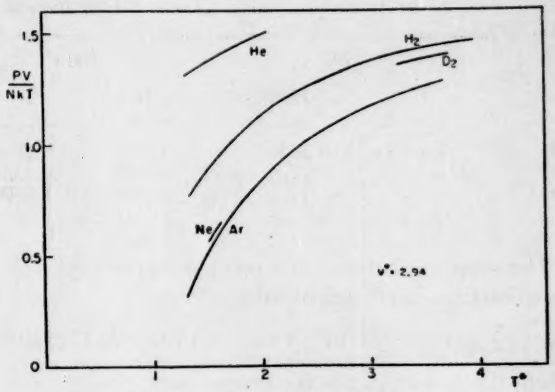

FIG. 1. Experimental compressibility factors.

$$\bar{V}(r)=C\epsilon\sigma^{12}\left\{\frac{1}{5ar}\left[\frac{1}{(a-r)^{10}}-\frac{1}{(a+r)^{10}}\right]-\frac{4}{a^{12}}\right\} +C\epsilon\sigma^6\left\{\frac{1}{2ar}\left[\frac{1}{(a+r)^4}-\frac{1}{(a-r)^4}\right]+\frac{4}{a^6}\right\}, \tag{5}$$

where $C=12$, and r is the distance from the center of the cell. Here the zero point of potential energy is chosen in the center of the cell. The free volume then follows from

$$v_f=\int_{\text{cell}} \exp(-\bar{V}(r)/kT)4\pi r^2dr, \tag{6}$$

where the integration extends between 0 and r_m. Here r_m is chosen such that the volume of the cell equals the volume per molecule

$$\tfrac{4}{3}\pi r_m^3=V/N. \tag{7}$$

However, since the potential rises very steeply at the edge of the cell, the exact choice of r_m is not critical (Fig. 2).

From the free volume and its temperature and volume derivatives, the thermodynamic properties of the system can be readily deduced, as will be shown in Sec. IV.

To obtain a quantum mechanical cell theory, the classical partition function

$$Z_{cl}=(1/N!)\,(2\pi mkT/h^2)^{3N/2} \times\int\cdots\int \exp(-\phi(r)/kT)d\tau_1\cdots d\tau_N, \tag{8}$$

must be replaced by the Slater sum

$$Z_{qu}=\sum_n g_n \exp(-E_n/kT), \tag{9}$$

where the summation extends over all energy eigenvalues of which the system is capable, and g_n is the weight factor or degeneracy of each level.

TABLE I. Experimental PV product of H_2 and D_2.

	−175°C		−100°C		0°C		+150°C	
d_{am}	H_2	D_2	H_2	D_2	H_2	D_2	H_2	D_2
200	0.3660	0.3606	0.7086	0.7040	1.1545	1.1494	1.8105	1.8044
400	...	...	0.8470	0.8327	1.3917	1.3766	2.1744	2.1573
600	...	...	1.0829	1.0500	1.7448	1.7119	2.6733	2.6379

The simple cell theory is a one particle theory. The partition function therefore reduces to

$$Z_{qu}=(\sum g_n \exp[-\lambda_n/kT])^N \exp(-NV(0)/2kT), \quad (10)$$

where the λ_n and g_n are the energy levels and the degeneracy, respectively, for one particle in a cell.

The energy levels are obtained by solving the Schroedinger equation for a particle moving in the sphericalized potential in the cell

$$(-\hbar^2/2m)\Delta\psi+(\bar{V}-\lambda)\psi=0, \quad (11)$$

with the boundary condition that ψ equals zero at

$$r=r_m=(3V/4\pi N)^{1/3}. \quad (12)$$

When this equation is solved, and a sufficient number of energy levels is obtained, the partition function and its derivatives with respect to volume and temperature can be determined; then the thermodynamic properties follow as will be shown in Sec. IV.

III. METHODS AND CALCULATIONS

A. Solution of the Eigenvalue Problem

The Schroedinger equation [Eq. (11)] for the present problem is first simplified and made tractable for numerical solution by introduction of new units. Thus, it is convenient to define

$$\rho=r/\sigma, \qquad \rho_m=(r_m/\sigma)=(3/4\pi\sqrt{2})^{1/3}\alpha, \quad (13)$$

$$\alpha=a/\sigma, \quad (14)$$

and Λ, the "quantum parameter" by,

$$\Lambda=h/(m\epsilon)^{\frac{1}{2}}\sigma. \quad (15)$$

In these new units Eq. (11) becomes

$$-\Delta\psi+(8\pi^2/\Lambda^2\epsilon)[\bar{V}(\rho)-\lambda]\psi=0, \quad (16)$$

where the potential $\bar{V}(\rho)$, Eq. (5), is then given by

$$\bar{V}(\rho)=\frac{C\epsilon}{\alpha\rho}\left\{\tfrac{1}{2}\left[\frac{1}{(\rho+\alpha)^4}-\frac{1}{(\rho-\alpha)^4}\right]+\tfrac{1}{5}\left[\frac{1}{(\rho-\alpha)^{10}}-\frac{1}{(\rho+\alpha)^{10}}\right]\right\}+C\epsilon\left(\frac{4}{\alpha^6}-\frac{4}{\alpha^{12}}\right). \quad (17)$$

Since $\bar{V}(\rho)$ is spherically symmetric, the Schroedinger equation can be shown[10] to have solutions of the form

$$\psi=Y_{l,m}(\theta,\phi)R(\rho). \quad (18)$$

[10] L. I. Schiff, *Quantum Mechanics* (McGraw-Hill Book Company, Inc., New York, 1955), p. 69.

Here the functions $Y_{l,m}(\theta, \phi)$ are the well-known spherical harmonics, and $R(\rho)$ satisfies the equation

$$(1/\rho^2)(d/d\rho)[\rho^2(dR/d\rho)]+\{-[l(l+1)/\rho^2]+(8\pi^2/\Lambda^2\epsilon)[\lambda-\bar{V}(\rho)]\}R=0, \quad (19)$$

where $l=0, 1, 2, 3, \cdots$.

Additional simplification in Eq. (19) is gained by introducing the substitution

$$R=S/\rho, \quad (20)$$

so that one obtains

$$(d^2S/d\rho^2)+\left\{-\frac{l(l+1)}{\rho^2}+W-\frac{8\pi^2}{\Lambda^2\epsilon}\bar{V}(\rho)\right\}S=0 \quad (21)$$

and

$$W=8\pi^2\lambda/\Lambda^2\epsilon. \quad (22)$$

Further, since we require that $R(\rho)$ be finite within the cell and restrict the motion of the wandering particle to the interior of the cell our boundary conditions become

$$S(W,0)=S(W,\rho_m)=0. \quad (23)$$

It is perhaps well to mention at this point that the choice of methods to be used in solving Eq. (21) is strongly influenced by the fact that the energy levels are rather close together. In order to obtain reliable thermodynamic properties from the partition function one must therefore have reasonably accurate eigenvalues even for the higher levels. This is particularly true for higher levels associated with large l values because of the correspondingly large statistical weight factors. Thus a method which gives accurate eigensolutions for Eq. (21) is highly desirable despite the fact that it may be difficult to use.

Since $(8\pi^2/\Lambda^2\epsilon)\bar{V}(\rho)$ contains only even powers of ρ, a Taylor series expansion for this quantity could contain only even powers of ρ. Further, since the other terms of Eq. (21) also contain only even powers of ρ one is led to suspect that the recursion relations for a power series expansion of S would be sufficiently simple so that the power series method of solution would be tractable. This has proven to be the case. Thus

$(8\pi^2/\Lambda^2\epsilon)\bar{V}(\rho)$ is represented by the Taylor series expansion which we have shown to be convergent for $\rho<1$ where

$$(8\pi^2/\Lambda^2\epsilon)\bar{V}(\rho)=4C\sum_{n=1}^{\infty}C_{2n}\rho^{2n} \tag{24}$$

and

$$C_{2n}=\frac{8\pi^2}{\Lambda^2}\left[\frac{1}{\alpha^{2n+12}}\frac{(2n+10)!}{10!(2n+1)!}-\frac{1}{\alpha^{2n+6}}\frac{(2n+4)!}{4!(2n+1)!}\right]. \tag{25}$$

We next try for a solution to Eq. (21) of the form

$$S=\sum_{i=0}^{\infty}a_i\rho^{i+s}. \tag{26}$$

On substitution of Eq. (26) into Eq. (21) one finds that the condition

$$S(0)=0$$

implies

$$a_{2i}=0 \tag{27}$$

where

$$i=0, 1, 2, 3, \cdots.$$

Further, after truncating the expansion for

$$(8\pi^2/\Lambda^2\epsilon)\bar{V}(\rho)$$

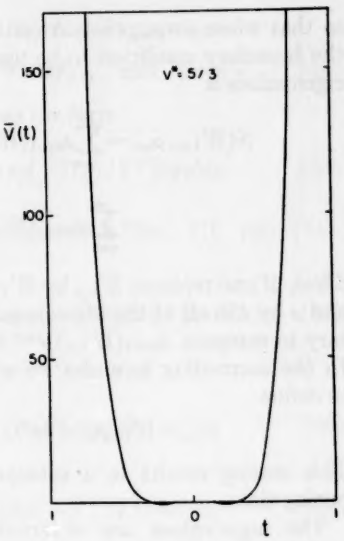

FIG. 2. Reduced potential in liquid cell at $v^*=5/3$.

to include M terms, i.e.,

$$(8\pi^2/\Lambda^2\epsilon)\bar{V}(\rho)=4C\sum_{n=1}^{M}C_{2n}\rho^{2n}, \tag{28}$$

one obtains the following recursion relations between the coefficients in the series chosen to represent S:

$$a_1 \text{ (arbitrary)} \tag{29a}$$

$$a_3=\{-Wa_1/[(l+3)(l+2)-l(l+1)]\} \tag{29b}$$

$$a_5=\{(C_2a_1-Wa_3)/[(l+5)(l+4)-l(l+1)]\} \tag{29c}$$

$$a_7=\{(C_4a_1+C_2a_3-Wa_5)/[(l+7)(l+6)-l(l+1)]\} \tag{29d}$$

$$a_9=\{(C_6a_1+C_4a_3+C_2a_5-Wa_7)/[(l+9)(l+8)-l(l+1)]\} \tag{29e}$$

$$\vdots \qquad\qquad \vdots$$

$$a_{2M+2m+3}=\frac{C_{2M}a_{2m+1}+C_{2M-2}a_{2m+3}+\cdots+C_2a_{2M+2m-1}-Wa_{2M+2m+1}}{(l+2M+2m+3)(l+2M+2m+2)-l(l+1)} \tag{29f}$$

where $m=0, 1, 2, 3, \cdots$.

Since one can show that $s=l$ we have

$$S(W,\rho)=\sum_{i=0}^{\infty}a_{2i+1}(W)\rho^{2i+l+1}. \tag{30}$$

This series converges for positive values of W and for $\rho\leq\rho_m$. In particular, those values of W which satisfy the boundary condition at the extremity of the cell, i.e., $S(W,\rho_m)=0$, are the eigenvalues to which the corresponding eigenfunctions R are given by Eq. (20)

$$R=S/\rho. \tag{31}$$

Further, we adopt the convention that those values of W and functions R which are the eigenfunctions and eigenvalues, respectively, will be denoted by subscripts l and n. Thus, $R_{l,n}$ is associated with $W_{l,n}$ where $l=0, 1, 2, 3\cdots$ and $n=1, 2, 3\cdots$. Again, the eigensolutions to the Schroedinger equation of the present problem are given by

$$\psi_{l,m,n}=Y_{l,m}(\theta,\phi)R_{l,n}(\rho), \tag{32}$$

where $Y_{l,m}(\theta,\phi)$ are spherical harmonics, $R_{l,n}(\rho)$ are given by Eqs. (30) and (31), and where

$$W_{l,n}=8\pi^2\lambda_{l,n}/\Lambda^2\epsilon. \tag{33}$$

For computational convenience we introduce the variable

$$t=\rho/\rho_m \tag{34}$$

so that when $\rho=\rho_m$, $t=1$. After this change in scaling the boundary condition to be used in determining the eigenvalues is

$$S(W_{l,n},\rho_m)=\sum_{i=0}^{\infty}a_{2i+1}(W_{l,n})\rho_m{}^{2i+1+l} \tag{35}$$

$$=\sum_{i=0}^{\infty}a_{2i+1}'(W_{l,n})=0. \tag{35}$$

Thus, if one replaces $W_{l,n}$ by $W_{l,n}\rho_m{}^2$, C_{2n} by $C_{2n}\rho_m{}^{2n+2}$ and ρ by t in all of the above equations it is not necessary to compute $a_{2i+1}(W_{l,n})\rho^{2i+1}$ but only $a_{2i+1}'(W_{l,n})$. In the succeeding formulas we will find it convenient to define

$$E_{l,n}=W_{l,n}\rho_m{}^2=8\pi^2\lambda_{l,n}\rho_m{}^2/\Lambda^2\epsilon. \tag{36}$$

This scaling results in a substantial saving in computing time.

The eigenvalues are determined on the Bendix G–15D computer in the following way. First, $S(E^1,\rho_m)$ is computed for a given choice E^1 of the energy parameter. Next, E^1 is incremented by an arbitrary amount Δ i.e., $E^2=E^1+\Delta$ and $S(E^2,\rho_m)$ is evaluated. Then, the ratio $S(E^2,\rho_m)/S(E^1,\rho_m)$ is computed and tested for sign. If the sign is negative an eigenvalue must lie between E^2 and E^1. In this case control is transferred to a routine which automatically iterates for the indicated eigenvalue with Newton's method. The iterations are generally continued until the eigenvalues are accurate to at least six places.

On the other hand, if the ratio $S(E^2,\rho_m)/S(E^1,\rho_m)$ is positive no eigenvalue has been located. In this latter case the energy parameter is incremented and as before the sign of the ratio $S(E^3,\rho_m)/S(E^2,\rho_m)$ is tested for the presence of an eigenvalue between E^3 and E^2. Again, if an eigenvalue has been found control is transferred to the automatic iteration routine. If an eigenvalue has not been found, the energy parameter is incremented to give E^4, and the same sequences of operations are performed as before. The entire process of locating the eigenvalues by the changes in sign of S and later iterating to determine the eigenvalues precisely is entirely automatic so that it is possible for the computer to determine all eigenvalues below a set maximum E without being attended.

In the present work for H_2 and D_2 it was found to be sufficient to take between 10 and 20 terms in the expansion for the potential [Eq. (28)] and between 125 and 150 terms in the expansion for S [Eq. (26)]. Results of these calculations are given in Sec. V.

B. The Volume Derivative of the Eigenvalues

As will be shown in Sec. IV, in order to determine the pressure one must know $\partial E_{l,n}/\partial v^*$ for all energy levels.

Since α and the reduced volume v^* are related by

$$\alpha^3=v^*\sqrt{2} \tag{37}$$

we have

$$\partial E_x/\partial v^*=(\sqrt{2}/3\alpha^2)(\partial E_x/\partial\alpha). \tag{38}$$

In Eq. (38) and in subsequent equations of the rest of this paper the double subscript l, n is replaced by a single index x or y. Further $\psi_{l,m,n}$ is denoted by $\psi_{m,x}$ or $\psi_{m,y}$. Thus, the problem reduces to devising a means for computing $\partial E_n/\partial\alpha$. This is obtained from the following considerations.

Let $H^{(1)}$ be the Hamiltonian of the system with α fixed at α_1. Similarly, $H^{(2)}$ is the Hamiltonian with $\alpha=\alpha_2$. Then one can treat the difference between $H^{(2)}$ and $H^{(1)}$ as a small perturbation H', that is

$$H^{(2)}=H^{(1)}+H'. \tag{39}$$

If

$$H^{(1)}\psi_{m,x}{}^{(1)}=E_x{}^{(1)}\psi_{m,x}{}^{(1)}, \tag{40}$$

then, according to second order perturbation theory,[11] we have

$$E_x{}^{(2)}-E_x{}^{(1)}=H_{xx}'-\sum_{y}^{y\neq x}[H_{xy}'H_{yx}'/(E_y{}^{(1)}-E_x{}^{(1)})], \tag{41}$$

where

$$H_{x,y}'=H_{yx}'=\int\psi_{m,x}{}^{(1)}H'\psi_{m,y}{}^{(1)}d\tau$$

and

$$H'=\Delta[(8\pi^2/\Lambda^2\epsilon)\bar{V}(t,\alpha)]$$
$$=(8\pi^2/\Lambda^2\epsilon)[\bar{V}(t,\alpha_2)-\bar{V}(t,\alpha_1)]. \tag{43}$$

If we replace H' by the differential, we obtain

$$H'\approx\frac{8\pi^2}{\Lambda^2\epsilon}\frac{d\bar{V}}{d\alpha}\bigg|_{\alpha=\alpha_1}\Delta\alpha. \tag{44}$$

Equation (41) can then be written (considering high-order perturbation terms)

$$\frac{E_x{}^{(2)}-E_x{}^{(1)}}{\alpha_2-\alpha_1}=h_{xx}'-\Delta\alpha\sum_{y}^{y\neq x}\frac{h_{xy}'h_{yx}'}{E_y{}^{(1)}-E_x{}^{(1)}}+0(\Delta\alpha)^2, \tag{45}$$

where

$$h_{xy}'=h_{yx}'=\frac{8\pi^2}{\Lambda^2\epsilon}\int\psi_{mx}\frac{d\bar{V}}{d\alpha}\bigg|_{\alpha=\alpha_1}\psi_{my}d\tau \tag{46}$$

and

$$\frac{8\pi^2}{\Lambda^2\epsilon}\frac{d\bar{V}}{d\alpha}\bigg|_{\alpha=\alpha_1}=4C\frac{d}{d\alpha}[\sum_{n=1}^{\infty}C_{2n}\rho_m{}^{2n+2}f^{2n}]\big|_{\alpha=\alpha_1} \tag{47}$$

$$=-4C\sum_{n=1}^{\infty}B_{2n}f^{2n}. \tag{48}$$

In this case

$$B_{2n}=\frac{8\pi^2G^{2n+2}}{\Lambda^2}\left[\frac{(2n+10)!}{9!(2n+1)!\alpha_1{}^{11}}-\frac{(2n+4)!}{3!(2n+1)!\alpha_1{}^{5}}\right], \tag{49}$$

[11] L. Pauling and E. B. Wilson, *Introduction to Quantum Mechanics* (McGraw-Hill Book Company, New York, 1935), p. 176.

where

$$G=(3/4\pi\sqrt{2})^{1/3}. \tag{50}$$

Since

$$\lim_{\alpha_2\to\alpha_1}\frac{E_x^{(2)}-E_x^{(1)}}{\alpha_2-\alpha_1}=\frac{\partial E_x}{\partial\alpha}\bigg|_{\alpha=\alpha_1}=\frac{8\pi^2}{\Lambda^2\epsilon}\int\psi_{m,x}\frac{d\bar{V}}{d\alpha}\bigg|_{\alpha=\alpha_1}\psi_{m,x}d\tau, \tag{51}$$

we have

$$\frac{\partial E_x}{\partial v^*}=\frac{\sqrt{2}}{3\alpha^2}\int\psi_{m,x}\left[\frac{8\pi^2}{\Lambda^2\epsilon}\frac{d\bar{V}}{d\alpha}\right]\psi_{m,x}d\tau. \tag{52}$$

Equation (52) can be evaluated most conveniently by numerical integration.

IV. THE THERMODYNAMIC PROPERTIES

From the partition function Z, Eq. (1), the thermodynamic properties may be derived. As is usual, we compute internal functions, which are the difference between the values of the thermodynamic quantities for the substance under consideration, and those for an ideal gas at the same density and temperature.

The formulas used for both classical and quantum-mechanical computations are:

(the internal energy)

$$U_i=kT^2(\partial\ln Z/\partial T)-\tfrac{3}{2}NkT, \tag{53}$$

(the internal entropy)

$$S_i=k\ln Z+kT(\partial\ln Z/\partial T)$$
$$-Nk[\ln(V/N)+\tfrac{5}{2}+\ln(2\pi mkT/h^2)^{3/2}], \tag{54}$$

and (the internal specific heat)

$$C_{Vi}=2kT(\partial\ln Z/\partial T)+kT^2(\partial^2\ln Z/\partial T^2)-\tfrac{3}{2}Nk. \tag{55}$$

Moreover, the pressure may be obtained from

$$p=kT(\partial\ln Z/\partial V). \tag{56}$$

A. Classical Formalism

The classical partition function for the theory of Lennard-Jones and Devonshire is given by

$$Z=(2\pi mkT/h^2)^{3N/2}v_f{}^N\exp(-NV(0)/2kT). \tag{57}$$

Equations (53)–(56) therefore reduce to

$$U_i=NkT^2(\partial\ln v_f/\partial T)+NV(0)/2, \tag{58}$$

$$S_i=Nk[\ln v_f+\ln N/V+T(\partial\ln v_f/\partial T)-1], \tag{59}$$

$$C_{Vi}=NkT^2(\partial^2\ln v_f/\partial T^2)+2NkT(\partial\ln v_f/\partial T), \tag{60}$$

and

$$p=NkT(\partial\ln v_f/\partial V)-N/2(\partial V(0)/\partial V), \tag{61}$$

where the free volume v_f is given by

$$v_f=\int_0^{r_m}\exp[-\bar{V}(r)/kT]4\pi r^2dr. \tag{62}$$

After introduction of the reduced quantities

$$\bar{V}^*=\bar{V}/\epsilon,\quad T^*=kT/\epsilon,\quad\text{and}\quad\rho=r/\sigma, \tag{63}$$

the free volume assumes the form

$$v_f{}^*=v_f/\sigma^3=\int_0^{\rho_m}\exp[\bar{V}^*(\rho)/T^*]4\pi\rho^2d\rho. \tag{64}$$

The same scaling process as in Sec. III, Eq. (34), finally gives

$$(4\pi/3v^*)v_f{}^*=\int_0^1\exp[-\bar{V}^*(l)/T^*]4\pi l^2dl. \tag{65}$$

The quantities

$$A=\int_0^1\exp(-\bar{V}^*/T^*)4\pi l^2dl, \tag{66}$$

$$B=\int_0^1\bar{V}^*/T^*\exp(-\bar{V}^*/T^*)4\pi l^2dl, \tag{67}$$

$$C=\int_0^1(\bar{V}^*/T^*)^2\exp(-\bar{V}^*/T^*)4\pi l^2dl, \tag{68}$$

and

$$D=\int_0^1(\partial\bar{V}^*/\partial v^*)\exp(-\bar{V}^*/T^*)4\pi l^2dl \tag{69}$$

serve to compute the reduced thermodynamic properties and pressure as follows:

$$U_i{}^*=U_i/N\epsilon=(B/AT^*)+(NV^*(0)/2), \tag{70}$$

$$S_i{}^*=S_i/Nk=(B/A)+\ln A+\ln\tfrac{4}{3}\pi-1, \tag{71}$$

$$C_{Vi}{}^*=C_{Vi}/Nk=(C/A)-(B/A)^2, \tag{72}$$

$$p^*=p\sigma^3/\epsilon=T^*/v^*-(D/A)-\tfrac{1}{2}(\partial V_0{}^*/\partial v^*). \tag{73}$$

B. Quantized Cell Theory Partition Function

The partition function for the quantized cell theory is given by

$$Z=[\sum_x g_x\exp(-\lambda_x/kT)]^N\exp(-NV(0)/2kT), \tag{74}$$

where the energy levels λ_x follow from the eigenvalues E_x according to

$$\lambda_x=(\Lambda^2\epsilon/8\pi^2\rho_m{}^2)E_x. \tag{75}$$

After introducing the reduced units

$$\lambda_x{}^*=\lambda_x/\epsilon,\quad V^*(0)=V(0)/\epsilon,\quad\text{and}\quad T^*=kT/\epsilon, \tag{76}$$

the following quantities may be computed

$$K=\sum_x(2l+1)\exp(-\lambda_x{}^*/T^*), \tag{77}$$

$$L=\sum_x(2l+1)\lambda_x{}^*/T^*\exp(-\lambda_x{}^*/T^*), \tag{78}$$

$$M=\sum_x(2l+1)(\lambda_x{}^*/T^*)^2\exp(-\lambda_x{}^*/T^*), \tag{79}$$

$$N=\sum_x(2l+1)(\partial\lambda_x{}^*/\partial v^*)\exp(-\lambda_x{}^*/T^*). \tag{80}$$

TABLE II. Energy levels of H_2 and D_2 at $v^*=5/3$.

n \ l	0	1	2	3	4	5
			Hydrogen			
1	1.7611	3.5504	5.6998	8.1616	10.9060	13.9124
2	6.4680	9.3144	12.4085	15.7449	19.3150	
3	13.0252	16.7153	20.6159			
4	21.1588					
			Deuerium			
1	0.9955	2.0405	3.2997	4.7421	6.3485	8.1058
2	3.7602	5.4185	7.2171	9.1532	11.2218	13.4184
3	7.2770	9.7134	11.9656	14.3352		
4	12.1777	14.8324				
5	17.7731					

For the internal thermodynamic functions we find

$$U_i^*=(L/K-\tfrac{3}{2})T^*+NV^*(0)/2, \tag{81}$$

$$S_i^*=L/K+\ln K-\ln v^*-\tfrac{5}{2}-\tfrac{3}{2}\ln 2\pi T^*/\Lambda^2, \tag{82}$$

$$C_{Vi}^*=M/K-(L/K)^2-\tfrac{3}{2}, \tag{83}$$

whereas the pressure is given by

$$p^*=-(N/K)-\tfrac{1}{2}(\partial V^*(0)/\partial v^*). \tag{84}$$

It should be remarked that neither in Eq. (57) nor in Eq. (74) a correction for the communal entropy has been made. The expressions given for S_i therefore tend to -1 at low density and high temperature.

V. RESULTS

The theory given in the previous sections has been applied, and numerical results have been obtained for H_2 and D_2. For both isotopes the calculations were performed for a reduced volume $v^*=\frac{5}{3}$. Since the reduced crystal volumes at 0°K are 1.49 and 1.29 for H_2 and D_2, respectively, one should expect the reduced volume chosen for these calculations to be within the range where the cell theory applies.

The potential field within the cell as computed for this volume is pictured in Fig. 2.

For the computations, the quantum parameters were taken from Lunbeck,[8] who calculated these quantities for hydrogen and deuterium using $\sigma=2.928$ A and $\epsilon/k=37.00$°K for the parameters in an "effective" Lennard-Jones (6–12) potential. He assumed that deviations from spherical symmetry of the molecules, and differences in zero-point vibration of the nuclei of the isotopes, are negligible. Specifically, the calculations were based on the following values of the quantum parameter:

$$\text{for } H_2, \quad \Lambda=1.729,$$

and

$$\text{for } D_2, \quad \Lambda=1.223.$$

Following the methods described in Sec. IIIA, all energy eigenvalues below a maximum reduced energy of about 60 for H_2 and 50 for D_2 were obtained and used in the statistical-mechanical calculations of the thermodynamic properties. In general, enough terms were included in the calculation of S [cf. Eq. (26)] such that the ratio of the last term to the sum was smaller than 10^{-8}. Further, the Taylor expansion of

$$(8\pi^2/\Lambda^2\epsilon)\bar{V}(\rho),$$

Eq. (28), included enough terms, such that the energy

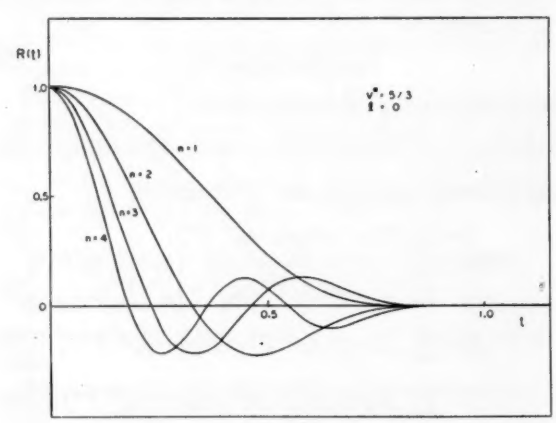

FIG. 3. Radial wave functions for $l=0$.

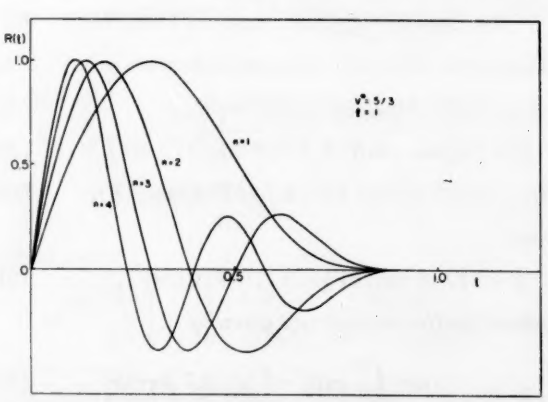

FIG. 4. Radial wave functions for $l=1$.

TABLE III. Reduced thermodynamic properties at $v^*=5/3$.

	$U_i^*-V^*(0)/2$			S_i^*			c_{vi}^*		
T^*	H_2	D_2	Class.	H_2	D_2	Class.	H_2	D_2	Class.
0.5	1.115 64	0.617 25	0.123 66	−2.712 3	−3.023 2	−3.253 1	−0.478 6	0.103 0	0.451 8
0.6	1.122 17	0.632 81	0.168 97	−2.775 5	−2.995 1	−3.170 5	−0.222 8	0.199 1	0.454 2
0.7	1.109 01	0.655 78	0.214 46	−2.796 1	−2.959 8	−3.100 4	−0.052 1	0.255 9	0.455 3
0.8	1.109 84	0.683 33	0.260 01	−2.795 2	−2.923 1	−3.039 5	0.061 1	0.292 7	0.455 7
0.9	1.120 02	0.713 94	0.305 58	−2.783 3	−2.887 1	−2.985 9	0.137 9	0.318 1	0.455 5
1.0	1.136 66	0.746 72	0.351 10	−2.765 8	−2.852 6	−2.937 9	0.191 8	0.336 5	0.455 0
1.1	1.157 88	0.781 10	0.396 56	−2.745 6	−2.819 8	−2.894 6	0.230 6	0.350 5	0.454 2
1.2	1.182 48	0.816 70	0.441 94	−2.724 2	−2.788 8	−2.855 1	0.259 9	0.361 2	0.453 3
1.3	1.209 64	0.853 27	0.487 21	−2.702 5	−2.759 6	−2.818 9	0.282 2	0.369 7	0.452 2
1.4	1.238 77	0.890 59	0.532 37	−2.680 9	−2.731 9	−2.785 4	0.299 8	0.376 5	0.451 1
1.5	1.269 47	0.928 52	0.577 42	−2.659 7	−2.705 8	−2.754 3	0.313 8	0.382 0	0.449 9
1.6	1.301 44	0.966 95	0.622 34	−2.639 1	−2.681 0	−2.725 3	0.325 2	0.386 5	0.448 6
1.7	1.334 44	1.005 78	0.667 15	−2.619 1	−2.657 4	−2.698 2	0.334 6	0.390 1	0.447 4
1.8	1.368 30	1.044 95	0.711 82	−2.599 7	−2.635 0	−2.672 6	0.342 4	0.393 2	0.446 1
1.9	1.402 87	1.084 40	0.756 37	−2.581 0	−2.613 7	−2.648 5	0.348 9	0.395 7	0.444 8
2.0	1.438 06	1.124 08	0.800 79	−2.563 0	−2.593 3	−2.625 8	0.354 5	0.397 8	0.443 6
2.1	1.473 75	1.163 94	0.845 08	−2.545 6	−2.573 9	−2.604 1	0.359 3	0.399 5	0.442 3
2.2	1.509 89	1.203 96	0.889 25	−2.528 8	−2.555 3	−2.583 6	0.363 4	0.400 9	0.441 1
2.3	1.546 40	1.244 11	0.933 30	−2.512 5	−2.537 4	−2.564 0	0.366 9	0.402 0	0.439 8
2.4	1.583 25	1.284 36	0.977 22	−2.496 9	−2.520 3	−2.545 3	0.369 9	0.403 0	0.438 6
2.5	1.620 37	1.324 70	1.021 02	−2.481 7	−2.503 8	−2.527 4	0.372 5	0.403 7	0.437 4
2.6	1.657 74	1.365 10	1.064 70	−2.467 0	−2.488 0	−2.510 3	0.374 8	0.404 3	0.436 2
2.7	1.695 33	1.405 56	1.108 26	−2.452 9	−2.472 7	−2.493 9	0.376 8	0.404 8	0.435 0
2.8	1.733 10	1.446 05	1.151 71	−2.439 1	−2.458 0	−2.478 1	0.378 6	0.405 1	0.433 9
2.9	1.771 04	1.486 58	1.195 04	−2.425 8	−2.443 8	−2.462 9	0.380 1	0.405 3	0.432 7
3.0	1.809 11	1.527 11	1.238 26	−2.412 9	−2.430 0	−2.448 2	0.381 4	0.405 4	0.431 6
3.1	1.847 31	1.567 66	1.281 36	−2.400 4	−2.416 7	−2.434 1	0.382 6	0.405 5	0.430 5
3.2	1.885 62	1.608 20	1.324 36	−2.388 2	−2.403 9	−2.420 4	0.383 6	0.405 4	0.429 4
3.3	1.924 02	1.648 73	1.367 25	−2.376 4	−2.391 4	−2.407 2	0.384 4	0.405 2	0.428 4
3.4	1.962 50	1.689 24	1.410 03	−2.364 9	−2.379 3	−2.394 5	0.385 2	0.405 0	0.427 3
3.5	2.001 06	1.729 73	1.452 71	−2.353 7	−2.367 6	−2.382 1	0.385 8	0.404 7	0.426 3
3.6	2.039 66		1.495 29	−2.342 9		−2.370 1	0.386 4		0.425 2
3.7	2.078 32		1.537 76	−2.332 3		−2.358 5	0.386 8		0.424 2
3.8	2.117 02		1.580 14	−2.322 0		−2.347 2	0.387 2		0.423 3
3.9	2.155 76		1.622 41	−2.311 9		−2.336 2	0.387 5		0.422 3
4.0	2.194 51		1.664 59	−2.302 1		−2.325 5	0.387 7		0.421 3
4.1	2.233 29		1.706 68	−2.292 5		−2.315 1	0.387 9		0.420 4
4.2	2.272 08		1.748 67	−2.283 2		−2.305 0	0.388 0		0.419 5
4.3	2.310 88		1.790 57	−2.274 0		−2.295 1	0.388 0		0.418 5
4.4	2.349 68		1.832 38	−2.265 1		−2.285 5	0.388 0		0.417 6
4.5	2.388 47		1.874 10	−2.256 4		−2.276 1	0.387 9		0.416 8
4.6	2.427 25		1.915 73	−2.247 9		−2.267 0	0.387 7		0.415 9
4.7	2.466 01		1.957 28	−2.239 5		−2.258 1	0.387 5		0.415 0
4.8	2.504 74		1.998 74	−2.231 4		−2.249 3	0.387 2		0.414 2
4.9	2.543 44		2.040 11	−2.223 4		−2.240 8	0.386 8		0.413 3
5.0	2.582 09		2.081 41	−2.215 6		−2.232 5	0.386 3		0.412 5

levels were correct to at least one part in 10 000. Generally, fewer than 5 iterations determined the eigenvalue to six places. A number of these eigenvalues, expressed in reduced units, cf. Eq. (76), are given in Table II.

Unnormalized radical eigenfunctions are presented graphically in Figs. 3 and 4 for several of the lower levels of H_2.

With the procedure described in Sec. IV, the internal energy, entropy, and specific heat were evaluated from the computed energy levels. These computations were not extended above temperatures at which the contribution of the neglected higher energy levels, to the internal specific heat, was greater than 1%. In general, the error introduced by neglecting higher energy levels is roughly a factor of 10 smaller for internal energy and entropy than for the specific heat.

For comparison, the corresponding classical values of the internal thermodynamic properties were computed, as outlined by Eq. (66)–(73). In computing these quantities, the integration over t was performed numerically. In this case, the interval from zero to one was divided into two sections and 16 Gaussian points were used in each section. This resulted in an

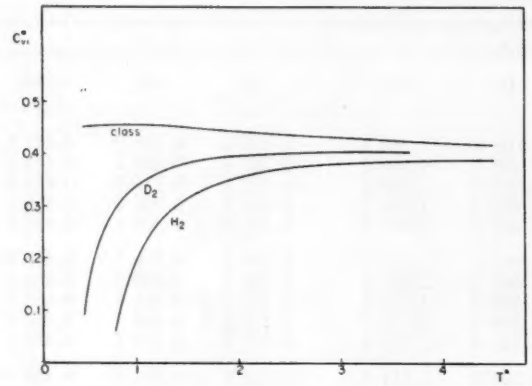

FIG. 5. Internal specific heats at $v^* = 5/3$.

accuracy of at least 5 places in the specific heat, and a greater accuracy for the other thermodynamic quantities.

The numerical results of the classical and quantum calculations of the thermodynamic functions are compiled in Table III, and the internal specific heats are shown graphically in Fig. 5.

VI. DISCUSSION

In Sec. V of this paper the theory and methods developed in the earlier parts have been applied to the special case of H_2 and D_2 at one value of the reduced density. The theory, however, is general and can be readily applied to gases with other values of the quantum parameter and at various densities. The computations on H_2 and D_2, and some preliminary calculations for Ar, show that the smaller the quantum effect, the slower the convergence of the expansion for $S(\rho)$ in Eq. (35).

The theoretical values for the thermodynamic properties of H_2 and D_2, as shown in Table III and Fig. 5, are appreciably different for the two isotopes, and these in turn show increasing deviations from classical behavior with decreasing temperature. Even at a temperature as high as $-144°C$ ($T^* = 3.5$), the computed internal specific heats of H_2 and D_2 differ by approximately 0.04 cal/mole deg. From accurate P–V–T measurements differences of this order of magnitude should be detectable. The differences in entropy and energy are larger and should reveal themselves readily.

Experimental data to compare the results with are not yet available. The present theory must be expected to share the usual deficiencies of the cell model. However, if one considers the deviations from classical behavior, rather than the absolute value of the quantities involved, the errors might well cancel to some extent.

Since the present theory is based on a one-particle model, it resembles Einstein's theory of the solid state rather than Debye's. Now it is well known that both theories give good representations of the experimental behavior at temperatures which are not too low. The Einstein model fails, however, for temperatures[12] below $\theta_E/2$, where $\theta_E = (h\nu_E/k)$. For 3-dimensional harmonic oscillators the zero-point energy λ_0 is given by $\lambda_0 = \frac{3}{2}h\nu_E = \frac{3}{2}k\theta_E$ and the Einstein model therefore holds for temperatures above $\theta_E/2 = \frac{1}{3}\lambda_0/k$.

If this estimate may be extended to the computations performed for H_2 and D_2, with $\lambda_0 = 1.8\epsilon$ and ϵ, respectively, one would expect that deficiencies of the nature described would be negligible for hydrogen at temperatures exceeding $1.2\epsilon/k$, that is, $T^* > 0.6$, and for deuterium for T^* larger than 0.33. Therefore, an Einstein-like theory should be justified for the temperature range of Table III.

ACKNOWLEDGMENT

The authors wish to express their gratitude to Professor J. O. Hirschfelder and to Dr. I. Shavitt for their aid and for many helpful discussions and suggestions.

[12] E. Katz, J. Chem. Phys. **19**, 488 (1951).

Dipole Moment of HD*†

S. M. BLINDER‡

Department of Chemistry, Harvard University, Cambridge 38, Massachusetts

(Received June 12, 1959)

The HD molecule has a small permanent electric dipole moment as a consequence of the asymmetry of nuclear vibration. The complete molecular Hamiltonian contains a term which is not invariant to inversion of electronic coordinates through the molecular center. This gives rise to an axial asymmetry of electronic charge. Treating the term as a perturbation, it is found that the $^1\Sigma_g^+$ electronic ground state is perturbed only by states of $^1\Sigma_u^+$ symmetry. Assuming that only the lowest such state (the B state) contributes, an upper bound on the permanent moment is established. For the ground vibrational state this is computed to be 8.89×10^{-4} Debye unit, directed in the sense H^+D^-.

I. INTRODUCTION

THE HD molecule exhibits a small permanent electric dipole moment as a result of an inertial perturbation of the electronic system by asymmetric nuclear vibration. The existence of this moment was first inferred by Wick.[1] Herzberg[2] was able to observe the very weak rotation-vibration spectrum—a necessary consequence of the existence of a moment dependent on vibrational state.

HD is almost, though not quite, a homonuclear diatomic molecule with regard to its electronic structure. The probability distribution of the proton, in oscillation about its equilibrium position, is more diffuse than that of the deuteron. The electron cloud is thereby perturbed asymmetrically, giving rise to a dipole along the internuclear axis. From a classical point of view, one might picture the nuclei as vibrating in phase, the proton having twice the amplitude of the deuteron. The characteristic shape of the vibrational potential well favors configurations of nuclear separation R greater than the equilibrium value R_0. Consider now the two extremes in electronic motion with respect to the nuclei:

(i) the electron cloud follows instantaneously the motion of the nuclei with no slippage;

(ii) the electronic configuration remains completely independent of nuclear motion.

Case (i) we designate as perfect following, case (ii) as complete slippage. Obviously, the truth lies somewhere between. For case (i) the electron distribution always has a center of inversion at the oscillating center of nuclear charge and there is no axial asymmetry in this moving coordinate system. In case (ii), however, the center of inversion in the moving system is lost. If any slippage does occur, then for $R>R_0$ the H end of the molecule is positive; for $R<R_0$, the opposite orientation holds. Since, as we have noted, the anharmonic vibration favors configurations of the former type, we conclude that there is a net dipole in the sense H^+D^-.

We shall next attempt a crude estimate of the magnitude of the permanent moment. For complete slippage, there would be an oscillating dipole of order $e\kappa a_0$, where κ is the Born-Oppenheimer parameter $(m/M)^{1/4}$,[3] a_0 is the first Bohr radius, and $a_0\kappa$ is a typical nuclear vibration amplitude. We shall guess that the degree of slippage is of order 1%, which seems reasonable from general considerations of electronic-vibrational interaction.[4] The moment must now be averaged over the vibrational probability distribution. Since the latter function is normalized and sharply peaked, it follows that the integral is closely approximated by the amplitude $e\kappa a_0$ of the dipole. The foregoing considerations indicate a permanent moment of roughly $0.01\ e\kappa a_0\sim 10^{-3}$ Debye unit.

There are additional perturbations due to rotational slippage and asymmetry in molecular rotation—a consequence of the noncoincidence of the center of mass and the center of nuclear charge. However, we shall show that these terms are of higher order. Wick neglects these effects on physical grounds.[1]

We proceed now to a quantitative treatment of the problem.

II. MOLECULAR HAMILTONIAN

The Hamiltonian for the system of a proton, a deuteron, and two electrons may be written

$$\mathcal{H}=-(\hbar^2/2m)(\nabla_1^2+\nabla_2^2)+V(\mathbf{r}_1\mathbf{r}_2\mathbf{r}_P\mathbf{r}_D)-(\hbar^2/2m)_P\nabla_P^2-(\hbar^2/2m_D)\nabla_D^2, \quad (1)$$

where $\mathbf{r}_1$, $\mathbf{r}_2$, $\mathbf{r}_P$, $\mathbf{r}_D$ denote the coordinates with respect to some arbitrary space-fixed set of axes. If the system forms a stable molecule, its motions are conventionally classified as: (i) translation of the molecular center of mass, (ii) relative motion of the nuclei, (iii) motion of

* Part of a thesis presented in fulfillment of the requirements for the degree of Doctor of Philosophy in chemical physics.

† This work was reported at the Symposium on Molecular Structure and Spectra, Ohio State University, June 15–19, 1959.

‡ Present address: Applied Physics Laboratory, Johns Hopkins University, Silver Spring, Maryland.

[1] G. C. Wick, Atti reale accad. naz. Lincei (Ser. 6) **21**, 708 (1935).

[2] G. Herzberg, Nature **166**, 563 (1950).

[3] See, for example: M. Born and J. R. Oppenheimer, Ann. Physik **84**, 457 (1927); Schiff, *Quantum Mechanics* (McGraw-Hill Book Company, Inc., New York, 1949), p. 289.

[4] See, for example, J. H. Van Vleck, J. Chem. Phys. **4**, 327 (1936).

the electrons with respect to a coordinate system defined by the nuclei. Accordingly, we transform coordinates of (1) to the set $\mathbf{R}_0$, $\mathbf{R}$, $\mathbf{R}_1$, $\mathbf{R}_2$: $\mathbf{R}_0$ represents the center of mass; $\mathbf{R}=\mathbf{r}_P-\mathbf{r}_D$ in terms of the spherical polar coordinates R, θ, ϕ; $\mathbf{R}_1$, $\mathbf{R}_2$ are the electron positions with respect to a set of coordinate axes rotating with the molecule with origin at the midpoint of the internuclear axis (the center of positive charge) and so oriented that the unit vectors u_X, u_Y, u_Z coincide with the instantaneous spherical unit vectors u_θ, u_ϕ, u_R, respectively. The nuclei then lie on the Z axis, the deuteron at $-R/2$, the proton at $R/2$.

Subtracting out the translational motion, which is of no interest here, the transformed Hamiltonian assumes the form

$$\mathcal{H}=\mathcal{H}^{(0)}+\mathcal{H}^{(2)}+\mathcal{H}^{(3)}+\mathcal{H}_a^{(4)}+\mathcal{H}_b^{(4)}+\mathcal{H}_c^{(4)}, \quad (2)$$

with

$$\mathcal{H}^{(0)}=-(\hbar^2/2m)(\nabla_1^2+\nabla_2^2)+V(\mathbf{R}_1, \mathbf{R}_2, R), \quad (3)$$

$$\mathcal{H}^{(2)}=-\tfrac{1}{2}\hbar^2[(1/m_P)+(1/m_D)](1/R^2)D_R R^2 D_R, \quad (4)$$

$$\mathcal{H}^{(3)}=\tfrac{1}{2}\hbar^2[(1/m_P)-(1/m_D)]D_R(D_{Z_1}+D_{Z_2}), \quad (5)$$

$$\mathcal{H}_a^{(4)}=-\tfrac{1}{2}\hbar^2[(1/m_P)+(1/m_D)]\{(R^2\sin\theta)^{-1}\bar{D}_\theta \sin\theta \bar{D}_\theta + (R^2\sin^2\theta)^{-1}\bar{D}_\phi^2\}, \quad (6)$$

$$\mathcal{H}_b^{(4)}=-(\hbar^2/8)[(1/m_P)+(1/m_D)](\nabla_1+\nabla_2)^2, \quad (7)$$

$$\mathcal{H}_c^{(4)}=\tfrac{1}{2}\hbar^2[(1/m_P)-(1/m_D)]\{(1/R)\bar{D}_\theta(D_{X_1}+D_{X_2}) - (R\sin\theta)^{-1}\bar{D}_\phi(D_{Y_1}+D_{Y_2})\}. \quad (8)$$

We have employed the notation:

$$D_q=\partial/\partial q, \quad (9)$$

$$\nabla_1=u_X D_{X_1}+u_Y D_{Y_1}+u_Z D_{Z_1}, \quad (10)$$

etc.,

$$\bar{D}_\theta=D_\theta-M_Y, \quad (11)$$

$$\bar{D}_\phi=D_\phi-\cos\theta M_Z+\sin\theta M_X, \quad (12)$$

$$M_X=(Y_1 D_{Z_1}-Z_1 D_{Y_1})+(Y_2 D_{Z_2}-Z_2 D_{Y_2}), \quad (13)$$

etc. The details of the transformation are given in Appendix A. The superscripts of the terms indicate their order with respect to the Born-Oppenheimer parameter.[3] $\mathcal{H}^{(0)}$ is the ordinary electronic Hamiltonian for fixed nuclei of infinite mass. $\mathcal{H}^{(2)}$ represents the nuclear vibration; $\mathcal{H}_a^{(4)}$ the nuclear rotation; $\mathcal{H}_b^{(4)}$ is a reduced mass correction. $\mathcal{H}^{(3)}$ and $\mathcal{H}_c^{(4)}$ represent, respectively, electronic-vibrational and electronic-rotational interactions. These would vanish in the homonuclear case ($m_P=m_D$), hence we shall designate them as heteronuclear perturbations. Their significance resides in the fact that they do not commute with inversion of the electronic coordinates through the molecular center. This means that the eigenfunctions of $\mathcal{H}$ cannot rigorously have even or odd symmetry and consequently, that the molecule will have an asymmetric electron distribution, hence a dipole.

The operators M_X, M_Y represent electronic angular momenta with respect to the rotating system. If there were no slippage of the electron cloud with nuclear rotation these would vanish.[5] In any case, they are smaller than the corresponding nuclear operators D_θ, D_ϕ by a factor of order κ^4. M_Z is the electronic angular momentum about the internuclear axis. This is of the same order in κ as the nuclear operators; however, should we restrict our consideration to Σ states of the molecule, terms in M_Z would vanish. Thus we may, to good approximation, replace the operators $\bar{D}_\theta$, $\bar{D}_\phi$ by their unbarred analogs.

Regarding terms of order κ^3 and higher as a perturbation we may write

$$\mathcal{H}=\mathcal{H}_0+\mathcal{V}, \quad (14)$$

with

$$\mathcal{H}_0=\mathcal{H}^{(0)}+\mathcal{H}^{(2)}, \quad (15)$$

$$\mathcal{V}=\mathcal{H}^{(3)}+\mathcal{H}_a^{(4)}+\mathcal{H}_b^{(4)}+\mathcal{H}_c^{(4)}. \quad (16)$$

We presume that the eigenfunctions of H_0, at least for the ground electronic state, may be factorized as follows:

$$\Phi_{nvr}(\mathbf{R}_1\mathbf{R}_2, R\theta\phi)=\phi_n(\mathbf{R}_1\mathbf{R}_2, R)\alpha_{nv}(R)\rho_{nvr}(\theta\phi), \quad (17)$$

where n, v, r denote the electronic, vibrational, and rotational quantum numbers, respectively. This requires that the R dependence of ϕ_n is such that terms containing $\partial\phi_n/\partial R$ are negligibly small in comparison with terms in the $\partial\alpha_{nv}/\partial R$, at least in their averages. The above is known as the adiabatic approximation and corresponds to the physical situation whereby: (i) the electron cloud in the unperturbed molecule follows instantaneously the motion of the nuclei; (ii) the vibration-averaged molecular system rotates rigidly.

III. ELECTRIC DIPOLE MOMENT

In a constant electric field $\mathbf{E}$, the molecular Hamiltonian becomes

$$\mathcal{H}=\mathcal{H}_0+\mathcal{V}-\boldsymbol{\mu}\cdot\mathbf{E}, \quad (18)$$

where

$$\boldsymbol{\mu}=-e(\mathbf{R}_1+\mathbf{R}_2). \quad (19)$$

Applying perturbation theory based on the eigenstates of $\mathcal{H}_0$, we find for the molecular energy to second order of the state A'

$$E_{A'}=E_A+\mathcal{V}_{AA}-\boldsymbol{\mu}_{AA'}\cdot\mathbf{E}+\sum_N{}'[\mathcal{V}_{AN}\mathcal{V}_{NA}/(E_A-E_N)] - \mathbf{E}\cdot\left\{\sum_N{}'\frac{\boldsymbol{\mu}_{AN}\mathcal{V}_{NA}+\mathcal{V}_{AN}\boldsymbol{\mu}_{NA}}{E_A-E_N}\right\} + \mathbf{E}\cdot\{\sum_N{}'[\boldsymbol{\mu}_{AN}\boldsymbol{\mu}_{NA}/(E_A-E_N)]\}\cdot\mathbf{E}. \quad (20)$$

[5] The work of Wick and Ramsey on spin-rotational interaction indicates that the rotational slippage in H_2 may be quite sizable: N. Ramsey, Phys. Rev. **58**, 226 (1940); G. C. Wick, *ibid.* **73**, 51 (1948).

Primed labels denote the eigenstates of the complete molecular Hamiltonian $\mathcal{H}$, their unprimed analogs denote the corresponding eigenstates of $\mathcal{H}_0$. These are composite labels containing implicitly electronic, vibrational, and rotational quantum numbers.

The permanent electric dipole moment of a system may be defined by the operator equation§

$$\boldsymbol{\mu} = -\lim_{\mathbf{E}\to 0} \partial\mathcal{H}/\partial\mathbf{E}. \tag{21}$$

By applying this to (20), we find for the expectation value in state A'

$$\langle\boldsymbol{\mu}\rangle_{A'} = \lim_{\mathbf{E}\to 0} (\partial E_{A'}/\partial\mathbf{E})$$

$$= \boldsymbol{\mu}_{AA} + \sum_N{}' \frac{\boldsymbol{\mu}_{AN}\mathcal{V}_{NA} + \mathcal{V}_{AN}\boldsymbol{\mu}_{NA}}{E_A - E_N}. \tag{22}$$

It is necessary to take the limit of zero field to exclude induced moments arising from the last term of (20) (the energy of polarization).

We now take A to represent a rotation-vibration level of the $^1\Sigma_g^+$ ground electronic state and determine the restrictions thereby placed on the states N. Considering separately the components of $\boldsymbol{\mu}$, it may be readily shown that $(\mu_Z)_{AN} = 0$ unless N is a $^1\Sigma_u^+$ state, $(\mu_Y)_{AN}$, $(\mu_X)_{AN} = 0$ unless N is a $^1\Pi_u$ state. It immediately follows then that

$$\boldsymbol{\mu}_{AA} = 0, \tag{23}$$

$$(\mathcal{H}_b^{(4)})_{AN} = (\mathcal{H}_a^{(4)})_{AN} = 0, \tag{24}$$

$$\mathcal{H}_{AN}^{(3)} = 0 \quad \text{unless} \quad N = {}^1\Sigma_u^+, \tag{25}$$

$$(\mathcal{H}_c^{(4)})_{AN} = 0 \quad \text{unless} \quad N = {}^1\Pi_u, \tag{26}$$

and the expectation values for the components of $\boldsymbol{\mu}$ become

$$\langle\mu_Z\rangle_{A'} = \sum_N{}' \frac{(\mu_Z)_{AN}\mathcal{H}_{NA}^{(3)} + \mathcal{H}_{AN}^{(3)}(\mu_Z)_{NA}}{E_A - E_N}, \qquad (N = {}^1\Sigma_u^+) \tag{27}$$

$$\langle\mu_X\rangle_{A'} = \sum_N{}' \frac{(\mu_X)_{AN}(\mathcal{H}_c^{(4)})_{NA} + (\mathcal{H}_c^{(4)})_{AN}(\mu_X)_{NA}}{E_A - E_N}, \qquad (N = {}^1\Pi_u) \tag{28}$$

with an identical expression for $\langle\mu_Y\rangle_A'$.

Since $\mathcal{H}^{(4)}$ terms are smaller than $\mathcal{H}^{(3)}$ terms by a factor of order κ, we might expect (μ_Z) to be large in comparison to $\langle\mu_X\rangle$ or $\langle\mu_Y\rangle$. However, it is conceivable, although not likely here, that the latter terms are of comparable magnitude since the parameter κ is rather large for so light a molecule as HD ($\kappa \approx 1/7$). In any case, we shall confine all further considerations to the Z component. Since this quantity has no dependence on orientation, we may hereafter completely disregard rotational structure, considerable simplification resulting.

The expression (27) may be generalized to give, as well, off-diagonal elements of μ, e.g., $(\mu_Z)_{A'B'}$. This is done in straightforward fashion by computing $\Phi_{A'}$, $\Phi_{B'}$ to first order in zero field, e.g.,

$$\Phi_{A'} = \Phi_A + \sum_N{}' [\Phi_N \mathcal{V}_{NA}/(E_A - E_N)]. \tag{29}$$

This yields, through terms of second order,

$$(\mu_Z)_{A'B'} = \sum_N{}' \frac{(\mu_Z)_{AN}\mathcal{H}_{NB}^{(3)}}{E_B - E_N} + \sum_N{}' \frac{\mathcal{H}_{AN}^{(3)}(\mu_Z)_{NB}}{E_A - E_N}. \tag{30}$$

We shall confine ourselves to the case when A, B are vibrational levels in the ground electronic state.

On substituting into (30) from (5) and (19), with the abbreviations Z for $Z_1 + Z_2$, D_Z for $D_{Z1} + D_{Z2}$, and noting that

$$\mathcal{H}_{AN}^{(3)} = \tfrac{1}{2}\hbar^2[(1/m_P) - (1/m_D)] \sum_M (D_R)_{AM}(D_Z)_{MN}$$

$$= \tfrac{1}{2}\hbar^2[(1/m_P) - (1/m_D)] \sum_M (D_Z)_{AM}(D_R)_{MN}, \tag{31}$$

we find

$$(\mu_Z)_{A'B'} = -(e\hbar^2/2)[(1/m_P) - (1/m_D)]$$

$$\times \sum_{NM, N\neq B} \frac{Z_{AN}(D_Z)_{NM}(D_R)_{MB}}{E_B - E_N}$$

$$+ \sum_{NM, N\neq A} \frac{(D_R)_{AM}(D_Z)_{MN}Z_{NB}}{E_A - E_N}, \tag{32}$$

where the index M runs over the complete orthonormal set of eigenstates of $\mathcal{H}_0$.

By virtue of the momentum-velocity relationship,

$$D_Z = -(m/\hbar^2)[\mathcal{H}_0, Z], \tag{33}$$

$$(D_Z)_{NM} = (m/\hbar^2)(E_M - E_N)Z_{NM}, \tag{34}$$

writing $(E_M - E_N)$ as $(E_M - E_B) + (E_B - E_N)$ in the first summation and as $(E_M - E_A) + (E_A - E_N)$ in the second, and noting that Z and D_R commute, (32) becomes

$$(\mu_Z)_{A'B'} = -(em/2)[(1/m_P) - (1/m_D)]$$

$$\times \sum_{NM, N\neq B} \frac{Z_{AN}Z_{NM}(E_M - E_B)(D_R)_{MB}}{E_B - E_N}$$

$$+ \sum_{NM, N\neq A} \frac{(E_A - E_M)(D_R)_{AM}Z_{MN}Z_{NB}}{E_A - E_N}. \tag{35}$$

Furthermore

$$(E_A - E_M)(D_R)_{AM} = [\mathcal{H}_0, D_R]_{AM} = -(\partial\mathcal{H}_0/\partial R)_{AM}. \tag{36}$$

The derivative is effectively $-(\partial V/\partial R)_{AM}$, where V is

§ This equation refers to the molecule-fixed coordinate system. Averaged over the rotation, this moment would vanish.

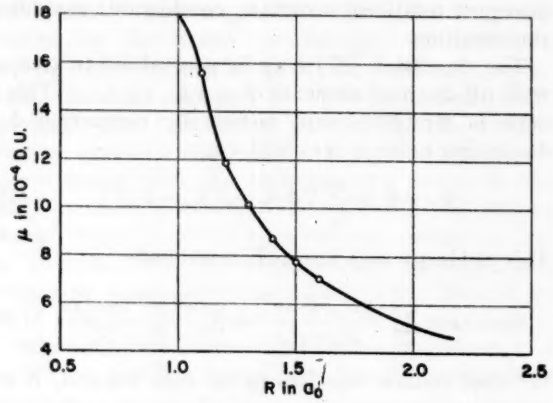

FIG. 1. $\mu_Z(R)$.

the electronic potential energy in (3). Summing now over the index M and defining the operator

$$W \equiv Z(-\partial V/\partial R), \tag{37}$$

we obtain finally for our dipole matrix element

$$(\mu_Z)_{A'B'} = -(em/2)[(1/m_P)-(1/m_D)] \cdot \sum_N{}' \left\{ \frac{Z_{AN}W_{NB}}{E_B - E_N} + \frac{W_{AN}Z_{NB}}{E_A - E_N} \right\}. \tag{38}$$

IV. SOLUTION BY PERTURBATION THEORY

An approximate evaluation of the matrix elements (38) is possible if the following assumptions are made: (i) only the lowest $^1\Sigma_u^+$ excited state perturbs the ground electronic state; (ii) the vibrational energies contained in the terms E_A, E_B, E_N are negligible compared to electronic energies. The former refers to the B state of H_2 with energy minimum about 91 700 cm^{-1} above the ground state energy minimum.[6] We must bear in mind, however, that contributions from unstable or continuum states of the same symmetry are also possible. Their unfavorable energy denominators would, in all probability, make their contributions secondary. Applying assumption (ii), we may set $E_A = E_B = E_0$, $E_N = E_1$ where E_0 is the electronic energy of the ground state (the minimum of the potential curve) and E_1 is the corresponding energy of the B state. The error in neglecting vibrational structure is at most several percent. In view of the above, we may remove the energy denominator from the summation (38) and sum over the states N. Recalling that A is a composite label representing the electronic and vibrational quantum numbers 0 and a, respectively, we may write for the diagonal element of μ_Z

$$\langle \mu_Z \rangle_{A'} = em[(1/m_P)-(1/m_D)] \frac{\{(ZW)_{00}\}_{aa}}{E_1 - E_0}, \tag{39}$$

where we have also taken the ground state function to be real, assumed the validity of the adiabatic approximation (17), and noted that Z_{00} vanishes.

Since the integral $(ZW)_{00}$ is not conveniently represented as an analytic function of R, we shall evaluate it separately for several representative R values and perform a graphical integration with respect to the vibrational function α_a.

We take as our ground state electronic function, one of the James and Coolidge[7] type in order to take advantage of certain tabulated integrals. In view of the large number of approximations to this point, use of one of their more accurate functions (11- or 13-term) would be unreasonably laborious. We use instead a four-term function: a linear combination of the four leading basis functions at the equilibrium internuclear distance ($1.40a_0$). Optimal coefficients are evaluated for nuclear separations of 1.10, 1.20, 1.30, 1.40, 1.50, and 1.60 Bohr radii. The method used is completely analogous to that of James and Coolidge,[7] to which the reader is referred for details. Our ground state function, by way of comparison, gives a total molecular energy within 2% of the experimental value and a binding energy >85% of that observed. As this function may be of use in other problems involving the H_2 molecule where dependence on the parameter R is required, we tabulate the energy values and normalized coefficients in Appendix B.

Integrating over the electronic coordinates for each value of R, we obtain the function $\mu_Z(R)$ represented in Fig. 1. The permanent moment in the ground vibrational state is found by graphical integration of $\mu_Z(R)$ over the square of the Morse eigenfunction for $v=0$. This yields

$$\langle \mu_Z \rangle_{v=0} = 8.89 \times 10^{-4} \text{ D.U.}$$

The positive sign of the moment, in accordance with our convention for the Z direction, indicates that the H end of the molecule is positive, consistent with our earlier expectation. The vibrational eigenfunctions for a Morse potential with parameters suitable for HD are discussed in Appendix C.

Our value for the permanent moment probably represents an upper bound within the framework of our system of approximations. This is indicated by the likelihood that all $^1\Sigma_u^+$ contributions (including the neglected ones) are of the same sign. By the summation procedure, all terms $Z_{0n}W_{n0}$ are implicitly added with the factor $(E_1-E_0)^{-1}$, larger than their factors $(E_n-E_0)^{-1}$ in the rigorous perturbation expansion.

Further work is now in progress on a more accurate computation taking implicit account of the other excited $^1\Sigma_u^+$ states by a modification of perturbation theory.[8] Complete computational details including

[6] G. Herzberg: *Spectra of Diatomic Molecules* (D. Van Nostrand Co., Inc., Princeton, New Jersey, 1950, p. 530 ff. There is evidence of another state of the same symmetry. Labeled $x^1\Sigma_u^+$, this lies about 113 800 cm^{-1} above the ground state.

[7] H. M. James and A. S. Coolidge, J. Chem. Phys. **1**, 825 (1933).

[8] S. M. Blinder, J. Chem. Phys. **32**, 111 (1960) (this issue).

those relevant to the present discussion will also be presented in the forthcoming work.

ACKNOWLEDGMENTS

This work was performed under the direction of the late Professor William Moffitt. The author also wishes to thank Milton Baker, Harold Salwen, Theodore Sarachman, and Professor William A. Klemperer for helpful discussions.

APPENDIX A

Transformation of the Molecular Hamiltonian

The transformation from Eq. (1) to Eq. (2) is most easily carried out in two steps. First we perform the linear transformation from the set $\mathbf{r}_1$, $\mathbf{r}_2$, $\mathbf{r}_P$, $\mathbf{r}_D$ to the set $\mathbf{R}_1'$, $\mathbf{R}_2'$, $\mathbf{R}$, $\mathbf{R}_0$ according to the matrix

$$\begin{array}{c|cccc} & \mathbf{r}_1 & \mathbf{r}_2 & \mathbf{r}_P & \mathbf{r}_D \\ \mathbf{R}_1' & 1 & 0 & -\frac{1}{2} & -\frac{1}{2} \\ \mathbf{R}_2' & 0 & 1 & -\frac{1}{2} & -\frac{1}{2} \\ \mathbf{R} & 0 & 0 & -1 & 1 \\ \mathbf{R}_0 & m/M & m/M & m_P/M & m_D/M \end{array}, \tag{A1}$$

where $M=m_P+m_D+2m$. Denoting the gradient operators with respect to the new coordinates by ∇_1, ∇_2, ∇_R, and ∇_0, the original gradients transform by the inverse matrix

$$\begin{array}{c|cccc} & \nabla_1' & \nabla_2' & \nabla_R & \nabla_0 \\ \nabla_1 & 1+(m/M) & m/M & \dfrac{m_P-m_D}{2M} & 1 \\ \nabla_2 & m/M & 1+(m/M) & \dfrac{m_P-m_D}{2M} & 1 \\ \nabla_P & m/M & m/M & -\dfrac{m+m_D}{M} & 1 \\ \nabla_D & m/M & m/M & \dfrac{m+m_P}{M} & 1 \end{array}, \tag{A2}$$

and (1) becomes

$$\mathfrak{H}=\begin{cases} -(\hbar^2/2M)\nabla_0^2-(\hbar^2/2m)[(\nabla_1')^2+(\nabla_2')^2]+V \\ -(\hbar^2/2)[(1/m_P)+(1/m_D)]\nabla_R^2 \\ \quad +(\hbar^2/2)[(1/m_P)-(1/m_D)]\nabla_R\cdot(\nabla_1'+\nabla_2') \\ -(\hbar^2/8)[(1/m_P)+(1/m_D)](\nabla_1'+\nabla_2')^2. \end{cases} \tag{A3}$$

Next, we discard the first term of (A3), corresponding to translation, and express R in spherical polar coordinates R, θ, ϕ. The second transformation, a rigid rotation of the $X'Y'Z'$ axes, is effected by the unitary matrix T:

$$T=\begin{bmatrix} \cos\phi\cos\theta & \sin\phi\cos\theta & -\sin\theta \\ -\sin\phi & \cos\phi & 0 \\ \cos\phi\sin\theta & \sin\phi\sin\theta & \cos\theta \end{bmatrix}, \tag{A4}$$

$$\begin{cases} \xi=T\xi' \\ \xi=\begin{pmatrix} X \\ Y \\ Z \end{pmatrix}, \quad \xi'=\begin{pmatrix} X' \\ Y' \\ Z' \end{pmatrix}, \end{cases} \tag{A5}$$

This is most easily arrived at by considering the cartesian components of the spherical unit vectors u_θ, u_ϕ, u_R and setting the latter equal to u_X, u_Y, u_Z, respectively.

The operators $(\nabla_1')^2$, $(\nabla_2')^2$, $(\nabla_1'\cdot\nabla_2')$ are invariant as a consequence of the unitary property of T; these we simply replace by their unprimed analogs. The derivatives with respect to θ and ϕ, however, are changed as follows:

$$D_\theta\rightarrow D_\theta+\sum_{i=1}^{6}(\partial\xi_i/\partial\theta)D_{\xi_i}(\xi_i=X_1,\cdots,Z_2). \tag{A6}$$

Using the matrix relationships

$$\begin{cases} \xi=T\xi', \\ \xi_\theta=T_\theta\xi', \\ \xi'=\tilde{T}\xi, \end{cases} \tag{A7}$$

where the subscript θ indicates the derivative with respect to θ, we find

$$D_\theta\rightarrow D_\theta+\sum_{i,k=1}^{6}A_{ik}\xi_k D_{\xi_i}, \tag{A8}$$

where the matrix A is defined by

$$A=T_\theta\tilde{T}, \tag{A9}$$

and its elements given explicitly by

$$A=\begin{pmatrix} 0 & 0 & -1 \\ 0 & 0 & 0 \\ 1 & 0 & 0 \end{pmatrix}. \tag{A10}$$

This yields finally

$$D_\theta\rightarrow D_\theta-M_Y\equiv\tilde{D}_\theta. \tag{A11}$$

TABLE I. Energies and normalized coefficients: four-term H_2 function.

R in a_0	E_0 in e^2/a_0	C_1	C_2	C_3	C_4
1.10	1.1233	2.4031	1.1939	0.2956	−0.9050
1.20	1.1391	2.4505	1.0961	−0.04575	−0.8052
1.30	1.14748	2.352711	1.002622	−0.236998	−0.716332
1.40	1.150005	2.176276	0.913044	−0.333346	−0.636162
1.50	1.14767	1.966938	0.828716	−0.371950	−0.564484
1.60	1.1413	1.7532	0.7507	−0.3771	−0.5009

By a completely analogous procedure, we obtain

$$D_\phi \rightarrow D_\phi + \sum B_{ik}\xi_k D_{\xi_i}, \tag{A12}$$

with

$$B = T_\phi \tilde{T} = \begin{vmatrix} 0 & \cos\theta & 0 \\ -\cos\theta & 0 & -\sin\theta \\ 0 & \sin\theta & 0 \end{vmatrix}, \tag{A13}$$

and

$$D_\phi \rightarrow D_\phi - \cos\theta M_Z + \sin\theta M_X \equiv \tilde{D}_\phi. \tag{A14}$$

After substituting (A12) and (A14) into (A3), the molecular Hamiltonian (2) is obtained.

APPENDIX B

Four-Parameter H_2 Ground State

James and Coolidge[7] represent the ground state of H_2 by a series:

$$\phi_0(\mathbf{R}_1\mathbf{R}_2, R) = \sum C_{MNJKP}(R)\phi_{MNJKP}, \tag{B1}$$

where

$$\begin{cases} \phi_{MNJKP} = (1/2\pi)\ \exp[-\delta(\lambda_1+\lambda_2)] \\ \qquad \cdot (\lambda_1{}^M\lambda_2{}^N\mu_1{}^J\mu_2{}^K\rho^P + \lambda_1{}^N\lambda_2{}^M\mu_1{}^K\mu_2{}^J\rho^P), \\ P = 2N_{12}/R, \qquad \delta = 0.75, \\ M, N, J, K, P = 0, 1, 2, \cdots, \quad J+K = \text{even}. \end{cases} \tag{B2}$$

The electronic positions are expressed in prolate spheroidal coordinates. For a given set of basis functions and a particular R, the coefficients are determined by the variational principle such as to minimize E_0. We have chosen the four basis functions which contribute most significantly in the equilibrium configuration, $R = 1.40a_0$, namely,

$$\begin{cases} \phi_{00000} \equiv \phi_1 \\ \phi_{00020} \equiv \phi_2 \\ \phi_{10000} \equiv \phi_3 \\ \phi_{00110} \equiv \phi_4. \end{cases}$$

We next compute the optimal coefficients for each of the six values of the parameter R. The energies and normalized coefficients are summarized in Table I.

APPENDIX C

Morse Eigenfunctions for HD

The solutions of the vibrational eigenvalue equation for a Morse potential in a nonrotating molecule are given by[9]

$$\begin{cases} R_n(y) = A_n e^{-\frac{1}{2}y} y^{\frac{1}{2}(k-2n-1)} L_{kn}(y) \\ y = k\exp[-\beta(R-R_0)] \\ A_n = \left[\dfrac{\beta(k-2n-1)}{n!(k-n-1)!}\right]^{\frac{1}{2}}, \end{cases} \tag{C1}$$

where $L_{kn}(y)$ is a generalized Laguerre polynomial ($L_{k0}(y) = 1.$). We use empirical parameters β and k obtained from the observed vibrational constants of the molecule.[10] Thus

$$\beta = [8\pi^2 c\mu\omega\chi/h]^{\frac{1}{2}}, \tag{C2}$$

$$k = w/w\chi, \quad \text{to the nearest integer}, \tag{C3}$$

where ω is the fundamental vibrational frequency, $\omega\chi$, the anharmonicity; and μ, the reduced nuclear mass. For the ground electronic state of HD we obtain $k = 40$, $\beta = 1.945 \times 10^8$ cm^{-1}.

[9] P. M. Morse, Phys. Rev. **34**, 57 (1929); J. L. Dunham, Phys. Rev. **34**, 438 (1929).

[10] G. Herzberg, reference 6, p. 101 ff., etc.

Generalized Perturbation Method Employing Nonorthogonal Functions*

S. M. BLINDER*†

Department of Chemistry, Harvard University, Cambridge, Massachusetts

(Received June 23, 1959)

A method is developed for solving second-order perturbation problems without explicit knowledge of the higher molecular states. This method involves, in principle, a transformation of basis from the set of orthonormalized eigenfunctions of the unperturbed molecular Hamiltonian to an arbitrary set of functions not, in general, either normalized or mutually orthogonal, but of such symmetry that perturbation matrix elements connecting them to the ground state do not vanish. If the new basis is chosen expediently, convergence to second-order eigenvalues may be attained with a small number of functions. The method is related to the conventional perturbation and variational approaches. As an illustration, the perturbed harmonic oscillator is treated.

I. INTRODUCTION

WE suppose the eigenvalue problem,

$$\{\mathcal{H}_0 - E^{(0)}\}\psi^{(0)} = 0, \tag{1}$$

to have been solved exactly for some particular state of a system. We further suppose that the system is subjected to a small perturbation such that

$$\mathcal{H} = \mathcal{H}_0 + \lambda \mathcal{V}, \tag{2}$$

and we wish now to compute the energy of the corresponding state.

Calculation of first-order eigenvalues requires only that we know $\psi^{(0)}$. Second-order contributions, however, require knowledge of eigenfunctions of other states of the unperturbed system. In molecular problems these would include formally all the discrete as well as the continuum solutions of the appropriate Schroedinger equation.[1] Dissociated states of the molecule might also contribute. Since these required eigenfunctions are little known and less tractable, even for the simplest of molecules, unmodified second-order perturbation theory is not effectively applicable, unless it can be shown that only a small number of states contribute to the perturbation.

We propose below a method in which functions more convenient than the eigenfunctions of $\mathcal{H}_0$ can be used in the calculation of second-order eigenvalues. The idea of using such a set of functions was due originally to Epstein.[2] His approach involved, in principle, diagonalization of the complete Hamiltonian in a suitable orthonormal basis not necessarily related to the unperturbed system. He applied his method to an accurate computation of the Stark effect in atomic hydrogen. Similar methods have been used by others in the solution of various molecular problems.[3] The extension we propose is the removal of the restriction that the basis be orthonormalized. This formalism has been developed specifically in connection with two problems involving perturbations on molecular hydrogen: the electric dipole moment of HD‡ and the nuclear spin interaction in HD.§ In these computations, we have employed basis functions of the form,

$$(1/2\pi)\exp[-\delta(\lambda_1+\lambda_2)](\lambda_1^M\lambda_2^N\mu_1^J\mu_2^K\rho^P \pm \lambda_1^N\lambda_2^M\mu_1^K\mu_2^J\rho^P), \tag{3}$$

first used by James and Coolidge[4] and by Present[5] in their studies of the ground and excited states of H_2. These functions form a complete, though not orthonormal, set. In order to make use of them and of various matrix elements computed by the above authors we have extended the generalized perturbation method of Epstein.[2] We present the method apart from its applications, since it is perhaps of interest in itself.

II. DERIVATION OF THE GENERALIZED PERTURBATION FORMULA

We seek a solution for the perturbed problem,

$$(\mathcal{H} - E)\psi = 0, \tag{4}$$

by developing ψ linearly as follows‖:

$$\psi = \psi^{(0)} + \sum_n{}' c_n \phi_n, \tag{5}$$

---

* Part of a thesis presented in fulfillment of the requirements for the degree of Doctor of Philosophy in Chemical Physics.

† Present address: Applied Physics Laboratory, The Johns Hopkins University, Silver Spring, Maryland.

[1] The importance of the continuum in atomic problems has most recently been pointed out by: Green *et al.*, Phys. Rev. **96**, 319 (1954); H. Shull and P.-O. Löwdin, J. Chem. Phys. **23**, 1362 (1955); **30**, 617 (1959). In the last reference, Shull and Löwdin estimate that the 2*s* orbital function in helium contains about 43% continuum character with reference to discrete hydrogen-like functions.

[2] P. S. Epstein, Phys. Rev. **28**, 695 (1926). We are indebted to Professor E. B. Wilson for bringing this reference to our attention. The method is discussed in detail also in L. Pauling and E. B. Wilson, *Introduction to Quantum Mechanics* (McGraw-Hill Book Company, Inc., New York, 1935), p. 190.

[3] J. E. Lennard-Jones, Proc. Roy. Soc. (London) **A129**, 598 (1930); E. Hylleraas, Z. Physik **65**, 209 (1930); H. R. Hassé, Proc. Cambridge Phil. Soc. **26**, 542 (1930); J. C. Slater and J. G. Kirkwood, Phys. Rev. **37**, 682 (1931).

‡ S. M. Blinder, J. Chem. Phys. **32**, 105 (1960). This work was reported at the Symposium on Molecular Spectroscopy, Ohio State University, June 15–19, 1959.

§ To be published in J. Chem. Phys.

[4] H. M. James and A. S. Coolidge, J. Chem. Phys. **1**, 825 (1933).

[5] R. D. Present, J. Chem. Phys. **3**, 122 (1935).

‖ We shall use throughout the convention that a prime on the summation sign indicates exclusion of the index 0.

where the $\phi_n (n=1, \cdots, N)$ represent a set of functions orthogonal to $\psi^{(0)}$ but not necessarily normalized, mutually orthogonal, or solutions of the unperturbed problem.¶ We assume the set $\psi^{(0)}, \phi_1, \cdots, \phi_N$ (where N may be ∞) to be complete in the domain of ψ. In practice, it need be only as nearly complete as the degree of accuracy requires. $\psi^{(0)}$, the normalized solution to Eq. (1), is, of course, a close approximation to ψ, presuming the perturbation to be small.

Substituting our linear development for ψ in Eq. (4) we find

$$(\mathcal{H}-E)\psi^{(0)}+\sum_n{}'c_n(\mathcal{H}-E)\phi_n=0. \tag{6}$$

Multiplying on the left by $\psi^{(0)*}$ and integrating, we obtain

$$E=H_{00}+\sum_n{}'H_{0n}c_n. \tag{7}$$

Similarly, multiplication by $\phi_k{}^*$ yields

$$H_{k0}+\sum_n{}'(H-E)_{kn}c_n=0. \tag{8}$$

We have employed the notation

$$\left.\begin{aligned} H_{0n}&=\int dq\psi^{(0)*}\mathcal{H}\phi_n, \quad \text{etc.,} \\ (H-E)_{kn}&=\int dq\phi_k{}^*\mathcal{H}\phi_n-E\int dq\phi_k{}^*\phi_n \end{aligned}\right\}. \tag{9}$$

Next we multiply Eq. (8) by $[(H-E)^{-1}]_{jk}$ and sum over the index k,** so that

$$\sum_k[(H-E)^{-1}]_{jk}H_{k0} +\sum_k\sum_n{}'[(H-E)^{-1}]_{jk}(H-E)_{kn}c_n=0. \tag{10}$$

Since

$$\sum_k[(H-E)^{-1}]_{jk}(H-E)_{kn}=\delta_{jn},$$

we find

$$c_j=-\sum_k{}'[(H-E)^{-1}]_{jk}H_{k0}. \tag{11}$$

Applying Eq. (11) to Eq. (7),

$$E-H_{00}-\sum_{n,k}{}''H_{0n}[(H-E)^{-1}]_{nk}H_{k0}. \tag{12}$$

Now we make use of the perturbation assumption, Eq. (2), and separate Eq. (12) into terms of various order. The energy of a perturbed system may be expanded as a power series in the parameter λ,

$$E=E^{(0)}+\lambda E^{(1)}+\lambda^2E^{(2)}+\cdots, \tag{13}$$

and all we need know of the development of $(H-E)^{-1}$ is that

$$[(H-E)^{-1}]_{nk}=[(H^{(0)}-E^{(0)})^{-1}]_{nk}\{1+0(\lambda)+\cdots\}. \tag{14}$$

Denoting the matrix elements of $\mathcal{H}_0$ and $\mathcal{V}$ in analogous fashion with Eq. (9) and noting that

$$H_{0n}{}^{(0)}=H_{n0}{}^{(0)}=0 \tag{15}$$

because of the assumed orthogonality of $\psi^{(0)}$ on the ϕ_n, we may write Eq. (12) through terms of second-order in λ as

$$H_{00}{}^{(0)}+\lambda V_{00}-\lambda^2\sum_{nk}{}''V_{0n}[(H^{(0)}-E^{(0)})^{-1}]_{nk}V_{k0}. \tag{16}$$

The summation contributes no other terms of first- or second-order by virtue of Eq. (15).

If we employ the notation

$$\mathfrak{R}\equiv\mathcal{H}_0-E^{(0)}, \tag{17}$$

we may write finally for the second-order energy[6]

$$E^{(2)}=-\sum_{nk}{}''V_{0n}(R^{-1})_{nk}V_{k0}. \tag{18}$$

Formally, all we require to find the second-order eigenvalue are the perturbation matrix elements connecting $\psi^{(0)}$ with each of the basis functions ϕ_n and the $\mathfrak{R}$ matrix elements between all pairs of such functions. The set $\{\phi_n\}$ need, of course, include only functions of such symmetry that the V_{0n} do not vanish identically. We observe that nowhere, as required by conventional perturbation theory, need we know anything of the structure of any state of the system other than the one in question.

III. CONNECTION WITH CONVENTIONAL PERTURBATION THEORY

Since the domain of ψ may be spanned by an infinite number of complete sets of functions, any two of which are connected by some linear transformation, we can, in principle, regard Eq. (18) as the result of a change in basis from the set of eigenvalues of the unperturbed Hamiltonian to the set $\{\phi_n\}$. (We write $\psi^{(0)}$ alternatively as ϕ_0, and regard it as a member of $\{\phi_n\}$ also.) In particular, we shall now show that if $\psi_k{}^{(0)} (k=0, 1, \cdots, N)$ represent orthonormalized eigenfunctions of $\mathcal{H}_0$, then the usual equation,

$$E_0{}^{(2)}=-\sum_k{}'\frac{v_{0k}v_{k0}}{E_k{}^{(0)}-E_0{}^{(0)}} \tag{19}$$

for the second-order energy of the state labeled by subscript 0 reduces to Eq. (18); if the $\psi_k{}^{(0)}$ are linearly

¶ We have placed the restriction on our basis that the first function be a solution to the unperturbed problem. This is not required by Epstein, reference 2.

** In this paper we use the notation $(A^{-1})_{jk}$ to indicate the inverse of the matrix representing the operator A. When we are dealing with a nonorthogonal basis this is not, in general, identical with the matrix of the inverse operator A^{-1}.

[6] This expression is somewhat similar to one derived by Shull and Simpson, J. Chem. Phys. **28**, 925 (1958), for a consolidated variation-perturbation approach. They use orthonormal functions, however.

dependent on the ϕ_n,

$$\psi_k^{(0)}=\sum_n c_{kn}\phi_n. \tag{20}$$

Note that this is not, in general, a unitary transformation since the orthonormality of the set $\{\phi_n\}$ is not required. Matrix elements with respect to the orthonormal basis are written in lower case.

The matrix r_{kl} is, by virtue of the orthonormality of the $\psi_k^{(0)}$, of diagonal form,

$$r_{kl}=(E_k^{(0)}-E_0^{(0)})\,\delta_{kl}. \tag{21}$$

Furthermore,

$$(r^{-1})_{kl}=(r_{kl})^{-1}=\frac{\delta_{kl}}{E_k^{(0)}-E_0^{(0)}}. \tag{22}$$

Multiplying by v_{l0} and summing over the index l we obtain

$$\sum_l{}'(r^{-1})_{kl}v_{l0}=\sum_l{}'\frac{\delta_{kl}v_{l0}}{E_k^{(0)}-E_0^{(0)}}=\frac{v_{k0}}{E_k^{(0)}-E_0^{(0)}}; \tag{23}$$

Eq. (19) may be written in a form analogous to Eq. (18), and

$$E_0^{(2)}=-\sum_{kl}{}''v_{0k}(r^{-1})_{kl}v_{l0}. \tag{24}$$

We need only show now that this form is invariant under the transformation in Eq. (20).

Matrix elements in the two representations are related by

$$\left.\begin{aligned} v_{0k}&=\sum_n c_{kn}V_{0n},\\ v_{l0}&=\sum_m c_{lm}{}^*V_{m0},\end{aligned}\right\} \tag{25}$$

and,

$$r_{kl}=\sum_{sr}c_{ks}{}^*R_{sr}c_{lr}. \tag{26}$$

The inverse of Eq. (26) is given by

$$(r^{-1})_{kl}=\sum_{sr}(c^{-1})_{sk}(R^{-1})_{sr}(c^{-1})_{rl}{}^*. \tag{27}$$

Substituting Eqs. (25) and (27) into Eq. (24) and summing over indices k, l we obtain Eq. (18). Conversely, it is easily shown by an analogous procedure that Eq. (18) becomes Eq. (19) when the ϕ_n are linearly dependent on the $\psi_k^{(0)}$.

IV. RELATION TO THE VARIATIONAL METHOD

It is instructive to consider also an alternative derivation of Eq. (18) from the standpoint of the variational principle. We begin, as before, with a linear development for ψ

$$\psi=\psi^{(0)}+\sum_{n=1}^{N}c_n\phi_n, \tag{28}$$

but recognize, however, the fact that the set $\{\phi_n\}$ in practice is but a small finite one and nowhere near complete. Consistent with this, we shall attempt to find the best second-order energy, determining the c_n by the variational principle.

For an arbitrary trial function χ of suitable symmetry characteristics,

$$\mathfrak{F}(\chi)=\int dq\chi^*\mathfrak{H}\chi-E\int dq\chi^*\chi\geq 0, \tag{29}$$

where E is the eigenvalue for the perturbed problem; the lowest one, in the event the original state is degenerate. Should the exact solution of the Schroedinger equation, Eq. (4), be substituted for χ, $\mathfrak{F}$ would vanish and moreover assume a stationary value with respect to all parameters in χ.

Our procedure shall be to substitute our linear development of ψ for χ and minimize $\mathfrak{F}$ with respect to the c_n. The inequality in Eq. (29) will then delimit the value for E. By using Eq. (28) in Eq. (29),

$$\mathfrak{F}(c_1,\cdots,c_N)=\left\{\begin{aligned}&H_{00}-E+\sum_n{}'(c_n{}^*H_{n0}+H_{0n}c_n)\\&+\sum_{mn}{}''c_n{}^*c_m(H_{nm}-ES_{nm}),\end{aligned}\right. \tag{30}$$

where we have defined

$$S_{nm}\equiv\int dq\phi_n{}^*\phi_m,$$

and noted the orthogonality of the ϕ_m to $\psi^{(0)}$. We apply now the usual power series expansions in the perturbation parameter λ,

$$\left.\begin{aligned} H_{ij}&=H_{ij}^{(0)}+\lambda V_{ij},\\ c_n&=\lambda c_n{}^{(1)}+\lambda^2 c_n{}^{(2)}+\cdots\end{aligned}\right\}. \tag{31}$$

Substituting Eqs. (13), (15), (17), and (31) into Eq. (30), and recalling that $H_{00}{}^{(0)}=E^{(0)}$ and $V_{00}=E^{(1)}$, we obtain, to terms of second order in λ,

$$\mathfrak{F}(c_1,\cdots,c_N)=\left\{\begin{aligned}&\lambda^2\{-E^{(2)}+\sum_n{}'(c_n{}^*V_{n0}+V_{0n}c_n)\\&+\sum_{mn}{}''c_n{}^*c_mR_{nm}\}+0(\lambda^3).\end{aligned}\right. \tag{32}$$

We now apply the variational conditions

$$\partial\mathfrak{F}/\partial c_k=0,\qquad k=1,\cdots,N, \tag{33}$$

obtaining the set of equations

$$V_{0k}+\sum_n{}'c_n{}^*R_{nk}=0,\qquad k=1,\cdots,N, \tag{34}$$

apart from terms of order λ^3. These are equivalent to the set,

$$V_{k0}+\sum_n{}'R_{kn}c_n=0,\qquad k=1,\cdots,N, \tag{35}$$

obtained by minimizing with respect to the $c_k{}^*$. The

nontrivial solutions of Eq. (35) are

$$c_n = -\sum_k{}'(R^{-1})_{nk}V_{k0}, \quad k=1, \cdots, N. \tag{36}$$

Applying the inequality $\mathfrak{F}\geq 0$, we establish finally the equation delimiting the second-order perturbation energy,

$$E^{(2)} \leq -\sum_{nk}{}''V_{0m}(R^{-1})_{nk}V_{k0}, \tag{37}$$

the equality holding only when the set $\{\phi_n\}$ is rigorously complete.

V. DISCUSSION

Little can be said regarding the form of the ϕ_n, or the number of such functions required to approximate $E^{(2)}$ to a given degree of accuracy without reference to some particular problem. A good indication of the relative importance of some ϕ_n may be obtained from its contribution were it the sole perturbing state,

$$E_n^{(2)} = -\,|\,V_{0n}\,|^2/R_{nn}. \tag{38}$$

Strictly speaking, however, each function must be tested in combination with others before it may be neglected validly. To obtain an idea of how well convergence to the true $E^{(2)}$ is proceeding, one might enlarge the basis by adding some "good" function ϕ_n, i.e., one with relatively large $E_n^{(2)}$. If the resulting change in $E^{(2)}$ is small, the accuracy of $E^{(2)}$ is strongly indicated.

Just as the variational result in Eq. (37) gives an upper bound on the value of $E^{(2)}$, the second-order perturbation in Eq. (19) can provide a lower one if the state labelled by subscript 0 is the ground state. This follows from the inequality,

$$\sum_n{}'[V_{0n}V_{n0}/(E_n-E_0)] \leq [1/(E_1-E_0)]\sum_n{}'V_{0n}V_{n0}$$
$$= [(V^2)_{00}-(V_{00})^2]/(E_1-E_0), \tag{39}$$

where E_1 is the energy of the lowest contributing excited state and

$$(V^2)_{00} = \int d\tau\psi_0^{(0)*}\mathcal{V}^2\psi_0^{(0)}. \tag{40}$$

Thus

$$E_0^{(2)} = -\sum_n{}'[V_{0n}V_{n0}/(E_n-E_0)]$$
$$\geq -[(V^2)_{00}-(V_{00})^2]/(E_1-E_0), \tag{41}$$

and $E_0^{(2)}$ is bracketed by Eqs. (37) and (41).††

Unless there is good reason to believe that the major constribution to $E^{(2)}$ is from a single state, Eq. (41) can not be regarded too seriously from a quantitative point of view. However, Eq. (41) almost certainly indicates the correct order of magnitude. Furthermore, it may indicate the behavior of a second-order eigenvalue with respect to some parameter.

Next we shall write out Eq. (37) explicitly for the case of two basis functions. Assuming that we have computed the requisite matrix elements, we find

$$E_{1,2}^{(2)} = -\frac{V_{01}^2R_{22}-2V_{01}V_{02}R_{12}+V_{02}^2R_{11}}{R_{11}R_{22}-R_{12}^2}, \tag{42}$$

choosing, for convenience, all matrix elements to be real.

For the case $R_{12}=0$, Eq. (42) reduces to

$$E_{1,2}^{(2)} = -(V_{01}^2/R_{11})-(V_{02}^2/R_{22}) = E_1^{(2)}+E_2^{(2)}, \tag{43}$$

using the notation of Eq. (38). Hence we may generalize that when basis functions of different symmetry are involved, the R matrix of each type may be inverted separately, and the energy contributions are additive.

We consider finally the evaluation of second-order properties other than that of the energy. Referring to our original expansion Eqs. (5) or (28), the expectation value of some operator $\mathcal{Q}$ for the perturbed state in question is found from

$$\langle\mathcal{Q}\rangle = \int d\tau\psi^*\mathcal{Q}\psi \Big/ \int d\tau\psi^*\psi. \tag{44}$$

Substituting the optimal expansion coefficients from Eq. (36), we find the second-order contribution,

$$Q^{(2)} = -\sum_{nk}{}''\{Q_{0n}(R^{-1})_{nk}V_{k0}+V_{0n}(R^{-1})_{nk}Q_{k0}\}. \tag{45}$$

Since no extremum properties hold, in general, for the operator $\mathcal{Q}$, we may state merely that Eq. (45) approximates $Q^{(2)}$ without specification as to whether this is an upper or a lower bound. However, since a function having a more accurate energy eigenvalue generally gives more dependable values for other properties, we may, with little additional labor, compute $E^{(2)}$ also, and observe its convergence properties as a test of our basis.

VI. A SIMPLE APPLICATION: THE PERTURBED HARMONIC OSCILLATOR

As a somewhat trivial though illustrative example of our perturbation method we shall consider the ground state of the harmonic oscillator perturbed by a small cubic potential term.

The Hamiltonian for an unperturbed one-dimensional harmonic oscillator in an appropriately scaled system of units may be written

$$\mathcal{H}_0 = -(d^2/dx^2)+x^2. \tag{46}$$

†† It should perhaps be noted that the concepts of upper and lower limit are here employed in the algebraic sense. Since, for nondegenerate ground states, second-order perturbation energies are always negative, absolute magnitudes of these quantities must be interpreted in the opposite sense as regards upper and lower limit.

The eigensolutions are[7]

$$\psi_n^{(0)}=[\pi^{-1/4}/(2^n n!)^{\frac{1}{2}}]\exp(-x^2/2)H_n(x),$$
$$E_n^{(0)}=2n+1, \quad (47)$$

where $H_n(x)$ is the nth Hermite polynomial. The only states we shall require explicitly are the following:

$$\left.\begin{aligned}\psi_0^{(0)}&=\pi^{-1/4}\exp(-x^2/2), & E_0^{(0)}&=1;\\ \psi_1^{(0)}&=\pi^{-1/4}2^{-1/2}x\exp(-x^2/2), & E_1^{(0)}&=3;\\ \psi_3^{(0)}&=\pi^{-1/4}3^{-1/2}(2x^3-3x)\exp(-x^2/2), & E_3^{(0)}&=7.\end{aligned}\right\} \quad (48)$$

We consider now a cubic anharmonicity, corresponding to a perturbation

$$\mathcal{U}=\kappa x^3, \quad (49)$$

where, in order for perturbation methods to be valid, we require $\kappa \ll 1$.

We compute the energy first by ordinary perturbation theory. This is possible here since only two states perturb the ground state, the first and third excited states, as follows readily from the properties of Hermite polynomials. To compute the necessary matrix elements requires only the integrals

$$\left.\begin{aligned}&\int_{-\infty}^{\infty}dx\exp(-x^2)=\pi^{\frac{1}{2}},\\ &\int_{-\infty}^{\infty}dx x^{2n}\exp(-x^2)=\frac{1\cdot3\cdot5\cdots(2n-1)\pi^{\frac{1}{2}}}{2^n},\\ &\qquad n=1, 2, \cdots.\end{aligned}\right\} \quad (50)$$

The perturbation energy to second-order is given by

$$E^{(2)}=-\{[V_{01}^2/(E_1-E_0)]+[V_{03}^2/(E_3-E_0)]\}$$
$$=-\tfrac{11}{16}\kappa^2. \quad (51)$$

For purposes of comparison, we estimate the energy by the summation procedure of Eq. (41),

$$E^{(2)}\geq-[(V^2)_{00}/(E_1-E_0)]=-\tfrac{15}{16}\kappa^2, \quad (52)$$

which is certainly of the correct magnitude.

We proceed now to a computation of $E^{(2)}$ by our method. We use three trial functions:

$$\left.\begin{aligned}\phi_a&=x\exp(-x^2/2)\\ \phi_b&=x^3\exp(-x^2/2)\\ \phi_c&=x^5\exp(-x^2/2).\end{aligned}\right\} \quad (53)$$

From symmetry considerations it is evident that only odd functions contribute in second order. We may anticipate immediately that the two-function basis ϕ_a, ϕ_b is equivalent to $\psi_1^{(0)}$, $\psi_3^{(0)}$, and should immediately yield the correct energy; it will be of interest to observe how closely each one alone predicts $E^{(2)}$, as well as to note the effect of the admittedly extraneous function ϕ_c.

The necessary matrix elements are readily computed using Eq. (50). They appear in Table I. The second-order energy is computed by Eqs. (38) and (42) for all possible one and two-function bases. The results are given in Table II together with the percentage of the correct value, $-\frac{11}{16}\kappa^2$. All but $E_c^{(2)}$ must be termed respectable results. Evidently, addition of ϕ_c to the basis affords considerable improvement nevertheless.

The foregoing example illustrates that the modified method can be as convenient and as accurate as ordinary perturbation theory, even when the latter is applicable. Moreover, when trial functions are suitably chosen, rapid convergence is obtained.

TABLE I

$V_{0a}=(3/4)\pi^{1/4}\kappa$	$R_{aa}=\pi^{1/2}$	$R_{ab}=(3/2)\pi^{1/2}$
$V_{0b}=(15/8)\pi^{1/4}\kappa$	$R_{bb}=(27/4)\pi^{1/2}$	$R_{ac}=(15/4)\pi^{1/2}$
$V_{0c}=(105/16)\pi^{1/4}\kappa$	$R_{cc}=(25/16)105\pi^{1/2}$	$R_{bc}=(225/8)\pi^{1/2}$

TABLE II.

$E_{ab}^{(2)}=-0.6875\kappa^2[-(11/16)\kappa^2]$	100%
$E_{ac}^{(2)}=-0.6563\kappa^2$	95%
$E_a^{(2)}=-0.5625\kappa^2[-(9/16)\kappa^2]$	82%
$E_{bc}^{(2)}=-0.5542\kappa^2$	81%
$E_b^{(2)}=-0.5208\kappa^2$	76%
$E_c^{(2)}=-0.2625\kappa^2$	38%

ACKNOWLEDGMENT

The author wishes to dedicate this paper to the late Professor William Moffitt of Harvard University, under whose direction this work was performed. The generous assistance of Professor E. B. Wilson with the manuscript is also acknowledged.

[7] See, for example, L. Pauling and E. B. Wilson, *Quantum Mechanics* (McGraw-Hill Book Company, Inc., New York, 1935), Chap. III.

Temperature Dependence of Quadrupole Resonance Frequencies under Constant Pressure

R. J. C. BROWN*

Department of Physical Chemistry, University of Sydney, Sydney, Australia

(Received August 31, 1959)

The theory of the temperature dependence of pure quadrupole frequencies under constant volume conditions is modified when constant pressure conditions apply. For the case of molecular crystals the first and second derivatives of frequency with respect to temperature have been calculated assuming that (i) the quadrupole coupling constant is independent of volume, and (ii) the lattice frequencies vary linearly with temperature. These derivatives have been evaluated experimentally for the α phase of p-dichlorobenzene, and comparisons made with the theory; good agreement with previous work on the pressure dependence of quadrupole frequencies is obtained.

I. INTRODUCTION

EARLY studies of the temperature dependence of nuclear quadrupole resonance frequencies (ν) showed discrepancies between the observed and predicted values of $d\nu/dT$. The theoretical interpretation was not complete until Kushida, Benedek, and Bloembergen[1] showed that the quadrupole frequency is a function of pressure as well as temperature, and pointed out that the theory proposed by Bayer,[2] and generalized by Kushida,[3] predicted the temperature dependence measured under conditions of constant volume. Previous measurements of the temperature dependence had been made under constant pressure conditions, and variations of the quadrupole coupling constant and lattice frequencies with volume had been neglected. A number of measurements of the pressure dependence under isothermal conditions were carried out by Kushida, Benedek, and Bloembergen,[1] Dean and Lindstrand,[4] and Gutowsky and Williams[5]; using published values for the thermal expansion coefficient and compressibility, complete analyses of contributions to the temperature and pressure dependence were made.

If appropriate volume dependence functions for the quadrupole coupling constant and the lattice frequencies are assumed, the temperature dependence of the quadrupole frequency under constant pressure conditions can be calculated; the assumptions made will depend markedly on the type of crystal involved. The present work deals with molecular crystals, for which suitable assumptions greatly simplify the calculations, in particular the α phase of p-dichlorobenzene will be considered.

II. THEORY

Kushida[3] calculated the temperature dependence using the normal lattice coordinates,

$$\xi_i=\xi_i^0 \sin(\omega_i t+\Delta_i), \tag{1}$$

where ξ_i^0, ω_i are the amplitude and angular frequency, respectively, of the ith normal coordinate. The angular displacement of a particular molecule and the coupling constant are expressed as series in the normal coordinates, ξ_i, and the known properties of normal coordinates in a crystal lattice[6] are used to complete the analysis. Under constant volume conditions the temperature dependence is given by

$$\nu(T)=\nu_0[1+bT+c/T], \tag{2}$$

where

$$b=-\tfrac{3}{2}k\sum_{i=1}^{M}(A_i/\omega_i^2), \tag{3}$$

$$c=-(\hbar^2/8k)\sum_{i=1}^{M}A_i, \tag{4}$$

and ν_0 = quadrupole frequency in a stationary molecule.

In these expressions, A_i are constants arising from the series expansions mentioned above; each A_i is related to an equivalent moment of inertia, Θ_i, associated with each coordinate ξ_i:

$$A_i \doteq \Theta_i^{-1}. \tag{5}$$

The summations in Eqs. (3) and (4) are carried out over the M modes which contribute significantly to the temperature dependence; usually frequencies above about 150 cm^{-1} are neglected.

The temperature dependence function [see Eq. (2)] approaches linearity at high temperatures, and except for molecules with small moments of inertia $\nu(T)$ is very closely linear near room temperatures. For p-dichlorobenzene the moments of inertia about the two axes perpendicular to the Cl–Cl direction can be calculated from x-ray data,[7] and the constant c can be estimated from these figures, using Eqs. (4) and (5) and assuming $M=2$. In the temperature range 250 to 320°K the term $\nu_0 c/T$ changes by 0.6 Kc/s, while the linear term $\nu_0 bT$ changes by about 160 Kc/s over the same range.

Kushida, Benedek, and Bloembergen[1] proceeded with the analysis on the assumption that ν_0, A_i, and

* Present address: Department of Chemistry and Chemical Engineering, University of Illinois, Urbana, Illinois.

[1] Kushida, Benedek, and Bloembergen, Phys. Rev. **104**, 1364 (1956).

[2] H. Bayer, Z. Physik. **130**, 227 (1951).

[3] T. Kushida, J. Sci. Hiroshima Univ. **A19**, 327 (1955).

[4] C. Dean and E. Lindstrand, J. Chem. Phys. **24**, 1114 (1956).

[5] H. S. Gutowsky and G. A. Williams, Phys. Rev. **105**, 464 (1957).

[6] M. Born and K. Huang, *Dynamical Theory of Crystal Lattices* (Clarendon Press, Oxford, 1954).

[7] Croatto, Bezzi, and Bua, Acta Cryst. **5**, 825 (1952).

ω_i are all volume dependent. In a molecular crystal the volume-dependent contribution of lattice fields to the quadrupole coupling constant is small, and hence ν_0 is approximately independent of volume. The equivalent moments of inertia of the molecules (A_i^{-1}) can be calculated from molecular dimensions alone, and will be assumed to be independent of volume. The volume dependence of the lattice frequencies ω_i can be introduced as follows. Ichishima[8] has measured the temperature dependence of the low frequency Raman lines in naphthalene under constant pressure conditions between -190 and $+25$°C. The frequencies were found to be linear functions of temperature.

$$\omega_i=\omega_i^0(1-g_it), \tag{6}$$

where t is the temperature measured from any fixed temperature and ω_i^0 is the frequency at $t=0$; the constants g_i lie between 0.0050 and 0.0015 deg^{-1}. It is assumed now that Eq. (6) holds generally for molecular crystals; the "constant" b is temperature dependent and the quadrupole frequency is expected to be a nonlinear function of temperature when measured under constant pressure conditions.

Let t be the temperature measured from 27°C; then $T=t+300$ and ω_i^0 should approximate the Raman frequencies measured by Saksena.[9] The quadrupole frequency is a function of the $M+1$ variables ω_i, t, and the total derivative with respect to temperature can be written

$$d\nu/dt=(\partial\nu/\partial t)+\sum_{i=1}^{M}(\partial\nu/\partial\omega_i)\cdot(d\omega_i/dt). \tag{7}$$

After carrying out the differentiations, using Eqs. (2), (3), and (6), and neglecting the term $\nu_0 c/T$ in the expression for $\nu(T)$, we obtain

$$(1/\nu_0)(d\nu/dt)=-\tfrac{3}{2}k\sum_{i=1}^{M}(A_i/\omega_i^2)$$

$$-3k(t+300)\sum_{i=1}^{M}(A_i/\omega_i^3)g_i\omega_i^0. \tag{8}$$

Similarly, $d\nu/dt$ is a function of ω_i and t, so that

$$d^2\nu/dt^2=(\partial/\partial t)(d\nu/dt)+\sum_{i=1}^{M}(\partial/\partial\omega_i)(d\nu/dt)\cdot(d\omega_i/dt), \tag{9}$$

and

$$(1/\nu_0)(d^2\nu/dt^2)=-6k\sum_{i=1}^{M}(A_i/\omega_i^3)g_i\omega_i^0$$

$$-9k(t+300)\sum_{i=1}^{M}(A_i/\omega_i^4)g_i^2\omega_i^{02}. \tag{10}$$

[8] I. Ichishima, J. Chem. Soc. Japan, Pure Chem. Sect. **71**, 607 (1950).

[9] B. D. Saksena, J. Chem. Phys. **18**, 1653 (1950).

TABLE I. Cl^{35} Quadrupole frequency in p-dichlorobenzene (α phase).

Temperature (°C)	$t(=T-300)$	Quadrupole frequency (Kc/s)
5	−22	34 337.2
7	−20	34 331.6
9	−18	34 324.9
11	−16	34 318.0
13	−14	34 311.2
15	−12	34 304.4
17	−10	34 297.2
19	−8	34 290.9
21	−6	34 283.7
23	−4	34 276.2
25	−2	34 269.1
27	0	34 261.3
29	2	34 253.8
31	4	34 246.2
33	6	34 238.4
35	8	34 231.0
37	10	34 224.3
39	12	34 216.8
41	14	34 208.8
43	16	34 201.8
45	18	34 193.9

The values of these derivatives at 300°K are:

$$(1/\nu_0)[d\nu/dt]_0=(1+600\langle g\rangle)b_0 \tag{11}$$

$$(1/\nu_0)[d^2\nu/dt^2]_0=(4\langle g\rangle+1800\langle g^2\rangle)b_0 \tag{12}$$

where the weighted averages $\langle g\rangle$, $\langle g^2\rangle$, are defined by

$$\langle g\rangle=[\sum_{i=1}^{M}(A_i/\omega_i^{02})\cdot g_i]/[\sum_{i=1}^{M}(A_i/\omega_i^{02})] \tag{13}$$

$$\langle g^2\rangle=[\sum_{i=1}^{M}(A_i/\omega_i^{02})\cdot g_i^2]/[\sum_{i=1}^{M}(A_i/\omega_i^{02})] \tag{14}$$

and b_0 is the value of b at $t=0$. In order to make use of Eqs. (11) and (12) it is necessary to assume all g_i values equal, so that $\langle g\rangle=g$ and $\langle g^2\rangle=g^2$; then Eqs. (11) and (12) are simultaneous equations in g and b_0 which can be solved if experimental values for the two derivatives are determined.

III. EXPERIMENTAL

The temperature dependence of the pure quadrupole frequency in the α phase of p-dichlorobenzene has been determined between 5 and 45°C. A frequency modulated continuous wave oscillator similar to that used by Wang[10] gave a signal/noise ratio of about five; frequencies were measured to ±0.5 Kc/s with a disposals BC221 wavemeter. The sample was recrystallized from ethyl alcohol and placed in a sealed tube; the coil of the oscillator was immersed in a kerosene thermostat bath which maintained the temperature constant to within 0.02°C. Two mercury thermometers were used for temperature measurement so that the required temperature range could be covered at constant immersion. The thermometers and wave-

[10] T. C. Wang, Phys. Rev. **99**, 566 (1955).

meter were calibrated at the National Standards Laboratory of the C.S.I.R.O. in Sydney.

The quadrupole frequency was determined at intervals of two degrees, and the results, shown in Table I, were subjected to a least squares analysis[11]; comparison of Table I with the results of Wang verify that the sample was in the α phase. The sums of squares of residuals about the linear and quadratic curves are, respectively,

$$\sum v_1^2 = 24.2\ (\text{Kc/s})^2,$$

and

$$\sum v_2^2 = 4.7\ (\text{Kc/s})^2.$$

A parabola fits the data significantly better than a straight line; the least squares quadratic expression for the quadrupole frequency is

$$\nu = (34261.5 \pm 0.1) - (3.62 \pm 0.01)t - (0.0074 \pm 0.0006)t^2\ \text{Kc/s}. \quad (15)$$

From this equation the derivatives $d\nu/dt$ and $d^2\nu/dt^2$ are found, and Eqs. (11) and (12) can be solved, yielding the values

$$g = 0.0011\ \text{deg}^{-1} \quad \text{and} \quad b_0 = -0.62 \times 10^{-4}\ \text{deg}^{-1}.$$

[11] R. T. Birge, Revs. Modern Phys. **19**, 298 (1947).

Wang has calculated the theoretical value for b_0 from Eq. (3) as -0.71×10^{-4} deg^{-1}; Kushida, Benedek and Bloembergen[1] found $b_0 = -0.60 \times 10^{-4}$ deg^{-1} for the γ phase. If the temperature variation of the lattice frequencies is neglected, and a straight line is fitted to the experimental data, the slope $d\nu/dt$ gives the value of b_0 directly as -1.05×10^{-4} deg^{-1}. Thus the introduction of temperature-dependent lattice frequencies gives closer agreement between theoretical and observed values of b_0; the experimental value of g falls in the range of g_i values for naphthalene.

IV. CONCLUSION

In the case of p-dichlorobenzene, the form of the temperature dependence at constant pressure can be accounted for by assuming that (i) the quadrupole coupling constant is independent of volume, and (ii) the lattice frequencies ω_i are linear functions of temperature. The values of g and b_0 can be determined from the temperature dependence curve near room temperature.

V. ACKNOWLEDGMENT

This work was carried out during the tenure of a University Research Studentship. The author wishes to acknowledge the helpful supervision of Dr. T. Iredale.

THE JOURNAL OF CHEMICAL PHYSICS VOLUME 32, NUMBER 1 JANUARY, 1960

Aspects of the Statistical Thermodynamics of Real Fluids

HOWARD REISS, H. L. FRISCH, AND E. HELFAND, *Bell Telephone Laboratories, Incorporated, Murray Hill, New Jersey*

AND

J. L. LEBOWITZ,* *Stevens Institute of Technology, Hoboken, New Jersey*

(Received July 6, 1959)

By extending the ideas previously applied to the statistical mechanical theory of hard sphere fluids of Reiss, Frisch, and Lebowitz, an approximate expression has been determined for the work of creating a spherical cavity in a real fluid. In turn the knowledge of this entity permits an evaluation of properties such as the surface tension and the normal heats of vaporization of fluids and the Henry's law constants of fluid mixtures. The agreement between the calculated and experimental properties is satisfactory.

I. BASIC CONSIDERATIONS

In a recent paper Reiss, Frisch, and Lebowitz[1] (henceforth referred to as I) obtained an approximate analytical expression for the equation of state of a hard sphere fluid which compared very favorably at all fluid densities with the results of previous machine computations[2–4] and which gave the first five virial coefficients quite accurately—the first three being in fact exact.

The techniques of this theory can be extended to the treatment of real fluids in a systematic manner, and at present this is being done. On the other hand the hard sphere results furnish a great deal of physical insight and suggest an approximate treatment of certain aspects of real fluids which can be carried out at once. The present paper will be devoted to this treatment.

The central idea of the development is that it is possible to write a very good estimate for the reversible work extended in the production of a spherical cavity of radius r in a fluid, $W(r)$. The work of expanding the spherical cavity's radius from r to $r+dr$ can be written as a sum of a volume and surface contribution

$$dW(r)=p\cdot 4\pi r^2 dr+\sigma(r)\cdot 8\pi r dr,$$

with p the pressure of the fluid. For sufficiently large r, $\sigma(r)=\sigma_0$, a surface tension, so that

$$W(r)\approx\tfrac{4}{3}\pi r^3 p+4\pi r^2\sigma_0. \tag{1.1}$$

The first term on the right-hand side of (1.1) is the volume work expended in creating the cavity of volume $(4/3)\pi r^3$. One may imagine this to be accomplished by the introduction of a hollow *rigid* sphere whose radius increases to the size r. During this expansion the total volume of the system remains constant at V and the pressure also remains constant when V is chosen in such a way that

$$\lim_{N,V\to\infty} N/V=\rho, \tag{1.2}$$

where N is the number of molecules in the system and ρ is the number density.

The surface tension σ_0 is then the interfacial tension between the fluid and a perfect rigid wall, and should not be confused with the surface tension at a liquid-vapor interface.

As r become somewhat smaller a term must be added which accounts for the curvature dependence of the surface work. We therefore write in place of (1.1) [cf. Eq. (6.2) of I],

$$W(r)=(\tfrac{4}{3}\pi r^3)p+4\pi r^2\sigma_0[1-(2\delta/r)], \tag{1.3}$$

where δ is a distance of the order of the thickness of the inhomogeneous layer near the interface.

If the real molecules in the fluid are regarded as having rigid cores of diameter a, it is actually possible to compute $W(r)$ exactly for $r\leq a/2$. This is so because a cavity of such small dimensions can contain at most the center of one molecule. For the details of the calculation the reader is referred to Eq. (3.1) through (3.3) of I. The work is given by

$$W(r)=-kT\ln(1-\tfrac{4}{3}\pi r^3\rho),\quad r\leq a/2, \tag{1.4}$$

where k is Boltzmann's constant and T is temperature. This is obviously different from Eq. (1.3), and the two must be matched at $r=a/2$.

Now the statistical considerations of reference I suggest that the density $\rho G(r)$ just outside a cavity of radius r is specified very closely by

$$G(r)=A+(B/r)+(C/r^2) \tag{1.5}$$

for $r>a/2$, where A, B, and C may depend upon density and temperature. This form should apply to both large and small cavities provided that $r>a/2$. Furthermore it is true [see Eq. (6.1) of I] that

$$G(r)=(4\pi r^2 kT\rho)^{-1}(\partial W/\partial r). \tag{1.6}$$

Insertion of (1.3) for W into (1.6) gives the form (1.5), and thus supports the conclusion that (1.3) which is

* Supported by the Air Force Office of Scientific Research.

[1] Reiss, Frisch, and Lebowitz, J. Chem. Phys. **31**, 369 (1959).

[2] M. N. Rosenbluth and A. W. Rosenbluth, J. Chem. Phys. **22**, 881 (1954).

[3] W. W. Wood and J. D. Jacobsen, J. Chem. Phys. **27**, 1207 (1957).

[4] T. E. Wainwright and B. J. Alder, U. S. Atomic Energy Comm. Report, Contract No. W-7405-eng-48, Radiation Laboratory, Livermore, University of California.

asymptotically correct for large r is also valid for very small r. As a matter of fact (1.6) would still yield (1.5) if an arbitrary function of temperature and density were added to the right member of (1.3). The value of the function should be small enough so it can be ignored when r achieves macroscopic dimensions in which case the asymptotic equation (1.1) holds. Calling this arbitrary function K_0, we now have

$$W(r)=(\tfrac{4}{3}\pi r^3)p+4\pi r^2\sigma_0[1-(2\delta/r)]+K_0,\quad r>a/2. \tag{1.7}$$

Equation (1.7) can be written for $r\geq a/2$ as

$$W(r)=k_0+k_1[r-(a/2)]+k_2[r-(a/2)]^2+k_3[r-(a/2)]^3$$
$$=K_0+K_1r+K_2r^2+K_3r^3, \tag{1.8}$$

where the K's (and the k's) may be functions of density and temperature. This is just an expansion of $W(r)$ with terms up to cubic order retained. Actually we know[1] that W is nonanalytic at $r=a/\sqrt{3}$ and other points beyond $a/\sqrt{3}$ but there is strong evidence that the discontinuities occur in terms of higher order than those retained in (1.8) (see Sec. III of reference I).

In practice we will not need to know W for r very much greater than $a/2$ (usually for $r\leq a$) so that (1.8) may be regarded simply as an extrapolation formula. It should be emphasized that by (1.4) we know W *exactly* up to the point $r=a/2$, so we are already in possession of an appreciable part of W for larger values of r.

Comparison of Eq. (1.8) with Eq. (1.3) reveals that

$$K_3=\tfrac{4}{3}\pi p. \tag{1.9}$$

The three remaining coefficients K_0, K_1, and K_2 can be determined by matching W and its first and second derivatives at $r=a/2$ to the values obtained from Eq. (1.4). This is made possible by the fact that W and its first two derivatives are continuous. For the proof of this the reader is referred to Sec. III of reference I. There reference is made to hard spheres but it is easily seen that the same proof can be given for cavities in real fluids, although in Eq. (3.27) of reference I, $G(a)$ must be replaced by $g(a)$ (since $G(a)\neq g(a)$ for real fluids).

When the coefficients are determined by this procedure, we obtain

$$K_0=kT\{-\ln(1-y)+\tfrac{9}{2}[y/(1-y)]^2\}-(\pi pa^3/6),$$
$$K_1=-(kT/a)\{[6y/(1-y)]+18[y/(1-y)]^2\}+\pi pa^2,$$
$$K_2=(kT/a^2)\{[12y/(1-y)]+18[y/(1-y)]^2\}-2\pi pa,$$
$$K_3=\tfrac{4}{3}\pi p, \tag{1.10}$$

where

$$y=\pi a^3\rho/6. \tag{1.11}$$

From the correspondence between the forms (1.7) and (1.8) for W we obtain, by using Eqs. (1.10),

$$\sigma_0=(kT/4\pi a^2)\{[12y/(1-y)]+18[y/(1-y)]^2\}-(pa/2),$$
$$\delta=(a/4)\left\{\frac{[6y/(1-y)]+18[y/(1-y)]^2-(\pi pa^3/kT)}{[6y/(1-y)]+9[y/(1-y)]^2-(\pi pa^3/kT)}\right\}. \tag{1.12}$$

We now note that the introduction of a rigid sphere of diameter b into the fluid of real molecules is equivalent to the introduction of a cavity of radius

$$r=(a+b)/2, \tag{1.13}$$

since such a sphere excludes the centers of molecules (whose hard cores are of diameter a) from a region of such radius. Thus (1.8) with r given by (1.13) is the reversible work expended in the introduction of a rigid sphere solute molecule of diameter b. To obtain the chemical potential μ_h of such a solute we must add to the work W a term representing the free energy of mixing of the solute with solvent. This leads to the expression

$$\mu_h=kT\ln\rho_2\Lambda_2^3+W, \tag{1.14}$$

where ρ_2 is the density of solute and Λ_2 is

$$\Lambda_2=h/(2\pi m_2kT)^{\frac{1}{2}}, \tag{1.15}$$

m_2 being the mass of a solute molecule, and h Planck's constant. Of course, Eq. (1.14) only applies to dilute solutions in which the solute molecules remain independent of one another. By introducing Eq. (1.10) into Eq. (1.8) and the result into Eq. (1.14) we obtain,

$$\mu_h/kT=\ln\rho_2\Lambda_2^3+(W/kT),$$
$$W=kT\{[6y/(1-y)][2(r/a)^2-(r/a)]+[18y^2/(1-y)^2][(r/a)^2-(r/a)+\tfrac{1}{4}]-\ln(1-y)\}+\pi pa^3[\tfrac{4}{3}(r/a)^3-2(r/a)^2+(r/a)-\tfrac{1}{6}], \tag{1.16}$$

where r is given by Eq. (1.13) and y by Eq. (1.11).

For such a hard sphere solute, the partial pressure p_2 can be computed, assuming the vapor phase to be ideal, for then the chemical potential μ_2 of the solute in the vapor must be given by

$$\mu_2/kT=\ln p_2\Lambda_2^3/kT. \tag{1.17}$$

Since in equilibrium $\mu_2=\mu_h$ we have by equating the right sides of (1.16) and (1.17)

$$p_2=[kT\rho_2/(1-y)]\exp\{(\pi pa^3/kT)\cdot[\tfrac{4}{3}(r/a)^3-2(r/a)^2+(r/a)-\tfrac{1}{6}]+6[y/(1-y)][2(r/a)^2-(r/a)]+18[y/(1-y)]^2[(r/a)^2-(r/a)+\tfrac{1}{4}]\}. \tag{1.18}$$

From (1.18) the constant of Henry's law

$$k_H = p_2/\rho_2 \tag{1.19}$$

can easily be deduced.

II. COMPARISON WITH EXPERIMENT

At this stage it is possible to test the validity of our expression for $W(r)$, the work required for the creation of a cavity of radius r by appeal to experiment. For example, by combining (1.14) with (1.17), using $\mu_2 = \mu_h$, and (1.19) we can derive

$$W(r) = kT \ln(k_H/kT), \tag{2.1}$$

which allows computation of $W(r)$ from measured values of the constant of Henry's law. Comparison of the right sides of Eqs. (2.1) and (1.16) furnishes the necessary test.

Of course it is necessary to have a solution containing a rigid sphere solute and approximately spherical solvent molecules, with effectively rigid cores. In any real solution the solute will have a partly attractive potential, which leads to a negative valued interaction free energy to be discussed more fully in Sec. III. Therefore, we expect our computed result to be higher than that found experimentally.

Two solutions for which data exist and which very nearly satisfy the requirements outlined above are helium in argon studied by Karasz and Halsey[5] and helium in benzene studied by Clevor *et al.*[6] The benzene molecule is not truly spherical and we must rely upon angular averaging to provide such behavior. If it is assumed spherical and appeal is made to some independent phenomenon such as viscosity or second virial coefficient measurements, an internally consistent value of a should be derived.

If the solvent-solvent interaction is assumed to be described by a Lennard-Jones 6–12 potential, then a good choice for a is the point at which the rising potential, showing repulsion, is zero. The potential rises so steeply here that an increase of several kT in energy occurs with almost negligible decrease of distance between the two molecules. We have made this choice of a. The diameter b of the solute is chosen in the same manner.

The necessary data is available in Table 1-A of the Appendix of Hirschfelder, Curtiss, and Bird.[7] We find

$$\begin{aligned} &\text{helium} \quad b = 2.56\times10^{-8}\ \text{cm} \\ &\text{argon} \quad a = 3.40\times10^{-8}\ \text{cm} \\ &\text{benzene} \quad a = 5.27\times10^{-8}\ \text{cm}. \end{aligned} \tag{2.2}$$

The first two quantities are obtained from second virial coefficient measurements and the third from viscosity. Densities were obtained from the critical tables.[8] Indicating $W(r)$ obtained from Henry's law data by $W(k_H)$, and that obtained using (2.2), the proper values of density (concentration), and (1.16) by W we obtain the following:

$$\begin{aligned} &\text{Helium in argon } (T = 86.6°\text{K}) \\ &W(k_H) = 3.46\times10^{-14}\ \text{erg} \\ &W = 6.07\times10^{-14}\ \text{erg} \\ &\text{Helium in Benzene } (T = 288°\text{K}) \\ &W(k_H) = 1.59\times10^{-13}\ \text{erg} \\ &W = 1.73\times10^{-13}\ \text{erg}. \end{aligned} \tag{2.3}$$

In the calculations leading to Eqs. (2.3) the term in Eq. (1.16) containing the pressure was neglected since at pressures of the order of an atmosphere it is entirely negligible. We see that $W(k_H)$ is less than W, which is to be expected by the considerations of Sec. III.

The agreement between the calculated and experimental values of the constants of Henry's law may appear to be less satisfactory than that shown in (2.3). This arises from the logarithmic relation in Eq. (2.1). For example, if we denote k_H computed by combination of Eqs. (1.16) and (2.1) as $k(W)$, then we find for the cases exhibited by (2.3):

Helium in argon

$$k(W)/k_H = 8.8$$

Helium in benzene

$$k(W)/k_H = 1.42. \tag{2.4}$$

Nevertheless the real standard of agreement must be found in Eq. (2.3) since we are testing the validity of our expression for $W(r)$.

Another test of the validity of our relations is furnished by consideration of σ_0 given in Eq. (1.12). It will be recalled that this represents the interfacial tension where the fluid contacts a perfectly rigid wall. This is not the same as σ, the interfacial tension between a liquid and its vapor, but ought to be of similar magnitude. This is especially true far below the critical temperature where the vapor is highly attenuated, for example at or below the normal boiling point. In Table I we compare σ_0 and σ for a number of substances. The values of σ were taken from the handbook[9] and σ_0 is calculated using (1.12) together with values of a from Table I-A in Hirschfelder, Curtiss, and Bird and values of density from the critical tables.[8] Once again, the term in p is negligible.

The temperatures have been chosen in Table I to correspond as closely as possible to measurements of

[5] F. E. Karasz and G. D. Halsey, J. Chem. Phys. **29**, 173 (1958).
[6] Clevor, Battino, Saylor, and Gross, J. Phys. Chem. **61**, 1078 (1957).
[7] Hirschfelder, Curtiss, and Bird, *Molecular Theory of Gases and Liquids* (John Wiley & Sons, Inc., New York, 1954), p. 1110.
[8] *International Critical Tables* (McGraw-Hill Book Company, Inc., New York, 1926).
[9] Lange, *Handbook of Chemistry* (Handbook Publishers, Sandusky, Ohio, 1941), fourth edition.

TABLE I. Comparison of σ and σ_0 at or below the boiling points of various liquids.

Substance	Temp °K	σ(dynes/cm)	σ_0(dynes/cm)
Ne	27.2 °K	4.80	6.09
Ar	85.1 °K	13.2	16.4
He	4.2 °K	0.098	0.223
H_2	20.4 °K	1.80	1.91
N_2	70.1 °K	10.5	14.9
O_2	70.1 °K	18.3	23.6
C_6H_6	273.1 °K	29.02	34.3

σ under conditions of low vapor pressure. For very high vapor densities the agreement is less satisfactory.

III. NONRIGID SPHERE SOLUTES

Until now we have been dealing with rigid sphere solutes whose potential energy of interaction with solvent molecules ϕ_h, could be represented by

$$\phi_h=\infty, \quad r\leq\tfrac{1}{2}(a+b); \qquad \phi_h=0, \quad r>\tfrac{1}{2}(a+b), \tag{3.1}$$

where r is the distance between the centers of the solute and solvent molecules. Real solute molecules have a nonrigid or soft potential in addition to ϕ_h. If we call this part ϕ_s, then the potential ϕ is

$$\phi=\phi_h+\phi_s. \tag{3.2}$$

We will now compute the chemical potential of such an added solute molecule by using the coupling parameter method. We introduce coupling parameters[10] ξ_h and ξ_s as follows:

$$\phi(r, \xi_h, \xi_s)=\phi_h(r, \xi_h)+\xi_s\phi_s(r). \tag{3.3}$$

For ξ_h it is convenient to chose the radius of the hard core (as in reference I). Then the hard core is fully coupled to the rest of the system when $\xi_h=\frac{1}{2}(a+b)$ so that (3.1) applies. The soft potential will be fully coupled when $\xi_s=1$, i.e., when the second term on the right of (3.3) is just ϕ_s.

We can now add the solute molecule to the solution in two stages. In the first ξ_h is charged from 0 to $\frac{1}{2}(a+b)$, while $\xi_s=0$. The reversible work in this stage is simply μ_h. Thus if the chemical potential of the added solute is represented as $\mu(\xi_h, \xi_s)$

$$\mu_h=\mu[\tfrac{1}{2}(a+b), 0]. \tag{3.4}$$

In the next step the soft potential is brought into play by charging ξ_s from 0 to 1. Denoting the corresponding change in chemical potential by μ_s we have

$$\mu_s=\mu[\tfrac{1}{2}(a+b), 1]-\mu[\tfrac{1}{2}(a+b), 0]. \tag{3.5}$$

Obviously the chemical potential of the added solute is

$$\mu=\mu_h+\mu_s. \tag{3.6}$$

[10] T. L. Hill, *Statistical Mechanics* (McGraw-Hill Book Company, Inc., New York, 1956), p. 191.

The quantity μ_h has been discussed in the two previous sections and an approximation expression, Eq. (1.16), has been derived for it. Using a simple extension of the usual coupling parameter technique[10] it can be shown that

$$\mu_s=\rho\int_0^1 d\xi_s\int_0^\infty 4\pi r^2\phi_s g[r, \xi_h=\tfrac{1}{2}(a+b), \xi_s]dr, \tag{3.7}$$

in which $g[r, \xi_h=\frac{1}{2}(a+b), \xi_s]$ is the radial distribution function of solvent molecules about a solute whose rigid core is fully coupled and whose soft potential is coupled to the extent ξ_s. The evaluation of μ_s therefore requires detailed knowledge of $g(r, \xi_h, \xi_s)$. Since g is positive and ϕ_s is negative we can say that μ_s is negative.

IV. μ_h AND HEATS OF VAPORIZATION

In this section we apply what should be an even more severe criterion for testing the validity of μ_h as given by (1.16). First (1.16) is specialized to the case in which $r=a$ so that the solute now is a solvent molecule. Thus

$$\mu_h/kT=\ln[\rho\Lambda^3/(1-y)]+6[y/(1-y)]+\tfrac{9}{2}[y/(1-y)]^2+(\pi a^3p/6kT). \tag{4.1}$$

If it is assumed that (4.1) applies to a liquid phase in equilibrium with an ideal vapor then [cf. Eq. (1.17)]

$$\mu=\mu_h+\mu_s=kT\ln(p\Lambda^3/kT). \tag{4.2}$$

If we use (4.1) in (4.2), we obtain

$$\mu/kT=\ln(p\Lambda^3/kT)=\ln\{(6\Lambda^3/\pi a^3)[y/(1-y)]\}+6[y/(1-y)]+\tfrac{9}{2}[y/(1-y)]^2+(\pi a^3p/6kT)+(\mu_s/kT). \tag{4.3}$$

The process in Eq. (3.7) in which ξ_s is charged from 0 to 1 may be approximated by setting $\xi_s=1$ in g from the beginning. It is asymptotically correct for that part of the integral in which ξ_s is approaching 1 and should not introduce a large error. In general μ_s can be decomposed as follows:

$$\mu_s=e_s+pv_s-Ts_s, \tag{4.4}$$

where e_s is the internal energy change during charging of the soft potential, v_s is a volume associated with the process and s_s an entropy. The term in pv_s may be shown to be small for a condensed system and will be neglected.

Now the change in internal energy during charging is obviously.

$$e_s=\rho\int_a^\infty 4\pi r^2\phi_s g(r, \xi_h=\tfrac{1}{2}(a+b), \xi_s=1)dr, \tag{4.5}$$

so that e_s is just what is obtained by setting ξ_s equal to unity in g in Eq. (3.7). Thus the error in doing this involves neglect of the entropy of charging. The

system becomes more organized upon charging since the attractive forces lead to greater correlation between molecules. As a result

$$s_s<0 \tag{4.6}$$

and

$$\mu_s>e_s. \tag{4.7}$$

Further, if the vapor is ideal it can be shown[11] that

$$e_s=2kT-2\lambda_v, \tag{4.8}$$

where λ_v is the heat of vaporization per molecule. Thus

$$\mu_s=2kT-2\lambda_v-Ts_s\approx 2kT-2\lambda_v. \tag{4.9}$$

Substituting (4.9) into (4.3) we obtain, with neglect of terms of the order pv,

$$\lambda_v/kT=1-\tfrac{1}{2}\{\ln(\pi a^3 p/6kT)[(1-y)/y]-6[y/(1-y)] -\tfrac{9}{2}[y/(1-y)]^2\}-(s_s/2k). \tag{4.10}$$

In view of (4.6) the last term on the right is positive. If we then approximate λ_v by λ_v' which we define to be equal to the first two terms on the right (i.e., we ignore the entropy contribution) then

$$\lambda_v'<\lambda_v. \tag{4.11}$$

If the measured vapor pressure and the measured density are used (in Eq. 4.10) together with values of a obtained by the procedure used previously, then λ_v' can be computed. This can be compared with the measured λ_v which it should approximate on the low side. In Table II we list values of λ_v' computed in this manner together with measured values of λ_v for various substances. The data all refer to the boiling points of the various substances.

The agreement between λ_v' and λ_v is really quite good. In all cases λ_v' is lower than λ_v by about 15%. This agrees with Eq. (4.11) and furthermore shows that the entropy contribution is small. The successful approximate compution of $\lambda_v(\lambda_v')$ by this technique strengthens the validity of Eq. (1.16) since the method is based on this expression for μ_h.

What is perhaps an even more stringent test of Eq. (1.16) is possible. This depends on the fact that if μ_s is known over a range of values of the state variables

TABLE II. Comparison of λ_v' and λ_v, the heat of vaporization.

Substance	λ_v' (cal)	λ_v (cal)
Ar	1 360	1 558
Ne	361	416
Xe	2 830	3 200
He	23.2	24
CH_4	1 850	2 218
N_2	1 260	1 340
H_2	188	218
C_6H_6	6 300	7 360

[11] Reference 10, p. 189.

TABLE III. Comparison of λ_v calculated by (4.18) with experimental values at the boiling point.

Substance	λ_v (cal.) calc.	λ_v (cal.) exp.
Ar	1510	1558
CH_4	2280	2218

then s_s and v_s can be computed from the thermodynamic formulas

$$s_s=-(\partial\mu_s/\partial T)_p, \tag{4.12}$$

$$v_s=(\partial\mu_s/\partial p)_T. \tag{4.13}$$

For reasons connected with the Clapeyron-Clausius relation it will be useful to examine the temperature derivative of μ_s along the line of coexistence between liquid and vapor phases. Using subscript c for such derivatives we have

$$(d\mu_s/dT)_c=-s_s+v_s(dp/dT)_c. \tag{4.14}$$

Another expression for this quantity, obtained by solving (4.3) for μ_s and differentiating, is

$$(d\mu_s/dT)_c=-s_s+(e_s/T)+(pv_s/T)+(\pi a^3 p/6T)-k +[(kT/p)-(\pi a^3/6)](dp/dT)_c-kT\frac{(1+2y)^2}{y(1-y)^3}(dy/dT)_c. \tag{4.15}$$

All coexistence derivatives can be written in terms of $(dp/dT)_c$ if T and p are regarded as the independent variables. The value of this arises from the fact that the Clapeyron-Clausius relation says

$$(d\ln p/dT)_c=\lambda_v/kT^2. \tag{4.16}$$

Recall that e_s is also given in terms of λ_v by (4.8).

The quantity v_s can be written as

$$v_s=v-v_h, \tag{4.17}$$

where $v_h=(\partial\mu_h/\partial p)_T$ by Eq. (4.1) is

$$v_h=kT[(1+2y)^2/y(1-y)^3](\partial y/\partial p)_T+(\pi a^3/6). \tag{4.18}$$

If we use the facts that $pa^3/kT\ll 1$, $v=0(a^3)$, and $(\partial\ \ln y/\partial\ \ln p)_T\ll 1$ then combination of (4.8) and (4.14–18) yields

$$\lambda_v=kT+kT^2\alpha[(1+2y)^2/(1-y)^3], \tag{4.19}$$

where α is the coefficient of thermal expansion,

$$(1/v)(\partial v/\partial T)_p=-(1/y)(\partial y/\partial T)_p.$$

This expression for the heat of vaporization is essentially an exact consequence of the assumed form of μ_h and thus serves as an important criterion for the validity of the latter. To apply it, however, requires reliable data for α and the molecular core diameter of simple liquids. For argon and methane the coefficients

of thermal expansion at the boiling point are available from the critical tables,[8] while a may be taken from Hirschfelder, Curtiss, and Bird.[7] Comparison of the calculated and experimental heats of vaporization are made in Table III. The agreement seems to be very good.

V. SUMMARY

It appears that it is possible to give an excellent approximation for the chemical potential of (or the work of adding) a hard sphere in a real fluid. Systems exist, such as helium in benzene, which are close to this model so that an experimental test of the theoretical expression may be obtained directly from Henry's law constants. In addition, for very large hard spheres the work of expanding the sphere can be related to the surface tension. Thus this rigid wall-liquid surface tension can be calculated. Lastly, the heat of vaporization can be related to the difference between the work of adding a real molecule and the work of adding a hard sphere to a fluid, and in this way determined. The agreement between these calculations and experimental data lends support to the basic concept involved in the estimation of μ_h.

THE JOURNAL OF CHEMICAL PHYSICS VOLUME 32, NUMBER 1 JANUARY, 1960

Evaluation of One-Center Electron Repulsion Integrals between Certain s-Type Atomic Orbitals*

WALTER D. JONES† AND F. L. BROOKS, JR.

Department of Chemistry, University of Washington, Seattle, Washington

(Received June 25, 1959)

A general formula is derived for one center s-type electron repulsion integrals for the set of basic atomic orbitals which involve the complete set of associated Laguerre functions of order $(2l+1)$ and degree $(n+l+1)$ with a single orbital exponent.

SEVERAL investigators have suggested the orthonormal set of functions

$$\psi_{nlm}=R_{nl}(r)\,Y_l^m(\theta,\varphi),$$

where, in atomic units,

$$R_{nl}(r)=\frac{(2Z)^{\frac{1}{2}}}{(n+l+1)\,!}\left[\frac{(n-l-1)\,!}{(n+l+1)\,!}\right]^{\frac{1}{2}}\cdot(2Zr)^l L_{n+l+1}^{2l+2}(2Zr)\exp-(Zr),$$

and

$$Y_l^m(\theta,\varphi)=\left[\frac{(2l+1)\,(l-|\,m\,|)\,!}{4\pi(l+|\,m\,|)\,!}\right]^{\frac{1}{2}}P_l^m(\cos\theta)\,\exp(im\phi)^1,$$

as a useful set of basic atomic orbitals.

In the early days of quantum mechanics it was pointed out by E. Schrödinger that this set might have advantages for variational treatments in as much as it is a discrete *and* complete set, in contrast to the set of hydrogenic orbitals. Recently, Löwdin and Shull have successfully used this basis for certain problems.

In order to use these functions in a variation or second-order perturbation theory treatment one must evaluate kinetic energy, potential energy, and electron repulsion integrals. Kinetic and potential energy integrals may be evaluated by using formulas which may be trivially obtained from the formulas derived for a hydrogen atom by Hirschfelder and Löwdin.[2] However, general formulas for the electron repulsion integrals do not seem to be available.

Although a single general formula for all electron repulsion integrals is not readily obtainable, a formula may be derived for each set of angular types not zero by symmetry. We have derived a formula for electron repulsion integrals of the s type ($l=m=0$ for all four functions) and other derivations may be patterned accordingly.

First we abbreviate as follows:

$$\langle ac\,|\,1/r_{12}\,|\,bd\rangle\equiv\iint a^*(1)c^*(2)\,(1/r_{12})b(1)d(2)d\tau_1 d\tau_2,$$

where

$$x(\mu)=\psi_{x00}(\mu),\qquad x=a,\,b,\,c,\,d.$$

Next we introduce the customary expansion for $1/r_{12}$

* This research was supported in part by the U. S. Air Force through the Air Office of Scientific Research of the Air Research and Development Command under Contract No. 18(600)-375.

† Address after September, 1959, Department of Physics, Bowdoin College, Brunswick, Maine.

[1] The associated Laguerre polynomials L_{n+l+1}^{2l+2} and associated Legendre polynomials P_l^m are defined as in L. C. Pauling and E. B. Wilson, *Introduction to Quantum Mechanics* (McGraw-Hill Book Company, Inc., New York, 1935).

[2] J. O. Hirschfelder and P.-O. Löwdin, *Long Range Interaction of Two 1s Hydrogen Atoms Expressed in Terms of Natural Spin Orbitals*, Technical Report of the Quantum Chemistry Group, Uppsala University (1957).

and integrate over the angular coordinates,

$$\langle ac \mid 1/r_{12} \mid bd \rangle = N\int_0^\infty L_{a+1}^2(2Zr_1)\, L_{b+1}^2(2Zr_1)\, \exp(-2Zr_1)$$
$$\cdot\left[(1/r_1)\int_0^{r_1} L_{c+1}^2(2Zr_2)\, L_{d+1}^2(2Zr_2)\, \exp(-2Zr_2)\, r_2^2 dr_2 + \int_{r_1}^\infty L_{c+1}^2(2Zr_2)\, L_{d+1}^2(2Zr_2)\, \exp(-2Zr_2)\, r_2 dr_2\right] r_1^2 dr_1,$$

where

$$N = (2Z)^6 \frac{[(a-1)\,!(b-1)\,!(c-1)\,!(d-1)\,!]^{\frac{1}{2}}}{[(a+1)\,!(b+1)\,!(c+1)\,!(d+1)\,!]^{\frac{1}{2}}}.$$

The integral may now be evaluated by making use of the generator function for the associated Laguerre polynomials, namely,

$$\sum_{\alpha=\beta}^\infty [L_\alpha^\beta(x)/\alpha\,!]\, t^\alpha = [(-1)^\beta t^\beta/(1-t)^{\beta+1}] \exp(-xt/1-t).$$

By using the generator function four times, one obtains

$$\sum_{s=2}^\infty \sum_{t=2}^\infty \sum_{u=2}^\infty \sum_{v=2}^\infty \frac{s^{a+1}t^{b+1}u^{c+1}v^{d+1}}{(a+1)\,!(b+1)\,!(c+1)\,!(d+1)\,!} \int_0^\infty L_{a+1}^2(2Zr_1)\, L_{b+1}^2(2Zr_1)\, \exp(-2Zr_1)$$
$$\times\left[(1/r_1)\int_0^{r_1} L_{c+1}^2(2Zr_2)\, L_{d+1}^2(2Zr_2)\, \exp(-2Zr_2)\, r_2^2 dr_2 + \int_{r_1}^\infty L_{c+1}^2(2Zr_2)\, L_{d+1}^2(2Zr_2)\, \exp(-2Zr_2)\, r_2 dr_2\right] r_1^2 dr_1$$
$$\equiv \frac{(-1)^2(-1)^2(-1)^2(-1)^2 s^2 t^2 u^2 v^2}{(1-s)^3(1-t)^3(1-u)^3(1-v)^3} \int_0^\infty \exp\left[-2Zr_1\left(\frac{s}{1-s}+\frac{t}{1-t}+1\right)\right]\left\{(1/r_1)\int_0^{r_1} \exp\left[-2Zr_2\left(\frac{u}{1-u}+\frac{v}{1-v}+1\right)\right] r_2^2 dr_2 + \int_{r_1}^\infty \exp\left[-2Zr_2\left(\frac{u}{1-u}+\frac{v}{1-v}+1\right)\right] r_2 dr_2\right\} r_1^2 dr_1$$
$$= \frac{(stuv)^2}{[(1-s)(1-t)(1-u)(1-v)]^3}\left\{-\frac{(1-s)^3(1-t)^3(1-u)^5(1-v)^5}{16Z^5(1-uv)^2[(1-st)(1-u)(1-v)+(1-uv)(1-s)(1-t)]^3}\right.$$
$$\left.-\frac{(1-s)^2(1-t)^2(1-u)^5(1-v)^5}{16Z^5(1-uv)^3[(1-st)(1-u)(1-v)+(1-uv)(1-s)(1-t)]^2}+\frac{(1-s)^2(1-t)^2(1-u)^3(1-v)^3}{16Z^5(1-st)^2(1-uv)^3}\right\}.$$

After equating coefficients of like powers of s, t, u, and v on both sides of the preceding equation and comparing with the expression for the integral, we find that the integral is given by the coefficient of $s^{a+1}t^{b+1}u^{c+1}v^{d+1}$ in the expansion of

$$N\left[\frac{(a+1)\,!(b+1)\,!(c+1)\,!(d+1)\,!(stuv)^2}{16Z^5}\right]\left[-\frac{(1-u)^2(1-v)^2}{(1-uv)^2[(1-st)(1-u)(1-v)+(1-uv)(1-s)(1-t)]^3}\right.$$
$$\left.-\frac{(1-u)^2(1-v)^2}{(1-s)(1-t)(1-uv)^3[(1-st)(1-u)(1-v)+(1-uv)(1-s)(1-t)]^2}+\frac{1}{(1-st)^2(1-s)(1-t)(1-uv)^3}\right]$$
$$= N'(stuv)^2[A+B+C],$$

where A, B, and C stand, respectively, for the three fractions inside the square brackets, and

$$N' = 4Z\left[\frac{(a-1)\,!(b-1)\,!(c-1)\,!(d-1)\,!}{(a+1)\,!(b+1)\,!(c+1)\,!(d+1)\,!}\right]^{\frac{1}{2}}.$$

Since $s^2t^2u^2v^2$ is a factor outside the brackets, one must find the $s^{a-1}t^{b-1}u^{c-1}v^{d-1}$ term inside the brackets, that is for A, B, and C.

To obtain the $s^{a-1}t^{b-1}u^{c-1}v^{d-1}$ term in the expansion of A and B, we note that

$$[(1-st)(1-u)(1-v)+(1-uv)(1-s)(1-t)]^{-m} = (1-s)^{-m}(1-t)^{-m} \times (1-u)^{-m}(1-v)^{-m}\left[\frac{1}{1-s}+\frac{1}{1-t}+\frac{1}{1-u}+\frac{1}{1-v}-2\right]^{-m}. \quad (1)$$

It may be demonstrated by induction that

$$\frac{\partial^x}{\partial w^x}\left((1-w)^{-n}\left[\frac{1}{1-w}+D\right]^{-m}\right)\Big|_{w=0}=\sum_{\alpha=0}^{x}(-1)^\alpha\binom{x}{\alpha}\frac{(n+x-1)!(m+\alpha-1)!}{(n+\alpha-1)!(m-1)!}[1+D]^{-m-\alpha}, \tag{2}$$

where D is any arbitrary quantity not a function of w.

After factoring A according to Eq. (1) and applying Eq. (2), successively allowing w to equal s, t, u, and v, we find that the coefficient of $s^{a-1}t^{b-1}u^{c-1}v^{d-1}$ in the expansion of A is given by

$$A'=\frac{1}{(d-1)!}\frac{\partial^{d-1}}{\partial v^{d-1}}\left\{\frac{1}{(c-1)!}\frac{\partial^{c-1}}{\partial u^{c-1}}\left[\frac{1}{(b-1)!}\frac{\partial^{b-1}}{\partial t^{b-1}}\left(\frac{1}{(a-1)!}\frac{\partial^{a-1}}{\partial s^{a-1}}A\right)_{s=0}\right]_{t=0}\right\}_{u=0}\Bigg|_{v=0}$$

$$=-\frac{(a+1)!(b+1)!}{16(a-1)!(b-1)!}\sum_{\epsilon=0}^{c-1}(\epsilon+1)\sum_{\alpha=0}^{a-1}\sum_{\beta=0}^{b-1}\sum_{\gamma=0}^{c-1-\epsilon}\sum_{\delta=0}^{d-1-\epsilon}(-\tfrac{1}{2})^{\alpha+\beta+\gamma+\delta}$$

$$\times\binom{a-1}{\alpha}\binom{b-1}{\beta}\binom{c-1-\epsilon}{\gamma}\binom{d-1-\epsilon}{\delta}\frac{(2+\alpha+\beta+\gamma+\delta)!}{(2+\alpha)!(2+\beta)!\gamma!\delta!}.$$

where $c\leqslant d$.

In the same manner we obtain the coefficient of $s^{a-1}t^{b-1}u^{c-1}v^{d-1}$ in the expansion of B. It is

$$B'=-\frac{(a+1)!(b+1)!}{4(a-1)!(b-1)!}\sum_{\epsilon=0}^{c-1}(\epsilon+1)(\epsilon+2)\sum_{\alpha=0}^{a-1}\sum_{\beta=0}^{b-1}\sum_{\gamma=0}^{c-1-\epsilon}\sum_{\delta=0}^{d-1-\epsilon}(-\tfrac{1}{2})^{\alpha+\beta+\gamma+\delta}$$

$$\times\binom{a-1}{\alpha}\binom{b-1}{\beta}\binom{c-1-\epsilon}{\gamma}\binom{d-1-\epsilon}{\delta}\frac{(1+\alpha+\beta+\gamma+\delta)!}{(2+\alpha)!(2+\beta)!\gamma!\delta!}$$

$$\times\left\{1+\frac{2}{(1+\alpha+\beta+\gamma+\delta)}\left(\frac{\gamma^2}{c-1-\epsilon}+\frac{\delta^2}{d-1-\epsilon}\right)+\frac{4\gamma^2\delta^2}{(1+\alpha+\beta+\gamma+\delta)(\alpha+\beta+\gamma+\delta)(c-1-\epsilon)(d-1-\epsilon)}\right\}$$

where $c\leqslant d$.

For the coefficient of the same term in the expansion of C, we obtain

$$C'=\delta_{cd}\binom{c+1}{c-1}\sum_{\zeta=0}^{a-1}\binom{\zeta+1}{\zeta}$$

where $a\leqslant b$.

Now combining the three parts we have the final result:

$$\langle ac\mid 1/r_{12}\mid bd\rangle=N'(A'+B'+C').$$

Note that the terms $\gamma^2/c-1-\epsilon$ and $\delta^2/d-1-\epsilon$ vanish when the denominator is zero.

Ionization of Strong Electrolytes. VIII. Temperature Coefficient of Dissociation of Strong Acids by Proton Magnetic Resonance

G. C. Hood and C. A. Reilly

Shell Development Company, Emeryville, California

(Received June 29, 1959)

The proton magnetic resonance of nitric and perchloric acid solutions over the entire concentration range has been used for determining the dissociation constants at 0, 25, and 70°C. Excellent agreement with earlier data for nitric acid derived from Raman spectra was obtained.

THE present investigation extends former results[1] on the dissociation of nitric and perchloric acids to lower and higher temperatures. The improvement of the experimental technique has allowed increased accuracy of the immediate observations and extension of the range to lower concentrations thereby sharpening the required extrapolations.

EXPERIMENTAL

Anhydrous nitric and perchloric acids were prepared by vacuum distillation of mixtures of commercial acids with sulfuric acid.[2] The various solutions were prepared by dilution and individually analyzed by titration with standard base. Concentrations are expressed as moles/l at 25°C.

NMR measurements were made at 40.01 Mcps with a modified Varian V-4310 high resolution spectrometer equipped with a flux stabilizer. A simple thermostat, which allowed measurements to be made on spinning samples at any temperature between 5 and 100°C, was built inside a Varian probe of the "straight-through" type. All measurements were made with the aid of a precision coaxial cell[3] using benzene in the annulus of the cell as a reference. Temperatures were measured to ±1°C by means of a thermocouple inserted (at the receiver coil height) in the air stream used for spinning and heating or cooling the cell.

CALCULATIONS

The assumptions involved in obtaining dissociation information from proton magnetic resonance measurements have been described previously.[1,4]

The frequency shifts of the solutions referred to benzene given in Tables I and II were plotted *vs* temperature. The shifts at 0, 25, and 70°C were obtained from these close-to-linear curves. The proton shift s (Tables III and IV) in units of 10^{-6} of the field strength referred to water was obtained from the frequency shift $\Delta\nu$ according to

$$s=(\Delta\nu-\Delta\nu')/40.01+g, \qquad (1)$$

where the frequency shift in cps between benzene and water $\Delta\nu'$ was determined from measurements at 8.5, 24.5, and 71.5°C to have the values 57.8 at 0°C, 68.0 at 25°C and 85.7 at 70°C. The bulk magnetic shielding correction g (Tables III and IV) was obtained from

$$g=2.60(\kappa-\kappa_0)\times10^6,$$

where 2.60 is an empirical constant used in preference to the theoretical value $2\pi/3$, κ is the volume magnetic susceptibility of the solution and κ_0 is that of water. The values of κ_0 used were -0.720 at 0°C, -0.721 at 25°C and -0.725 at 70°C and were obtained from[5]

$$\kappa_0=-0.7205\cdot10^6[1+1.15\times10^{-4}(t-20)], \qquad (2)$$

where t is the temperature in °C. The values of κ were obtained from the temperature-independent gram magnetic susceptibilities χ_g measured previously and given in Tables I and II by using the densities of the acid solutions at the appropriate temperatures with the relation $\kappa=\chi_g d$.

As described previously[1] the degree of dissociation α of nitric acid can be calculated from

$$s/p=s_1\alpha+s_2(1-\alpha) \qquad (p<1) \qquad (3)$$

and that of perchloric acid from

$$s/p=s_1\alpha+s_2(1-\alpha)/3, \qquad (4)$$

where p is the stoichiometric mole fraction of hydrogen in H_3O^+ on a total hydrogen basis, s_1 is the shift of H_3O^+ and s_2 is the shift of the undissociated acid. Values of s_1 were obtained for each acid at each temperature from

$$s_1=\lim_{p\to0} s/p. \qquad (5)$$

The value of s_2 for nitric acid was obtained previously[1] from a curve of s *vs* p at the 50 mole % point ($p=1$) with the somewhat arbitrary assumption that at this point the solution contains only undissociated nitric acid monomer ($\alpha=0$). As a first approximation this is a good assumption in terms of previous Raman studies and the generally accepted view of the constitution

[1] Hood, Redlich, and Reilly, J. Chem. Phys. **22**, 2067 (1954).
[2] Redlich, Holt, and Bigeleisen, J. Am. Chem. Soc. **66**, 13 (1944).
[3] Manufactured by Wilmad Glass Company, Buena, New Jersey.
[4] G. C. Hood and C. A. Reilly, J. Chem. Phys. **27**, 1126 (1957).
[5] *Tables of Constants and Numerical Data* (I.U.P.A.P.), *Vol. 7: Diamagnetism and Paramagnetism*, G. Foex. (Masson and Company, Paris, 1957).

TABLE I. Nitric acid.

C, 25°C	t	Δv	t	Δv	t	Δv	t	Δv	χ_0
23.98	8.2	−202.7	30.5	−193.8	51.2	−185.6	65.0	−180.2	−0.314
23.00	8.2	−167.2	30.5	−157.9	49.8	−150.0	76.5	−138.8	−0.316
21.51	8.5	−131.2	30.5	−122.4	49.8	−114.8	77.0	−104.0	−0.325
21.36	10.0	−125.7	30.5	−117.7	50.8	−109.2	76.1	−98.9	−0.336
19.12	8.2	−100.2	30.5	−91.2	50.2	−83.2	75.6	−72.9	−0.351
17.20	9.8	−87.6	30.5	−77.0	49.5	−66.8	76.3	−60.6	−0.385
15.95	9.0	−81.0	29.0	−69.3	...	...	72.5	−50.2	−0.407
14.13	11.7	−71.9	29.0	−62.6	...	...	72.0	−43.6	−0.431
12.02	9.0	−61.7	29.0	−51.0	...	...	72.0	−30.1	−0.448
9.90	7.7	−49.9	29.0	−39.8	...	...	71.5	−20.2	−0.471
8.02	9.0	−30.1	28.0	−21.2	...	...	72.0	−3.5	−0.504
6.01	11.7	−8.9	28.3	−2.8	...	...	72.7	+14.2	−0.532
4.01	9.0	+14.0	28.5	+20.4	...	...	72.7	+34.7	−0.574
3.01	10.5	+27.5	29.0	+34.2	...	...	72.7	+47.3	−0.596
2.01	6.3	+40.1	29.0	+46.9	...	...	72.7	+60.6	−0.623
1.00	8.7	+51.8	28.5	+58.8	...	...	70.2	+72.1	−0.668

TABLE II. Perchloric acid.

C, 25°C	t	Δv	t	Δv	t	Δv	χ_0
17.59	10.0	−140.2	30.2	−137.3	49.8	−133.8	−0.340
16.76	10.0	−152.3	30.2	−148.0	50.0	−142.8	−0.352
16.18	...	...	...	...	50.5	−147.5	−0.360
15.61	...	...	...	...	50.5	−145.5	−0.366
13.44	10.0	−116.5	30.2	−114.8	50.0	−113.2	−0.398
12.05	10.2	−96.6	30.5	−94.2	49.8	−92.2	−0.416
10.48	11.3	−74.8	27.1	−72.2	72.0	−64.1	−0.440
9.01	11.3	−53.5	26.7	−50.2	72.5	−41.0	−0.464
7.50	9.7	−32.9	26.7	−29.1	73.0	−18.5	−0.490
6.03	11.5	−11.8	27.3	−7.8	73.0	+3.8	−0.518
4.26	12.0	+9.0	27.5	+13.5	71.5	+26.5	−0.551
3.02	12.5	+30.0	27.0	+35.0	72.0	+50.2	−0.587
1.51	9.5	+46.9	28.0	+53.6	73.0	+69.8	−0.634
0.755	8.7	+55.4	27.0	+61.0	73.0	+78.4	−0.666

TABLE III. Nitric acid.

		g			s			α			$\log a/c$	$\log K\beta$		
C, 25°C	p	0°C	25°C	70°C	0°C	25°C	70°C	0°C	25°C	70°C		0°C	25°C	70°C
23.98	2.979	0.61	0.64	0.65	7.20	7.23	7.24	...	...	...	...	...	...	...
23.00	2.358	0.61	0.64	0.65	6.33	6.34	6.33	...	...	...	...	...	...	...
21.51	1.820	0.58	0.61	0.63	5.40	5.44	5.44	...	...	...	...	...	...	...
21.36	1.775	0.57	0.57	0.61	5.26	5.27	5.28	...	...	...	...	...	...	...
19.12	1.212	0.54	0.55	0.56	4.58	4.59	4.58	...	...	...	...	...	...	...
17.20	0.913	0.40	0.44	0.45	4.15	4.19	4.05	0.118	0.110	0.081	3.00	3.05	3.05	3.04
15.95	0.779	0.34	0.37	0.39	3.93	3.88	3.81	0.176	0.151	0.123	2.80	2.88	2.87	2.86
14.13	0.606	0.29	0.32	0.35	3.69	3.64	3.60	0.301	0.260	0.218	2.51	2.67	2.64	2.62
12.02	0.464	0.28	0.30	0.33	3.39	3.33	3.26	0.445	0.386	0.318	2.17	2.43	2.38	2.34
9.90	0.348	0.25	0.28	0.30	3.04	3.03	2.95	0.614	0.546	0.450	1.84	2.25	2.18	2.10
8.02	0.264	0.22	0.24	0.26	2.52	2.51	2.52	0.710	0.632	0.548	1.55	2.08	1.98	1.90
6.01	0.186	0.20	0.22	0.24	1.98	2.02	2.05	0.840	0.775	0.680	1.18	1.98	1.82	1.68
4.01	0.118	0.17	0.18	0.18	1.34	1.40	1.46	0.923	0.880	0.806	0.74	1.85	1.68	1.45
3.01	0.086	0.153	0.164	0.148	1.01	1.06	1.13	0.950	0.929	0.876	0.48	1.80	1.63	1.38
2.01	0.056	0.130	0.143	0.117	0.659	9.705	0.765	0.974	0.958	0.925	0.17	1.76	1.55	1.29
1.00	0.027	0.086	0.091	0.040	0.322	0.347	0.383	0.988	0.985	0.974	−0.23	1.69	1.59	1.36

TABLE IV. Perchloric acid.

C, 25°C	p	g 0°C	g 25°C	g 70°C	s 0°C	s 25°C	s 70°C	α 0°C	α 25°C	α 70°C	log a/c	log Kβ 0°C	log Kβ 25°C	log Kβ 70°C
17.59	3.000	0.29	0.31	0.32	5.27	5.46	5.70	0	0	0	...	...	...	...
16.76	1.630	0.19	0.21	0.22	5.49	5.64	5.80	0.203	0.194	0.179	...	...	...	...
16.18	1.350	0.14	0.16	0.17	5.56	5.70	5.89	0.299	0.283	0.265	...	...	...	...
15.61	1.143	0.11	0.14	0.15	5.51	5.64	5.82	0.388	0.366	0.343	...	...	...	...
13.44	0.678	0.08	0.10	0.12	4.46	4.68	5.07	0.612	0.600	0.577	...	...	...	...
12.05	0.548	0.02	0.06	0.07	3.91	4.13	4.46	0.682	0.675	0.672	...	...	...	...
10.48	0.438	0.01	0.03	0.05	3.37	3.55	3.81	0.752	0.742	0.730	...	...	...	...
9.01	0.350	...	0.03	0.05	2.84	3.00	3.24	0.805	0.796	0.781	5.49	6.20	6.18	6.15
7.50	0.275	...	0.02	0.04	2.32	2.46	2.66	0.848	0.841	0.826	3.97	4.79	4.77	4.74
6.03	0.207	...	0.01	0.02	1.81	1.92	2.09	0.885	0.880	0.871	2.84	3.78	3.76	3.73
4.26	0.144	...	...	0.01	1.30	1.38	1.50	0.922	0.915	0.905	1.62	2.73	2.69	2.64
3.02	0.086	...	...	...	0.795	0.844	0.916	0.949	0.944	0.931	1.06	2.35	2.31	2.22
1.51	0.038	...	...	...	0.361	0.384	0.419	0.981	0.977	0.969	0.27	1.99	1.91	1.78
0.755	0.019	...	...	...	0.114	0.193	0.212	0.990	0.988	0.983	−0.18	1.83	1.73	1.58

of nitric acid solutions as a function of concentration. However, with the present improved precision of the NMR method a better evaluation of s_2 is desirable. Unfortunately, there is no way to obtain this evaluation from the NMR data alone. The recent Raman data of Krawetz[6] show that a small but significant amount of dissociation takes place beyond the 50 mole % point. The degree of dissociation approaches approximately 0.01 at 22–23 moles/l and then appears to increase again as the concentration increases. This latter effect is probably caused by dissociation into NO_2^+ and NO_3^-. The best basis for the determination of s_2 for nitric acid appears to be the degree of dissociation found at 15.95 moles/l by Krawetz[6] (for 70°C an extrapolation of the data is required).

The value of s_2 for perchloric acid was taken as the shift for the pure acid. The values of s_1 and s_2 are given in Table V.

The dissociation constant K was obtained by extrapolation of log $K\beta$ according to

$$K\beta = a/c(1-\alpha), \qquad (6)$$

where β is the activity coefficient of the undissociated acid, a is the activity of the acid, and c is the stoichiometric acid concentration in moles/l at the appropriate temperature. The activities were calculated from activity coefficient data at 25°C.[7,8] Data for both acids at 0 and 70°C are insufficient. As an approximation the 25°C coefficients were also used at the other temperatures. The thermodynamic dissociation constants and related quantities are given in Fig. 1 and Table VI where the nitric acid results of Krawetz,[6] who used the Raman technique, are shown for comparison. The values of K calculated with $s_2=3.55$ are given in Fig. 1 as filled circles. The values of K for nitric acid shown in parentheses in Table VI and in large open circles in Fig. 1 were calculated by means of the value $s_2=4.20$ based on $\alpha=0$ at the 50 mole % point. These values are therefore independent of Raman results. The values of $\Delta H°$ were estimated from the slopes of curves of log K *vs* $1/T$ at 25°C. The values of $\Delta S°$ at 25°C were calculated with $\Delta F° = \Delta H° - T\Delta S°$.

TABLE V. Values of s_1 and s_2.

Temperature °C	Nitric acid s_1	Nitric acid s_2	Perchloric acid s_1	Perchloric acid s_2
0	12.00	3.55	9.65	5.27
25	13.00	3.55	10.30	5.46
70	14.50	3.55	11.30	5.70

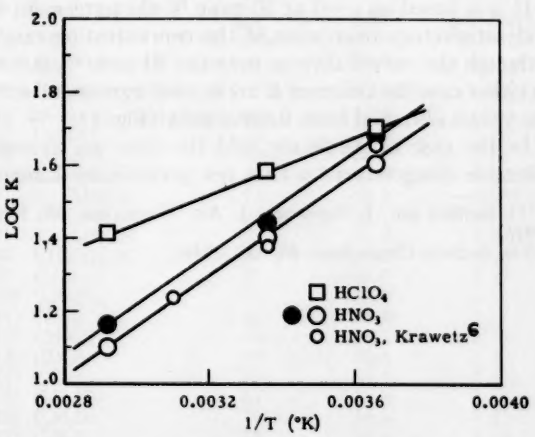

FIG. 1. Variation of dissociation constants with temperature.

[6] A. Krawetz, Thesis, University of Chicago, 1955; presented at Am. Chem. Soc. Meeting, April 1957, Miami, Florida. See also Young, Marenville, and Smith in Chap. 4 of *Structure of Electrolytic Solutions* edited by Walter J. Hamer (John Wiley & Sons, Inc., New York, 1959).

[7] Landolt-Börnstein, *Physikalische-Chemische Tabellen* (Verlag, Julius Springer, Berlin, 1936), fifth edition.

[8] R. A. Robinson and O. J. Baker, Trans. Roy. Soc. New Zealand **76**, 250 (1946).

TABLE VI. Dissociation constants.

Acid	Temp. °C	K (This investigation)	K Krawetz[6]	$\Delta F°$ (cal mole^{-1})	$\Delta H°$ (cal mole^{-1})	$\Delta S°$ (cal mole^{-1} deg^{-1})
Nitric	0	48(40)	45	−2100	...	...
	25	27.5(25)	23.5	−1970	−3300	−4.46
	50	...	17.5	...	...	...
	70	15(12.5)	...	−1840	...	...
Perchloric	0	50	...	−2120	...	...
	25	38	...	−2160	−1800	+1.20
	70	26	...	−2220	...	...

DISCUSSION

It has been indicated previously[9,10] that from 0 to 50 mole % a solution of nitric acid contains predominantly dissociated ions and undissociated monomeric acid while from 50 to 100 mole % the solution contains few hydrated protons but mixtures of undissociated monomer, dimer, and possibly higher polymers. Further confirmation of this general picture is given by the variation of s as a function of concentration and temperature. From 50 to 100 mole % the value of s at a given concentration shows practically no variation with temperature which should be the case if little or no dissociation takes place. Perchloric acid, however, which does dissociate even in concentrated solutions and does not polymerize yields values of s which vary with temperature at a given concentration.

In the case of nitric acid the curves of α *vs* concentration at different temperatures are in very good agreement with Raman data at all concentrations if the calculation of α from NMR data is calibrated by means of the Raman value at 15.95 moles/l by adjustment of s_2.

If s_2 is based on $\alpha=0$ at 50 mole % the agreement is still satisfactory over most of the concentration range although the curves diverge near the 50 mole % point. In either case the values of K are in good agreement with the values obtained from Raman data (Fig. 1).

In the case of perchloric acid the data are in considerable disagreement with a few preliminary Raman results[11] which, if confirmed by further research, will indicate a considerably higher degree of dissociation than that obtained here. A discrepancy if fully established, could be due to the failure of some assumption introduced in the interpretation of either Raman or NMR data. The least certain assumption is probably that of Eq. (4). It takes no account of the variation in hydration[12–14] of the hydrogen ion from $H^+\cdot 4H_2O$ to $H^+\cdot H_2O$. Moreover, the assumption that the magnetic field around the proton in $HClO_4$ is equally screened in anhydrous perchloric acid and in nearly completely dissociated acid may introduce an appreciable error.

The somewhat crude interpretation, which has been very satisfactory for the data so far obtained, probably has to be developed soon into a more elaborate and necessarily more complicated model since a considerably higher level of precision is now being attained in both experimental techniques.

ACKNOWLEDGMENT

The authors express their appreciation to Professor T. F. Young, University of Chicago, for a copy of the unpublished data presented in the thesis of Dr. A. A. Krawetz and for preliminary Raman results concerning perchloric acid.

[9] O. Redlich and J. Bigeleisen, J. Am. Chem. Soc. **65**, 1883 (1943).

[10] O. Redlich, Chem. Revs. **39**, 333 (1946).

[11] T. F. Young, University of Chicago (personal communication).

[12] K. N. Bascombe and R. P. Bell, Discussions Faraday Soc. **24**, 158 (1957.

[13] P. A. H. Wyatt, Discussions Faraday Soc. **24**, 162 (1957).

[14] van Eck, Mendel, and Boog, Discussions Faraday Soc. **24**, 200 (1957).

Diffusion of Impurities in Amorphous Polymers

A. W. LAWSON

Department of Physics and Institute for the Study of Metals, University of Chicago, Chicago 37, Illinois

(Received July 23, 1959)

The data of Ryskin on diffusion of impurities into amorphous polymers appear to be consistent with the prediction of elastic continuum theory that the ratio of the entropy of activation, $\Delta S^{\ddagger}$, to the enthalpy of activation, $\Delta H^{\ddagger}$, is independent of the nature of the diffusing impurity. The ratio, $\Delta S^{\ddagger}/\Delta H^{\ddagger}$, depends only on the host polymer, and is approximately equal to 4α, where α is the volume thermal expansion coefficient of the polymer. The concentration dependence of the diffusion coefficient is roughly explained by the continuum theory on the basis of swelling.

THE purpose of this note is to point out that the diffusion of various impurities in amorphous polymers appears to obey the type of empirical relations which describe self-diffusion in inorganic systems. The pertinent relations are

$$\Delta S^{\ddagger}=\alpha/\beta\Delta V^{\ddagger}, \tag{1}$$

and

$$\Delta V^{\ddagger}=4\beta\Delta H^{\ddagger}. \tag{2}$$

Here α is the isobaric coefficient of volume expansion; β the isothermal compressibility; and $\Delta S^{\ddagger}$, $\Delta V^{\ddagger}$, and $\Delta H^{\ddagger}$ are, respectively, the entropy, volume, and heat of activation at constant pressure. Equation (1) has been justified approximately by the author[1]; Eq. (2), first given by Keyes,[2] can be understood in terms of the surface tension[3] and continuum models[2,4,5] of diffusion. It is also possible to give a thermodynamical justification in simple one-component systems.[6]

The empirical basis of Eqs. (1) and (2) is confined to those materials in which diffusion has been studied as a function of pressure, so that experimental values of $\Delta V^{\ddagger}$ are available. Such data are scarce. However, the two equations imply that

$$\Delta S^{\ddagger}=4\alpha\Delta H^{\ddagger}, \tag{3}$$

and this equation, previously given by Keyes,[2] may be tested in systems for which pressure data are unavailable. For instance, in a particular host material, the ratio $\Delta S^{\ddagger}/\Delta H^{\ddagger}$ should be independent of the particular diffusing impurity and should be determined only by the quantity, α.

The extensive data of Ryskin[7] on the diffusion of a variety of impurities into several amorphous polymers, both above and below the glassy transition temperature T_g, afford a test of Eq. (3). In Table I, we exhibit Ryskin's data, reformulated to conform with the Eyring framework, on the diffusion of various impurities in polyvinyl acetate. The values of $\Delta H^{\ddagger}$ and $\Delta S^{\ddagger}$, which are strongly temperature dependent, are those appropriate to temperatures just above and just below T_g, extrapolated to zero impurity concentration. In order to estimate the values of $\Delta S^{\ddagger}$, it is necessary to know the pre-exponential factor $a^2\nu$ in Eyring's diffusion equation. We have taken the jump distance as equal to 10^{-7} cm and the attempt frequency ν equal to 10^{12} sec^{-1}. These values are consistent with Ryskin's estimates. Fortunately, uncertainties in $\Delta S^{\ddagger}$ arising from errors in a and ν are small because the former depend only logarithmically on the choice of $a^2\nu$. The earlier, but less extensive, data of Kokes and Long[8] on diffusion in polyvinyl acetate have not been included in Table I. Their data, however, are in substantial agreement with those of Ryskin.

The surprising constancy of the ratio $\Delta S^{\ddagger}/\Delta H^{\ddagger}$ in Table I tends to support Eq. (3). The small but dis-

TABLE I. $\Delta S^{\ddagger}$ and $\Delta H^{\ddagger}$ for various impurities diffusing into polyvinyl acetate $T_g=303°$K.

	Impurity	$\Delta S^{\ddagger}$ cal/mole °C	$\Delta H^{\ddagger}$ kcal/mole	$\Delta S^{\ddagger}/\Delta H^{\ddagger}$ °C$^{-1}\times10^3$
			$T>T_g$	
(1)	H_2O	27	13.8	1.9
(2)	CH_3OH	40	20.5	1.95
(3)	C_2H_5OH	59	28.5	2.06
(4)	C_3H_7OH	63	31.0	2.03
(5)	1—C_4H_9OH	75	35.9	2.08
(6)	2—C_4H_9OH	74	36.0	2.06
(7)	3—C_4H_9OH	73	36.2	2.03
(8)	CH_3COCH_3	67	32.0	2.10
(9)	C_6H_6	81	38.0	2.13
(10)	C_5H_5N	75	35.0	2.14
(11)	C_6H_{12}	82	38.6	2.12
(12)	CH_2Cl_2	68	31.7	2.14
(13)	$CHCl_3$	80	36.4	2.19
(14)	CCl_4	83	38.5	2.15
(15)	C_2H_5Cl	67	31.9	2.10
(16)	C_2H_5Br	74	34.0	2.17
(17)	C_2H_5I	78	36.4	2.14
			$T<T_g$	
(1)	H_2O	1.16	6.4	0.180
(2)	CH_3OH	1.23	7.6	0.162

[1] A. W. Lawson, J. Phys. Chem. Solids **3**, 250 (1957).
[2] R. W. Keyes, J. Chem. Phys. **29**, 467 (1958).
[3] H. Brooks, *Impurities and Imperfections* (American Society for Metals, Cleveland, 1955), pp. 1–27.
[4] A. W. Lawson, J. Chem. Phys. **30**, 1114 (1959).
[5] R. A. Swalin, Acta Met. **5**, 443 (1957).
[6] Corneliussen, Lawson, Nachtrieb and Rice, J. Chem. Phys. (to be published).
[7] G. Y. Ryskin, Zhur. Tekh. Fiz. **25**, 458 (1955).
[8] R. J. Kokes and F. A. Long, J. Am. Chem. Soc. **75**, 6142 (1953).

TABLE II. Average ratio $\Delta S^{\ddagger}/\Delta H^{\ddagger}$ for diffusion of impurities into various amorphous polymers for temperatures above and below the glassy transition temperature T_g.

Polymer	T_g °K	Impurities studied[a]	$\Delta S^{\ddagger}/\Delta H^{\ddagger}$ °C$^{-1}\times 10^3$ $T>T_g$	$\Delta S^{\ddagger}/\Delta H^{\ddagger}$ °C$^{-1}\times 10^3$ $T<T_g$
polyvinyl acetate	303	(See Table I)	2.11±0.06	0.17±0.01
polyvinyl alcohol	400	1, 2	1.77±0.02	...
polystyrene	361	(2), (3), (12), (16)	1.71±0.02	0.55±0.28
polyethyl methacrylate	313	(1), (2), 3, 9, 10	1.63±0.07	0.98±0.26
polymethacrylate	280	(1), 2, 3, 9	1.96±0.07	0.92
polymethyl methacrylate	360	(1), (2), (3)	1.69±0.03	1.09±0.21
polybutyl methacrylate	283	(1), 2	1.72±0.03	1.11

[a] Numbers refer to impurities listed in Table I. All those listed were investigated for $T>T_g$; those in parentheses were investigated for $T<T_g$.

cernible trend to lower values of $\Delta S^{\ddagger}/\Delta H^{\ddagger}$ for smaller molecules may be real or may be the result of an inadequate value for $a^2\nu$. Similar, but sparser, data have been obtained by Ryskin for other polymers. Summary data for these polymers are given in Table II. The relatively greater scatter in the values of $\Delta S^{\ddagger}/\Delta H^{\ddagger}$ for $T<T_g$ may be ascribed to the greater uncertainty in $\Delta S^{\ddagger}$ arising from the greater effect of an uncertainty in $a^2\nu$. The fact that $\Delta S^{\ddagger}/\Delta H^{\ddagger}$ changes abruptly at $T=T_g$ is associated with the abrupt change in α at this transition temperature. The order of magnitude of the observed ratios is consistent with the range of values of 4α for polymers commercially available in this country. Because α is dependent on the rate of measurement, the molecular weight of the polymer and the amount of plasticizer in solution, no better than order-of-magnitude agreement can be expected.

Specific interactions between dissolved impurities and the host polymer, ignored by the continuum theory, appear to affect $\Delta S^{\ddagger}$ and $\Delta H^{\ddagger}$ in such a way that their ratio is unaffected. Assuming that Eq. (1) is valid for these systems, which seems likely in view of the empirical success of Eq. (3) and the correlation noted by Kokes and Long[8] between $\Delta H^{\ddagger}$ and the molal volume of the diffusing impurity, we are able to make some general statements about the concentration dependence of the diffusion coefficient.

Experimentally, one finds

$$D(c)=D(0)e^{+\delta c}, \tag{4}$$

where D is the diffusion coefficient at impurity concentration c, δ is a dimensionless constant, and $D(0)$ is the value of $D(c)$ at $c=0$. The value of δ may be estimated from continuum theory as follows. As the impurity concentration is increased, the polymer swells and there is a concomitant change in the compressibility which may be estimated in terms of the Gruneisen constant, $\gamma=(1\partial\ln\beta/2\partial\ln\nu)+\frac{1}{6}$.

Then, using Eq. (2) and assuming $\Delta V^{\ddagger}$ is a constant, we calculate a value for δ in rough agreement with experiment, namely, $(2\gamma-\frac{1}{3})\Delta H^{\ddagger}(0)/RT$. In this expression, we have omitted a small term (estimated to be usually less than 10% of the value of δ) which depends on the Flory-Huggins interaction parameter μ for swelling. In this connection, we note that Kokes and Long[8] have reported a correlation between δ and μ. The experimental work of Flory[9] on the effect of swelling on elastic modulus, which is roughly consistent with the Gruneisen theory, lends further credence to this model.

[9] P. J. Flory, Chem. Revs. **35**, 51 (1944); Ind. Eng. Chem. **38**, 417 (1946).

Matrix Isolation Studies: Infrared Spectra of Intermediate Species in the Photolysis of Hydrazoic Acid. II

MATHIAS VAN THIEL* AND GEORGE C. PIMENTEL

Department of Chemistry, University of California, Berkeley, California

(Received January 27, 1959)

Further infrared studies of the photolysis of hydrazoic acid in solid nitrogen at 20°K confirm the spectroscopic detection of unusual molecular species, as postulated earlier. Neither hydrogen bonding nor tautomerism of HN_3 can account for the new bands detected. The two most prominent of these, at 1325 and 1290 cm^{-1}, are shifted by a factor near $\sqrt{2}$ when DN_3 is photolyzed. The data tend to confirm the presence of imine radical NH_2 but two alternate interpretations, diimide N_2H_2, or azide amine NH_2N_3, cannot be eliminated at this time.

BECKER, Pimentel, and Van Thiel[1] applied the matrix isolation method to the detection of intermediate species in the photolysis of hydrazoic acid (hereafter this work will be called reference 1). These authors detected ammonia and, in addition, absorptions attributed to species intermediate in the formation of ammonia. The following possible reactions were offered[1]:

$$HN_3+h\nu\rightarrow NH+N_2 \quad (1)$$

I.
$$NH+HN_3\rightarrow NH_2+N_3 \quad (2)$$
$$NH_2+HN_3\rightarrow NH_3+N_3 \quad (3)$$

II.
$$NH+HN_3\rightarrow N_2H_2+N_2 \quad (4)$$
$$N_2H_2+HN_3\rightarrow NH_3+2N_2 \quad (5)$$

III.
$$NH+HN_3\rightarrow 2HN_2 \quad (6)$$

Reference 1 summarizes earlier work but three other reports have appeared which pertain.

1. Thrush[2] independently has proposed reactions (1–3) to account for the spectral features observed in the flash photolysis of gaseous HN_3. He assigns absorptions near 2700 A to the N_3 radical.

2. Milligan, Brown, and Pimentel[3] detected an absorption at 2150 cm^{-1} by the film obtained on condensing at 4°K the products of nitrogen passed through a 60-cycle electrode discharge. Since this absorption appeared as a multiplet in an experiment using nitrogen enriched with N^{15}, it was assigned to N_3 radical, in agreement with reference 1.

3. McCarty and Robinson[4] detected a number of lines in the visible-ultraviolet absorption spectrum of condensed products from an argon-N_2H_4 mixture passed through an electrodeless discharge. These authors associate three of these lines with spectral features of gaseous NH_2 as identified by Ramsay.[5]

Each of these reports encourages an interpretation of the results of reference 1 in terms of reaction scheme I. We have sought more direct evidence concerning the identities of the species responsible for the infrared absorptions observed by Becker *et al.*[1] We present here data pertaining to three aspects of this problem: (1) possible alternative explanations based upon the formation of hydrogen bonded species; (2) the growth of photolysis products as a function of photolysis time; (3) the effect of deuteration.

EXPERIMENTAL

The experimental techniques were identical to those of reference 1 except as noted. Photolysis was conducted with a high-pressure mercury arc, General Electric A-*H*6.

The sample was usually held at 20°K with liquid hydrogen coolant. In some experiments the sample temperature was reduced to about 15°K by placing the liquid hydrogen coolant under vacuum. After irradiation the effects of diffusion were investigated by successive "diffusion operations." In this operation the liquid hydrogen coolant is evaporated and the temperature is allowed to rise. When the temperature reaches the desired value, coolant is rapidly introduced to restore the sample temperature to 20°K. Each diffusion operation is characterized by the maximum temperature reached by the salt window upon which the sample is laid.

HN_3 was prepared as described by Dows and Pimentel[6] but DN_3 was prepared by a more elaborate process. In a vacuum line yellow phosphorous was distilled to a thin layer on the walls of the tube. The line was carefully flushed with D_2O and then oxygen (dried by P_2O_5) was introduced at a rate controlled to avoid over-

* Present address: School of Chemistry, University of Minnesota, Minneapolis, Minnesota.

[1] Becker, Pimentel, and Van Thiel, J. Chem. Phys. **26**, 145–50 (1957).

[2] B. A. Thrush, Proc. Roy. Soc. (London) **A235**, 143 (1956).

[3] Milligan, Brown, and Pimentel, J. Chem. Phys. **25**, 1080 (1956).

[4] G. W. Robinson and M. McCarty, Jr., J. Chem. Phys. **28**, 349 (1958).

[5] D. A. Ramsay, Mem. soc. roy. sci. Liège, **18**, 471 (1957).

[6] D. A. Dows and G. C. Pimentel, J. Chem. Phys. **23**, 1258 (1955).

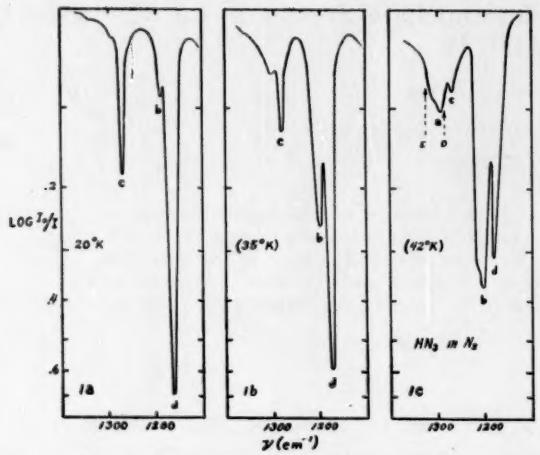

FIG. 1. Effect of diffusion on the infrared spectrum of HN_3 in solid N_2, Experiment 1, $M/R=650$, $T=20°K$.

heating. Then D_2O was distilled into the tube containing the resulting P_2O_5. With suitable explosion shielding, the deuterated phosphoric acid was poured into a tube containing sodium azide without breaking vacuum connections. Gaseous DN_3 was evolved at a rate controlled with an ice bath intermittently placed around the reaction tube. The DN_3 was slowly passed through a still kept at $-17°C$ (removing excess D_2O) and collected in a trap at $-78°C$.[7] Infrared analysis of this product showed it to contain 97% DN_3 and 3% HN_3. No phosphine, a possible by-product, was detected.

Deuterated ammonia, ND_3, was prepared by the reaction of magnesium nitride with D_2O. The nitride was heated under vacuum by flaming the reaction tube to remove traces of water. Then D_2O vapor was passed slowly through the powdered nitride and through a glass coil cooled to $-78°C$ to remove excess D_2O. The first product was discarded to ensure complete deuteration.

Spectra were recorded on a Perkin-Elmer Model 21 spectrometer equipped with a NaCl prism. Frequency accuracy is probably better than in reference 1 and some frequencies are slightly different from the earlier values, the present numbers being preferred. Accuracy is estimated to be ± 10 at 3000, ± 5 at 2000, ± 3 at 1000, and ± 3 at 800 cm^{-1}.

RESULTS

Hydrogen bonded species.—Careful matrix studies were made of the hydrogen bonding effect on the spectra of HN_3, NH_3, DN_3, and mixtures of HN_3 and NH_3 in nitrogen matrices. These studies follow the pattern of earlier work[8,9] and will be reported separately. We present here only those results pertaining directly to the assignments of the new absorptions reported in reference 1, particularly of 2140, 1325, and 1290 cm^{-1}, the bands designated as species *K*, *E*, and *D*.

HN_3 *in* N_2.—The hydrogen bonding of HN_3 was studied thoroughly but only one experiment (Experiment 1) need be described here. HN_3 was suspended in solid nitrogen at $M/R=650$ (M=moles matrix, R=moles suspended compound) at a window temperature of 14°K. After a spectrum was recorded, a diffusion operation was carried out, the temperature reaching a maximum value of 28°K. A second spectrum was then recorded. This process was repeated four more times, each time to a slightly higher temperature.

Two observations are of particular interest. First, the asymmetric stretching mode of HN_3 at 2160 cm^{-1} (2140 cm^{-1} in reference 1) increased in intensity by a factor of almost 2.5 with the formation of hydrogen bonded aggregates. Secondly, the diffusion operations resulted in the growth of a broad absorption band centered at 1299 cm^{-1}. These spectral changes could contribute to the absorptions assigned to *K*, *E*, and *D*.

Figure 1(a) shows the spectral region 1350–1100 cm^{-1} for the sample of Experiment 1 after deposition. The two prominent absorptions *c* and *d* are caused by monomeric HN_3. Figures 1(b) and 1(c) show the effect of successive diffusion operations. Aggregation is revealed by the loss of the monomer bands and the growth of the absorption near 1299 cm^{-1} (designated *a*) accompanied by the growth of two more intense bands, *b*, near 1191 cm^{-1} and *e*, near 3100 cm^{-1} (not shown). The band *b* remains approximately six times as intense as *a*. These spectra show decisively that the absorptions *E* and *D* (see reference 1) cannot be assigned to the H bonded HN_3 polymers produced by diffusion.

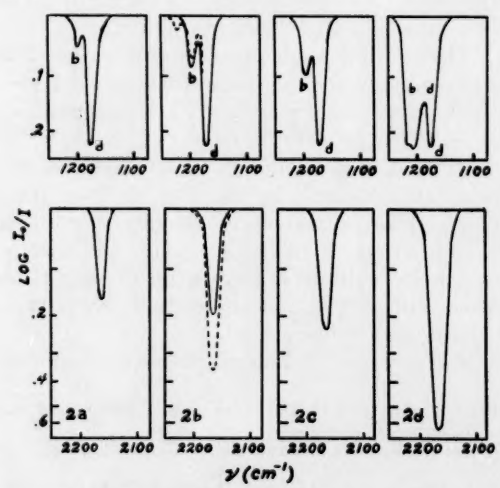

FIG. 2. Comparison of effects of diffusion and photolysis on the relative intensities of 2160, 1191, and 1168, (a) no diffusion, (b) diffusion, $T=32.5°K$ (solid curve), photolysis (dashed curve), (c) diffusion, $T=35°K$, (d) diffusion, $T=42°K$.

[7] Use of a dry ice trap was advised by Dr. M. M. Davies (University College, Aberystwyth, Wales) to avoid the explosive danger accompanying the solid-liquid transition (private communication).

[8] Van Thiel, Becker, and Pimentel, J. Chem. Phys. **27**, 95–9 (1957).

[9] Van Thiel, Becker, and Pimentel, J. Chem. Phys. **27**, 486–90 (1957).

First, *a* is broad and centered at 1299 cm^{-1} whereas the *E* and *D* bands are sharp and centered at 1325 and 1290 cm^{-1}. Secondly, the bands of *E* and *D* are formed without evidence of either band *b* or *e* (see Fig. 4 of reference 1).

It is more difficult to prove that HN_3 polymers do not contribute to the absorption at 2160 cm^{-1} (species *K*). Careful analysis of the intensities of *a* and *b* in reference 1 indicates, however, that the photolytic enhancement of the band at 2160 cm^{-1} cannot be explained solely on the basis of production of HN_3 polymers. Figure 2 gives graphic support for this contention. Four of the spectra of Experiment 1 have been normalized (by using Beer's law) to the same peak absorption of band *d* at 1168 cm^{-1} (solid curves). The increasing absorption near 2160 cm^{-1} is associated with the increased concentration of HN_3 polymers (*a*, *b*, and *e*). Superimposed on Fig. 2(b) is one of the spectra obtained by Becker (unpublished) by photolyzing HN_3 in nitrogen at $M/R=300$ (dotted curve). This spectrum is reported here because it reveals the largest production of species *E* and *D* recorded (1325 cm^{-1}, $\log I_0/I=0.32$; 1290 cm^{-1}, $\log I_0/I=0.25$). Whereas the absorption at *b* is quite similar in Fig. 2(b), the absorption near 2160 cm^{-1} is much more intense for the sample which had been photolyzed. The discrepancy must be assigned to another species, species *K*. This is consistent with the conclusions of reference 1 even though the absorption attributed to *K* was overestimated there.

NH_3 *in* N_2.—A complete study of the hydrogen bonding of NH_3 in solid nitrogen matrix showed that NH_3 polymers have no absorption bands between 1200 and 1550 cm^{-1} and none between 1700 and 3100 cm^{-1}. The absorption of the symmetric bending mode of NH_3 is extremely sensitive to hydrogen bond formation and permits a clear identification of monomeric NH_3 by its sharp absorption at 973 cm^{-1} and of dimeric NH_3 by two sharp absorptions at 990 and 1008 cm^{-1}. This region shows that the NH_3 produced by photolysis of HN_3 is in the monomeric state, again a reassurance that hydrogen bonding is relatively unimportant in the experiments of reference 1.

HN_3+NH_3 *in* N_2.—Two experiments were performed in which both HN_3 and NH_3 were present in equal amounts in the same matrix ($M/R=549$, 128). In each experiment diffusion operations were carried out. Although the spectra are complicated, it is possible to assign spectral features at 1220, 1062, and 1070 cm^{-1} to a hydrogen bonded complex of HN_3 with NH_3. Bands attributable to ammonium azide or high aggregates grew in slowly after successive diffusion operations: 2040, 1236, 1094, and 1450 cm^{-1}. The 2040 cm^{-1} band of NH_4N_3 did not appear during any experiment involving photolysis of HN_3 until a diffusion operation was performed. The most intense band of the $HN_3 \cdot NH_3$ complex, 1220 cm^{-1}, presumably corresponds to the band at 1225 cm^{-1} reported in reference 1 and classified as Type *G*.

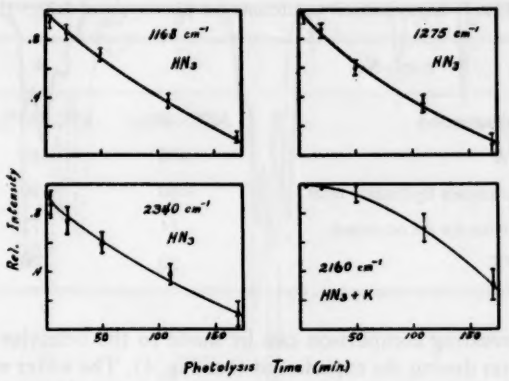

FIG. 3. Loss of HN_3 bands during photolysis, Experiment 2, $M/R=1600$, $T=20°K$, maximum absorbances: 1168 (1.46), 1275 (0.28), 2340 (0.08), 2160 (0.38).

Photolysis of HN_3.—An experiment will be described which reproduces the work of reference 1 but at a higher value of M/R and at a lower temperature. In this experiment (Experiment 2), the amount of HN_3 was estimated to be 30 μmoles from the intensity of the band at 1275 cm^{-1} and corresponds to M/R near 1600. Both water ($M/R\sim10^4$) and CCl_4 ($M/R\sim10^4$) were present as undesired impurities. The sample was deposited at 15°K and held at this temperature during photolysis and the accompanying spectral study. The aggregated photolysis times were 5, 20, 50, 110, and 170 min. Following the last photolysis approximately 90% of the sample had been decomposed. Three successive diffusion operations were conducted, reaching temperatures of 30, 35, and 40°K, respectively.

The results are presented graphically in Figs. 3 and 4. For each band each intensity datum is normalized by division by the absorbance of that band at its maximum intensity (which is given parenthetically in the caption). The loss of some of the bands of HN_3 during photolysis is shown in Fig. 3. The curvatures of the bands clearly indicate the unique behavior of the band at 2160 cm^{-1}, behavior also shown to some extent by the polymer band at 1191 cm^{-1}.

Figure 4 shows the growth of products during photolysis and also the behavior of each band after each diffusion operation. The band at 973 cm^{-1} is caused by monomeric NH_3 and the characteristic doublet of dimeric ammonia (at 990 and 1008 cm^{-1}) is not observed. The 973 cm^{-1} band shows growth appropriate to a tertiary product of photolysis, as proposed in reaction scheme I. In contrast, the growths of the bands 1325 and 1290 cm^{-1} are more rapid, consistent with an assignment to a product intermediate in the reactions giving NH_3. Equally revealing is the loss on diffusion of these three features. The more rapid loss of the bands at 1325 and 1290 cm^{-1} suggests that species *E* and *D* diffuse and react more rapidly than monomeric NH_3. An

TABLE I. Experimental conditions for photolysis of DN_3—HN_3.

Expt. No.	3	4
% deuterated	50% (40%)	85% (85%)
M/R	400	515
micromoles hydrazoic acid	~60	~90
micromoles decomposed	54	72
T, °K	20	20

interesting comparison can be made to the behavior of water during the experiment (see Fig. 4). The water was initially present as monomer, as revealed by the single sharp band at 1600 cm^{-1}.[9] Approximately half of this monomer was lost during photolysis, and the remainder is lost during the diffusion operations in a manner quite similar to E and D. The apparent loss of water is attributed to reaction with NH and to hydrogen bond formation during diffusion.

The growths of seven other absorptions, 2358, 2047, 1346, 1305, 1205, 1136, and 1085 cm^{-1} are shown in Fig. 4. The band at 2358 cm^{-1} grew continuously during photolysis and at an accelerated rate during diffusion. The band at 1136 cm^{-1} was observed in four separate experiments and in every one of these experiments a small amount of water was present (as revealed by absorption at 1600 cm^{-1}). In four other experiments the absorption at 1136 cm^{-1} was *not* observed and in these experiments water had been carefully removed (as verified by the absence of absorption at 1600 cm^{-1}). The absorption at 2047 cm^{-1} can be assigned to an identified product, NH_4N_3.

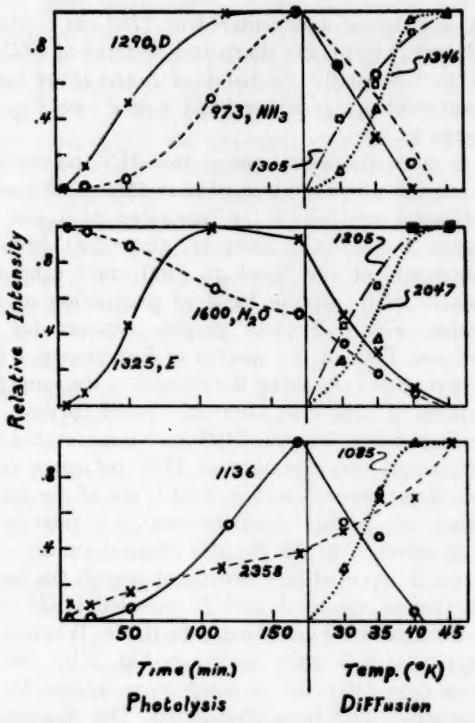

FIG. 4. Growth of products during photolysis, Experiment 2, M/R=1600, T=20°K, maximum absorbances: 973 (0.09), 1290 (0.09), 1325 (0.08), 1600 (0.16), 1136 (0.08), 2358 (0.13), 2047 (0.04), 1346 (0.05), 1305 (0.05), 1205 (0.09), 1085 (0.04).

Three of these bands, 1346, 1305, and 1085 cm^{-1}, were classified as Type G in reference 1, bands which appeared during photolysis (at the lower M/R used there) but which grow upon diffusion. The four H bands

TABLE II. Intensities of spectral features caused by photolysis of DN_3 and HN_3 in N_2 ($\log I_0/I$).

Phot. time (min)	Experiment 3, 40% DN_3				Experiment 4, 85% DN_3				
	0	5	15	25	1	6	21	51	
ν (cm^{-1})									Identity
2350	...	~0.02	0.04	0.05	...	...	...	...	
2311	...	...	...	0.01	0.01	0.04	0.025	0.02	
2250	...	...	...	...	...	0.01	0.015	0.015	
1325	...	0.05	0.035	0.03	...	...	...	...	*E*
1290	...	0.06	0.04	0.04	...	...	...	0.005	*D*
1137	...	0.025	0.025	0.02	...	0.01	0.01	0.01	
1128	...	0.03	0.02	0.01	0.005	0.02	0.015	0.02	
1085	0.02	0.03	0.035	0.04	...	...	...	...	
1060	...	0.05	0.04	0.03	0.005	0.02	0.02	0.02	
1040	0.015	0.02	0.02	0.035	...	...	...	0.005?	
980[a]	...	...	...	...	...	...	...	...	
973	?	?	(0.03–0.04)	(0.04–0.05)	?	?	?	?	NH
950	...	0.025	0.02	0.02	...	(0.15–0.26)	(0.16–0.24)	(0.16–0.20)	*D*
915	...	...	...	...	0.005	0.02	0.025	0.025	
905	...	0.03	0.05	0.095	...	...	...	...	NH_2D
828	...	0.015	0.025	0.03	0.005	0.03	0.055	0.065	NHD_2
790	...	...	...	...	...	0.005	0.015	0.025	
758	...	...	...	0.005	...	0.04	0.09	0.10	ND_3
749	...	...	...	...	...	...	0.02	0.015	

[a] Presence of the absorption of a product superimposed on the absorption of DN_3 is inferred from Fig. 6 (see text, point 12).

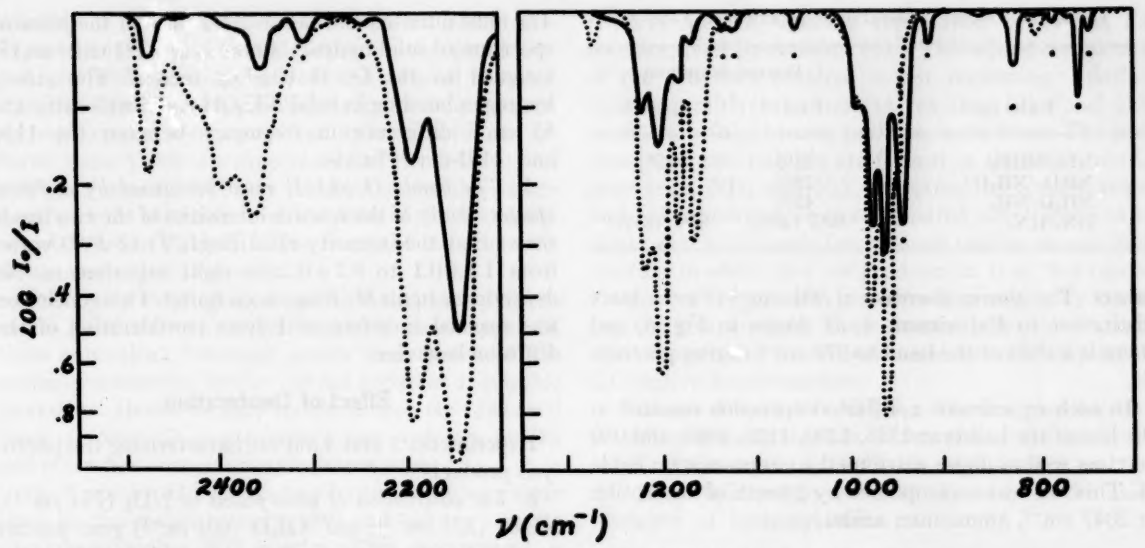

FIG. 5. Photolysis of DN_3 and HN_3 in nitrogen, Experiment 4, $M/R=515$, $T=20°K$, 85%D ..... before photolysis, ——— after 21 min photolysis. Dots identify bands produced by photolysis, as listed in Table II, column 8.

of uncertain intensity behavior (reference 1) were not observed (832, 847, 1062, and 3020 cm^{-1}).

Photolysis of DN_3-HN_3 *mixtures.*—Four experiments were performed in which DN_3-HN_3 mixtures were suspended in solid nitrogen and photolyzed. Two of these (Experiments 3 and 4) are described in detail. Table I shows the conditions used. The DN_3/HN_3 ratios were estimated in two ways. The intensities of the bands of hydrazoic acid coupled with pressure measurements provide one estimate. The instability of HN_3 together with doubt about the reproducibility of the area of deposition make this estimate of uncertain reliability. In addition we have derived the percent deuteration from the relative intensities of the HN_3 band at 1168 cm^{-1} and the analogous DN_3 band at 968 cm^{-1} with the assumption that the absorption coefficient of HN_3 (at 1168 cm^{-1}) exceeds that of DN_3 (at 968 cm^{-1}) by a factor of two in accordance with the isotopic mass effect on a pure hydrogen motion.[10] The values based on estimated absorption coefficients, given parenthetically in Table I, may be the more accurate.

Table II lists the bands produced during photolysis and their intensities. Figure 5 shows representative spectra from Experiment 4. Figure 6 shows for Experiment 3 the loss of bands of hydrazoic acid during photolysis while Fig. 7 shows the growth behavior of the new bands. (The intensities plotted for the polymer band at 981 cm^{-1} are the measured values without correction for overlap of the monomer band at 968 cm^{-1}. The band at 1275 cm^{-1} is caused by monomeric HN_3; see band *c* in Fig. 1.) The effects of photolysis in Experiment 4 are similar. In Fig. 6 the behavior of the band at 981 cm^{-1} differs qualitatively from the

[10] B. Crawford, Jr., J. Chem. Phys. **20**, 977–81 (1952).

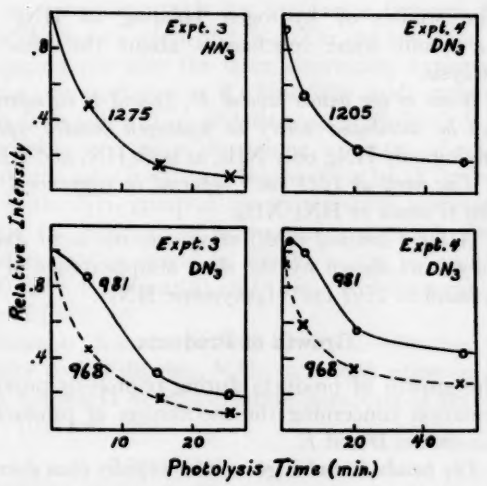

FIG. 6. Loss of HN_3 and DN_3 bands during photolysis, Experiment 3, $M/R=400$, $T=20°K$, 40–50%D, Experiment 4, $M/R=515$, $T=20°K$, 85%D.

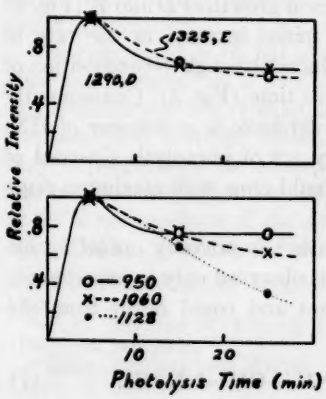

FIG. 7. Growth of products during photolysis of DN_3 and HN_3, Experiment 3, $M/R=400$, $T=20°K$, 40–50%D.

TABLE III. Percent deuteration in experiments 3 and 4.

Ratio used	Percent deuterium Expt. 3	Expt. 4
ND_3/NHD_2	35%	85%
NHD_2/NH_2D	25%	...
NH_2D/NH_3	45%	...
DN_3/HN_3	50% (40%)	85% (85%)

others. The slower decrease of 981 cm^{-1} is even more distinctive in Experiment 4, as shown in Fig. 6, and there is a shift of the band to 977 cm^{-1} during photolysis.

In each experiment a diffusion operation resulted in the loss of the bands at 1325, 1290, 1128, 1060, and 950 cm^{-1} as well as those attributed to ammonia in Table II. This loss was accompanied by growth of absorption at 2047 cm^{-1}, ammonium azide.

DISCUSSION

Hydrogen-Bonded Species

The studies of hydrogen bonding of HN_3 and NH_3 permit some conclusions about the effect of photolysis.

1. *None of the bands labeled K, D and E in reference 1 can be attributed solely to hydrogen bonded species* involving only HN_3, only NH_3, or both HN_3 and NH_3.

2. *The band at 1225 cm^{-1} reported in reference 1 and labeled G could be* $HN_3 \cdot NH_3$.

3. *A large amount of diffusion does not occur during photolysis* as shown by the slow disappearance of the HN_3 band at 1191 cm^{-1} (polymeric HN_3).

Growth of Products

The growth of products during photolysis provides information concerning the mechanism of production of the species *D* and *E*.

4. *The bands D and E grow more rapidly than does the ammonia band at 973 cm^{-1}* (see Fig. 4). This is consistent with the statement that *D* and *E* are caused by intermediates in the formation of NH_3.

5. The *S* shaped curves of growth of *D* and *E* (Fig. 4) show that there is an initial increase in the rate of production of these products although decomposition of HN_3 is most rapid at zero time (Fig. 3). Consequently *neither D nor E can be attributed to a tautomer of* HN_3 produced in the primary act of photolysis (instead of reaction). A tautomer would grow with maximum slope at zero photolysis time.

6. *The band at 1136 cm^{-1} is probably caused by hydroxylamine.* This band is observed only in experiments in which water is present and could result from the reactions:

$$NH + H_2O \rightarrow NH_2 + OH \rightarrow NH_2OH. \quad (7)$$

The most intense band below 2000 cm^{-1} in the infrared spectrum of solid hydroxylamine is at 1191 cm^{-1} and is assigned to the O—H bending mode.[11] The strong hydrogen bonding in solid NH_2OH could well cause the 55 cm^{-1} difference in frequency between the 1136 and 1191-cm^{-1} bands.

7. *The bands D and E must be caused by different species.* Study of the relative intensities of the two bands shows that the intensity ratio ($\log I_0/I$) of *E/D* varies from 1.3 ± 0.1 to 0.7 ± 0.2 in eight experiments. No dependence upon M/R has been found. This conclusion was reached in reference 1 from consideration of the diffusion behavior.

Effect of Deuteration

Experiments 3 and 4 aid in characterizing the photolysis products.

8. *The observation of absorptions of* ND_3 (*758 cm^{-1}*), NHD_2 (*828 cm^{-1}*), *and* NH_2D (*905 cm^{-1}*) *gives positive proof of the identification of ammonia as a matrix photolysis product.* These frequencies coincide with absorptions of the deuterated ammonias (produced by the reaction of magnesium nitride with D_2O) suspended in solid nitrogen at 20°K.

Furthermore, the intensity ratios of the various species give separate estimates of percent deuteration. Assuming equal absorption coefficients for all species, the observed intensities lead to the results shown in Table III. Since the assignments of the ammonia species are not in any doubt, the discrepancies in Table III must be attributed to the uncertainties in the intensity measurements and in the assumption of equal absorption coefficients.

9. Both *E* and *D* are lost in Experiment 4 and the only feature of appropriate intensity to be assigned as a deuterated counterpart is the band at 950 cm^{-1}. This association represents an isotopic shift by a factor of 1.40 if 950 cm^{-1} is assigned to species *E* (1325 cm^{-1}) and by a factor of 1.36 if it is assigned to species *D* (1290 cm^{-1}). While the larger ratio is possible, the second figure is a normal ratio for relatively pure hydrogen motions and is the more likely. *Consequently the band 950 cm^{-1} is assigned as species D in Table* II.

10. The relative intensities of the 1290 and 950 cm^{-1} bands provide a basis for deciding how many hydrogen atoms are influential in the reduced mass of the mode. Assuming again that the hydrogen species has double the absorption coefficient of the deuterium species (a reasonable guess for a relatively pure hydrogen motion), we can calculate the expected intensity of one band from the observed intensity of the other. For example, if only one hydrogen atom is involved in the motion, the intensity of 950 cm^{-1} divided by that of 1290 cm^{-1} should be one-half the ratio of the fraction of deuterium to the fraction of hydrogen. Thus in Experiment 4 the

[11] E. R. Nightingale and E. L. Wagner, J. Chem. Phys. **22**, 203–8 (1954).

intensity of 1290 would be in the range 0.06–0.08. The observed intensity of 0.005 eliminates the possibility that one hydrogen only affects the reduced mass of the 1290—950 mode. A similar calculation based on the assumption that two equivalent hydrogens fix the reduced mass yields an expectation of the intensity of 1290 cm^{-1} near 0.01. Surely this is in acceptable agreement with the observed results in view of the discrepancies observed in Table III. The results of Experiment 3 do not contradict this result.

Continuing this argument, we find that both Experiments 3 and 4 are incompatible with the assumption of three equivalent hydrogen atoms since bands of the partially deuterated species are not apparent at suitable intensities. Hence we may conclude that *the 1290 cm^{-1} band of species D is a relatively pure hydrogen motion and it involves two equivalent hydrogen atoms.*

11. If species *D* includes two hydrogen atoms, there must be absorption between 1290 and 950 cm^{-1} due to the corresponding HD species. This requirement is qualitatively satisfied in Experiments 3 and 4 by the bands at 1128 and 1060 cm^{-1}. Furthermore, these bands have growth behaviors parallel to those of 1325, 1290, and 950 cm^{-1}, as can be seen in Fig. 7.

12. No band of comparable intensity to 950 cm^{-1} which can be assigned to 1325 cm^{-1} is evident in Experiment 4. If 1325 cm^{-1} were shifted on deuteration by the factor 1.35, it would be expected at 980 cm^{-1}. This directs attention to the behavior of the absorption at 981 cm^{-1} during photolysis. Figure 6 compares the loss of DN_3 bands at 968 and 981 cm^{-1} both in Experiments 3 and 4. The behavior of 981 cm^{-1} is indeed distinctive and the effect cannot be attributed to NH_3 since a negligible amount of NH_3 is formed in Experiment 4. *The data indicate that the deuterated counterpart of 1325 cm^{-1} absorbs in the region near 980 cm^{-1}.*

Identities of *D* and *E*

The several conclusions just listed add much to our knowledge of the identities of *D* and *E*. While positive identification is not possible, we can list evidence concerning likely possibilities.

Reaction Scheme I: NH_2.—The proposal that *D* could be NH_2 formed in reaction (2) (as proposed in reference 1) is not in serious disagreement with any known facts. The presence of two H atoms in a relatively pure hydrogen motion (conclusions 9, 10, and 11) and the growth prior to growth of NH_3 (conclusion 4) are required by this reaction scheme. Furthermore, a calculation of the bending frequencies of NHD and ND_2 from a single force constant based on assignment of species *D* to NH_2 reproduces the frequencies of the observed absorptions at 1128 and 950 cm^{-1} within the accuracy which this approximation permits (as verified by a similar calculation for H_2O, HDO, and D_2O).

On the other hand, there are factors which detract from this assignment. Identification of *D* as NH_2 requires quite a separate explanation of *E* [as, for instance, N_2H by reaction (6)]. This added complexity of the processes required is not reassuring. Another equally intuitive objection to reaction (2) [and also to reaction (6)] carries, perhaps, more force. The proposal that two radicals are formed in the same matrix cage (e.g., NH_2 and N_3) is opposed by a substantial body of experience we have acquired which leads us to doubt that two simple free radicals readily escape from the cage in which they are produced or that they can be "stabilized" together in a matrix cage merely by lowering the temperature. These factors leave doubt sufficient to necessitate a critical examination of all possible alternative interpretations.

Reaction Scheme IV: NH_2N_3.—On the premise that retention without reaction of two radical species in the same matrix cage is unlikely, we might expect reaction (2) to be followed by reaction (8) to form the azide analogue of hydroxylamine.

IV. $$NH_2+N_3=NH_2N_3 \qquad (8)$$

Except for the premise just mentioned, there seems to be no compelling basis for preference between NH_2 and NH_2N_3 to explain the data. On the one hand this compound provides the more convenient explanation of the proposed species *K*. Since the azide groups of both HN_3 and CH_3N_3 absorb near 2140 cm^{-1}, [12] it is reasonable to expect the amine azide to absorb at nearly the same frequency. On the other hand, the bonding in the NH_2 group of the hypothetical azide amine would be expected to be normal and the hydrogen bending motion would be sought in the region 1600–1700 cm^{-1}. Reaction (8) still offers no obvious explanation of *E*.

Reaction Schemes II *and* V: N_2H_2.—Another possibility is that diimide, N_2H_2, is formed either in reaction scheme II or V, the latter consisting of reactions (1), (9), and (10).

V. $$NH+NH=N_2H_2 \qquad (9)$$

$$NH+N_2H_2=NH_3+N_2 \qquad (10)$$

Since this proposal is in accord with almost all the known facts, it has sufficient merit to warrant a detailed examination.

The compound N_2H_2 has already been suggested by Rice and Freamo[13] as a possible reaction intermediate in the decomposition of gaseous hydrazoic acid. Dows, Pimentel, and Whittle[14] agreed, proposing that diimide may be responsible for absorption bands at 3230 and 860 cm^{-1} in the spectrum of the solid formed by freezing at 90°K the products of the glow discharge decomposition of HN_3. The absence of an inert matrix and the

[12] E. H. Eyster and R. H. Gillette, J. Chem. Phys. **8**, 369 (1940).
[13] F. O. Rice and M. Freamo, J. Am. Chem. Soc. **73**, 5529 (1951); **75**, 548 (1953).
[14] Dows, Pimentel, and Whittle, J. Chem. Phys. **23**, 1606–9 (1955).

much higher temperature (90°K) in the experiment of Dows *et al.* make their experiment sufficiently complicated that we are not inhibited in examining the possibility that N_2H_2 is responsible for *D* or *E* in the present work, an assignment which would contradict the earlier work.[15]

One basis for testing the proposal that N_2H_2 is responsible for *D* or *E* is to predict its infrared spectrum. We may do so on the assumption that this molecule, isoelectronic with ethylene, will have similar bonding: H–N=N—H. This proposed planar and nonlinear structure of diimide would have cis and trans isomers. The infrared spectra of these isomeric molecules would include prominent absorptions by the N—N—H in-plane deformations. The trans isomer would have one infrared active deformation mode whereas the cis form would have two. We may seek evidence concerning the frequencies for these modes in the spectra of the intensively studied deuteroethylenes.[16] The ν_{12} vibrations of cis and trans dideuteroethylene serve as model vibrational modes. These are labelled by Golike *et al.* as CHD deformations and are predominantly hydrogen (not deuterium) motions, as is revealed by the *L* matrices.[16] The ν_{12} mode for *cis*-$C_2H_2D_2$ is found at 1344 cm^{-1} and for *trans*-$C_2H_2D_2$ at 1300 cm^{-1}. These are sufficiently close to the frequencies 1325 and 1290 cm^{-1} to encourage the interpretation that diimide formed in reaction (4) or (9) accounts for *both E* and *D*.

There are, however, arguments that detract from this explanation.

(a) Foner and Hudson[17] have identified N_2H_2 in mass spectrometric studies of the products resulting from passing HN_3 through a glow discharge. This, by itself, encourages the proposal that N_2H_2 has been formed in the present work. Less in accord, however, is their observation that N_2H_2 is reasonably stable. In contrast, the spectral features *D* and *E* are lost at 35°K. In order to assign *D* and *E* to N_2H_2, we must attempt to rationalize this diffusion behavior in terms of hydrogen bonding or reaction with some other stored reactive species (e.g., NH).

(b) The cis form of N_2H_2 has two active bending modes, though only one is assigned here. The absence of the second band must be attributed to a low absorption coefficient or to spectral interference by the parent HN_3.

(c) The bands assignable to N_2HD, 1128 and 1060 cm^{-1}, are roughly midway between those assigned to N_2H_2 and N_2D_2. A more reasonable expectation would be that the two bending modes would be decoupled to give one frequency nearer 1300 cm^{-1} and one nearer 950 cm^{-1}.

(d) The satisfaction afforded by the simultaneous identification of *D* and *E* is neutralized somewhat by the fact that species *K* is left unexplained.

CONCLUSIONS

The present work confirms the most interesting conclusion of reference 1: some of the new spectral features produced by photolysis of HN_3 in solid nitrogen must be attributed to unusual molecular species. Another proposal of reference 1 is that NH_2 or N_2H_2 could be produced. The data presented here add substantial support to this deduction. Alternate proposals have been found to be untenable and the crucial deuteration results confirm the assignment of bands *D* and *E* to modes with reduced mass determined by two hydrogen atoms. The identifications of *D* as NH_2 and *K* as N_3 are entirely consistent with the data, but there are no decisive arguments which eliminate N_2H_2 and the third alternate explanation, NH_2N_3.

ACKNOWLEDGMENT

Grateful appreciation is expressed for research support by the American Petroleum Institute Research Project 50 and the United States Air Force through the AFOSR of the Air Research and Development Command, under Contract No. 49(638)-1. Reproduction in whole or in part is permitted for any purpose of the U. S. Government. We would like to thank the Texaco Company, Beacon, New York, for predoctoral fellowship support (to M.V.T.).

[15] It must be noted that the 90°K spectrum recorded by Dows *et al.*[14] included a weak ($\log I_0/I = .02$) but distinct absorption in the region 1290–1300 cm^{-1}. They ascribed this to HN_3 but this assignment seems improbable in view of the present work. The band was almost completely lost on the first temperature rise (to 120–124°K) in contradiction to the HN_3 diffusion behavior shown in our Fig. 1. It could be that this absorption is the one labeled *D* here and in reference 1.

[16] Golike, Mills, Person, and Crawford, J. Chem. Phys. **25**, 1266–75 (1956); see references given here to earlier work of Crawford *et al.*

[17] S. N. Foner and R. L. Hudson, J. Chem. Phys. **28**, 719–20 (1958).

THE JOURNAL OF CHEMICAL PHYSICS VOLUME 32, NUMBER 1 JANUARY, 1960

Kinetics of the Surface Degradation of Polymethylmethacrylate*

R. F. Chaiken, W. H. Andersen, M. K. Barsh, E. Mishuck, G. Moe, and R. D. Schultz

Aerojet-General Corporation, Azusa, California

(Received August 13, 1959)

The surface degradation of both linear and crosslinked polymethylmethacrylate (PMM) has been studied over the surface temperature range of 550° to 910°K by means of a hot-plate pyrolysis technique. It was demonstrated that surface gasification due to the high heat flux at the decomposing PMM surface involves a depolymerization process and surface desorption of methylmethacrylate monomer. The apparent activation energy for the linear rate of regression of the solid PMM surface (linear pyrolysis rate) was found to decrease with increasing surface temperature, approaching a limiting constant value of 11.2±0.6 kcal/mole at ~650°K for linear PMM and at ~770°K for crosslinked PMM. The mechanism for the surface degradation is depicted as (1) formation of monomer in the surface substrate, (2) diffusion of monomer to the surface, and (3) desorption of monomer from the surface. The linear pyrolysis rate data are correlated by means of an absolute rate theory treatment of surface decomposition. The experimental results are in good agreement with the theory.

INTRODUCTION

THE thermal degradation of polymethylmethacrylate (PMM) has been studied by various investigators[1] using the standard techniques of heating a bulk sample to a constant temperature, and analyzing the decomposition products as a function of time. Under these reaction conditions, the over-all energy of activation for monomer production has been found to increase from about 30 to 40 kcal/mole between the start and finish of the reaction. The decomposition mechanisms have been generally interpreted in terms of breaking of certain critical bonds in the polymer chain, followed by a rapid "unzipping" of monomer units from the chain. Thus, the value of the activation energy is identified with that required to initiate the rupture of the polymer chain. The reaction may be initiated by (1) splitting at any point along the chain,[2] (2) splitting at the chain ending,[3] or (3) action of the polymerization catalyst.[4]

Schultz and Dekker,[5] utilizing a new experimental technique, obtained preliminary kinetic data on surface depolymerization of PMM under the conditions of large heat flux at the decomposing surface. The solid polymer was pressed against a heated surface (an electrically heated wire) maintained at constant temperature. A steady-state linear rate of regression of the surface (linear pyrolysis) was obtained which was taken as a measure of the rate of thermal degradation of the solid. From these surface pyrolysis studies, Schultz and Dekker tentatively suggested that the rate of surface reaction under the above conditions is probably controlled by the same mechanism as that prevailing in bulk thermal degradation.

In the present paper, the authors describe surface-depolymerization studies which have been extended over the surface temperature range of 550°–910°K with the use of an improved flat hot-plate surface-heating apparatus.[6,7] The measured linear pyrolysis rate data for both linear and crosslinked PMM suggest that the rate-controlling mechanism for surface depolymerization at high surface temperature actually differs from that for the bulk depolymerization. It is further suggested that desorption of monomer units from the heated surface controls the rate of surface regression under the conditions of large heat flux at the surface (high surface temperatures), while formation and diffusion of monomer through polymer is rate controlling at lower surface temperatures (<700–800°K).

HOT PLATE PYROLYSIS OF POLYMETHYLMETHACRYLATE

Samples of PMM containing 5 different percentages of the crosslinking agent ethylene glycol diacrylate were prepared under identical conditions. The methylmethacrylate (MM) and ethylene glycol diacrylate (EGDA) monomer were purified by distillation just prior to polymerization. A 50% solution of benzoyl peroxide in tricresyl phosphate was used as the polymerization catalyst. The procedure followed was that of dissolving the catalyst (0.1 wt. %) in the MM, adding the EGDA while stirring, and then polymerizing the whole mixture for one week at 60°C. A 24-hr post cure at 82°C was given to all samples. The resulting

* This work was supported by the U. S. Air Force under Contract No. AF18(603)-74 monitored by the Air Force Office of Scientific Research of the Air Research and Development Command.

[1] See for example N. Grassie, *Chemistry of High Polymer Degradation Processes* (Interscience Publishers, Inc., New York, 1956), pp. 1–50; and H. H. G. Jellinek, *Degradation of Vinyl Polymers* (Academic Press, New York, 1955), pp. 3–90.

[2] H. S. Taylor and A. V. Tabolsky, J. Am. Chem. Soc. **45**, 2063 (1945).

[3] N. Grassie and H. W. Melville, Proc. Roy. Soc. (London) **A199**, 1 (1949).

[4] S. L. Madorsky, J. Polymer Sci. **11**, 491 (1953).

[5] R. D. Schultz and A. O. Dekker, *Fifth Symposium (International) on Combustion* (Reinhold Publishing Corporation, New York, 1955), pp. 260–267.

[6] Barsh, Andersen, Bills, Moe, and Schultz, Rev. Sci. Instr. **29**, 392–395 (1958).

[7] R. F. Chaiken and D. K. Van de Mark, Rev. Sci. Instr. **30**, 375–376 (1959).

TABLE I. Composition of polymethylmethacrylate samples.

Sample designation	Wt. % catalyst	Wt. % EGDA	Crosslinking density[a] (moles of chains/cm³)
PMM-0	0.1	0	Sample dissolved
PMM-½	0.1	½	4×10^{-3}
PMM-1	0.1	1	2×10^{-3}
PMM-2	0.1	2	2×10^{-3}
PMM-5	0.1	5	2×10^{-3}
Plexiglas IIUVA[b]	...	...	Sample dissolved

[a] Determined from swelling ratios in ethyl acetate.
[b] Commercial polymethylmethacrylate cast sheet from Rohm & Haas Company.

hard polymer was then machined into strands measuring 0.6×0.6×5.0 cm for pyrolysis on the hot-plate apparatus. Table I lists the composition of the PMM polymers (including a commercial PMM) studied.

The linear pyrolysis measurements were obtained with the use of the hot-plate pyrolysis apparatus described in detail elsewhere.[6,7] The rate data are plotted in the conventional semi-log form in Fig. 1. Briefly, surface pyrolysis is accomplished by pressing the end of a sample strand against an electrically heated hot-plate. A small Pt (Pt–10%Rh) thermocouple junction, which is imbedded in the hot-plate and positioned at the strand-hot-plate interface, enables the surface temperature (T_s) to be recorded, while the linear rate of regression of the strand surface (B) is measured. Each point on the rate plot of Fig. 1 corresponds to a steady-state condition of constant T_s and B. Varying the electrical power expended in the hot-plate causes a variation in T_s, and hence B.

It was found by using methods described by Barsh *et al.*[6] that for PMM a strand loading force(force exerted against the hot-plate by the strand) of 640 g was sufficient to maintain good thermal contact between the gasifying surface and the hot-plate over the temperature range studied.

Most of the pyrolysis rate data of Fig. 1 were measured at an environmental pressure of 1 atmos; however, several PMM strands were pyrolyzed at lower environmental pressure (~ 2 mm Hg). The variation in pressure did not appear to have any significant effect on the rate of linear pyrolysis. During these low-pressure experiments, the products of the surface gasification were condensed in a liquid-nitrogen cold trap. Product analysis of the condensate by infrared absorption techniques indicated that the surface gasification of both the linear and crosslinked PMM yields for all practical purposes only methylmethacrylate monomer.

It is seen from Fig. 1 that the rate data for the linear and crosslinked strands appear to follow two rate curves whose slopes decrease with increasing temperature ($1/T_s$ decreasing), while approaching a limiting value (2440±130 deg for linear PMM, and 2310±350 deg for crosslinked PMM). The effect of crosslinking on the linear pyrolysis rate of PMM appears to be primarily one of increasing the rate of change of B with $1/T_s$ at surface temperatures less than ~800°K rather than affecting the value of the limiting slope. There is no significant difference between the rate data for the various crosslinked samples studied. This is not surprising in view of the small differences in the measured crosslinking densities for these materials. Likewise, there is little difference between the pyrolysis rates for the PMM–0 and for the Plexiglas IIUVA samples.

DISCUSSION

Referring to Schultz and Dekker's treatment of the thermal decomposition of solids,[5] the linear rate of regression of a reacting surface can be expressed as

$$B = n_s(M/\rho N)k_s \text{ cm/sec}, \qquad (1)$$

where n_s = number of decomposing molecules/cm² surface; M = molecular weight, g/mole; ρ = density of solid, g/cm³; N = Avogadro number, molecules/mole; and k_s = first-order reaction rate constant, sec⁻¹. If we express k_s in terms of the absolute reaction rate theory,[8]

$$B = n_s(M/\rho N)(kT_s/h)(F^{\ddagger}/F)\exp(-E_s/RT_s)\text{cm/sec}, \qquad (2)$$

where T_s refers to the surface temperature and the other terms have their usual meaning.

When n_s is relatively insensitive to surface temperature changes, such as would be the case for a saturated surface, $n_s \simeq (\rho N/M)^{2/3}$, the surface reaction is essentially zero order, and the linear pyrolysis rate [Eq. (2)] can be approximated by an Arrhenius-type rate equation

$$B = A_s \exp(-E_s/RT_s) \text{ cm/sec}, \qquad (3)$$

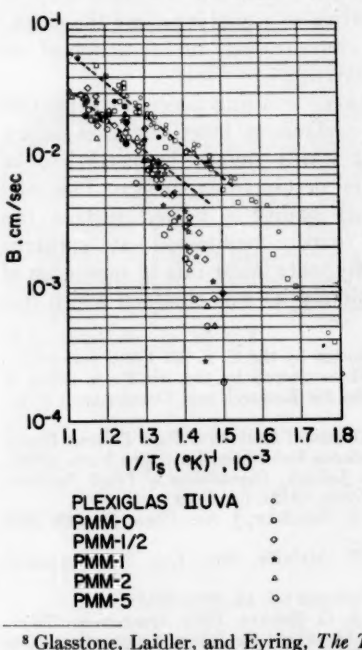

FIG. 1. Linear pyrolysis rate for polymethylmethacrylate. Ambient pressure: open points, 760 mm Hg; shaded points, ~2 mm Hg.

[8] Glasstone, Laidler, and Eyring, *The Theory of Rate Processes* (McGraw-Hill Book Company, Inc., New York, 1941).

where for a surface saturated by the decomposing molecules

$$A_s = (M/\rho N)^{1/3}(kT/h)(F^{\ddagger}/F) \simeq \text{const, cm/sec.} \quad (4)$$

Equation (3) has been applied successfully in describing rate data for the linear pyrolysis of ammonium chloride[5] and ammonium nitrate.[9] In both cases the measured values of E_s were consistent with a gas desorption process at the surface as the rate-controlling step in the surface regression.

In attempting to apply Eq. (3) to the data of Fig. 1, it is apparent that no single set of values of A_s and E_s could be consistent with all the data. This differs considerably from Schultz and Dekker's preliminary results for linear PMM (see Fig. 2).[5]

The question then arises as to what type of reaction mechanisms could be controlling the rate of linear pyrolysis of PMM. It is apparent from the semi-log rate plot that the rate-controlling reaction is changing with surface temperature (or heat flux into the surface). The apparent limiting value of the slope (corresponding to a value, $E_s = 11.2 \pm 0.6$ kcal/mole) is too low to suggest formation of monomer by chain rupture as the rate-controlling mechanism. Rather, it is more consistent with a surface process of surface desorption of monomer. The heat of vaporization of liquid monomer at 100°C has been estimated from vapor pressure data[10] to be 9.2 kcal/mole.

Since crosslinking would not be expected to alter significantly the value for the heat of vaporization of monomer from polymer, a surface desorption process is consistent with the fact that the rate curves for both crosslinked and linear PMM appear to tend toward the same slope. However, the fact that $d^2(\ln B)/d(1/T_s)^2$ is negative suggests that a reaction mechanism on the surface is not rate controlling over the entire range of surface temperatures studied, since it is unlikely that increasing temperature would slow down such a surface reaction mechanism. Also, the fact that E_s at high temperature is less than the endothermicity of the total depolymerization reaction (the heat of polymerization of gaseous monomer to condensed polymer is ~20 kcal/mole),[11] indicates that surface depolymerization occurs as a step wise process. Therefore, it is possible that a bulk reaction step (reaction in the surface substrate) is rate controlling at low surface temperature.

Referring to Eq. (1), it is seen that the concept of a slope which decreases (Fig. 1) toward a limiting value would be consistent with n_s increasing exponentially with surface temperature toward its surface saturation value, $(\rho N/M)^{2/3}$. Thus, the apparent order of the surface-regression reaction would be first order at low surface temperatures and zero order at high surface temperatures. This suggests that Schultz and Dekker's treatment of thermal decomposition of solids can be extended to fit the present PMM pyrolysis data by utilizing a modification of Langmuir's treatment of gas reactions on solid surfaces.[12]

Consider that during pyrolysis monomer molecules form in the solid (or liquid) substrate and diffuse to the surface. At the surface, the monomer molecules occupy desorption sites prior to "evaporation" (i.e., leaving the surface and entering the gas phase). Denoting θ as the fraction of desorption sites filled by the desorbing species; J as the rate of diffusion in molecules/cm² sec; and ξ as the "evaporation" rate constant in units of molecules/cm² sec, then under the condition of steady-state surface regression,

$$(1-\theta)J = \theta\xi. \quad (5)$$

Since the total number of desorption sites is approximately $(\rho N/M)^{2/3}$, θ can be defined as

$$\theta = n_s(M/\rho N)^{2/3}. \quad (6)$$

By combining Eqs. (2–6) we obtain the following modified expressions for the rate of surface regression

$$B = \theta A_s \exp(-E_s/RT_s) \text{ cm/sec,} \quad (7)$$

and

$$B = (J/\xi/1 + J/\xi) A_s \exp(-E_s/RT_s) \text{ cm/sec.} \quad (8)$$

Since θ refers to the rate of evaporation

$$-dn_s/dt = k_s n_s = \theta\xi \text{ molecules/cm}^2 \text{ sec} \quad (9)$$

and

$$\xi = k_s(M/\rho N)^{-2/3} \text{ molecules/cm}^2 \text{ sec.} \quad (10)$$

Assuming the diffusion flux to be Fickian, J is directly proportional to the diffusion coefficient D and concentration of diffusing species (M). An approximate expression for J would be

$$J \simeq cD(M) \text{ molecules/cm}^2 \text{ sec,} \quad (11)$$

where c is a proportionality constant, cm^{-1}.

Although the diffusion of small molecules through high-polymer systems may be Fickian there is evidence that at temperatures of ~50°C the diffusion process would involve a diffusion coefficient which is very sensitive to changes in monomer concentration.[13,14] The concentration dependence has been interpreted in terms of transition state "hole" theory[3] as a "loosening" of the polymer matrix by the penetrant molecules.[13] At the high temperatures and monomer concentrations involved in surface pyrolysis, the polymer matrix should already be relatively "loose," and it is reasonable to expect that under these conditions the dependence of

[9] Andersen, Bills, Dekker, Mishuck, Moe, and Schultz, Jet Propulsion **28**, 831–832 (1958).

[10] E. R. Blout and H. Mark, *Monomers* (Interscience Publishers, Inc., New York, 1949).

[11] P. A. Small, Trans. Faraday Soc. **49**, 441–447 (1953).

[12] See S. Glasstone, *Textbook of Physical Chemistry* (D. Van Nostrand Company, Inc., New York, 1946), second edition, pp. 1118–1120.

[13] G. S. Park, Trans. Faraday Soc. **46**, 684–697 (1950).

[14] R. J. Kokes and F. A. Long, J. Am. Chem. Soc. **75**, 6142–6146 (1953).

the diffusion coefficient on monomer concentration should be slight. Therefore, it can be considered that D and (M) in Eq. (11) are explicitly independent of each other, but both dependent upon temperature. It is further assumed that (M) refers to the equilibrium concentration of decomposing species which for the case of PMM corresponds to the concentration of monomer in the polymerization-depolymerization equilibrium reaction[1]

$$P_m + M \underset{k_d}{\overset{k_p}{\rightleftarrows}} P_{m+1}, \tag{12}$$

where P_m is a polymer chain containing m monomer units, and k_p and k_d are the respective rate constants for propagation and depropagation of the polymer chain. Therefore

$$(M) = (k_d/k_p)\,\text{molecules/cm}^3. \tag{13}$$

By utilizing Eqs. (10), (11), and (13), and expressing k_d, k_p, D, and k_s as Arrhenius-type rate expressions, the temperature sensitivity of J/ξ can now easily be described:

$$J/\xi = \alpha \exp[(E_s + E_p - E_d - E_D)/RT_s]. \tag{14}$$

Here, E_s, E_p, E_d, and E_D are the respective activation energies for desorption of monomer from polymer, chain propagation, chain depropagation, and diffusion of monomer in polymer; the constant α is a composite of all factored terms which are approximately independent of temperature.

If we combine Eqs. (8) and (14) we obtain the following expression for the rate of surface regression:

$$B = \frac{\alpha A_s \exp[(E_p - E_d - E_D)/RT_s]}{1 + \alpha \exp[(E_s + E_p - E_d - E_D)/RT_s]}\,\text{cm/sec}. \tag{15}$$

For suitable values of α and E_i ($i = s$, p, d, or D) it is seen that at low surface temperatures the exponential term in the denominator of Eq. (15) would be much smaller than unity. At high temperatures the same term would be large compared to unity, in which case the expression for B is the same as that given by Schultz and Dekker [Eq. (3)].

In correlating Eq. (15) with the data of Fig. 1, it is possible to use literature values for E_d, E_D, and E_p. The values for A_s and E_s can be determined by fitting a straight line to the pyrolysis rate data in Fig. 1 in the region of linearity (high surface temperature region).

It would be possible to calculate the constant α if accurate kinetic data on diffusion, depropagation, and propagation were available. Unfortunately, such data are not available at this time. Alternatively, α can be considered as an arbitrary constant whose value can be calculated from the experimental pyrolysis rate data by assuming that $\theta \simeq 1$ at a particular finite T_s. Within the experimental accuracy of the data of Fig. 1, it is reasonable to assume that $\theta \simeq 1$ when the ratio $J/\xi = 10$. Thus, determination of the value of T_s for $J/\xi = 10$ enables one to calculate α utilizing Eq. (14).

TABLE II. Values for the constants of Eq. (15).

Parameter	Linear PPM	Crosslinked PMM
E_s	11 kcal/mole	11 kcal/mole
E_p	5.5 kcal/mole[a,b]	5.5 kcal/mole
E_d	18.5 kcal/mole[a,b]	18.5 kcal/mole
E_D	30 kcal/mole[a]	35 kcal/mole
A_s	27 cm/sec	14 cm/sec
α	5.6×10^{11}[a]	3.1×10^{11}[b]

[a] Calculated by setting $J/\xi = 10$ at $T_s = 650$°K.
[b] Calculated by setting $J/\xi = 10$ at $T_s = 770$°K.

The second column in Table II lists the values for the constants of Eq. (15) when applied to the linear PMM rate data. Substitution of these values yields the following surface-regression rate expression:

$$B_{(\text{linear})} = \frac{1.5\times10^{13} \exp(-43000/RT_s)}{1 + 5.6\times10^{11} \exp(-32000/RT_s)}\,\text{cm/sec}. \tag{16}$$

It is probable that the major effect of crosslinking on the linear pyrolysis rate will be associated with an increase in the activation energy for diffusion of monomer molecules through the stiffer polymer matrix. Therefore, it can be expected that at a given surface temperature the diffusion flux through the polymer substrate to the surface will be less in the case of crosslinked PMM than in the case of uncrosslinked PMM. It is also reasonable to expect that the desorption, and depropagation mechanisms will remain essentially unchanged. Equation (15) suggests that the linear pyrolysis rate of crosslinked PMM would therefore be different from the linear PMM as the result of an effective increase in E_D (which in later calculations is arbitrarily assumed to be $\sim$5 kcal/mole), and of an increase in the value of the effective surface temperature at which $\theta \simeq 1$ (or $J/\xi = 10$).

By utilizing the values listed in the last column of Table II, the following expression for the rate of surface regression of crosslinked PMM is obtained:

$$B_{(\text{x link})} = \frac{4.4\times10^{12} \exp(-48000/RT_s)}{1 + 3.1\times10^{11} \exp(-37000/RT_s)}\,\text{cm/sec}. \tag{17}$$

Equations (16) and (17) are plotted in Fig. 2 along with the experimental rate data. The observed agreement is reasonable in view of the data scatter and approximations used in deriving the theoretical curves.

It is interesting to compare the measured pyrolysis rate of PMM at high surface temperature to the rate which can be approximated from simple considerations utilizing absolute rate theory. The approach taken is the same as that used to describe the rate of linear pyrolysis of ammonium nitrate.[15]

[15] Schultz, Green, and Penner, *Third AGARD Colloquium—Combustion and Propulsion* (Pergamon Press, New York, 1958), pp. 367–427.

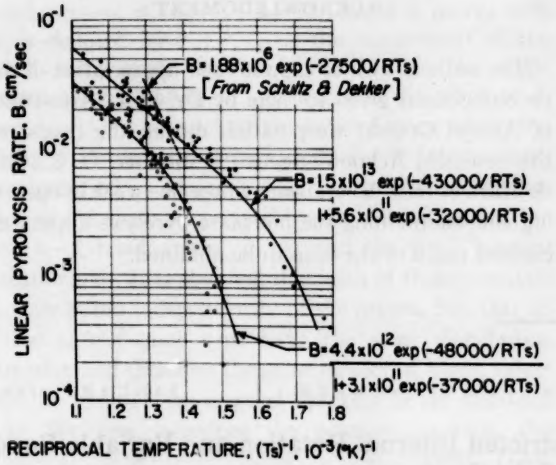

FIG. 2. Linear pyrolysis rate for polymethylmethacrylate. ●, linear PMM; O, cross-linked PMM; —, theoretical curves.

It is considered that at surface temperatures greater than ~700°K the polymer surface is covered by a thin liquid monomer layer and that desorption of monomer is the rate-controlling step for surface pyrolysis. The assumed model corresponds to a physically adsorbed surface molecule which passes into the gaseous state with little change in its modes of vibration. It is further assumed that the torsional frequencies for rotational degrees of freedom of the molecule in the normal state are roughly the same as those which exist when the molecule is in the activated (transition) state. For these conditions, the absolute rate expression for the rate of linear pyrolysis of PMM can be approximated[15] as

$$B=e(M/\rho N)^{1/3}(kT_s/h)[f(\nu_x^*)f(\nu_y^*)/f(\nu_x)f(\nu_y)f(\nu_z)\cdot\exp(-\Delta H_{c_0}/RT_s)\text{cm/sec}, \quad (18)$$

where ΔH_{c_0} is the enthalpy of the vaporization process, kcal/mole; e is the Napierian constant; $f(\nu)$ is a partition function for one vibrational mode of the normal state of the adsorbed molecule $=[1-\exp(-h\nu/kT)]^{-1}$; $f(\nu^*)$ is similar to $f(\nu)$ except that the partition function refers to the frequency ν^* of the activated complex instead of the corresponding frequency ν of the normal state; and ν_x, ν_y, ν_z are vibration frequencies for the normal state translational oscillation of the center of gravity of the monomer molecule in the x and y directions parallel to the surface, and in the z direction perpendicular to the surface (the reaction coordinate is taken along the z direction in the activated state).

If the escape direction for the physically adsorbed monomer molecule is taken as that which is exactly perpendicular to the reaction surface, then $f(\nu_x^*)=f(\nu_y^*)=1$. If we make the reasonable assumptions that $\nu_x\approx\nu_y\approx\nu_z$ and $kT_s\gg h\nu$, Eq. 18 becomes

$$B=e(M/\rho N)^{1/3}(h/kT_s)^2\nu^3\exp(-\Delta H_{c_0}/RT_s)\text{cm/sec}. \quad (19)$$

For methylmethacrylate monomer $e(M/\rho N)^{1/3}\approx 10^{-7}$ cm, and ΔH_{c_0} can be estimated as 9.2 kcal/mole.[10]

From the work of Hill[16] on the vibration frequencies of physically adsorbed molecules, it can be estimated that ν is approximately 10^{11} sec^{-1}. Therefore, the equation for the rate of linear pyrolysis of PMM is

$$B_{T_s>700°K}\approx 50\exp(-9200/RT_s)\text{cm/sec}, \quad (20)$$

as compared to the experimentally determined expression

$$B_{\text{linear}}=27\exp(-11200/RT_s)\text{cm/sec} \quad T_s<700°\text{K}. \quad (21)$$

In view of the many assumptions and approximations made in evaluating the partition functions, and the uncertainty in the experimental data, the agreement between the theoretical and experimental rate expressions for monomer desorption is probably as good as one can expect.

CONCLUSIONS

It has been shown that the thermal depolymerization of polymethylmethacrylate during surface heating involves a rate-controlling process which differs from that which one might expect on the basis of isothermal bulk-depolymerization data. This duality of rate processes is probably associated with the surface-heating technique in which superheating of the surface layer is possible. The experimental pyrolysis rate data suggest a surface-depolymerization mechanism involving the formation of a monomer layer on the polymer surface. At high temperatures, the polymer surface is saturated with monomer, and desorption of monomer is the rate-controlling step in the pyrolysis process. At lower temperatures, the polymer surface is not saturated with monomer, so that monomer formation and diffusion processes in the surface substrate are rate controlling. Although the proposed reaction scheme allows the derivation of rate expressions which are in good agreement with the data, the possibility that another treatment can yield similar consistent results has not been eliminated.

The discrepancies between the results of this investigation and those of Schultz and Dekker's[5] probably lies in the type of surface-heating element employed. The hot-wire technique of Schultz and Dekker could introduce a cutting action as the PMM strand is pressed against it. Thus, the measured surface regression rates would be influenced by shear forces and viscous flow as well as the rate of gasification. In connection

[16] T. L. Hill, J. Chem. Phys. **16**, 181–189 (1948).

with this, it is worthwhile to mention the unpublished data of Marklund and Grahm[17] who repeated Schultz and Dekker's work with hot wires of varying diameter. They found that the linear pyrolysis rate of PMM at equivalent surface temperatures decreased as wire diameter increased. This result is consistent with a cutting action by the hot wire.

[17] P. T. Marklund and L. Grahm, Research Institute of National Defense, Stockholm, Sweden (private communication, 1958).

ACKNOWLEDGMENT

The authors wish to express their appreciation of the encouragement given to them by Dr. D. L. Armstrong of Aerojet-General Corporation during the course of this research. Acknowledgment is due Mr. D. K. Van de Mark of these laboratories whose fine work in operating and maintaining the hot-plate pyrolysis apparatus enabled much of the data to be obtained.

THE JOURNAL OF CHEMICAL PHYSICS VOLUME 32, NUMBER 1 JANUARY, 1960

Dimensions of Long-Chain Molecules with Restricted Internal Rotation and Variable Bond Length and Angle

WILLIAM J. TAYLOR

McPherson Chemical Laboratory, Ohio State University, Columbus, Ohio

(Received August 5, 1959)

Exact formulas are obtained for the mean square length and radius of an unbranched chain molecule of n equivalent bonds, with restricted internal rotation about each bond and variable bond length and angle. It is assumed only that each of the internal coordinates is distributed independently of the others. This model is not entirely realistic, but is justified for the bond stretching and bending motions because of the small effect they have on the chain dimensions, shown to be of the order of a few tenths of one percent at normal temperatures.

IN 1932 Eyring[1] obtained a formula for the mean square length of an unbranched chain molecule of n equivalent bonds with free internal rotation about each bond. Eyring's formula is valid for finite n, and we will consider only calculations exact in this sense, as opposed to formulas valid asymptotically for $n \to \infty$.[2] Eyring's method was extended to a chain with restricted internal rotation by Oka,[3] although he carried the calculation to completion only for a symmetrical hindering potential. Benoit[4] obtained independently* a compact formula for the case of free rotation within a finite angular range. An equivalent formula was shown to be valid for general hindering potentials by Kubo.[5] More recently the general case has been treated by Wolkenstein and Ptitsyn.[6] The mean square radius of a chain with a symmetrical potential has been calculated by Suzuki.[7]

All the preceding calculations refer to chains with fixed bond lengths and valence angles. Recently Borsellino[8] has generalized the formulas to the case of variable valence angle, θ. Provided the angle θ is distributed independently of the internal rotations, it is only necessary to replace $\cos\theta$ and $\sin\theta$ by their mean values in the previous formulas. Borsellino also obtained a more compact formula for the mean radius than that of Suzuki.[7]

The purpose of this note is to present the further natural generalization to the case of variable bond length. It will be shown that the alteration in chain dimensions is, in part, a result of the change in mean bond length arising from the anharmonicity of the vibrations, but that there is an additional increment proportional to the mean square amplitude of vibration which is present even for harmonic vibrations. Both effects will increase the chain dimensions, thus counteracting the some extent the usual contraction of the chain produced by internal rotation as the temperature increases.[9]

The chain of $n+1$ atoms is characterized by the n

[1] H. Eyring, Phys. Rev. **39**, 746 (1932).

[2] For more general reviews, see H. A. Stuart, *Die Struktur des Freien Moleküls* (Springer-Verlag, Berlin, Germany, 1952), and M. W. Wolkenstein and O. B. Ptitsyn, Fortschr. Physik **1**, 596 (1954).

[3] S. Oka, Proc. Phys.-Math. Soc. Japan **24**, 657 (1942).

[4] H. Benoit, J. chim. phys. **44**, 18 (1947).

* Perhaps it is not amiss to point out that there was no communication between the Japanese workers in this field and those in Europe and the United States during the war and for some time thereafter.

[5] R. Kubo, J. Phys. Soc. Japan **3**, 119 (1948).

[6] M. W. Wolkenstein and O. B. Ptitsyn, J. Phys. Chem. (U.S.S.R.) **26**, 1061 (1952).

[7] K. Suzuki, Bull. Chem. Soc. Japan **20**, 19 (1947).

[8] A. Borsellino, Ricerca sci. **29**, 496 (1959); J. Chem. Phys. **30**, 857 (1959).

[9] W. J. Taylor, J. Chem. Phys. **15**, 412 (1947); **16**, 257 (1948). The present discussion is based on the general treatment of the length and radius referred to in the first of these papers, but not previously published. *Erratum*: The several references to 22a which appear in the text of the second paper listed should be to reference 21.

bond vectors, $\mathfrak{d}_1, \mathfrak{d}_2, \cdots, \mathfrak{d}_n$. The angle $\mathfrak{d}_j$ makes with $\mathfrak{d}_i$ is denoted by θ_{ij}; $\theta_{i,i+1}$ is the supplement of the usual bond angle between $\mathfrak{d}_i$ and $\mathfrak{d}_{i+1}$. The angle between the plane of $\mathfrak{d}_{i-1}$ and $\mathfrak{d}_i$ and the plane of $\mathfrak{d}_i$ and $\mathfrak{d}_{i+1}$ in the sense of a right-handed screw advancing along $\mathfrak{d}_i$ is denoted by ϕ_i, with $\phi_i=0$ for the *trans* configuration of $\mathfrak{d}_{i-1}$ and $\mathfrak{d}_{i+1}$. The internal configuration of the chain is specified by the n bond lengths, σ_i, the $n-1$ bond angles, $\theta_{i,i+1}$, and the $n-2$ internal rotations, ϕ_i. It is assumed that each of these variables is distributed independently of the others, but that all those of the same type have the same distribution function and therefore the same moments. Mean values will be denoted by angular brackets or an overhead bar. We now introduce the notation $\langle\sigma_i\rangle=\bar{\sigma}$, $s^2=\langle(\sigma_i-\bar{\sigma})^2\rangle=\langle\sigma_i^2\rangle-\bar{\sigma}^2$, $\langle\cos\theta_{i,i+1}\rangle=\alpha$, $\langle\sin\theta_{i,i+1}\rangle=\beta$, $\langle\cos\phi_i\rangle=a$, $\langle\sin\phi_i\rangle=b$, and $\langle\cos\theta_{i,i+k}\rangle=\alpha_k(\alpha_1=\alpha)$. It follows from the preceding assumptions that $\langle\cos\theta_{i,i+k}\rangle$ depends only on k, and the explicit form of α_k is obtained subsequently. The mean square length and radius of the chain are defined by

$$\langle L^2\rangle=\langle(\sum_{i=1}^{n}\mathfrak{d}_i)^2\rangle, \tag{1}$$

$$\langle R^2\rangle=(n+1)^{-1}\sum_{k=0}^{n}\langle\mathbf{r}_k^2\rangle, \tag{2}$$

with $\mathbf{r}_k$ the vector from the center of mass to the kth atom, so that

$$\mathbf{r}_k=\sum_{i=1}^{k}\mathfrak{d}_i-(n+1)^{-1}\sum_{i=1}^{n}(n+1-i)\,\mathfrak{d}_i \tag{3}$$

(omit the first sum in Eq. (3) for $k=0$). On using the relations $\langle\mathfrak{d}_i\cdot\mathfrak{d}_i\rangle=\langle\sigma_i^2\rangle=\bar{\sigma}^2+s^2$ and $\langle\mathfrak{d}_i\cdot\mathfrak{d}_{i+k}\rangle=\bar{\sigma}^2\alpha_k(k>0)$, we obtain

$$\langle L^2\rangle=\bar{\sigma}^2[n(1+2S_0)-2S_1]+ns^2, \tag{4}$$

and

$$\langle R^2\rangle=\bar{\sigma}^2\{[n(n+2)/6(n+1)](1+2S_0)-[1-(\tfrac{1}{3})(n+1)^{-2}]S_1+(n+1)^{-1}S_2-(\tfrac{1}{3})(n+1)^{-2}S_3\}+[n(n+2)/6(n+1)]s^2, \tag{5}$$

where

$$S_\mu=\sum_{k=1}^{n-1}k^\mu\alpha_k$$

[for $n=1$ omit the terms containing S_μ in Eqs. (4) and (5)].

The mean value of the rotation matrix which transforms the components of a vector from axes fixed in the ith bond to axes in the $(i-1)$th bond is[1] (note that Eyring defined $\phi=0$ for the *cis* configuration)

$$\mathbf{A}=\begin{pmatrix}\alpha & -\beta & 0\\ -\beta a & -\alpha a & b\\ -\beta b & -\alpha b & -a\end{pmatrix}, \tag{6}$$

and it follows from the independent distribution of the coordinates that $\alpha_k=(\mathbf{A}^k)_{11}$. Define the polynomials

$$P_\mu(x)=\sum_{k=1}^{n-1}k^\mu x^k,$$

where x is a square matrix or a scalar. Then in Eqs. (4) and (5) $S_\mu=[P_\mu(\mathbf{A})]_{11}$. The characteristic equation of $\mathbf{A}$ is $|\lambda\mathbf{I}-\mathbf{A}|=\lambda^3-(\alpha-\alpha a-a)\lambda^2+[\alpha(a^2+b^2)-(\alpha+\alpha^2+\beta^2)a]\lambda-(\alpha^2+\beta^2)(a^2+b^2)=0$. Denote the roots of this equation by $\lambda_j, j=1, 2, 3$. For nondegenerate roots the corresponding eigenvectors of $\mathbf{A}$ are

$$\mathbf{u}_j=\begin{pmatrix}U_{1j}\\ U_{2j}\\ U_{3j}\end{pmatrix}=\begin{pmatrix}\beta(\lambda_j+a)\\ (\alpha-\lambda_j)(\lambda_j+a)\\ (\alpha\lambda_j-\alpha^2-\beta^2)b\end{pmatrix}, \tag{7}$$

each being indeterminate to the extent of a multiplicative constant. Let $\mathbf{U}$ be the square matrix having the eigenvectors [Eq. (7)] as its columns. Then $\mathbf{AU}=\mathbf{U\Lambda}$, where $\mathbf{\Lambda}$ is a diagonal matrix with elements $\Lambda_{ij}=\lambda_j\delta_{ij}$. It follows immediately that $\mathbf{A}=\mathbf{U\Lambda U}^{-1}$, $\mathbf{A}^k=\mathbf{U\Lambda}^k\mathbf{U}^{-1}$, and $P_\mu(\mathbf{A})=\mathbf{U}P_\mu(\mathbf{\Lambda})\mathbf{U}^{-1}$, where $[P_\mu(\mathbf{\Lambda})]_{ij}=P_\mu(\lambda_j)\delta_{ij}$. Finally

$$S_\mu=[P_\mu(\mathbf{A})]_{11}=\sum_{j=1}^{3}Z_jP_\mu(\lambda_j), \tag{8}$$

with $Z_j=U_{1j}(\mathbf{U}^{-1})_{j1}$. This diagonalization technique[10] has been used by several authors.[2,3,6] Borsellino[8] has suggested an alternative procedure based on Sylvester's theorem[10] (a form of Lagrange's interpolation formula) according to which

$$Z_j=\{\prod_{i\neq j}[(\lambda_i\mathbf{I}-\mathbf{A})/(\lambda_i-\lambda_j)]\}_{11}.$$

This method does not require the calculation of the eigenvectors, but on the other hand the latter are obtained easily from Eq. (7). The two relations for Z_j are identically equivalent.[10]

Substitution of Eq. (8) in Eqs. (4) and (5), and use of the relations $P_0(\lambda)=\lambda(1-\lambda^{n-1})/(1-\lambda)$ and $P_\mu(\lambda)=[\lambda(d/d\lambda)]^\mu P_0(\lambda)$, $\mu>0$, now yields

$$\langle L^2\rangle=\bar{\sigma}^2\sum_{j=1}^{3}Z_j\{[n(1-\lambda_j^2)-2\lambda_j(1-\lambda_j^n)]/(1-\lambda_j)^2\}+ns^2 \tag{9}$$

[10] R. A. Frazer, W. J. Duncan, and A. R. Collar, *Elementary Matrices* (Cambridge University Press, London, 1938), Chap. 3.

$$\langle R^2\rangle=\bar{\sigma}^2\sum_{j=1}^{3}Z_j\{(n/6)[(1+\lambda_j)/(1-\lambda_j)]$$
$$+[n/6(n+1)][(1-6\lambda_j-\lambda_j^2)/(1-\lambda_j)^2]$$
$$+[2/(n+1)^2][\lambda_j^2/(1-\lambda_j)^4][n(1-\lambda_j)-\lambda_j(1-\lambda_j^n)]\}$$
$$+[n(n+2)/6(n+1)]s^2. \quad (10)$$

These formulas are identical with those of Borsellino[8] except for the replacement of his constant bond length, l, by mean length, $\bar{\sigma}$, and the additional terms in the mean square amplitude of vibration, s^2.

The anharmonic potential for bond stretching may be approximated as $V=(K/2)(\Delta\sigma)^2(1-\gamma\Delta\sigma)$, where $\Delta\sigma=\sigma-\sigma_0$, and σ_0 is the value of σ at the minimum of the potential. Then for a given vibrational state of energy E relative to the minimum of V, the mean value of $\Delta\sigma$ averaged over the motion is approximately $(\gamma/K)E$. On carrying out a further thermal average over all states we obtain $\Delta\bar{\sigma}=(\gamma/K)\bar{E}$, with $\bar{E}=h\nu[(e^x-1)^{-1}+(\frac{1}{2})]$ as the average energy of the oscillator in the harmonic approximation. Here ν is the harmonic frequency of the oscillator, $x=h\nu/kT$, h is Planck's constant, and k is Boltzmann's constant. Finally, the mean bond length is $\bar{\sigma}=\sigma_0+\Delta\bar{\sigma}$. The mean square amplitude of vibration, $s^2=\langle(\sigma-\bar{\sigma})^2\rangle$, may be written in the form $s^2=s_0^2-(\Delta\bar{\sigma})^2$, where $s_0^2=\langle(\sigma-\sigma_0)^2\rangle$. These averages also represent an average for each state followed by a thermal average over all states, and it has been shown by Bloch[11] that in the harmonic approximation $s_0^2=(1/K)\bar{E}$.

Application of the preceding equations to a polymethylene chain shows that the effect of bond stretching vibrations on the chain dimensions is very small. Using the values $\nu/c=990$ cm^{-1}, $K=4.5\times10^5$ erg cm^{-2}, and $\gamma=1.9\times10^8$ cm^{-1}, one calculates, at 400°K, $\bar{E}=1.04\times10^{-13}$ erg, $\Delta\bar{\sigma}=0.0045$ A, and $s=0.048$ A. With $\sigma_0=1.54$ A, $(\Delta\bar{\sigma})/\sigma_0=0.0029$, representing an increase of 0.29% in the dimensions of the chain due to anharmonicity. On the other hand, even though the root-mean-square amplitude of vibration, s, is 3.1% of σ_0, the increase in chain dimensions from this cause is only 0.015%. Comparable values are obtained for the bending vibrations. Thus, the present analysis justifies the neglect of the vibrational effects in the previous calculations of the dimensions of polymethylene chains with restricted internal rotation.[9,12]

[11] F. Bloch, Z. Physik **74**, 295 (1932).
[12] H. Benoit and C. Sadron, J. Polymer Sci. **4**, 473 (1949).

The model of independent internal coordinates on which the present calculation is based is of course not entirely realistic. The interaction of the internal rotations, particularly the so-called excluded-volume effect, has been discussed extensively in the literature in recent years. For a molecule without internal rotation a treatment of the small vibrational displacements leads, in the harmonic approximation, to the concept of normal coordinates, and it is the latter, rather than the valence coordinates, which are distributed independently in quantum statistics. However, for a molecule which undergoes internal rotation one is faced with the much more difficult problem of the interaction of the vibrations with the large-amplitude rotations, and the wave equation is no longer separable in any strict sense. Even if the rotational coordinates are treated as slowly varying parameters in the vibrational problem (adiabatic approximation) there remains the task of averaging the vibrational states or eigenvalues over the internal rotations. In the present problem the vibrational effects are so small that it seems sensible to avoid these difficulties by assuming the valence coordinates are independent. The present analysis is a mathematically exact treatment of this model. That is, exact relations have been obtained between the mean square length and radius and the mean parameters for the independent variables, $\bar{\sigma}$, s, a, b, α, and β.[13] The calculation of the latter mean values is a separate problem, which may be approached in quantum statistics through the evaluation of the Slater sum,[14] or the solution of Bloch's differential equation.[11] If a quantum mechanical calculation appears impractical, classical statistics may be used as in an earlier calculation of $a=\langle\cos\phi\rangle$.[9]

[13] At several points in the proof use has been made of the theorem that the mean value of a product of independent random variables (or functions of such variables) is equal to the product of the mean values of the factors (provided the latter mean values exist). For a rigorous proof of this theorem see H. Cramér, *Mathematical Methods of Statistics* (Princeton University Press, Princeton, New Jersey, 1946), Chaps. 14 and 15. A set of quantum mechanical observables, such as the internal coordinates of the chain considered here, which are represented by commuting operators and are thus simultaneously observable, constitute a set of random variables in the sense used by Cramér, with the square of the amplitude function playing the role of the probability density function. The necessary and sufficient condition that they be *independent* random variables is that the wave equation be separable, so that the amplitude function factors into a product of functions each depending on a single observable.
[14] J. C. Slater, Phys. Rev. **38**, 237 (1931).

THE JOURNAL OF CHEMICAL PHYSICS VOLUME 32, NUMBER 1 JANUARY, 1960

Mass Spectrum of Propane: Isotope Effect and Metastable Ions*

ALLEN KROPF,† EDWARD M. EYRING, AUSTIN L. WAHRHAFTIG, AND HENRY EYRING

Department of Chemistry, University of Utah, Salt Lake City, Utah

(Received July 29, 1959)

The mass spectra of propane and of propane-2,2-d_2 have been calculated assuming that the mass spectra result from successive and competing unimolecular reactions following initial vertical ionization of the parent molecules. Reasonable agreement with experiment is found for the change in mass spectral pattern with deuterium substitution. The metastable ion peaks are shown to be a normal part of the mass spectrum.

I. INTRODUCTION

IT was suggested by Rosenstock *et al.*,[1] in order to account for the characteristic mass spectral patterns of hydrocarbons, that the fragment ions observed following electron bombardment arose from competing and successive unimolecular decompositions of excited molecule-ions. These excited molecule-ions were assumed to decompose adiabatically from stable electronic states, the excess electronic energy which was imparted to the ions at the time of electron impact having been converted into vibrational energy through many radiationless transitions. Using the methods of statistical mechanics, they arrived at an expression for the rate constant for the decomposition of a collection of isolated systems, each represented by L internal rotors and $N-L$ harmonic oscillators.

The expression given contained two errors, a simple arithmetical error in the power of π, and the neglect of the double degeneracy of a rotational energy level. Also, the number of ways in which a reaction could occur and the effect of symmetry upon energy level density were not specifically included in the general equation but were introduced in the discussions of the specific reactions. With these corrections, one obtains

$$k(E)=z(1-\epsilon/E)^p(E-\epsilon)^q \tag{1}$$

in which

$$p=N-\tfrac{1}{2}L-1, \qquad q=\tfrac{1}{2}(L-L^\ddagger),$$

and

$$z=\sigma(2\pi)^{\frac{1}{2}q}\frac{\Gamma(N-\frac{1}{2}L)\prod_{i=1}^{L^\ddagger}\frac{I_i^{\frac{1}{2}}}{n_i^\ddagger}\prod_{k=1+L}^{N}\nu_k}{\Gamma(N-\frac{1}{2}L^\ddagger)\prod_{j=1}^{L}\frac{I_j^{\frac{1}{2}}}{n_j}\prod_{l=L^\ddagger+1}^{N-1}\nu_l^\ddagger} \tag{2}$$

where σ = number of equivalent ways of picking the reaction coordinate, considering each atom labeled and free rotations frozen,

L = number of internal rotational degrees of freedom,

N = total number of internal degrees of freedom (for nonlinear molecules $N=3N'-6$, where N' is the number of atoms),

$\Gamma(N)$ = gamma function of N,

I_i = reduced moment of inertia for the ith internal rotor,

n_i = number of equivalent positions for the ith internal rotor,

ν_i = frequency of vibration for the ith normal mode,

E = total energy of the molecule,

ϵ = energy of activation for the reaction, and

‡ indicates quantity for the activated complex configuration.

After the unimolecular reaction rate constants for all possible reactions have been calculated, the probability of formation of the several product ions from parent ions of a given energy can be determined. The relative abundances (R.A.'s) of the product ions are then given by the integrals over energy of the above probabilities multiplied by the assumed energy function for the parent molecule-ions.

It was demonstrated by Rosenstock[1,2] that this theory permitted the calculation of the mass spectrum of propane, but the number of arbitrary assumptions required was large. In principle, the calculation of the mass spectra of all deuterium substituted propanes follows readily from the calculation for the nondeuterated molecule. As good data were available for propane-2,2-d_2, calculations were made for this molecule.[3]

II. THE REACTIONS

The set of reactions assumed for propane-d_2, Fig. 1, is the simplest set that will yield reasonable R.A.'s for all major peaks in the mass spectrum. Certainly, other reactions occur, but it is believed that they will have higher activation energies and thus will be of little importance. The addition of reactions 1 and 6 to the scheme used by Rosenstock[1,2] was required by the existence of mass peaks 45 and 29 in the mass spectrum

* This research was assisted by the U. S. Atomic Energy Commission under Contract AT(11-1)-82, Project No. 5.

† From a dissertation in partial fulfillment of the requirement for the Ph.D. degree, University of Utah, 1954. Now at Department of Chemistry, Amherst College, Amherst, Massachusetts.

[1] Rosenstock, Wallenstein, Wahrhaftig, and Eyring, Proc. Natl. Acad. Sci. U.S. **38**, 667 (1952).

[2] H. M. Rosenstock, Ph.D. thesis, University of Utah (1952).

[3] Schissler, Thompson, and Turkevitch, Discussions Faraday Soc. **10**, 46 (1951).

TABLE I. Calculated and observed mass spectra of propane and propane-2,2-d_2.

	Propane			Propane-2,2-d_2		
m/e	Reactions producing the ions[a]	R.A.[b] Calc.	R.A.[c] Obs.	Reactions producing the ions[a]	R.A.[b] Calc.	R.A.[c] Obs.
46				Parent	10.4	13.1
45				1	2.3	1.9
44	Parent	10.3	12.7	2	4.9	3.6
43	1 and 2	14.4	10.6	3 and (0.4) of 7	1.6	2.0
42	3	1.9	1.5			
42–36				8, 9, and (0.6) of 7	5.9	9.0
41–36	7, 8, and 9	9.8	12.5			
31				4	30.7	28.9
30				5	24.2	20.6
29	4	25.7	31.1	6 and (0.3) of 10	9.0	9.2
28	5 and 6	22.3	19.2	(0.6) of 10	6.9	8.0
27	10	12.8	10.5	(0.1) of 10, 11, and (0.5) of 12	3.5	3.1
26	11 and 12	2.8	1.9	(0.5) of 12	0.6	0.6

[a] Reaction numbers are given in Fig. 1.
[b] Calculated and observed relative abundances are both normalized to a total ionization of 100 for the masses listed.
[c] Schissler, Thompson, and Turkevich.[3]

of propane-d_2.‡ The mass 29 peak is so large that it is extremely unlikely that it results entirely from loss of H_2 from mass 31. It has been assumed here that H—D exchange on the parent molecule-ion does not occur to any appreciable extent even though data obtained on several deuterated butanes casts some doubt on this assumption.[4] The agreement obtained in these calculations, neglecting such exchange, cannot be considered conclusive evidence that it does not occur. Additional data at low electron energies is required.

In contrast to rearrangement processes in the parent molecule-ion, which we believe to be slow, rearrangement reactions are probably very rapid in fragment ions, especially ones containing an odd number of hydrogen plus deuterium atoms. In such ions, rearrangement can occur by repeated shifts of single atoms, while hydrogen must exchange pairwise on the molecule-ion. The resulting plethora of possible secondary reactions and products can be treated approximately by neglecting isotope effects in calculating the reaction rates for the secondary reactions, and by lumping together many of the possible secondary products.

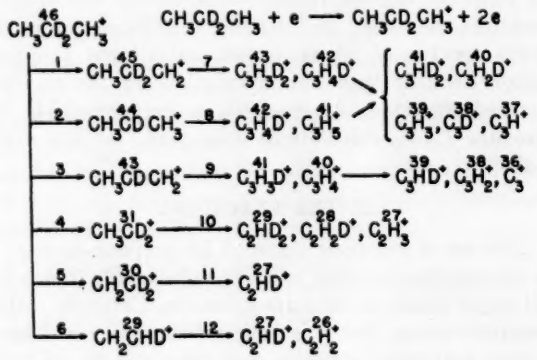

FIG. 1. Unimolecular decomposition scheme for 2,2-dideuteropropane under electron bombardment.

The calculation of R.A.'s of ions in the propane-2, 2-d_2 mass spectrum that will be described fails to distinugish between the relative amounts of mass 43 and 42 produced by reaction 7. Since these are major peaks in the mass spectrum, resolution of these peaks in the calculated spectrum is desirable as a check of these calculations. We have assigned the fractions of the calculated product from reactions 7, 10, and 12 to the several possible ions according to purely statistical considerations. As an example, consider reaction 10. Assuming complete randomization of hydrogens and deuteriums in the ethyl ion produced by reaction 4, the probability that reaction 10 involves the loss of two hydrogens and the production of $C_2HD_2^+$ is $\frac{3}{5}\times\frac{3}{4}=0.3$. The analogous probability that $C_2H_2D^+$ is produced is $\frac{2}{5}\times\frac{3}{4}+\frac{3}{5}\times\frac{2}{4}=0.6$. Similarly, the probability of $C_2H_3^+$ formation is $\frac{2}{5}\times\frac{1}{4}=0.1$. The sum of these three fractions is, of course, unity. The fractions calculated for the three reactions, 7, 10, and 12, are given in Table I where the values for reaction 7 are averages of several calculations based upon more detailed assumptions as to mechanism.

Further extension of this process to the tertiary reactions indicated in Fig. 1 would lead to an absurd compounding of approximations. Consequently, the fragment ions with masses 36 through 42 are lumped together, and those with masses below 26 (experimentally, 2% of the total) are ignored.

‡ Since only singly charged ions are considered in this paper, the cumbersome "peak of mass to charge ratio . . ." is abbreviated to "mass peak."

[4] W. H. McFadden and A. L. Wahrhaftig, J. Am. Chem. Soc. 78, 1572 (1956).

TABLE II. Frequencies and activation energies used in the rate expressions for the decomposition of propane and propane-2,2-d_2.

[a]	[b]	Frequencies changed in the activated complex	σ	z	[c]	$(L-L^\ddagger)/2$	$[N-(\frac{1}{2}L)-1]$
1	ν_3		6	2.70×10^{14}	1.18	0	25
2	ν_1		2	9.00×10^{13}	.83	0	25
2D	ν_1		2	6.30×10^{13}	.92	0	25
3	ν_1	$\nu_3^\ddagger=300$; $\nu_9^\ddagger$, $\nu_{10}^\ddagger$, $\nu_{11}^\ddagger=1000$ $\nu_{26}^\ddagger=500$; $\nu_{18}^\ddagger=1200$ $\nu_{23}^\ddagger=600$; $\nu_{19}^\ddagger=700$	4	2.03×10^{21}	1.70	$\frac{1}{2}$	25
3D	ν_1	$\nu_3^\ddagger=300$; $\nu_9^\ddagger$, $\nu_{10}^\ddagger$, $\nu_{19}^\ddagger=700$ $\nu_{11}^\ddagger=1000$; $\nu_{18}^\ddagger=1200$ $\nu_{23}^\ddagger=400$; $\nu_{26}^\ddagger=500$	4	1.55×10^{21}	1.82	$\frac{1}{2}$	25
4	ν_{17}	$\nu_{19}^\ddagger$, $\nu_{20}^\ddagger$, $\nu_{25}^\ddagger=100$	2	2.03×10^{16}	1.63	0	25
5	ν_{17}	$\nu_{18}=1200$; $\nu_{26}^\ddagger$, $\nu_{27}^\ddagger=500$ $\nu_{19}^\ddagger$, $\nu_{20}^\ddagger=100$	2	5.34×10^{25}	.87	1	25
6	ν_{17}	$\nu_{18}^\ddagger=1200$; $\nu_{19}^\ddagger$, $\nu_{20}^\ddagger=100$ $\nu_{23}^\ddagger=1400$; $\nu_{26}^\ddagger$, $\nu_{27}^\ddagger=500$	4	7.65×10^{25}	1.17	1	25
6D	ν_{17}	Same as 6 except for $\nu_{23}^\ddagger=1000$	4	7.49×10^{25}	1.16	1	25
7 & 8	ν_1	$\nu_3^\ddagger=300$; $\nu_{18}^\ddagger=1200$ $\nu_{19}^\ddagger=700$; $\nu_{23}^\ddagger=600$ $\nu_{26}^\ddagger=500$; $\nu_9^\ddagger$, $\nu_{10}^\ddagger$, $\nu_{11}^\ddagger=1000$	2	1.08×10^{21}	3.80	$\frac{1}{2}$	22
7D & 8D	ν_1	$\nu_3^\ddagger=300$; $\nu_{11}^\ddagger=1000$ $\nu_{18}^\ddagger=1200$; $\nu_{23}^\ddagger=400$ $\nu_{26}^\ddagger=500$; $\nu_9^\ddagger$, $\nu_{10}^\ddagger$, $\nu_{19}^\ddagger=700$	2	8.29×10^{20}	3.92	$\frac{1}{2}$	22
9	ν_1	Same as 7 & 8	2	1.17×10^{21}	3.33	$\frac{1}{2}$	19
9D	ν_1	Same as 7D & 8D	2	8.92×10^{20}	3.45	$\frac{1}{2}$	19
10	ν_1	Same as 7 & 8	2	1.29×10^{21}	4.92	$\frac{1}{2}$	27/2
10D	ν_1	Same as 7D & 8D	2	9.85×10^{20}	5.04	$\frac{1}{2}$	27/2
11 & 12	ν_1	$\nu_3^\ddagger=300$; $\nu_{28}^\ddagger=1800$ $\nu_{19}^\ddagger=700$; $\nu_{23}^\ddagger=600$ $\nu_9^\ddagger$, $\nu_{12}^\ddagger=1000$	2	7.45×10^{15}	4.41	0	11
11D & 12D	ν_1	Same as 11 & 12 except $\nu_9^\ddagger=700$ and $\nu_{23}^\ddagger=400$	2	5.58×10^{15}	4.52	0	11

[a] Reaction as in Fig. 1.
[b] The vibrational frequency in the molecule-ion which is taken to be the reaction coordinate in the decomposition.
[c] Activation energy ϵ in ergs/molecule$\times10^{12}$.

(a) Activation Energies

The activation energies for reactions 2–5 and 8–11 in propane were taken directly as differences in the corresponding appearance potentials indicated to be the "best values" by Field and Franklin.[5] This assumption, not entirely consistent with the quasi-equilibrium theory used in these calculations, is discussed in Sec. V of this paper.

Activation energies for reactions 1, 6, 7, and 12 had to be estimated since the necessary appearance potential measurements have not been made on deuterated molecules. The activation energy for reaction 1 was taken as greater than that for reaction 2 by the difference in primary and secondary C—H bond energies given by Szwarc.[6] This is equivalent to assuming the ionization potentials for primary and secondary propyl radicals are equal. Stevenson[7] has determined values for these quantities which are slightly different, but the uncertainties are such that the simpler assumption was used here. The activation energy for reaction 6 was taken to be 0.3×10^{-12} erg/molecule§ greater than that for reaction 5; this small difference was found to be necessary in the calculations and is reasonable. The activation energies for reactions 7 and 12 were assumed equal to those for reactions 8 and 11, respectively; the calculated results are insensitive to small changes in these values.

[5] F. H. Field and J. L. Franklin, *Electron Impact Phenomena and the Properties of Gaseous Ions* (Academic Press, Inc., New York, 1957), pp. 252–260.

[6] M. Szwarc, Discussions Faraday Soc. **10**, 336 (1951).
[7] D. P. Stevenson, Trans. Faraday Soc. **49**, 867 (1953).
§ 1.0×10^{-12} erg/molecule = 0.624 v.

TABLE III. Frequency groups for propane and propane-2,2-d_2 ions.

Designation	Type of vibration	Frequency (cm^{-1}) propane	propane-2,2-d_2
ν_1, ν_2	C—X[a] stretching	3000	2100
ν_3–ν_8	C—H stretching	3000	3000
ν_9, ν_{10}	C—X bending	1400	1000
ν_{11}–ν_{16}	C—H bending	1400	1400
ν_{17}, ν_{18}	C—C stretching	900	900
ν_{19}–ν_{22}	CH_3 rocking	1000	1000
ν_{23}, ν_{24}	CX_2 rocking	1000	1000
ν_{25}	C—C—C bending	375	375
ν_{26}, ν_{27}	CH_3 rotation	$I_{CH_3}=4.7\times10^{-40}$ g-cm^2	
ν_{28}[b]	C=C stretching	1600	1600

[a] X represents H in propane and D in propane-2, 2-d_2.
[b] Not a frequency in propane but used in the representation of the ground state of the reactant in the secondary reactions 11 and 12.

The activation energies for the reactions of propane-d_2 are the same as the corresponding values for the nondeuterated molecule, corrected for the changes in zero point energy in ground and activated complex states

$$\epsilon_D=\epsilon_H+\tfrac{1}{2}h\Big[\sum_{i=L+1}^{N}(\nu_{iH}-\nu_{iD})-\sum_{i=L^\ddagger+1}^{N-1}(\nu_{iH}{}^\ddagger-\nu_{iD}{}^\ddagger)\Big],$$

where $\epsilon_H=\Delta H^\ddagger$ for the undeuterated molecule and the symbols have the meanings given following Eqs. (1) and (2). The frequencies used in these calculations are discussed in the following paragraphs. The resulting values for the activation energies ϵ_D and ϵ_H for the several reactions are listed in Table II.

(b) Frequency Factors

While good values are available for the vibrational frequencies of the propane molecule, no data are available for the molecule-ion, either ground state or activated complex. If it is assumed that the electron lost in forming the ion comes from a molecular orbital spread out over the entire molecule, then the loss of one electron out of twenty should have relatively little effect upon the normal mode frequencies. Consequently, the frequencies for propane-d_0 ion are taken as those for propane,[8] rounded off and grouped together as indicated in Table III. The frequencies for propane-d_2 are taken to be the same except for the C—D frequencies which are reduced by a factor of $1/\sqrt{2}$.

There is certainly some hindrance to methyl group rotation in propane ion. However, it is probable that the barrier is much lower than the mean energy per degree of freedom in a molecule with sufficient energy to dissociate by any path. Hence, the free rotor approximation seems most suitable.

The activated complex frequencies are merely reasonable guesses. In general, all frequencies not directly affected by the change in structure in going to the activated complex configuration are assumed to remain unchanged. Those frequencies which are changed and their values in the activated complexes of the several reactions are given in Table II. In reactions 1 and 2, a C—H or C—D stretching vibration becomes the reaction coordinate, but all other frequencies are assumed to remain the same. For a reasonable fit of the experimental data a factor of $\frac{1}{2}$ is also required in the frequency factors for these two reactions. The need for an electronic transition to a higher potential energy surface before a lone hydrogen atom can leave the propane molecule-ion would account for such a factor. This means that it cannot be assumed that the basic equation of Rosenstock *et al.*[1],

$$k'(E)=\int_0^{E-\epsilon_0}\frac{\rho^\ddagger(E,\epsilon_0,\epsilon_t)}{\rho(E)}(1/h)d\epsilon_t, \qquad (3)$$

simplifies to Eq. (1), but that a dependence on electronic wave functions must also be included.

In reaction 4, a C—C bond stretching becomes the reaction coordinate, the two CH_3 rocking frequencies associated with the departing methyl radical are greatly lowered, and the C—C—C bending frequency is also lowered. In similar calculations of the mass spectra of aliphatic alcohols, Friedman *et al.*[9] used a frequency factor for C—C bond breakage 100 times as large as that for H abstraction. In the present calculation the frequency factor for reaction 4 is 75 times as large as that for reaction 1, in good agreement with the choice made by Friedman *et al.* for the alcohols.

The remaining reactions, all of which involve the loss of a hydrogen or methane molecule, necessarily proceed through more complicated activated complexes. The small value of the excess of $\Delta H^\ddagger$ over ΔH for these reactions[2] indicates that the activated state must be a tight ring complex in which relatively strong new bonds form as the initial bonds lengthen and weaken. For example, in reaction 3 in the d_2 compound, a C—D and a C—H stretching combine to yield the reaction coordinate and an oscillation of H—D relative to C—C. Two C—D bending frequencies and a C—H bending frequency are reduced due to the lengthening of the C—D and C—H bonds. A CH_3 rocking frequency is also assumed to decrease in the activated complex. A C—C stretching goes over part way into a C=C stretching vibration and is thus increased in frequency. Finally, the formation of the "tight" ring complex will stop the free rotation of one methyl group and replace it by a torsional oscillation.

In reaction 5, loss of methane, one C—C stretching becomes the reaction coordinate while the other such frequency increases. The two CH_3 rocking frequencies associated with the departing methyl group are assumed to decrease markedly. The formation of a "tight"

[8] G. Herzberg, *Infrared and Raman Spectra of Polyatomic Molecules* (D. Van Nostrand Company, Inc., New York, 1945).

[9] Friedman, Long, and Wolfsberg, J. Chem. Phys. **27**, 620 (1957).

ring activated complex stops the free rotation of both methyl groups. Reaction 6, the last of the primary reactions, is assumed to differ from 5 only in the increase of a C—D rocking frequency resulting from a second link to the departing deuterium atom in the activated complex. Clearly, these choices are quite arbitrary and other choices giving the same frequency factors could be made. We prefer this method over the simpler method of Friedman *et al.*[9] in that it does insure that the frequency factors are reasonable in terms of a physical picture, and also in order to be able to discuss quantitatively the effect of deuterium substitution.

(c) Secondary Reactions

The selection of activated complex frequencies for the secondary reactions proceeds in an analogous manner. However, the calculated R.A.'s in Table I are much less sensitive to a variation in secondary reaction frequency factors than to variation in those just discussed. Secondary reaction rate constants are used only in determining the energy E_a necessary in the parent propane molecule-ion for a secondary reaction to follow its corresponding primary reaction. Before demonstrating the above mentioned insensitivity, we will consider the method of calculating E_a.

The time scale for mass analysis in a mass spectrometer is such that if the rate constant, k, for a reaction is much greater than 10^6 sec^{-1}, only product is observed. Similarly, if $k \ll 10^6$, only reactant is observed. As k changes very rapidly with E when k is about 10^6 sec^{-1} (see Fig. 2), negligible error is introduced by assuming $k=10^6$ as a cutoff point below which only reactant and above which only product is formed in cases where competing reactions do not exist. Then, for primary product ions to have the critical energy, E_b, necessary to undergo secondary decomposition with $k=10^6$ sec^{-1}, the parent ion must have had, on the average, some larger energy, E_a. This energy is given by

$$E_b=(n_b/n_a)(E_a-\epsilon_p+\Delta H_r), \qquad (4)$$

where n_a = number of internal degrees of freedom in the reactant molecule-ion of the primary reaction, n_b = number of internal degrees of freedom in the ionic product of the primary reaction, ϵ_p = activation energy of the primary reaction in the forward direction, and ΔH_r = activation energy for the reverse process. The ratio of degrees of freedom in Eq. (4) results from assuming an approximate equipartition of energy between the degrees of freedom of the ionic and neutral products of the unimolecular decomposition. Large statistical fluctuations in energy distribution between primary product ion and neutral fragment certainly occur, and some energy must be transferred to the new rotational and translational degrees of freedom resulting from the dissociation. To modify Eq. (4) to include these effects would only require the introduction of more approximations and computational difficulties without any certain increase in reliability of the calculations.

The value of E_b is given directly by Eq. (1) with $k=10^6$ sec^{-1}. For simple bond break, as in reactions 1, 2, and 4, ΔH_r is taken as 0. In reactions 3, 5, and 6, the same expression is used with a ΔH_r of 10 kcal/mole as suggested by the tabulations of Rosenstock.[2] The reason for such an activation energy is more readily understood by visualizing, for example, the reversal of reaction 3. The neutral hydrogen molecule is forced to surmount a steric potential energy barrier as it approaches the double bond in the $C_3H_5D^+$ molecule-ion. This barrier is only partially compensated for by the ion-induced dipole interaction of the reactants.

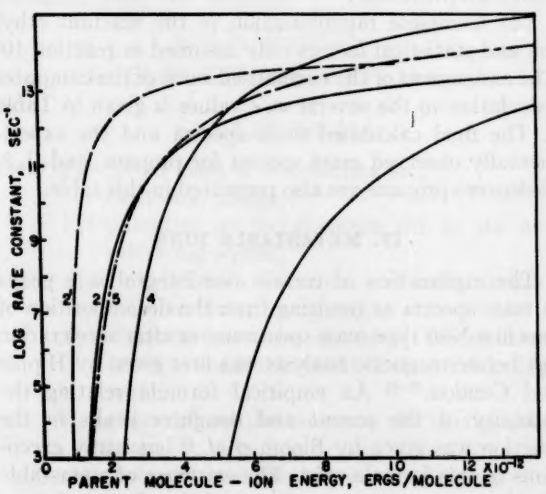

FIG. 2. Semilog plot of unimolecular decomposition rate constants *vs* energy E of the parent molecule-ion, $C_3H_8^+$. The curve numbers are the same as the reaction numbers of Fig. 1. The 2′ curve is a plot of the rate constant for reaction 2 *vs* E with the value of the exponent $N-(\frac{1}{2}L)-1$ of Eq. (1) reduced from 25 to 8 following the suggestion of Chupka.[17]

III. CALCULATIONS

The actual numerical calculations were performed on a high speed digital computer (Datatron Model 205). The values for z_i and $(L-L^\ddagger)/2$ as given in Table II were introduced into the computer which then calculated

$$k_i(E)=z_i(1-\epsilon_i/E)^{25}(E-\epsilon_i)^q, \quad q=\tfrac{1}{2}(L-L^\ddagger),$$

for the six primary reactions at values of E from 0 to 20×10^{-12} erg/molecule at intervals of 0.2×10^{-12} erg/molecule. Figure 2 is a plot of the rate constants for several of the propane reactions *vs* energy in the parent molecule-ion. Parent ions having an E such that $\sum_i k_i < 10^6$ sec^{-1} were assumed to be collected as such. Parent ions having energies greater than that giving $\sum_i k_i = 10^6$ sec^{-1} yield the several primary product ions in the ratios of $k_j/\sum_i k_i$. For energies in the parent greater than E_a, each primary product ion was assumed

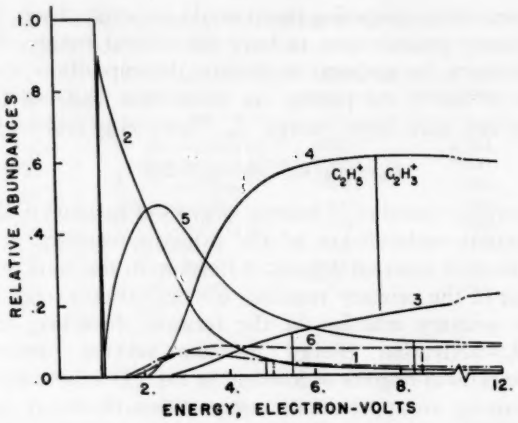

FIG. 3. Breakdown diagram for $C_3H_8^+$. The numbers adjacent to the curves are the same as the reaction numbers of Fig. 1.

to decompose completely to give its secondary product. For example, since $E_a = 12.10 \times 10^{-12}$ erg/molecule for reaction 4, the expression

$$I_4 = k_4(E) / \sum_{i=1}^{8} k_i(E)$$

gives the relative abundance of $C_2H_5^+$ in the mass spectrum of propane from propane ions having an excitation energy $E < 12.10 \times 10^{-12}$ ergs/molecule, and gives the relative abundance of $C_2H_3^+$ for $E > 12.10 \times 10^{-12}$ erg/molecule. If z_{10}, the frequency factor for this secondary reaction, were increased by a factor of ten, E_a would be decreased to 11.67×10^{-12}. This ΔE_a of 0.43×10^{-12} erg/molecule would make a negligible difference in the R.A.'s of the reactant and the product of the secondary reaction, 10, as calculated in the final integration. The resulting curves indicating the fraction of the parent ion yielding the several products are plotted as a function of energy in Fig. 3. The breakpoints above which the decompositions to secondary products are assumed to occur are indicated by vertical lines.

Following the calculation of the R.A.'s at the one hundred values of E, a probability function weighting each parent energy is introduced. The function used, which is consistent with what little is known concerning the excess excitation given molecules on ionization,[1] is

E, erg$\times 10^{12}$/molecule	$P(E)$
0.0 − 12.0	1.0
12.0 − 20.0	0.4
> 20.0	0.0.

The required numerical integration is performed by simply obtaining the sums of the several products

$$\sum_{E} P(E) I_i(E),$$

where each summation is taken over the energy range appropriate to a given primary or secondary product; the parent ion is given by $\sum P(E)$ over the range where $\sum k_i < 10^6$ sec^{-1}, as previously discussed. The final step in the machine calculation is the normalization of these sums to a "total ionization" of 100.

In the propane mass spectrum the calculated products of the several reactions are combined in giving the intensities of some ions. For example, reactions 1 and 2 are combined to give the calculated R.A. of mass 43. On the other hand, in the calculated propane-d_2 mass spectrum it is necessary in several instances to split up the calculated product of a reaction among several mass ratios.

An exact treatment would require the consideration of the rates of all possible rearrangement reactions of all reactant ions and of all possible decomposition reactions for the several rearranged species. It is easily seen that such a calculation for the loss of H_2 and analogs from, say $CH_3CD_2CH_2^+$ would be difficult even with the Datatron and with the necessary data. Here, the simplifying approximations previously discussed with reference to Fig. 1 were made:

(a) No rearrangement in parent molecule-ion, nor in ethylene ion.

(b) Fragment ions with mass 42 to 36 (propane-d_2) or 41 to 36 (propane-d_0) lumped together in the final comparison.

(c) In reaction 7, H_2 loss to give mass 43 from propane-d_2 assumed to occur in 0.4 of the dissociations, as calculated assuming loss of any pair of atoms, H_2, HD, or D_2, from $CH_3CD\ CH_2D^+$. (Approximately the same factor, between 0.3 and 0.5, is obtained for such loss from other rearranged structures and by more restricted processes.)

(d) Complete randomization in the reactant ethyl ion and statistical factors only assumed in reaction 10. The assignment of the normalized sums of the computer calculation to the several m/e values is given in Table I. The final calculated mass spectra and the experimentally observed mass spectra for propane and 2,2-di-deutero-propane are also presented in this table.

IV. METASTABLE IONS

The explanation of certain non-integral m/e peaks in mass spectra as resulting from the decomposition of ions in a Nier type mass spectrometer after acceleration but before magnetic analysis was first given by Hipple and Condon.[10-12] An empirical formula relating the intensity of the parent and daughter peaks in the reaction was given by Bloom *et al.*,[13] but many exceptions to this formula exist. The existence of metastable ions is a necessary consequence of the theory of mass

[10] J. A. Hipple and E. U. Condon, Phys. Rev. **68**, 54 (1945).
[11] Hipple, Fox, and Condon, Phys. Rev. **69**, 347 (1946).
[12] J. A. Hipple, Phys. Rev. **71**, 594 (1947).
[13] Bloom, Mohler, Lengel, and Wise, J. Research Natl. Bur. Standards **40**, 437 (1948).

spectra assumed in this paper,[1,14] and the calculation of the R.A.'s of the metastable ion peaks requires no further assumptions over those necessary to calculate the normal peaks.

According to the assumptions made concerning energy transfer during the inelastic collision between an electron and a molecule, molecule-ions will be found with all degrees of excitation energy, from zero to the energy of the incident electron minus the ionization potential. Thus, depending upon their energies E, ions will be formed which are capable of decomposing with rate constants having values from 0 to about 10^{14} sec^{-1} as given by Eq. (1). The geometry and accelerating voltages of the mass spectrometer are such that only those ions with $k \approx 10^6$ sec^{-1} have a reasonable probability of decomposing in the proper region to be collected as metastable ions. Those ions having rate constants in the range 10^6 $sec^{-1} < k < 10^7$ sec^{-1} will mostly decompose in the accelerating and focusing region and contribute to the background, while those ions having k in the neighborhood of 10^5 sec^{-1} will mostly collide with the walls of the analyzer tube and be lost.

The fraction of the parent ions decomposing by a particular primary reaction path, at a specific internal energy E of the parent, that are collected as metastable ions is given by

$$D_i = [k_i(E)/\sum k_i(E)] \exp[-\sum k_i(E) t_2] \{1-\exp[-\sum k_i(E)\tau]\}.$$

In this equation, t_2 is the time between formation of an ion and its entrance into the region in which decomposition will result in the ion being collected as a "metastable" ion, and τ is the time spend by the ion in this latter region. For a 180° mass spectrometer, these times are calculated from the relations

$$t_1 = (2s_1{}^2 M_0/eV_1)^{\frac{1}{2}},$$

$$t_2 = (s_2/V_2)(2M_0/e)^{\frac{1}{2}}[V_2^{\frac{1}{2}} - V_1^{\frac{1}{2}}] + t_1,$$

and

$$\tau = (M_0{}^2\theta^2/2eV_2)^{\frac{1}{2}},$$

where M_0 = initial mass of the reacting ion,
e = electronic charge,
V_1 = potential on the entrance slit to the accelerating region,
t_1 = time between ionization and entrance into main accelerating region,
s_1 = distance from the center of the electron beam to the entrance slit of the accelerating region,
V_2 = potential on the entrance slit to the analyzer,
s_2 = distance across the accelerating region,
r = radius of the ion beam in the analyzer, and
θ = angular region of the analyzer in which dissociation yields metastable ions.

[14] Rosenstock, Wahrhaftig, and Eyring, J. Chem. Phys. **23**, 2200 (1955).

TABLE IV. Calculated and observed relative abundances of metastable ions in the mass spectrum of propane-d_0.

$m^* = m_f{}^2/M_0$[a]	R.A.[b] Calc.	R.A.[c] Obs.	R.A.[d] Obs.
$42.02 = 43^2/44$	0.32		
$39.09 = 41^2/43$	0.17	0.043	0.04
$38.1 = 40^2/42$	0.054		
$37.1 = 39^2/41$			0.02
$35.1 = 37^2/39$			0.007
$25.1 = 27^2/29$	0.34	0.074	0.06
$24.1 = 26^2/28$	0.17	0.009	0.010
$17.8 = 28^2/44$	0.047		0.008

[a] m^* = apparent mass of ion, M_0 = mass of the ion during acceleration, and m_f = mass of the ion during analysis.
[b] Calculated and observed relative abundances are both normalized to a total ionization of 100.
[c] Serial No. 3 from the *Catalog of Mass Spectral Data*, Am. Petroleum Institute Research Project 44 (National Bureau of Standards, Washington, D. C., 1947).
[d] Private communication from H. M. Rosenstock and C. E. Melton at Oak Ridge, Tennessee, 1955. The area of a peak was taken as the peak height times the half-width. These data were obtained after initial calculations indicated that the peak at $m/e = 17.8$ should be observable.

The fraction of the parent ions that produce metastable ions by a secondary reaction with rate constant k_{is}, following a primary reaction with rate constant k_i, at a given value of E is

$$D_{is} = [k_i(E)/\sum_i k_i(E)]\{1 - \exp[-\sum k_i(E) t_1]\} \cdot \exp[-k_{is} t_2][1 - \exp(-k_{is}\tau)],$$

where the terms are as previously defined. For values of k_{is} of the order of 10^6 sec^{-1}, $\sum_i k_i t_i > 10^4$, and the second term of this expression is essentially unity.

Since electrostatic scanning was used in determining the experimental relative abundances of the metastable ions,[15] the potentials V_1 and V_2 are first determined for the apparent masses of the "metastable ions" of the several reactions. The foregoing quantities, D_i and D_{is}, were then calculated at intervals in E of 0.04×10^{-12} ergs/molecule for each reaction over the range of E of interest, summed, and normalized to give the relative intensity of a specific metastable peak. The results are listed in Table IV.

The expressions given above are those for a 180° instrument such as the Consolidated Electrodynamic Corporation Model 21-102, in which there is no field free region between accelerating region and magnetic analyzer. The value used for θ in these calculations, 8°, is the one suggested by Hipple[12] as appropriate for his apparatus. The corresponding equation for D_i in a Nier type sector instrument will be the same, except for differences in the expressions for t_2 and τ. The resulting changes in time scale will be small and not change the results significantly.

In the calculation of the major peaks, the value of 10^6 sec^{-1} for the summation of the primary rate con-

[15] *Catalog of Mass Spectral Data*, Am. Petroleum Institute Research Project 44 (Carnegie Institute of Technology, Pittsburgh, Pennsylvania, 1947).

stants, or for a secondary rate constant was taken as a sharp cutoff determining whether collected ions were product or reactant. Actually, as indicated in this section, the situation for 10^5 sec$^{-1}<k_i<10^7$ is more complicated. However, as may be seen from the curves of Fig. 2 and the intensities tabulated in Table IV, the energy region over which such a change occurs is such a small fraction of the total that negligible error results in the calculation of the major peaks.

It is seen that the calculated R.A.'s for the metastable peaks listed in Table IV are all larger than the observed R.A.'s for both sets of data. The ratios, R.A. (calc.) to R.A. (obs.), are between three and six for all peaks except $m^*=24.1$, for which the ratio is about 19. No detailed studies of collection efficiencies for metastable ions have been made, but a low efficiency is quite possible so that the above ratios are reasonable, except for the reaction $C_2H_4^+\rightarrow C_2H_2^+ + H_2$.

V. CONCLUSIONS

It may be seen from the results tabulated in Tables I and IV that these calculations based upon the quasi-equilibrium theory of mass spectra are in reasonable agreement with experiment. In particular, no special assumptions are required to obtain the agreement noted for the effect of deuterium substitution and for the relative abundances of the "metastable ions." While the number of parameters to be assigned in calculating the frequency factors z_i is large, and the range of activation energies consistent with the appearance potentials obtained by the various investigators is considerable,[5] it was found that the nature of the theory places very definite limits upon the range possible for the calculated relative abundances of the ions. No choice of frequencies and energies that seemed to us to be consistent with present experimental evidence and knowledge of activated complex structures gave a sufficiently low value for the rate of C—H bond break. A previous assertion, based upon the first calculations, that "much better agreement with the data could be obtained by several recalculations, slightly modifying the assumed frequencies and the initial energy distribution of the parent ions"[16] was overly optimistic. As long as one assigns plausible values to parameters such as the vibration frequencies in the activated state, the calculated propane mass spectra do not agree with the observed spectra to within the experimental error although good qualitative agreement is obtained.

In an article appearing since the completion of these calculations Chupka[17] has shown, using data obtained by photoionization studies with a mass spectrometer, that the quasi-equilibrium theory is qualitatively correct but that more satisfactory quantitative agreement is obtained if the exponent $N-\frac{1}{2}L-1$ in Eq. (1) is divided by approximately three and the range of values of E is reduced by a factor of two. Such a reduction in the effective number of oscillators implies that some of the ionic states are only slowly accessible. Following Chupka's suggestions, we have repeated the propane calculations on the Datatron 205 using the same values of z and ϵ in Eq. (2) as previously, but employing the exponent $(N-\frac{1}{2}L-1)/3$ and the following probability function:

E, ergs$\times 10^{12}$/molecule	$P(E)$
0.0–6.0	1.0
6.0–10.0	0.4
>10.0	0.0.

The calculated R.A.'s of ions in both the propane and propane-2, 2-d_2 mass spectra were in nearly as good agreement with observed values as those listed in Table I. This agreement is surprising since it was obtained on the first calculation, without the laborious readjustments of frequency factors and repeated Datatron 205 calculations that led to the only slightly superior results listed in Table I.

As is also discussed by Chupka, the decrease in the exponent of Eq. (2) will decrease the calculated R.A. of a metastable ion. This, too, is consistent with our calculated results which are all too high. It may be concluded that the agreement obtained in these calculations demonstrates that the quasi-equilibrium theory is capable of explaining isotope effects and metastable ion peaks but that the quantitative agreement obtained cannot be taken as evidence for the particular activation energies and frequency factors selected.

More general objections to the theory applied here have been raised by Friedman *et al.*[18] Certainly, some complicating factors enter in, factors which are not included in the simple approximation of the dissociating ion by a collection of oscillators and rotors. However, we believe that the discussion of Chupka[17] does adequately explain why appearance potentials consistent with bond energies are obtained even though the quasi-equilibrium theory leads to the prediction that for an "ideal" measurement (monoenergetic electrons, gas at 0°K) the observed appearance potential should be well above the thermochemical value. It then follows that the difference in appearance potentials for product ion and reactant ion is the activation energy ϵ in reactions 2–5, the primary reactions of the parent molecule-ion, as was assumed in Sec. II (a).

The situation is far less certain for the secondary reactions. The excess of energy required in the parent molecule-ion to yield a secondary product ion is

[16] Krauss, Wahrhaftig, and Eyring, Ann. Rev. Nuclear Sci. **5**, 253 (1955).
[17] W. A. Chupka, J. Chem. Phys. **30**, 191 (1959).
[18] Friedman, Long, and Wolfsberg, J. Chem. Phys. **30**, 1605 (1959).

several times larger than that required for a primary reaction only, so that the observed appearance potential is likely to be higher than the minimum energy for the process.[17] Also, since the neutral fragment of the primary reactions usually will have some internal energy, the probability of detection of the secondary fragment with electrons of minimum energy for its production will be further reduced. If the activation energy for the primary reaction is greater than the equilibrium ΔH for the reaction, as is assumed for reactions 3, 5, and 6, another complication exists. The excess ΔH_r will appear statistically only in part as internal energy in the primary fragment ion, but should be added, in toto, to the calculated activation energy of the second reaction, if the appearance potentials truly correspond to the lowest possible potentials for the reactions involved. This last effect will in part compensate for the greater error in the secondary product ion appearance potential, if the secondary reaction activation energy is taken as the difference in the appearance potentials determined for propane. Thus, the assumption made is certainly not exact for the secondary reaction activation energies, but is not unreasonable.

In these numerical computations, which are for the mass spectra produced by relatively high energy electrons, the energy spread in electron energy and the thermal energy in the parent molecule change the energy distribution function for the parent molecule-ions by a negligible amount. The effect of energy loss in the neutral fragment and of a ΔH_r in a primary reaction is approximated quite closely by the treatment of Sec. II (c).

Microwave Spectrum and Molecular Structure of Formamide

C. C. COSTAIN AND J. M. DOWLING*

Division of Pure Physics, National Research Council, Ottawa 2, Canada

(Received August 3, 1959)

The microwave spectra of ten isotopic species of formamide (H_2N—CHO) have been investigated. Type *a* and type *b* transitions have been identified and measured for all ten species. The inertial defect is found to decrease whenever a heavier isotope is substituted for any atom in the NH_2 group, and in fact is negative for four of the species studied. It is concluded that the molecule is nonplanar with the H_2N—C group forming a shallow pyramid. The structural parameters deduced from the rotational constants are: r(N—H′, where H′ is *trans* to the aldehyde hydrogen) = 1.014±0.005 A, r(N—H″, where H″ is *cis* to the aldehyde hydrogen) = 1.002±0.005 A, r(N—C) = 1.376±0.010 A, r(C—H) = 1.102±0.010 A, r(C=O) = 1.19$_3$±0.020 A, ∠H′NH″ = 118°53′ ±40′, ∠H″NC = 120°37′±40′, ∠H′NC = 117°9′±40′, ∠NCO = 123°48′±40′, ∠NCH = 113°14′±40′ and ∠OCH = 122°58′±40′. The dihedral angles between the H′NC plane and the NCO plane, and between the H″NC plane and the NCH plane, are 7°±5°, and 12°±5°, respectively.

In all the spectra investigated each line was accompanied by a vibrational satellite line of anomalously high intensity. Measurements of relative intensities were carried out for H_2N^{14}—CHO, *cis*- and *trans*-HDN^{14}—CHO, and D_2N^{14}—CHO. The energy levels (above the zero point) deduced from these measurements show a very large isotope shift, and are interpreted as being due to the first excited state of the NH_2 wagging frequency. A pyramidal model for formamide will have two equilibrium configurations separated by a potential barrier. With a Manning type potential, a barrier of 370±50 cm^{-1}, hindering the "inversion-wagging" type of motion, is determined. The equilibrium value of the normal coordinate calculated from the Manning potential is found to be in good agreement with that found in the structure determination.

1. INTRODUCTION

THE structure of formamide is important not only spectroscopically, but also biologically. From a biological viewpoint it is the simplest molecule containing an N−C−O linkage characteristic of amides and polypeptides. From the spectroscopic as well as chemical viewpoint the N—C bond distance is of particular interest because of its partial double bond character in formamide.

In 1954 Evans[1] reported a study of the vibrational infrared spectrum of gaseous formamide. He concluded from the band envelopes that the two hydrogens bonded to the nitrogen were not coplanar with the N−CHO group, but rather were symmetrically placed above and below this plane. This was in disagreement with an x-ray diffraction study of crystalline formamide carried out by Post and Ladell[2] also in 1954. Their data were consistent with a planar or nearly planar model. In 1955 Kurland[3] reported preliminary results for the microwave spectrum of formamide. This was followed in 1957[4] by a more complete study which included data (type *a* transitions only) for *cis*- and *trans*-HDN^{14}—CHO and D_2N^{14}—CHO. For H_2N^{14}—CHO both the *a* and *b* type spectra were observed, which allowed accurate values of all three rotational constants A_0, B_0, and C_0 to be determined. From the very small positive value of the inertial defect it was concluded that the molecule was planar and with the data from these four species a structure was determined. In a study of the nuclear magnetic resonance of solid formamide Kromhaut and Moulton[5] in 1956 also favored a planar structure for formamide.

The original object of this investigation of formamide was to study the effect of isotopic substitution on the inertial defect. For planar molecules studied in the past, where all three rotational constants have been accurately determined, the inertial defect was found to be positive in sign, and to range[6] from 0.05 (for H_2O)[7] to 0.18 amu A^2 (for propynal).[8] When deuterium was substituted for a hydrogen the inertial defect was usually found to increase by about 0.008 amu A^2. Since formamide has three nonequivalent hydrogens this molecule should provide an excellent opportunity for a study of the inertial defect. However, it was found that the inertial defects were quite anomalous, and could be explained only by a nonplanar structure, with the NH_2—C group forming a shallow pyramid. A study of the intense "inversion" satellites provided a confirmation of the pyramidal structure.

II. EXPERIMENTAL METHODS

The spectra of formamide and its isotopic species were studied in the frequency range 9 kMc/sec to 43 kMc/sec using a square wave Stark modulation spectrograph, details of which have been described elsewhere.[9]

The isotopic species H_2N^{14}—CDO, H_2N^{15}—CHO, and H_2N^{15}—CDO were prepared by Dr. L. C. Leitch

* National Research Council Postdoctorate Fellow, 1957–1959. Present address: Department of Physics, Arizona State University, Tempe, Arizona.

[1] J. C. Evans, J. Chem. Phys. **22,** 1228 (1954).

[2] C. Post and J. Ladell, Acta Cryst. **7,** 559 (1954).

[3] R. J. Kurland, J. Chem. Phys. **23,** 2202 (1955).

[4] R. J. Kurland and E. B. Wilson, Jr., J. Chem. Phys. **27,** 585 (1957).

[5] R. A. Kromhout and G. W. Moulton, J. Chem. Phys. **25,** 35 (1956).

[6] Somewhat smaller values are found for large cyclic compounds containing many hydrogens.

[7] Benedict, Gailor, and Plyler, J. Chem. Phys. **24,** 1139 (1956).

[8] C. C. Costain and J. Morton, J. Chem. Phys. **31,** 389 (1959).

[9] C. C. Costain and B. P. Stoicheff, J. Chem. Phys. **30,** 777 (1959).

TABLE I. Frequencies (in Mc/sec) of rotational lines.

Transition	H_2N^{14}—CHO	H_2N^{14}—CDO	*c*-HDN^{14}—CHO	*t*-HDN^{14}—CHO	D_2N^{14}—CHO
$1_{01}\leftarrow 0_{00}$	21 207.47[a]	20 792.77[a]	20 344.00[a]	19 605.77[a]	18 903.93[a]
$2_{12}\leftarrow 1_{11}$	40 874.91	39 632.17	39 012.18	37 870.71	36 324.63
$2_{02}\leftarrow 1_{01}$	42 386.07	41 521.85	40 646.67	39 189.45	37 774.83
$2_{11}\leftarrow 1_{10}$			42 363.74	40 552.04	39 290.02
$1_{11}\leftarrow 2_{02}$	18 956.06		9 689.15	21 516.74	11 747.37
$3_{03}\leftarrow 2_{12}$		20 435.77	12 166.33		
$4_{04}\leftarrow 3_{13}$	26 924.05[b]		34 639.00	20 751.45	29 328.44
$5_{05}\leftarrow 4_{14}$				42 642.30	
$3_{22}\leftarrow 4_{13}$		40 883.81			
$4_{23}\leftarrow 5_{14}$			39 492.18		
$6_{15}\leftarrow 5_{24}$					22 209.24
$7_{16}\leftarrow 6_{25}$	16 960.96[b]	37 765.17	11 423.09	28 596.20	
Transition	H_2N^{15}—CHO	H_2N^{15}—CDO	*c*-HDN^{15}—CHO	*t*-HDN^{15}—CHO	D_2N^{15}—CHO
$1_{01}\leftarrow 0_{00}$	20 644.33	20 245.78	19 846.70	19 159.33	18 505.25
$2_{12}\leftarrow 1_{11}$	39 824.19	38 632.02	38 096.52	37 031.65	35 586.15
$2_{02}\leftarrow 1_{01}$	41 262.58	40 433.42	39 655.90	38 298.26	36 980.00
$2_{11}\leftarrow 1_{10}$			41 290.30	39 605.82	38 434.56
$1_{11}\leftarrow 2_{02}$	20 131.44		10 897.20	22 298.92	12 649.10
$3_{03}\leftarrow 2_{12}$		18 625.75	10 397.83		
$4_{04}\leftarrow 3_{13}$	24 470.30	41 117.81	32 289.71	18 964.62	27 516.69
$5_{05}\leftarrow 4_{14}$				40 332.08	
$3_{22}\leftarrow 4_{13}$					
$4_{23}\leftarrow 5_{14}$		19 029.94			
$6_{15}\leftarrow 5_{24}$			18 679.65		25 418.95
$7_{16}\leftarrow 6_{25}$	21 933.95	32 595.74			

[a] Corrected for quadrupole coupling.
[b] Taken from Kurland and Wilson.

of the Pure Chemistry Division, N.R.C. The isotopic species *cis*- and *trans*-HDN^{14}—CHO and HDN^{15}—CHO, D_2N^{14}—CHO, and D_2N^{15}—CHO were prepared by mixing suitable quantities of D_2O with the corresponding hydrogen compound.[4] The amide hydrogens (bonded to the nitrogen) are labile, whereas the aldehyde hydrogen (bonded to the carbon) is not. The optimum concentration of cis and trans isomers is 25%, the H_2 and D_2 species making up the rest of the sample. Concentrations of the D_2 species greater than 90% were achieved quite easily by repeated mixings with D_2O followed by removal of the water.

The spectra were recorded at room temperature and at pressures of 4 to 30 μ of Hg. No attempt was made to cool the cell to dry ice temperature in view of the low vapor pressure of formamide. It was found that formamide reacted with the walls of the cell to the extent that it could not be removed by pumping. It was necessary to alternately heat (70–80°C) and cool the cell, and flush the cell with the new species until the undesired species was no longer in evidence.

Attempts were made to locate lines due to the C^{13} and O^{18} species present in natural abundance. These attempts were unsuccessful since the cell could not be cooled to eliminate the many vibrational satellites having the expected intensity of lines due to C^{13} and O^{18} species.

III. OBSERVED SPECTRA AND ROTATIONAL CONSTANTS

Ten isotopic species of formamide were investigated. These are listed in Table I along with the measured frequencies of the rotational transitions. All *a* type transitions were positively identified by their Stark effect. At least one of the *b* type lines (usually the $4_{04}\leftarrow 3_{13}$ or $3_{03}\leftarrow 2_{12}$) was also identified by its Stark effect. In order to further ensure the correctness of the assignments at least two additional *b* type transitions were predicted from the rotational constants and measured. This proved to be a necessity when the spectra of the cis and trans isomers were being investigated, since with four species in the cell at the same time the correct assignment of the type *b* transitions was very difficult.

In part the complexity of the spectrum arises from the presence of a strong satellite line accompanying each main line. For the *a* type spectra these were readily identified, but the satellites of the *b* lines were very difficult to locate because of the large shift from the main line. For H_2N^{14}—CHO the satellite intensity was about 25% of the main line. For D_2N^{14}—CHO the satellite intensity was about 50% of the main line. Quantitative results will be given in another section. The high intensity of these satellites made identification of the type *b* transitions somewhat more difficult.

The quadrupole structure of the $1_{01}\leftarrow 0_{00}$ lines was resolved for the N^{14} species. For the $J=2\leftarrow 1$ transitions however the structure was not resolved. The quadrupole constants reported by Kurland and Wilson[4] were confirmed and the $1_{01}\leftarrow 0_{00}$ transition corrected accordingly.

For all the isotopic species investigated it was possible to identify and measure the $1_{01}\leftarrow 0_{00}$ transition ($\nu = B_0+C_0$) and the $2_{12}\leftarrow 1_{11}$ transition ($\nu = B_0+3C_0$).

TABLE II. Rotational constants and moments of inertia.

Constant	H_2N^{14}—CHO	H_2N^{14}—CDO	c-HDN^{14}—CHO	t-HDN^{14}—CHO	D_2N^{14}—CHO
A_0 Mc/sec	72 716.12	54 948.39	61 345.91	71 179.61	59 715.99
B_0	11 373.75	11 373.07	11 009.91	10 473.30	10 193.58
C_0	9 833.72	9 419.70	9 334.09	9 132.47	8 710.35
I_A^0 amu A^2	6.9521	9.2001	8.2407	7.1022	8.4656
I_B^0	44.447_2	44.449_8	45.916_0	48.268_5	49.593_1
I_C^0	51.407_9	53.667_4	54.159_6	55.355_3	58.038_0
Δ	$+0.008_6$	$+0.017_5$	$+0.002_9$	-0.015_4	-0.020_7
Constant	H_2N^{15}—CHO	H_2N^{15}—CDO	c-HDN^{15}—CHO	t-HDN^{15}—CHO	D_2N^{15}—CHO
A_0 Mc/sec	72 448.61	54 733.59	61 275.15	70 820.47	59 594.17
B_0	11 054.40	11 052.66	10 721.79	10 223.17	9 964.80
C_0	9 589.93	9 193.12	9 124.91	8 936.16	8 540.45
I_A^0 amu A^2	6.9778	9.2362	8.2502	7.1382	8.4829
I_B^0	45.731_2	45.738_4	47.149_9	49.449_5	50.731_7
I_C^0	52.714_8	54.990_1	55.401_2	56.571_4	59.192_5
Δ	$+0.005_8$	$+0.015_5$	$+0.001_1$	-0.016_8	-0.022_1

Neglecting the small effects due to centrifugal distortion these transitions were used to determine B_0 and C_0. The rotational constant A_0 was then determined from the $1_{11}\leftarrow 2_{02}$ transition ($\nu = A_0 - 3B_0 - 2C_0 +$ terms in the asymmetry parameter b_p) when possible. When this transition was not in the range of the spectrometer the $3_{03}\leftarrow 2_{12}$ transition ($\nu = -A_0 + 5B_0 + 2C_0 +$ terms in the asymmetry parameter b_p) was used. Since all these transitions involve low quantum numbers ($J \leq 3$, $K_a \leq 1$) the energy levels are only slightly affected by centrifugal distortion and should give quite accurate values for the ground state rotational constants. The rotational constants are given in Table II along with the corresponding moments of inertia[10] and inertial defects.

The behavior of the inertial defect is clearly anomalous. Not only does the inertial defect decrease when a heavier atom is substituted on the NH_2 group, but in four of the species studied it is negative. Such behavior would be expected if formamide were slightly nonplanar. The inertial defect does increase when deuterium is substituted for the aldehyde hydrogen. This indicates that this atom is very close to the *ab* (principal) plane.

IV. MOLECULAR STRUCTURE

In 1953 Kraitchman[11] formulated the problem of structure determination in terms of the changes in the moments of inertia between isotopically substituted molecules. For a nonplanar asymmetric top Kraitchman's formulation can be summarized as follows:

$$c^2 = \langle (1/\mu)(P_c' - P_c)[1 + (P_a' - P_a)/(P_a - P_c)] \cdot [1 + (P_b' - P_b)/(P_b - P_c)] \rangle, \quad (1)$$

where

$$1/\mu = [(M + \Delta M)/M\Delta M], \quad (2)$$

and

$$P_a = \sum_i m_i a_i^2 = \tfrac{1}{2}[I_c - I_a - I_b]. \quad (3)$$

Here I_a, I_b, and I_c are the principal moments of inertia, the P's are the second moments, defined by Eq. (3), M is the total mass of the "original" molecule, and ΔM is the mass change on isotopic substitution. In Eq. (1) the primed quantities refer to the isotopically substituted molecule and the unprimed quantities to the "original" molecule; Eqs. (1) and (3) are cyclical in a, b, and c. The quantities a, b, and c are the coordinates of the substituted atom in the principal axis system of the "original" molecule. While Eq. (1) gives only the absolute value of the coordinates of the substituted atom, it is usually a simple matter to decide the relative signs of the coordinates using first moment and cross moment equations along with any chemical evidence for the structure.

Although the coordinates obtained from Kraitchman's equations will not, in general, reproduce the experimentally determined moments of inertia, strong arguments[12] (experimental and theoretical) have been advanced that these coordinates are probably closer to the equilibrium values than those obtained from direct solution of the moment of inertia equations. Inspection of Eq. (1) shows that the requirement for obtaining a real coordinate α (as opposed to an imaginary one) for a positive ΔM is that the quantity $(P_\alpha' - P_\alpha)$ be positive, (where $\alpha = a$, b, or c). For the H to D and N^{14} to N^{15} substitutions on the NH_2 group, this condition is met (although some of the P's are negative) and Kraitchman's equations will therefore give real values for all three coordinates. On the other hand even if $(P_\alpha' - P_\alpha)$ is negative (which for the out-of-plane coordinate of a planar molecule would mean an increased inertial defect) it can only be argued that the

[10] The conversion factor $B_0 \times I_0 = 5.05531 \times 10^5$ Mc/sec/amu A^2 was used.

[11] J. Kraitchman, Am. J. Phys. **21**, 17 (1953).

[12] C. C. Costain, J. Chem. Phys. **29**, 864 (1958).

atom in question must be quite close to a principal plane or axis.[13]

In the case of formamide substitution was made at all hydrogen positions and the nitrogen position. The absolute values of their coordinates were determined by Kraitchman's equations. The c (or out-of-plane) coordinate for the aldehyde hydrogen is imaginary and was taken as zero. Two difficulties in determining relative signs of coordinates were encountered. From the data of H_2N^{14}—CHO, H_2N^{15}—CHO, H_2N^{14}—CDO, and *cis*- and *trans*-HDN^{14}—CHO it was impossible to determine whether the aldehyde hydrogen (H_{a1}) was on the same side or the opposite side of the b axis as the NH_2 group. Likewise it was also impossible to determine whether the two amide hydrogens were on the same side or opposite sides of the *ab* plane. In these instances the data from the other N^{15} species were invaluable.

Regardless of which molecule is chosen as the "original" molecule the structural parameters should be invariant with respect to this choice.[12] This invariance property was used to determine the relative signs of the a coordinate of the N and H_{a1} nuclei. First the N—H_{a1} distance was computed by assuming the two nuclei were on opposite sides of the b axis, and using H_2N^{14}—CHO as the original molecule and H_2N^{15}—CHO and H_2N^{14}—CDO as the substituted species. The result was

$$r(\text{N—H}_{a1}) = 2.076_0\text{A}.$$

Now using H_2N^{15}—CHO as the original molecule and H_2N^{14}—CHO and H_2N^{15}—CDO as the substituted species (again assuming the two nuclei were on opposite sides of the b axis), one obtains

$$r(\text{N—H}_{a1}) = 2.072_4\text{A}.$$

Then exactly the same calculations were carried out assuming both nuclei were on the same side of the b axis. The two results are

r(N—H_{a1}, N^{14} formamide as the original molecule) = 1.983_1A,

r(N—H_{a1}, N^{15} formamide as the original molecule) = 1.952_5A.

Clearly the two nuclei are on opposite sides of the b axis.

The same type of analysis was carried out for the H—H distance in the NH_2 group. The results are summarized in Table III. The invariance of the H—H distance for both hydrogen nuclei being on the same side of the *ab* plane is within the experimental error, whereas the invariance for the two nuclei being on opposite sides of the *ab* plane is just outside the experimental error. The same results are obtained if one considers each of the N—H distances separately. In analogy with the structure of molecules such as ammonia and methylamine a pyramidal model for the H_2N—C group would be favored over a planar (or almost planar) NH_2 group twisted with respect to the HCO group. It is therefore concluded that the H_2N—C group forms a shallow pyramid.

[13] See for instance D. K. Coles and R. H. Hughes, Phys. Rev. **76**, 178A (1949).

TABLE III. The invariance of the H—H distance.

Original molecule	r(H—H), hydrogens on same side of *ab* plane	r(H—H), hydrogens on opposite side of *ab* plane
H_2N^{14}—CHO	1.735_6 A	1.743_5 A
D_2N^{14}—CHO	1.733_6 A	1.739_0 A
H_2N^{15}—CHO	1.737_7 A	1.744_8 A
D_2N^{15}—CHO	1.733_8 A	1.739_4 A

Since no isotopic substitution was made for the carbon or oxygen atoms, these atoms were located by using first moment equations, cross moment equations, and $P_b(=\sum_i m_i b_i^2)$ for H_2N^{14}—CHO. P_b was used rather than P_a since it was quite evident that the a coordinate of the carbon nucleus was quite small, and as pointed out previously[12] this could lead to a large error in the determination of this coordinate. The errors introduced by using the moments of inertia directly (or the P's) will be the least when locating heavy atoms not too close to a principal plane or axis. The results gave a complete structural determination for formamide. This preliminary structure proved the N—CHO group to be planar within the experimental error.

A second determination of the structure was made in which the planarity of the N—CHO group was used in place of the cross moment equations containing the small inaccurate out-of-plane c coordinates. In addition an attempt was made to correct the P_c moments for the effects of zero point vibration. This was done by adding 0.0047 amu A^2 to each P_c' in which D substitution had been made; i.e., for H_2N^{14}—CDO, H_2N^{15}—CDO, *cis*- and *trans*-HDN^{14}—CHO, and HDN^{15}—CHO. This is the order of magnitude correction one would have to apply to a planar molecule for $(P_c'-P_c)$ to be zero for a single hydrogen-deuterium substitution. The particular value of 0.0047 amu A^2 was derived from the H_2N^{14}—CHO and H_2N^{14}—CDO pair, and the H_2N^{15}—CHO and H_2N^{15}—CDO pair. This small correction did not affect the gross structural parameters (bond lengths and interbond angles) to any large extent, but as expected did have a considerable effect on the out-of-plane coordinates. Independent determinations of the preliminary and corrected structures were also made using the N^{15} species as the original molecule. The four sets of structural parameters are listed in Table IV along with those reported in previous investigations.

V. SATELLITES AND "INVERSION"

As mentioned previously the spectra of all the species investigated were complicated by the presence of a

TABLE IV. The structural parameters of formamide.

Parameter	Preliminary structure		Final structure			
	N^{14} coord. system	N^{15} coord. system	N^{14} coord. system	N^{15} coord. system	Kurland and Wilson[a]	Others
r(N—H′)	1.010 A	1.010	1.014	1.014	0.995	1.036[b]
r(N—H″)	0.999	0.999	1.002	1.001	0.995	1.036[b]
r(N—C)	1.376	1.377	1.375	1.376	1.343	1.300[c]
r(C—O)	1.194	1.192	1.194	1.192	1.243	1.255[c]
r(C—H″)	1.102	1.103	1.102	1.103	1.094	
∠H′NH″	119°31′	119°50′	118°43′	119°3′	118°58′	120°[b]
∠H″NC	120°21′	120°19′	120°35′	120°38′	120°31′	
∠H′NC	117°6′	117°6′	117°10′	117°9′	120°31′	
∠NCO	123°39′	123°39′	123°48′	123°48′	123°35′	121°30′[c]
∠NCH	113°20′	112°53′	113°27′	113°1′	103°54′	
∠OCH	122°41′	123°7′	122°45′	123°11′	132°31′	
$\angle_D$H′N—CO	11°21′	10°56′	7°12′	6°43′	...	
$\angle_D$H″N—CH	15°1′	14°25′	12°52′	11°18′	...	

[a] See reference 4.
[b] See reference 5.
[c] See reference 2.

TABLE V. Frequencies of the $1_{01}\leftarrow 0_{00}$ transitions (ground and first excited states), relative intensities, and deduced "vibrational" frequencies for H_2N^{14}—CHO, *c*-HDN^{14}—CHO, *t*-HDN^{14}—CHO, and D_2N^{14}—CHO.

	H_2N^{14}—CHO	*c*-HDN^{14}—CHO	*t*-HDN^{14}—CHO	D_2N^{14}—CHO
$1_{01}\leftarrow 0_{00}$ Mc/sec	21 207.5	20 344.0	19 605.8	18 903.9
Sat $1_{01}\leftarrow 0_{00}$	21 190.7	20 341.2	19 621.6	18 929.5
δ	+16.8	+2.8	−15.8	−25.6
I (relative)	$0.23_3\pm0.05$	$0.33_3\pm0.05$	$0.30_7\pm0.05$	$0.44_3\pm0.05$
ν (cm^{-1})	304±45	229±35	246±35	170±25

strong satellite accompanying each line. Quantitative measurements were made for four molecules, H_2N^{14}—CHO, D_2N^{14}—CHO, and *cis*- and *trans*-HDN^{14}CHO for the $1_{01}\leftarrow 0_{00}$ lines, and their respective satellites. The results are given in Table V. The relative intensities are based on the measurement of integrated absorption curves, with at least four runs made for each line. The error quoted represents at least twice the average deviation for the average of all measurements for a particular species. Since there are no equivalent atoms, and thus no degeneracy, the energy levels are given directly by the Boltzman factor. These energy levels (in cm^{-1}) are given in the last column of Table V.

The vibration must involve primarily the hydrogen nuclei in view of the large isotope shift. In fact the isotopic ratio between the H_2 and D_2 species is 1.79, far more than the maximum expected ratio of 1.414 for a pure harmonic vibration. Then too the positions of the satellite lines with respect to the main lines are somewhat anomalous. In the case of the H_2 species the satellite is 17 Mc/sec below the main line, whereas in the D_2 species the satellite line is 26 Mc/sec above the main line. In extreme cases (such as Q branch lines and some b type transitions) the satellite lines were found displaced as much as 400 Mc/sec from the main line. Although extensive measurements were not carried out on the satellite lines, it does appear that the α associated with this vibration are quite large for at least one of the rotational constants (and possibly two) and are affected greatly by H—D isotopic substitution on the NH_2 group. If the vibration responsible for the satellites were of the typical kind[14] found in polyatomic molecules one would expect the vibrations and its overtones to give rise to a series of equally spaced lines ($B_v=B_0-\alpha_B v$, etc.), with relative intensities given by the Boltzman factor. For the H_2 species a series with the relative intensities 1: $\sim\frac{1}{4}$; $\sim\frac{1}{16}$; ··· would be expected; for the HD species 1: $\sim\frac{1}{3}$; $\sim\frac{1}{9}$; ···; and for the D_2 species 1: $\sim\frac{1}{2}\sim\frac{1}{4}$; $\sim\frac{1}{8}$; ···. Several of these overtone lines should have been readily detected. In fact, only the first satellite corresponding to the fundamental vibration could be identified. This could be due to the intensity falling off faster than expected, and/or the α associated with this vibration being quite different for each energy level. Both of these possibilities imply a very anharmonic potential energy function for this vibration. It can therefore be concluded that the formamide molecule must have a very low energy vibration, involving primarily hydrogen atoms, which is very anharmonic in nature.

[14] That is, with a potential energy function having a single deep minimum, and expressable, for small displacements about the equilibrium configuration of the molecule, in terms of a harmonic oscillator force field perturbed by small anharmonic terms.

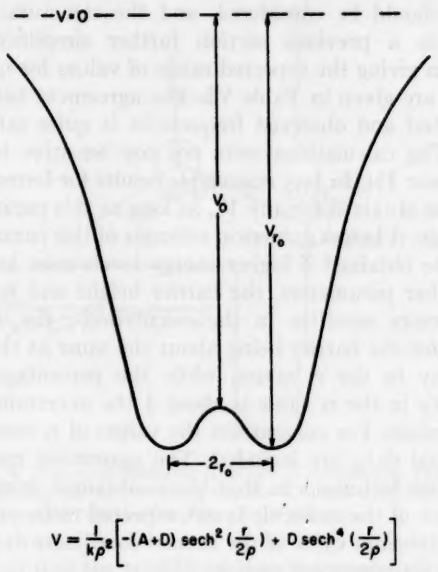

FIG. 1. The (Manning) double minimum potential energy function.

All these facts would be quite difficult, if not impossible, to explain on the basis of a planar model for formamide. For a planar model for formamide the lowest lying fundamental would be expected to correspond largely to a torsion about the N—C bond. In view of the partial double bond character of the N—C bond and the small reduced mass, this vibration should lie at ~ 600 cm^{-1} for the H_2 species and at ~ 500 cm^{-1} for the D_2 species.[15] The only other candidate would be the vibration corresponding to the deformation of the N—C—O angle. This vibration should lie between 500 and 600 cm^{-1} and should show a negligible isotope shift. In addition none of these vibrations would be expected to show extreme anharmonicity.

On the basis of a nonplanar, pyramidal H_2N—C model for formamide all the anomalies can be interpreted. With this model the wagging type frequency of the NH_2 group (the two hydrogen atoms moving against the nitrogen atom perpendicular to the *ab* plane) will be perturbed by a hump or barrier at the bottom of the potential well. This will of course give rise to two equilibrium positions for the hydrogen atoms (on opposite sides of the N—CHO plane). This effect is quite well known in many molecules, the best known and understood being ammonia.

In 1935 Manning[16] was able to obtain an excellent fit for the energy levels of the ammonia inversion spectrum by using the potential energy expression

$$V(r) = (1/k\rho^2)[-(A+D)\,\mathrm{sech}^2(r/2\rho) + D\,\mathrm{sech}^4(r/2\rho)], \quad (4)$$

where A, D, and ρ are arbitrary constants, k the appropriate reduced mass parameter for the type of vibration considered, and r the normal coordinate describing the type of motion. A graph of this potential energy expression is shown in Fig. 1. In order that the potential function have a double minimum at $r=\pm r_0$ (the equilibrium value of the normal coordinate), the following relation must hold:

$$\mathrm{sech}^2(r_0/2\rho) = (A+D)/2D. \quad (5)$$

Thus if r_0 is known (i.e., from structural data) Eq. (5) can be used to eliminate one of the arbitrary constants, or conversely if the three arbitrary parameters have been determined the value of r_0 is fixed by Eq. (5). The values of the potential $V(r)$ at $r=0$, V_0, and at $r=\pm r_0$, Vr_0 are given in terms of the constants A, D, and ρ by

$$V_0 = -A/k\rho^2, \quad (6)$$

$$V_{r_0} = -(A+D)^2/4Dk\rho^2. \quad (7)$$

Since the potential energy should be isotopically invariant the constants A and D will have to be changed in the same ratio as k.

Since r_0 is strictly the equilibrium value of the normal coordinate describing the vibration, it may not be simply related to the geometry of the molecule. If the form of the vibration is known, however, (inversion for ammonia and formamide) a very good approximate value for r_0 can be obtained from the structure of the molecule. In a very symmetrical molecule such as ammonia r_0 is very nearly the height of the NH_3 pyramid. For formamide where the HCO group can be considered as a single heavy mass for the "inversion-wagging" vibration, r_0 will be approximately the distance between the nitrogen nucleus and the two amide hydrogen nuclei measured perpendicular to the *ab* plane.

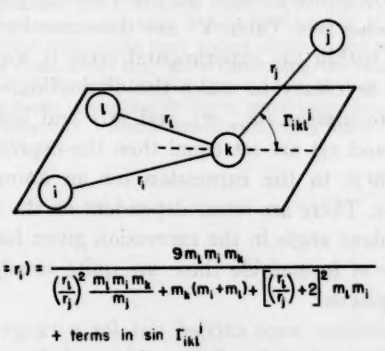

FIG. 2. Assumed molecular model, and reduced mass for the "wagging-inversion" type vibration of formamide.

[15] In a private communication, Dr. W. Schneider (Division of Pure Chemistry, National Research Council of Canada) reports, from a nuclear magnetic resonance study of liquid formamide, a preliminary value of 18±3 kcal/mole for the barrier hindering internal rotation. This barrier gives a torsional frequency for the H_2 species of 600±50 cm^{-1} and for the D_2 species 490±40 cm^{-1}.

[16] M. F. Manning, J. Chem. Phys. **3**, 136 (1935).

TABLE VI. Calculated and observed "inversion-wagging" type frequencies for H_2N^{14}—CHO, *cis*- and *trans*-HDN^{14}—CHO, and D_2N^{14}—CHO, and deduced parameters for Manning type potential.

Molecule	ν_{obs} (cm^{-1})	ν_{calc} (cm^{-1})
H_2N^{14}—CHO	304±45	299
c-HDN^{14}—CHO	229±35	236
t-HDN^{14}—CHO	246±35	236
D_2N^{14}—CHO	170±25	171

Barrier $V_0 - V_{r_0} = 370 \pm 50$ cm^{-1}
$V_{r_0} = 32\ 043$ cm^{-1}
$r_0 = 0.151 \pm 0.009$ A
r_0 (preliminary structure) $= 0.13 \pm 0.02$ A
r_0 (final structure) $= 0.15_5 \pm 0.02$ A

The advantages of using the expression given in Eq. (4) for the double minimum problem are numerous. First of all the Schrödinger wave equation for this potential has been solved exactly and thus recourse to perturbation techniques need not be made. The energy levels are given in terms of the roots of a continued fraction, and can be obtained very accurately. Secondly the expression has been used quite successfully for ammonia and ammonia-d_3. Using the data available at that time (1935), Manning determined the constants in Eq. (4). In order to obtain a reasonable fit for the higher energy levels he found that the inversion splitting of the ground state to be 0.83 cm^{-1} as compared to the experimental value of 0.62 cm^{-1} available at that time. The accepted value at present is 0.793 cm^{-1}. In addition his results gave $r_0 = 0.37$ A as compared with the modern value of 0.3810 A. The agreement between calculated and observed values is indeed striking.

For formamide, a simplified form for the reduced mass was assumed. It is given, apart from a factor of $8\pi^2 c/h$, in Fig. 2 along with the molecular model assumed for describing the vibration. Two simplifications were made, the first being that the heavy end of the molecule can be treated as a single mass (m_j), and the second that the two nitrogen-hydrogen bond distances are equal. Because of these simplications the model chosen will not distinguish between the cis and trans HD isomers. Since the experimentally determined frequencies (see Table V) are the same for these two species within the experimental error it was not considered necessary to make the distinction. If the appropriate masses (m_i, m_j, and m_l) and bond lengths (r_i, r_j, and r_l) are set equal then the expression given will reduce to the expression for an ammonia type molecule. There are terms dependent on the sine of the out-of-plane angle in the expression given for k, but in the case of formamide these are quite small and have been neglected.

Calculations were carried out for a range of values of A, D, and ρ for formamide and its deuterated species. Manning's results for ammonia indicated which range should be considered, and the structural data given in a previous section further simplified the problem giving the expected range of values for r_0. The results are given in Table VI. The agreement between calculated and observed frequencies is quite satisfactory. The calculations were not too sensitive to the parameter V_{r_0}. In fact reasonable results for formamide could be obtained for any V_{r_0} as long as this parameter was large. A better numerical estimate of this parameter could be obtained if higher energy levels were known. The other parameters, the barrier height and r_0 were much more sensitive in the calculations, the uncertainty for the barrier being about the same as the uncertainty in the ν values, while the percentage uncertainty in the r_0 value is about $\frac{1}{2}$ the uncertainty in the ν values. For comparison the values of r_0 from the structural data are included. The agreement may be somewhat fortuitous in that the r_0 obtained from the structure of the molecule is not expected to be exactly the equilibrium value of the normal coordinate describing the wagging type motion.

The lower portion of the Manning potential as fitted to the data of formamide and its deuterated species is given in Fig. 3, along with the final numerical form of the potential energy expression. The lowest three levels of the H_2, HD, and D_2 species are included. The lowest level for each species is below the top of the barrier, whereas the subsequent levels are above. With this very anharmonic potential energy one would expect the α for each of the lowest lying energy levels to be quite different. Also these lowest energy levels deviate quite markedly from the evenly spaced harmonic energy levels. Thus one can explain qualitatively the anomalous behavior of the α associated with this vibration and

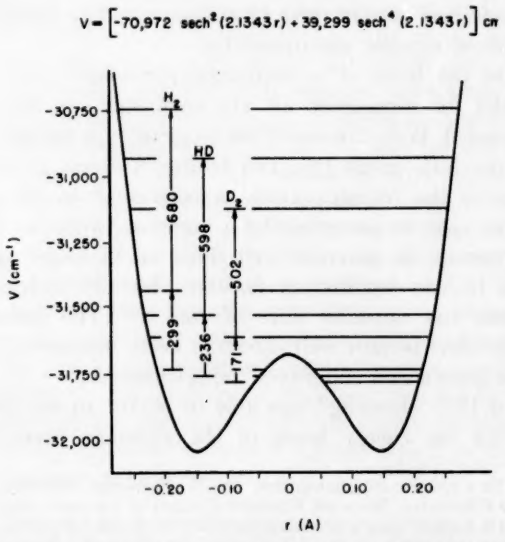

FIG. 3. The lower portion of the (Manning) double minimum potential energy function as fitted to formamide. The three lowest energy levels for the H_2, HD, and D_2 species are shown.

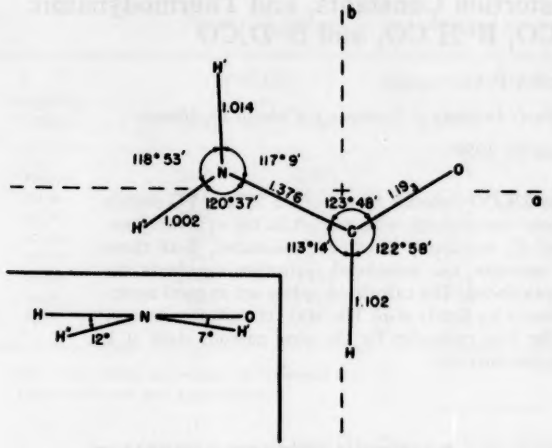

FIG. 4. The most probable structure of formamide. Inset shows the molecule as viewed along the N—C bond with the N–CHO plane perpendicular to the plane of the page.

the fact that the satellites due to the second vibrational state were not detected.

VI. CONCLUSIONS AND DISCUSSION

It is seen that all the data are consistent with a nonplanar structure for formamide, whereas the assumption of a planar model cannot explain some of the gross features in its microwave spectrum. In particular it is concluded that the H_2N—C group forms a shallow pyramid while the N—CHO group is planar. A most probable structure is proposed with the following structural parameters: r(N—H′, where H′ is trans to the aldehyde hydrogen) = 1.014±0.005 A, r(N—H″, where H″ is cis to the aldehyde hydrogen) = 1.002±0.005 A, r(N—C) = 1.376±0.010 A, r(C—H) = 1.102±0.010 A, r(C=O) = 1.19₃±0.020 A, ∠H′NH″ = 118°53′±40′, ∠H″NC = 120°37′±40′, ∠H′NC = 117°9′±40′, ∠NCO = 123°48′±40′, ∠NCH = 113°14′±40′, and ∠OCH = 122°58′±40′. The dihedral angles between the H′NC plane and the NCO plane, and between the H″NC plane and the NCH plane are 7°±5°, and 12°±5°, respectively. These structural parameters were obtained by averaging the corrected (or final) structures in Table III. In Fig. 4 the formamide molecule is shown located in the $H_2N^{14}C^{12}HO^{16}$ principal axis system.

An estimate of the double-bond character of the C—O bond and the N—C bond can be obtained from an empirical formula proposed by Pauling,[17] which is a function of idealized single and double bonds and the bond distance for the molecule in question. With the idealized single and double bond data of Cox and Jeffrey[18] (r(N=C) = 1.28 A, r(N—C) = 1.47 A, r(C=O) = 1.18 A, and r(C—O) = 1.43 A), and the bond lengths given in Fig. 4, one obtains for formamide a C—O bond of 86% double-bond character and a N—C bond of 25% double-bond character.

In the past if a molecule exhibited a positive inertial defect it was considered a proof of, or at least a strong suggestion for, the planarity of the molecule. The results of this investigation clearly show the danger of using this criterion without other evidence. In general any slightly nonplanar molecule might be expected to show a small positive inertial defect when the contribution from the out-of-plane c coordinate is not large enough to completely counter-balance the inertial defect. It is indeed unfortunate that no theoretical criteria are available in order to ascertain if an observed inertial defect is of the correct order of magnitude to warrant using a planar model for the determination of a molecular structure. The calculation of the inertial defect for molecules other than triatomic may be quite formidable, but as pointed out by Nielsen[19] the inertial defect is not principally a function of the anharmonic part of the potential energy, but rather a function only of the geometry and of the quadratic (force) constants of the molecule.

Finally it should be pointed out that other molecules containing an NH_2 group, formerly thought to be planar, may actually be nonplanar. Such effects should be looked for in such molecules as urea and cyanamide.[20] In addition to the evidence provided by the microwave spectrum for the structures of these molecules, the investigation of the far infrared spectrum should lead to the direct observation of the "wagging-inversion" type frequencies and therefore much improved data for use in calculating the barrier hindering this motion.

[17] L. Pauling, *The Nature of the Chemical Bond* (Cornell University Press, Ithaca, 1948), second edition, p. 171 ff.

[18] E. G. Cox and G. A. Jeffrey, Proc. Roy. Soc. (London) **A207**, 110 (1951).

[19] H. H. Nielsen, Revs. Modern Phys. **23**, 90 (1951).

[20] In a private communication from J. K. Tyler, L. F. Thomas, and J. Sheridan concerning their recent study of the microwave spectrum of cyanamide, they state concerning the intensities of satellite lines, "These intensities also suggest that at least one deformation mode of cyanamide has a lower frequency than any previously assigned . . . further studies are being made."

Potential Energy Constants, Rotational Distortion Constants, and Thermodynamic Properties of $B^{11}H_3CO$, $B^{11}D_3CO$, $B^{10}H_3CO$, and $B^{10}D_3CO$

S. SUNDARAM AND FORREST F. CLEVELAND

Spectroscopy Laboratory, Department of Physics, Illinois Institute of Technology, Chicago 16, Illinois*

(Received August 11, 1959)

Potential energy constants have been obtained for the BH_3CO molecule by use of the Wilson **FG** matrix method. The derivatives of the moments of inertia tensor components, with respect to the symmetry coordinates, of an axially symmetric ZX_3YW molecule of C_{3v} symmetry have been evaluated. With these derivatives and the elements of the potential energy matrices, the rotational distortion constants for $B^{11}H_3CO$, $B^{11}D_3CO$, $B^{10}H_3CO$, and $B^{10}D_3CO$ have been calculated. The calculated values are in good agreement with the values obtained in the microwave experiments by Gordy *et al.* The heat content, free energy, entropy, and heat capacity have been calculated for the four molecules for the ideal gaseous state at 1 atmos pressure, with a rigid-rotor harmonic-oscillator approximation.

INTRODUCTION

THE electron diffraction work of Bauer[1] on BH_3CO has established a symmetric C_{3v} structure for this molecule and this has been confirmed by the microwave experiments of Gordy *et al.*[2] Rotational distortion constants have been reported by Strandberg *et al.*[3] and by Gordy *et al.*[4]

The earliest report of a few of the infrared bands of BH_3CO was made by Cowan.[5] Bethke and Wilson[6] have reported the complete infrared spectral data of gaseous $B^{11}H_3CO$, $B^{11}D_3CO$, $B^{10}H_3CO$, and $B^{10}D_3CO$. These authors have also partially investigated the Raman spectra of these compounds in the gaseous phase and the infrared spectra of the solid. They have carried out a normal coordinate treatment also, and obtained a set of potential energy constants. Taylor[7] has reported the Raman spectral data for $B^{11}H_3CO$ and $B^{11}D_3CO$ in the liquid state together with the results of a normal coordinate treatment.

However, it may be seen that in both the above investigations,[6,7] the symmetry coordinate describing the angle bending motion under the a_1 type is not orthogonal to the redundant coordinate. It was, therefore, one of the objectives of the present investigation to use a proper orthonormalized set of symmetry coordinates and to obtain the potential energy constants for the molecule.

Further, as a check on the potential energy constants, another objective has been to calculate the rotational distortion constants for these molecules, using the first-order perturbation theory of Kivelson and Wilson.[8]

POTENTIAL ENERGY CONSTANTS

The BH_3CO molecule has 4 vibrations of the a_1 type and 4 of the e type. There are 13 internal coordinates and the redundant coordinate is set up using the changes in the valence angles around the boron atom. The symmetry coordinates used in this investigation are the same as those given by Bethke and Wilson,[6] except for S_4 which was given the form,

$$S_4=[b(\Delta\alpha_1+\Delta\alpha_2+\Delta\alpha_3)-(\Delta\beta_1+\Delta\beta_2+\Delta\beta_3)]/(3+3b^2)^{\frac{1}{2}},$$

where α=H−B−H, β=H−B−C, $b=-2\cos\beta(1-\cos\alpha)/(\sin\alpha\sin\beta)$, and S_4 is orthogonal to S_0, the redundant coordinate.

The elements of the kinetic energy matrices were obtained by use of the s_{kt} vectors by methods given by Meister and Cleveland[9] and Ferigle and Meister.[10] As a check, these elements were modified using tetra-

TABLE I. Potential energy constants for BH_3CO and BD_3CO.[a]

Bond stretching and bond-bond interaction constants (md/A)	Bond-angle interaction constants (md/rad)	Angle bending and angle-angle interaction constants (md A/rad²)
$f_D=18.04500$	$f_{D\alpha}=0$	$f_\alpha=0.29194$
$f_R=2.72830$	$f_{D\beta}=0$	$f_{\alpha\alpha}=-0.05336$
$f_r=3.20589$	$f_{D\delta}=0$	$f_{\alpha\beta}=-0.07711$
$f_{DR}=0$	$f_{R\alpha}=-0.10944$	$f_{\alpha\beta'}=-0.07711$
$f_{Dr}=0$	$f_{R\beta}=0.13669$	$f_{\alpha\delta}=0$
$f_{Dr}=0$	$f_{R\delta}=0$	$f_{\alpha\delta'}=0$
$f_{rr}=0.04949$	$f_{r\alpha}=0$	$f_\beta=0.32335$
	$f_{r\alpha'}=0$	$f_{\beta\beta}=-0.01721$
	$f_{r\beta}=0$	$f_{\beta\delta}=-0.13889$
	$f_{r\beta'}=0$	$f_{\beta\delta'}=0.06944$
	$f_{r\delta}=0$	$f_{\beta\delta''}=0.12028$
	$f_{r\delta'}=0$	$f_\delta=0.40598$
	$f_{r\delta''}=0$	

[a] The number of significant figures is not justified except to have internal consistency in the calculations. D=the CO internuclear distance, R=BC, r=BH α=the HBH angle, β=HBC, δ=BCO; and the primes (′) and double primes (″) indicate that the bond and the angle, or the two angles, are in different planes.

* Publication No. 130.

[1] S. H. Bauer, J. Am. Chem. Soc. **59**, 1804 (1937).

[2] Gordy, Ring, and Burg, Phys. Rev. **74**, 1191 (1948).

[3] Strandberg, Pearsall, and Weiss, J. Chem. Phys. **17**, 429 (1949).

[4] Gordy, Ring, and Burg, Phys. Rev. **78**, 512 (1950).

[5] R. D. Cowan, J. Chem. Phys. **17**, 218 (1949).

[6] G. W. Bethke and M. K. Wilson, J. Chem. Phys. **26**, 1118 (1957); **27**, 978 (1957).

[7] R. C. Taylor, J. Chem. Phys. **26**, 1131 (1957); **27**, 979 (1957).

[8] D. Kivelson and E. B. Wilson, Jr., J. Chem. Phys. **20**, 1575 (1952); **21**, 1229 (1953).

[9] A. G. Meister and F. F. Cleveland, Am. J. Phys. **14**, 13 (1946).

[10] S. M. Ferigle and A. G. Meister, J. Chem. Phys. **19**, 982 (1951).

TABLE II. Calculated and observed wave numbers (c/cm) for the various molecules.[a]

Frequency Symbol	$B^{11}H_3CO$		$B^{11}D_3CO$		$B^{10}H_3CO$		$B^{10}D_3CO$	
	Calc.	Obs.	Calc.	Obs.	Calc.	Obs.	Calc.	Obs.
$\nu_1(a_1)$	2401	2380	1707	1679	2411	2385	1714	1695
$\nu_2(a_1)$	2201	2169	2205	2169	2207	2166	2205	2169
$\nu_3(a_1)$	1088	1073	874	862[b]	1091	1083	892	883[b]
$\nu_4(a_1)$	684	692	614	625	695	707	618	630
$\nu_5(e)$	2444	2434	1858	1837	2440	2456	1873	1852
$\nu_6(e)$	1084	1101	814	801	1084	1100	814	802
$\nu_7(e)$	824	816	720	709	806	819	732	718
$\nu_8(e)$	323	317	261	266	321	314	261	266

[a] Calc. = calculated, obs. = observed (reference 6).
[b] These values are only approximate.

TABLE III. The $[J_{\alpha\beta}{}^i]_0$ for an axially symmetric ZX_3YW molecule.[a]

Symmetry coordinate	$[J_{xx}{}^i]_0$	$[J_{zz}{}^i]_0$	$[J_{xz}{}^i]_0$
S_1	$2m_3(D+R-l)$	0	0
S_2	$2[m_3(D+R-l)+m_2(R-l)]$	0	0
S_3	$2\sqrt{3}m[\frac{1}{2}r(1+c^2)-lc]$	$2\sqrt{3}mrs^2$	0
S_4	$3rsm(rc-2l)/(3+3b^2)^{\frac{1}{2}}$	$-6mscr^2/(3+3b^2)^{\frac{1}{2}}$	0
S_{5a}	$-(6)^{\frac{1}{2}}mrs^2/2$	0	$(6)^{\frac{1}{2}}ms[lI_{yy}{}^x-rc]$
S_{6a}	$mr^2s^2\Gamma/2^{\frac{1}{2}}$	0	$-\sqrt{2}mrs\Gamma(rc-l)I_{yy}{}^x$
S_{7a}	0	0	$4I_{yy}{}^x[m_2R(R-l)+m_3(D+R)(D+R-l)]/6^{\frac{1}{2}}$
S_{8a}	0	0	$2m_3D(D+R-l)I_{yy}{}^x$
S_{5b}	0	0	0
S_{6b}	0	0	0
S_{7b}	0	0	0
S_{8b}	0	0	0

[a] D=Y—W bond distance; R=Z—Y bond distance; r=Z—X bond distance; $c=\cos\beta$, $s=\sin\beta$; m=mass of X atom; m_2=mass of Y atom; m_3=mass of W atom; $\Gamma=(1+4\cot^2\beta)^{\frac{1}{2}}$; $b=-2\cos\beta(1-\cos\alpha)/\sin\alpha\sin\beta$; α=X—Z—X angle; β=X—Z—Y angle; $M=\Sigma m_i$, the molecular mass; $I_{yy}{}^x=I_x(I_{yy}{}^{-1})=\Sigma m_i x_i{}^2/\Sigma m_i(x_i{}^2+z_i{}^2)$; $l=[m_2R+m_3(D+R)+3mrc]/M$.

hedral values for the angles around the boron atom, and compared with those for methyl acetylenes given by Meister[11] and modified by Davidson and Bernstein.[12]

The molecular parameters used are the same as those given by Bethke and Wilson.[6] From the symmetry force constants obtained here, using the theory of Gold, Dowling, and Meister,[13] analytical expressions for the potential energy constants were set up. Thus the valence force constants for the molecule have been evaluated. These are listed in Table I. The notation used is the same as that used by Bethke and Wilson.[6] Table II summarizes the wave numbers calculated for the molecules using the potential energy constants given in Table I. These are also compared with the observed wave numbers and the maximum difference is about 2%.

MOMENTS OF INERTIA DERIVATIVES

It may be seen from the Kivelson-Wilson[8] theory for the rotational distortion constants, that in the case of a molecule of symmetry C_{3v}, we need only $[J_{xx}{}^i]_0$, $[J_{zz}{}^i]_0$, and $[J_{xz}{}^i]_0$. These are, respectively, the partial derivatives (evaluated at the equilibrium position), of the xx, zz, and xz components of the moment of inertia tensor with respect to the ith symmetry coordinate. These were obtained by assuming arbitrary displacements of the internal coordinates of the molecule. The $[J_{\alpha\beta}{}^i]_0$ evaluated for the various symmetry coordinates are given in Table III, where α or $\beta = x$ or y or z.

ROTATIONAL DISTORTION CONSTANTS

The potential energy matrix F obtained here has been used to obtain the values of t_{xxxx}, t_{zzzz}, t_{xxzz}, and t_{xzzz},

TABLE IV. Rotational distortion constants in Mcps.

Molecule	D_J Calc.	D_J Obs.	D_{JK} Calc.	D_{JK} Obs.	D_K Calc.
$B^{11}H_3CO$	0.0059	<0.0100[a]	0.3841	0.36[a]	1.7656
$B^{11}D_3CO$	0.0043		0.2305	0.24	0.2963
$B^{10}H_3CO$	0.0063	0.177[b]	0.4093	0.39	1.7054
$B^{10}D_3CO$	0.0046		0.2450	0.29	0.2818

[a] Reference 4.
[b] Reference 3.

[11] A. G. Meister, J. Chem. Phys. **16**, 950 (1948).
[12] D. W. Davidson and H. J. Bernstein, Can. J. Chem. **33**, 1226 (1955).
[13] Gold, Dowling, and Meister, J. Mol. Spectroscopy **2**, 9 (1958).

TABLE V. Heat content, free energy, entropy, and heat capacity for $B^{11}H_3CO$ for the ideal gaseous state at 1 atmos pressure.[a]

T(°K)	$(H°-E_0°)/T$	$-(F°-E_0°)/T$	$S°$	$C_p°$
100	8.15	39.41	47.56	8.87
200	9.15	45.35	54.50	11.49
273.16	10.05	48.33	58.38	13.54
298.16	10.38	49.23	59.61	14.24
300	10.40	49.29	59.69	14.29
400	11.70	52.46	64.16	16.85
500	12.93	55.20	68.13	18.89
600	14.08	57.66	71.74	20.64
700	15.12	59.91	75.03	22.13
800	16.08	61.99	78.07	23.41
900	16.96	63.94	80.90	24.47
1000	17.76	65.77	83.53	25.42

[a] The values are in cal deg^{-1} mole^{-1}.

using the relation,[8]

$$t_{\alpha\beta\gamma\delta}=\sum_{ik}[J_{\alpha\beta}{}^{i}]_0(F^{-1})_{ik}[J_{\gamma\delta}{}^{k}]_0,$$

where each one of the α, β, γ, and δ may be x, y, or z, and $(F^{-1})_{ik}$ is an element of the matrix F^{-1}, the inverse of F. The rotational distortion constants calculated by the above procedure are compared with the values obtained from the microwave investigations in Table IV.

The D_J values obtained here are less than 10 kc/s, in agreement with Gordy *et al.*[4] For $B^{10}H_3CO$, the value of 177 kcps for D_J given by Strandberg *et al.*[3] differs widely from the present results. The values of D_{JK} are in good agreement with the microwave data.[4] This agreement together with the agreement between the calculated and observed wave numbers (as shown in Table II) supports the conclusion that the potential energy constants determined in this investigation form a valid set.

TABLE VI. Heat content, free energy, entropy, and heat capacity for $B^{11}D_3CO$ for the ideal gaseous state at 1 atmos pressure.[a]

T(°K)	$(H°-E_0°)/T$	$-(F°-E_0°)/T$	$S°$	$C_p°$
100	8.29	40.63	48.92	9.31
200	9.59	46.75	56.34	12.57
273.16	10.74	49.90	60.64	15.15
298.16	11.14	50.86	62.00	15.97
300	11.17	50.93	62.10	16.02
400	12.75	54.36	67.11	18.81
500	14.19	57.37	71.56	21.02
600	15.48	60.07	75.55	22.80
700	16.63	62.54	79.17	24.25
800	17.66	64.83	82.49	25.43
900	18.58	66.96	85.54	26.39
1000	19.40	68.97	88.37	27.16

[a] The values are in cal deg^{-1} mole^{-1}.

THERMODYNAMIC PROPERTIES

For all the 4 molecules studied here, the thermodynamic properties—heat content, free energy, entropy, and heat capacity—have been calculated. The wave numbers used are the observed values listed in Table II. The calculations are for the ideal gaseous state at atmospheric pressure for a rigid-rotor, harmonic-oscillator approximation. The results are summarized in Tables V to VIII.

TABLE VII. Heat content, free energy, entropy, and heat capacity for $B^{10}H_3CO$ for the ideal gaseous state at 1 atmos pressure.[a]

T(°K)	$(H°-E_0°)/T$	$-(F°-E_0°)/T$	$S°$	$C_p°$
100	8.15	39.25	47.40	8.87
200	9.14	45.20	54.34	11.44
273.16	10.03	48.18	58.21	13.48
298.16	10.35	49.07	59.42	14.17
300	10.37	49.14	59.51	14.22
400	11.66	52.30	63.96	16.73
500	12.89	55.03	67.92	18.83
600	14.03	57.48	71.51	20.58
700	15.07	59.73	74.80	22.08
800	16.03	61.80	77.83	23.36
900	17.65	63.74	81.39	24.45
1000	17.71	65.56	83.27	25.37

[a] The values are in cal deg^{-1} mole^{-1}.

TABLE VIII. Heat content, free energy, entropy, and heat capacity for $B^{10}D_3CO$ for the ideal gaseous state at 1 atmos pressure.[a]

T(°K)	$(H°-E_0°)/T$	$-(F°-E_0°)/T$	$S°$	$C_p°$
100	8.29	40.50	48.79	9.31
200	9.57	46.61	56.19	12.52
273.16	10.71	49.76	60.47	15.13
298.16	11.11	50.72	61.83	15.89
300	11.15	50.78	61.93	15.94
400	12.70	54.21	66.91	18.72
500	14.13	57.20	71.33	20.92
600	15.42	59.89	75.31	22.72
700	16.57	62.36	78.93	24.18
800	17.60	64.63	82.23	25.37
900	18.52	66.76	85.28	26.33
1000	19.34	68.76	88.10	27.11

[a] The values are in cal deg^{-1} mole^{-1}.

ACKNOWLEDGMENT

This work has been aided by a grant from the National Science Foundation. The authors are thankful for this assistance.

Kinetics of the Hydrolysis of Acetyl Chloride

E. J. CAIRNS* AND J. M. PRAUSNITZ

Department of Chemical Engineering, University of California, Berkeley, California

(Received April 20, 1959)

The hydrolysis of acetyl chloride in mixed solvent of acetone-water was investigated by means of an electrical conductance method. The temperature was varied over the range of −35°C to +10°C, and the solvent composition was varied over the range of 10 to 25% of water by volume. The reaction was found to be first order with respect to water and first order with respect to acetyl chloride over the range investigated. A strong dielectric constant influence was found, manifesting itself in an influence on the isodielectric entropy of activation. This effect was consistent with electrostatic theory and followed the dipole-dipole type of dielectric constant dependence. The dipole moment of the activated complex was estimated to be 16 debyes.

INTRODUCTION

THE purpose of this work was to investigate more completely the kinetics of the hydrolysis of acetyl chloride in media of various dielectric constants. This reaction has been studied by Gold and Hilton[1] in pure water and by Swain and Scott,[2] and Zimmerman and Yuan[3] in acetone-water mixed solvents. Swain's[4] proposal of a termolecular "push-pull" type of mechanism which explained results of kinetic studies on triphenyl methyl halides reacting with various hydroxylating agents suggested to Zimmerman and Yuan a similar termolecular mechanism for the hydrolysis of acetyl chloride in acetone. Archer and Hudson[5] indicated that this reaction in dioxane also gave third-order results (first-order with respect to acetyl chloride, second-order with respect to water).

Gold and Hilton,[1] by means of some approximations and comparison to a reaction of known second-order mechanism, proposed that their results for the hydrolysis of acetyl chloride in pure water were characteristic of a bimolecular reaction. Using the results of Zimmerman and Yuan for their calculations, Gold and Hilton[6] supported their previous indications in favor of a bimolecular reaction.

Benzoyl chloride is known to follow a predominately bimolecular mechanism[7–9] for its hydrolysis in the presence of acetone, at water concentrations up to 50% by weight. At higher water concentrations, there is an appreciable unimolecular ionization contribution. This information supports the bimolecular mechanism proposal, since benzoyl chloride more closely approximates the structure of acetyl chloride than does a trityl halide.

This paper presents kinetic data in the region of 10 to 30 weight percent water and over a wide temperature range. These data help to complete the information necessary to reach a more certain decision regarding the mechanism and influence of electrostatic forces on the rate of acetyl chloride hydrolysis.

THEORY

According to the theory of absolute reaction rates, an equation of the general form

$$k=(RT/N_0h)\exp(-\Delta F^{\ddagger}/RT) \qquad (1)$$

describes the temperature dependence of the reaction rate, where $\Delta F^{\ddagger}$ is the free energy of activation, and k is the reaction rate constant. In reactions which involve strongly dipolar molecules and a separation of charges during the reaction, the dielectric constant of the medium plays an important part in determining the rate of reaction.

In a system composed of dipoles, the dielectric constant of the medium strongly influences the free energy of the system. This is expressed by Kirkwood's formula[10] as reported by Amis[11]

$$\Delta F=(RT/N_0)\ln f=(-\mu^2/r_0^3)[(D-1)/(2D+1)]. \qquad (2)$$

Equation (2) gives the free energy change on moving a dipole of dipole moment μ and radius r_0 from a vacuum into a medium of dielectric constant D. If we apply this principle to Eq. (1)

$$\ln k=\ln(RT/N_0h)$$

$$-\frac{\Delta F_{D=1}^{\ddagger}-N_0\Delta(\mu^2/r_0^3)^{\ddagger}[(D-1)/(2D+1)]}{RT}, \qquad (3)$$

* Present address: General Electric Company Research Laboratory, Schenectady, New York.

[1] V. Gold and J. Hilton, J. Chem. Soc. (1955), 838.

[2] C. G. Swain and C. B. Scott, J. Am. Chem. Soc. 75, 246 (1953).

[3] G. Zimmerman and C. Yuan, J. Am. Chem. Soc. 77, 332 (1955).

[4] C. G. Swain, J. Am. Chem. Soc. 70, 1124 (1948).

[5] B. L. Archer and R. F. Hudson, J. Chem. Soc. (1950), 3259.

[6] V. Gold and J. Hilton, J. Chem. Soc. (1955), 3303.

[7] M. J. Kelly and G. M. Watson, J. Phys. Chem. 62, 260 (1958).

[8] Gold, Hilton, and Jefferson, J. Chem. Soc. (1954), 2756.

[9] D. A. Brown and R. F. Hudson, J. Chem. Soc. (1953), 3352; *ibid.* p. 883.

[10] J. G. Kirkwood, J. Chem. Phys. 2, 351 (1934).

[11] E. S. Amis, *Kinetics of Chemical Change in Solution* (The MacMillan Company, New York, 1949).

where $\Delta(\mu^2/r_0^3)^\ddagger$ represents the summation over the product of the activation step minus the summation over the reactants and $\Delta F_{D=1}^\ddagger$ is the free energy of activation extrapolated to the reference state of a dielectric constant of unity. Since it is difficult to obtain any data on the activated complex, it is assumed as was done in Kirkwood's development[10] that the term (μ^2/r_0^3) for each species is constant for a given temperature over the region of dielectric constant studied.

Since the free energy of activation may be separated into its components

$$\Delta F^\ddagger = \Delta H^\ddagger - T\Delta S^\ddagger \tag{4}$$

we find on combining Eqs. (3) and (4)

$$\ln k = \ln(RT/N_0 h) + (\Delta S_{D=1}^\ddagger/R) - (\Delta H_{D=1}^\ddagger/RT) + \frac{N_0\Delta(\mu^2/r_0^3)^\ddagger[(D-1)/(2D+1)]}{RT}. \tag{5}$$

In applying Eq. (5) to experimental results it is necessary that data be available for sets of isodielectric runs at various temperatures. It has been customary to evaluate $\Delta H_c^\ddagger$ and $\Delta S_c^\ddagger$, where the subscript c refers to isocomposition conditions. There is a difference between the values of $\Delta H^\ddagger$ and $\Delta S^\ddagger$ when measured for isocompositional and isodielectric media. This difference is due to the fact that in isocompositional solvent has a dielectric constant with a finite temperature coefficient. The quantitative expressions for these differences are obtained by differentiating $\Delta F^\ddagger/T$ with respect to reciprocal temperature:

$$-\Delta H^\ddagger = -\frac{\partial(\Delta F^\ddagger/T)}{\partial(1/T)} = \frac{R\partial[\ln k - \ln(RT/N_0 h)]}{\partial(1/T)}. \tag{6}$$

The differentiation is carried out first holding D constant, then allowing T and D to vary, and then taking the difference. The result is given in Eq. (7). In this calculation $\Delta(\mu^2/r_0^3)^\ddagger$ is independent of D (following Kirkwood) but not independent of T:

$$\Delta H_c^\ddagger - \Delta H_D^\ddagger = -N_0\Delta(\mu^2/r_0^3)^\ddagger[3D\delta T/(2D+1)^2]. \tag{7}$$

A similar procedure, operating on $\Delta F^\ddagger$, yields

$$\Delta S_c^\ddagger - \Delta S_D^\ddagger = -N_0\Delta(\mu^2/r_0^3)^\ddagger[3D\delta/(2D+1)^2] \tag{8}$$

where δ is the temperature coefficient of the dielectric constant D in the empirical equation $D = a\exp(-\delta T)$, and a is a constant.

Another effect which is present, but usually too small to be detected, is the change in the energy of interaction of two dipoles on change of the dielectric constant of the medium. This would be manifested in the enthalpy of activation, and may have a maximum value of

$$E = -2\mu_A\mu_B\Delta D/r_0^3 D_1 D_2. \tag{9}$$

This effect is too small to be detected in the present experiments.

EXPERIMENTAL

Materials

Acetone.—Commercial grade, with water as its main impurity (0.5%), was dried for a period of several days over $CaSO_4$ (drierite), which has been found capable of reducing water content to 0.001%,[12] and was then distilled from the drierite at a reflux ratio of about 8:1 in a 15-plate Oldershaw column under a dry nitrogen atmosphere. The acetone was refluxed for 2–3 hr and then distilled. A center cut (about 80%) was taken for the product in such a manner that it did not contact the air.

Acetyl chloride.—Baker analyzed reagent grade (98%) was purified under a dry nitrogen atmosphere in a still having a 2-ft packed section. The material was refluxed for two hours in order to drive off any HCl that might be present and then distilled at a reflux ratio of 10:1, taking a center cut as above. The product was received in about $\frac{1}{3}$-cc quantities in special Pyrex ampules which were vacuum-sealed after freezing the acetyl chloride by immersing the container in liquid nitrogen.

Water.—Doubly distilled conductivity water having a specific resistance of about 10^6 ohm-cm was used.

Apparatus

A one-liter round-bottomed flask was modified for use as a batch reactor by depressing the walls of the flask in such a manner that four baffles were formed. Four necks were mounted at the top of the flask to accommodate a thermometer, a stopper (for charging the reactor), a mechanical stirring device of Teflon, and an electrical conductivity cell. The reactor was immersed in a constant-temperature bath of kerosene.

Temperatures in the range of −40° to +5°C were obtained by use of a $\frac{3}{4}$-hp, two-cylinder York refrigeration unit, with Freon 22 as a refrigerant. Thermal regulation was attained by use of an automatic diaphragm-type expansion valve for the Freon 22, adjusted so that a temperature about 0.02 or 0.03° below the desired temperature would eventually be obtained. To compensate for the overcooling, an incandescent bulb was used as a heater and its off-on cycle was determined by a mercury thermal regulator coupled with an electronic relay. Temperature regulation was ±0.005°C.

[12] *Techniques of Organic Chemistry* edited by Arnold Weissberger (Interscience Publishers, Inc., New York, 1956), Vol. VIII.

TABLE I. Slopes of conductance *vs* concentration plots: equation: $C=\beta L^{\alpha}$.[a]

Solvent Composition Vol % H_2O	Solvent Composition Wt % H_2O	Concentration range of acids (each), normality	Temperature range, °C	α
10	12.35	10^{-3}–10^{-2}	−35 to +25	1.305
10	12.35	10^{-4}–10^{-3}	−35 to +25	1.083
10	12.35	10^{-5}–10^{-4}	−35	1.010
10	12.35	10^{-5}–10^{-4}	−20	0.920
10	12.35	10^{-5}–10^{-4}	0	0.900
10	12.35	10^{-5}–10^{-4}	+22	0.980
25	29.71	10^{-5}–2×10^{-2}	−35 to +25	1.053
40	45.80	10^{-5}–2×10^{-2}	−25 to +25	1.022

[a] Only the α's are listed here, since an accurate knowledge of β is not necessary for kinetics analysis. β depends on the cell constant; α does not.

Conductivity Measurements

The conductivity cell for use in the reactor was constructed such that two platinum plates, one centimeter square and one centimeter apart, were rigidly attached to glass tubes with provisions for electrical contact through mercury pools (which were immersed in the bath) to the Wheatstone bridge and for mounting in the neck of the reactor. The conductivity cell was placed in the flask in such a manner that it allowed the reacting mixture to flow freely between the electrodes without cavitation or stagnation.

The Wheatstone bridge itself consisted of a 1000-cycle audio oscillator as a voltage source, Rubicon decade resistance boxes, Kohlrausch student-type slidewire potentiometer, a decade-type capacitance box, and an oscilloscope. Careful shielding and grounding practices were utilized.

The products of the reaction are equal quantities of acetic acid and hydrochloric acid. It was therefore desirable to have accurate data relating the electrical conductivity of solutions containing equal concentrations of acetic acid and hydrochloric acid in aqueous solvents of varying acetone content. For calibration of the conductivity cells solutions of both hydrochloric acid and acetic acid were prepared having solvent compositions of 10, 25, and 40% water by volume and having normalities of 1.0, 10^{-1}, 10^{-2}, 10^{-3}, 10^{-4}, and 10^{-5}, all concentrations expressed at room temperature.

Logarithmic plots of conductance *vs* normality were prepared for each temperature and solvent composition. These plots were used in the interpretation of conductance data taken during the reaction; it was assumed that the contribution of unreacted acetyl chloride to the conductance is negligibly small [the specific conductance of pure acetyl chloride at 20°C is about 10^{-8} $(\text{ohm-cm})^{-1}$]. Table I summarizes the slopes α of the standardization plots. The constant β is determined by measuring the conductivity of a solution of known strength at a given temperature. Accurate values of β are not necessary for kinetic determinations, as will be shown later. Detailed data of conductivity-concentration relationships are available elsewhere.[13]

PROCEDURE

The reactor filled with mixed solvent was placed in the bath and fitted with the conductivity cell, Beckmann thermometer, and paddle mixer. The speed of the mixer was always regulated so as to obtain a maximum of agitation without excessive cavitation in the region of the conductivity cell. The reactor was kept closed at all times to prevent evaporation.

The reaction rate was independent of mixer speed in the operating range utilized. The mixer paddle was approximately rectangular, measuring 2 by $\frac{7}{8}$ in., and operated in the range of 500 to 750 rpm in the $4\frac{1}{2}$-in. i.d. spherical reactor. According to mixing efficiency studies performed under very similar geometrical situations and mixer speeds by Kramers *et al.*,[14] 25 revolutions of the paddle completes the mixing process. This indicates that for the experimental situation utilized in this work, the mixing was essentially complete in about two seconds.

The temperature of the solvent in the reactor was monitored with the Beckman thermometer and the bridge. Since the bridge gave an extremely sensitive test of thermal equilibrium through the conductivity of the mixed solvent, the bridge readings were taken as indicative of establishment of equilibrium.

After thermal equilibrium was reached, the conductivity of the solvent was recorded, and balanced out at the bridge. The reactor neck was opened, an ampule of acetyl chloride was broken open, quickly dumped through the neck of the reactor, and the reactor was again closed.

It was not found necessary to refrigerate the acetyl chloride, since its volume was only 1/2000 of the volume of the solvent, and the specific heat effects are small compared to the heat of reaction.

At the instant that the acetyl chloride entered the reactor, the timing device was started, the bridge was adjusted to the first resistance reading, and the balance condition was awaited. At the proper instant when the bridge was in balance, the timer switch was thrown and the next anticipated balance point was set on the resistance boxes. The previous value of resistance and its corresponding time interval were recorded.

The above procedure was continued for eight to ten reaction half-lives, taking careful note of the final conductivity values.

REDUCTION OF DATA

The reaction rate determination procedure outlined above was carried out so that the kinetics were pseudo

[13] E. J. Cairns, Dissertation, University of California, Berkeley, California (1959).

[14] Kramers, Baars, and Knoll, Chem. Eng. Sci. **2**, 35 (1953).

TABLE II. Results: hydrolysis of acetyl chloride in the presence of acetone.

Wt. % H_2O	Water conc.[a] mole/l	Temp. °C	Dielectric constant[b]	$k_1=k_{obs}$ sec^{-1}	k_2 l/mole-sec	$\Delta H_c^{\ddagger}$[c] kcal/mol	$\Delta S_c^{\ddagger}$[c] e.u.
12.34	4.748	+9.45	27.15	1.327×10^{-2}	2.308×10^{-3}		
12.34	5.862	−4.90	29.03	3.978×10^{-3}	6.785×10^{-4}		
12.34	5.941[d]	−14.95	30.45	1.471×10^{-3}	2.475×10^{-4}		
12.34	5.941[d]	−14.95	30.45	1.443×10^{-3}	2.420×10^{-4}		
12.34	6.019	−24.99	31.86	5.084×10^{-4}	8.446×10^{-5}		
						13.15±.14	−23.80±.24
20.61	9.975	+0.12	33.55	2.955×10^{-2}	2.962×10^{-3}		
20.61	10.038	−4.75	34.37	1.828×10^{-2}	1.821×10^{-3}		
20.61	10.620	−14.88	36.00	6.460×10^{-3}	6.352×10^{-4}		
20.61	10.300	−24.99	37.68	2.020×10^{-3}	1.961×10^{-4}		
20.61	10.427	−34.88	39.48	6.024×10^{-4}	5.777×10^{-5}		
						14.06±.14	−18.49±.24
29.71	14.939	−9.86	41.75	4.113×10^{-2}	2.753×10^{-3}		
29.71	15.028	−14.80	42.74	2.447×10^{-2}	1.628×10^{-3}		
29.71	15.191	−25.40	44.95	7.032×10^{-3}	4.629×10^{-4}		
29.71	15.310	−29.90	45.90	4.180×10^{-3}	2.730×10^{-4}		
						14.26±.45	−15.83±.39

[a] Computed from extrapolated density data on acetone-water mixtures, International Critical Tables, Vol. III, pp. 112, 113.
[b] Estimated from data by G. Ackerlöf, J. Am. Chem. Soc. **54**, 4125 (1932).
[c] These values calculated by method of least squares; 95% confidence intervals are reported.
[d] Duplicate runs made at two mixer speeds.

first-order, since at all times the water concentration was very great compared to the acetyl chloride concentration. Since only about $\frac{1}{3}$ cc of acetyl chloride was used, the water concentration and the dielectric constant of the medium were constant throughout the run.

The kinetic equation is

$$dC_a/dt=k_2[H_2O]\left(CH_3C(=O)Cl\right)=k_1\left(CH_3C(=O)Cl\right), \quad (10)$$

where C_a=concentration of HCl or acetic acid, mole/l, k_2=second-order reaction rate constant, and k_1=pseudo first-order reaction rate constant.

From the conductivity data of the reacting mixture the exact concentration of the products may be determined with the aid of the calibration curves already discussed.

It is of interest to determine the quantity

$$d\log(C_{a_\infty}-C_{a_t})/dt.$$

After substituting

$$C=\beta L^{\alpha}, \quad (11)$$

we find

$$d\log(C_{a_\infty}-C_{a_t})/dt=[d\log(L_\infty^{\alpha}-L_t^{\alpha})/dt] + d\log\beta/dt. \quad (12)$$

The last term in Eq. (12) vanishes indicating that an accurate knowledge of β is not required. An order of magnitude of accuracy in concentration is all that is necessary to establish the value of α, which is listed in Table I. In view of the magnitude of the values of α listed in the table it is necessary to plot $\log(C_{a_\infty}-C_{a_t})$ *vs* time rather than $\log(L_\infty-L_t)$ *vs* time.

The procedure followed in this work was to find the concentration corresponding to each conductivity reading by use of large-scale plots of the calibration data, and then to plot $\log(C_\infty-C_t)$ *vs* t, and to take the slope of the straight line obtained. This slope yields k_2 when multiplied by $2.303/[H_2O]$. These

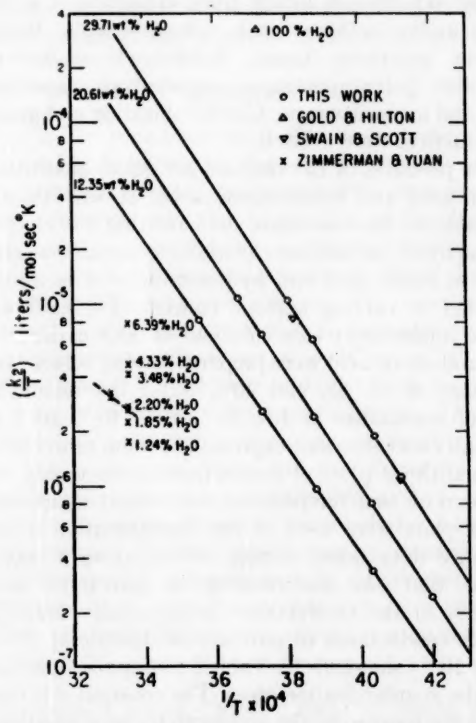

FIG. 1. Effect of temperature on hydrolysis of acetyl chloride in acetone solutions.

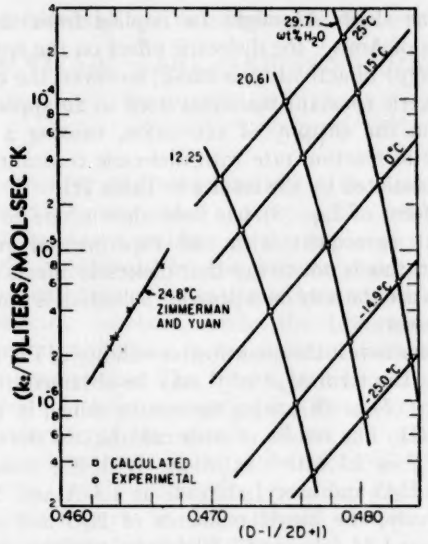

FIG. 2. Effect of dielectric constant of solvent on reaction rate constant.

primary results are reported in Table II. The subscript "C" denotes isocompositional runs.

Because of the nature of the experiments, the temperature effect as well as the effect of dielectric constant of the mixed solvent should be taken into account. The viscosity effect of the solvent, which is much more difficult to separate, is not accounted for because of the indefinite state of the theory.[15]

The temperature effect is expressed in terms of the enthalpy of activation, which is determined by plotting $\log(k_2/T)$ *vs* $1/T$ and taking the slope of the line obtained (see Fig. 1).

Enthalpies of activation are commonly expressed in terms of sets of isocomposition runs. When relatively large ranges of dielectric constant are encountered, it is interesting to determine the enthalpy of activation for sets of runs isodielectric with respect to the medium. The primary results of this work are isocompositional (see Table II). The equivalent sets of results for the isodielectric case are obtained by plotting the isocomposition results *vs* a function of dielectric constant, using temperature as a parameter (see Fig. 2). From this set of curves, a dielectric constant is selected, and the reaction rate constant is obtained at various temperatures. These rate constants may then be plotted in the usual manner to obtain the isodielectric enthalpies of activation. These results are reported in Table III.

Similar procedures may be employed for the entropies of activation, since the entropies are contained in the expression for the intercept of the plot of $\log(k_2/T)$ *vs* $1/T$. All results which were obtained using the experimentally determined reaction rate constants have been calculated using the least-squares technique and expressing the probable error in terms of the 95% confidence interval.

If, as suggested in Eq. (3), it is postulated that this reaction is predominately influenced by electrostatic forces, a plot having the coordinates shown in Fig. 2 would be expected to show a straight line for various isotherms. This is the case to within experimental error over the range of variables investigated here. From the results shown in Table III, a plot of the isodielectric entropy of activation *vs* $(D-1)/(2D+1)$ shows a straight line relationship, the entropy of activation increasing with the dielectric constant (see Fig. 3). The maximum deviation of the enthalpies of activation

TABLE III. Isodielectric enthalpies and entropies of activation.

Dielectric constant D	$\Delta H_D^{\ddagger}$ kcal/mole	$\Delta S_D^{\ddagger}$ e.u.
26.3	17.68	−8.18
30.8	17.72	−5.73
37.0	17.93	−3.04
46.4	17.74	−0.362

$$\Delta H_{D=48.5}^{\ddagger} = 17.77 \text{ kcal/mole at } 0°\text{C}$$

$$\Delta S_{D=48.5}^{\ddagger} = 0.0 \text{ eu}$$

$D = 48.5$ is the reference state.

$$\Delta(\mu^2/r_0^3)^{\ddagger} = +2.72\times10^{-19} \text{ cal/molecule at } -15°\text{C}$$

$$N_0\frac{\partial[\Delta(\mu^2/r_0^3)^{\ddagger}]}{\partial T} = \frac{\partial(\Delta S_D^{\ddagger})}{\partial[(D-1)/(2D+1)]} = 653.612 \text{ e.u.}$$

Dipole moment of activated complex $= 16\times10^{-18}$ esu-cm

$$\ln k_2 = \ln(RT/N_0h) - (\Delta H_{D=48.5}^{\ddagger}/RT) + (\Delta S_{D=48.5}^{\ddagger}/R) - \frac{N_0\Delta[\mu^2/r_0^3]^{\ddagger}\{[(D-1)/(2D+1)]-0.4847\}}{RT}$$

$$\Delta H_D^{\ddagger} = \Delta H_{ref}^{\ddagger} + N_0\Delta(\mu^2/r_0^3)^{\ddagger}\left[\frac{D-1}{2D+1}-0.4847\right] - TN_0\frac{\partial(\Delta[\mu^2/r_0^3]^{\ddagger})}{\partial T}\left[\left(\frac{D-1}{2D+1}\right)-0.4847\right]$$

$$\Delta S_D^{\ddagger} = \Delta S_{ref}^{\ddagger} - N_0\frac{\partial[\Delta(\mu^2/r_0^3)^{\ddagger}]}{\partial T}\left(\frac{D-1}{2D+1}-0.4847\right)$$

[15] E. A. Moelwyn-Hughes, *The Kinetics of Reactions in Solution* (Oxford University Press, New York, 1947).

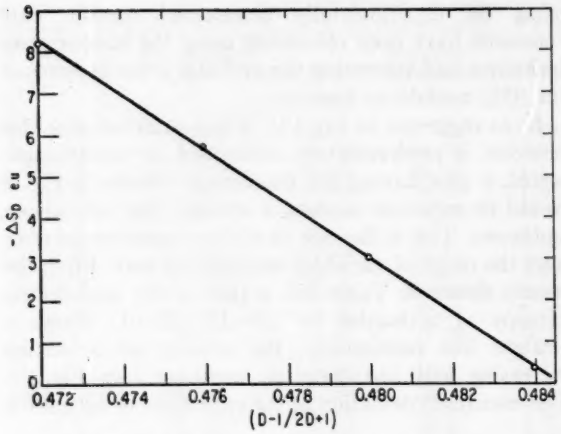

FIG. 3. Effect of dielectric constant on isodielectric entropy of activation.

in isodielectric media is about one percent; therefore, this work reports an average value representing an enthalpy of activation which is constant over the range of dielectric constant investigated here. Table III also shows the values for a reference value of the enthalpy of activation, a reference value of the isodielectric entropy of activation, and the rate of change of entropy of activation with respect to $(D-1)/(2D+1)$, as well as $N_0\Delta[\mu^2/r_0^3]^\ddagger$.

DISCUSSION OF RESULTS

Since there are more than just the variables of temperature and concentrations of various components influencing this reaction, it becomes difficult to separate clearly all of the effects which determine the reaction rate. Zimmerman and Yuan were led to believe that this reaction was third-order because a plot of log k_1 *vs* log[H_2O] in the region of one to five percent H_2O by volume had a slope of very nearly two. Using Zimmerman and Yuan's data, logk_2 plotted against $(D-1)/(2D+1)$ gave a straight line, while k_1 and k_3 did not.

In this investigation, the slopes of the plot of log k_1 *vs* log[H_2O] were much greater than two and were not constant; however, a plot of $\log(k_2/T)$ *vs* $(D-1)/(2D+1)$ gave a straight line at each temperature and over the whole range of dielectric constant investigated, showing the applicability of the form proposed in Eq. (3).* The slopes of these lines were the same for all temperatures investigated, and data extrapolated with respect to temperature also yielded the same slope. As might be implied from the discussions of Amis,[11] the dielectric effect on the enthalpy (or energy) of activation is small; however, the change of dielectric constant manifests itself in an appreciable effect on the entropy of activation, causing a rapid increase in reaction rate with dielectric constant. This is substantiated by the results in Table III.

The form of Eq. (3) has been shown here to be in excellent agreement with the experimental results; however, this is not to say that dielectric effects of the medium are the only ones present. Solvation is probably also present.

In order to test the quantitative validity of Eq. (3) or Eq. (5), the term $\Delta[\mu^2/r_0^3]^\ddagger$ may be obtained directly from Eq. (7) or (8), using the results shown in Tables II and III. The results of such calculations show that $\Delta[\mu^2/r_0^3]^\ddagger$ is 2.7×10^{-19} cal/mole. With the molecular radii of H_2O and acetyl chloride as 1.4 A and 2.5 A, respectively, the dipole moments of H_2O and acetyl chloride as 1.84 debyes and 2.0 debyes, respectively, the value of $[\mu^2/r_0^3]$ for the activated complex is 9.95×10^{-12} ergs/molecule. Estimating the radius of the activated complex as 3 A, which is reasonable for a reaction involving a separation of charges, the dipole moment of the activated complex amounts to 16.4 debyes. This compares very favorably with the value of 15 debyes reported by Kirkwood[10] for glycine.

The entropy effect may also be thought of in terms of solvation. The activated complex tends to solvate, as shown by the increase of rate with an increase in water concentration, causing a decrease in entropy for the reactant going to the activated complex. The expected negative entropies of activation were found (see Tables II and III). The more meaningful results for discussions from the solvation standpoint would be those for isocomposition runs (Table II). For electrostatic considerations, Table III is more instructive.

Qualitatively speaking, most of the isocompositional energies and entropies of activation for truly third-order reactions are considerably smaller in absolute value than those encountered here. The present results fall in the range of those encountered for bimolecular reactions.

SUMMARY AND CONCLUSIONS

The hydrolysis of acetyl chloride in the presence of acetone was investigated over the temperature range of -35°C to $+10$°C and dielectric constant range corresponding to a solvent composition range of 10 to 25% of water by volume ($D=26$ to $D=47$). The kinetics were found to be best analyzed on a basis of first order with respect to water and first order with respect to acetyl chloride, having a strong dielectric constant influence on the isodielectric entropy of activation, as described by electrostatic theory.

* The electrostatic theory as presented here is limited in its applicability as discussed by Winstein *et al.*[16,17] This theory applies well over the somewhat limited ranges of solvent composition due, in some cases, to competing mechanisms for the same overall reaction. An example is hydrolysis of benzoyl chloride in the presence of acetone.

[16] Fainberg, Robinson, and Winstein, J. Am. Chem. Soc. **78**, 2770 (1956).

[17] S. Winstein and A. H. Fainberg, J. Am. Chem. Soc. **79**, 5937 (1957).

The results may best be expressed in the form

$$\ln k_2 = \ln(RT/N_0h) - (\Delta H_{D=1}^{\ddagger}/RT) + (\Delta S_{D=1}^{\ddagger}/R) + \frac{N_0\Delta[\mu^2/r_0^3]^{\ddagger}[(D-1)/(2D+1)]}{RT}.$$

This method of analyzing kinetic data is more useful for determining the order of reaction than the usual methods in that it emphasizes the importance of isodielectric conditions. In the present case, the isodielectric enthalpy of activation is constant with varying dielectric constant, while the isocompositional enthalpy of activation is not constant with varying solvent composition. The theory used here, based on Kirkwood's formula accounting for the dielectric constant influence of the solvent, allows the calculation of the dipole moment of the activated complex, giving interesting insight concerning reaction mechanisms. The dipole moment of the activated complex in this reaction is estimated at 16.4 debyes.

ACKNOWLEDGMENTS

The authors are grateful to H. S. Johnston for helpful discussion and to the Dow Chemical Company for financial support in the form of a fellowship.

NOMENCLATURE

a = constant in empirical equation $D = ae^{-\delta T}$
C = instantaneous concentration
D = dielectric constant
e = constant, 2.718 . . . .
F = free energy
H = enthalpy
h = Planck's constant
k = reaction rate constant
L = specific conductance, ohm-centimeter
N = normality
N_0 = Avogadro's number
R = universal gas constant
r_0 = radius of dipole
S = entropy
t = time, seconds; temperature, degrees centigrade
T = absolute temperature

Greek Letters

α = empirical constant ($C = \beta L^{\alpha}$)
β = empirical constant
Δ = operator denoting difference, or change
δ = temperature coefficient of dielectric constant: $D = ae^{-\delta T}$
μ = dipole moment
ρ = density

Superscripts

0 = reference state

Subscripts

∞ = value at infinite time
a = acids
S = solvent
c = isocompositional
D = isodielectric constant
t = value at time t.

Spin Densities in Odd Alternant Hydrocarbon Radicals*

ROLAND LEFEBVRE,† HENRY H. DEARMAN,‡ AND HARDEN M. MCCONNELL§

Gates and Crellin Laboratories of Chemistry,|| California Institute of Technology, Pasadena, California

(Received August 10, 1959)

The spin densities at the starred and unstarred carbon atoms of odd alternant hydrocarbon radicals have been calculated using the method of alternant molecular orbitals introduced by Löwdin. The spin densities at unstarred positions are shown to be negative in sign and to depend upon the electron correlation parameter θ. Observed spin densities on one carbon atom can be used to estimate θ and to calculate spin densities on other carbon atoms. Illustrative calculations for the cases of triphenylmethyl and perinaphthenyl are described.

INTRODUCTION

SIMPLE Hückel molecular orbital theory has been successfully applied in the interpretation of the proton hyperfine splitting of the electron resonance spectra of the singly charged ions of even alternant hydrocarbons.[1-3] The principle upon which this interpretation is based is that the coupling constant due to a particular proton in hydrocarbon ions is directly proportional to the density of unpaired electron spin at the carbon atom to which the proton is bonded.[4-6] Within the Hückel approximation, the theoretical spin density at carbon atom C is the square of the coefficient of the atomic orbital centered on C in the singly occupied molecular orbital.

In this paper, we will be concerned with the estimation of electron spin densities in neutral odd alternant hydrocarbon radicals. For these molecules simple Hückel MO theory predicts zero coefficients for the singly occupied molecular orbital at the unstarred carbon atoms.[7] However, this prediction of zero spin densities at the unstarred carbon atoms cannot be correlated with the experimental electron resonance spectra of the odd alternant radicals, either quantitatively or qualitatively. The failure of this simple theory implies that the calculation should be carried out using a wave function which more correctly correlates the electrons.

It has been shown that elementary valence bond theory, or molecular orbital theory with π–π configuration interaction, can lead to negative spin densities at the unstarred positions.[6,8] McConnell[9] has carried out the calculation of the spin density for the allyl radical using these two types of wave functions and has shown that this is indeed the case. Since the total spread of an electron resonance spectrum of a conjugated radical or ion is a measure of the sum of the absolute values of the spin densities at the various carbon atoms, introduction of negative density into odd alternant radicals requires that the spread of the spectrum of these molecules be greater than that arising from the even alternant ions. This result has been borne out by experiment for the cases of the triphenylmethyl,[10] dimesitylmethyl,[10] and perinaphthenyl[11] radicals.

Hoijtink[12] has reported the results of the calculation of the spin densities in odd alternant radicals using a wave function obtained by first order π–π configuration interaction and finds negative density at the unstarred positions. McLachlan[13] has recently found a general proof that valence bond theory (without long bonds or ionic structures) leads to an alternation in the sign of spin densities in all odd alternant radicals. We wish to report in this paper the results obtained by employing the type of wave function proposed by Löwdin which is constructed from the so-called alternant molecular orbitals.[14] Formulas for the spin densities at the starred and unstarred atoms will be derived and the sign of the density at the unstarred positions shown to be negative in this approximation.

WAVE FUNCTION

Alternant hydrocarbons are conjugated molecules whose carbon atoms can be labeled such that no starred atom is bonded to any other starred atom. In odd alternant systems there are $2n+1$ π electrons, and $2n+1$ carbon atoms will be labeled such that there are $n+1$ starred and n unstarred atoms.

* Supported in part by the Office of Ordnance Research, U. S. Army and by the National Science Foundation.

† On leave from Centre de Mecaniqué Ondulatoire Appliquée, Paris.

‡ National Science Foundation Summer Fellow.

§ Alfred P. Sloan Fellow.

|| Contribution No. 2489.

[1] Tuttle, Ward, and Weissman, J. Chem. Phys. **25,** 189 (1956).

[2] E. de Boer, J. Chem. Phys. **25,** 290 (1956).

[3] E. de Boer and S. I. Weissman, J. Am. Chem. Soc. **80,** 4550 (1958).

[4] H. M. McConnell, J. Chem. Phys. **24,** 764 (1956).

[5] S. I. Weissman, J. Chem. Phys. **25,** 890 (1956).

[6] H. M. McConnell and D. B. Chesnut, J. Chem. Phys. **27,** 984 (1957); **28,** 107 (1958).

[7] C. A. Coulson and H. C. Longuet-Higgins, Proc. Roy. Soc. (London) **A192,** 16 (1948); H. C. Longuet-Higgins, J. Chem. Phys. **18,** 265 (1950).

[8] P. Brovetto and S. Ferroni, Nuovo cimento **5,** 142 (1957).

[9] H. M. McConnell, J. Chem. Phys. **28,** 1188 (1958).

[10] H. S. Jarrett and G. J. Sloan, J. Chem. Phys. **22,** 1783 (1954).

[11] Sogo, Nagazaki, and Calvin, J. Chem. Phys. **26,** 1343 (1957).

[12] G. J. Hoijtink, Mol. Phys. **1,** 157 (1958).

[13] A. D. McLachlan, Mol. Phys. **2,** 223 (1959).

[14] P. O. Löwdin, *Advances in Physics* (Taylor and Francis, Ltd., London, 1956) Vol. 5, p. 161 (1956); Phys. Rev. **97,** 1509 (1955).

It is a characteristic feature of the molecular orbital theory of alternant systems that the LCAO MO's occur in pairs of bonding and antibonding orbitals, ϕ_i and $\phi_{i'}$. The antibonding orbital $\phi_{i'}$ is obtained from the bonding orbital ϕ_i by changing the sign of the coefficients of the AO's centered on the unstarred atoms. The orbital energies ϵ_i and $\epsilon_{i'}$ belong to symmetrical places in the bonding and antibonding level diagram.

For the case of an odd alternant molecule, there is also a nonbonding orbital ϕ_0, having an orbital energy ϵ_0, ϵ_i and $\epsilon_{i'}$ are symmetrically disposed about ϵ_0. Also, as was mentioned before, the coefficients of the AO's centered on the unstarred atoms making up ϕ_0 are zero. The symmetrical disposition of orbital energies, pairwise correspondence of bonding and antibonding orbitals, and zero amplitude at unstarred atoms in nonbonding orbital can also be proved in a self-consistent field approximation.[15]

The wave function with which the matrix elements of the spin density operator will be calculated is obtained by applying the doublet state projection operator to the single determinant

$$T_0=|\,(a\phi_1+b\phi_{1'})(a\phi_2+b\phi_{2'})\cdots(a\phi_n+b\phi_{n'})\phi_0 \cdot(a\bar{\phi}_1-b\bar{\phi}_{1'})(a\bar{\phi}_2-b\bar{\phi}_{2'})\cdots(a\bar{\phi}_n-b\bar{\phi}_{n'})\,| \qquad a=\cos\theta,\ b=\sin\theta,\ a^2+b^2=1. \quad (1)$$

Here θ is the parameter which mixes excited configurations with the lowest molecular orbital configuration. Inspection of Eq. (1) shows that for the case $\theta=0°$ T_0 is the basic antisymmetrized MO product. $\theta=45°$ gives rise to a wave function in which the electrons with α spin are confined to spatial orbitals centered on the starred atoms and those with β spin to spatial orbitals with zero amplitude everywhere except on the unstarred atoms. In the case of physical interest θ lies somewhere between these two limits and may be obtained from the variation principle.

It should be pointed out that the present case can be generalized by replacing the single parameter θ with a set of θ_i's, one such parameter for each pair of conjugate bonding and antibonding orbitals. In the appendix use of the function

$$T_0'=|\,(a_1\phi_1+b_1\phi_{1'})(a_2\phi_2+b_2\phi_{2'})\cdots(a_n\phi_n+b_n\phi_{n'})\phi_0 \cdot(a_1\bar{\phi}_1-b_1\bar{\phi}_{1'})(a_2\bar{\phi}_2-b_2\bar{\phi}_{2'})\cdots(a_n\bar{\phi}_n-b_n\bar{\phi}_{n'})\,| \quad (2)$$

will be justified by a simple generalization of the procedure to be described. It will be shown that the conclusion drawn from function (1) about the signs of the spin densities at the various positions is unchanged by this generalization.

It is a simple matter to show that the result of applying the doublet state projection operator to T_0 is

$${}^2\mathbf{O}T_0=C_0\sum_{K=0}^{n}(-1)^K\binom{n+1}{K}^{-1}T_K. \quad (3)$$

Here both the operator ${}^2\mathbf{O}$ and the determinants T_K have been thoroughly defined by Löwdin.[14] C_0 is obtained by the direct application of the doublet projection operator. The procedure which will be described here will make use of this general result only for a small number of electrons, namely the cases of three and five electrons. For three electrons C_0 has the value of $\frac{2}{3}$ and for five electrons C_0 has the value of $\frac{1}{2}$.

We now make the assumption that b is a small quantity. This can be justified on a physical basis, as will be shown later. If terms in b^2 are retained in the development of T_0 one obtains

$$\begin{aligned}T_0=a^{2n}&|\,\phi_1\phi_2\cdots\phi_n\phi_0\bar{\phi}_1\bar{\phi}_2\cdots\bar{\phi}_n\,|\\&+a^{2n-1}b\sum_{i=1}^{n}\{|\,\phi_1\phi_2\cdots\phi_{i'}\cdots\phi_n\phi_0\bar{\phi}_1\bar{\phi}_2\cdots\bar{\phi}_i\cdots\bar{\phi}_n\,|\\&\quad-|\,\phi_1\phi_2\cdots\phi_i\cdots\phi_n\phi_0\bar{\phi}_1\bar{\phi}_2\cdots\bar{\phi}_{i'}\cdots\bar{\phi}_n\,|\}\\&\quad+a^{2n-2}b^2\sum_{i>j}\{|\,\phi_1\phi_2\cdots\phi_{i'}\cdots\phi_{j'}\cdots\\&\qquad\cdot\phi_n\phi_0\bar{\phi}_1\bar{\phi}_2\cdots\bar{\phi}_i\cdots\bar{\phi}_j\cdots\bar{\phi}_n\,|\\&\quad-|\,\phi_1\phi_2\cdots\phi_{i'}\cdots\phi_j\cdots\phi_n\phi_0\bar{\phi}_1\bar{\phi}_2\cdots\bar{\phi}_i\cdots\bar{\phi}_{j'}\cdots\bar{\phi}_n\,|\\&\quad-|\,\phi_1\phi_2\cdots\phi_i\cdots\phi_{j'}\cdots\phi_n\phi_0\bar{\phi}_1\bar{\phi}_2\cdots\bar{\phi}_{i'}\cdots\bar{\phi}_j\cdots\bar{\phi}_n\,|\\&\quad+|\,\phi_1\phi_2\cdots\phi_i\cdots\phi_j\cdots\phi_n\phi_0\bar{\phi}_1\bar{\phi}_2\cdots\bar{\phi}_{i'}\cdots\bar{\phi}_{j'}\cdots\bar{\phi}_n\,|\}\\&\quad-a^{2n-2}b^2\sum_{i=1}^{n}\{|\,\phi_1\phi_2\cdots\phi_{i'}\cdots\phi_{j'}\cdots\\&\qquad\cdot\phi_n\phi_0\bar{\phi}_1\bar{\phi}_2\cdots\bar{\phi}_{i'}\cdots\bar{\phi}_j\cdots\bar{\phi}_n\,|\}. \quad (4)\end{aligned}$$

The function (4) now contains only Slater determants made up of orthogonal molecular orbitals. Retention of terms of order b^2 in the wave function will lead to a result for the spin density which includes terms in b up to fourth order. This is equivalent to the assumption, in configuration interaction language, that only configurations up to those corresponding to two-electron excitations contribute significantly to the wave function.

We now apply the doublet projection operator to (4) and note that the determinantal functions

$$|\,\phi_1\phi_2\cdots\phi_n\phi_0\bar{\phi}_1\bar{\phi}\cdots\bar{\phi}_n\,| \text{ and}$$

$$\sum_{i=1}^{n}\{|\,\phi_1\phi_2\cdots\phi_{i'}\cdots\phi_j\cdots\phi_n\phi_0\bar{\phi}_1\bar{\phi}\cdots\bar{\phi}_{i'}\cdots\bar{\phi}_j\cdots\bar{\phi}_n\,|$$

are already eigenfunctions of S^2. We must extract the doublet component from the functions in

$$\sum_{i=1}^{n}\{|\,\phi_1\phi_2\cdots\phi_{i'}\cdots\phi_n\phi_0\bar{\phi}_1\bar{\phi}_2\cdots\bar{\phi}_i\cdots\bar{\phi}_n\,| -|\,\phi_1\phi_2\cdots\phi_i\cdots\phi_n\phi_0\bar{\phi}_1\bar{\phi}_2\cdots\bar{\phi}_{i'}\cdots\bar{\phi}_n\,|\}$$

[15] R. Lefebvre, J. Chem. Phys. **54**, 168 (1957).

which contain three singly filled orbitals and from the functions in

$$\sum_{i>j}\{|\phi_1\phi_2\cdots\phi_{i'}\cdots\phi_{j'}\cdots\phi_n\phi_0\bar{\phi}_1\bar{\phi}_2\cdots\bar{\phi}_i\cdots\bar{\phi}_j\cdots\bar{\phi}_n|$$
$$-|\phi_1\phi_2\cdots\phi_{i'}\cdots\phi_j\cdots\phi_n\phi_0\bar{\phi}_1\bar{\phi}_2\cdots\bar{\phi}_i\cdots\bar{\phi}_{j'}\cdots\bar{\phi}_n|$$
$$-|\phi_1\phi_2\cdots\phi_i\cdots\phi_{j'}\cdots\phi_n\phi_0\bar{\phi}_1\bar{\phi}_2\cdots\bar{\phi}_{i'}\cdots\bar{\phi}_j\cdots\bar{\phi}_n|$$
$$+|\phi_1\phi_2\cdots\phi_i\cdots\phi_j\cdots\phi_n\phi_0\bar{\phi}_1\bar{\phi}_2\cdots\bar{\phi}_{i'}\cdots\bar{\phi}_{j'}\cdots\bar{\phi}_n|\}$$

which contain five such orbitals. The result of the application of the doublet projection operator to Eq. (4) is

$$^2\mathbf{O}T_0=a^{2n}|\phi_1\phi_2\cdots\phi_n\phi_0\bar{\phi}_1\bar{\phi}_2\cdots\bar{\phi}_n|$$
$$+(\tfrac{2}{3})^{\frac{1}{2}}a^{2n-1}b\sum_{i=1}^{n}\frac{1}{(6)^{\frac{1}{2}}}\{|\phi_1\phi_2\cdots\phi_{i'}\cdots\phi_n\phi_0\bar{\phi}_1\bar{\phi}_2\cdots\bar{\phi}_i\cdots\bar{\phi}_n|$$
$$-|\phi_1\phi_2\cdots\phi_i\cdots\phi_n\phi_0\bar{\phi}_1\bar{\phi}_2\cdots\bar{\phi}_{i'}\cdots\bar{\phi}_n|$$
$$+2|\phi_1\phi_2\cdots\phi_i\cdots\phi_n\bar{\phi}_0\bar{\phi}_1\bar{\phi}_2\cdots\phi_{i'}\cdots\bar{\phi}_n|\}$$
$$-\frac{(12)^{\frac{1}{2}}}{3}a^{2n-2}b^2\sum_{i>j}\frac{1}{(12)^{\frac{1}{2}}}$$
$$\cdot\{2|\phi_1\phi_2\cdots\phi_i\cdots\phi_{i'}\cdots\phi_n\phi_0\bar{\phi}_1\bar{\phi}_2\cdots\bar{\phi}_{j'}\cdots\bar{\phi}_j\cdots\bar{\phi}_n|$$
$$+2|\phi_1\phi_2\cdots\phi_{j'}\cdots\phi_j\cdots\phi_n\phi_0\bar{\phi}_1\bar{\phi}_2\cdots\bar{\phi}_i\cdots\bar{\phi}_{i'}\cdots\bar{\phi}_n|$$
$$-|\phi_1\phi_2\cdots\phi_{i'}\cdots\phi_{j'}\cdots\phi_n\phi_0\bar{\phi}_1\bar{\phi}_2\cdots\bar{\phi}_i\cdots\bar{\phi}_j\cdots\bar{\phi}_n|$$
$$+|\phi_1\phi_2\cdots\phi_{i'}\cdots\phi_j\cdots\phi_n\phi_0\bar{\phi}_1\bar{\phi}_2\cdots\bar{\phi}_i\cdots\bar{\phi}_{j'}\cdots\bar{\phi}_n|$$
$$+|\phi_1\phi_2\cdots\phi_i\cdots\phi_{j'}\cdots\phi_n\phi_0\bar{\phi}_1\bar{\phi}_2\cdots\bar{\phi}_{i'}\cdots\bar{\phi}_j\cdots\bar{\phi}_n|$$
$$-|\phi_1\phi_2\cdots\phi_i\cdots\phi_j\cdots\phi_n\phi_0\bar{\phi}_1\bar{\phi}_2\cdots\bar{\phi}_{i'}\cdots\bar{\phi}_{j'}\cdots\bar{\phi}_n|$$
$$-a^{2n-2}b^2\sum_{i=1}^{n}\{|\phi_1\phi_2\cdots\phi_{i'}\cdots\phi_j\cdots$$
$$\cdot\phi_n\bar{\phi}_1\bar{\phi}_2\cdots\bar{\phi}_{i'}\cdots\bar{\phi}_j\cdots\bar{\phi}_n|\}. \quad (5)$$

However function (5) is no longer normalized and must be divided by $(N)^{\frac{1}{2}}$ where

$$N=a^{4n}+(2n/3)a^{4n-2}b^2+a^{4n-4}b^4(2n^2+n)/3.$$

SPIN DENSITY RELATIONS

We are interested in two types of quantities, the molecular orbital spin density and the atomic orbital spin density. The spin density operator is

$$(1/m_s)\sum_{\mu}\delta(r-r_\mu)\mathbf{S}\mu z.^{5,6}$$

Calculation of the expectation value of the spin density operator is carried out with the application of the well-known Slater-Condon rules. For the molecular orbital density we obtain

$$\rho(r)=N^{-1}\{a^{4n}\delta_{00}+\tfrac{4}{3}a^{4n-1}b\sum_{i=1}^{n}\delta_{ii'}$$
$$+\tfrac{1}{9}a^{4n-2}b^2\sum_{i=1}^{n}[4\delta_{i'i'}-2\delta_{00}+4\delta_{ii}]$$
$$+(\tfrac{8}{9}n+\tfrac{4}{9})a^{4n-3}b^3\sum_{i=1}^{n}\delta_{ii'}$$
$$+[(2n^2+n)/3]a^{4n-4}b^4\delta_{00}\}. \quad (6)$$

in which

$$\delta_{00}=\phi_0^2(r),$$
$$\delta_{ik}=\phi_i(r)\phi_k(r).$$

In the calculation of the atomic orbital spin density, we neglect differential overlap which here means that we retain only diagonal elements of the atomic orbital spin density matrix.[9] However, this procedure is likely to lead, in the present case, to the spin densities which would be calculated using the "atomic orbital delta function,"[16] rather than to the diagonal elements of the atomic orbital spin density matrix. This is because of the nature of the "atomic orbitals" involved in such a calculation. Pairing of the molecular orbitals arises either in the Hückel method or in a semi-empirical scheme similar to that proposed by Pariser and Parr.[17] It is likely that the orthogonal atomic orbitals used in these schemes are really some sort of localized linear combinations of nonorthogonal AO's similar to those defined by Löwdin.[18] The atomic charge density can be calculated either by using the nonorthogonal AO's with a definition of the charge density including overlap[19] or by first expressing the AO's in terms of the Löwdin orbitals and then calculating the charge densities from the formula suitable for orthogonal AO's. These two procedures lead to the same value in the case of conjugated alternant hydrocarbons.[18] The same result applies here. Therefore, the diagonal elements of the spin density matrix calculated from orthogonalized AO's represent in fact the unpaired spin density calculated with inclusion of overlap.

If we express the density on the starred atoms ρ_A and the density on the unstarred atoms ρ_B as a function of the parameter θ, we arrive at the relations

$$\rho_A=(N')^{-1}\{C_{0A}{}^2\cdot Y+\tfrac{2}{3}\tan\theta+\tfrac{4}{9}\tan^2\theta$$
$$+[(4n+2)/9]\tan^3\theta\}\chi_A{}^2(r) \quad (7)$$
$$\rho_B=(N')^{-1}\{-\tfrac{2}{3}\tan\theta+\tfrac{4}{9}\tan^2\theta$$
$$-[(4n+2)/9]\tan^3\theta\}\chi_B{}^2(r) \quad (8)$$

in which

$$N'=1+(2n/3)\tan^2\theta+[(2n^2+n)/3]\tan^4\theta,$$

[16] H. M. McConnell, J. Mol. Spectroscopy **1**, 11 (1957).
[17] R. Pariser and R. G. Parr, J. Chem. Phys. **21**, 466, 767 (1953).
[18] P. O. Löwdin, J. Chem. Phys. **18**, 365 (1950).
[19] B. H. Chirgwin and C. A. Coulson, Proc. Roy. Soc. (London) **A201**, 196 (1950).

and

$$Y=1-\tfrac{2}{3}\tan\theta-[(2n+4)/9]\tan^2\theta-[(4n+2)/9]\tan^3\theta+[(2n^2+n)/3]\tan^4\theta,$$

$X_A(r)$ is the atomic orbital centered on starred atom A, and $X_B(r)$ is the atomic orbital centered on unstarred atom B. In passing from the molecular orbital spin density to the atomic orbital spin density, advantage has been taken of the fact that the coefficients of the molecular orbitals obey the relation[20]

$$2\sum_{i=1}^{n}C_{iA}^2+C_{0A}^2=1.$$

Inspection of Eq. (8) shows that the sign of the spin density at an unstarred atom ρ_B is governed by the sign of $\tan\theta$. In order to demonstrate the presence of a negative sign of spin density at an unstarred atom we must show that $\tan\theta$ is a positive quantity. To carry this out we will calculate the value of the quantity b/a which is obtained by first-order configuration interaction.

If the function (5) be restricted to terms linear in b, it can be considered as having arisen from a configuration interaction of the basic molecular orbital determinant, $|\phi_1\phi_2\cdots\phi_n\phi_0\bar{\phi}_1\bar{\phi}_2\cdots\bar{\phi}_n|=\psi_0$, with the normalized combinations of excited configurations

$$\frac{1}{(n)^{\frac{1}{2}}}\sum_i\frac{1}{(6)^{\frac{1}{2}}}\{|\phi_1\phi_2\cdots\phi_{i'}\cdots\phi_n\phi_0\bar{\phi}_1\bar{\phi}_2\cdots\bar{\phi}_i\cdots\bar{\phi}_n|-|\phi_1\phi_2\cdots\phi_i\cdots\phi_n\phi_0\bar{\phi}_1\bar{\phi}_2\cdots\bar{\phi}_{i'}\cdots\bar{\phi}_n|+2|\phi_1\phi_2\cdots\phi_i\cdots\phi_n\bar{\phi}_0\bar{\phi}_1\bar{\phi}_2\cdots\phi_{i'}\cdots\bar{\phi}_n|=\psi_1.$$

By using first-order perturbation theory, we have

$$\Psi_{\text{ground state}}=\psi_0+\lambda\psi_1 \tag{9}$$

in which

$$\lambda=-\mathcal{H}_{01}/(E_1-E_0), \tag{10}$$

and

$$\mathcal{H}_{01}=\int\psi_0\mathcal{H}\psi_1 d\tau,$$

where $\mathcal{H}$ is the total Hamiltonian for the system and E_0 and E_1 are the zeroth-order energies corresponding to ψ_0 and ψ_1. It is readily shown that

$$\mathcal{H}_{01}=-[1/(n)^{\frac{1}{2}}](\tfrac{3}{2})^{\frac{1}{2}}\sum_{i=1}^{n}\zeta_{i'0}^{i0}, \tag{11}$$

where

$$\zeta_{i'0}^{i0}=\iint\phi_i(1)\phi_0(1)(e^2/r_{12})\phi_{i'}(2)\phi_0(2)d\tau_1 d\tau_2.$$

It has been further shown that[15]

$$\zeta_{pq}^{mn}=\zeta_{p'q'}^{mn}. \tag{12}$$

[20] C. A. Coulson and G. S. Rushbrooke, Proc. Cambridge Phil. Soc. **36**, 193 (1940).

Therefore we can write

$$\zeta_{i'0}^{i0}=\zeta_{i0'}^{i0}=\zeta_{i0}^{i0}$$

since $\phi_{0'}=\phi_0$.

ζ_{i0}^{i0} is the familiar exchange integral K_{i0}, and we can now apply the general theorem of Roothaan[21] by which all such exchange integrals arising from orthogonal molecular orbitals are necessarily positive. Therefore $\mathcal{H}_{01}$ is a negative quantity and by Eq. (10) λ has a positive value. λ in turn can be identified with $[(n)^{\frac{1}{2}}\cdot(\frac{3}{2})^{\frac{1}{2}}]b/a$ which completes the demonstration of the fact that $\tan\theta$ calculated in this manner is a positive quantity. Furthermore E_1 represents an average monoexcitation energy. A similar first-order perturbation calculation of the quantity b^2/a^2 would show that it is inversely proportional to an average two-electron excitation energy.

ILLUSTRATIVE CALCULATIONS

At least two examples of the experimental determination of the electron-proton coupling constants in odd alternate hydrocarbon radicals are available. The EPR spectra of triphenylmethyl[22] and perinaphthenyl radicals[11,23] have been interpreted in terms of negative spin density at the unstarred carbon atoms. We shall take the values of the spin density at the unstarred carbon atoms of these radicals and calculate a value of the parameter θ. With this quantity the value of the spin density at the starred carbon atom will be determined and compared with those deduced from the experimental measurements.

For ease of numerical computation we assume that b is such a small quantity that terms of order b^2 [Eqs. (7) and (8)] can be neglected. We shall see later that this assumption is justified. Neglecting all but terms linear in b, we have

$$\rho_A=(1-\tfrac{2}{3}\tan\theta)C_{0A}^2+\tfrac{2}{3}\tan\theta,$$

$$\rho_B=-\tfrac{2}{3}\tan\theta.$$

For the case of triphenylmethyl radical experiment[24] shows that $|\rho_3|=|\rho_5|=2|\rho_4|$ with the numbering shown below.

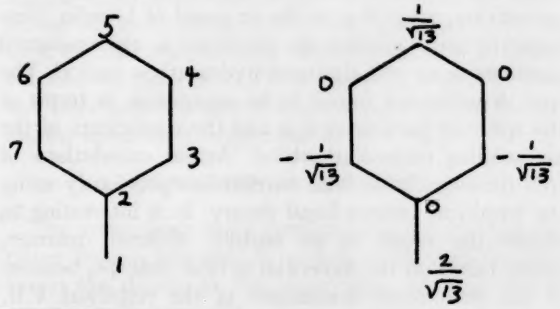

[21] C. C. J. Roothaan, Revs. Modern Phys. **23**, 69 (1951).

[22] F. C. Adam and S. I. Weissman, J. Am. Chem. Soc. **80**, 2057 (1958).

[23] H. M. McConnell and H. H. Dearman, J. Chem. Phys. **28**, 51 (1958).

[24] D. C. Reitz, J. Chem. Phys. **30**, 1364 (1959).

The values of the coefficients of the nonbonding orbital are also included.

The sum of all the absolute values of the spin density at carbon atoms linked to a proton has been shown to be 1.57.[22] From a comparison of these two results we find that

$$3\{2\,|\,\rho_3\,|+2\,|\,\rho_4\,|+|\,\rho_5\,|\}=24\,|\,\rho_4\,|=1.57,$$

$$|\,\rho_4\,|=0.065,$$

$$\rho_4=-0.065.$$

The value of ρ_4 is also the value of the quantity $-2b/3a$ which enters the calculation of the positive spin density. Using the coefficients shown, we obtain in this way $\rho_3=\rho_5=0.137$, which is very nearly twice the value of $|\,\rho_4\,|$. The spin density on the methyl carbon atom is calculated to be 0.360.

For the perinaphthenyl radical $|\,\rho_1\,|$ is measured as 0.098. Thus $\rho_1=-0.098$ from which we calculate $\rho_2=0.247$ instead of the experimental value of 0.327.

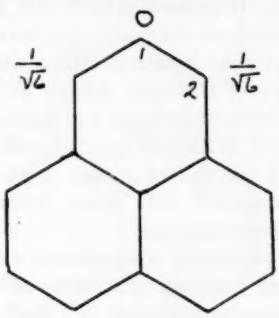

Considering that for triphenylmethyl $b/a=0.097$ and for perinaphthenyl $b/a=0.147$, it can be seen that neglect of higher powers of b/a in the spin density relations is justified.

CONCLUSION

It has been shown that if the conventional MO scheme is extended in such a way as to include electron correlation, according to the proposal of Löwdin, then negative spin densities are predicted at the unstarred positions in an odd alternant hydrocarbon radical. The spin densities are found to be expressible in terms of the splitting parameter b/a and the coefficients of the nonbonding molecular orbital. Actual calculations of spin densities have been carried out previously using the empirical valence bond theory. It is interesting to obtain the result in an entirely different manner, firmly based on the molecular orbital concept, because of the well-known limitations of the empirical V.B. theory.

A value of the spin density at a particular carbon atom deduced from the experimental proton coupling constant via the linear relationship between this constant and the spin density at the adjacent carbon atom can then be used to determine the parameter entering the total wave function, thus affording a way to a quantity which would otherwise involve a lengthy variational calculation. The rather good agreement between the other calculated spin densities and their experimental counterparts can be taken as an indication of the general validity of such a scheme.

If the constraint of a single splitting parameter is lifted the spin density at the unstarred carbon atoms are still found to be negative, as shown in the appendix, but the formulas there obtained appear to be less useful for practical applications.

APPENDIX

A more general form for T_0 is

$$T_0'=|\,(a_1\phi_1+b_1\phi_{1'})(a_2\phi_2+b_2\phi_{2'})\cdots(a_n\phi_n+b_n\phi_{n'})\phi_0$$
$$\cdot(a_1\bar{\phi}_1-b_1\bar{\phi}_{1'})(a_2\bar{\phi}_2-b_2\bar{\phi}_{2'})\cdots(a_n\bar{\phi}_n-b_n\bar{\phi}_{n'})\,|. \quad (13)$$

Application of the same procedure described in the text has the effect of leading to different coefficients for the various functions which arise from expansion and projection of T_0.

The molecular orbital spin density now takes on the form

$$\rho(r)=(N'')^{-1}\{\delta_{00}+\tfrac{4}{3}\sum_{i=1}^{n}(b_i/a_i)\delta_{ii'}$$
$$+\tfrac{1}{9}\sum_{i=1}^{n}(b_i/a_i)^2[4\delta_{i'i'}+4\delta_{ii}-2\delta_{00}]$$
$$+\tfrac{8}{9}\sum_{i>j}(b_i/a_i)(b_j/a_j)^2\delta_{ii'}+\tfrac{4}{3}\sum_{i>j}(b_i/a_i)^2(b_j/a_j)^2\delta_{00}$$
$$+\tfrac{4}{3}\sum_{i=j}^{n}(b_i/a_i)^3\delta_{ii'}+\sum_{i=j}^{n}(b_i/a_i)^4\delta_{00}\}. \quad (14)$$

in which

$$N''=1+\tfrac{2}{3}\sum_{i=1}^{n}(b_i/a_i)^2+\tfrac{4}{3}\sum_{i>j}(b_i/a_i)^2(b_j/a_j)^2$$
$$+\sum_{i=1}^{n}(b_i/a_i)^4.$$

The formulas for atomic orbital spin densities which correspond to Eqs. (7) and (8) are

$$\rho_A(r)=(N'')^{-1}\{C_{0A}{}^2-\tfrac{2}{9}\sum_{i=1}^{n}(b_i/a_i)^2C_{0A}{}^2$$
$$+\tfrac{4}{3}\sum_{i>j}(b_i/a_i)^2(b_j/a_j)^2C_{0A}{}^2+\sum_{i}(b_i/a_i)^4C_{0A}{}^2$$
$$+\sum_{i=1}^{n}C_{iA}{}^2[\tfrac{4}{3}(b_i/a_i)+\tfrac{8}{9}(b_i/a_i)^2+\tfrac{8}{9}(b_i/a_i)^2\sum_{i>j}(b_j/a_j)^2$$
$$+\tfrac{4}{3}(b_i/a_i)^3]\}\chi_A{}^2(r) \quad (15)$$

and

$$\rho_B(r)=(N'')^{-1}\{\sum_{i=1}^{n}C_{iA}^2[-\tfrac{4}{9}(b_i/a_i)^2+\tfrac{8}{9}(b_i/a_i)^2 -\tfrac{4}{9}(b_i/a_i)^3-\tfrac{8}{9}(b_i/a_i)\sum_{>j}(b_j/a_j)^2]\}\chi_B^2(r). \quad (16)$$

To determine the sign of b_i/a_i the same type of argument as proposed in the text can be applied.

$$\Psi_{\text{ground state}}=\psi_0+\sum_{K=1}^{n}\lambda_K\psi_K,$$

where

$$\lambda_K=-\mathcal{H}_{0K}/E_K-E_0,$$

$$\mathcal{H}_{0K}=-(\tfrac{3}{2})^{\frac{1}{2}}\zeta_{K0^{K0}},$$

λ_K, thus b_K/a_K, is a positive quantity because of positive value which $\zeta_{K0^{K0}}$ must have.

Inclusion of different θ_i's has the effect of weighing the excited configurations differently, which is certainly the more reasonable case. We note that the conclusion of negative spin density at the unstarred atom is still valid in this more general treatment. However, in this approximation the spin density at different unstarred atoms is not the same. Unfortunately no experimental results are available for the case of proton-electron coupling on more than one unstarred carbon atom.

THE JOURNAL OF CHEMICAL PHYSICS VOLUME 32, NUMBER 1 JANUARY, 1960

Vibrational Spectra of OsF_6 and PtF_6*

BERNARD WEINSTOCK, HOWARD H. CLAASSEN,† AND JOHN G. MALM

Argonne National Laboratory, Lemont, Illinois

(Received July 28, 1959)

Infrared absorption spectra of gaseous OsF_6 and PtF_6 from 6–50μ and the Raman spectrum of liquid OsF_6 are reported. These are interpreted in terms of the octahedral point group O_h, and the six fundamental frequencies are determined. Their values and symmetry species are for OsF_6 733 (a_{1g}), 632 (e_g), 720 (f_{1u}), 268 (f_{1u}), 252 (f_{2g}), and 230 (f_{2u}); for PtF_6 655 (a_{1g}), 601 (e_g), 705 (f_{1u}), 273 (f_{1u}), 242 (f_{2g}), and 211 (f_{2u}). Thermodynamic functions, including electronic contributions, are calculated for the ideal gaseous state of both compounds.

A comparison of the details of the vibrational spectra of eleven hexafluorides reveals certain characteristic features for OsF_6 and ReF_6. Since only these two molecules have appropriately degenerate electronic ground states these differences are interpreted as evidence of a Jahn-Teller effect.

INTRODUCTION

THE characteristic volatility of the inorganic hexafluorides offers the possibility for the study of the behavior of nonbonding electrons in molecular environments of well-defined symmetry. In the vapor phase where molecular distortions due to neighboring molecules are largely avoided, these compounds have been found to have the high symmetry of the octahedral point group O_h. There is the interesting possibility, however, that a distortion due to the Jahn-Teller effect can arise for those compounds in which the nonbonding electrons produce degenerate ground states.[1]

In the infrared spectra of NpF_6 and PuF_6, which we previously reported,[2] no evidence for distortion of the molecular configuration due to the nonbonding 5*f* electrons in these molecules was apparent. In the present paper the vibrational spectra of OsF_6 and PtF_6, which contain two and four nonbonding 5*d* electrons, respectively, are reported. This study of OsF_6 contributed to the demonstration that the volatile yellow fluoride of Os is actually a hexafluoride and not the unique octafluoride that it had been erroneously called during the forty years since its first preparation.[3] Also, these infrared measurements with the recently prepared, volatile, red fluoride of Pt[4] supported its identification as a hexafluoride molecule and consequently as the only known hexavalent compound of Pt.

EXPERIMENTAL TECHNIQUE

The compounds were prepared by the reaction between fluorine gas and the metals at elevated temperatures; the details of the preparation and purification are given elsewhere.[3,4]

The infrared absorption spectra of OsF_6 and PtF_6

* Based on work performed under the auspices of the U. S. Atomic Energy Commission.

† Permanent address, Wheaton College, Wheaton, Illinois.

[1] H. A. Jahn and E. Teller, Proc. Roy. Soc. (London) **A161**, 220 (1937).

[2] Malm, Weinstock, and Claassen, J. Chem. Phys. **23**, 2192 (1955).

[3] B. Weinstock and J. G. Malm, J. Am. Chem. Soc. **80**, 4466 (1958).

[4] Weinstock, Claassen, and Malm, J. Am. Chem. Soc. **79**, 5832 (1957).

were studied using a Model 21 Perkin-Elmer spectrophotometer from 4000 to 400 cm^{-1} with NaCl and KBr optics and a Beckman IR-4 spectrophotometer from 1000 to 300 cm^{-1} with CsBr optics. The range from 350 to 200 cm^{-1} was studied with a grating spectrometer at Ohio State University. We are indebted to Dr. R. A. Oetjen for the use of this far infrared spectrograph[5] and to his students, Miles Vance and Raymond Brown, for their help in obtaining the spectra.

Two 1-in. i.d. absorption cells were used: a nickel cell, 10.3 cm long and fitted either with AgCl or with polyethylene windows, and a brass cell 11.0 cm long with BaF_2 windows. The BaF_2 windows were very brittle and cracked upon the application of even slight pressure against soft gasket materials. For this reason the windows were cemented to the cell with a thermal setting Araldyte resin. The resin was set by maintaining it overnight at 140°C. To prevent cracking of windows due to unequal thermal contraction upon cooling, a thin-walled ($\frac{1}{32}$ in.) metal tube was used. Brass was chosen rather than Ni because its expansion coefficient more nearly matches that of CaF_2, which in turn has physical properties close to those of BaF_2.

Considerable difficulty was encountered in obtaining the spectra because of attack or deposition on the window materials. In general, BaF_2 was found to be superior to AgCl out to its practical cutoff frequency of 800 cm^{-1}. Although both hexafluorides are strong fluorinating agents, polyethylene was again successfully used as the window material in the region 450 to 200 cm^{-1} as had been done with ClF_3.[6] It was therefore not necessary to use KRS-5 windows, which show rapid attack by other hexafluorides.[2]

The Raman spectrum of liquid OsF_6 was obtained using a Hilger E612 spectrograph with $f/6.3$ camera and Eastman 103 a−C plates. Excitation was by the 5461A line from a water cooled mercury arc filtered by a 3-cm thickness of 13 wt % aqueous Na_2CrO_4. The filtering solution and sample tube were kept about five degrees above the melting point of OsF_6, 32°C. Exposure times were 15, 45, and 150 min. The green Hg line was used rather than the blue in order to minimize possible photochemical decomposition of the yellow liquid. The sample tube for the Raman experiment consisted of a 2-cm length of 6-mm o.d. Pyrex tubing with a plane window that contained the liquefied sample during the irradiations. Joined to this was a 10-cm length of 12-mm tubing that was used to condense the sample during the filling and served as a ballast volume for possible fluorine pressure build-up arising from photochemical decomposition. The concern about photochemical decomposition was a consequence of our experiences with NpF_6 and PuF_6 where the photochemical decomposition even with the vapor was too severe to allow a study of the Raman effect.[2] However, OsF_6, in spite of its yellow color in the liquid phase, appeared to be relatively insensitive to photochemical decomposition.[7] No attempt was made to obtain the Raman spectrum of the intensely colored dark red PtF_6.

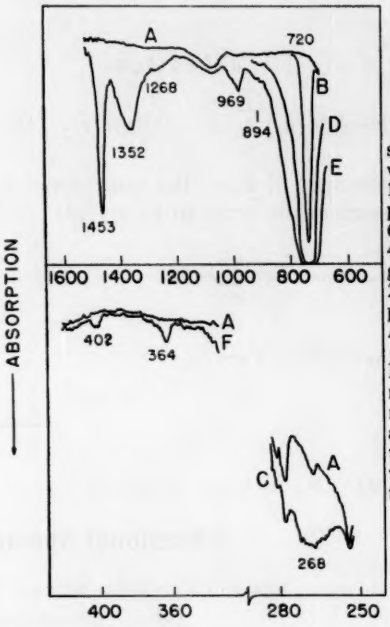

FIG. 1. Infrared spectrum of OsF_6 vapor (cell length, 10.3 cm) using NaCl prism from 1500 to 650 cm^{-1}, CsBr from 450 to 300 cm^{-1}, and grating from 300 to 250 cm^{-1}. The sample pressures were: A (background), B (5 mm), C (13 mm), D (90 mm), E (300 mm), and F (600 mm). The cell was at room temperature except for F when it was maintained at 45°C.

SPECTRA AND INTERPRETATION

Two Raman bands were observed for OsF_6 shifted 252 and 733 cm^{-1} from the exciting line. The former is clearly visible on the 15-min. exposure where the latter is barely seen, and the 733-cm^{-1} band appears clear and sharp on the 45-min exposure where the 252-cm^{-1} is hidden in the high background near the exciting line. It is difficult to make even a qualitative estimate of relative intensities because the sample absorbs in the visible and because of the high background at the 252-cm^{-1} band. Although the third Raman-active fundamental would lie in a favorable region for observation, it is neither observed in these exposures nor in a 150-min. exposure and therefore it is clearly weaker or much more diffuse than those observed.

The tracings of the infrared spectra are shown in Figs. 1 and 2. These were obtained only after much difficulty because of the reactive nature of the compounds under study. Two kinds of spurious absorption bands resulted, one due to nonvolatile deposits on the window and the other to contamination of the gas with volatile reaction products. This seasoning of the cell eventually ceased or became very slow so that it was possible to interpret the spectra reliably. To avoid false interpretations due to window deposits no spec-

[5] Oetjen, Haynie, Ward, Hansler, Schauwecher and Bell, J. Opt. Soc. Am. **42**, 559 (1952).

[6] Claassen, Weinstock, and Malm, J. Chem. Phys. **28**, 285 (1958).

[7] The 1.5-g sample of OsF_6 used for the Raman experiment was quantitatively recovered about a year later; the upper limit of photochemical decomposition was estimated to be 0.3%.

tral scan was taken as reliable unless the background scan was the same before and after the sample scan. For example in the PtF_6 spectrum shown in Fig. 2 the large background absorptions between 500–700 cm^{-1} and 1100–1200 cm^{-1} resulted from the initial exposure of the gas to the windows but did not sensibly alter during the further measurements. The absorption bands due to the volatile impurities were identified in the course of increasing the sample pressure by raising the temperature of the condensed phase in the sidearm; a point being reached where the intensity of the spurious bands increased very little while the sample bands continued to increase. It was possible to obtain spectra that were free from this type of impurity by repeated seasoning of the cell and repurification of the samples by vacuum fractional sublimation. The spectra shown in Figs. 1 and 2 are believed to be representative of the pure compounds. An uncertainty remains for some very weak absorption bands observed for OsF_6 at 325, 352, 544, 644, and 800 cm^{-1}. These were observed in scans other than those shown in Fig. 1 and although they very likely are due to impurities they cannot be ruled out with certainty because of their weakness.

The main features of the spectra for OsF_6 and PtF_6 are similar to those observed for the other 5*d* transition

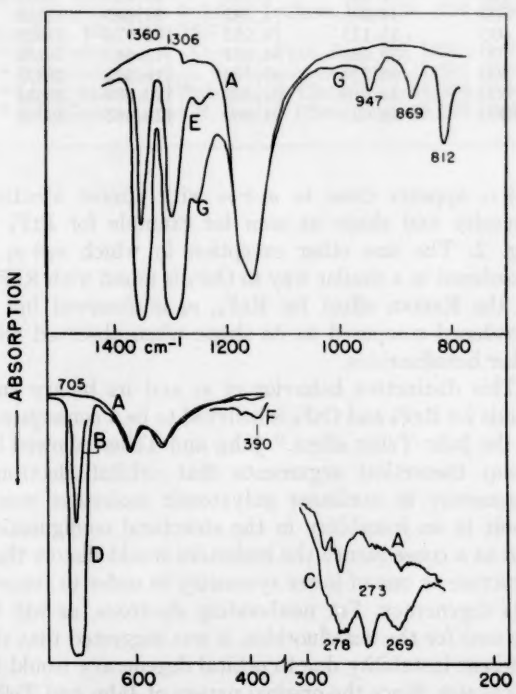

FIG. 2. Infrared spectrum of PtF_6 vapor (cell length, 10.3 cm), using NaCl prism from 1500 to 800 cm^{-1}, KBr from 750 to 375 cm^{-1}, and grating from 300 to 250 cm^{-1}. The sample pressures were: A (background), B (1 mm), C (20 mm), D (27 mm), E (110 mm), F (240 mm), and G (370 mm). The cell was at room temperature except for F and G when it was maintained at 50°C.

TABLE I. The vibrational spectra (cm^{-1}).

OsF_6		PtF_6		
Observed	Calculated	Observed	Calculated	Assignment
252	(Raman)	...	...	σ_5
268 *S*	...	269, 273, 278 *VS*	...	σ_4
364 *VW*	364	...	328	$\sigma_2-\sigma_4$
402 *VW*	402	390 *VW*	390	$\sigma_2-\sigma_6$
720 *VS*	...	705 *VS*	...	σ_3
733	(Raman)	...	...	σ_1
...	862	812 *W*	812	$\sigma_2+\sigma_6$
894 *VW*	900	869 *W*	874	$\sigma_2+\sigma_4$
969 *W*	972	947 *W*	947	$\sigma_3+\sigma_5$
1268 *VW*	1256	1250 *VW*	1251	$2\sigma_4+\sigma_3$
1352 *W*	1352	1306 *M*	1306	$\sigma_2+\sigma_3$
1453 *M*	1453	1360 *M*	1360	$\sigma_1+\sigma_3$

series hexafluorides, WF_6,[8] ReF_6,[9] and IrF_6,[10] and on this basis the spectra are interpreted successfully in terms of the structure of a regular octahedron, point group O_h. The infrared-active binary combinations for molecules of this type are tabulated in reference 8. The two infrared-active fundamentals σ_3 and σ_4 are easily recognized because of their great intensity. Two moderately strong bands for both OsF_6 and PtF_6 at roughly twice the frequency of σ_3 can be assigned unambiguously as $\sigma_1+\sigma_3$ and $\sigma_2+\sigma_3$ and serve to locate σ_1 and σ_2. Similarly, σ_5 can be evaluated for both from the sum band $\sigma_3+\sigma_5$. For OsF_6 both σ_1 and σ_5 thus obtained agree well with the values obtained directly in the Raman spectrum. For PtF_6, σ_6 can be located from the binary combination $\sigma_2+\sigma_6$ as well as from the corresponding difference band. The sum band $\sigma_2+\sigma_6$ was not observed in OsF_6 and although the difference band was observed it was necessary to heat the cell above room temperature. Although the failure to observe $\sigma_2+\sigma_6$ for OsF_6 may in part be due to its proximity to the strong fundamental σ_3 we shall presently offer another explanation.

The observed vibrational frequencies of OsF_6 and PtF_6, their assignments, and the calculated values for the combination bands are listed in Table I. In Table II are listed the derived fundamental frequencies as well as their spectral activity and symmetry species.

THERMODYNAMIC PROPERTIES

The thermodynamic properties of OsF_6 and PtF_6 in the ideal gaseous state at one atmosphere pressure from 250 to 1000°K are given in Tables III and IV, respectively. These have been calculated by means of statistical mechanics with the usual approximations and include contributions from the excited electronic levels as well as from the degeneracy of the ground state.

[8] Burke, Smith, and Nielsen, J. Chem. Phys. **20**, 447 (1952).
[9] J. Gaunt, Trans. Faraday Soc. **50**, 209 (1954).
[10] Mattraw, Hawkins, Carpenter, and Sabol, J. Chem. Phys. **23**, 985 (1955).

TABLE II. Fundamental vibrational frequencies (cm^{-1}).

Designation	Symmetry species	Spectral activity	OsF_6	PtF_6
σ_1	a_{1g}	Raman, p	733	655
σ_2	e_g	Raman, dp	632	601
σ_3	f_{1u}	Infrared	720	705
σ_4	f_{1u}	Infrared	268	273
σ_5	f_{2g}	Raman, dp	252	242
σ_6	f_{2u}	Inactive	230	211

For OsF_6 the following data were used: molecular weight 304.2 on the chemical scale; Os−F distance, 1.831 A;[11] and the pertinent electronic states a fivefold degenerate ground state, a singlet level at 3900 cm^{-1} and a triplet level at 4300 cm^{-1}.[12] For PtF_6 the data were: molecular weight, 309.09;[13] Pt−F distance (extrapolated from values for WF_6, OsF_6, and IrF_6)[11] 1.829 A; and the pertinent electronic states a nondegenerate ground state, a triplet at 3300 cm^{-1} and a quintet at 5500 cm^{-1}.[12] The fundamental constants used in these calculations were taken from the American Petroleum Institute tabulation.[14] For OsF_6 the contribution to the entropy due to the degeneracy of the ground state is $R\ln 5 = 3.198$ cal $mole^{-1}$ deg^{-1}; the contribution due to the excited electronic levels at 1000°K is 0.028 cal $mole^{-1}$ deg^{-1} additionally. For PtF_6 the ground state is nondegenerate and makes no contribution to the entropy; the contribution from the excited electronic levels is 0.321 cal $mole^{-1}$ deg^{-1} at 1000°K.

JAHN-TELLER EFFECT

As previously mentioned, σ_6, the frequency of the inactive fundamental vibration, was difficult to evaluate for OsF_6 because the sum band $\sigma_2+\sigma_6$ from which it is derived for the other hexafluorides was not observed. Furthermore, detailed comparisons of the vibrational spectra show that for OsF_6 the vibration of symmetry e_g, σ_2, and its other allowed binary sum bands appear to be less intense or markedly broader than in the corresponding bands for nine other hexafluorides SF_6, SeF_6, MoF_6, TeF_6, WF_6, UF_6, PtF_6, NpF_6, and PuF_6.[2,8,15,16] Thus, σ_2 was not observed in the Raman effect under conditions where σ_1 and σ_5 were observed whereas σ_2 is usually more easily observed than σ_5 because of the latter's proximity to the exciting line. In addition, $\sigma_2+\sigma_4$ is so weak as to be uncertain and $\sigma_2+\sigma_3$, although intense, is greatly broadened. This broadening of $\sigma_2+\sigma_3$ is particularly noteworthy because a characteristic feature of the infrared spectra of the above mentioned nine hexafluorides is the fact that $\sigma_2+\sigma_3$ appears close to $\sigma_1+\sigma_3$ with almost identical intensity and shape as seen for example for PtF_6 in Fig. 2. The one other exception in which $\sigma_2+\sigma_3$ is broadened in a similar way to OsF_6 is found with ReF_6.[9] In the Raman effect for ReF_6, σ_2 is observed but is broadened compared to its shape when observed with other hexafluorides.

This distinctive behavior of σ_2 and its binary sum bands for ReF_6 and OsF_6 is believed to be a consequence of the Jahn-Teller effect.[17] Jahn and Teller[1] showed by group theoretical arguments that orbital electronic degeneracy in nonlinear polyatomic molecules would result in an instability in the structural configuration and as a consequence the molecules would distort their structure to one of lower symmetry in order to remove this degeneracy. For nonbonding electrons, as will be the case for the hexafluorides, it was suggested that the inherent instability due to orbital degeneracy would be less severe. Since the original papers of Jahn and Teller there have appeared numerous extensions and amplifi-

TABLE III. Thermodynamic properties of OsF_6 in the ideal gaseous state at one atmosphere pressure.

T °K	C_p^0 cal $mole^{-1}$ deg^{-1}	$-(F^0-E_0^0)/T$ cal $mole^{-1}$ deg^{-1}	S^0 cal $mole^{-1}$ deg^{-1}	$(H^0-E_0^0)$ cal $mole^{-1}$
250	26.711	63.782	80.658	4219.0
273.15	27.825	65.315	83.073	4850.5
298.15	28.880	66.909	85.556	5559.6
350	30.657	70.031	90.332	7105.3
400	31.955	72.834	94.514	8672.0
500	33.728	77.925	101.852	11964
600	34.830	82.447	108.106	15396
700	35.558	86.510	113.534	18918
800	36.073	90.192	118.318	22500
900	36.457	93.558	122.589	26128
1000	36.761	96.644	126.431	29786

TABLE IV. Thermodynamic properties of PtF_6 in the ideal gaseous state at one atmosphere pressure.

T °K	C_p^0 cal $mole^{-1}$ deg^{-1}	$-(F^0-E_0^0)/T$ cal $mole^{-1}$ deg^{-1}	S^0 cal $mole^{-1}$ deg^{-1}	$(H^0-E_0^0)$ cal $mole^{-1}$
250	27.222	60.923	78.180	4314.2
273.15	28.312	62.490	80.639	4957.4
298.15	29.355	64.119	83.165	5678.6
350	31.080	67.306	88.013	7247.6
400	32.330	70.164	92.250	8834.2
500	34.046	75.343	99.663	12160
600	35.175	79.935	105.976	15625
700	36.026	84.057	111.465	19186
800	36.750	87.792	116.324	22825
900	37.410	91.209	120.689	26534
1000	38.027	94.360	124.665	30306

[11] Schomaker, Kimura, Smith, and Weinstock (unpublished results).
[12] Moffitt, Goodman, Fred, and Weinstock, Mol. Phys. **2**, 109 (1959).
[13] E. Wichers, J. Am. Chem. Soc. **78**, 3235 (1956).
[14] Rossini, Pitzer, Arnett, Braun, and Pimentel, *Selected Values of Physical and Thermodynamic Properties of Hydrocarbons and Related Compounds* (Carnegie Press, Pittsburgh, 1953).
[15] Yost, Steffens, and Gross, J. Chem. Phys. **2**, 311 (1934).
[16] J. Gaunt, Trans. Faraday Soc. **49**, 1122 (1953).
[17] B. Weinstock and H. H. Claassen, J. Chem. Phys. **31**, 262 (1959).

cations of their theory,[18–23] however, none have detailed the type of effect in the rotation-vibration spectra described in the foregoing.

Of the eleven hexafluorides for which vibrational spectra have been reported in sufficient detail, only ReF_6 and OsF_6 have the appropriate electronic degeneracy to participate in the Jahn-Teller effect. ReF_6 and OsF_6 contain $5d^1$ and $5d^2$ nonbonding electronic configurations which give rise to fourfold and fivefold degenerate ground states, respectively.[12] SF_6, SeF_6, MoF_6, TeF_6, WF_6, and UF_6 use all of their valence electrons in the six bonding orbitals of the molecule and therefore have nondegenerate electronic ground states. For PtF_6[12] and PuF_6[24] which have $5d^4$ and $5f^2$ nonbonding electronic configurations, respectively, the degeneracy of the ground state is removed under the influence of the octahedral ligand field. For NpF_6[25] with a $5f^1$ configuration the ground state is a Kramers doublet which does not participate in the Jahn-Teller effect. IrF_6 also has a degenerate electronic ground state capable of showing a Jahn-Teller coupling but its spectra have not been reported in sufficient detail to be discussed.[10]

Thus, since only ReF_6 and OsF_6 have suitable degenerate ground states it appears very likely that the distinct behavior of σ_2 and its binary combination bands for these molecules is a consequence of the Jahn-Teller effect. This conclusion is substantiated by the fact that σ_2 has the symmetry e_g, which was predicted to result in a nonvanishing contribution to the first-order perturbation energy for point group O_h to which the hexafluorides belong.[1] This observation is in agreement with the view first detailed by Van Vleck[18] and since developed by several others that the Jahn-Teller effect for nonbonding electrons need not evidence itself by a static distortion but rather may appear as a special vibronic coupling. It is also significant that σ_5, the vibration of symmetry f_{2g}, may give rise to similar linear terms in the potential energy but according to these experimental observations the effect is much smaller than that of the e_g vibration in ReF_6 and OsF_6.

FORCE CONSTANTS

When the force constant calculations for hexafluorides[26] were done, σ_6 for OsF_6 had not yet been definitely located and several force constants were left out. With the present value of 230 cm^{-1} for σ_6 we obtain

$$f_\alpha-\gamma-2\kappa+2\epsilon=0.296 \text{ md/A},$$

$f_\alpha-\gamma=0.299$ md/A, $f_{\alpha\alpha}-\gamma=+0.053$ md/A, and

$$\kappa-\epsilon=+0.002 \text{ md/A}.$$

[18] J. H. Van Vleck, J. Chem. Phys. **7** 61, 72 (1939).
[19] U. Öpik and M. H. L. Pryce, Proc. Roy. Soc. (London) **A238**, 425 (1957).
[20] Longuet-Higgins, Öpik, Pryce, and Sack, Proc. Roy. Soc. (London) **A244**, 1 (1958).
[21] W. Moffitt and A. D. Liehr, J. Chem. Phys. **25**, 1074 (1956); Phys. Rev. **106**, 1195 (1957).
[22] W. Moffitt and W. Thorson, Phys. Rev. **108**, 1251 (1957).
[23] A. D. Liehr and C. J. Ballhausen, Ann. Phys. **3**, 304 (1958).
[24] Gruen, Malm, and Weinstock, J. Chem. Phys. **24**, 905 (1956).
[25] G. L. Goodman and M. Fred, J. Chem. Phys. **30**, 849 (1959).
[26] H. H. Claassen, J. Chem. Phys. **30**, 968 (1959).

Elastic and Inelastic Scattering of Low-Velocity D^+ and D_2^+ in Deuterium*†

W. H. CRAMER, *College of Engineering, University of Florida, Gainesville, Florida*

AND

A. B. MARCUS,‡ *Department of Chemistry, University of Florida, Gainesville, Florida*

(Received August 14, 1959)

Results are presented of the measurement in the energy range 4 to 400 ev of elastic and charge exchange cross sections for D^+ and D_2^+ ions in D_2. Ordinary ionization was not observed. Charge exchange was detected above 65 ev for D^+ in D_2 and over the entire range of energies for D_2^+ in D_2. The present results are compared with measurements of collisions of hydrogen ions in H_2.

INTRODUCTION

THE apparatus and methods used in studying collisions of rare gas ions and atoms[1-3] were employed in the present investigation of scattering of deuterium ions in deuterium gas. α_T, the total cross section, was evaluated from the attentuation by target gas molecules of a beam of ions which was produced in a mass spectrometer. α_S, the elastic cross section, was determined from the results of electrostatic separation of slow ions formed by charge exchange from fast elastically scattered ions. A helical grid is coaxial with the axis of the beam in the collision region. By making the outside wall of the collision chamber about 0.25 volt positive with respect to the grid slow ions formed by charge exchange from molecules with thermal energies are repelled from the wall and collected on the grid. Since there is negligible transfer of kinetic energy during the process of charge exchange the ions so formed have energies orders of magnitude less than those ions scattered elastically. α_I, the inelastic (charge exchange) cross section, was taken as the difference between α_T and α_S.

The deuterium which was used as both source gas and target gas was stated to be 99.5% pure. It was introduced into the system through activated charcoal held at liquid-air temperature.

RESULTS

The results of the scattering as functions of the ion energies W are presented in Tables I and II and are exhibited graphically in Figs. 1 and 2. Charge exchange for D^+ ions was detected only at energies greater than 65 ev. No ordinary ionization, i.e., production of free electrons, was observed in collisions involving either D^+ or D_2^+.

In Figs. 3 and 4 are shown plots of log α_S *vs* log W. If it is assumed that the potential energy of interaction may be represented by $V=Kr^{-n}$ then n may be determined from the slope and K from the intercept of these plots.[1]

Potential functions for the interactions of the various systems are collected in Table III.

TABLE I. Elastic and inelastic collision cross sections for D^+ in D_2.

W (ev)	α_T (cm^{-1})	α_S (cm^{-1})	α_I (cm^{-1})
3.2	135	135	0.0
4	109	109	0.0
5	97.9	97.9	0.0
6.5	83.7	83.7	0.0
8	76.6	76.6	0.0
10	73.0	73.0	0.0
12.5	68.7	68.7	0.0
16	56.7	56.7	0.0
20	49.6	49.6	0.0
25	39.9	39.9	0.0
32	29.7	29.7	0.0
40	23.6	23.6	0.0
50	16.6	16.6	0.0
65	12.1	12.0	0.1
80	10.8	10.3	0.5
100	8.32	7.58	0.74
150	4.04	3.18	0.86
200	2.52	1.73	0.79
250	2.13	1.32	0.81
300	1.96	1.03	0.93
400	2.10	1.05	1.05

DISCUSSION

Simons and co-workers[4,5] have measured the elastic and charge exchange cross sections for H^+, H_2^+, and H_3^+ in H_2. Their method of separating ion current due to charge exchange from elastically scattered current was based on applying a draw-out voltage for slow ions to an electrode at the entrance to the scattering region. They did not detect any charge exchange for H^+ in H_2 for energies up to 135 ev. Their elastic cross sections and derived potential energy functions for H^+ in H_2 agree quite well with the present values for D^+ in D_2.

The present results for the elastic scattering of D_2^+ in D_2 also agree rather well with the earlier measurements

* Supported by a grant from the National Science Foundation.

† Based in part on a thesis submitted by one of us (A.B.M.) to the Graduate School at the University of Florida in partial fulfillment of the requirements for the degree of Master of Science.

‡ Present address: Department of Chemistry, Massachusetts Institute of Technology, Cambridge, Massachusetts.

[1] W. H. Cramer and J. H. Simons, J. Chem. Phys. **26**, 1272 (1957).

[2] W. H. Cramer, J. Chem. Phys. **28**, 688 (1958).

[3] W. H. Cramer, J. Chem. Phys. **30**, 641 (1959).

[4] Simons, Fontana, Muschlitz, and Jackson, J. Chem. Phys. **11**, 307 (1943).

[5] Simons, Fontana, Francis, and Unger, J. Chem. Phys. **11**, 312 (1943).

TABLE II. Elastic and inelastic collision cross sections for D_2^+ in D_2.

W (ev)	α_T (cm^{-1})	α_S (cm^{-1})	α_I (cm^{-1})
4	109.4	58.0	51.4
5	117.2	62.6	54.6
6.5	100.5	51.7	48.8
8	99.8	51.0	48.8
10	96.3	49.4	46.9
12.5	92.2	47.9	44.3
16	85.6	43.6	42.0
20	77.8	37.2	40.6
25	75.8	35.9	39.9
32	65.5	30.2	35.4
40	60.7	24.9	35.8
50	55.6	19.7	35.9
65	47.7	16.6	31.1
80	45.5	15.1	30.4
100	40.6	13.0	27.6
150	34.3	10.7	23.6
200	30.2	8.97	21.2
250	27.0	6.97	20.0
300	25.2	6.30	18.9
400	21.6	5.55	16.1

of Simons and co-workers on H_2^+ in H_2. The agreement in the case of charge exchange cross sections is much poorer, D_2^+ in D_2 exhibiting considerably larger inelastic cross sections than does H_2^+ in H_2. The discrepancy increases with decreasing ion energy. The reason for this lack of agreement is not apparent. There is very little difference in the ionization energies of H_2 and D_2. Charge exchange in these cases is not necessarily an exact resonance process; the equilibrium separations of the molecular ion and the respective molecule are not the same. Furthermore, the zero point energies and vibrational levels of the two isotopic molecules are different. Therefore, the energy change for the most probable transition involving charge transfer according to the Franck-Condon principle may not be the same for D_2^+ in D_2 as for H_2^+ in H_2.

A possible reaction, exothermic by some tens of kilocalories per mole,[6] which might contribute to the measured inelastic cross section is the following:

$$D_2^+ + D_2 \rightarrow D_3^+ + D.$$

Stevenson and Schissler[7,8] have studied such ion-molecule reactions at much lower energies than those employed in the present investigation, and they find that the cross sections decrease with increasing energy. Such a reaction cannot absolutely be ruled out of consideration in the present experiments since mass analysis of the collision products cannot be accomplished in the apparatus. If such a reaction did occur ions with kinetic energies between thermal energy and beam energy would be formed. The behavior of grid current as a function of grid voltage did not indicate the presence of ions with such intermediate energies. A chemical kinetics treatment by the method of Eyring[9] predicts that the rate of such a reaction should be higher for the system involving hydrogen. Since the cross sections are higher for the system involving deuterium it appears unlikely that this type of reaction is contributing to the observed cross section.

The actual potential distribution about a hydrogen or deuterium molecule is not spherically symmetrical,

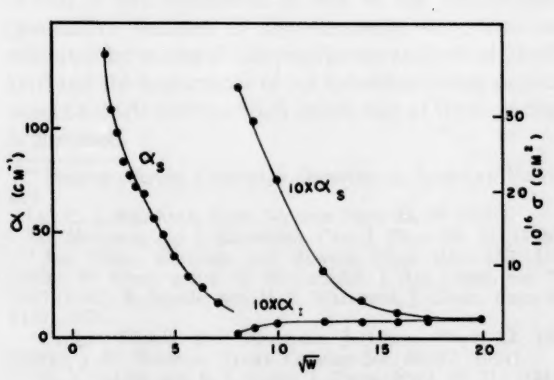

FIG. 1. Scattering data for D^+ in D_2.

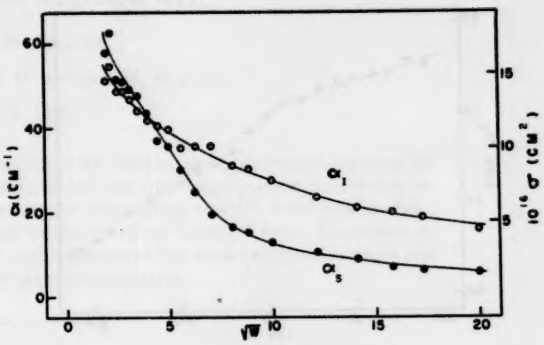

FIG. 2. Scattering data for D_2^+ in D_2.

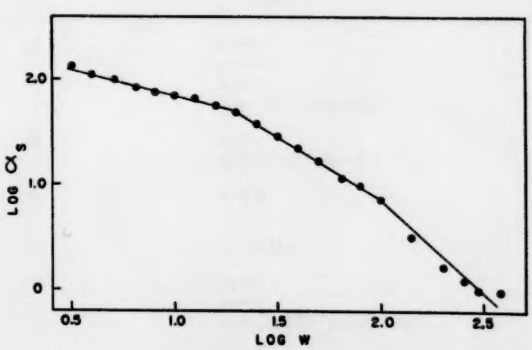

FIG. 3. Elastic scattering of D^+ in D_2.

[6] Hirschfelder, Curtiss, and Bird, *Molecular Theory of Gases and Liquids* (John Wiley & Sons, Inc., New York, 1954).

[7] D. P. Stevenson and D. O. Schissler, J. Chem. Phys. **23**, 1353 (1955).

[8] D. P. Stevenson and D. O. Schissler, J. Chem. Phys. **29**, 282 (1958).

[9] Eyring, Hirschfelder, and Taylor, J. Chem. Phys. **4**, 479 (1936).

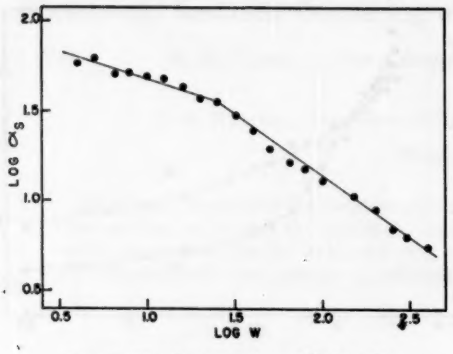

FIG. 4. Elastic scattering of D_2^+ in D_2.

but is angle-dependent; the functions listed in Table III thus represent some sort of average over all possible angular orientations. In the case of the atomic ion and the molecule it is reasonable to assume, at least at the lower energies, that the potential is attractive. This is in accord with the fact that the H_3^+ and D_3^+ molecular ions are well-known entities. Mason and Vanderslice[10] have pointed out that the interaction of H_2^+ and He is repulsion over the range of internuclear separations involved in these experiments, and it is reasonable to assume that the forces are also repulsive for H_2^+ in H_2 and D_2^+ in D_2. The value of n in the potential function $V=Kr^{-n}$ in the approximation employed in this work is the same whether attraction or repulsion is assumed. The value of K, however, calculated on the basis of attraction differs in magnitude and sign from the value obtained on the assumption of repulsion. If it is assumed that the interaction is attraction then K is taken to be negative, and for repulsion K is positive. It is not possible to distinguish experimentally between attractive and repulsive forces. Values based on both assumptions are given in Table III in order to afford ready comparison with the results of Simons and co-workers,[4,5] who assumed attraction in all cases.

TABLE III. Summary of potential functions.

	D^+ in D_2	
$V=-22.4\,r^{-4.03}$	3–20 ev	3.2–2.0 A
$V=-6.56\,r^{-1.69}$	20–100 ev	2.0–0.8 A
	D_2^+ in D_2	
$V=-47.7\,r^{-7.02}$	4–25 ev	2.2–1.7 A
$V=+211\,r^{-7.02}$	4–25 ev	2.7–2.0 A
$V=-8.16\,r^{-3.00}$	25–400 ev	1.7–0.6 A
$V=+14.3\,r^{-3.00}$	25–400 ev	2.0–0.8 A
	H^+ in H_2[a]	
$V=-20.4\,r^{-4.0}$	2–24 ev	>1.7 A
$V=-7.10\,r^{-1.74}$	24–135 ev	1.7–1.5 A
	H_2^+ in H_2[b]	
$V=-10.0\,r^{-1.0}$	10–25 ev	2.1–1.7 A
$V=-6.96\,r^{-3.0}$	25–70 ev	<1.7 A

(r in Angstrom units, V in electron volts)

[a] Reference 4.
[b] Reference 5.

Amdur, Kells, and Davenport[11] found considerable difference in the behavior of hydrogen atoms with hydrogen molecules and deuterium atoms with deuterium molecules at energies above a few hundred ev, where the dominant force is repulsion. It is interesting to note that in the present investigation very little difference was observed in elastic scattering of the isotopic ions by the respective gas molecules.

[10] E. A. Mason and J. T. Vanderslice, J. Chem. Phys. **27**, 917 (1957).

[11] Amdur, Kells, and Davenport, J. Chem. Phys. **18**, 1676 (1950).

Electronic Structure of CH_2 and CH_3

A. PADGETT* AND M. KRAUSS

National Bureau of Standards, Washington 25, D. C.

(Received April 9, 1959)

The self-consistent field molecular orbital method is applied to the calculation of the ground states of the CH_2 and CH_3 molecules. All electrons are explicitly considered but the three- and four-center electron repulsion integrals were approximated. Results are reported for the dissociation energies, excitation energies, ionization potentials, and the hyperfine splitting constants for the Fermi or "contact" term. The values reported for the dissociation energies are in poor agreement with experiment but some qualitative insight into the bonding of these molecules is obtained by an electron population analysis.

I. INTRODUCTION

THE increased interest in free radical research suggests that even approximate self-consistent field linear combination of atomic orbital (SCF-LCAO)[1] calculations of the radicals CH_2 and CH_3 would be of value, particularly since experimental studies of the electronic structure of these molecules are so difficult. The CH_3 radical has been investigated with a flash photolysis technique by Herzberg and Shoosmith,[2] but the spectra of the CH_2 radical have not yet been identified. Observation of the CH_3 radical has been reported several times in electron spin resonance experiments.[3] Both radicals have been extensively studied by mass spectrometric techniques.[4] There is also a considerable literature on experiments where the radicals are identified by recourse to some kinetics scheme. One of the outgrowths of this type of investigation has been the observation[5] of two apparently different species of CH_2 and a continuing discussion regarding the multiplicity of the ground state.[6]

In this paper we report the results of a calculation of the heat of atomization, excitation energies, and hyperfine splitting. A comparison with the results of an extensive calculation of the CH_3 radical by Higuchi[7] reveals some serious discrepancies, but it is difficult to resolve these differences because of the different basis sets that were used. The nonplanarity of the CH_3 radical is not considered in any of the calculations. Qualitative features of the electronic structures are exhibited by means of the population analysis of Mulliken[8] and the importance of s-p hybridization or promotion in a single configuration description of the molecules is discussed.

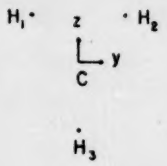

FIG. 1. Coordinate system.

II. METHOD OF CALCULATION

The molecular orbitals are formed from a linear combination of all the atomic orbitals in the basis set which are of the same symmetry species. A limited set of Slater orbitals[9]

$$\begin{aligned} 1s&=h,\ c=(\zeta_1^3/\pi)^{\frac{1}{2}}\exp-\zeta_1 r,\\ s^*&=(\zeta_2^5/3\pi)^{\frac{1}{2}} r\exp-\zeta_2 r,\\ z&=(\zeta_2^5/\pi)^{\frac{1}{2}} r\cos\theta\exp-\zeta_2 r,\\ x&=(\zeta_2^5/\pi)^{\frac{1}{2}} r\cos\phi\sin\theta\exp-\zeta_2 r,\\ y&=(\zeta_2^5/\pi)^{\frac{1}{2}} r\sin\phi\sin\theta\exp-\zeta_2 r, \end{aligned} \qquad (1)$$

are arranged into symmetry orbitals for CH_2 and CH_3 with the coordinate system chosen as in Fig. 1. We have

TABLE I. Symmetry orbitals.

	CH_2
a_1	$\sigma_1=c$
	$\sigma_2=s$
	$\sigma_3=z$
	$\sigma_4=(1/\sqrt{2})(h_1+h_2)$
b_2	$\sigma_5=y$
	$\sigma_6=(1/\sqrt{2})(h_2-h_1)$
b_1	$\sigma_7=x$
	CH_3
a_1'	$\sigma_1=c$
	$\sigma_2=s$
	$\sigma_3=(1/\sqrt{3})(h_1+h_2+h_3)$
e'	$\sigma_4=z$
	$\sigma_5=[1/(6)^{\frac{1}{2}}](-2h_3+h_2+h_1)$
	$\sigma_6=y$
	$\sigma_7=(1/\sqrt{2})(h_2-h_1)$
a_2''	$\sigma_8=x$

[9] The orbital parameters are H, $\zeta_1=1.0$; C, $\zeta_1=5.7$, $\zeta_2=1.625$.

* Present address, Chemistry Department, American University.

[1] C. C. J. Roothaan, Revs. Modern Phys. **23**, 69 (1951).

[2] G. Herzberg and J. Shoosmith, Can. J. Phys. **34**, 523 (1956).

[3] Jen, Foner, Cochran, and Bowers, Phys. Rev. **112**, 1169 (1958); W. Gordy and C. G. McCormick, J. Am. Chem. Soc. **78**, 3243 (1956). B. Smaller and M. S. Matheson, J. Chem. Phys. **28**, 1169 (1958).

[4] Langer, Hipple, and Stevenson, J. Chem. Phys. **22**, 1836 (1954); J. D. Waldron, Trans. Faraday Soc. **50**, 97 (1954).

[5] K. J. Laidler and E. J. Casey, J. Chem. Phys. **17**, 213 (1949).

[6] B. F. Gray, J. Chem. Phys. **28**, 1252 (1958); D. A. Galleys, J. Chem. Phys. **28**, 1252 (1958).

[7] J. Higuchi, J. Chem. Phys. **23**, 2197 (1955); **28**, 527 (1958).

[8] R. S. Mulliken, J. Chem. Phys. **23**, 1833 (1955).

TABLE II. SCF—LCAO solutions.

		CH_2			
90°	$a_{11}=1.00_1$	$a_{12}=0.02_1$	$a_{13}=0.00_6$	$a_{14}=-0.00_8$,	$\epsilon=-11.289$[a]
	$a_{21}=-0.04_4$	$a_{22}=0.64_7$	$a_{23}=0.22_5$	$a_{24}=0.32_2$,	$\epsilon=-0.895$
	$a_{31}=-0.04_2$	$a_{32}=-0.82_0$	$a_{33}=0.60_0$	$a_{34}=0.49_3$,	$\epsilon=-0.405$
	$a_{41}=-0.11_7$	$a_{42}=-1.03_4$	$a_{43}=-0.99_6$	$a_{44}=1.25_2$,	$\epsilon=0.469$
	$a_{55}=0.65_8$	$a_{56}=0.58_6$,			$\epsilon=-0.449$
	$a_{65}=-1.02_5$	$a_{66}=1.38_5$,			$\epsilon=0.341$
120°	$a_{11}=1.00_1$	$a_{12}=0.02_0$	$a_{13}=0.00_5$	$a_{14}=-0.00_8$,	$\epsilon=-11.286$
	$a_{21}=-0.04_3$	$a_{22}=0.69_9$	$a_{23}=0.17_6$	$a_{24}=0.30_5$,	$\epsilon=-0.859$
	$a_{31}=-0.05_0$	$a_{32}=-0.77_6$	$a_{33}=0.67_0$	$a_{34}=0.55_7$,	$\epsilon=-0.366$
	$a_{41}=-0.11_7$	$a_{42}=-1.04_5$	$a_{43}=-0.85_2$	$a_{44}=1.24_6$,	$\epsilon=0.340$
	$a_{55}=0.62_7$	$a_{56}=0.54_2$,			$\epsilon=-0.495$
	$a_{65}=-1.14_2$	$a_{66}=1.38_4$,			$\epsilon=0.383$
150°	$a_{11}=1.00_1$	$a_{12}=0.02_0$	$a_{13}=0.00_3$	$a_{14}=-0.00_7$,	$\epsilon=-11.236$
	$a_{21}=-0.04_3$	$a_{22}=0.72_2$	$a_{23}=0.12_5$	$a_{24}=0.30_5$,	$\epsilon=-0.817$
	$a_{31}=-0.05_1$	$a_{32}=-0.68_8$	$a_{33}=0.78_4$	$a_{34}=0.55_7$,	$\epsilon=-0.305$
	$a_{41}=-0.11_3$	$a_{42}=-1.06_8$	$a_{43}=-0.65_0$	$a_{44}=1.21_3$,	$\epsilon=0.234$
	$a_{55}=0.62_6$	$a_{56}=0.50_6$,			$\epsilon=-0.509$
	$a_{65}=-1.23_2$	$a_{66}=1.43_7$,			$\epsilon=0.443$
180°	$a_{11}=1.00_1$	$a_{12}=0.02_1$	$a_{14}=-0.00_7$,		$\epsilon=-11.118$
	$a_{21}=-0.04_9$	$a_{22}=0.68_9$	$a_{24}=0.35_5$,		$\epsilon=-0.739$
	$a_{31}=-0.12_1$	$a_{32}=-1.27_9$	$a_{34}=1.30_7$,		$\epsilon=0.185$
	$a_{45}=0.64_5$	$a_{46}=0.47_3$,			$\epsilon=-0.483$
	$a_{55}=-1.26_0$	$a_{56}=1.47_1$,			$\epsilon=0.487$
		CH_3			
	$a_{11}=1.00_1$	$a_{12}=0.02_4$	$a_{13}=-0.00_8$,		$\epsilon=-11.058$
	$a_{21}=-0.05_3$	$a_{22}=0.66_7$	$a_{23}=0.31_9$,		$\epsilon=-0.766$
	$a_{31}=-0.15_1$	$a_{32}=-1.49_5$	$a_{33}=1.32_2$,		$\epsilon=0.154$
	$a_{44}=a_{66}=0.69_0$	$a_{45}=a_{67}=0.46_3$,			$\epsilon=-0.396$
	$a_{54}=a_{76}=-1.10_5$	$a_{55}=a_{77}=1.41_2$,			$\epsilon=0.414$

[a] In a.u.; 1 a.u.=27.210 ev.

assumed that the nuclear framework of CH_2 has the symmetry C_{2v} and that CH_3 is planar with D_{3h} symmetry. This configuration for CH_3 is probably not far enough from equilibrium[2] to warrant the additional effort that would be needed to treat the nonplanar case. The symmetry orbitals are given in Table I. The nodeless s^* atomic orbital has been replaced by the function

$$s=(1-S^2)^{-\frac{1}{2}}(s^*-S\cdot 1s). \qquad (2)$$

The ground state configurations of CH_2 and CH_3 may be represented by

$$CH_2,\ ^1A_1,\ (1a_1)^2(2a_1)^2(1b_2)^2(3a_1)^2;$$
$$CH_3,\ ^2A_2'',\ (1a_1')^2(2a_1')^2(1e')^4(1a_2'')^1, \qquad (3)$$

where

$$ia_1=\sum_j a_{ij}\sigma_j \qquad i,j=1,2,3,4$$
$$ib_2=\sum_j a_{ij}\sigma_j \qquad i,j=5,6$$
$$ia'_1=\sum_j a_{ij}\sigma_j \qquad i,j=1,2,3$$
$$ie'_x=\sum_j a_{ij}\sigma_j \qquad i,j=4,5$$
$$ie'_y=\sum_j a_{ij}\sigma_j \qquad k,j=6,7. \qquad (4)$$

For CH_2 the SCF-LCAO procedure developed by Roothaan is directly applicable and for CH_3 the parameters are varied in the closed shell configuration $(1a_1')^2(2a_1')^2(1e')^4$, considering the $1a_2''$ orbital fixed. All one- and two-center integrals had previously been obtained for a calculation of the CH radical,[10] and the CH internuclear distance, 2.124 a.u., therefore was retained. The three-center nuclear attraction integrals were computed by the method of Coulson.[11] Those two-center electron interaction integrals involving exclusively hydrogenic function were obtained by standard techniques. The major problem of evaluating the three- and four-center electron interaction integrals was avoided by employing the approximation suggested by Mulliken[12] and formalized by Ruedenberg.[13] We shall not attempt to discuss the adequacy of this approximation except to note that some experimentation for CH_3 with other approximations[14] indicates little change in qualitative information.

Iterative solution of the secular determinants leads to the results given in Table II. The molecular orbitals determined by variation of the ground state were used

[10] M. Krauss, J. Chem. Phys. **28**, 1021 (1958).
[11] C. A. Coulson, Proc. Camb. Phil. Soc. **33**, 104 (1937).
[12] R. S. Mulliken, J. chim. phys. **46**, 497 (1949).
[13] K. Ruedenberg, J. Chem. Phys. **19**, 1433 (1951).
[14] F. O. Ellison, J. Chem. Phys. **23**, 2358 (1955).

to calculate the energies of the following excited electronic states:

CH_2

$^3B_1$, $(1a_1)^2(2a_1)^2(1b_2)^2(3a_1)^1(1b_1)^1$
$^1B_1$, $(1a_1)^2(2a_1)^2(1b_2)^2(3a_1)^1(1b_1)^1$
$^3A_2$, $(1a_1)^2(2a_1)^2(3a_1)^2(1b_2)^1(1b_1)^1$
$^1A_2$, $(1a_1)^2(2a_1)^2(3a_1)^2(1b_2)^1(1b_1)^1$
$^3B_2$, $(1a_1)^2(2a_1)^2(3a_1)^1(1b_2)^1(1b_1)^2$
$^1B_2$, $(1a_1)^2(2a_1)^2(3a_1)^1(1b_2)^1(1b_1)^2$
$^3A_1$, $(1a_1)^2(2a_1)^2(1b_2)^2(3a_1)^1(4a_1)^1$
$^1A_1$, $(1a_1)^2(2a_1)^2(1b_2)^2(1b_1)^2$;

CH_3

$^2E'$, $(1a_1')^2(2a_1')^2(1e_y')^2(1e_x')^1(1a_2'')^2$
$^2A_1'$, $(1a_1')^2(2a_1')^2(1e_y')^2(1e_x')^2(3a_1')^1$.

The states of linear CH_2 which correlate with these states were also obtained. Further improvement in the energies of the excited and ground states was then effected by means of a second-order perturbation treatment. A list of the excited configurations considered in the second-order perturbation calculation is given below. Neither the form of the symmetry state or states that arise from the configuration nor the importance of the state in the energy calculation is considered except that those states with identically zero matrix elements in this approximation are omitted:

CH_2

$^1A_1$, $(1a_1)^2(2a_1)^2(3a_1)^2(4a_1)^2$
$(1a_1)^2(2a_1)^2(3a_1)^2(2b_2)^2$
$(1a_1)^2(2a_1)^2(3a_1)^2(1b_1)^2$
$(1a_1)^2(2a_1)^2(4a_1)^2(1b_2)^2$
$(1a_1)^2(2a_1)^2(1b_2)^2(2b_2)^2$
$(1a_1)^2(2a_1)^2(1b_2)^2(1b_1)^2$
$(1a_1)^2(3a_1)^2(1b_2)^2(1b_1)^2$
$(1a_1)^2(3a_1)^2(4a_1)^2(1b_2)^2$
$(1a_1)^2(3a_1)^2(1b_2)^2(2b_2)^2$

$^3A_1$, $(1a_1)^2(2a_1)^2(3a_1)^2(1b_2)^1(2b_2)^1$
$(1a_1)^2(2a_1)^2(3a_1)^1(4a_1)^1(1b_1)^2$
$(1a_1)^2(2a_1)^1(3a_1)^2(4a_1)^1(1b_2)^2$
$(1a_1)^2(2a_1)^1(3a_1)^1(1b_2)^2(1b_1)^2$
$(1a_1)^2(2a_1)^1(4a_1)^1(1b_2)^2(1b_1)^2$

$^1B_1, {}^3B_1$, $(1a_1)^2(2a_1)^2(4a_1)^1(1b_2)^2(1b_1)^1$
$(1a_1)^2(2a_1)^2(3a_1)(4a_1)^2(1b_1)^1$
$(1a_1)^2(2a_1)^2(3a_1)^1(2b_2)^2(1b_1)^1$
$(1a_1)^2(2a_1)^1(3a_1)^2(1b_2)^2(1b_1)^1$
$(1a_1)^2(3a_1)^2(4a_1)^1(1b_2)^2(1b_1)^1$
$(1a_1)^2(2a_1)^1(3a_1)^1(4a_1)^1(1b_2)^2(1b_1)^1$
$(1a_1)^2(2a_1)^2(3a_1)^1(1b_2)^1(2b_2)^1(1b_1)^1$
$(1a_1)^2(2a_1)^1(3a_1)^2(1b_2)^1(2b_2)^1(1b_1)^1$

$^1A_2, {}^3A_2$, $(1a_1)^2(2a_1)^2(3a_1)^2(2b_2)^1(1b_1)^1$
$(1a_1)^2(2a_1)^2(3a_1)^1(4a_1)^1(1b_2)^1(1b_1)^1$
$(1a_1)^2(2a_1)^2(4a_1)^2(1b_2)^1(1b_1)^1$
$(1a_1)^2(2a_1)^2(1b_2)^2(2b_2)^1(1b_1)^1$
$(1a_1)^2(2a_1)^1(3a_1)^2(4a_1)^1(1b_2)^1(1b_1)^1$

$^1B_2, {}^3B_2$, $(1a_1)^2(2a_1)^2(3a_1)^2(4a_1)^1(1b_2)^1$
$(1a_1)^2(2a_1)^2(3a_1)^1(4a_1)^2(1b_2)^1$
$(1a_1)^2(2a_1)^2(3a_1)^1(2b_2)^1(1b_1)^2$
$(1a_1)^2(2a_1)^2(4a_1)^1(1b_2)^1(1b_1)^2$
$(1a_1)^2(2a_1)^2(4a_1)^1(2b_2)^1(1b_1)^2$
$(1a_1)^2(2a_1)^1(3a_1)^1(4a_1)^1(1b_2)^1(1b_1)^2$;

CH_3

$^2A_2''$, $(1a_1')^2(2a_1')^1(3a_1')^1(1e_y')^2(1e_x')^2(1a_2'')^1$
$(1a_1')^2(3a_1')^2(1e_y')^2(1e_x')^2(1a_2'')^1$
$(1a_1')^2(2a_1')^2(1e_y')^2(1e_x')^1(2e_x')^1(1a_2'')^1$
$(1a_1')^2(2a_1')^2(1e_x')^2(1e_y')^1(2e_y')^1(1a_2'')^1$
$(1a_1')^2(2a_1')^2(1e')^2(2e')^2(1a_2'')^1$

$^2A_2'$, $(1a_1')^2(2a_1')^1(1e_y')^2(1e_x')^2(1a_2'')^2$
$(1a_1')^2(2a_1')^2(3a_1')^1(1e_y')^2(1e_x')^1(2e_x')^1$
$(1a_1')^2(2a_1')^2(3a_1')^1(1e_x')^2(1e_y')^1(2e_y')^1$
$(1a_1')^2(2a_1')^2(3a_1')^1(1e')^2(1a_2'')^2$
$(1a_1')^2(2a_1')^1(3a_1')^2(1e_y')^2(1e_x')^2$

$^2E'$, $(1a_1')^2(2a_1')^2(1e_y')^2(1e_x')^2(2e_x')^1$.

The two configurations for which the component of the e' orbitals is not designated are composed of all possible combinations of the two components. For the $^2E'$ state the two levels arising from the listed configurations have energies sufficiently close to each other that it was felt that the solution of the secular determinant for these states would suffice.

III. DISSOCIATION AND EXCITATION ENERGIES

We shall accept the values of the heats of atomization proposed by Laidler and Casey.[5] Our calculated atomization energies, listed in Table III, are very inaccurate while Higuchi, who employs a variant of the atom-in-molecule concept, obtains a much more accurate value of 0.463 a.u. for CH_3. The poor values obtained for the dissociation energies may arise from the use of approximate integrals, since a similar calculation for diborane made by Yamazaki[15] gave only 35% of binding, while a calculation for NH_3 by Duncan[16] involving exact integrals gave 72% of the experimental value. We must

TABLE III. Heat of atomization.[a]

	CH_2	CH_3
A_t[b] (This work)	0.05_3	-0.00_9
A_t[c] (This work)	0.08_7	0.02_0
A_t[d] (Higuchi)		0.463
A_t[e] (Exptl.)	0.345	0.470

[a] In a.u.
[b] Zero-point energy was not deducted from calculated values.
[c] Second-order perturbation calculation.
[d] See reference 7.
[e] See reference 5.

[15] M. Yamazaki, J. Chem. Phys. **27**, 1401 (1957).
[16] A. B. F. Duncan, J. Chem. Phys. **27**, 423 (1957).

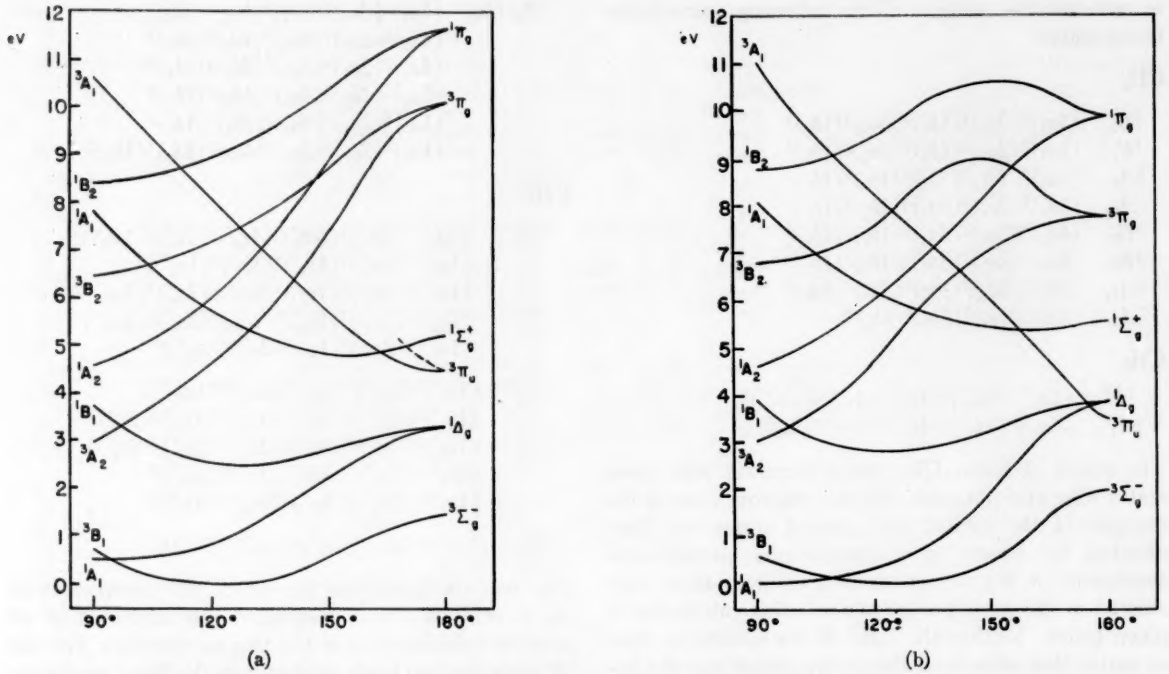

FIG. 2(a). Energy level diagram for CH_2 as a function of angle. Single configuration calculation; (b) second-order configuration interaction perturbation calculation.

remember, however, that all calculations are relative to the calculated and not experimental atomic energies and the results for diatomic molecules,[17] where all integrals are calculated exactly, are generally poor.

The excitation energies found for CH_3 differed in one major respect from those calculated by Higuchi or predicted by Walsh.[18] The first excited state, $^2A_1'$, $(1a_1')^2(2a_1')^2(1e')^4(3a_1')^1$, is only 1.8 or 0.4 ev from the ground state for a single configuration or a second-order perturbation calculation, respectively. Higuchi calculated this state to be 10.5 ev above the ground state and identified it as the upper level of the lowest $^2A_1'$–$^2A_2''$ transition observed by Herzberg and Shoosmith. In a more refined calculation in which $3s_C$ orbitals were used, Higuchi found the excitation energy of the $^2A_1'$ level to be 7.4 ev while there is an observed $^2A_1'$ state at 8.3 ev. We must conclude, however, on the basis of our calculations that the observed level can be identified with one of the $^2A_1'$ states arising from the configurations $(1a_1')^2(2a_1')^2(1e')^3(2e')^1(3a_1')^1$ and

$$(1a_1')^2(2a_1')^2(1e')^2(1a_2'')^2(3a_1')^1.$$

The $^2E'$–$^2A_2''$ transition is calculated to be 6.5 and 7.7 ev for the single configuration and second-order second-order perturbation cases. This is in agreement with the results of Higuchi who obtained 6.8 and 7.3 ev where the latter value includes the effect of the $3s_C$ orbital. Qualitative agreement is also found with the experimental value of 5.7 ev which is identified with this transition.

The ionization potential of CH_3 can be identified with the a_2'' orbital energy to a second-order approximation. Higuchi obtained a value of approximately 12 ev for all his computations and we obtained 8.3 ev; the experimental value is 9.95 ev. Part of this error is undoubtedly related to the uncertainty of the a_2'' $2p$ effective nuclear charge which will profoundly affect the ionization potential regardless of the method used to obtain the atomic integrals.

We note that the identity of the ground state of CH_2 is still an open question. This statement includes our work, as is shown by Fig. 2. The $^1A_1$ and $^3B_1$ curves lie so close at their equilibrium positions that it is impossible to predict the ground state on the basis of such a qualitative calculation. The equilibrium position of the $^3B_1$ level is in the neighborhood of 120° which is considerably different than the much larger angle of 140° found by Niira and Oohata[19] and predicted qualitatively by several investigators.[18,20] In general we observe that there are additional qualitative differences between our curves and those exhibited by Niira and Oohata, but the qualitative nature of both calculations make further analysis unwarranted. However, we may note that these calculations support the assignment

[17] A. J. Freeman, J. Chem. Phys. **28**, 230 (1958); J. E. Faulkner, J. Chem. Phys. **27**, 369 (1957).
[18] A. D. Walsh, J. Chem. Soc. **1953**, 2260.
[19] K. Niira and K. Oohata, J. Phys. Soc. Japan **7**, 61 (1952).
[20] J. Lennard-Jones and J. A. Pople, Discussions Faraday Soc. **10**, 9 (1951).

TABLE IV. Atomic population $CH_3(^1A_1)$.

		$N(i,c)$	$N(i,s)$	$N(i,z)$	$N(i,ah)$	$N(i,bh)$	$N(i,y)$
90°	$1a_1$	2.001	0.001	0.000	−0.002		
	$2a_1$	0.001	1.163	0.168	0.668		
	$3a_1$	−0.001	0.714	0.992	0.294		
	$1b_2$					0.798	1.202
		2.001	1.878	1.160	0.960	0.798	1.202
			s-p promotion = 6.0%				
120°	$1a_1$	2.001	0.001	0.000	−0.002		
	$2a_1$	0.001	1.309	0.097	0.593		
	$3a_1$	−0.001	0.531	1.141	0.329		
	$1b_2$					0.832	1.168
		2.001	1.841	1.238	0.920	0.832	1.168
			s-p promotion = 7.9%				
150°	$1a_1$	2.001	0.001	0.000	−0.002		
	$2a_1$	0.001	1.384	0.044	0.571		
	$3a_1$	−0.000	0.351	1.375	0.274		
	$1b_2$					0.818	1.182
		2.002	1.736	1.419	0.843	0.818	1.182
			s-p promotion = 13.1%				
180°	$1\sigma_g$	2.001	0.001		−0.002		
	$2\sigma_g$	0.001	1.329		0.670		
	$1\sigma_u$					0.772	1.228
		2.002	1.330		0.668	0.772	1.228
			s-p promotion = 33.4%				

of $^1B_1$–$^1A_1$ as the longest wavelength transition with a separation of about 3 ev at the equilibrium position. The $^3A_2$–$^3B_1$ separation is about 1.5 ev larger. Since the $^1A_2$–$^1A_1$ and $^3B_1$–$^3B_2$ transitions are forbidden, the transitions which would be observed next are the $^1A_1$–X^1A_1 and $^3B_1$–$^3A_1$ at 7–8 ev, which would result in highly excited vibrational levels.

If we identify the orbital energy of the $3a_1$ orbital for the 120° case with the ionization potential we obtain 10 ev which is to be compared with the experimental value of 12 ev.[6] A calculation of the $^2A_1$ ground state of the CH_2 ion using functions for the neutral molecule also indicates a minimum for this level in the neighborhood of 120°. However some allowance for vibrational excitation in the Franck-Condon transition may be inferred from the bond shortening which presumably occurs upon ionization of the antibonding $3a_1$ orbital.

IV. HYPERFINE STRUCTURE OF THE CH_2 AND CH_3 RADICAL

The Fermi contact Hamiltonian may be represented by

$$H = h a_N S_z I_{nz},$$

where

$$a_N = (8\pi g\beta\mu_N/3I)\,\delta_N$$

and

$$\delta_N = \langle\Psi \mid \sum_k \delta(r_{kN})\, S_{kz} \mid \Psi\rangle / S_z.$$

Of the functions considered in a second-order perturbation calculation, only the interaction between the ground state and two excited states, arising from the electron configurations $(1a_1')^2(2a_1')^1(3a_1')^1(1e')^4(1a_2'')^1$ and $(1a_1')^2(2a_1')^2(1e')^3(2e')^1(1a_2'')$, results in an appreciable contribution to H. We obtain $a_H = -67.2$ Mc/sec which yields a value of about 72 gauss for the total spread of the quartet of lines due to the protons. This value compares favorably with the experimental values of 75 gauss observed by Gordy, 68 gauss reported by Jen *et al.* and 80 gauss reported by Smaller and Matheson.[3] A calculation of the hyperfine contact interaction constant for CH[21] where all terms were included showed that the sum of matrix elements of two excited states were as important as those considered in the foregoing. Contributions of the carbon functions at the proton are about 20 to 30% of each term considered for CH_3 but the over-all effect on the total is only about 5% due to cancellation. The value obtained from the straightforward configuration interaction function was approximately twice that calculated from the atoms-in-molecule[22] function. The latter was approximately equal to that obtained in the truncated calculation.

A calculation of the doublet splitting, 211 gauss, due to the C^{13} isotope is, however, in poor agreement with the experimental value of 41 gauss.[23] It is interesting that the calculated value is larger. The configuration interaction uncoupling mechanism seems quite able to account for the splitting qualitatively; an appreciable s-p mixing due to the possible nonplanarity of the molecule need not be invoked. The extremely large value for the C^{13} splitting indicates that the good agree-

[21] M. Krauss and F. Wehner, J. Chem. Phys. **29**, 1287 (1958).
[22] W. Moffitt, Proc. Roy. Soc. (London) **A210**, 245 (1951); A. C. Hurley, Proc. Phys. Soc. (London) **A69**, 49 (1956), and subsequent publications.
[23] Cole, Pritchard, Davidson, and McConnell, Mol. Phys. **1**, 406 (1958).

TABLE V. Atomic population $CH_2(^3A_2'')$.

	$N(i,c)$	$N(i,s)$	$N(i,ah)$	$N(i,eh)$	$N(i,y)$	$N(i,z)$	$N(i,x)$
$1a_1'$	2.001	0.001	−0.002				
$2a_1'$	0.001	1.297	0.701				
$1e_y'$				0.689	1.311		
$1e_z'$				0.689		1.311	
$1a_2''$							1.000
	2.002	1.298	0.699	1.378	1.311	1.311	1.000
			s-p promotion = 35.0%				

TABLE VI. Overlap population $CH_2(^1A_1)$.

		$n(i;c;ah)$	$n(i;s;ah)$	$n(i;z;ah)$	$n(i;ah;ah)$	$n(i;bh;bh)$	$n(i;y;bh)$	$n(i)$
90°	$1a_1$	−0.003	−0.001	0.000	0.000			−0.004
	$2a_1$	−0.006	0.649	0.133	0.072			0.848
	$3a_1$	−0.008	−1.259	0.543	0.169			−0.555
	$1b_2$					−0.239	0.701	0.462
		−0.017	−0.611	0.676	0.241	−0.239	0.701	0.751
				$n(^3B_1) = 1.030$				
120°	$1a_1$	−0.003	−0.000	0.000	0.000			−0.003
	$2a_1$	−0.005	0.664	0.070	0.043			0.772
	$3a_1$	−0.011	−1.346	0.484	0.144			−0.729
	$1b_2$					−0.136	0.763	0.627
		−0.019	−0.682	0.554	0.187	−0.136	0.763	0.667
				$n(^3B_1) = 1.030$				
150°	$1a_1$	−0.003	−0.000	0.000	0.000			−0.003
	$2a_1$	−0.005	0.685	0.013	0.033			0.726
	$3a_1$	−0.011	−1.193	0.293	0.110			−0.801
	$1b_2$					−0.091	0.794	0.703
		−0.019	−0.508	0.306	0.143	−0.091	0.794	0.625
				$n(^3B_1) = 1.037$				
180°	$1\sigma_g$	−0.003	−0.000		0.000			−0.003
	$2\sigma_g$	−0.007	0.761		0.081			0.835
	$1\sigma_u$					−0.072	0.792	0.720
		−0.010	0.761		0.081	−0.072	0.792	1.552

TABLE VII. Overlap population. $CH_2(^3A_2'')$.

	$n(i;c,ah)$	$n(i;s,ah)$	$n(i;ah,ah)$	$n(i,eh,eh)$	$n(i;y,eh)$	$n(i;z,eh)$	$n(i)$
$1a_1'$	−0.004	−0.001	0.000				−0.005
$2a_1'$	−0.008	0.813	0.095				0.900
$1e_y'$				−0.100	0.718		0.618
$1e_z'$				−0.100		0.718	0.618
	−0.012	0.812	0.095	−0.200	0.718	0.718	2.131

ment for the proton spectrum is probably fortuitous since it is not to be expected that the $3a_1'$ orbital adequately represents the first excited orbital. We also note that the spin density at the carbon nucleus is positive for both the configuration interaction and nonplanar pictures.

For CH_2, a calculation of the largest terms of the hyperfine Hamiltonian for the $^3B_1$ level at 120° predicts a triplet with a total spread of 102 gauss and $a_H = 71.2$ Mc/sec. We note that in this case the hyperfine interaction constant is positive; the ground $^3B_1$ level exhibits a hyperfine splitting without configuration interaction and the terms due to configuration interaction are negative, tending to reduce the contact term.

V. DISCUSSION

The importance of $s-p$ hybridization or promotion in the bonding of diatomic hydride molecules has been

emphasized by several investigators.[24] This phenomenon is equally important in the polyatomic hydrides for similar reasons, mainly the reduction of the s antibonding. This is seen very clearly in the increasing values for the promotion calculated for the $^1A_1$ state as the angle increases. Even with a rapidly decreasing contribution to the s population from the $3a_1$ orbital, the antibonding negative overlap population decreases only slightly from 90 to 150°. The very large increase in $s-p$ promotion and decrease in the absolute value of the negative overlap population between 150 and 180° is indicative of the large change in orbital character for small deviations from linearity.

The very large promotion for CH_3 may also be explained by assuming a rapid rise in the s population upon distortion from planarity. For the more realistic nonplanar case we would certainly have a smaller value. We must also consider the large transfer of charge to the carbon atom which tends to obscure any simple picture of atomic promotion. For the $^2A_2'$ state, which in a single configuration approximation is only 1.8 ev above the ground state, the promotion is only 18%. This large promotion decrease, accompanying a relatively small energy difference, is also reflected in the tremendous change in the total overlap population which goes from 2.132 to −0.872. We also observe for CH_2 an increase in the total overlap population for the $^3B_1$ state over the $^1A_1$ which is deceptive in any absolute sense since for the 90° case the $^3B_1$ state is not the more stable one. However the relative variation of the $3a_1$ overlap population with angle certainly indicates that promotion out of the antibonding $3a_1$ orbital into the nonbonding $1b_1$ orbital is favored as the angle increases.

The unusually large population changes may be ascribed to two difficulties. The first is the difficulty of defining the bonding properties of orbitals such as the π in linear CH_2 or the a_2'' in planar CH_3, which, due to the high molecular symmetry, are orthogonal to the majority of the orbitals. According to Mulliken's definitions we must regard the a_2'' and π orbitals as nonbonding and it is likely that these orbitals do not differ much from this characterization. However the rapid variation of the overlap population for these orbitals as the symmetry of the molecules is reduced does not seem to reflect the actual variation in the energy of the state. For the CH_3 case there is the additional difficulty of the unusually large values which orthonormality considerations force on the $3a_1'$ coefficients. The inappropriateness of this orbital for use as an excited molecular orbital may be seen by noting the large changes in orbital coefficients for the excited orbitals that Higuchi finds by introducing a $3s_C$ atomic orbital into the basis set.

[24] R. S. Mulliken, J. Phys. Chem. **56**, 295 (1952); W. Moffitt, Proc. Roy. Soc. (London) **A202**, 534 (1950).

Electron Spin Resonance Studies of Semiquinones and the C—F Bond*

D. H. ANDERSON,† PETER J. FRANK,‡ AND H. S. GUTOWSKY

Noyes Chemical Laboratory, University of Illinois, Urbana, Illinois

(Received June 15, 1959)

The electron spin resonance spectrum has been observed for a solution of tetrafluoro *p*-benzosemiquinone and a value, $a_F = 4.14 \pm 0.08$ gauss, obtained for the fluorine hyperfine splitting. It is concluded that this splitting is caused by the $\sigma-\pi$ configuration interaction proposed for protons attached to an aromatic free radical. The results show that the fluorine orbital in the C—F bond contains about 5% *s* character. The relationship between the hyperfine splitting constants and the contact contribution to the electron coupling of nuclear spins is commented upon. The electron spin density ρ_C at a carbon atom in an aromatic free radical is related to a_F, for a fluorine bonded to the carbon, by the approximate relation $a_F \cong -40\rho_C$. Data are presented which can be explained by assuming the semiquinone free radicals produced by air oxidation of hydroquinones in alcoholic KOH dimerize or otherwise react in concentrated solution to give radicals with oxygen linkages, while dibenzosemiquinone radicals are produced from quinones under reducing conditions. An *X*-band spectrometer was used; a brief description is given of it and of an electronic sweep unit for the electromagnet.

1. INTRODUCTION

EXTENSIVE experimental[1–4] and theoretical[5–12] studies have been made of the electron spin resonance spectra of *p*-benzosemiquinones and other aromatic free radicals in solution. One of the most interesting aspects of these studies is the hyperfine splitting of the electron resonance by magnetic nuclei[13–15] which are bonded to the aromatic ring. In solution the hyperfine constant a_N may be written for nucleus N as

$$a_N = (4\hbar/3)\gamma_e\gamma_N[\Psi(0)]_N^2, \qquad (1)$$

where γ_e and γ_N are the nuclear and electron gyromagnetic ratios and $[\Psi(0)]_N^2$ is the density of the unpaired electron at nucleus N. Only *s* electrons have a nonzero density at a nucleus and, therefore, the measurement of a hyperfine constant provides a means of estimating *s* character in a chemical bond.

The *p*-semiquinones, with which this paper deals, are the reaction intermediates in the general quinone-hydroquinone oxidation-reduction system.[16] Schematically, the reaction is the following:

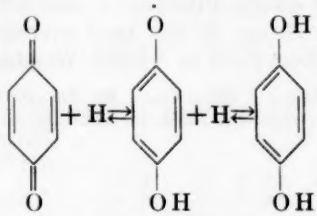

quinone *p*-semiquinone hydroquinone.

Semiquinones are stabilized in basic solution by the formation of a semiquinone ion. The negative charge and the unpaired electron are delocalized over the π-electron system as indicated below by representative conjugate structures for the tetrafluoro *p*-semiquinone anion.

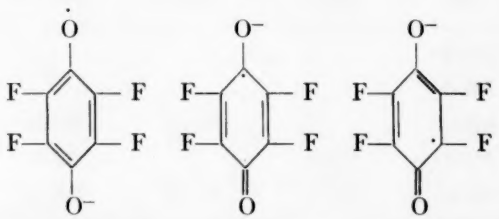

However, this description of conjugated aromatic radicals places the unpaired electron in a π state, which has a node in the plane of the molecule. Thus one predicts that $[\Psi(0)]^2$ is zero at carbon, hydrogen, fluorine, or other atoms in or attached to the ring, and they should produce no hyperfine splitting.

To account for the splittings observed in the case of protons, it was suggested originally that zero-point

* This research was supported in part by a grant from The Petroleum Research Fund aministered by the American Chemical Society. Grateful acknowledgment is hereby made to the donors of said fund. Also, the work was supported by the Office of Naval Research and by a Grant-in-Aid from E. I. du Pont de Nemours and Company.

† Now at Sandia Corporation, Albuquerque, New Mexico.

‡ Now at Institute of Experimental Physics, University of Geneva, Geneva, Switzerland.

[1] Venkataraman, Segal, and Fraenkel, J. Chem. Phys. **30**, 1006 (1959), and prior work cited there.

[2] Adams, Blois, and Sands, J. Chem. Phys. **28**, 774 (1958).

[3] J. E. Wertz and J. L. Vivó, J. Chem. Phys. **23**, 2441 (1955); **24**, 479 (1955).

[4] E. de Boer and S. I. Weissman, J. Am. Chem. Soc. **80**, 4549 (1958).

[5] S. I. Weissman, J. Chem. Phys. **22**, 1378 (1954).

[6] H. M. McConnell, J. Chem. Phys. **24**, 764 (1956).

[7] R. Bersohn, J. Chem. Phys. **24**, 1066 (1956).

[8] S. I. Weissman, J. Chem. Phys. **25**, 890 (1956).

[9] H. S. Jarrett, J. Chem. Phys. **25**, 1289 (1956).

[10] Weissman, Tuttle, and de Boer, J. Phys. Chem. **61**, 28 (1957).

[11] H. M. McConnell and R. E. Robertson, J. Phys. Chem. **61**, 1018 (1957).

[12] H. M. McConnell and D. B. Chesnut, J. Chem. Phys. **28**, 107 (1958).

[13] A. Abragam and M. H. L. Pryce, Proc. Roy. Soc. (London) **205**, 135 (1951).

[14] N. Bloembergen and W. C. Dickinson, Phys. Rev. **79**, 179 (1950).

[15] For a review of the magnetic properties of free radicals see J. E. Wertz, Chem. Revs. **55**, 829 (1955).

[16] L. Michaelis and M. P. Schubert, Chem. Revs. **22**, 437 (1938).

out-of-plane vibrations could be responsible.[17] But later, the same electron spin densities were found at deuterium nuclei which were substituted for the protons.[18] The vibrational amplitude of D should be less than that of H, so it was concluded that this mechanism was probably incorrect for protons. It was then proposed[18] that a $\sigma-\pi$ interaction allows some of the unpaired electrons in the π system to leak into the σ bonds of the carbon ring and thence to the protons. Order of magnitude calculations have been made which demonstrate that such a mechanism is plausible for protons.[6-8] The work which we describe here was prompted by two considerations: (1) The observation of hyperfine splitting by fluorine nuclei in free radicals similar to the protonated species already studied could provide a better understanding of the interaction mechanism. (2) Because of the dependence of the hyperfine constant on s character, we might learn something about the nature of the C—F bond.

2. EXPERIMENTAL

Apparatus and Methods

The X-band spectrometer is of fairly conventional design.[19] The source is a klystron, Varian model VA-260. The sample cavity, of reflection type, is placed in one arm of a magic-T bridge, and detection is by means of a crystal. The magnetic field is modulated by an amplitude stabilized $R-C$ tuned oscillator operated at 34.5 cps.[20] After suitable amplification, the audio signal is fed into a lock-in detector of somewhat unusual design[21] and thence to a strip chart recorder. There is of course the usual provision for oscilloscope display of the audio signal. Initially, the klystron was unregulated except for a high quality power supply, but later we installed[22] the automatic frequency control circuits of the Varian V-4500 EPR spectrometer and inserted a Tektronix Type 122 preamplifier after the crystal detector. All measurements reported here were made with the unregulated klystron, except for those on the tetrafluoro p-semiquinone.

The main magnetic field is supplied by a Varian V-4007 electromagnet[23] having a 2-in. gap and shimmed 6-in. diameter pole caps. The V-2200 regulated power supply for the magnet has provision for an input voltage to sweep the magnetic field through a resonance. A useful feature of our system is the versatile electronic device used to generate the sweep, which covers an arbitrary range of fields without requiring resetting the range controls of the power supply. The sweep circuit itself is shown in Fig. 1. A voltage which varies linearly in time is provided by discharging an exceptionally leakproof capacitor, C_4, through a resistor. The device includes a switching network and a marker circuit. The network provides independent adjustments of the sweep duration, from 10 to 2000 sec, and of sweep amplitude, from about 1 gauss to the maximum range of the magnet. There is provision for a ten-second return to either the beginning or end of the sweep and also for stopping the sweep and holding the field at any point. The marker circuit provides sharp pips at two adjustable points on the recorded output of the spectrometer. A detailed description complete with the other circuits and the necessary adjustments is given elsewhere.[21] The spectrometer includes an electronic integrator which is used on occasion for direct recording of the absorption itself rather than of the first derivative as is customary.

The splittings in a spectrum were obtained by calibrating the sweep conditions. The markers are set near the beginning and the end of the sweep, the sweep stopped at each marker and the magnetic field measured with a proton magnetic resonance field meter. The line widths are the main factor limiting the accuracy of this procedure; the estimated error in the splittings usually is ± 0.03 gauss. Two procedures were used to measure g values. In one, the field is swept through the resonance until its center, the "crossover" of the derivative, is reached. The sweep is then stopped, the microwave frequency measured with a wavemeter, and the magnetic field measured with the proton field meter. This procedure has the disadvantage that systematic errors can result from the difference in position of the proton and free radical samples. In the second procedure, the electron resonance of the unknown and of a reference are observed consecutively under standardized calibrated conditions, and the difference between the positions of their centers gives the difference in g values. This latter procedure, with p-semiquinone ($g=2.0047$)[2] as the reference was used to measure the g value of the tetrafluoro p-semiquinone. The other g values were measured by the first procedure or by both procedures with powdered hydrazyl ($g=2.0037$) as the reference. The estimated error of the g-value measurements is ± 0.0006.

Samples and Their Preparation

In general, the free radicals were prepared by either air oxidation of the hydroquinone in ethanolic KOH or by reduction of the quinone with an ethanol-glucose solution. Only a very small sample of the tetrafluoro p-benzoquinone was available and, therefore, several exploratory experiments were performed upon the hydrogen analogue, p-benzoquinone. It was found that in order to produce the simple five-line spectrum of the p-benzosemiquinone ion, one had to oxidize hydro-

[17] Weissman, Townsend, and Paul, J. Chem. Phys. **21**, 2227 (1953).
[18] B. Venkataraman and G. K. Fraenkel, J. Chem. Phys. **24**, 737 (1956).
[19] A very similar spectrometer is discussed by D. J. E. Ingram, *Spectroscopy at Radio and Microwave Frequencies* (Butterworths Scientific Publications, London, 1955), Fig. 46.
[20] R. L. Rutledge, Ph.D. thesis, University of Illinois (1957).
[21] P. J. Frank, Ph.D. thesis, University of Illinois (1957).
[22] D. H. Anderson, Ph.D. thesis, University of Illinois (1959).
[23] Our experience with this unit suggests that it may develop shorts between the high-voltage coils and ground.

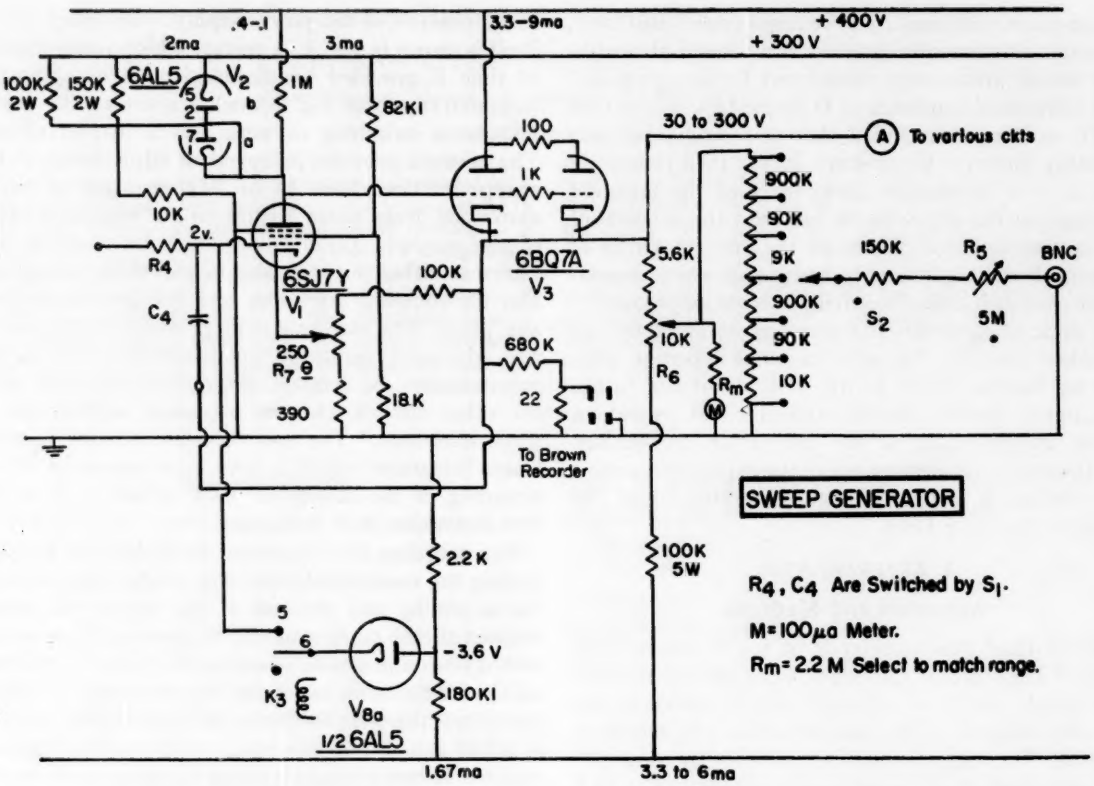

FIG. 1. Circuit diagram of an electronic unit used to sweep the field of an electromagnet. A switching network and marker circuit which are part of the assembly are described in reference 21.

quinone in basic solution.[24] Moreover, it appeared that the radical was most stable when produced by equimolar amounts of base and hydroquinone.

Our tetrafluoro sample was the quinone so it was reduced with SO_2 to the hydroquinone. The only departure from the standard procedure[25] was the addition of acetone to the solvent water to increase the solubility of the tetrafluoroquinone. The product was not recrystallized because of the small amount of starting material. The solutions examined initially were 0.1*M* in tetrafluoro hydroquinone and ethanolic KOH. Later experiments used 0.2*M* hydroquinone to increase the signal to noise ratio. However, the characteristic features of the spectra were the same in each case. The reactions were carried out and the spectra were observed at room temperature.

The sample of tetrafluoro *p*-benzoquinone was supplied by Dr. J. C. Tatlow of the University of Birmingham, Great Britain. The other fluorine containing quinones and hydroquinones were obtained from Dr. Glenn C. Finger of the Fluorocarbon Division of the Illinois State Geological Survey; these samples were several years old and of doubtful purity. In some instances the quinones were reduced to the hydroquinones and the latter oxidized to give the free radicals observed, as described for the tetrafluoro quinone. The *p*-benzoquinone, hydroquinone, and substituted (nonfluoro) *p*-benzoquinones were obtained commercially.

[24] B. Venkataraman and G. K. Fraenkel, J. Am. Chem. Soc. 77, 2707 (1955); J. Wertz (personal communication).

[25] W. J. Higginbottom, *Reactions of Organic Compounds* (Longmans, Green and Company, New York, 1948), second edition, p. 213.

3. SPECTRA AND THEIR ANALYSIS

Tetrafluoro *p*-Benzosemiquinone

There is reproduced in Fig. 2 the oscilloscope display of the electron spin resonance absorption of a free radical obtained from the air oxidation of tetrafluoro hydroquinone. The spectrum consists of a quintet with approximate intensities of 1:4:6:4:1, as predicted for hyperfine splitting by four equivalent nuclei with $I=\frac{1}{2}$. The spacing between components was measured to be 4.14 ± 0.08 gauss and g, 2.0048 ± 0.0006. The time behavior of this radical was much different from the others reported below. Approximately five minutes after preparation no resonance was observed, while, for example, the spectrum shown in Fig. 3 for the reduction product of 2-fluoro, 5-chloro hydroquinone was obtained 8 hr after the solution was prepared. Strip chart recordings were made in addition to oscilloscope photographs. The former were better for measuring the splittings; however, the intensities of the components

at the end of the sweep were smaller than those at the beginning, independent of sweep direction, because of the relatively fast decomposition rate of the radical. The recorded derivatives of the absorption are more sensitive to unresolved structure than the oscilloscope display. No evidence of absorption other than the quintet was found in our sample. Moreover, the splitting of 4.14 gauss is greater by a factor of 2 than the 2 gauss proton splittings found in *p*-benzosemiquinones, including methyl derivatives, while the *g* value of 2.0048±0.0006 equals that of the *p*-semiquinone ion,[2] within experimental error. We conclude, therefore, that the spectrum shown in Fig. 2 is due to the tetrafluoro *p*-semiquinone and that $a_F = 4.14$ gauss.

Oxidation of Hydroquinones

Before the value for a_F was obtained[22] as described in the foregoing paragraph, a number of attempts were made to produce fluorine containing *p*-benzosemiquinones from partially fluorinated hydroquinones and quinones. These early experiments[21] were unsuccessful in that no clear example of a fluorine hyperfine splitting was found. In retrospect, the main reason for this is that the then lower sensitivity of the spectrometer required the use of concentrated solutions in which the fluoro-substituted *p*-benzosemiquinone radicals either dimerize or react rapidly with the parent hydroquinone or quinone to give more complex radicals. Venkataraman and Fraenkel[24] and also Wertz[24] have commented on the formation of complex radicals during air oxidation of hydroquinone in alcoholic KOH, but no detailed study has been reported. Our main concern here is not the nature of these complex radicals; however, some of our observations bear on this question and may lead to the proper answers.

One of the most interesting observations is that virtually identical spectra were obtained for the products of the air oxidation in ethanolic KOH solution of five different hydroquinones: 2-fluoro; 2,5-difluoro; 2-fluoro, 5-chloro; 2-fluoro, 5-bromo; and hydroquinone itself. The derivative of the absorption by the 2-fluoro,5-chloro hydroquinone solution is reproduced in Fig. 3. It consists of a 1-4-6-4-1 quintet with splittings of 1.10 gauss, while each component of the quintet is a 1-2-1 triplet with splittings of 0.30 gauss. The *g* values (2.006),[26] splittings, and relative intensities are the same within experimental error for the radicals derived from all five compounds except that in some cases the outer pair of triplets is too weak to discern clearly. Also, the spectrum from the 2-fluoro hydroquinone product(s) has a weak satellite symmetrically placed on each side of the main spectrum; the separation of this pair of lines is 6.3 gauss.

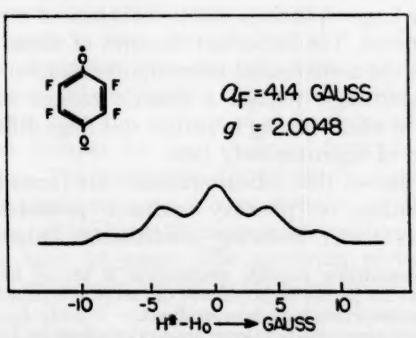

FIG. 2. Oscilloscope display of the electron spin resonance absorption of the free radical produced by the air oxidation of an ethanolic KOH solution of tetrafluoro hydroquinone. The spectrum was observed in the solution at room temperature, with an *X*-band spectrometer. The value for a_F is 4.14±0.08 gauss and for *g*, 2.0048±0.0006.

FIG. 3. First derivative of the electron spin resonance absorption of the product produced by air oxidation of an ethanolic KOH solution of 2-fluoro,5-chloro hydroquinone. The spectrum was observed in the solution at room temperature with an *X*-band spectrometer. The separation between markers corresponds to 6.08 gauss; the modulation amplitude was 0.1 gauss.

Hydroquinone itself, when treated with weak base such as that used on the substituted hydroquinones, gave the simple five-line spectrum characteristic of the *p*-benzosemiquinone ion. A complex spectrum such as that shown in Fig. 3 was obtained only after the solution was made strongly basic. Moreover, the character of the spectrum for this solution changed continuously with time as different radicals were formed and destroyed. In contrast, the spectra of the products from the substituted hydroquinones, in weak base, showed no time variation after the first few minutes other than a gradual decay in intensity as the radicals were destroyed.

The simplest interpretation of the spectrum in Fig. 3 is that the quintet results from the hyperfine splitting by four nuclei with $I = \frac{1}{2}$ and $a_N = 1.1$ gauss, and the triplet substructure from two nuclei with $I = \frac{1}{2}$ and $a_N = 0.3$ gauss. It is probable that in some of the solu tions more than one kind of radical contributes to the spectrum. Even so, it is difficult to explain the number of components and their splittings without postulating some type of dimeric species. In chloro- and methyl-

[26] These values are consistently higher by about 0.001 than those reported in reference 2 for semiquinones, possibly as a result of systematic errors in the correction for the difference in magnetic field between the radical and the field meter samples.

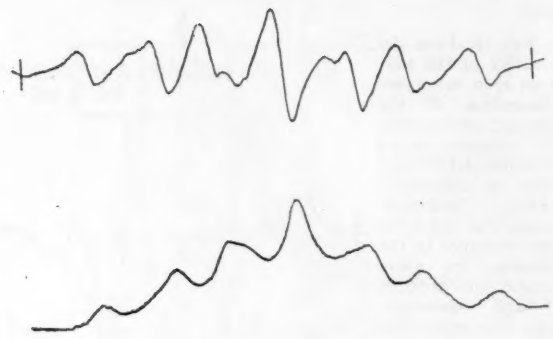

FIG. 4. The electron spin resonance absorption of the product obtained upon reduction of 2-fluoro, 5-chloro *p*-benzoquinone. The spectrum was observed in solution at room temperature, with an *X*-band spectrometer. The upper curve is the first derivative obtained with a modulation amplitude of 0.1 gauss; the separation between markers is 6.08 gauss. The lower curve is the absorption itself obtained by recording an electronic integration of the derivative.

substituted *p*-benzosemiquinones[1] a_H for ring protons ranges between 1.76 and 2.46 gauss, and for CH_3 group protons, between 1.71 and 2.25 gauss. Thus, for example, a 2-fluoro *p*-benzosemiquinone ion would be expected to give a spectrum with at most sixteen lines of equal intensity. Moreover, the separation of the outermost lines, which is $\Sigma_N a_N$, should be about 10 gauss, i.e., $3a_H+a_F$, instead of the 5 gauss observed. Similar arguments rule out *p*-benzosemiquinones in which one or more of the ring substituents has been replaced by an ethoxy or other proton containing group.

If a dimeric species is formed, delocalization of one unpaired electron over two ring systems would decrease a_H to about 1 gauss from the 2 gauss values found in *p*-benzosemiquinones. This would account for the quintet splitting observed. Phenols undergo a wide variety of coupling reactions under oxidative conditions and semiquinone radicals have very similar reactions.[27] The coupling reactions could yield products such as I and II, including the several possible substituted versions of each, depending upon the starting material, the reaction mechanism, and the displacement of substitutents:

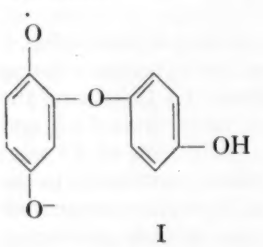

I

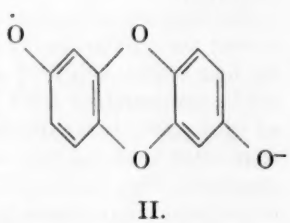

II.

Structure I has enough adjustable parameters, including substituents and the relative values of a_H and a_F on the two different rings, that it can be stretched to account for the spectra of all the products, except possibly that from hydroquinone, which would have seven ring protons unless one were displaced. Structure II has the advantage that it could be produced, upon loss of substituents,[28] from all the substituted hydroquinones and also from hydroquinone itself. Moreover, one would expect[4] the four protons ortho to the exocyclic oxygens to have nearly equal and significantly larger splitting constants than the two meta protons,§ in good accord with experiments. In structures I and II conjugated forms can not be written which transfer the odd electron from one ring to the other; however, the experiments on paracyclophane anions[29] leave no doubt that the electron transfer in I and II should be fast enough for both rings to participate in the hyperfine splitting.

Reduction of Quinones

The spectra obtained from the reduction products of quinones differ greatly from those found for the oxidation products of the hydroquinones. The products from 2, 5-dichloro and 2-chloro, 5-bromo *p*-benzoquinone gave the simple 3-line spectra with splittings of 2 gauss reported for the corresponding substituted semiquinones.[1,3] The relative, derivative peak heights of the components in the spectra from these two compounds were particularly sensitive to the microwave power applied, as noted previously for other semiquinones.[1] The most extreme deviation we found from the theoretical 1:2:1 ratio is 1:4.7:1 at high power and the least, 1:2.2:1 at low power.

The spectrum of the product(s) from 2-fluoro, 5-chloro *p*-benzoquinone is given in Fig. 4 which includes the derivative and the recorded integral of the derivative. Except for unresolved structure in components 2, 3, 5, and 6, the spectrum is a septet with approximately equal splittings of 0.8 gauss and relative intensities 1:2:3:4:3:2:1. The spectrum of the reduction product from 2-fluoro, 5-bromo *p*-benzoquinone is also a septet with the same relative intensities, but having slightly larger splittings and no evidence of unresolved components. The important features of these spectra, namely the nonbinomial intensity distribution and the small splittings, require a dimeric radical with two groups of nuclei having hyperfine splittings differing by a factor of approximately two.

It is known that dibenzoquinones are formed by the dimerization of phenoxy radicals produced from quinones under reducing conditions.[30] Dibenzosemi-

[27] D. H. R. Barton and T. Cohen, *Festschrift Arthur Stoll* (Birkhäuser, Basel, Switzerland, 1957), pp. 117, 129.

[28] In considering possible mechanisms it should be kept in mind that the parent hydroquinone can serve as a reducing agent for molecules which have been oxidized.

§ Recent approximate valence bond calculations by John Schug (personal communication) give equal electron spin densities at the carbons ortho to the exocyclic oxygen atoms and densities about half as large at the meta carbons.

[29] S. I. Weissman, J. Am. Chem. Soc. **80**, 6462 (1958).

[30] R. H. Thompson, *Naturally Occurring Quinones* (Academic Press, Inc., New York, 1957), p. 47.

quinone radicals such as III and IV will account for the spectra observed:

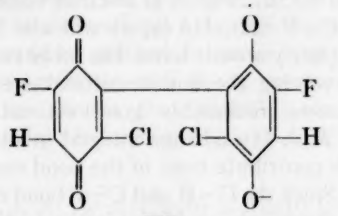

III

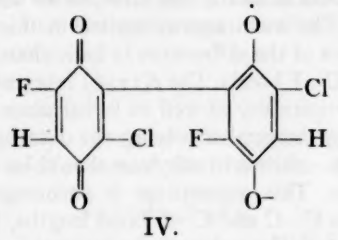

IV.

A value of $a_F \cong 1.6$ gauss for the two equivalent fluorines in III would give a 1:2:1 triplet. A value of $a_H \cong 0.8$ gauss for the two equivalent hydrogens in III would split each component of the fluorine triplet also into triplets which overlap to give seven components with intensities and splittings corresponding to those observed. The unresolved structure in the spectrum from the 2-fluoro, 5-chloro *p*-benzoquinone product(s) could arise from the nonequivalence of the fluorine and proton splittings in IV, from a_F not being exactly $2a_H$, from a mixture of III and IV, or from some combination of these reasons. The hyperfine splitting constants, $a_F \cong 1.6$ and $a_H \cong 0.8$ are reasonable for radicals such as III and IV. To a first approximation these values correspond to $a_F \cong 3.2$ and $a_H \cong 1.6$ for the monomeric *p*-benzosemiquinone. The value $a_H \cong 1.6$ is compatible with the 1.76 to 2.46 range found for a_H in substituted semiquinones[1] and $a_F \cong 3.2$ is compatible with the value of 4.14 gauss found in tetrafluoro *p*-benzosemiquinone inasmuch as a_F probably has much the same fractional dependence upon substituents as does a_H.

The products from the reduction of 2,5-dibromo *p*-benzosemiquinone gave an unsymmetrical spectrum with at least 10 components and extending over 7 gauss. It appears that the mixture of radicals includes some in which bromine has been displaced from the ring by hydrogen. The product(s) from 2-fluoro, 5-methyl *p*-benzosemiquinone gave a very complex, symmetrical spectrum with about 40 components resolved and extending over 13 gauss. The spectrum of the semiquinone monomer should contain no more than 32 lines and should extend over about 15 gauss ($\Sigma_N a_N$; assuming $a_F = 4$, and $a_H = 2.2$ gauss for ring and CH_3 group protons). The number of components in the spectrum would be increased by formation of a dibenzosemiquinone radical such as III, with F and CH_3 substituents. Moreover, if the a_N values in the dimer are about ½ their values in the monomer, the loss of two protons upon dimerization would decrease the predicted breadth of the spectrum to 13 gauss, as observed. This argument assumes that a_F is between 3 and 4 gauss in the semiquinone monomer and, along with the results for the products from 2-fluoro, 5-chloro and the 2-fluoro, 5-bromo *p*-benzosemiquinones, supports the value $a_F = 4.14$ gauss from the tetrafluoro derivative.

Wertz has suggested[24] that dibenzosemiquinone, the parent of III and IV, may be the species giving the quintet of triplets spectrum shown in Fig. 3. However, the chemical evidence[27,30] that dibenzoquinones are formed more readily by reducing quinones than by oxidizing hydroquinones leads us to favor the different interpretations presented here. The problem certainly warrants further study.

4. DISCUSSION OF a_F

Hyperfine Splitting Mechanisms

Several conclusions can be drawn from the fluorine hyperfine constant. First let us consider the mechanism by which the unpaired electron arises at the fluorine nucleus. One possibility is the zero-point vibration model[17] mentioned previously. In the case of protons, calculation of the vibrational effects[18] gives a value for a_H in *p*-benzosemiquinone of only about 0.05 gauss, compared with the experimental value of about 2 gauss. However, this probably cannot be considered unambiguous evidence against the mechanism because of the approximate nature of the calculation. The experimental evidence consists of finding upon deuterium substitution a value for a_H/a_D of approximately $\gamma_H/\gamma_D = 6.51$, whereas it is stated[18] that the vibration model leads to a ratio $a_H/a_D \cong (m_D/m_H)^{\frac{1}{2}}(\gamma_H/\gamma_D) = 9.2$. This last argument is not as strong as it appears at first glance because of the contributions to a_H and a_D from excited vibrational states, which were neglected. The relaxation time for excited vibrational states[31] is short compared with $1/(\gamma_e a_H$ or $_D)$; therefore, only *one* splitting constant will be discernible, the average over all vibrational states, $\langle a \rangle_v$. Upon deuterium substitution the amplitudes of vibration are less; however, the populations of the excited vibrational states are greater because the vibrational frequencies are lower. The two effects tend to cancel and lead to a value for $\langle a_H \rangle_v / \langle a_D \rangle_v$ closer to γ_H/γ_D.

The fluorine nucleus has a mass nineteen times that of the proton and the C—F bond length (1.33 A) is greater than the C—H (1.08 A), so we would expect a much larger discrepancy between the vibration theory and experiment if this model is incorrect for fluorine. Upon making an approximate calculation, analogous to that for protons in semiquinone ions,[18] we find this is actually the case. Using 200 cm^{-1} as an approximate frequency for the perpendicular C—F bending mode,[32]

[31] It is important here to note that vibrational relaxation will occur in events which do not produce electron spin relaxation.

[32] L. Delbouille, J. Chem. Phys. **25**, 182 (1956).

we obtain for a_F a value of about 2×10^{-3} gauss. This is over three orders of magnitude smaller than the 4.14 gauss observed and we conclude that the vibration mechanism cannot account for the fluorine hyperfine splitting in aromatic radicals.

The combined interactions between the magnetic moments due to the electron orbital, electron spin, and nuclear spin angular momenta can yield an isotropic component of the hyperfine interaction,[14] the so-called pseudo contact term. While this term is difficult to calculate accurately, we can expect that the approximate model proposed by McConnell[12] for protons bonded to π-electron systems will apply as well to fluorine. The main difference is that the C—F distance is longer than the C—H. This reduces the 0.04 gauss contribution estimated[12] for a_H to 0.02 gauss for a_F. Again, the effect is even less likely to be important for fluorine than for hydrogen. The only other plausible mechanism for the fluorine hyperfine splitting in a π radical is the $\sigma-\pi$ configuration interaction mechanism which was found to be reasonable for protons.

The σ-π Configuration Interaction

The amount of $\sigma-\pi$ configuration interaction in an aromatic radical is a difficult quantity to estimate for a ring hydrogen and can be expected to be even more difficult for fluorine. The reason for this is that off-diagonal elements must be calculated in the secular equation for the electronic wave functions of the radical. These are small relative to the diagonal elements and since the diagonal elements are not usually known to any great degree of accuracy, reliable estimates of the off-diagonal elements will be even harder to obtain. However, if relative values of the important exchange integrals were known, fairly reliable comparisons could be made of the configuration interaction to be expected for hydrogen and fluorine in aromatic compounds. Estimates have been made[6-8] of the $\sigma-\pi$ configuration interaction for hydrogen; here we restrict ourselves to the relative values for H and F.

To a good approximation, it appears that the amount of $\sigma-\pi$ interaction for fluorine should be approximately equal to that for hydrogen. This may be seen by considering the C—H radical as a three electron problem: the unpaired electron in the carbon $2p_\pi$ orbital (π), and the bonding electrons in the carbon sp^2 hybridized orbital (σ) and the hydrogen $1s$ orbital (h). In order to evaluate the configuration interaction constant, or the deviation from perfect $\sigma-h$ pairing, we require three exchange integrals: $K(\pi, \sigma)$, $K(\pi, h)$, and $K(\sigma, h)$. The values of these integrals determine the amount of configuration interaction in an approximate valence bond formulation. For the C—F radical, there is the fluorine orbital (f), the carbon π and σ orbitals, and the analogous exchange integrals, $K(\pi, \sigma)$, $K(\pi,f)$, and $K(\sigma,f)$. In considering the methyl radical, Karplus[33] used the following values[34] for the C—H exchange integrals: $K(\pi, \sigma)=1.26$, $K(\pi, h)=0.60$, and $K(\sigma, h)=3.92$, in units of electron volts.

For the C—F radical $K(\pi, \sigma)$ will also be 1.26 ev, since it is a purely atomic term. The other two exchange integrals involving the fluorine orbital are not available, but some reasonably good estimates can be made. The $K(\sigma, f)$ exchange integral involves the orbitals which contribute most of the bond energy of the two atoms. Since the C—H and C—F bond energies are almost the same,[35] the exchange integrals $K(\sigma, h)$ and $K(\sigma, h)$ should be nearly the same, so we use 3.9 ev for the latter. The main approximation in this procedure is the neglect of the differences in ionic character of the C—H and C—F bonds. The $K(\pi, f)$ integral is difficult to obtain empirically as well as to calculate. However, the exchange integral involving the 1-carbon $2p_\pi$ and 2-carbon $2p_\sigma$ orbitals in ethylene should be a good approximation. This assumption is encouraged by the similarity in C—C and C—F bond lengths, 1.35 A and about 1.33 A.[36] The value of the integral in ethylene is 0.58 ev[37] and, therefore, for $K(\pi, f)$ we use a value of 0.6 ev. These approximate values for the C—F exchange integrals are virtually the same as those for C—H, so the amount of configuration interaction in $\cdot$(C—H) should be roughly the same as in $\cdot$(C—F).

CONCLUSIONS

C—F *bond character.*—In order to simplify the discussion, let us relate the coupling constant a_N to the bonding orbital ψ centered on the nucleus which is bound to the aromatic ring. We can rewrite Eq. (1) as

$$a_N=\tfrac{4}{3}\hbar\gamma_e\gamma_N C_N[\psi(0)]_N^2. \qquad (2)$$

In this expression, $[\psi(0)]_N^2$ is the *electron* density at N rather than the *spin* density as in Eq. (1), while C_N is a constant which converts the electron density at nucleus N to spin density. The value of C_N is determined by the π-electron spin density and by the mechanism which transfers some of that spin density to the carbon σ orbital employed in bonding N to the aromatic ring. In other words, once there is a given spin density in the carbon σ orbital, the extent of its transferal via ψ to N is governed by the value of $[\psi(0)]_N^2$.

We have already concluded that the $\sigma-\pi$ interaction should be approximately equal for C—H and C—F.

[33] M. Karplus, J. Chem. Phys. **30**, 15 (1959).

[34] Note that these values differ from Jarrett's in reference 9; he used values for $K(\pi, \sigma)$ and $K(\sigma, h)$ based on a pure p orbital rather than on an sp^2 hybrid. $K(\pi, h)$ is difficult to evaluate and we feel that empirical techniques are more reliable; see J. H. van Vleck, J. Chem. Phys. **2**, 20 (1934).

[35] T. L. Cottrell, *The Strengths of Chemical Bonds* (Academic Press, Inc., New York, 1954). However, the C—F bond energy is still in doubt, especially in view of the recent report on fluorobenzene by P. Smith, J. Chem. Phys. **29**, 681 (1958).

[36] *Tables of Interatomic Distances and Configuration in Molecules and Ions* (The Chemical Society, Burlington House, London, 1958).

[37] M. Karplus (personal communication).

Moreover, the tetrafluoro and tetrahydro semiquinones are sufficiently similar that we would expect approximately equal π-electron spin densities in the carbon orbitals of the two radicals. The validity of these assumptions could be checked by measuring the C^{13} hyperfine splittings in the radicals; at present it appears reasonable to assume that $C_F \cong C_H$. Consequently, upon writing Eq. (2) for a_F and a_H and dividing, we can assert that

$$a_F/a_H \cong (\gamma_F/\gamma_H)\{[\psi(0)]_F^2/[\psi(0)]_H^2\}. \quad (3)$$

By using our measured value for a_F with the known values of a_H and the gyromagnetic ratios γ_H and γ_F, we then obtain

$$[\psi(0)]_F^2 \cong 1.86[\psi(0)]_H^2. \quad (4)$$

However, only s electrons have a nonzero density at the nucleus so ψ for F must be of the form

$$\psi_F = c_0 F_{2p_\sigma} + \lambda F_{2s}, \quad (5)$$

where F_{2p_σ} and F_{2s} are $(2p_\sigma)$ and $(2s)$ orbitals on fluorine. Equation (5) leads to the result

$$[\psi(0)]_F^2 \cong \lambda^2 F_{2s}^2(0). \quad (6)$$

The self-consistent field function for F^- gives a value[38] for the electron density, $F_{2s}^2(0)$, at the fluorine nucleus of $(1/4\pi)$ $(11.75)^2$ atomic units. Upon combining this value with Eqs. (4) and (6) and using a hydrogen $1s$ function to evaluate the electron density, $[\psi(0)]_H^2$, at the proton, we obtain a value for λ^2 of 0.053. This means that the fluorine orbital in the C—F bond of the tetrafluoro p-benzosemiquinone ion contains roughly 5% $2s$ character.

It should be emphasized that this value depends upon three major approximations. Two of these are the assumptions already mentioned of equal $\sigma-\pi$ configuration interaction and of equal unpaired electron densities in the carbon π orbitals in the semiquinone and tetrafluorosemiquinone ions. The third involves the Löwdin value[38] for $F_{2s}^2(0)$, often called the contact term, which is needed to calculate the s character. There are, in addition, two minor approximations in Eq. (5). The F_{1s} and F_{3s} functions are neglected even though a_F depends upon the total s character. Also, it is assumed, in effect, that the electron densities in ψ_F and ψ_H are those of filled orbitals in nonradical species even though we are dealing with semiquinone free radicals.

The "basic" quantity which is obtained from a_F in the manner just described is $[\psi(0)]_F^2$, the product of the fluorine s character λ^2 and the fluorine contact term $F_{2s}^2(0)$ as shown in Eq. (6). The numerical value obtained for $[\psi(0)]_F^2$ in the tetrafluoro semiquinone is 0.58 atomic unit. This is to be compared with a value of about 1.0 found for the same quantity from an analysis of the electron coupling of nuclear spins in fluorobenzenes.[39] The agreement between these independently determined values is not too bad when one considers all the approximations. Moreover, if a higher C—F bond energy[15] were used, the $\sigma-\pi$ interaction would be less for C—F than for C—H; and, in Eq. (2), C_F would be less than C_H. In consequence, the constant in Eq. (4) and also $[\psi(0)]_F^2$ would be increased by the ratio C_H/C_F, improving the agreement. In any event, the two values for $[\psi(0)]_F^2$ are close enough that there is little doubt about the $\sigma-\pi$ interaction being the mechanism governing a_F, and also a_H.

It should be remembered that the accuracy of our result for the fluorine s character is no better than the accuracy with which the fluorine contact term $F_{2s}^2(0)$ is known. Bersohn has pointed out[40] that recent hyperfine structure experiments with atomic fluorine[41] support a value for the fluorine contact term which is a factor of 1.5 to 2 times as large as the Löwdin value, and which would reduce the estimate of the s character by a reciprocal factor. The best guess at present gives about 5% fluorine s character in the C—F bond of aromatic systems.

Contact contribution to electron coupling of nuclear spins.—As mentioned in the preceeding section, the contact terms in the hyperfine interaction and in the electron coupling of nuclear spins are closely related. In addition to the support which this relation provides for the $\sigma-\pi$ interaction mechanism, it can be used to make predictions about one set of coupling constants from a knowledge of the other set. Equation (2) can be modified very simply[33,42] to give the following expression for the contact contribution to $A_{NN'}$, the constant describing the electron coupling of nuclei N and N′:

$$A_{NN'}{}^c \equiv A_{NN'}(\text{contact}) = \gamma_N \gamma_{N'} K_{N'} [\psi(0)]_{N'}^2. \quad (7)$$

The assumptions and approximations in Eq. (7) are much the same as those in Eq. (2). However, the physical significance of $K_{N'}$ differs from that of C_N because the magnitude of $A_{NN'}{}^c$ is related to the correlation of electron spins.[39] We assume that N and N′ are separated by at least two bonds and, as a specific example, that N is H and that N′ can be either H′ or F. The constant $K_{N'}$ contains the correlation of electron spins in the bonding orbitals centered on N and on the atom (C) to which N′ is bonded, while the effect upon nucleus N′ of this spin correlation is governed by $[\psi(0)]_{N'}^2$. If the nature of N′ does not affect the spin correlation, i.e., if $K_{H'} = K_F$, then by writing Eq. (7) for the parent and substituted compounds, we obtain the analog of Eq. (3),

$$A_{HF}{}^c/A_{HH'}{}^c \cong (\gamma_F/\gamma_H)\{[\psi(0)]_F^2/[\psi(0)]_H^2. \quad (8)$$

[38] P.-O. Löwdin, Phys. Rev. **90**, 120 (1953).

[39] G. A. Williams and H. S. Gutowsky, J. Chem. Phys. **30**, 717 (1959).

[40] R. Bersohn (personal communication). See also reference 39.

[41] H. E. Radford, Bull. Am. Phys. Soc. Ser. II, **3**, 325 (1958).

[42] M. Karplus, J. Chem. Phys. **30**, 11 (1959).

This result can be used in several ways. Upon combining it with Eq. (3) and substituting the experimental values for a_H and a_F in semiquinone and its tetrafluoro derivative, we find that

$$A_{HF}^{c}/A_{HH'}^{c} \cong (a_F/a_H) = 1.75 \qquad (9)$$

We expect the numerical value in Eq. (9) to be most accurate for quinones, but it should also be a fair approximation for compounds in which H′ and F are bonded to a carbon atom which has π bonds to other atoms. An interesting example is provided by fluoroacetylene and acetylene, for which A_{HF} and $A_{HH'}$ have been observed, respectively,[43,44] to be about 21 cps and 9.1±2 cps. The contact term is the only important one in $A_{HH'}$ for acetylene,[44] and the closeness of the ratio, 2.3, of the observed constants to the 1.75 value predicted by Eq. (9) suggests that the contact term also dominates A_{HF}.

Also, one can use Eq. (3) or (4) to obtain a numerical value for $[\psi(0)]_F^2$ to substitute in the general theoretical expressions for A_{NF}^{c}, as has been done by Karplus[42] to approximate A_{FF}^{c} and A_{HF}^{c} in fluoroethylenes. However, Eq. (9) is a simpler procedure which may well be more accurate because the errors introduced in Eq. (3) by assuming that $C_{H'}=C_F$ are probably partially compensated in Eq. (9) by the added assumption that $K_{H'}=K_F$. Accurate calculations of the $\sigma-\pi$ interaction, i.e., of C_H and C_F, would be very helpful.

Relation between a_F and ρ_C.—Finally, the fluorine hyperfine constant a_F can be related to the electron spin density, ρ_C, on the carbon to which the fluorine is bonded. In the case of protons, McConnell[12] proposed the following approximate linear relationship

$$a_H = Q_H \rho_C, \qquad (10)$$

where Q_H was found to be -22.5 gauss from empirical data. If the ρ_C's are the same for the carbon atoms in the semiquinone and tetrafluoro semiquinone ions, then (a_F/a_H) equals $(Q_F/-22.5)$. The values observed for a_F and a_H lead to the relation

$$a_F = -39.3\rho_C \text{ gauss}. \qquad (11)$$

This expression should apply to fluorine nuclei which are substituted on aromatic rings and is of potential value in the valence theory of fluoro aromatics. However, it is by no means clear that even the approximate constancy of Q in the proton case[1] will be shown for fluorine nuclei; at present, we cannot vouch for the accuracy of Eq. (11).

[43] W. J. Middleton and W. H. Sharkey, J. Am. Chem. Soc. **81**, 803 (1959); we are indebted to G. R. Miller for calling this value to our attention.

[44] Karplus, Anderson, Farrar, and Gutowsky, J. Chem. Phys. **27**, 597 (1957); T. C. Farrar, Ph.D. thesis, University of Illinois, 1959 (unpublished).

ACKNOWLEDGMENTS

We wish to express our appreciation to Dr. J. C. Tatlow of the University of Birmingham, Great Britain, for the sample of tetrafluoro *p*-benzoquinone and to Dr. G. C. Finger of the Illinois State Geological Survey, Urbana, for all the other fluorine compounds used in this investigation. We are also indebted to Dr. Martin Karplus for many interesting and helpful discussions on the theory of the electronic structure of semiquinones and to Dr. N. J. Leonard and Dr. E. J. Corey for their comments on the feasibility of the reactions leading to the complex radicals suggested. The design and construction of the apparatus were made possible by the aid of Dr. John C. Buchta.

Microwave Spectrum, Structure, Dipole Moment, and Nuclear Quadrupole Effects in Vinyl Chloride*

DANIEL KIVELSON† AND E. BRIGHT WILSON, JR.,

Mallinckrodt Chemical Laboratory, Harvard University, Cambridge, Massachusetts

AND

DAVID R. LIDE, JR., *National Bureau of Standards, Washington, D. C.*

(Received July 23, 1959)

The microwave spectra of nine isotopic species of vinyl chloride have been measured and analyzed, yielding moments of inertia from which a molecular structure was calculated. The bond lengths found are (in A) C=C 1.33$_2$, C—Cl 1.72$_6$, average C—H 1.08. The bond angles are C_2C_1Cl 122°, $C_2C_1H_1$ 124°, $C_1C_2H_3$ (cis to Cl) 121°, $C_1C_2H_2$ (trans to Cl) 120°. Planarity was assumed.

The chlorine nuclear quadrupole hyperfine lines were reexamined. From the data for several isotopic species it was shown that the C—Cl bond direction is within five degrees of a principal axis of the field gradient tensor. The lack of cylindrical symmetry of the field gradient about the C—Cl bond was confirmed. This is evidence that the observed shortening of the C—Cl bond is at least in part due to conjugation with the C=C double bond and not solely to hybridization effects.

The component of dipole moment along the *a* inertial axis was found to be 1.42±0.02 *D*.

VINYL chloride, CH_2CHCl, is the simplest molecule in which the question of conjugation between a carbon-carbon double bond and an adjacent carbon-chlorine bond can be investigated. Early electron diffraction studies[1] indicated a considerable shortening of the C—Cl bond, which was interpreted as an effect of the structure

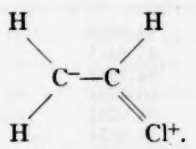

In the first microwave spectroscopy investigation of an asymmetric rotor with quadrupole coupling, Goldstein and Bragg[2] observed and analyzed part of the spectrum of the normal isotopic species, obtaining moments of inertia and particularly the hyperfine structure due to the interaction of the nuclear electrical quadrupole moment of the chlorine nucleus with the electrical field gradient from the other charges. They demonstrated that the field gradient at the chlorine is not cylindrically symmetrical about the C—Cl bond axis.

The purpose of the present paper is to report some measurements on various isotopic species of vinyl chloride, which enable a structure to be determined. The principal component of the dipole moment has also been obtained from the Stark effect, and the hyperfine structure data have been extended and refined, permitting a test of the assumption that the C—Cl bond direction is a principal axis of the field gradient tensor.

EXPERIMENTAL

The several deuterated species were prepared as a mixture by the catalytic reaction[3] of DCl with C_2D_2, the latter being obtained from D_2O and CaC_2. Enough light hydrogen was present so that several partially deuterated species were formed as well as the totally deuterated form. They were not separated.

The observations on the deuterated species were made on a standard Stark modulated microwave spectrograph[4] and the frequencies determined by comparison with a frequency standard checked against the National Bureau of Standards Station WWV. These older measurements should have an accuracy of ±0.2 Mc.

TABLE I. Observed frequencies[a] in deuterated species (Mc).

Species	$1_{11}\rightarrow 2_{12}$	$1_{01}\rightarrow 2_{02}$	$1_{10}\rightarrow 2_{11}$
D_2CCDCl^{35}	19 500.15	20 161.10	20 847.59
	(19 496.72)	(20 159.92)	(20 844.28)
D_2CCDCl^{37}	19 109.40	19 744.98	
	(19 106.73)	(19 744.04)	
$HDCCDCl^{35}$(trans)[b]	20 938.70	21 701.78	22 497.05
	(20 935.27)	(21 700.59)	(22 493.74)
$HDCCDCl^{37}$(trans)	20 523.55	21 257.18	22 021.70
	(20 520.88)	(21 256.22)	(22 019.12)
$DHCCDCl^{35}$(cis)	20 232.40	20 837.33	21 461.10
	(20 228.97)	(20 836.14)	(21 457.79)

[a] Figures given are principal hyperfine component ($F=5/2\rightarrow 7/2$); hypothetical unsplit frequency in parentheses, accuracy ±0.2 Mc.

[b] Trans means H trans to Cl.

* The research reported in this paper was made possible by support extended Harvard University by the Office of Naval Research under Office of Naval Research Contract Nonr 1866, Task Order XIV.

† Now at the University of California, Los Angeles, California.

[1] Brockway, Beach, and Pauling, J. Am. Chem. Soc. **57**, 2693 (1935).

[2] J. H. Goldstein and J. K. Bragg, Phys. Rev. **75**, 1453 (1949).

[3] D. H. R. Barton and M. Mugdan, J. Soc. Chem. Ind. (London) **69**, 74 (1950).

[4] McAfee, Hughes, and Wilson, Rev. Sci. Instr. **20**, 821 (1949).

TABLE II. Observed frequencies[a] in hydrogen species (Mc).

Rot. Trans.	$F \rightarrow F'$	H_2CCHCl^{35}	H_2CCHCl^{37}	$H_2CC^{13}HCl^{35}$	$H_2C^{13}CHCl^{35}$
$1_{11} \rightarrow 2_{12}$	3/2→5/2	22 355.06	21 918.85	22 204.76	[b]
	3/2→3/2	360.71			
	5/2→5/2	361.47			
	5/2→7/2	369.38	930.15	219.16	
	1/2→1/2	380.11	938.65		
		(22 365.83)	(21 927.36)	(22 215.59)	
$1_{01} \rightarrow 2_{02}$	1/2→3/2	22 931.02			
	5/2→5/2	932.24	22 474.53		
	3/2→5/2 }	946.55	485.81	22 805.33	22 199.21
	5/2→7/2 }				
	3/2→3/2	956.74	493.89		
		(22 945.31)	(22 484.85)	(22 804.49)	(22 198.00)
$1_{10} \rightarrow 2_{11}$	3/2→5/2	23 524.30	23 043.39	23 392.21	22 744.21
	3/2→3/2	528.86	047.00		
	5/2→5/2	532.19	049.57		
	5/2→7/2	538.58	054.65	406.72	758.33
	1/2→3/2	543.09	058.19		
	1/2→1/2	549.45	063.29		
		(23 535.17)	(23 051.96)	(23 403.27)	(22 754.96)

[a] Estimated uncertainty is ±0.02 Mc for H_2CCHCl^{35} and H_2CCHCl^{37}, and ±0.10 Mc for $H_2CC^{13}HCl^{35}$ and $H_2C^{13}CHCl^{35}$. Hypothetical unsplit frequencies in parentheses.

[b] Experimental difficulties prevented measurement; rotational constants for this species were calculated by assuming the same inertial defect as in the major species.

TABLE III. Rotational constants (Mc) and moments of inertia (amu A^2) (conversion factor 505 531 amu $A^2 \times$Mc).

Species	b	c	I_b	I_c
H_2CCHCl^{35}	6 029.96±.01	5 445.29±.01	83.8365	92.8382
H_2CCHCl^{37}	5 903.56±.01	5 341.26±.01	85.6315	94.6463
$H_2CC^{13}HCl^{35}$	5 999.28±.03	5 405.44±.03	84.2653	93.5226
$H_2C^{13}CHCl^{37}$	5 826.82±.03	5 274.51±.03	86.7593	95.8442
D_2CCDCl^{35}	5 379.52	4 705.74	93.9733	107.4286
D_2CCDCl^{37}	5 261.84	4 614.71	88.8134	102.2734
$DHCCDCl^{35}$ (trans)	5 818.24	5 039.01	86.8873	100.3235
$DHCCDCl^{37}$ (trans)	5 692.06	4 942.94	88.8134	102.2734
$HDCCDCl^{35}$ (cis)	5 518.05	4 903.64	91.6141	103.0930
H_2CCHCl^{35}	(calc. from structure)		(83.6415)	(92.5273)

The $J=1\rightarrow2$ transitions of $H_2CC^{13}HCl^{35}$ and $H_2C^{13}CHCl^{35}$ were measured in natural abundance on the 80-kc Stark-modulation spectrometer at the National Bureau of Standards. The complete Cl^{35} hyperfine pattern was observed, but only the stronger components were accurately measured. Lines from the C^{13} species were distinguished from those of excited vibrational states by observing the temperature dependence of the relative intensities. The $J=1\rightarrow2$ transitions of the major isotopic species were also remeasured with greater accuracy.

OBSERVED FREQUENCIES

The observed frequencies and the detailed transitions to which they were assigned are given in Tables I and II. The quantum number assignments are based primarily on the frequencies expected for a reasonable model but are confirmed by the hyperfine pattern, isotope shifts, Stark effect, and rough relative intensities. The identification of the particular deuterated species responsible for each spectral line is based on calculations from an approximate structure. For the deuterated species, hyperfine doublets were observed in most cases but only the strongest component ($F=\frac{5}{2}-\frac{7}{2}$) is listed in Table I. Some $J=2\rightarrow3$ transitions were also observed and serve as an additional check on the assignments.

To obtain the rotational constants listed in Table III it was first necessary to correct the observed frequencies for the effect of the hyperfine structure, which was analysed by the usual methods.[5] The corrected transitions $1_{10}\rightarrow2_{11}$ and $1_{11}\rightarrow2_{12}$ were then used to obtain values of b and c. These a type transitions (no other type was observed) are not very sensitive to a, which was therefore only roughly determined. The agreement between the calculated and observed frequencies for

[5] C. H. Townes and A. L. Schawlow, *Microwave Spectroscopy* (McGraw-Hill Book Company, Inc., New York, 1955), Chapter 6. Note, however, that the sign of η should be reversed in Eqs. (6-22a) through (6-22e).

$1_{01}\rightarrow 2_{02}$ served as a check on the assignment (the assumption of planarity provided the needed rough value of a). In the case of both the H_2CCHCl^{35} and H_2CCHCl^{37} species, where the measurements were most accurate, the $1_{01}\rightarrow 2_{02}$ frequency calculated on the assumption that $I_c=I_a+I_b$ is 0.11 Mc higher than the observed frequency, which implies a negative inertial defect ($\Delta=-0.2$ amu A^2). This discrepancy appears to be slightly outside the experimental uncertainty. However, it could be explained by the presence of a centrifugal distortion term of the form $-D_{JK}K^2J(J+1)$, with $D_{JK}=-27$ kc. Centrifugal distortion terms of this magnitude and sign have been found in several molecules similar to vinyl chloride.

STRUCTURE

The structure was obtained from the changes in moments of inertia on isotopic substitution, as recommended by Costain.[6] The cartesian coordinates, relative to principal axes for H_2CCHCl^{35}, were determined directly for the two carbon atoms and the chlorine from the equations[7]

$$b_i^2+a_i^2=\Delta I_c/\mu, \quad (1)$$

$$a_i^2=(\Delta I_b/\mu)[1+(\Delta I_c-\Delta I_b)/(I_c-2I_b)], \quad (2)$$

where b_i is the coordinate of the substituted atom (along the b axis), a_i along the a axis, μ is $M\Delta m/(M+\Delta m)$, ΔI_c and ΔI_b are the changes in I_c and I_b on substitution of atom i with an isotope heavier by Δm_i, and M is the total mass of the unsubstituted molecule. Planarity was assumed.

The location of the hydrogens required a more complex calculation involving successive approximations because no singly deuterated species were observed. The details will be omitted but account was taken of the rotation of the axes and shift of the center of mass with the result that hydrogen positions were determined which fitted the changes in moments observed. The resulting interatomic distances and angles are listed in Table IV, and are shown in Fig. 1. The values obtained were checked‡ by calculating the moments of inertia of all species from the cartesian coordinates and masses of the atoms and comparing the differences between the normal and each substituted species with the differences of the observed values. The worst disagreement was 0.009 amu. On the other hand, as expected, the *absolute* values of the calculated and observed moments differed by as much as 0.3 amu, and rather systematically, presumably due to the effect of zero point vibrations.

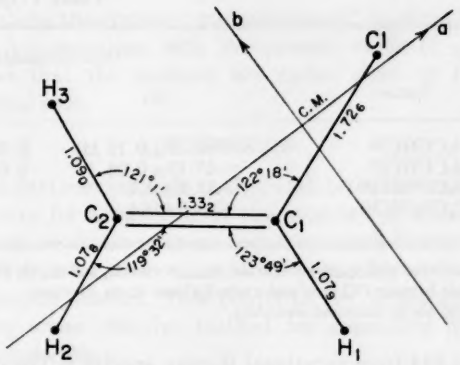

FIG. 1. Structural parameters for vinyl chloride, with principal axes for normal species CH_2CHCl^{35}.

The uncertainty in the structure arises primarily from these vibrational effects. The inertial defect Δ is defined by

$$\Delta=I_c-I_a-I_b. \quad (3)$$

If this did not change on isotopic substitution, the results obtained would not depend on which pair I_a, I_b; I_b, I_c; or I_c, I_a was used. It was not possible to obtain I_a accurately and thus evaluate the changes in Δ. However, the results available in other molecules suggest that Δ may change by as much as 0.01 amu A^2 on substitution, at least when hydrogen is involved, thereby introducing an ambiguity into the structural calculations. Since except for Cl, $\mu\sim\sim 1$, Eq. (2) shows that approximately (in A and amu)

$$\delta a_i=\delta\Delta I_b/2a_i. \quad (4)$$

Consequently, an uncertainty $\delta\Delta I_b$ of 0.01 amu will give an uncertainty of 0.005 A for an atom 1 A from the axis. A better knowledge of the effect of vibration is required to improve upon this.

The C=C distance agrees excellently with that reported for vinyl fluoride.[8] The C—H distances agree within the differences between nonequivalent hydrogens.

The C=C distance 1.332±0.005 A found here can be compared with the values for ethylene of 1.337 from recent infrared work,[9] 1.334 from electron diffraction,[10]

TABLE IV. Structural parameters (masses used from reference 5).

Bonds		Angles	
C_1H_1	1.07_9 A	$C_1C_2H_2$	119° 32′
C_2H_2	1.07_8	$C_1C_2H_3$	121° 1′
C_2H_3	1.09_0	$H_2C_2H_3$	119° 27′
C_1C_2	1.33_2	C_2C_1Cl	122° 18′
C_1Cl	1.72_6	$C_2C_1H_1$	123° 49′
		H_1C_1Cl	113° 53′

[6] C. C. Costain, J. Chem. Phys. **29**, 864 (1958).
[7] J. Kraitchman, Am. J. Phys. **21**, 17 (1953).
‡ We are grateful to Dr. L. C. Krisher for carrying through these check calculations on an IBM 650 computer.

[8] Bak, Christensen, Hansen-Nygaard, and Rastrup-Andersen, Spectrochim. Acta **13**, 120 (1958).
[9] H. C. Allen and E. K. Plyler, J. Am. Chem. Soc. **80**, 2673 (1958).
[10] L. S. Bartell and R. A. Bonham, J. Chem. Phys. **27**, 1414 (1957).

TABLE V. Quadrupole coupling constants.

Species	Obs. constants		Calc. constants[a]		
	χ_{aa}	η	χ_{aa}	η	θ[b]
H_2CCHCl^{35}	-57.15 ± 0.10 Mc	0.0528 ± 0.0005	-57.16	0.0528	20°5′
H_2CCHCl^{37}	-45.19 ± 0.08	0.0502 ± 0.0009	-45.17	0.0501	19°58′
$H_2CC^{13}HCl^{35}$	-57.8 ± 0.4	[c]	-57.47	0.0472	19°50′
$H_2C^{13}CHCl^{35}$	-56.5 ± 0.4	[c]	-56.70	0.0614	20°27′

[a] Calculated with $\chi_{aa}^{35}=-70.16$ Mc, $\eta_{\text{bond}}=-0.1422$, and $Q_{35}/Q_{37}=1.2628$.
[b] Angle between CCl bond and a principal axis (from structure).
[c] Could not be measured accurately.

and 1.344 from rotational Raman spectra.[11] The C—H distances can be compared with 1.086 reported for ethylene from the infrared.[9] The differences are probably not physically significant. The H—C—C angle in ethylene is reported as 117° 22′ from infrared.[9]

QUADRUPOLE COUPLING CONSTANTS

The results of the hyperfine structure analysis are conveniently expressed in terms of χ_{aa} and $\eta=(\chi_{bb}-\chi_{cc})/\chi_{aa}$, where $\chi_{aa}=eQ(\partial^2V/\partial a^2)$, etc., are diagonal elements of the quadrupole coupling tensor in the principal inertial axis system. In order to relate the observed constants to actual bond properties in an asymmetric molecule, it is usually assumed that a principal axis of the quadrupole tensor coincides with the bond to the atom in question. Since constants are available for several isotopic species of vinyl chloride, a rough test of this assumption is possible. We define a system α, β, γ such that the α axis coincides with the CCl bond and the γ axis is perpendicular to the plane of the molecule. Then if α is a principal axis of the quadrupole tensor, the coupling constants for all species should be predictable from the two parameters χ_{aa} and $\eta_{\text{bond}}=(\chi_{\beta\beta}-\chi_{\gamma\gamma})/\chi_{aa}$. The angle θ between the α and a axes may be computed from the known molecular structure.

The constants predicted in this way are compared with the observed constants in Table V. Although the agreement is entirely satisfactory, the isotope shifts are so small that the test is not extremely critical. A detailed analysis shows that we can conclude only that the principal axis of the quadrupole tensor lies within about 5° of the CCl bond.

The best fit from the above calculation is obtained with bond constants (for Cl^{35}): $\chi_{aa}=-70.16$ Mc, $\chi_{\beta\beta}=40.07$ Mc, and $\chi_{\gamma\gamma}=30.09$ Mc ($\eta_{\text{bond}}=-0.1422$). In view of the more accurate experimental measurements and the improved structure, these bond constants are believed to be more precise than the values reported previously.[12] The value of χ_{aa} may be compared with -70.07 Mc in ethyl chloride,[13] and -74.77 in methyl chloride.[14] As pointed out by Goldstein,[12] the observed value of η_{bond} suggests about 6% double bond character for the CCl bond.

The experimental uncertainty in the angle θ is about 20′, which leads to an uncertainty of about 0.7% in χ_{aa} and of 5% in η_{bond}. However, the values of the bond constants are rather sensitive to the assumption that the principal axis of the quadrupole tensor coincides with the C—Cl bond. If the angle between the principal axes of the inertial and quadrupole tensors were 5° less than θ (which we cannot rule out on existing experimental evidence), χ_{aa} would become -63 Mc while $\eta_{\text{bond}}=-0.05$. Therefore, some caution must be exercised in the quantitative interpretation of bond coupling constants in an asymmetric molecule such as vinyl chloride.

STARK EFFECT

The Stark effect of vinyl chloride is complicated by the presence of hyperfine structure. Accurate measurements may be obtained only on selected components, and these must in general extend into the intermediate field region where calculations are often tedious. It is well known, however, that the combined Stark and quadrupole energy of certain components may be simply expressed. For a nucleus of spin $I=\frac{3}{2}$ and a general asymmetric rotor level J_τ these expressions take the following form. We assume that in the absence of hyperfine structure the Stark energy would be given by $W_S=(A+BM_J^2)\epsilon^2$; and that in the absence of the Stark perturbation the quadrupole energy would be $W_Q=q_J'f(I,\ J,\ F)(2J+3)/J$, where $f(I,\ J,\ F)$ is Casimir's function.[5] Then the combined energy for the level $F=J+\frac{3}{2}$, $M_F=J+\frac{3}{2}$ is

$$W_{Q,S}=(q_J'/4)+(A+BJ^2)\epsilon^2; \tag{5}$$

while for $F=J+\frac{3}{2}$, $M_F=J+\frac{1}{2}$ (upper sign) and $F=J+\frac{1}{2}$, $M_F=J+\frac{1}{2}$ (lower sign)

$$W_{Q,S}=(-3q_J'/8J)+[A+B(J^2-J+\tfrac{1}{2})]\epsilon^2 \pm(1/8J)[(2J+3)^2q_J'^2-8J(2J-1)(2J-3)q_J'B\epsilon^2+16J^2(2J-1)^2B^2\epsilon^4]^{\frac{1}{2}}. \tag{6}$$

[11] B. P. Stoicheff, Current Science **27**, 1 (1958).
[12] J. H. Goldstein, J. Chem. Phys. **24**, 106 (1956).
[13] R. S. Wagner and B. P. Dailey, J. Chem. Phys. **26**, 1592 (1957).
[14] J. Kraitchman and B. P. Dailey, J. Chem. Phys. **22**, 1477 (1954).

TABLE VI. Stark shifts in weak field limit.

Trans.	$F \rightarrow F'$	$M_F \rightarrow M_F'$	Obs.[a] $\Delta\nu/\epsilon^2$	Calc.[b] $\Delta\nu/\epsilon^2$
$1_{01} \rightarrow 2_{02}$	$5/2 \rightarrow 7/2$	$5/2 \rightarrow 5/2$	4.16 Mc(kv/cm)$^{-2}$	4.15
$1_{01} \rightarrow 2_{02}$	$5/2 \rightarrow 5/2$	$5/2 \rightarrow 5/2$	3.70	3.70
$2_{02} \rightarrow 3_{03}$	$7/2 \rightarrow 9/2$	$7/2 \rightarrow 7/2$	1.69	1.71
$2_{02} \rightarrow 3_{03}$	$7/2 \rightarrow 7/2$	$7/2 \rightarrow 7/2$	1.26	1.29

[a] Estimated uncertainty is 3%.
[b] Calculated with $\mu_a = 1.420$ D, $\mu_b = 0$.

The Stark coefficients[15] A and B and the quadrupole factor[5,16] $q_J' = eQ(\partial^2 V/\partial z^2)_{hr}$ may be computed by well-known methods. It is assumed that the spacing between asymmetric rotor levels is much greater than W_Q and W_S.

Stark shifts were measured for several vinyl chloride transitions which could be analyzed with the above expressions. The limiting slopes for small fields are given in Table VI. Unfortunately, the Stark effects of these transitions (and of all others which can be conveniently measured) are quite insensitive to the μ_b component of the dipole moment. A satisfactory fit may be obtained with $\mu_b = 0$ and $\mu_a = 1.42$ D, as shown in Table VI. The detailed analysis shows that μ_b is undetermined (although probably less than 1.0 D) and that $\mu_a = 1.42 \pm 0.02$ D.

A total dipole moment of 1.45 D has been determined from dielectric-constant measurements[17] on vinyl chloride. A comparison with the present value of μ_a indicates that the moment lies rather close to the a principal axis.

DISCUSSION

The first conclusion from this work is that interatomic distances for a molecule of this number of atoms are difficult to obtain with an accuracy much better than ± 0.01 A, even when a considerable number of isotopic species are studied. This points to the desirability of finding some effective method for correcting for vibrational effects.

The second conclusion is that the C—Cl bond is indeed considerably shortened (e.g. 0.05 A below CH_3Cl), presumably by being adjacent to C=C, but not so much shortened as suggested by the early electron diffraction study.

The third result is the confirmation of the idea that the field gradient at the Cl nucleus is at least approximately oriented with a principal axis along the C—Cl bond. As found before,[2] this gradient is not cylindrically symmetrical about the C—Cl bond. Although the shortening of the C—Cl bond might alternatively be ascribed to a change in hybridization of the carbon,[18] the lack of cylindrical symmetry is best accounted for in terms of double bond character, i.e., conjugation.

[15] S. Golden and E. Bright Wilson, Jr., J. Chem. Phys. **16**, 669 (1948).
[16] J. K. Bragg, Phys. Rev. **74**, 533 (1948).
[17] Hugill, Coop, and Sutton, Trans. Faraday Soc. **34**, 1518 (1938).
[18] M. J. S. Dewar and H. N. Schmeising, Tetrahedron **5**, 166 (1959).

Kinetics of Strontium Oxide on Tungsten*

J. A. CAPE† AND E. A. COOMES

University of Notre Dame, Notre Dame, Indiana

(Received July 10, 1959)

Field electron microscopy has been used to study the kinetics of strontium oxide on tungsten in the range 900–2200°K. Reactions take place on the {111} and {100} which have high concentrations of four nearest neighbor surface atoms. Below 1150°K there is some evidence for the dissociation of SrO and migration of Sr to the {110} edges where clusters of crystallites are formed. Two modifications of field emission patterns associated with the (Sr—O—W) complex within 1150–1550°K are tentatively identified with the basic and normal tungstate; apparently the first goes over to the second with an activation energy of ~60 kcal as determined from desorption data. An unusually sharp decrease in Fowler-Nordheim work function occurs during this reaction. In the later stages of desorption above 1550°K patterns identifiable with an oxygen-tungsten surface are obtained. Desorption at this stage takes place with an activation energy of ~140 kcal.

1. INTRODUCTION

THE physical and chemical kinetics of the alkaline earth oxides in contact with refractory metals at elevated temperatures are of interest in oxide cathode electronics.[1] While (BaSr)O on W, Mo, or Ni may simply migrate or evaporate when heated, chemical reactions between oxide and metal ending in complex compounds occur in certain temperature ranges.[1–3] Moore *et al.*[4] made a quantitative study for the solid state chemical reaction between SrO and W. They found that within the range 1150–1550°K, tungsten reduced SrO in vacuum with an evolution of Sr vapor and formation of a strontium tungstate as end products. The probable reactions[2] which govern this process are, (1) a reduction of the oxide to form the basic tungstate, according to the equation,

$$2\mathrm{SrO}(s)+\tfrac{1}{3}\mathrm{W}(s)=\tfrac{1}{3}\mathrm{Sr_3WO_6}(s)+\mathrm{Sr}(g), \qquad (1)$$

and (2) a further reduction of the basic tungstate ending in the normal tungstate and an evolution of strontium,

$$\tfrac{2}{3}\mathrm{Sr_3WO_6}(s)+\tfrac{1}{3}\mathrm{W}(s)=\mathrm{SrWO_4}(s)+\mathrm{Sr}(g), \qquad (2)$$

with reaction (2) occurring at a much slower rate than reaction (1). Since these reactions take place at a macroscopic metal surface, apparently unimpeded by diffusion in the bulk materials[4] the possibility of observing their occurrence in a field electron microscope (FEM) presents itself. This experiment has sought possible correlations between thin film kinetics and the bulk thermochemistry by this device.

II. EXPERIMENTAL METHOD

The experiment consisted in evaporating SrO molecules in measured amounts from a calibrated source‡ onto a clean W tip held at a *receiver temperature* T_R. The source was turned off, the emitter raised to a selected *activation temperature* T_A, and allowed to heat for chosen time intervals. At the end of each interval the FEM pattern was photographed with the tip at room temperature. An average work function ϕ was determined[5] from the relation

$$\phi=4.5(V/V_0)^{\frac{1}{2}}\ (\mathrm{ev}), \qquad (3)$$

where V_0 is the voltage required to draw a standard field emission current (usually 0.5 μa in this experiment) with the emitter tip clean, and V the voltage to draw the same current with the tip activated. While the fundamental significance of ϕ computed by Eq. (3) must always be weighed in view of the patchiness of a field emitter tip, and especially where preferential buildup may occur due to reactive adsorbants, this quantity is useful for a comparison of total electron emissivity at various states of adsorption. The accuracy of the comparison will depend upon the constancy of the pre-exponential term of the Fowler-Nordheim equation over these states. T_R was chosen greater than 900°K since boundary migration appeared below this temperature.

Figure 1 indicates the main features of the FEM tube. Emitter tips of radius greater than 3000 A were used to inhibit migration of tungsten.[6] The probable structure developed on the W tip by rigorous heating to the clean state is illustrated in Fig. 2; this sketch shows the surface structure formed by the four and five nearest neighbor atoms on the surface as they

* Supported in part by Office Naval Research.

† Now at the Physics Department, University of Illinois, Urbana, Illinois.

[1] See, for example, E. S. Rittner, Philips Research Rpts. **8**, (1953); Moore and Allison, Phys. Rev. **77**, 246 (1950).

[2] A. H. White, J. Appl. Phys. **20**, 856 (1949).

[3] Rutledge and Rittner, J. Appl. Phys. **28**, 167 (1957).

[4] Moore, Allison, and Morrison, J. Chem. Phys. **18**, 1579 (1950).

‡ The source filaments, prepared by spraying a coating of $SrCO_3$ in a nitrocellulose binder on highly refined platinum and converting to SrO by heating, were furnished by G. E. Moore, Bell Telephone Laboratories, Murray Hill, New Jersey. See reference 4.

[5] R. Gomer, Advances in Catalysis **7**, 93 (1955).

[6] E. W. Müller, Ergeb. Exakt. Naturw. **27**, 290 (1953).

appear on a tungsten point model.[7] Note in particular the symmetrical arrangements of four nearest neighbors {100} and {111} which probably develop as facets and the wide lattice steps at the {110} edges; the {110} containing only six nearest neighbor surface atoms are blank in the sketch. The emitter area represented in Fig. 2 correlates with approximately the upper left hand quadrant of each of the FEM photographs to follow.

Molybdenum film gettering and ion pumping, indicated in Fig. 1, reduced the background of adsorbable gases to a degree where contamination of the clean pattern did not appear for days after flashing the W point at 2300°K. Tube pressures were below 10^{-11} mm Hg, the limit of measurement with the Bayard-Alpert

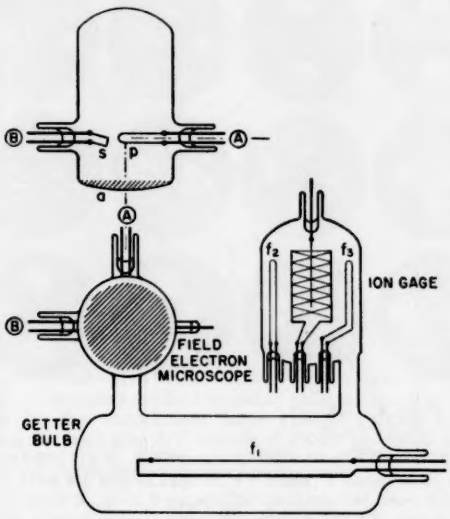

FIG. 1. The field electron microscope used for the SrO—W reactions. Note the convenient mounting for SrO source S and tungsten tip P. Final ion pumping was carried out with tube sealed off from vacuum system. Molybdenum filaments f_1 and f_2 were used for film gettering.

gauge. A temperature scale for the emitter point was established by taking optical pyrometer readings on a position 1 mm from the tip and computing the gradient to the tip; 10°K precision is estimated. The arrival rate of SrO at the tip was computed from the source temperature, the vapor pressure equation,[8] and the geometry. Since the sticking coefficient is unknown, the amount of SrO deposited on the tip for a chosen arrival rate can only be estimated. Sufficient SrO, however, was deposited to assure a uniform reaction over the entire tip, as illustrated in Fig. 3, for an arrival rate of 1×10^{-5} g/cm²-hr with $T_R=900$°K. Figures 3(a) to (f) show patterns symmetrical about the [110] direction as they occur with increasing reception time up to 56 min; ϕ decreases from 4.5 to 1.9 ev. Figures

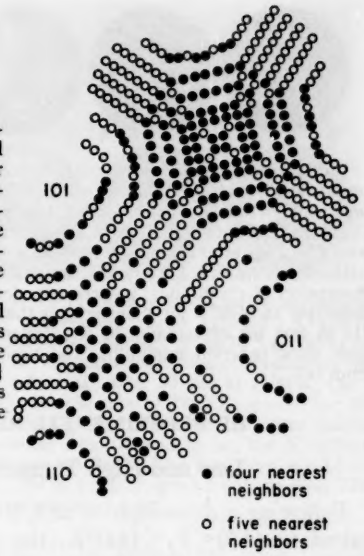

FIG. 2. Surface structure formed by four and five nearest neighbor atoms on a clean tungsten tip after heat treatment at 2300°K. The area mapped corresponds to about the upper right hand quadrant in each of the field emission micrographs which follow. A "marble model" of W with {111} and {100} developed as facets was used for the sketch.

3(g) to (h) for additional deposit of SrO are characterized by a buildup of crystallites on the {110} edges; in this range field currents are unstable and the FEM patterns show strong agitation. While this buildup could be associated with a migration of SrO deposited in excess of a monolayer, high temperature studies to follow offer the alternate suggestion that SrO on W dissociates at 900°K; the crystallites result from a migration of Sr to the {110} edges, the temperature being too low for complete evaporation.§ Whenever T_R is held at 900–1175°K and sufficient SrO is deposited to obtain crystallites as in Fig. 3(g), the FEM patterns at constant activation temperature which follow subsequent to the disappearance of the clustering are independent of the amount deposited.

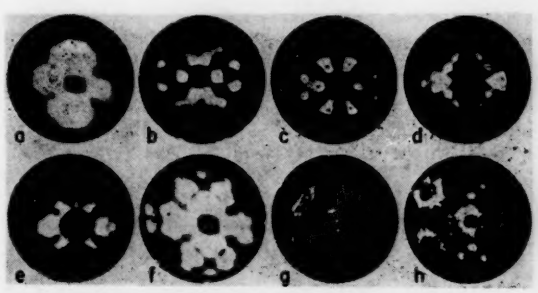

FIG. 3. Sequence of field emissions patterns for SrO deposited on W at $T_R=900$°K, arrival rate 1×10^{-5} g/cm²-hr: (a) clean tip, 9.2 kv at 0.5 μa, $\phi=4.5$ ev; (b) after 15-sec deposit, $\phi=2.9$ ev; (c) after 4-min deposit, $\phi=2.7$ ev; (d) after 16-min deposit, $\phi=2.2$ ev; (e) after 29-min deposit, $\phi=2.0$ ev; (f) after 45-min deposit, $\phi=1.9$ ev; (g) after 91-min deposit, i fluctuating; (h) after 135-min deposit, i fluctuating. The times are total from pattern (a). Direction of deposition was from upper left; note crystallite formation on {110} edges in (g)–(h).

[7] Becker and Brandes, J. Chem. Phys. **23**, 1323 (1955).
[8] Moore, Allison, and Struthers, J. Chem. Phys. **18**, 1572 (1950).

§ Barnaby has obtained the same crystallite formation when several monolayers of Sr are allowed to migrate into a symmetrical coverage on a clean W tip held at ~350°K, and then raised to 450°K (unpublished data).

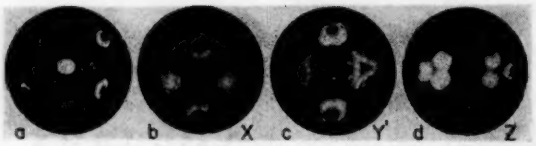

FIG. 4. Sequence of field emission patterns for activation temperature $T_A = 1460°K$: (a) after 10-hr deposit on clean point held at $T_R = 1075°K$, deposit rate 2×10^{-5} g/cm²-hr, i fluctuating; (b) after 2 min at 1460°K, $\phi = 4.2$ ev; (c) after 12 min at 1460°K, $\phi = 3.7$ ev; (d) after 30 min at 1460°K, $\phi = 4.2$ ev. V_0 for clean W pattern was 9.23 kv. Pattern (b), designated X, appears first after desorption of crystallites; pattern (d), designated Z, persists indefinitely at 1460°K for times greater than 30 min. Refer to Sec. III of text for explanation of (c), designated Y', which occurs near work function minimum. The times at 1460°K are total from (a).

III. EXPERIMENTAL RESULTS

Low and High Temperatures

Following a deposition of SrO, if the temperature is raised to $1150 \leq T_A \leq 1525°K$, the crystallites desorb, as illustrated in Fig. 4(a) to (b). The first pattern (*designated* X) which follows is Fig. 4(b); the work function associated with this pattern is 3.4 to 4.2 ev, apparently depending upon T_R. If the tip is now heated continuously at a constant T_A in the above range, patterns occur in a definite time sequence (Figs. 4, 5, 7, 8); ϕ decreases to a minimum at Fig. 4(c) and then rises rapidly to ~4.0 ev at Fig. 4(d). This last pattern (*designated* Z) terminates the sequence; it will persist indefinitely unless T_A is raised above 1525°K. The time to reach Z from X depends upon T_A: in Fig. 4(b) to (d) for $T_A = 1460°K$ the time interval is 28 min, while in Fig. 5(a) to (c), for $T_A = 1525°K$, Δt is 4 min. Figures 5(d) to (h) are typical of the changes brought about by now raising T_A to 1550°K or higher. For constant temperature in this high range gradual changes occur, with Fig. 5(d) most persistent for 1550–1700°K, Fig. 5(e) for 1700–1850°K, and Fig. 5(f) for 1850–2000°K. The clean W pattern develops in the 2000–2200°K range, as shown in Fig. 5(g) to (h). One may identify Figs. 5(d)–(f) with the FEM patterns obtained by Müller[9] on exposing a W point at room temperature to 10^{-3} mm Hg of O_2, and then heating in vacuum for 1 min at 1695, 1900, and 2060°K, respectively. A simple interpretation at this stage would associate the Z pattern with the normal tungstate, which decomposes above 1550°K leaving the tip oxidized or oxygen chemisorbed to it. The observed work function ϕ going from

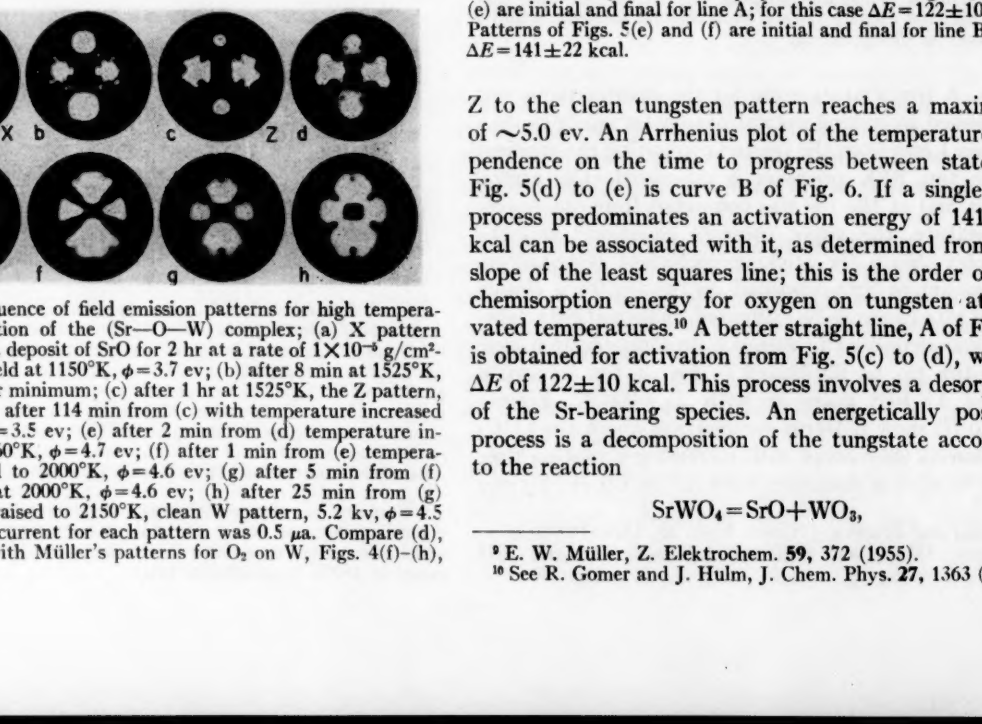

FIG. 5. Sequence of field emission patterns for high temperature modification of the (Sr—O—W) complex; (a) X pattern produced by a deposit of SrO for 2 hr at a rate of 1×10^{-5} g/cm²-hr on W tip held at 1150°K, $\phi = 3.7$ ev; (b) after 8 min at 1525°K, $\phi = 3.2$ ev-near minimum; (c) after 1 hr at 1525°K, the Z pattern, $\phi = 4.2$ ev; (d) after 114 min from (c) with temperature increased to 1550°K, $\phi = 3.5$ ev; (e) after 2 min from (d) temperature increased to 1760°K, $\phi = 4.7$ ev; (f) after 1 min from (e) temperature increased to 2000°K, $\phi = 4.6$ ev; (g) after 5 min from (f) temperature at 2000°K, $\phi = 4.6$ ev; (h) after 25 min from (g) temperature raised to 2150°K, clean W pattern, 5.2 kv, $\phi = 4.5$ ev. The field current for each pattern was 0.5 μa. Compare (d), (e), and (f) with Müller's patterns for O_2 on W, Figs. 4(f)–(h), reference 9.

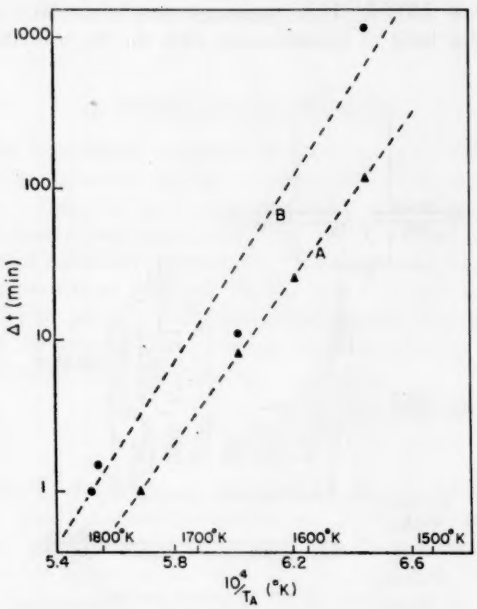

FIG. 6. Plots of $\log\Delta t$ *vs* $1/T_A$ for high temperature desorption, with the least squares lines displayed. Patterns of Figs. 5(c) and (e) are initial and final for line A; for this case $\Delta E = 122\pm10$ kcal. Patterns of Figs. 5(e) and (f) are initial and final for line B, and $\Delta E = 141\pm22$ kcal.

Z to the clean tungsten pattern reaches a maximum of ~5.0 ev. An Arrhenius plot of the temperature dependence on the time to progress between states of Fig. 5(d) to (e) is curve B of Fig. 6. If a single rate process predominates an activation energy of 141 ± 22 kcal can be associated with it, as determined from the slope of the least squares line; this is the order of the chemisorption energy for oxygen on tungsten at elevated temperatures.[10] A better straight line, A of Fig. 6, is obtained for activation from Fig. 5(c) to (d), with a ΔE of 122 ± 10 kcal. This process involves a desorption of the Sr-bearing species. An energetically possible process is a decomposition of the tungstate according to the reaction

$$SrWO_4 = SrO + WO_3, \qquad (4)$$

[9] E. W. Müller, Z. Elektrochem. **59**, 372 (1955).
[10] See R. Gomer and J. Hulm, J. Chem. Phys. **27**, 1363 (1957).

with an evolution of strontium oxide at 1550°K; the heat of formation of $SrWO_4$ by reaction (4) going from right to left[4] is 112 kcal.

Intermediate Temperatures

Intermediate activation temperatures are *defined* in this paper as $1150 \leq T_A \leq 1525$°K; this practically coincides with Moore's range[4] for chemical reaction between SrO and W. The sequence of FE micrographs for the coated tip held at constant T_A in this range starts with X and ends with Z. The X pattern [Figs. 4(b), 5(a), 7(a), 7(g), 8(a), and 8(e)] may be identified by the following characteristics: (1) high emission from the triangular {111} region of four nearest neighbor

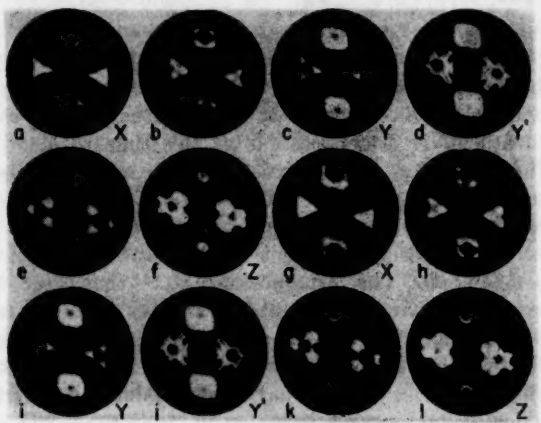

FIG. 7. Sequence of field emission patterns showing developments for the temperature range $1150 \leq T_A \leq 1525$°K: (a) X pattern obtained after SrO deposit of 2×10^{-5} g/cm²-hr for 10 hr, W point at 1175°K, $\phi = 3.6$ ev; (b) after 50 min at 1410°K, $\phi = 3.4$ ev; (c) after 110 min at 1410°K, $\phi = 3.0$ ev, Y pattern; (d) after 115 min at 1410°K, $\phi = 2.9$ ev, the Y′ pattern; (e) after 120 min at 1410°K, $\phi = 3.1$ ev; (f) after 180 min at 1410°K, the Z pattern, $\phi = 3.7$ ev; (g) after flashing to clean W at 2300°K and then depositing SrO at 2×10^{-5} g/cm²-hr for 10 hr on the point at 1175°K, the X pattern, $\phi = 3.5$ ev; (h) after 200 min at 1310°K [cf(b)], $\phi = 3.4$ ev; (i) after 280 min at 1310°K pattern, $\phi = 3.0$ ev; (j) after 300 min at 1310°K, the Y′ pattern, $\phi = 2.7$ ev; (k) after 340 min 1310°K [cf (e)], $\phi = 3.0$ ev; (l) after 900 min at 1310°K, the Z pattern, $\phi = 3.7$ ev.

atoms (see Fig. 2), and (2) emission from the vicinals of {100}, particularly the ring comprising the ⟨611⟩ and ⟨310⟩ directions. The Z pattern [Figs. 4(d), 5(c), 7(f), 7(l), 8(d) and 8(h)] develops from X on continued heating by a series of systematic modifications; notable is the gradual filling in of the [100] ring with high emission until the entire {100} area is bright; at this state [*designated* Y, Fig. 5(b), 7(c), 7(i), 8(b), and 8(f)], ϕ reaches its minimum value. On continued heating the emitting area in the {111} enlarges until it reaches the {110} edges and extends into the {211} regions whereas in the {100} there is a gradual recession to the central {100} plane; ϕ increases during these latter developments. Figures 7 and 8 illustrate in some detail the X to Z modifications as a function of T_R and T_A. In these cases SrO was deposited on a clean tip at an arrival rate of 2×10^{-5} g/cm²-hr for 10 hr;

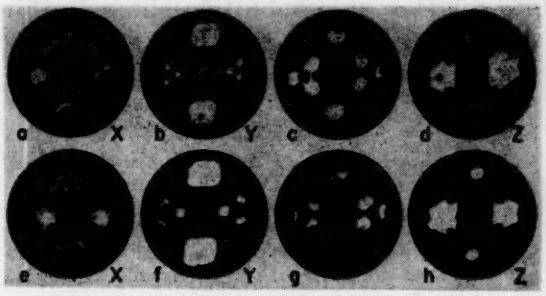

FIG. 8. Another sequence of field emission patterns showing developments for the temperature range $1150 \leq T_A \leq 1525$°K: (a) X pattern obtained after SrO deposit of 2×10^{-5} g/cm²-hr for 10 hr, W point at 1075°K, and then desorption of crystallites (see Fig. 4) at 1400°K, $\phi = 4.4$ ev; (b) after 30 min at 1400°K, the Y pattern, $\phi = 3.9$ ev; (c) after 50 min at 1400°K, $\phi = 3.9$ ev; (d) after 80 min at 1400°K, the Z pattern, $\phi = 4.4$ ev; (e) after flashing clean, and then reproducing conditions as in (a), the X pattern, $\phi = 4.2$ ev; (f) after 600 min at 1240°K, the Y pattern, $\phi = 3.5$ ev; (g) after 1200 min at 1240°K (cf (c)), $\phi = 3.8$ ev; (h) after 2200 min at 1240°K, the Z pattern, $\phi = 4.4$ ev.

$T_R = 1175$°K for Fig. 7, no crystallites were formed, and the X pattern appeared immediately at the end of deposition. For $T_R = 1075°$, Fig. 8, crystallites occurred [cf Fig. 5(a)–(b)], and X was obtained after desorption at higher temperatures. This would indicate that ~1150°K, Moore's lower limit for reaction, is the highest temperature at which Sr is physically adsorbed on the (Sr—O—W) complex, and suggests a correlation between the X pattern and the basic tungstate. Increase of T_A in the intermediate range steps up the rate at which the X to Z modification occurs, but effects no change of FEM pattern sequence: for $T_A = 1240$°K, Fig. 8(e) to (h), $\Delta t \sim 2000$ min; for $T_A = 1310$°K, Fig. 7(g) to (l), $\Delta t \sim 900$ min; and for $T_A = 1410$°K, Fig. 7(a) to (f), $\Delta t \sim 200$ min. Physical changes are significantly revealed in a display of ϕ *vs* Δt, as given in Fig. 9, on which the times of occurrence of the fiducial

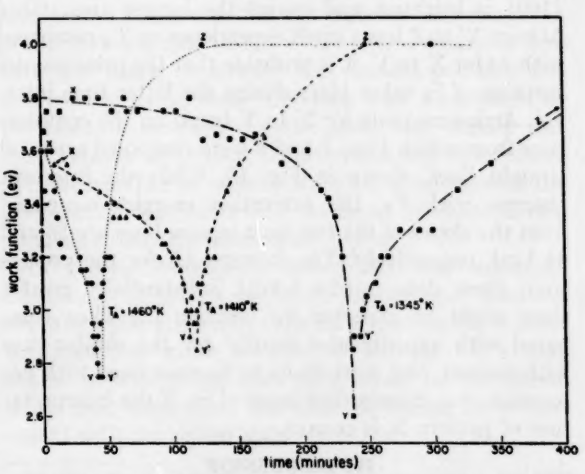

FIG. 9. Fowler-Nordheim work functions *vs* time, for the (Sr—O—W) complex activated in the range $1150 \leq T_A \leq 1525$°K. Positions of the fiducial X, Y, Y′, Z patterns, Fig. 7, are marked. The fine structure, which appears as steps in the plots, is real and may be associated with observed desorption effects.

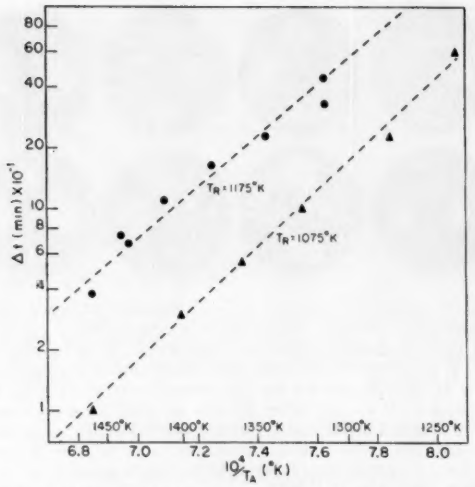

FIG. 10. Plots of $\log\Delta t$ *vs* $1/T_A$ for activation from X to Y state, Figs. 7 and 8. The least squares lines are given. The average activation energy from the two lines is $\Delta E = 61 \pm 3$ kcal.

X, Y, Z patterns are marked. Note the identical form of the plots with a shift to the right for lower T_A. Minimization of Fowler-Nordheim work function occurs with such suddenness that the resolving time of the present experiment is not good enough to detect the depth of the depression. During the short fall-rise interval, Fig. 9, the FEM pattern changes from Y, Fig. 7(c) and (i) to Y′, Fig. 7(d) and (j), marked by an inversion of the bright bands along the {223} and {221} regions. The groups of emitting planes comprising Y forms a threefold symmetry pointing outward from central {111}, while in Y′ emission is chiefly from the {332} and forms a threefold symmetry pointing inward. At the Y–Y′ inversion both groups of planes are briefly at nearly equal emitting intensity; this is also the instant at which emission from the {100} is brightest and covers the largest area. Since Δt from Y′ to Z has a small dependence on T_A compared with Δt for X to Y, it is probable that the principal desorption of Sr takes place during the latter time interval. Arrhenius plots for X to Y based on the complete runs from which Figs. 7 and 8 were composed are good straight lines, shown in Fig. 10. While the intercept changes with T_R, the activation energies computed from the slopes of the two least square lines are 58 and 64 kcal, respectively. The average ΔE for the process from these data is 61 ± 3 kcal, substantially greater than might be expected for reaction (2) when compared with experimental results[4] for the similar case with barium, and more likely to be associated with desorption of a chemisorbed layer of Sr, if the interpretation of pattern X is correct.

IV. DISCUSSION

The FEM observations of SrO on W were reproduced in three different tubes on three different tungsten points. They are consistent with the bulk reaction (1) within 1150–1150°K, followed by a reduction of the

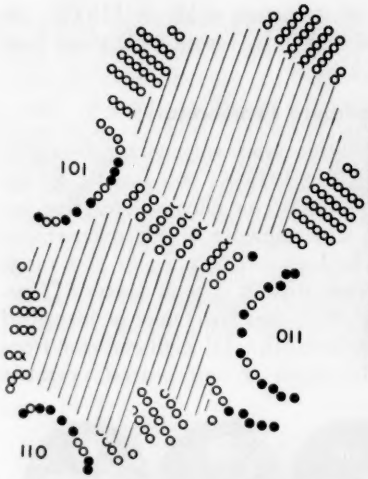

FIG. 11. Sketch of the crystal surface region on which the (Sr—O—W) reaction occurs suggesting epitaxy. The cross-hatched area is a superposition of all FEM patterns in the X to Z sequence (see text). In comparison with Fig. 2, note that this area outlines {111}, {100} regions composed of four nearest neighbor atoms.

basic tungstate according to reaction (2). Similar reactions for BaO and W have been studied[3] and well identified. It is not possible at this time to identify the X pattern as the basic tungstate with complete unambiguity, since the clustering observed in Fig. 3 might be attributed to physisorbed SrO, the X to Y activation energy representing a desorption of chemisorbed SrO. The experimental fact[4] that *only* Sr evaporates when SrO is heated in contact with tungsten in the range 1150–1550°K argues against this premise. However, we have performed the experiment in which all the patterns of Fig. 7 have been produced in reverse order by making successive small deposits of SrO on the tip held at 1050°K after the Z state had been formed; on heating to 1150–1525°K the X to Z pattern sequence and the X to Y activation energy as described in the last section were then reproduced. While a direct suggestion of this experiment is the formation and subsequent desorption of a chemisorbed SrO film, it more probably implies the buildup of a very thin $SrWO_4$ layer in epitaxy with the {111} and {100} facets. A superposition of all patterns of the X to Z sequence as sketched in Fig. 11 (cf. Fig. 2) would supplement the latter analysis.

Although the data in Fig. 9 were plotted principally as a display for obtaining accurate desorption times, an explanation of the sharp minima presents an interesting problem. In this range of strong buildup the connection of ϕ with an average thermionic work function may be remote, but a preliminary attempt to fit the current-voltage data near the minima to the Fowler-Nordheim equation did not reveal a corresponding extreme variation in pre-exponential term. The Y–Y′ transition patterns would associate the dip with a critical concentration of adatoms near the edges of the {111}, probably less than a monolayer of Sr on the {223} or {332} regions. A more precise study of this phenomena is anticipated.

The authors thank Ernest Parsons for building the FEM tubes, and appreciate the contribution of Jane Coomes and David Mead to photographic techniques.

THE JOURNAL OF CHEMICAL PHYSICS VOLUME 32, NUMBER 1 JANUARY, 1960

Hydrogen Ion Titration Curve of a Polynucleotide Capable of Undergoing a Helix-Coil Transition*

R. F. STEINER

Naval Medical Research Institute, National Naval Medical Center, Bethesda, Maryland

(Received July 13, 1959)

A theory is developed for the hydrogen ion titration curve of doubly stranded helical polynucleotides for which the two strands are nonidentical and very long. It is shown that for pronounced sharpening to occur the binding (or dissociation) of a proton must favor the rupture of the internucleotide hydrogen bonding and also the addition to a sequence of ruptured bonds must be energetically favored over the formation of a new sequence.

IN recent years a number of structural transitions have been observed for biosynthetic polynucleotides which have been interpreted as reflecting the change from an ordered helical structure to a random coil. Some examples are the transitions observed at alkaline *p*H for the equimolar complex of polyriboadenylic acid (poly A) with polyribouridylic acid (poly U)[1,2] or with polyriboinosinic acid (poly I)[3], and the transition occurring for poly A itself at acid *p*H's.[4]

The thermally induced helix-coil transition for polynucleotides has been discussed in detail by Hill,[5] by Rice and Wada,[6] and by Gibbs and Di Marzio.[7] However, relatively little theoretical attention has been paid to the effect of such a transition upon the hydrogen ion titration curve of a polynucleotide system. It would certainly be expected *a priori* that the influence would be profound, inasmuch as for all four bases the probable locus of proton attachment is to a site likely to serve as a donor or acceptor in forming a hydrogen-bonded base pair, such as has been postulated to account for the stability of doubly stranded helical polynucleotides.

Warner has reported that the alkaline branch of the titration curve of the poly A-poly U equimolar complex consists of a very sharp rise at a *p*H alkaline to the *pK* of uracil.[1] As this rise is exactly paralleled by a loss in the characteristic ultraviolet hypochromism of the complex[1,2] it appears quite likely that the enolization and subsequent dissociation of the N_1 hydrogen of uracil results in a disruption of the complex and that, as each uracil becomes ionized, its hydrogen bond-stabilized pairing with a complementary adenine base is ruptured. This is consistent with the postulated involvement of the N_1 of uracil as a donor in a hydrogen bond to the N_1 of adenine in the intact complex.[1]

Similar statements may be made about the alkaline denaturation of the equimolar poly A-poly I complex and the structural transition of poly A itself at acid *p*H's.[3,4] In both cases the close correspondence between the binding or dissociation of a proton and the spectral transition suggests that only one of the states of ionization of the particular base is consistent with its involvement in helical pairing.

In the case of native deoxyribonucleic acid (DNA) it has been known for some time that, at low temperatures, a considerable fraction of the bases may be titrated at acid *p*H's without producing any *irreversible* denaturation.[8] This might reflect simply the presence of sequences of ruptured bonds sufficiently limited in size as to be capable of spontaneous reformation upon back titration. The heterogeneous nature of DNA makes this plausible.

However Sturtevant *et al.* in a calorimetric study have found that, at 5°C and 0.1 ionic strength, no important enthalpy change for DNA occurs at acid *p*H's until about 65% of all possible protons have been bound.[9] This was taken to indicate that extensive proton binding may occur without the rupture of any hydrogen bonds. Peacocke[10] has pointed out that the uncertainty as to both the sign and magnitude of the heats of ionization of the bases may render this interpretation somewhat tentative. In any event there is evidence that at sufficiently high temperatures the discrepancy disappears and the onset of denaturation parallels closely the binding of protons.[8]

In general it may be stated that any adequate theoretical treatment of the hydrogen ion titration curve of a polynucleotide capable of undergoing a helix-coil transition must be able to account for a high degree of sharpening and must allow for the possibility that more than one state of ionization is consistent with the helical state.

* The opinions or assertions contained herein are the private ones of the author and are not to be construed as official or reflecting the views of the Navy Department or the naval service at large.

[1] R. Warner, Proc. Intern. Congr. Biochem. 4th Congr. Vienna, 9 (1958).

[2] R. Steiner and R. Beers, Biochim. et Biophys. Acta **33**, 470 (1959).

[3] R. Steiner (to be published).

[4] R. Steiner and R. Beers, Biochim. et Biophys. Acta **32**, 166 (1959).

[5] T. Hill, J. Chem. Phys. **30**, 383 (1959).

[6] S. Rice and A. Wada, J. Chem. Phys. **29**, 233 (1958).

[7] J. Gibbs and E. DiMarzio, J. Chem. Phys. **30**, 271 (1959).

[8] L. Cavalieri and B. Rosenberg, J. Am. Chem. Soc. **79**, 5353 (1957).

[9] Sturtevant, Rice, and Geiduschek, Discussions Faraday Soc. **25**, 130 (1958).

[10] A. Peacocke, Discussions Faraday Soc. **25**, (1958).

In what follows we shall consider the problem of the hydrogen ion titration curve of a synthetic polynucleotide which is capable of existing in either a helical or a random state. For the sake of concreteness the treatment will be limited to the doubly stranded case for which each of the two (nonidentical) strands is a linear polymer consisting of B single nucleotide units. This model corresponds to the equimolar complex of polyriboadenylic acid with polyribouridylic acid. An extension to the deoxyribonucleic acid case should not be too difficult.

The actual problem is simplified by the fact that the pK's of the purine and pyrimidine bases involved in each case are widely separated and the two zones of titration can therefore be analyzed independently.

At a molecular state intermediate to the completely helical and the completely random case the polynucleotide may be visualized as consisting of alternating regions of hydrogen-bonded pairs of helical subelements and rings of unbonded random subelements.[5-7] For purposes of analysis we may divide up the macromolecule into segments containing one or more pairs of helical residues on the left and one or more pairs of random residues on the right. For reasons cited in the foregoing we need consider the binding of protons by only one of the two strands. Thus, in the zone of titration of the D residues, we may visualize the polynucleotide thus:

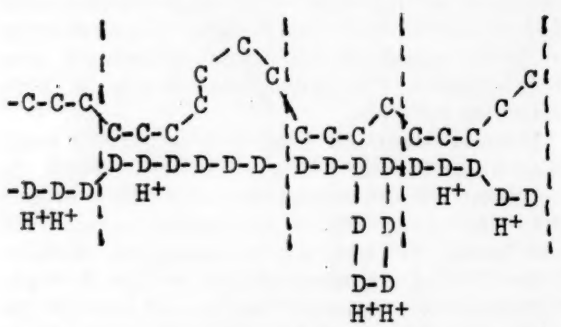

It is to be noted that, while identical pairing of C and D residues is required in the helical regions, it is possible for mismatching to occur in the random, unbonded regions.[5]

The problem is of a generalized Ising type[5] and may be attacked readily provided the following assumptions are made:

(a) The two strands are of equal length and are sufficiently long that "end effects" are insignificant and "unzippering" from the ends may be disregarded as a mechanism of helix disruption.[5,7]

(b) Only nearest neighbor (electrostatic) interactions are important for the bound hydrogen ions.

It is worthwhile to dwell briefly upon the justification for assumption (b). It is obvious that this degree of simplification is virtually essential in order to obtain tractible relationships, as the inclusion of higher order interactions results in very involved expressions even when the problem is not complicated by the occurrence of a helix-coil transition.[11]

Nevertheless it should be made clear that the assumption that only nearest neighbor interactions of bound protons are important is basically inexact and will inevitably lead to errors in the computed titration curves. However the computed results of Lifson *et al.*[11] indicate that for nearest neighbor interaction energies of the order of magnitude expected in this case ($<2kT$) the degree of distortion of the shape of the curve caused by neglect of higher order interactions is probably unimportant for the purposes of this paper.

(c) The first and higher order nearest neighbor Van der Waals interactions of the nucleotides themselves are not perturbed by the presence of bound protons.

Subject to the foregoing we may write for the partition function, in terms of the completely helical macromolecule as a reference state,

$$Q=\sum\{(\sum N_{<m>})!\prod(X'_{<m>}{}^{N_{<m>}}/N_{<m>}!)\}, \quad (1)$$

where $N_{<m>}=N_{r,sh\,ijkl}$=the number of segments (as defined earlier) containing h pairs of helical subelements, with j bound protons, and l nearest neighbor pairs of bound protons; r random residues of type D, with i bound protons, and k nearest neighbor pairs of bound protons; s random residues of type C, forming an $r+s$ membered ring with the r residues of type D. The combinatorial $(\sum N_{<m>})!/\prod N_{<m>}!$ is simply the number of ways of ordering the $\sum N_{<m>}$ segments:

$$X'_{<m>}=\sigma\subset_{i-k-1}^{i-1}\subset_{i-k}^{r-i+1}\subset_{j-l-1}^{j-1}\cdot\subset_{j-l}^{h-j+1}f(r+s)x_r{}^i x_h{}^j a_r{}^k a_h{}^l\phi_r(r+s)\phi_h(h) \quad (2)$$

where

$$\subset_{i-k-1}^{i-1}\text{etc.,}=\text{binomial coefficient}=(i-1)!/(i-k-1)!k!, \quad \text{etc.}$$

x_r, x_h=partition function for a proton bound to a random and to a helical D subelement, respectively. x_h includes a factor accounting for the free energy increment accompanying the formation (or rupture) of a hydrogen bond upon binding a proton.

a_r, $a_h=\exp(-w_{ii}/kt)$, $\exp(-w_{jj}/kt)$, respectively,

where w_{ii}, w_{jj}=free energies of interaction of nearest neighbor pairs of protons bound to random and to helical "D" subelements, respectively,

$$\sigma=\exp[-(2w_{rh}-w_{rr}-w_{hh})/kt],$$

where w_{rh}, w_{rr}, w_{hh}=free energies of interaction for nearest neighbor pairs of helical and random, random-random, and helical-helical subelements, respectively;

$\phi_r(r+s)$, $\phi_h(h)$=factors accounting for nearest neigh-

[11] Lifson, Kaufman, and Lifson, J. Chem. Phys. **27**, 1356 (1957).

bor interactions of order higher than the first for random and helical subelements, respectively;

$$f(r+s)=\exp-[(r+s)w_r/kt]Z(r+s),$$

where w_r = energy change *per subelement* upon rupturing a helically bonded pair;

$Z(r+s)$ = number of configurations available to a ring of $r+s$ random elements.

The product of the binomial coefficients

$$\subset_{i-k-1}^{i-1}\subset_{i-k}^{r-i+1}\subset_{j-l-1}^{j-1}\subset_{j-l}^{h-j+1}$$

is the modified Ising expression for the number of ways of ordering i protons upon r random residues and j protons upon h helical residues so that they possess k and l nearest neighbor pairs, respectively.

We may write for the grand partition function summing over all possible numbers of bound protons

$$\Xi=\sum Q\lambda^{(i+j)N_{<m>}} \tag{3}$$
$$=\sum\{(\sum N_{<m>})!\prod(X_{<m>}{}^{N_{<m>}}/N_{<m>}!)\},$$

where $X_{<m>}=X'_{<m>}\lambda^{i+j}$ and λ = absolute activity of hydrogen ion.

This must be evaluated subject to the two subsidiary conditions

$$\sum(r+h)N_{<m>}=B,$$
$$\sum(s+h)N_{<m>}=B. \tag{4}$$

Picking out the maximum term of Ξ (Ξ^*) and employing the method of undetermined multipliers, we have, using Sterling's approximation,

$$\ln\sum N_{<m>}-\ln N_{<m>}+\ln X_{<m>}+\ln\alpha(r+h)$$
$$+\ln\beta(s+h)=0, \tag{5}$$

where $\ln\alpha$, $\ln\beta$ = undetermined multipliers, or $N_{<m>}=(\sum N_{<m>})X_{<m>}\alpha^{r+h}\beta^{s+h}$. This yields for Ξ^*

$$\ln\Xi^*=\sum\{N_{<m>}(\ln\sum N_{<m>}-\ln N_{<m>}+\ln X_{<m>})\}$$
$$=-\ln\alpha\sum(r+h)N_{<m>}-\ln\beta\sum(s+h)N_{<m>},$$

or

$$\Xi^*=(\alpha\beta)^{-B} \tag{6}$$

and

$$\bar{N}_a=\text{number of hydrogen ions bound}$$
$$=(\partial\ln\Xi^*/\partial\ln\lambda)=(-B\partial\ln\alpha\beta)/\partial\ln\lambda,$$

or

$$\theta=\bar{N}_a/B=-\partial\ln(\alpha\beta)/\partial\ln\lambda=\text{fraction of "D"sites occupied.} \tag{7}$$

From Eq. (5) and the subsidiary relationships we have

$$\sum X_{<m>}\alpha^{r+h}\beta^{s+h}=1, \tag{8a}$$
$$\sum rX_{<m>}\alpha^r\beta^s=\sum sX_{<m>}\alpha^r\beta^s. \tag{8b}$$

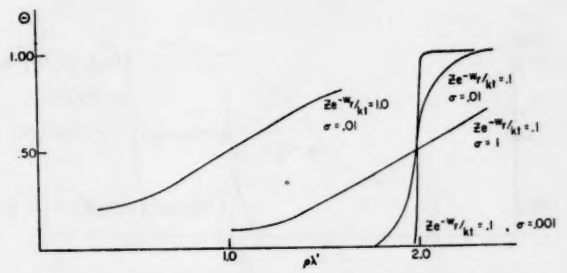

FIG. 1. Computed titration curves for varying values of σ, $ze^{-w_r/kt}$ ($a_r=1$, $\lambda''=0$).

These furnish the required relationship between λ, α, and β.

The exact form of the equations depends, of course, upon the form chosen for $\phi_r(r+s)$, $\phi_h(h)$, and $Z(r+s)$ [Eq. (3)]. A number of cases of varying exactness (and complexity) can be treated. In order of increasing complexity we have

(I) $$\phi_r(r+s)=\phi_h(h)=1,$$
$$r=s,$$
$$z(r+s)=Z(2r)=z^{2r},$$

where z = effective number of configurations available to a random residue.

This model corresponds to ignoring all nucleotide interactions except first nearest neighbors, to excluding the possibility of mismatching of the strands, and to ignoring the ringlike nature of the random segments, which prohibits many configurations.

Subject to the foregoing, the two parameters α and β may be replaced by the single parameter $\gamma(=\alpha\beta)$.

Thus

$$\theta=-\partial\ln\gamma/\partial\ln\lambda. \tag{9}$$

Upon summing Eq. (8a) over all values of r, i, k and h, j, l and using the binomial theorem we obtain

$$1=\sigma\left\{\frac{\gamma(1-\gamma\lambda''a_h+\lambda''+\gamma\lambda'')}{(1-\gamma)(1-\gamma\lambda''a_h)-\gamma^2\lambda''}\right\}$$
$$\cdot\left\{\frac{\gamma'(1-\gamma'\lambda'a_r+\lambda'+\gamma'\lambda')}{(1-\gamma')(1-\gamma'\lambda'a_r)-\gamma'^2\lambda'}\right\}, \tag{10}$$

where $\lambda'=\lambda x_r$, $\lambda''=\lambda x_h$, and $\gamma'=\gamma z^2\exp(-2w_r/kt)$.

The above yields a simple quadratic equation for λ as a function of γ. In the case for which the binding of a proton or its dissociation (regarded formally as the binding of a OH^- ion) is sufficient to rupture the internucleotide linkage a further simplification is possible. We then have $\lambda''=0$ and Eq. (10) reduces to

$$1=\sigma[\gamma/(1-\gamma)]\left\{\frac{\gamma'(1-\gamma'\lambda'a_r+\gamma'\lambda'+\lambda')}{(1-\gamma')(1-\gamma'\lambda a_r)-\gamma'^2\lambda'}\right\}. \tag{11}$$

In actuality the evidence is strong that this latter condition holds for several of the cases thus far

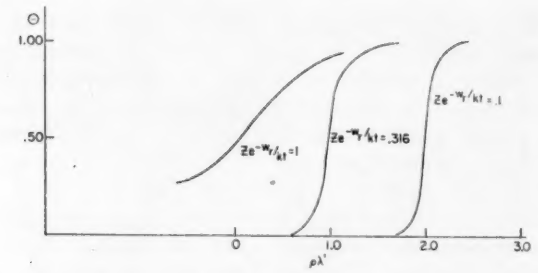

FIG. 2. Computed titration curves for varying values of $ze^{-w_r/kt}$ ($a_r=1$, $\lambda''=0$, $\sigma=0.01$).

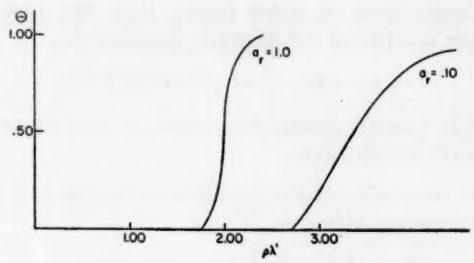

FIG. 3. Computed titration curves for two values of a_r($\lambda''=0$, $ze^{-w_r/kt}=0.1$, $\sigma=0.01$).

studied.[1–4] Computations have been made for this simplest case. Figures 1–3 show the variation of θ with $p\lambda'$ as a function of σ, $z\exp(-w_r/kt)$, and a_r, respectively.

In general it can be stated that, for a pronounced sharpening of the titration curve to occur, σ and $z\exp(-w_r/kt)$ must both be $\ll 1$. For a given value of σ the curve becomes sharper with decreasing values of $z^2\exp(-2w_r/kt)$ and vice versa. A value of σ less than unity means that it is easier to enlarge a sequence of broken bonds than to start a new sequence. A decrease in a_r has a broadening effect upon the titration curve, which also becomes asymmetric, as Fig. 3 shows. The midpoint of the curve is displaced to greater values of λ' as $z\exp(-w_r/kt)$ or a_r decreases.

Figure 4 shows two titration curves computed from Eqs. (9) and (10) for the case where a proton may be bound by either a helical or a random subunit. If the proton can be bound equally well by either ($\lambda'=\lambda''$) no sharpening occurs, irrespective of the values of σ and $z\exp(-w_r/kt)$. If binding by a helical subunit is much less favored ($\lambda''=0.0001\lambda'$) then considerable sharpening does occur. In the limit when $\lambda''=0$, the curves approach those shown in Figs. 1 and 2.

The influence of temperature is also accounted for by Eqs. (9)–(11) via the dependence upon $z\exp(-w_r/kt)$. An increase in temperature (corresponding to an increase in $z\exp(-w_r/kt)$ shifts the midpoint of the curve to lower values of λ', as has been observed experimentally (4).

Thus this crudest possible approximation appears capable of accounting for most of the features observed experimentally for the hydrogen ion titration curves of polynucleotides capable of undergoing a helix-coil transition.[1–4]

(II) $\phi_h(h)=\phi_r(r+s)=1$, $r=s$, $Z(r+s)=z^{2r}/(2r+1)^{\frac{1}{2}}$.

This case is analogous to (I), except that the refinement is made of introducing an expression of the Stockmayer-Jacobsen type to account for the constraint upon the available configurations of the random sections imposed by their ringlike nature.[12] We then have

$$\theta=-(\partial\ln\gamma/\partial\ln\lambda), \tag{12}$$

and

$$1=\sigma\left\{\frac{\gamma(1-\gamma\lambda''a_h+\lambda''+\gamma\lambda''}{(1-\gamma)(1-\gamma\lambda''a_h)-\gamma^2\lambda''}\right\}\sum^{i,k,r}\subset_{i-k-1}^{i-1}\subset_{i-k}^{r-i+1}a_r^k\lambda'^i[\gamma'^r/(2r+1)^{\frac{1}{2}}]. \tag{13}$$

If $\lambda''=0$ (as before)

$$1=[\sigma\gamma/(1-\gamma)]\sum^{i,k,r}\subset_{i-k-1}^{i-1}\subset_{i-k}^{r-i+1}a_r^k\lambda'^i[\gamma'^r/(2r+1)^{\frac{1}{2}}]. \tag{14}$$

Equations (13) and (14) give λ implicitly as a function of γ. Iterative machine computation would be required to obtain numerical values of λ' as a function of γ.

If a_r can be set equal to unity, as may be roughly valid at high ionic strengths, we then have, corresponding to Eq. (13)

$$1=\sigma\left\{\frac{\gamma(1-\gamma\lambda''a_h+\lambda''+\gamma\lambda'')}{(1-\gamma)(1-\gamma\lambda''a_h)-\gamma^2\lambda''}\right\}\sum^{r}[\gamma'(1+\lambda')]^r/(2r+1)^{\frac{1}{2}}. \tag{15}$$

If $\lambda''=0$, Eq. (15) becomes

$$1=\sigma[\gamma/(1-\gamma)]\sum^{r}[\gamma'(1+\lambda')]^r/(2r+1)^{\frac{1}{2}}. \tag{16}$$

[12] H. Jacobsen and W. Stockmayer, J. Chem. Phys. **18**, 1607 (1950).

After introducing $\phi[=\gamma(1+\lambda')]$, we have

$$\lambda'=\sigma\phi\sum^{r}[\phi'^{r}/(2r+1)^{\frac{1}{2}}]+\phi-1, \tag{17}$$

where

$$\phi'=\phi z^2\exp(-2w_r/kt);$$

and

$$\theta=-(\partial\ln\gamma/\partial\ln\lambda')=[\lambda'/(1+\lambda')]-(\lambda'/\phi)(\partial\phi/\partial\lambda'), \tag{18}$$

where

$$\partial\phi/\partial\lambda'=(\partial\lambda'/\partial\phi)^{-1}=1/[\sigma\{\sum^{r}[\phi'^{r}/(2r+1)^{\frac{1}{2}}]+\sum^{r}[r\phi'^{r}/(2r+1)^{\frac{1}{2}}]\}+1]. \tag{19}$$

This expression is readily computable.

(III) $$\phi_r(r+s)=\phi_h(h)=1, \qquad Z(r+s)=z^{r+s}.$$

This corresponds to ignoring the ringlike nature of the random segments. We then obtain, using the binomial theorem, setting $\alpha'=\alpha z\exp(-w_r/kt)$; $\beta'=\beta z\exp(-w_r/kt)$:

$$\beta'=\{\alpha'/\{\lambda'+[1+\alpha'\lambda'(1-a_r)]^2\}\}\{[1+\alpha'\lambda'(1-a_r)]^2+\lambda'+\lambda'(1+\lambda'a_r+2\alpha'\lambda'-2\alpha'\lambda'a_r)\} \tag{20}$$

and

$$1=\frac{\sigma\alpha'\beta'(1-\alpha'\lambda'a_r+\lambda'+\alpha'\lambda')\alpha\beta(1-\alpha\beta\lambda''a_h+\lambda''+\alpha\beta\lambda'')}{(1-\beta')\{(1-\alpha')(1-\alpha'\lambda'a_r)-\alpha'^2\lambda'\}\{(1-\alpha\beta)(1-\alpha\beta\lambda''a_h)-\alpha^2\beta^2\lambda''\}}. \tag{21}$$

If $a_r=1$ and $\lambda''=0$, these expressions reduce to

$$\beta'=\alpha'(1+\lambda') \tag{22}$$

and

$$1=\frac{\sigma\alpha'\beta'(1+\lambda')\alpha\beta}{(1-\beta')(1-\beta')(1-\alpha\beta)}; \tag{23}$$

$$\lambda'=[\sigma\beta'^2\beta^2/(1-\beta')^2]+\beta^2-1; \tag{24}$$

also

$$\theta=-(\partial\ln\alpha\beta/\partial\ln\lambda')=[\lambda'/(1+\lambda')]-(2\lambda'/\beta)(\partial\beta/\partial\lambda'). \tag{25}$$

Figure 5 compares titration curves computed using Eqs. (11) and (25). Similar values of σ and $z\exp(-w_r/kt)$ were assumed. As Fig. 5 shows, allowance for mismatching has no important effect upon the position of the midpoint, but does result in a slight broadening of the curve.

(IV) $$\phi_r(r+s)=\phi_h(h)=1, \qquad Z(r+s)=z^{r+s}/(r+s+1)^{\frac{1}{2}}.$$

We then have

$$\sigma\sum^{r,i,k,s}\subset^{i-1}_{i-k-1}\subset^{r-i+1}_{i-k}\lambda'^{i}a_r{}^{k}[\alpha'^{r}\beta'^{s}/(r+s+1)^{\frac{1}{2}}]\sum^{h,j,l}\subset^{j-1}_{j-l-1}\subset^{h-j+1}_{j-l}\lambda''^{j}a_h{}^{l}(\alpha\beta)^{h}=1$$

$$=\sigma\frac{\alpha\beta(1-\alpha\beta\lambda''a_h+\lambda''+\alpha\beta\lambda'')}{\{(1-\alpha\beta)(1-\alpha\beta\lambda''a_h)-\alpha^2\beta^2\lambda''\}}\sum^{r,i,k,s}\subset^{i-1}_{j-l-1}\subset^{r-i+1}_{i-k}\lambda'^{i}a_r{}^{k}[\alpha'^{r}\beta'^{s}/(r+s+1)^{\frac{1}{2}}] \tag{26}$$

and

$$\sum^{r,i,k,s}r\subset^{i-1}_{i-k-1}\subset^{r-i+1}_{i-k}\lambda'^{i}a_r{}^{k}[\alpha'^{r}\beta'^{s}/(r+s+1)^{\frac{1}{2}}]=\sum^{r,i,k,s}s\subset^{i-1}_{i-k-1}\subset\lambda''^{r-i+1}{}^{i}a_r{}^{k}[\alpha'^{r}\beta'^{s}/(r+s+1)^{\frac{1}{2}}]. \tag{27}$$

In this most general case there is nothing for it but to solve numerically for λ as a function of α and β by machine computation. However if $\lambda''=0$ and $a_r=1$, we have

$$\beta'=\alpha'(1+\lambda')$$

and

$$1=\sigma[\alpha\beta/(1-\alpha\beta)]\sum^{r,s}\{[\alpha'(1+\lambda')]^r\beta'^s\}/(r+s+1)!$$

$$=\sigma[\alpha\beta/(1-\alpha\beta)]\sum^{r,s}[\beta'^{r+s}/(r+s+1)!]$$

$$=\sigma[\beta^2/(1+\lambda'-\beta^2)]\sum^{r,s}[\beta'^{r+s}/(r+s+1)!]; \tag{28}$$

or

$$\lambda'=\sigma\beta^2\sum^{r,s}[\beta'^{r+s}/(r+s+1)!]+\beta^2-1 \tag{29}$$

and

$$\theta=[\lambda'/(1+\lambda')]-(2\lambda'/\beta)(\partial\beta/\partial\lambda'), \tag{30}$$

where

$$\partial\beta/\partial\lambda'=(\partial\lambda'/\partial\beta)^{-1}=1/[\sigma\{2\beta\sum^{r,s}[\beta'^{r+s}/(r+s+1)!]+\beta\sum^{r,s}[(r+s)\beta'^{r+s}/(r+s+1)!]\}+2\beta]. \tag{31}$$

This is readily evaluable.

It should be noted that, in the limit of zero binding, α becomes equal to β and a derivation similar to that of Eqs. (3)–(8) yields for the partition function

$$Q=\gamma^{-B} \qquad (\gamma=\alpha\beta),$$

where γ is obtainable from

$$\sigma\sum_{r,s,h=1}^{B} f(r+s)\phi_r(r+s)\phi_h(h)\gamma^{r+s+2h}=1, \tag{32}$$

or, if $\phi_r=\phi_h=1$,

$$\sigma\sum_{r,s,h=1}^{B} f(r+s)\gamma^{r+s+2h}=1. \tag{33}$$

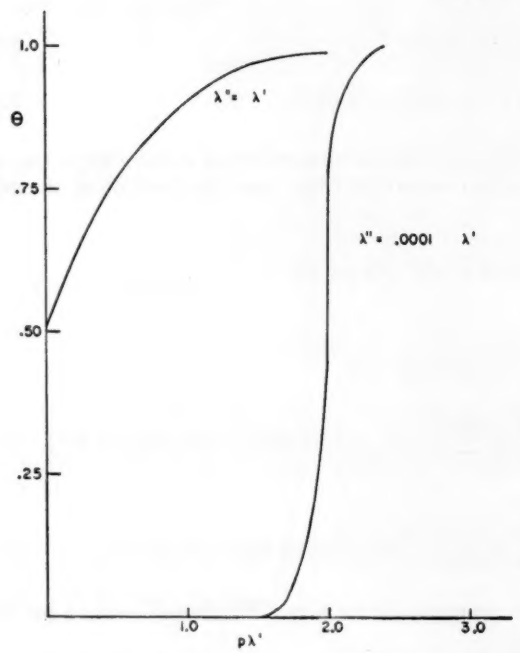

FIG. 4. Computed values of θ as a function of $\rho\lambda'$ for two values of λ''. $ze^{-w_r/kt}=0.1$, $\sigma=0.01$, and $a_r=a_h=1$ in each case.

Equations (32) and (33) are very analogous to the corresponding relationships obtained by Gibbs and Di Marzio for the DNA case.[7] The difference in form of Eq. (33) and their Eq. (12) arises from the neglect of mismatching in the latter case, as is probably permissible for DNA. Indeed if mismatching is ignored in the present case and r set equal to s, we obtain

$$Q=\delta^{-B} \tag{34}$$

and

$$[\sigma\delta/(1-\delta)]\sum_{r=1}^{B} f(2r)\delta^r=1; \tag{35}$$

or

$$1=\delta+\sigma\delta\sum_{r=1}^{B} f(2r)\delta^r$$

$$=\delta(1+\sigma\sum_{r=1}^{B} f(2_r)\delta^r). \tag{36}$$

In the case of DNA, the analogous expression of Gibbs and Di Marzio takes the form (in their notation)

$$1=\sum_{j=0}^{B}\mu^{j+1}A_j$$

$$=\mu\sum_{j=0}^{B}\mu^jA_j$$

$$=\mu(1+\sum_{j=1}^{B}\mu^jA_j) \quad (\text{as } A_0=1). \tag{37}$$

As μ is equivalent to δ and A_j to $\sigma f(2r)$, Eqs. (36) and (37) are essentially identical. Thus the present treatment reduces to that of Gibbs and Di Marzio in the limit of zero charge, if mismatching is neglected.

Rice and Wada[6] have treated the thermal transition of DNA by a similar procedure. While slightly different in form, their results are basically equivalent to those of Gibbs and Di Marzio for DNA, except for the explicit introduction of a Jacobsen-Stockmayer type factor.

While it is hoped that detailed computations for the most general case can be made, it is possible to make certain conclusions on the basis of the limited calculations which have been discussed previously. If $z \exp(-w_r/kt)$ is small compared with unity, so that the helical form of the polynucleotide is stable in the absence of any binding of protons, it can be stated that a definite sharpening of the titration curve is predicted if the following hold:

(a) The binding of a proton (or its dissociation, represented formally as the binding of a hydroxyl ion) favors the rupture of the internucleotide bonding. In the case of the alkaline titration of the poly A-poly U complex and of the poly A-poly I complex the available evidence appears to indicate that this is the case, in view of the close parallel of the spectral transition to the almost discontinuous titration curve. Indeed the observed sharpening may be regarded as evidence that this is the case. It should be noted that, as Fig. 4 shows, the binding of a proton by a helical subunit need not be prohibited absolutely for a high degree of sharpening to occur. Indeed Eqs. (9) and (10) predict a gradual increase in sharpness as binding by helical units becomes less favored.

It should be noted that, when $a_r = a_h = 1$ and $\lambda' = \lambda''$, Eqs. (7) and (8) reduce to the Langmuir equation $[\theta = \lambda'(1+\lambda')]$.

(b) σ must be small compared with unity. It is especially to be noted that if $\sigma = 1$ no sharpening occurs irrespective of the relative magnitudes of λ' and λ''. A similar statement may be made for the thermal transition. Thus the frequently made assertion that a high degree of order in a linear array of hydrogen bonded subunits is sufficient in itself to bring about a sharp helix-coil transition is incorrect.

Condition (b) may be compared with the similar conclusion reached by Zimm and Bragg,[13] who found that a necessary condition for a sharp thermal helix-coil transition was that the addition to an already formed unbonded sequence be much more probable than the initiation of a new sequence.

[13] B. Zimm and J. Bragg, J. Chem. Phys. **28**, 1246 (1958).

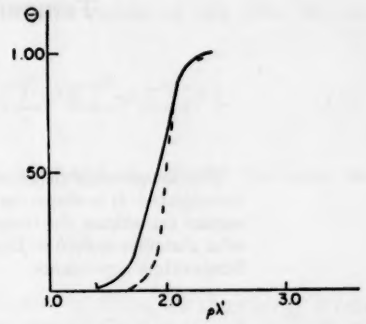

FIG. 5. Effect of mismatching upon the titration curve. In both cases $a_r = 1$, $\lambda'' = 0$, $ze^{-w_r/kt} = 0.1$, and $\sigma = 0.01$. ——— computed from Eq. (25), taking mismatching into account. – – – – computed from Eq. (11).

The origin of a low value of σ is less obvious than for the case of α-helical polypeptides, where it follows naturally from the requirement that, to form a sequence of m random residues, $m+2$ hydrogen bonds must be broken. In the polynucleotide case, perhaps the most plausible explanation is that the effect is primarily entropic in origin and reflects the steric restriction upon the rotational freedom of the terminal nucleotides of a random ring imposed by their close proximity.

The introduction of nearest neighbor interactions of bound protons has the effect of broadening the titration curve and rendering it asymmetrical, with a tendency toward flattening at large values of θ. This effect has been observed in the synthetic polynucleotide case.[4]

In general the preceding theory can account for most of the anomalous features of the titration curves observed for several synthetic polynucleotide systems. In particular the high degree of sharpening, the asymmetry, and the shifts with temperature (as reflected by changes in $z \exp(-w_r/kt)$ are all predictable in terms of this kind of treatment.

The existence of two kinds of hydrogen bonding of different strengths, the nonrandom base sequence, and the internal and molecular heterogeneity of DNA preclude application of the theory to this case, except in a very approximate manner. To the extent that DNA can be accommodated by the kind of model assumed here, the reversible portion of its titration curve can be roughly accounted for, with an appropriate choice of parameters.[3]

Temperature Dependence of Raman Intensities*

G. W. CHANTRY

Cornell University, Ithaca, New York

(Received July 27, 1959)

The temperature dependence of the intensity of the Raman lines of a polyatomic molecule has been investigated. It is shown that, when account is taken of all possible "hot" band transitions as well as fundamental transitions, the temperature dependence of each band is the same as that found for the single band of a diatomic molecule. Degenerate vibrations are also considered and likewise shown to have the same temperature dependence.

THE treatment of Raman intensities as given by Woodward and Long[1] involves the expansion of the molecular polarizability as a Taylor series in the normal coordinates. Thus, for a given coordinate Q_i, they write

$$\alpha=\alpha_0+(\partial\alpha/\partial Q_i)_0\cdot Q_i+\cdots. \tag{1}$$

In terms of this theory, the intensity of a Raman transition is determined by the integral

$$\int\psi_n Q_i\psi_m d\tau, \tag{2}$$

where n and m, respectively, represent the set of vibrational quantum numbers for the two states involved. For an assumed harmonic oscillator, this integral vanishes unless only one of the set of quantum numbers changes, and that by unity. As a consequence, combination and overtone transitions are forbidden but so-called "hot" bands of the form

$$l\nu_1+m\nu_2+n\nu_3+\cdots\rightarrow(l\pm1)\nu_1+m\nu_2+n\nu_3+\cdots \tag{3}$$

are permitted. Bands arising from these transitions are well known, for as a consequence of anharmonicity they do not always coincide exactly with the fundamental tone. Some particularly beautiful examples of this phenomenon are to be seen in the spectrograms included in the paper by Welsh *et al.* describing the Raman spectrum of ethane.[2]

If the conditions mentioned earlier are satisfied, the value of the integral (2) is

$$[(n+1)h/8\pi^2\mu\nu]^{\frac{1}{2}}, \tag{4}$$

where n is the quantum number of the lower state and μ and ν are the reduced mass and vibrational frequency, respectively. Since the intensity is proportional to the square of the change of polarizability, it follows that the intensity of a given transition from a state with quantum number n to that with quantum number $(n+1)$ will be proportional to the quantity

$$(n+1)\exp[-nh\nu/KT], \tag{5}$$

where the exponential term gives the population of the lower level with respect to the ground state. Woodward and Long[1] have considered the effect that temperature will have on the intensity of an observed Raman line by summing over all levels for a one-dimensional oscillator. They find that

$$I\alpha(1-\exp[-h\nu/KT])^{-1}. \tag{6}$$

For polyatomic molecules, Eq. (6) has likewise been used, though in view of the "hot" bands involving other frequencies than the one considered, this approach would seem to require justification. Another difficulty arises when degenerate states are being considered, for the overtone levels of a doubly degenerate oscillator have $(n+1)$ component sublevels and it might be thought that transitions among these increasingly degenerate levels would lead to an enhancement of the intensity of a doubly degenerate fundamental compared with the intensity of two fundamentals accidentally degenerate. In this discussion the temperature dependence of the Raman intensities for a hypothetical molecule having two vibrational degrees of freedom will be derived and the treatment extended to the general case. Finally, the situation in which two or more frequencies are degenerate by symmetry will be considered.

TWO ONE-DIMENSIONAL OSCILLATORS

Let the two frequencies of the oscillators be ν_1 and ν_2 and for convenience, let

$$x=\exp[-h\nu_1/KT]$$

$$y=\exp[-h\nu_2/KT]. \tag{7}$$

The energy levels of this system can be conveniently

* This research was supported by the United States Air Force through the Air Force Office of Scientific Research of the Air Research and Development Command, under Contract No. AF 49 (638) -279. Reproduction in whole or in part is permitted for any purpose of the United States Government.

[1] L. A. Woodward and D. A. Long, Trans. Faraday Soc. **45**, 1131 (1949); C. Placzek, Handbuch Radiol. **6**(2) 205 (1934).

[2] Romanko, Feldman, and Welsh, Can. J. Phys. **33**, 588 (1955).

represented by points on a square lattice:

	ν_1						
	00	01	02	03	04	05	..
	10	11	12	13	14	15	..
	20	21	22	23	24	25	..
ν_2	30	31	32	33	34	35	..
	40	41	42	43	44	45	..
	50	51	52	53	54	55	..
	..	..	..	..	..	..	..

Transitions contributing to ν_1 can only occur between adjacent points in the same row; transitions contributing to ν_2 can only occur between adjacent points in the same column. All diagonal transitions are forbidden. To find the resulting intensity for ν_1, it is necessary to sum over each column, and then to sum the columns. Hence,

$$I_{\nu_1}=\{1+2x+3x^2+\cdots+(n+1)x^n+\cdots$$
$$+y+2xy+3x^2y+\cdots+(n+1)yx^n+\cdots+\cdots$$
$$+y^m+2xy^m+3x^2y^m+\cdots(n+1)y^mx^n+\cdots+;\cdots\}xN_0. \tag{8}$$

where N_0 is the population of the ground state. Equation (8) is clearly equivalent to

$$I_{\nu_1}=N_0[\sum_0^\infty(n+1)x^n][\sum_0^\infty y^n], \tag{9}$$

i.e.,

$$I_{\nu_1}=N_0[1-x]^{-2}\times[1-y]^{-1}.$$

By summing over all the levels of Fig. 1 and equating the total to N, the number of molecules present, it is found that

$$N_0=N[1-x][1-y]. \tag{10}$$

So finally

$$I_{\nu_1}=N[1-x]^{-1}. \tag{11}$$

GENERAL CASE

Consider first a molecule having three vibrational degrees of freedom. Its energy levels can be plotted as points in an infinite cube. It is readily seen that Fig. 1 is, in fact, a section of such a cube—that with $n_3=0$. The intensity of ν_1 is now obtained by summing over each two-dimensional section ($n_3=0$, $n_3=1$, $n_3=2$, etc.) and then summing the totals. Clearly

$$I_{\nu_1}=N_0[\sum_0^\infty(n+1)x^n][\sum_0^\infty y^n][\sum_0^\infty z^n], \tag{12}$$

where

$$z=\exp[-h\nu_3/KT]. \tag{13}$$

By summing over all the points of the cube we see that

$$N=N_0[\sum_0^\infty x^n][\sum_0^\infty y^n][\sum_0^\infty z^n]. \tag{14}$$

The intensity of ν_1 is, therefore, exactly the same as before, i.e.,

$$I_{\nu_1}=N(1-x)^{-1}.$$

The generalization is now obvious, for the energy levels of the four oscillator system can be plotted as points in a hypercube and summation will lead as before to a factor involving $\exp[-h\nu_4/KT]$ which is identical in both the expression for the intensity and that for the population. As a consequence, this factor cancels and the expression reduces once more to Eq. (11). Clearly this procedure can be extended to cover any case, and, therefore, Eq. (11) is valid for all cases.

The conclusion, therefore, is that when account is taken of all possible vibrational levels in determining the fraction of molecules in any given level, the contribution of the "hot" band levels to the intensity and their effect on the ground state population just cancel and the equation derived for a one-dimensional oscillator likewise holds for each frequency of a polyatomic molecule separately. Likewise, the overtone levels of two accidentally degenerate oscillators which are such that their total quantum number is n have $(n+1)$ components and mirror exactly, so far as population and transition probability are concerned, the case of the doubly degenerate oscillator. Consequently, the equation derived for vibrations which are not degenerate by symmetry applies also to this case. However, the observed intensity of a degenerate fundamental is to be considered the sum of N equal parts where N is the degeneracy; consequently, the intensity should be divided by N before the calculation of molecular polarizability parameters is performed. Corrections of this kind have been applied by Long and his co-workers.[3]

An important practical consideration is that Eq. (11) is only valid if *all* hot bands are included. As they will in general be shifted slightly from the band center of the 0⟶1 transition due to anharmonicity, the band shape will not be gaussian. Consequently, meaningful intensity values can only be obtained from area determinations.

ACKNOWLEDGMENT

The author wishes to thank Dr. L. A. Woodward of the Inorganic Chemistry Laboratory, Oxford, and Dr. R. A. Plane, of the Department of Chemistry, Cornell University, for helpful discussion.

[3] Long, Milner, and Thomas, Proc. Roy. Soc. (London) **A237**, 197 (1956).

THE JOURNAL OF CHEMICAL PHYSICS VOLUME 32, NUMBER 1 JANUARY, 1960

Inhomogeneous Field Method for the Study of Large Polarizable Particles

ALFRED PROCK AND GLADYS MCCONKEY

Cornell University, Ithaca, New York

(Received August 3, 1959)

An inhomogeneous electric field applied to a solution of polarizable particles causes a movement of the particles toward the region of lowest potential energy. The resulting creation of concentration gradient can be observed, for large particles, by a method involving measurement of capacitance change of a cylinder containing a solution of the polymer.

This effect has been measured in terms of weight average molecular weight; the system investigated is polystyrene in cyclohexane. The basic Debye theory relating capacitance change at equilibrium to weight average molecular weight has been extended to make it applicable to experimental conditions found to be necessary in work with random coil polymers. The theory is substantiated by the agreement obtained between molecular weight calculated by this method and by the method of light scattering.

The polarizability of the particles present determines not only their equilibrium position, but also the rate at which they move. This idea is the basis of a theory presented here relating the time dependence of capacitance change to molecular weight distribution of a given sample. Another theory presented here shows how the shape of the curve for capacitance change as a function of applied field strength is related to the moments of the weight distribution function of the polarizable substance.

INTRODUCTION

CONCENTRATION gradients are produced in solutions of large polarizable particles by external application of an inhomogeneous electric field which causes the particles to move toward the region where their potential energy is smallest. A theory describing this process was presented by P. Debye and P. P. Debye,[1] who discussed the effect in terms of the capacitance change of a cylindrical condenser containing a solution of the particles, and showed how weight average molecular weight is related to such capacitance change. Working in the laboratory of P. Debye at Cornell University, we have extended the theory to make it applicable to random coil solutions under experimentally required conditions and have successfully determined the molecular weight of polystyrene, thus substantiating the validity of the theory.

Migration of polarizable particles in an inhomogenous field has thus been produced by artificial means. But it may be pointed out that this process occurs without external application of field in the well-known "salting out" effect in which the inhomogeneous field is supplied by the ions of the salt. A saturated solution of, for example, ether in water is made to separate into two phases upon the addition of salt. We suppose that the strong inhomogeneous field around each ion draws the more highly polarizable water from the bulk of the water-ether solution; the result is a solution supersaturated with ether which then separates out.

Also presented in this paper are two theories relating molecular weight distribution of samples of polarizable particles to capacitance change measurements. The first relates the shape of the graph of capacitance change *vs* the square of applied voltage to the moments of the weight distribution function. This is possible because the ratio of potential to kinetic energy of a particle $\alpha E^2/2kT$ can be made large compared to unity. Also dependent on size and polarizability is the rate at which particles move under the influence of the inhomogeneous field. This relationship, discussed qualitatively in the original paper, is the basis of a second theory which provides another potentially useful method for investigation of molecular weight distribution.

The simplest mathematical handling of these theories is possible if one assumes that there are no molecular interactions. Accordingly we shall first present the basic Debye theory as developed for ideal conditions, and then give the two molecular weight distribution theories, which also assume the absence of interaction. The effect of interactions in monodisperse random coil systems will then be considered in the development of an extended theory for the relationship of capacitance change to molecular weight. This theory is applicable to random coil solutions at concentrations and field strengths found to be experimentally useful, and it provides a reasonable basis for determining what conditions must be met for correct interpretation of data. The result is an accurate method for determining molecular weight (as compared with values obtained by light scattering).

THEORY OF CAPACITANCE CHANGE (ORIGINAL DEBYE THEORY)

The capacitance of a cylindrical condenser filled with a solution of polarizable particles is

$$C=\frac{L}{2\int_a^b (d\tau/\epsilon\tau)},$$

where L is the length of the condenser, a and b are the

[1] P. Debye and P. P. Debye, Jr., *The Collected Papers of Peter J. W. Debye* (Interscience Publishers, Inc., New York, 1954), p. 697.

radii of the inner and outer conductors, respectively, and ϵ is the dielectric constant.

If a concentration gradient is produced in the condenser there will be a corresponding change in capacitance according to the expression

$$(\Delta C/C)=\frac{4\pi n_0\alpha}{\epsilon_0 \ln b/a}\int_1^{b/a}[(n/n_0)-1](dx/x), \quad (1)$$

where n is the number of particles per cc, α represents the excess polarizability of a molecule, x is the dimensionless quantity r/a, and the subscript 0 refers to bulk property. The ratio of outer to inner diameter of the condenser b/a is in our case 250.

A concentration gradient is created by application of a voltage V which produces a field E of magnitude $E=V/[r\ln(b/a)]$. The field polarizes the particles and causes them to move toward the region where their potential energy is lowest. In the case of particles with positive excess polarizability, this region is at the central electrode.

If we assume that our solution is ideal, then at equilibrium the Maxwell-Boltzmann distribution law, $n=n_0\exp(\alpha E^2/2kT)$, should apply, and Eq. (1) can be written

$$\frac{\Delta C}{C}=\frac{4\pi n_0\alpha}{\epsilon_0 \ln b/a}\int_1^{b/a}\left[\exp\left(\frac{\alpha E_0^2}{2kT}\cdot\frac{1}{x^2}\right)-1\right]\frac{dx}{x}, \quad (2)$$

where E_0 is the field strength at the surface of the inner electrode. At any given distance from the inner electrode, the field strength is E_0/x.

Since polarizability is proportional to the amount of material in the particle (in the case of a polymer, to the number of monomer units in the molecule), the capacitance change is clearly affected by the molecular weight of the particle: the higher the molecular weight, the larger the gradient of dielectric constant throughout the solution. With very low field strengths, when the exponent is much less than unity, the final expression is

$$M=\frac{4\pi NkT}{(\partial\mu/\partial C)^2}a^2\ln^2(b/a)\,(1/cV^2)\,(\Delta C/C),$$

where N is Avogadro's number. The polarizability α has been expressed in terms of M, molecular weight, and of $\partial\mu/\partial C$, the change of refractive index with concentration. In a polydisperse polymer solution, the value obtained for M is the weight average molecular weight.

DETERMINATION OF MOLECULAR WEIGHT DISTRIBUTION FROM CAPACITANCE CHANGE AT HIGH FIELD STRENGTH: METHOD OF MOMENTS

Equation (2) is the fundamental equation for capacitance change in a monodisperse system. The integration can be performed by expanding the integrand in a Taylor series, and integrating term by term. The result is

$$\frac{\Delta C}{C}=\frac{4\pi n_0\alpha}{\epsilon_0 \ln b/a}\left[\tfrac{1}{2}\frac{\alpha E_0^2}{2kT}+\frac{1}{4\cdot 2!}\left(\frac{\alpha E_0^2}{2kT}\right)^2+\frac{1}{6\cdot 3!}\left(\frac{\alpha E_0^2}{2kT}\right)^3+\cdots\right].$$

If we factor out the term $\frac{1}{2}(\alpha E_0^2/2kT)$, write α as $\mu/2\pi\cdot\partial\mu/\partial c\cdot M/N$, and write E_0 as $V/(a\ln b/a)$, then the equation becomes

$$\frac{\Delta C}{C}=\frac{(\partial\mu/\partial c)^2}{4\pi kT}\cdot\frac{1}{a^2\ln^2 b/a}\,\frac{n_0M^2}{N^2}V^2 \cdot\left[1+\frac{1}{2\cdot 2!}\frac{\alpha E_0^2}{2kT}+\frac{1}{3\cdot 3!}\left(\frac{\alpha E_0^2}{2kT}\right)^2+\cdots\right].$$

If we divide both sides of the equation by the product of molecular weight M and concentration $c(c=nM/N)$, we obtain

$$\frac{1}{Mc}\frac{\Delta C}{C}=\frac{(\partial\mu/\partial c)^2}{4\pi NkT\cdot a^2\ln^2 b/a}V^2 \cdot\left[1+\frac{1}{2\cdot 2!}\frac{\alpha E_0^2}{2kT}+\frac{1}{3\cdot 3!}\left(\frac{\alpha E_0^2}{2kT}\right)^2+\cdots\right].$$

The first term in the right hand side of the equation is independent of molecular weight, and so curves of $1/Mc\ \Delta C/C$ *vs* V^2 have the same slopes at the origin for all values of molecular weight. If the ratio $\alpha E_0^2/2kT$ is small compared to unity, only this first term need be retained, and the equation is the one derived in the original paper.

But in a system of high molecular weight polystyrene in cyclohexane, the ratio $\alpha E_0^2/2kT$ can be large: for example, for a molecular weight of 6 million, an applied voltage of 10 kv, and a temperature of 35°C, $\alpha E_0^2/2kT$ is 7.5. In the equation terms beyond the first are significant and, moreover, are dependent on molecular weight (through α). Figure 1 is a plot of $1/Mc\cdot\Delta C/C$ *vs* $(\text{kv})^2$ for a series of molecular weights. All the curves exhibit positive curvature which increases rapidly with molecular weight. This phenomenon is the basis of a method for determination of distribution of molecular weight in a given sample, for polydispersity produces a significant change in the shape of the curve for capacitance change as a function of applied voltage.

Let us consider, for example, the plots for a monodisperse system and for a simple polydisperse system of the same weight average molecular weight. Let A and B be 0.1% cyclohexane solutions of polystyrene of 3 million weight average molecular weight; A is monodisperse and B contains equal parts of 2 million and 4 million molecular weight polymer as solute. The theoretically expected curves are shown in Fig. 2.

We shall now develop a theory relating the shape of such a curve to the moments of a weight distribution curve of a polydisperse system.

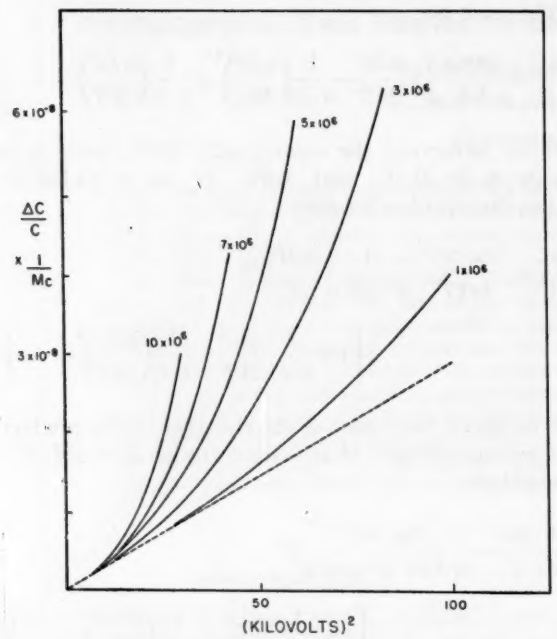

FIG. 1. Theoretical capacitance change of a cylindrical condenser containing solutions of polystyrene in cyclohexane, as a function of applied voltage. These values were calculated for ideal behavior of monodisperse solutions of various molecular weights. Because in the ordinate $\Delta C/C$ is divided by molecular weight and by concentration, the slope at the origin (dotted line) is the same for all curves.

The product $n_0\alpha$ is dependent on molecular weight, and so for a polydisperse system the equation for capacitance must be written

$$\frac{\Delta C}{C}=\frac{4\pi}{\epsilon_0 \ln b/a}\int_{M=0}^{\infty}\frac{d(n_0\alpha)}{dM}dM\int_1^{b/a}\left[\exp\left(\frac{\alpha E_0^2}{2kT}\cdot\frac{1}{x^2}\right)-1\right]\frac{dx}{x}.$$

By substituting the value $n_0=N/Mc$ and $\alpha=\mu/2\cdot d\mu/dc\cdot 1/N\cdot M$, we obtain

$$\frac{\Delta C}{C}=\frac{2\mu(\partial\mu/\partial c)}{\epsilon_0 \ln b/a}\int_0^c\int_1^{b/a}\left[\exp\left(\frac{\alpha E_0^2}{2kT}\cdot\frac{1}{x^2}\right)-1\right]\frac{dx}{x}dc.$$

With the second integral as a Taylor series,

$$\frac{\Delta C}{C}=\frac{2\mu(\partial\mu/\partial c)}{\epsilon_0 \ln b/a}\int_0^c\frac{\alpha E_0^2}{4kT}\left[1+\frac{1}{2\cdot 2!}\frac{\alpha E_0^2}{2kT}+(1/3\cdot 3!)(\alpha E_0^2/2kT)^2+\cdots\right]dc.$$

Substituting again for α, and for E_0 the value $V/(a\cdot\ln b/a)$, we obtain

$$\frac{\Delta C}{C}=\frac{(\partial\mu/\partial c)^2V^2}{4\pi NkT\cdot a^2\ln^3 b/a}\int_0^c M\left[1+\frac{1}{2\cdot 2!}\frac{\alpha E_0^2}{2kT}+(1/3\cdot 3!)(\alpha E_0^2/2kT)^2+\cdots\right]dc.$$

Since the polarizability α is proportional to the molecular weight of the particle, the quantity α/M is constant; hence the integral may be written

$$\int_0^c Mdc+(1/2\cdot 2!)(\alpha/M)(E_0^2/2kT)\int_0^c M^2dc+(1/3\cdot 3!)(\alpha/M)^2(E_0^2/2kT)^2\int_0^c M^3dc.$$

Each integral corresponds to a moment of the weight distribution function.

In order to express these moments in dimensionless form, let us characterize the molecule by its polymerization degree P which is the ratio of molecular to monomer weight M/ω. The nth integral is then of the form

$$\omega^n\int_0^c p^n dc,$$

which upon dividing by concentration becomes $\omega^n\mu_n$, where μ_n is the nth moment of the distribution function. The sum of integrals then becomes

$$c[\omega\mu_1+(\omega^2/2\cdot 2!)(\alpha/M)(E_0^2/2kT)\mu_2+(\omega^3/3\cdot 3!)(\alpha/M)^2(E_0^2/2kT)^2\mu_3+\cdots].$$

But $\omega\mu_1$ is the weight average molecular weight $\bar{M}_w$ which can be factored out. Also, the ratio α/M can be written in terms of weight average quantities as $\bar{\alpha}_w/\bar{M}_w$. By expressing $\bar{M}_w/\omega$ as μ_1, we obtain as the

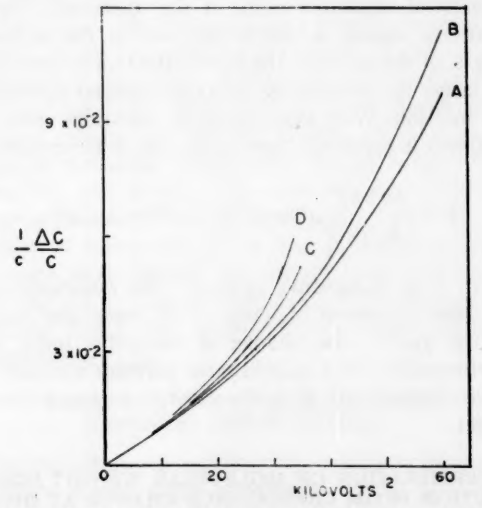

FIG. 2. Effect of polydispersity on capacitance change as a function of applied voltage. Theoretical values of $\Delta C/C$ divided by concentration for solutions of polystyrene in cyclohexane are plotted. All solutes have a weight average molecular weight of 3×10^6. Solute A is monodisperse; B is a mixture of equal parts of molecular weights 2×10^6 and 4×10^6; C and D are distributions corresponding to $b=1$ and $b=0$, respectively.

final expression for capacitance change

$$\frac{\Delta C}{C}=\frac{(\partial\mu/\partial c)^2V^2c\bar{M}_w}{4\pi NkT\cdot a^3\ln^3 b/a}\left[1+\frac{1}{2\cdot 2!}\frac{\bar{\alpha}_w E_0^2}{2kT}\frac{\mu_2}{\mu_1^2}\right.$$
$$\left.+(1/3\cdot 3!)(\bar{\alpha}_w E_0^2/2kT)^2(\mu_3/\mu_1^3)+\cdots\right].$$

For a monodisperse system the ratio μ_n/μ_1^n is unity, and so this equation reduces directly to the equation obtained above for the monodisperse system. For a polydisperse system, this ratio μ_n/μ_1^n is greater than unity: a monodisperse solution will always produce a smaller capacitance change than a polydisperse solution of the same weight average molecular weight (for the case of positive excess polarizability). This effect is illustrated in Fig. 2.

The moments of the weight distribution may be obtained from such graphs of $\Delta C/C$ *vs* V^2 by means of usual methods of curve fitting.

Curves C and D in Fig. 2 represent polydisperse systems typical of those which occur with thermally polymerized polystyrene. The distribution is well represented by the two-parameter equation of Schulz[2]:

$$W(P)dP=[(1-a)^{b+2}/(b+1)!]P^{b+1}\alpha^P dP,$$

where $W(P)$ is the weight fraction of material found in the interval dP, P is the polymerization degree, and a and b are constants. In the weight average molecular weight range of 3×10^6, the parameter b is mainly responsible for the shape of the curve, and distributions corresponding to $b=0$ (about the broadest obtained by thermal polymerization) and $b=1$ are shown.

The magnitude of the effect due to polydispersity is illustrated by the figure. For example, at 5.4 kv, where

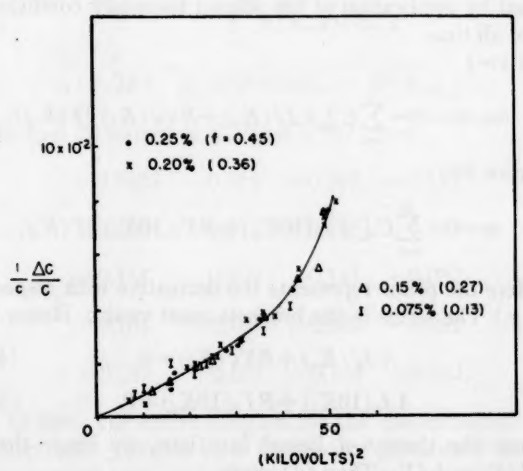

FIG. 3. Experimental measurements of capacitance change of the condenser containing solutions of polystyrene in cyclohexane. Data are divided by concentration and plotted as a function of applied voltage. Measurements were made at 34.8°C.

[2] G. V. Schulz, Z. physik. Chem. (Leipzig) **B43**, 25 (1939).

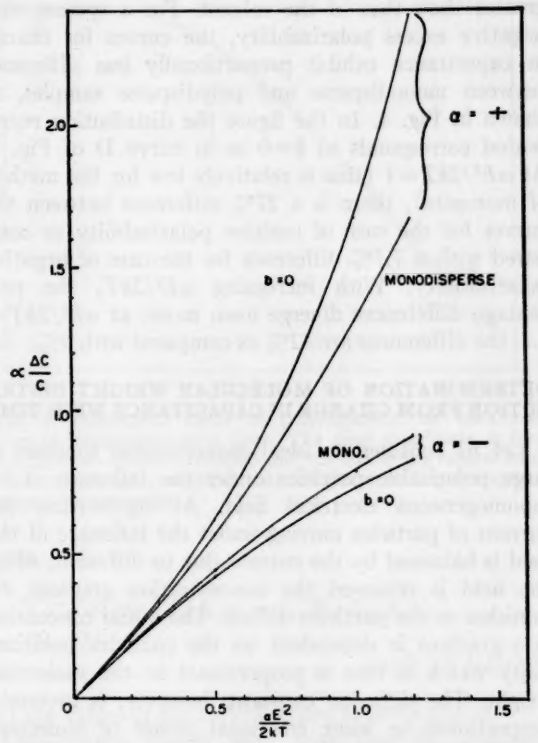

FIG. 4. The effect of the sign of excess polarizability on magnitude of capacitance change. Theoretical values proportional to $\Delta C/C$ are plotted *vs* $\alpha E^2/2kT$ for solutions having positive and negative excess polarizabilities. Monodisperse systems and polydisperse systems which can be characterized by the equation of Schulz are shown.

$\bar{\alpha}_w E_0^2/2kT$ is unity, there is a 28% greater capacitance change for the distribution $b=0$ than for the monodisperse system.

An experimental graph corresponding to these theoretical curves is shown in Fig. 3. For this work we used a sample of thermally polymerized polystyrene known to have a wide distribution of molecular weight. We measured solutions of four concentrations in the range from 0.25% to 0.075%, which is about the lowest range feasible with the sensitivity of our present equipment. Since change in capacitance is divided by concentration, the experimental points for the different solutions are directly comparable. We chose a temperature at which the solutions were sufficiently ideal so that the experimental curves for the various concentrations fell within a narrow band. Extrapolation of points at given voltages to zero concentration should yield the ideal curve, but because of instabilities inherent in our equipment, the reproducibility was not sufficient to permit us to do this. However, the curve is of the expected shape, and further refinement of measurement should make possible the determination of moments from such a graph.

In the system just discussed, excess polarizability is positive; i.e., the dielectric constant of the solute is

greater than that of the solvent. For a system with negative excess polarizability, the curves for change in capacitance exhibit proportionally less difference between monodisperse and polydisperse samples, as shown in Fig. 4. In the figure the distribution represented corresponds to $b=0$ as in curve D of Fig. 2. At $\alpha E^2/2kT=1$ (this is relatively low for the method of moments), there is a 27% difference between the curves for the case of positive polarizability as compared with a 7.7% difference for the case of negative polarizability. With increasing $\alpha E^2/2kT$, the percentage differences diverge even more: at $\alpha E^2/2kT=1.2$, the differences are 42% as compared with 9%.

DETERMINATION OF MOLECULAR WEIGHT DISTRIBUTION FROM CHANGE IN CAPACITANCE WITH TIME

Let us consider an ideal monodisperse solution of large polarizable particles under the influence of an inhomogeneous electrical field. At equilibrium the current of particles moving under the influence of the field is balanced by the current due to diffusion; when the field is removed the concentration gradient diminishes as the particles diffuse. The initial concentration gradient is dependent on the particles' polarizability which in turn is proportional to the molecular weight. The diffusion constant, however, is inversely proportional to some fractional power of molecular weight. This means that the time required for equilibrium to be established after removal of the field should not be the same for particles of different molecular weights. In an ideal polydisperse mixture, when it is assumed that the particles move independently of each other, this variation in "time effect" may be considered as a basis for measurement of polydispersity. With the system used in our experimental work the time required for reestablishment of equilibrium is easily measurable, being of the order of several minutes.

In considering the reestablishment of equilibrium upon removal of voltage, we need only the diffusion equation with suitable boundary conditions. This equation is: $\partial n/\partial t=D$ div grad n. Using cylindrical coordinates, we obtain

$$(1/D)(\partial n/\partial t)=(\partial^2 n/\partial r^2)+(1/r)(\partial n/\partial r).$$

The boundary conditions are

(a) At $t=0$, $n=n_0\exp(\alpha E^2/2kT)$. We shall assume that $\alpha E^2/2kT$ is small compared to unity, so that at $t=0$, $n=n_0(1+\alpha E^2/2kT)$.

(b) Because there can be no flow of particles across the confining boundaries, the gradient of concentration vanishes at the boundaries: $\partial n/\partial r=0$ at $r=a$ and $r=b$. The mathematical manipulations are greatly simplified if a slightly different boundary condition is assumed, and for our purposes the assumption is reasonable. The ratio b/a for the condenser used in our experimental work is 250; but since the concentration gradient falls off rapidly with distance from the inner radius, we assume that as before, $\partial n/\partial r=0$ at $r=a$, but that at a distance $b'=10a$, n is held at a constant value n_0.

Let us change to dimensionless variables. Let $n=n_0(1+m)$ where m represents the small fractional change in concentration. The equation then becomes

$$(1/D)(\partial m/\partial t)=(\partial^2 m/\partial r^2)+(1/r)(\partial m/\partial r).$$

If we let $x=r/a$, then

$$(a^2/D)(\partial m/\partial t)=(\partial^2 m/\partial x^2)+(1/x)(\partial m/\partial x).$$

In terms of x, the boundary conditions are:

(a′) At $t=0$, $m=\alpha E_0^2/2kT\cdot 1/x^2$,

(b′) $\partial m/\partial x=0$ at $x=1$, $m=0$ at $x\geqq 10$.

Variables can be separated by assuming $m=R(x)T(t)$. The solution for the time variable is

$$T=T_0\exp[-K^2(D/a^2)t]=T_0\exp[-K^2(t/\tau)],$$

where $\tau=a^2/D$ and K^2 is some positive constant. The expression involving distance is

$$(d^2R/dx^2)+(1/x)(dR/dx)+K^2R=0,$$

whose solution is

$$R=AJ_0(Kx)+BY_0(Kx), \tag{3}$$

where J_0 and Y_0 are the Bessel functions of zeroth order.

The general solution for m is a sum of such solutions, each for a different value of K,

$$m=\sum_{i=1}^{\infty}C_iR(K_ix)T(K_it).$$

The constants that appear in Eq. (3) can be evaluated by application of the second boundary condition. For all time
for $x=1$

$$\partial m/\partial x=0=\sum_{i=1}^{\infty}C_i[AJ_0'(K_i)+BY_0'(K_i)]T(K_it),$$

for $x=10$

$$m=0=\sum_{i=1}^{\infty}C_i[AJ_0(10K_i)+BY_0(10K_i)]T(K_it).$$

(Here the prime represents the derivative with respect to x.) The terms in the brackets must vanish. Hence

$$AJ_0'(K_i)+BY_0'(K_i)=0, \tag{4}$$

$$AJ_0(10K_i)+BY_0(10K_i)=0. \tag{5}$$

From the theory of Bessel functions, we know that $J_0'/Y_0'=J_1/Y_1$. Then (4) gives

$$A/B=-[Y_0'(K_i)/J_0'(K_i)]=-[Y_1(K_i)/J_1(K_i)].$$

On substituting the ratio A/B into (5), we find

$$Y_1(K_i)/J_1(K_i)=Y_0(10K_i)/J_0(10K_i).$$

The roots K_i are the solutions to this equation. Using a standard text on Bessel functions, we found the first twenty roots, which lie at almost equal intervals between 0.245 and 6.814.

We are now ready to evaluate the constants C_i*. At $t=0$, the first boundary condition is

$$(a'') \quad m=(\alpha E_0^2/2kT)(1/x^2)=\sum_{i=1}^{\infty} C_i R(K_i x).$$

We make use of the orthogonality relationship

$$\int_{x_a}^{x_b} xR(K_n x)\,R(K_m x)\,dx = \frac{[xR'(K_n)\,R(K_m)-xR(K_n)\,R'(K_m)]_{x_a}^{x_b}}{K_m^2-K_n^2}.$$

With our boundary conditions, this integral vanishes when $K_n \neq K_m$. When $K_n=K_m$

$$\int xR^2(Kx)\,dx=\tfrac{1}{2}[10^2R'^2(10K)-R^2(K)].$$

Multiplying (a'') by $xR(K_m x)$ and integrating from $x=1$ to $x=10$, we find

$$(\alpha E_0^2/2kT)\int_1^{10}(1/x^2)\cdot xR(K_m x)\,dx = \sum_{i=1}^{\infty}\int_1^{10} C_i R(K_i x)\,R(K_m x)\,x\,dx = C_m\cdot\tfrac{1}{2}[10^2R'^2(10K_m)-R^2(K_m)].$$

After solving this equation, we find

$$\frac{C_m}{\alpha E_0^2/2kT}=\frac{\int_1^{10} R(K_m x)\,(dx/x)}{\tfrac{1}{2}[10^2R'^2(10K_m)-R^2(K_m)]}.$$

The first 20 values of $C_m/(\alpha E_0^2/2kT)$ are

−0.0483	−0.165	−0.168	−0.151
−0.100	−0.176	−0.145	−0.130
−0.155	−0.093	−0.141	−0.082
−0.161	−0.107	−0.084	−0.082
−0.189	−0.107	−0.102	−0.083.

In sum, the entire solution for the concentration of polarizable particles as a function of distance x from the central wire and time t which has elapsed since removal of the electric field is

$$n=n_0(1+m),$$

* This includes the constant T_0.

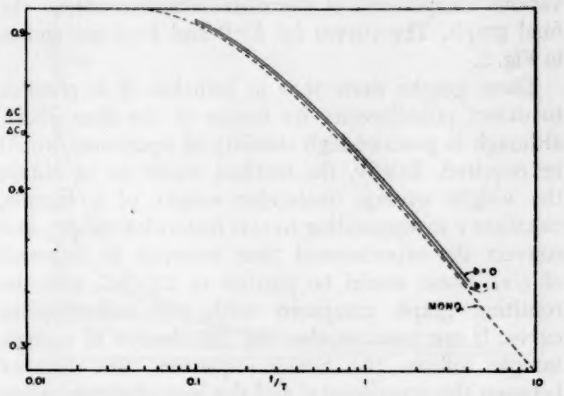

FIG. 5. Theoretical effect of polydispersity on fractional change in capacitance with time. The time coordinate is t/τ, which includes diffusion constant and the size of the central wire of the cylindrical condenser. Monodisperse and polydisperse systems are represented.

where

$$m=\sum_{i=1}^{\infty} C_i[Y_1(K_i)\,J_0(K_i x)-J_1(K_i)\,Y_0(K_i x)]\cdot\exp[-K_i^2(t/\tau)],$$

and the values of the constants are as given above.

Capacitance change with time may be obtained from Eq. (1). Thus we find

$$\Delta C/C=(4\pi n_0\alpha/\epsilon_0 \ln b/a)\int_1^{10} m(dx/x).$$

The integrations were performed graphically for various values of t/τ: results are shown in Fig. 5, where the dotted line is for any monodisperse system. For this curve, the ordinate $\Delta C/\Delta C_0$ represents the fraction of capacitance change at any time t (at time $t=0$, $\Delta C/\Delta C_0$ is unity). The properties of the system, diffusion constant and inner cylinder diameter, are incorporated into the constant τ of the coordinate t/τ.

This curve for monodisperse systems will now be compared with curves for two molecular weight distributions typical of those found in thermally polymerized polystyrene. These distributions are the same used above in the consideration of distribution determination by the method of moments; they are characterized by $b=0$ and $b=1$. To prepare the curves, we first constructed histograms of the distributions, using fifteen equally spaced values of molecular weight between zero and $3\bar{M}_w$. For each point on a histogram we then calculated the ratio $\tau_M \div \tau_{Mw}$ where τ_M represents the value for that particular molecular weight, and τ_{Mw} is the value for the weight average molecular weight. We assumed that τ is proportional to $M^{\frac{1}{2}}$. For any time t, we then had a set of values of t/τ which corresponded to values of molecular weight in the histograms. For any time we were able to add together the contributing values of $\Delta C/\Delta C_0$ for the

various components of the distribution to obtain the final graph. The curves for $b=0$ and $b=1$ are shown in Fig. 5.

These graphs show that in principle it is possible to detect polydisperity by means of the time effect, although in practice high stability of equipment would be required. Briefly, the method would be to obtain the weight average molecular weight of a sample, calculate τ corresponding to this molecular weight, and convert the experimental time intervals to intervals of t/τ. These would be plotted *vs* $\Delta C/\Delta C_0$ and the resulting graph compared with the monodisperse curve. If one assumes that the distribution of a given sample follows the Schulz equation, the distance between the experimental and the monodisperse curves should be a measure of the width of the distribution.

Experimentally, we encountered several difficulties. First of all, there is the requirement that $\alpha E_0^2/2kT$ be small for all molecular weights present; in a wide distribution, the higher molecular weights give rise to large values of $\alpha E_0^2/2kT$ unless the applied voltage is kept low. Secondly, to meet the requirement of ideality the concentration must be low. These two restrictions greatly limit the measureable frequency response. With the sensitivity of our apparatus, the time effect method was not practical for the system polystyrene in cyclohexane.

It may be helpful to make a brief comparison of the determination of distribution by the method of moments and by the time effect. First of all, the method of moments depends on large values of $\alpha E_0^2/2kT$, whereas for time effect studies (as outlined here) this quantity must be kept low. Of course, this means that much greater frequency response can be obtained with the method of moments. Furthermore, there is a difference in functional dependence of frequency response on molecular weight: in the time effect method, the parameter τ depends on only a fractional power of molecular weight, whereas in the method of moments there is a stronger dependence: molecular weight appears (in α) as a factor in an exponent which is of the order of unity. [See Eq. (2).] This means that the method of moments is more sensitive to molecular weight differences. Concentration restrictions are the same for both methods: theoretically, infinite dilution is required. Practically, this condition may be approached more closely by using the more sensitive method of moments.

It may also be pointed out that the theory for time effect might be modified to cover the situation for large values of $\alpha E_0^2/2kT$, but this development would be complicated and appears to offer no advantage over the simpler method of moments.

Of course, if the quantity $\alpha E_0^2/2kT$ cannot be made large (i.e., if the excess polarizability is small or if the properties of the solvent are such that high field strengths cannot be applied) only the time effect method can be considered. In this connection, it may be pointed out that a forthcoming publication by Crawford J. MacCallum, formerly associated with this laboratory, will present a more complete analysis, made possible by the use of a computer, of the time effect.

EFFECT OF INTERACTIONS IN RANDOM COIL SYSTEMS; CHOICE OF EXPERIMENTAL CONDITIONS FOR MOLECULAR WEIGHT STUDIES

The assumption of a Maxwell-Boltzmann distribution in concentration means that any effect of molecular interactions is ignored. But even when the bulk concentration in our cylindrical condenser is very low, the concentration in the important region around the central wire may be high and the effect of interactions may be significant. This effect may be taken into account through consideration of the way the thermodynamic potential changes with concentration and applied field strength. We can do this conveniently by means of the concentration dependence of osmotic pressure.

At equilibrium there is a balance between electrical and osmotic forces. At any point in the solution the gradient of osmotic pressure, π, is related to the gradient of the potential energy of the polarizable solute according to the equation

$$\text{grad}\pi = n\,\text{grad}(\alpha E^2/2),$$

where n is the number of particles of solute per cc of solution. In our cylindrical condenser the concentration n and the variables π and $(\alpha E^2/2)$ depend only on radial distance r; hence we may write

$$(1/n)(d\pi/dn)(dn/dr) = (d/dn)(\alpha E^2/2)(dn/dr),$$

or, in integrated form,

$$\int_{n_0}^{n} (d\pi/dn)(dn/n) = \alpha E^2/2. \tag{6}$$

Of course, if the Van't Hoff relationship for osmotic pressure, $\pi = nkT$, is used, the expression reduces to the Maxwell-Boltzmann law. However, for a better approximation we shall use Flory's equation[3] for osmotic pressure of a monodisperse random coil polymer solution. This is

$$\pi\omega_1/kT = -\ln(1-\phi_2) - [1-(1/x)]\phi_2 - (\Omega\omega_1/2kT)\phi_2^2, \tag{7}$$

where

ϕ_2 = volume fraction of polymer,
ω_1, ω_2 = volume of one solvent molecule, volume of one polymer molecule,
$x = \omega_2/\omega_1$ (for the system polystyrene-cyclohexane, $x = 0.91P$, where P is polymerization degree),
Ω = interaction parameter,

[3] Paul J. Flory, *Principles of Polymer Chemistry* (Cornell University Press, Ithaca, New York, 1953), p. 511.

n_1, n_2 = number of solvent molecules per cc, number of polymer molecules per cc.

In a mixture

$$\phi_2 = n_2\omega_2,$$

$$\phi_1 = n_1\omega_1.$$

Let us expand the term $-\ln(1-\phi_2)$ as $\phi_2+(\phi_2^2/2)+(\phi_2^3/3)$. Then Eq. (7) becomes

$$\pi\omega_1/kT = (1/x)\phi_2+\tfrac{1}{2}[1-(\Omega\omega_1/kT)]\phi_2^2+\tfrac{1}{3}\phi_2^3.$$

Equation (6) can be written

$$\alpha E^2/2 = \int_{n_0}^{n}(d\pi/dn)\cdot(dn/n)$$

$$= kTx\int_{\phi_2^0}^{\phi_2}(d/d\phi_2)(\pi\omega_1/kT)(d\phi_2/\phi_2).$$

After substituting and integrating we find

$$\alpha E^2/2kT = \ln(\phi_2/\phi_2^0)+x[1-(\Omega\omega_1/kT)](\phi_2-\phi_2^0) + \tfrac{1}{2}x(\phi_2^2-\phi_2^{02}). \quad (8)$$

This equation can be expressed in terms of certain experimental parameters. The critical temperature T_c and the critical concentration ϕ_{2c} have values such that $\partial\pi/\partial\phi_2=0$ and $\partial^2\pi/\partial\phi_2^2=0$. These values are

$$\Omega\omega_1/kT_c = \{1+[1/(x)^{\frac{1}{2}}]\}^2,$$

$$\phi_{2c} = 1/[1+(x)^{\frac{1}{2}}].$$

The so-called Θ temperature is defined, then, as $\Omega\omega_1/k\Theta=1$. (This corresponds to the critical temperature for infinite molecular weight.) If we introduce Θ into Eq. (8) and define ϕ_2/ϕ_2^0 as η and ϕ_2^0/ϕ_{2c} as f, we obtain

$$\ln\eta+(f^2/2)\{1-[2/(x)^{\frac{1}{2}}]\}(\eta^2-1) + f[(x)^{\frac{1}{2}}-1](\eta-1)[1-(\Theta/T)] = \alpha E^2/2kT. \quad (9)$$

For small values of field strength, when $\alpha E^2/2kT \ll 1$, η is close to unity. Then we can make the approximations

$$\ln\eta = \eta-1,$$

$$\eta^2-1 = 2(\eta-1).$$

Equation (9) becomes

$$\eta-1 = \{1+f^2\{1-[2/(x)^{\frac{1}{2}}]\}+f[(x)^{\frac{1}{2}}-1][1-(\Theta/T)]\}^{-1}\cdot(\alpha E^2/2kT). \quad (10)$$

For very low field strengths, then, the coefficient in (10) expresses the divergence from ideal behavior. We will refer to this expression in the discussion of an experimental determination of molecular weight, for in the calculations only the slope at the origin of the experimental curve $\Delta C/C$ *vs* kv^2 is used.

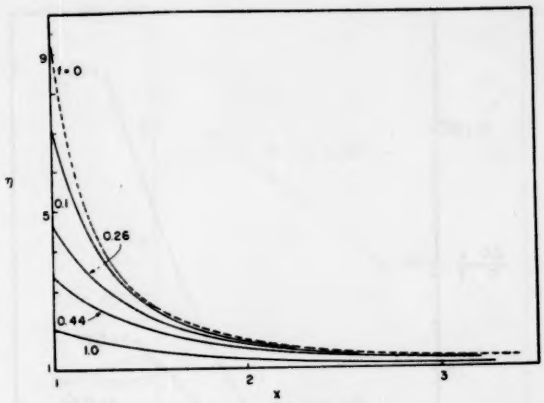

FIG. 6. Theoretical concentration profiles near the central wire for solutions of polystyrene in cyclohexane. These calculations were made for monodisperse solutions of polymer of molecular weight 3.6×10^6 at the theta temperature and at an applied voltage of 7 kv (this creates at the central wire a field strength of 866 esu). Concentrations are expressed as fractions of the critical concentration, 0.57%.

If we work at the temperature $T=\Theta$, the term involving f vanishes, and the deviation from ideality depends only on the term involving f^2. The experimental importance of concentration range can be investigated qualitatively using Eq. (9) at $T=\Theta$. Figure 6 is a plot of concentration profiles in our cylindrical condenser; for this illustration we have used a monodisperse polymer of molecular weight 3.6×10^6 at an applied voltage of 7 kv and at the theta temperature. In this case, $f=1$ corresponds to a concentration of 0.57%. In the graph x represents the distance r/a from the central wire, and η, which is ϕ_2/ϕ_2^0, is the same as n/n_0. The ideal situation, where $f=0$, is represented by the dotted line; as bulk concentration increases, there is proportionally less increase in concentration at the central wire (at given voltage). This would mean that capacitance change would not increase in proportion to concentration increase. This can be seen more clearly in Fig. 7 which was derived from plots similar to those in Fig. 6, for various voltages. This is a plot of $\Delta C/C\cdot 1/f$ *vs* (kv)^2; here again the dotted line represents ideal behavior. This shows that even at the theta temperature the effect of concentration is very large. Such a graph may be useful in choosing an experimental range of concentration and voltage.

Experimentally, it is not always feasible to work exactly at the theta temperature. This is partly because of the danger of precipitating the sample, especially if there are high molecular weight molecules present, and partly because unusual effects appear to occur at temperatures very close to Θ. (We observed that as the theta temperature was closely approached from above, measurements of $\Delta C/C$ increased very rapidly in a way not explained by the Flory equation. A calculation shows that such effects are not due to any change in Θ with field strength.) We shall, therefore, consider

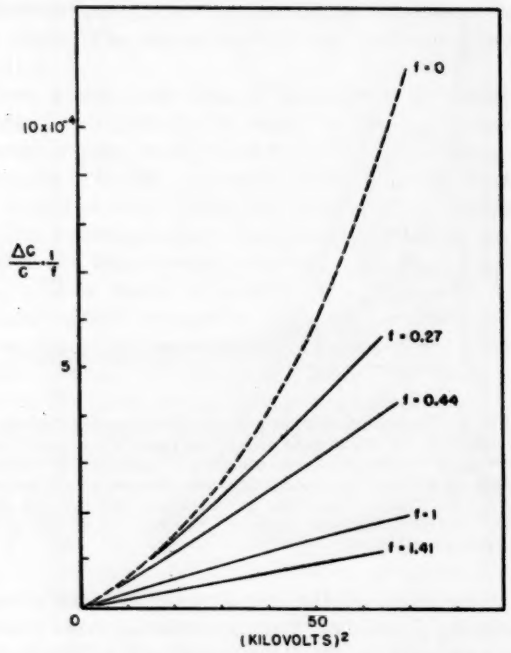

FIG. 7. Theoretical effect of molecular interactions in solutions of monodisperse polystyrene in cyclohexane at the theta temperature. The calculations were made for polymer of molecular weight 3.6×10^6; concentration is expressed as a fraction of the critical concentration, 0.57%.

next the effect of temperature variation on capacitance change.

Figure 8 shows the theoretical plot of $\Delta C/C$ *vs* $(\text{kv})^2$ for a monodisperse solution of polymer of molecular weight 3.6×10^6, at various temperatures. The concentration chosen corresponds to $f=1.414$, which for this

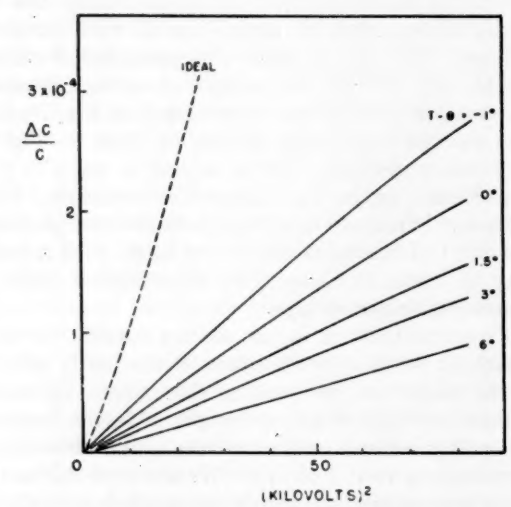

FIG. 8. Theoretical plot of capacitance change as a function of applied voltage, to show the effect of temperature. Calculations were made for a solution of polystyrene of molecular weight 3.6×10^6 at a concentration of 0.8% in cyclohexane. The effect of temperature in a narrow range around Θ is shown.

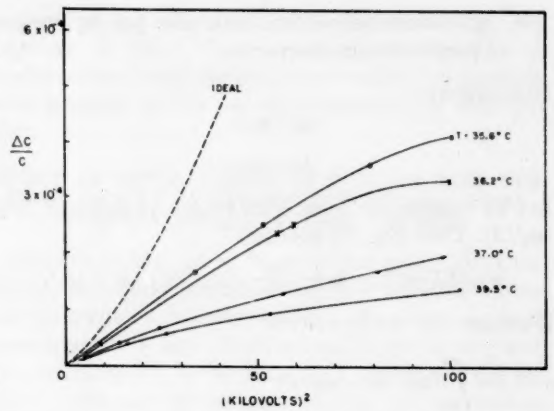

FIG. 9. Experimental graph of capacitance change as a function of applied voltage and temperature. The solution is polystyrene of molecular weight 3.6×10^6 at a concentration of 0.8% in cyclohexane.

molecular weight is 0.8%. An experimental graph for similar conditions is shown in Fig. 9. (The theta temperature for polystyrene in cyclohexane is usually reported as 34°C.) The two graphs are qualitatively comparable; complete agreement cannot be expected because the experimental measurements were made of a polydisperse system. At any rate, it can be concluded that temperature significantly affects the sensitivity of the method.

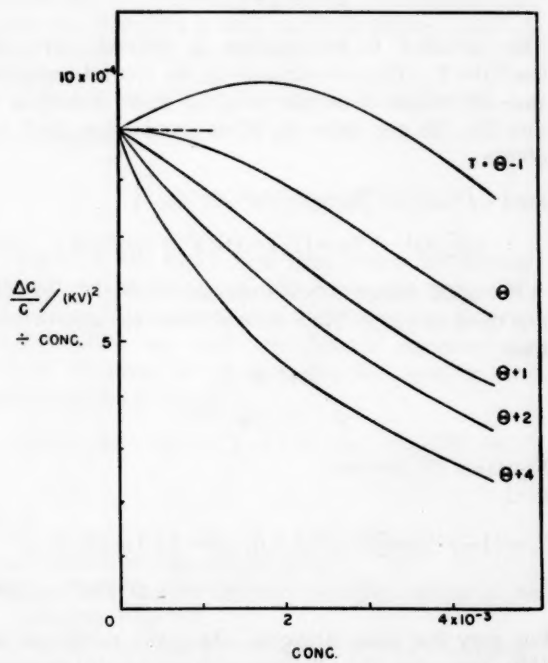

FIG. 10. Theoretical plot to show the dependence on temperature and concentration of the tangent at the origin of the graph $\Delta C/C$ *vs* $(\text{kv})^2$. The calculations are for solutions of polystyrene of molecular weight 3.6×10^6 in cyclohexane, at temperatures close to the theta temperature.

DETERMINATION OF WEIGHT AVERAGE MOLECULAR WEIGHT

In order to determine weight average molecular weight, one must obtain the slopes at the origin of the experimental graphs of $\Delta C/C \div$ concentration *vs* $(\text{kv})^2$, at a given temperature and various concentrations, and extrapolate to zero concentration. Theoretical counterparts of such extrapolations may be obtained by substituting into Eq. (1) the value for n/n_0-1 (i.e. $\eta-1$) as given by Eq. (10), solving for $\Delta C/C \div c \div (\text{kv})^2$, and plotting these values *vs* concentration. An example is shown in Fig. 10, which is for a monodisperse polymer of molecular weight 3.6×10^6; graphs for several temperatures close to Θ are plotted. It may be observed that as T approaches Θ, the slope at the origin approaches zero; the tangent is zero at $T=\Theta$ because there is no linear term in f present.

Figure 11 shows typical data for a molecular weight determination of polystyrene in cyclohexane. The tangents at the origin were extrapolated to zero concentration, as shown in the upper part of Fig. 12. The molecular weight calculated from the intercept is 3.6×10^6; a light-scattering determination also yielded a value 3.6×10^6 for this sample.

Figure 12 also shows experimental data for a different sample. The data were taken at three different temperatures and show the expected decrease in magnitude of slope with decreasing temperature. (Of course, these curves are only qualitatively comparable to theoretical ones such as shown in Fig. 10 because the experimental sample was polydisperse.) The molecular weight calculated from the intercept is 1.3×10^6, which agrees within experimental error with the value of 1.7×10^6, obtained by light scattering.

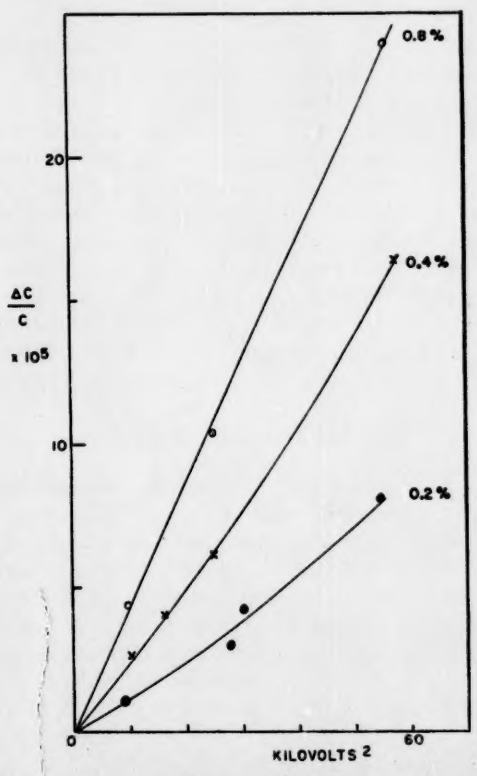

FIG. 11. Experimental data: capacitance change as a function of applied voltage for solutions of polystyrene in cyclohexane. The molecular weight is 3.6×10^6 and the temperature is 36°C.

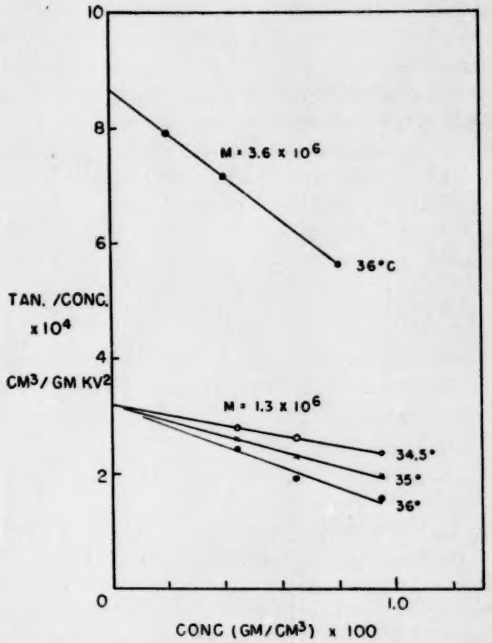

FIG. 12. Experimental data for molecular weight determinations. The plot for the sample of molecular weight 3.6×10^6 was constructed from Fig. 11; the plot for the sample of molecular weight 1.3×10^6 was obtained from similar data. The intercept at zero concentration is used in making the molecular weight calculation.

In summary, we may conclude that theoretical temperature and concentration studies, such as have been made here are qualitative aids in choosing usable experimental conditions, and in the interpretation of data.

MOLECULAR WEIGHT STUDIES OF OTHER SYSTEMS

Although we have worked only with the system polystyrene in cyclohexane, the inhomogeneous field theories and methods appear to be applicable to other systems of large polarizable particles.

Of course, there are certain requirements that must be met. As discussed in the original paper, the solvent must have a sufficiently high specific resistance, depending on how large a change in capacitance due to heating can be tolerated. In our system, for example, the specific resistance must be 10^{13} ohm cm, or greater. Also, the dielectric strength of the system must be sufficient to withstand the field strengths used.

We have considered several other phenomena which we thought might have an effect on frequency change,

but which were shown to be insignificant, at least for our system. Possible effects of electrostriction were discussed in the original paper. Another effect considered is change of polarizability with field strength. The dielectric constant is not a function of field strength in first approximation, but in our measurements, where very small changes in dielectric constant are important, it seemed that second-order effect might be significant. The dielectric constant is given by the expression

$$\epsilon=\epsilon_0[1+(E^2/E_0^2)],$$

where E is the field strength, ϵ_0 is the dielectric constant at the limit of no field strength, and E_0 is a constant. The expression for $\Delta C/C$ arising from this phenomenon is

$$\Delta C/C=\{1/[2\ln(b/a)]\}(E_w^2/E_0^2),$$

where E_w is the field strength at the wall of the central wire. Buckingham[4] has reported values of E_0 for a number of simple gases including methane. This value is given as 7.5 v per A. which we thought would be comparable in magnitude to E_0 for cyclohexane. Using this value, and a value for E_w of 400 kv per cm., $\Delta C/C$ is found to be 3×10^{-8}; our smallest measurements were of the order of 3×10^{-6}.

Even before dielectric breakdown, there may occur space charge phenomena which could alter the field strength.[5–7] In our experiments with cyclohexane solutions, using field strengths under 400 kv per cm., space charge effects were considered insignificant. But in other systems, especially with polar solvents, space charge phenomena might lower the maximum usable field strength. However, according to Vafiadis,[8] space charge effects are diminished by the use of alternating rather than direct voltage. Such a use of alternating voltage would, of course, necessistate alteration of the circuitry.

In order to decide whether inhomogeneous field measurements are applicable to specific systems, one would need to determine conditions necessary to produce measurable changes in capacitance (according to the sensitivity of the equipment to be used.) As can be seen from the equations for capacitance change, the quantity $\Delta C/C$ varies (for given equipment) primarily according to $\alpha E^2/2kT$. Limitations on field strength have been discussed. The quantity α is proportional to particle size. (Substances of suitably high molecular weight include colloids as well as polymers.) Or, for a given particle kind and size, the excess polarizability can be increased by changing the solvent. The value of α can be made especially large if one employs a polar solvent with a dielectric constant much higher than that of the solute: this would produce a large negative excess polarizability. However, the dielectric properties of such solvents limit the field strength which can be applied.

[4] A. D. Buckingham and J. A. Pople, Proc. Phys. Soc. (London) **A68**, 905 (1955).
[5] D. W. Goodwin and K. A. MacFadyen, Proc. Phys. Soc. (London) **B66**, 85 (1953).
[6] J. Dantscher, Ann. Physik. **9**, 179 (1931).
[7] W. Rogowski, Arch. Electrotech. **12**, 1 (1923).
[8] G. Vafiadis, Ann. Physik **35**, 23 (1935).

EQUIPMENT AND REAGENTS

Capacitance change to be measured is of the order of magnitude of one part in 10^5, and since this is out of the range of ordinary bridge methods, another system had to be devised. The condenser containing the polymer solution is made part of the resonant circuit of a radio frequency oscillator, and capacitance change is measured by a beat frequency method. The signal is mixed with the output from a standard crystal oscillator, and the resulting frequency difference is measured by a counter and automatically recorded on a tape. The components of the apparatus will be discussed.

Temperature Control

Because the capacitance change to be measured is so small, there must be very good frequency stability, and this requires stringent temperature control. With our equipment, there is a frequency change of about 300 cps for each degree of temperature change. We require that over the length of time needed for a measurement, which could be as long as an hour, there be no more than one cycle per second change due to temperature. Actually, the temperature stability achieved is better than this.

The resonant circuit components are enclosed in four nested boxes; the inside two, of $\frac{1}{4}$-in. aluminum, are tightly closed. The third box is a copper water jacket through which is circulated water controlled to 0.01°C. Insulating material fills the space between this jacket and the outer wooden box. The entire apparatus occupies a space of about 6 cubic ft. Temperature control is achieved by means of the water bath, plus the thermal inertia of the insulating boxes. In addition, the room is air conditioned.

Variable Frequency Oscillator

The basic circuit is the Colpitts oscillator which includes the condenser cell in the tank circuit, and is operated at 5 Mc. To make it possible to apply direct voltage to the cell, suitable blocking condensers and an input filter are employed. The filter and tank circuits are shown in schematic diagram in Fig. 13. The grid circuit is modified by the addition of a small phase-shifting inductance which enables the oscillator to be operated at the natural frequency of the tank circuit[9]; this minimizes the changes in frequency due to changes in tube properties.

[9] Llewellyn, Proc. I.R.E. **19**, 2063 (1931).

Condenser Cell

The condenser containing the polymer solution actually consists of four identical brass cells connected in parallel. Each cell is about 20 cm long and of 2.5-cm id. The central electrode is a tungsten wire of diameter 0.0095 cm., electroprocessed to produce a very uniform surface; this wire was obtained from the General Electric Company. The wire must be centrally mounted: we used a series of concentric hypodermic needles to facilitate the centering. The wire was put under tension of about 50 g by means of a steel spring $\frac{1}{2}$ in. long and about $\frac{1}{8}$ in. in diameter. The ends of the cells are Teflon disks. Included in the cell design are special chambers to facilitate filling; the cells are mounted at a slight angle and are filled and emptied (with nitrogen pressure) through vertical standpipes. The cell is diagrammed in Fig. 14.

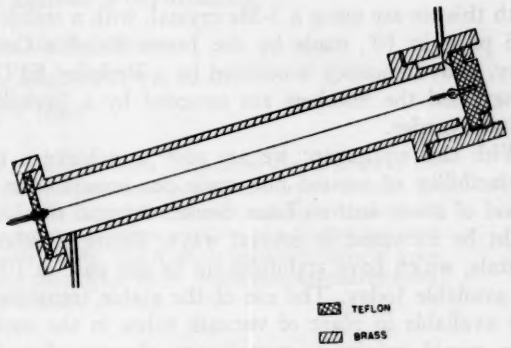

FIG. 14. Condenser cell.

It is essential that the wire be centered exactly. If it is just slightly off-center the electrical forces on the wire are unbalanced and it tends to move even more off-center. This changes the capacitance of the cell. This change of capacitance is directly proportional to the wire's distance from the axis of the cell and to the square of the applied voltage, and inversely proportional to the tension on the wire. At one time, with not as good a mounting system as is used in our present cells, we measured capacitance changes due to wire motion as large as 50 cps. This has been reduced to about 10% of that amount. Capacitance change due to wire motion is exhibited by the cell filled with pure solvent, and must be subtracted from the total capacitance change; therefore it must be kept low to avoid errors in measurement.

The cells were calibrated as follows. The cell capacitance includes an "active" capacitance between the wire and the outer cylinder wall, and a "passive" capacitance between the much thicker spring and the outer wall. We assume that upon application of voltage the field strength at the spring and mounting nuts is small compared with that at the wire, and hence that it has negligible effect on the polymer molecules. The proportion of active to passive capacitance was estimated in the following way. We constructed a dummy cell which included all parts (including an extended spring) except the central wire; by means of a Q meter we measured the difference between its capacity when filled with air and when filled with cyclohexane. The same procedure was followed using the experimental cell. From these measurements we found that the change in capacity due to cell parts other than the central wire accounted for one third of the total change. Next, with the experimental cell back in the variable frequency oscillator, we measured frequencies when the cell was filled with benzene, and then with cyclohexane. The difference in the measurements related frequency change to capacitance change. This relationship was corrected to give the change in just active capacitance in terms of frequency change. Our result was

$$\Delta C/C = 1.76 \times 10^{-6} \Delta\nu,$$

where $\Delta\nu$ is the frequency change.

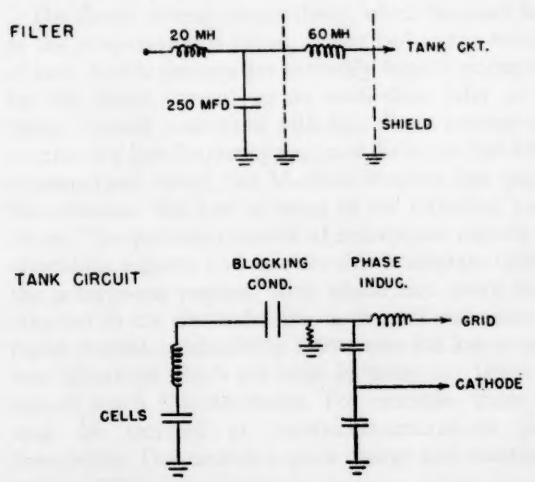

FIG. 13. Input filter circuit diagram, and simplified diagram of tank circuit.

Voltage Supplies

The needed voltage supplies are high voltage (0–10 kv) to apply to the cells; plate and filament supplies for the variable frequency oscillator, and a voltage supply for the crystal oscillator. Our high voltage supply was manufactured by the Beta Electric Corporation; it is regulated by a Stabiline voltage regulator made by the Superior Electric Company. For the plate supply we use an ac voltage stabilizer made by the Raytheon Manufacturing Company, and a simple rectifier using an OD4 regulator tube. Our filament supply is a heavy-duty 6-v storage battery equipped with a trickle charger. The voltage supply for the crystal oscillator is obtained from a 28-v storage battery equipped with a trickle charger.

Monitor, Counter, Printer

In our equipment we are using a frequency monitor manufactured by the Radio Corporation of America.

With this we are using a 5-Mc crystal, with a stability of 5 parts in 10^7, made by the James Knights Company. Beat frequency is counted by a Berkeley EPUT Meter, and the numbers are recorded by a Berkeley digital recorder.

With this equipment we are able to achieve a reproducibility of around one cycle per second over a period of about half an hour. Sensitivity and stability might be increased in several ways. Better standard crystals, which have stabilities up to one part in 10^{10}, are available today. The use of the stable transistors now available in place of vacuum tubes in the oscillator would minimize capacitance changes due to heating and to change of tube characteristics. Cell design could be improved by supplying tension with a spring mounted outside rather than inside the cell; by providing a mechanism for adjusting the position of the central wire; and by minimizing end effects by using one long cell rather than four shorter ones.

Our equipment was designed and assembled over a period of years by a number of people. A preliminary report was published by P. Debye, P. P. Debye, B. H. Eckstein, W. A. Barber, and G. J. Arquette.[10] Arquette, who built the final variable frequency oscillator and performed some preliminary experiments, will publish a detailed description of this apparatus in the near future.

Reagents

The solvent used is C. P. cyclohexane (Matheson Company), electrically treated to remove dust and possibly polar or ionic contaminants. This treatment is performed in an "electrocleaner" consisting of a cylinder with a centrally mounted wire to which a high voltage (about 5 kv) is applied. (This is roughly similar to the condenser cells in the variable frequency oscillator.) The cyclohexane is run through the electrocleaner very slowly—at about one drop per second. The product has a specific resistance of 10^{16} ohm cm and is dust-free as shown by lack of asymmetry in its light scattering.

The polystyrene is prepared by thermal polymerization of commercial styrene. To remove remaining monomer, the product is dissolved in cyclohexane to make a solution of about three percent, and this is further treated in small batches (about 100 cc). The bath is frozen rapidly with dry ice and acetone and volatiles removed under vacuum. Temperature is gradually raised during this process: after about 12 hours gentle heat is applied. This process is repeated several times until a fluffy white product is obtained.

In making the polymer solutions, we tried to keep them as dust-free as possible. We did this by either filtering the solution through sintered glass, or by electrocleaning the whole solution using a heated jacket around the electrocleaner.

It was our experience that apparently even trace amounts of monomer or other aromatics decrease the amount of capacitance change. For this reason we found it advisable to avoid the use of aromatic solvents in sample preparation.

ACKNOWLEDGMENTS

We wish to acknowledge the aid given us by the National Science Foundation, which financed this work. We also wish to acknowledge the always available help and advice of P. Debye, who instigated the research and guided its development.

[10] Debye, Debye, Eckstein, Barber, and Arquette, J. Chem. Phys. **22**, 152 (1954).

Dielectric Properties of Linear Polyamides

DAVID W. MCCALL AND ERNEST W. ANDERSON
Bell Telephone Laboratories, Inc., Murray Hill, New Jersey

(Received July 6, 1959)

The dielectric constant and loss have been measured for several linear polyamides over a range of frequency and temperature. At low frequencies and elevated temperatures, proton conduction through the amorphous regions gives rise to a Maxwell-Wagner loss, while at high frequencies and high temperatures dipole relaxation of the amide groups contained in the amorphous regions gives rise to a typical loss peak. Nylons 6, 6–6, 6–10, 7–9, 6–9, and 10–10 yield very similar results. The *N*-methylated derivative of nylon 10–10 exhibits a much smaller direct current conductivity than nylon 10–10 (when compared at temperatures of equivalent chain activity) owing to the absence of amide protons.

I. INTRODUCTION

THE study of dielectric relaxation is one of the oldest and most reliable means for revealing the nature of molecular motion. The relaxation spectrum can be measured over a wide range of frequency and often absorption regions appear which can be ascribed to particular types of molecular motion. This paper contains such data for a variety of linear polymers containing the amide group, i.e., the nylons. These materials are of special interest because of the great strength of the interchain forces and the importance of such structures in proteins and synthetic textiles.

Prior to the present study two excellent papers have been written on the dielectric properties of polyamides. Baker and Yager[1] made extensive measurements on both polyamides and polyesters, in the former case directing their attention, primarily, to nylon 6–10. (We adhere to the standard procedure of designating the polymers by two numbers which refer to the numbers of carbon atoms in the constituent diamine and dioic acid respectively. A single number is employed in ω amino acid nylons.) The essentials of the dielectric spectra were explained by Baker and Yager and to date no alternative explanation has been offered.

The direct current conductivity, which becomes large as the temperature is raised, is ascribed to the motions of ions. Amide protons are probably largely responsible for this direct current, as we shall show later in this paper. Closely associated with this direct current conduction is a low-frequency region of dielectric loss which is sometimes called the Maxwell-Wagner loss region. We visualize this loss in terms of the following mechanism. The polymers consist of amorphous regions and crystalline regions, and ions are able to migrate through the amorphous regions. Ions which can move unobstructed to the electrodes are discharged and cause the direct current conductivity. Other ions are free to move over distances which are large in molecular terms but cannot reach the electrodes. For example, these ions may be trapped at crystalline-amorphous phase boundaries. This creates a space charge and consequent polarization and, owing to the relatively long distances the ions travel, it is built up slowly, and thus corresponds to a low-frequency loss mechanism.

At higher frequencies there is a dielectric loss maximum which is ascribed to amide group rotation. It is assumed that the word "rotation" will be interpreted in its most general sense; in this connection it probably means quick jumps separated by relatively long pauses. The rotating amide groups are almost certainly confined to the amorphous regions of the polymer.

Boyd[2] has performed a number of interesting experiments relating to the dipolar loss in nylon 6–6. Boyd crosslinked nylon 6–6 and observed the effect on the intensity of the dipolar loss region. The loss maximum was observed to decrease in intensity and had virtually disappeared at a concentration of one crosslink for every 15 amide groups. Also, Boyd studied the effects of sorption by hydrogen bonding solvents; water, methanol, and ethanol. These liquids enter the amorphous regions of the polymer and act as plasticizers by reducing interchain forces and increasing segmental mobility.[2] This shifts the dipolar loss maximum to higher frequencies.

In the present study two aspects of the dielectric properties have been investigated. First, the number of methylene groups separating the amide groups was varied; measurements have been made on nylons 6, 6–6, 6–10, 6–9, 7–9, 10–10, and a terpolymer prepared from the monomers for nylons 6, 6–6, and 6–10. Second, the interpretations associated with the amide hydrogens have been checked by studying the *N*-methylated derivative of nylon 10–10.

II. EXPERIMENTAL

The polymers studied were obtained from W. P. Slichter who, in turn, either synthesized the polymers or obtained them commercially. The materials are of unknown molecular weight but they are fiber-forming. The densities have been determined by a flotation technique (Table I). The degree of crystallinity has been determined for nylons 6–6 and 6–10 from the

[1] W. O. Baker and W. A. Yager, J. Am. Chem. Soc. **64**, 2171 (1942).

[2] R. H. Boyd, J. Chem. Phys. **30**, 1276 (1959).

TABLE I.

Nylon	Amide groups/cm³	Density (g/cm³) (25°C)
6	6.1×10^{21}	1.146
6–6	6.2	1.153
6–9	4.7	1.110
7–9	4.7	1.095
6–10	4.7	1.107
10–10	3.8	1.070
10–10(*N*-methylated)	3.4	1.020
terpolymer	5.6	1.125

densities, using the limiting densities reported by Starkweather and Moynihan.[3] The nylon 6–6 was found to be 56% crystalline and the nylon 6–10 was found to be 60% crystalline.

Between 200 and 2×10^5 cps a standard Western Electric bridge circuit was used. From 10^5 to 5×10^7 cps a Boonton 160-A Q-meter was used. Special cells were constructed for operation above and below room temperature. Air and water are excluded from the cells either by pumping or by flushing with dry nitrogen gas. The specimens were subjected to pre-conditioning in the cells for periods of the order of one day at about 100°C. Measurements obtained after such treatment were reproducible even if the specimens were subsequently taken to temperatures above 150°C. for several hours. On the basis of this observation, we are led to believe that there is no important amount of low molecular weight material (especially water) present. Also, it is believed that sample degradation is negligible.

The specimens used were in the form of molded wafers. They were coated with silver paint electrodes. In computing the dielectric constant and loss the area and the thickness at room temperature were used. This results in values which are somewhat high at high temperatures but the differences are not important. The direct current conductivity (as measured by means of an Instruments for Industry Megohmeter) was subtracted from the alternating current conductivity in computing the dielectric loss.

No important discrepancies exist between the present data and the data reported by Baker and Yager[1] or by Boyd.[2] Differences may be noted in the derived quantities but these merely serve to put us on our guard lest we seek too detailed an explanation from the data which are poorly resolved.

III. RESULTS AND DISCUSSION

The dielectric constant ϵ' and loss ϵ'' have been mapped over the frequency range 200 to 5×10^7 cps and the temperature range 25 to 150°C for each of the polymers except for the *N*-methylated nylon 10–10. The *N*-methylated nylon 10–10 was measured from −20 to +60°C because of its low melting point (about 63°C). The most striking result is the great similarity which exists between plots for different polyamides. Figure 1 is a contour diagram[4] of ϵ'' *vs* frequency and temperature for nylon 6–9. The prominent features are a steep cliff in the low-frequency, high-temperature corner, and a ridge running from the center of the plot to the high-frequency, high-temperature corner, increasing in height as it nears the corner. The cliff represents the Maxwell-Wagner loss and the ridge represents the dipolar loss. Each of the polyamides studied yielded a contour diagram similar to Fig. 1. Figure 2 is a plot of ϵ'' *vs* log ν where ν is the frequency for nylon 6–9 at 90°C. This is one of the more favorable cases for the resolution of the Maxwell-Wagner and dipolar loss regions.

The dielectric constant ϵ' behaves in the expected manner, showing dispersion in regions of frequency corresponding to high dielectric loss. The limiting dielectric constant at high frequency ϵ_∞ was found to lie between 3 and 4 for the polymers studied. Figure 3 is a contour diagram for ϵ' *vs* frequency and temperature for nylon 6–9. As before, the other polymides behave similarly. The theory of dipole relaxation[5] finds that the dielectric relaxation time is given by

$$\tau = 1/\omega_m, \qquad (1)$$

where ω_m is the angular frequency of maximum loss. Dipole rotation is normally thought to be a thermally

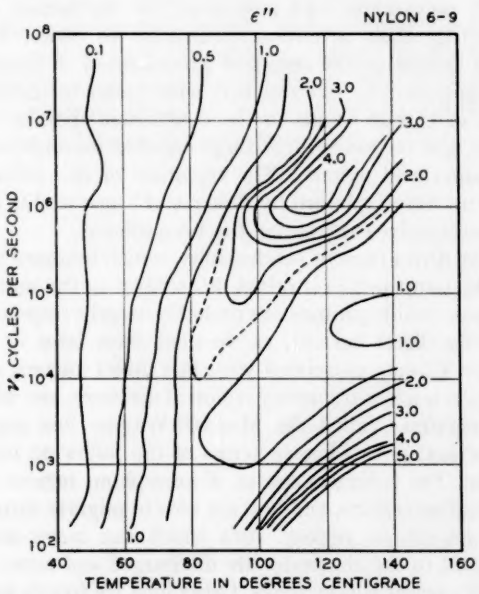

FIG. 1. Contour diagram of the dielectric loss ϵ'', as a function of frequency and temperature. This diagram represents data obtained for nylon 6–9 but the general features are common to all the polyamides studied.

[3] H. W. Starkweather and R. E. Moynihan, J. Polymer Sci. **22**, 363 (1956).

[4] W. Reddish, Trans. Faraday Soc. **46**, 459 (1950).

[5] C. J. F. Bottcher, *The Theory of Electric Polarization* (Elsevier Publishing Company, Amsterdam, 1952).

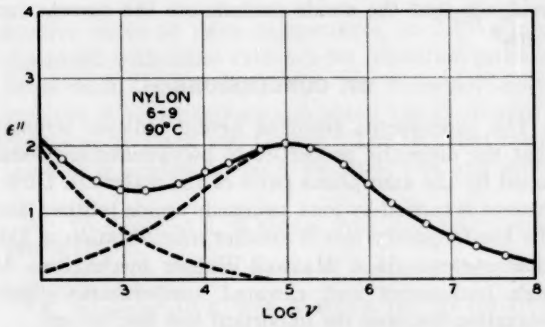

FIG. 2. A plot of ϵ'' *vs* log ν for nylon 6–9 at 90°C. The dashed lines have been sketched in to indicate how the two regions were resolved.

activated process and thus[6]

$$\tau=(h/\kappa kT)\exp(-\Delta S^{\ddagger}/R)\exp(\Delta H_{\text{dipole}}{}^{\ddagger}/RT). \quad (2)$$

$\Delta H_{\text{dipole}}{}^{\ddagger}$ and $\Delta S^{\ddagger}$ are the activation enthalpy and entropy and κ is the transmission efficient. $\Delta H_{\text{dipole}}{}^{\ddagger}$ has been determined from the slope of $\ln\omega_m$ *vs* $1/T$ plots. The temperature dependence of the direct current conductivity, σ_{dc}, can also be used to compute an activation energy which we denote E_{dc}.

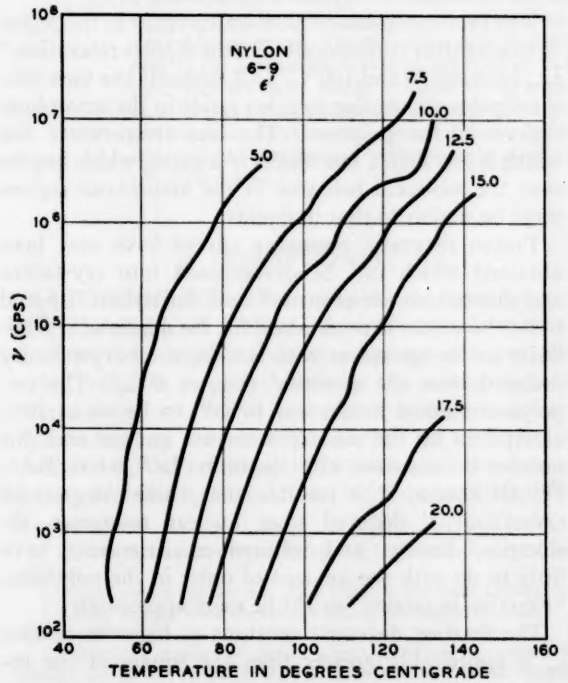

FIG. 3. Contour diagram of the dielectric constant ϵ' as a function of frequency and temperature. This diagram represents data obtained for nylon 6–9 but the general features are common to all the polyamides studied.

[6] W. Kauzman, Revs. Modern Phys. **14**, 12 (1942). Actually the macroscopic relaxation time is given by Eq. (1) and the intrinsic relaxation time is intended in Eq. (2). However, at the present state of our knowledge we can only assume that these are approximately the same.

TABLE II.

	E_{dc}(kcal)	$\Delta H_{\text{dipole}}{}^{\ddagger}$(kcal)
Baker and Yager,[1] nylon 6-10	30	23
This study, nylon 6–10	35	32
Boyd,[2] nylon 6–6	...	46
This study, nylon 66	40	35

In Table II values for $\Delta H_{\text{dipole}}{}^{\ddagger}$ and E_{dc} obtained in the present study are compared with the values determined previously.[1,2] The $\ln\sigma_{\text{dc}}$ *vs* $1/T$ plots are not linear, so the numbers quoted are averages. Over the temperature interval investigated E_{dc} varies by about 10 kcal. We believe that the discrepancies between corresponding numbers in Table II are to be attributed to experimental errors. It is perhaps worthy of note that with less than 1% water present Boyd[2] found that $\Delta H_{\text{dipole}}{}^{\ddagger}$ for nylon 6–6 had dropped from 46 to 22 kcal.

Table III exhibits the results for the various polyamides. The $\Delta H_{\text{dipole}}{}^{\ddagger}$ and E_{dc} are distinguished by their constancy with changing polar content. This is consistent with the view that the dipole rotation and direct current conductivity are features peculiar to the amorphous regions. This is further supported by the fact that the temperature at which ϵ'' has its maximum at 10^6 cps (t_1) does not vary much with polar content although the melting points differ considerably.

Sillars[5,7] has shown that the area under the dipolar part of an ϵ'' *vs* $\ln\omega$ plot, e.g. Fig. 2, is

$$\int_0^{\infty}\epsilon''d\ln\omega=(\epsilon_s-\epsilon_{\infty})/2, \quad (3)$$

where ϵ_s and ϵ_{∞} are the limiting values for the dielectric constant at low and high frequencies. This is useful because one may show that

$$N\mu^2=(9kT/4\pi)(\epsilon_s-\epsilon_{\infty})(2\epsilon_s+\epsilon_{\infty})/\epsilon_s(\epsilon_{\infty}+2)^2, \quad (4)$$

where N is the number of dipoles of moment μ per cm^3. This relation is based on the Onsager theory[5] and is independent of a distribution of relaxation times. Assuming $\mu=3.4$ Debye units, we have estimated the fraction of amide groups which are "free to rotate,"

TABLE III.

Nylon	$\Delta H_{\text{dipole}}{}^{\ddagger}$	E_{dc}	$t_1(\epsilon_{\max}'', 10^6$ cps, °C)	$10^{11}\sigma_{\text{dc}}(t_1)$ (ohm-cm)$^{-1}$
6–6	35	40	113	57
6–10	32	35	115	23
7–9	33	36	112	96
6–9	27	36	115	48
10–10	27	37	108	54
6	26	30	102	530
6, 6–6, 6–10	25	33	108	780
N-methylated	25	29	38	6

[7] R. W. Sillars, Proc. Roy. Soc. (London) **A169**, 66 (1939).

TABLE IV.

Nylon	β	range, t(°C)	N_r/N_t
6–6	0.5–0.7	100–130	0.3
6–10	0.5	80–120	0.3
6	0.5–1.0	90–110	0.3
6–9	0.4–1.0	80–120	0.4
7–9	0.5	80–130	0.4
6, 6–6, 6–10	0.4–0.8	80–110	0.6
10–10	0.3–0.6	80–130	0.5
10–10 (N-methylated)	0.3–0.4	10–50	0.3

N_r/N_t, and the results are presented in Table IV. Unfortunately, the accuracy of these ratios is difficult, is not impossible, to estimate. However, it is clear that they should be considered only semi-quantitative. The ratios are approximately independent of temperature in the range in which the dipolar loss maximum is resolvable. (In the present study this range is about 80 to 130°C except for the N-methylated nylon 10–10. In N-methylated nylon 10–10 the range is 10 to 50°C.) The ratio N_r/N_t increases somewhat with increasing temperature in nylon 7–9 and 6–10.

The ratio N_r/N_t is comparable with the fraction of amorphous material for the two cases for which the degree of crystallinity is known; for nylon 6–6, 0.3 *vs* 0.44 and for nylon 6–10, 0.3 *vs* 0.40. This is, of course, to be expected if all the amide dipoles in the amorphous regions contribute to the polarization. On the other hand, these results cannot establish that all the amide group in amorphous regions are rotating. In keeping with the general interpretation it is to be noted that the terpolymer, which is expected to be largely amorphous, has the highest N_r/N_t ratio.

The quantity β listed in Table IV is the Fuoss-Kirkwood[8] parameter which measures the width of the distribution of relaxation times. It has been computed from

$$\beta = 2\epsilon_{max}''/(\epsilon_s - \epsilon_\infty). \quad (5)$$

The ranges listed for β correspond to the temperature ranges. For a single relaxation time β is unity, and it decreases as the width of the distribution increases. The values given in Table IV show that the distributions are relatively narrow in the polyamides.

Consider now the results for nylon 10–10 and the N-methylated nylon 10–10. The activation energies for dipole rotation (27 and 25 kcal) and direct current conductivity (37 and 29) are not too different but the direct current conductivity, at the temperature t_1 which is equivalent as regards chain motion, is an order of magnitude lower for the methylated polymer [6×10^{-11} *vs* 54×10^{-11} (ohm-cm)$^{-1}$]. This result is good evidence that the amide protons are the current carriers.*

IV. CONCLUSIONS

The experiments reported herein indicate strongly that the dielectric properties of polyamides are dominated by the amorphous parts of the materials. Direct current is carried by ions, primarily amide protons, and the low-frequency loss is another manifestation of this ionic current via a Maxwell-Wagner mechanism. At high frequencies and elevated temperatures dipole relaxation becomes the important loss mechanism.

Slichter[9] has studied the proton magnetic resonance in polyamides. He finds a line width transition in each case and observes that the transition temperature increases with increasing polar content. No such relationship was found for the similar temperature t_1 (Table III) in the present study. Also, on the basis of the dielectric results, we should predict that the proton resonance curve should be a superposition of a broad (crystalline) resonance and a narrow (amorphous) resonance[10,11] at high temperatures. Slichter[9] observed a simple bell-shaped curve over the entire temperature range. However, it is well known[11] that the broad crystalline magnetic resonance is difficult to detect when the degree of crystallinity is below 60%.

The proton resonance narrows abruptly in the region of temperature corresponding to the dipolar relaxation,[12] i.e., between 50 and 100°C. This supports the view that the dipoles undergoing rotation reside in the amorphous regions of the polymers. The high-temperature line width is less than a few tenths of a gauss, which implies that the motional behavior in the amorphous regions must be similar to that in liquids.

Proton magnetic resonance curves have now been obtained which can be decomposed into crystalline and amorphous components[12] and, for nylons 6–6 and 6–10, the values thus obtained for the degree of crystallinity are in agreement with the degree of crystallinity deduced from the densities[3] (i.e., *ca* 60%). The terpolymer studied herein was found[12] to be about 70% amorphous by the nuclear resonance method and this number is consistent with the ratio $N_r/N_t=0.6$, Table IV. Of course, it is possible that these "degrees of crystallinity," deduced from nuclear resonance, dielectrics, density, and infrared measurements, have little to do with the amount of order in the polymers. "Fraction in motion" might be more appropriate.

The limiting dielectric constant at high frequencies ϵ_∞ is appreciably greater than the square of the re-

[8] R. M. Fuoss and J. G. Kirkwood, J. Am. Chem. Soc. **63**, 385 (1941). See also reference 5, p. 373.

* A referee has pointed out that this argument implies that the mobility of the charge carrier is controlled by the same mechanism as the dipole orientation. See R. M. Fuoss, J. Am. Chem. Soc. **63**, 378 (1941).

[9] W. P. Slichter, J. Appl. Phys. **26**, 1099 (1955).

[10] C. W. Wilson and G. E. Pake, J. Polymer Sci. **10**, 503 (1953).

[11] W. P. Slichter and D. W. McCall, J. Polymer Sci. **25**, 230 (1957).

[12] D. W. McCall (unpublished results).

fractive index at room temperature, *ca* 2.3.[13] This is consistent with other evidence for relaxation processes below room temperature.[2,9,14,15] The molecular motion involved is very likely torsion about the chain axes as suggested by Bunn and Garner.[13] The fact that the relaxation is evident in both dielectric loss and proton resonance data implies that both the dipolar and paraffinic parts of the molecules are moving, even at low temperatures.

[13] C. W. Bunn and E. V. Garner, Proc. Roy. Soc. (London) **189**, 39 (1947).
[14] A. J. Curtis, National Bureau of Standards, dielectrics results (unpublished).
[15] K. Schmieder and K. Wolf, Kolloid-Z. **134**, 149 (1953).

ACKNOWLEDGMENT

We take this opportunity to express our thanks to Dr. W. P. Slichter who, in addition to supplying the specimens, contributed many enlightening discussions. We are also indebted to Dr. R. H. Boyd, E. I. du Pont de Nemours Company, for making his manuscript available to us prior to publication.

THE JOURNAL OF CHEMICAL PHYSICS VOLUME 32, NUMBER 1 JANUARY, 1960

Determination of Atomic Distributions in Liquid Lead-Bismuth Alloys by Neutron and X-Ray Diffraction*

PAUL C. SHARRAH† AND JOHN I. PETZ,‡ *Department of Physics, University of Arkansas, Fayetteville, Arkansas*
AND
ROBERT F. KRUH, *Department of Chemistry, University of Arkansas, Fayetteville, Arkansas*

(Received July 7, 1959)

The intensity of scattered neutrons and x-rays has been measured for molten alloys and pure components in the system lead-bismuth. A specially designed diffraction spectrometer has been constructed for the x-ray determinations. The diffraction data have been treated to give atom distributions, and the first main peak in the distribution curves for solutions up to about 60 wt % bismuth corresponds to 12 nearest neighbors, with the value falling to about 7.7 for pure bismuth. No unusual features have been found in the eutectic region, but the density decrease on melting of lead-rich solids is puzzling in view of the retention of 12 nearest neighbors at a mean distance shorter than in the crystal. A model of average pentagonal dodecahedral coordination is suggested to account for this and for the spacing of first maxima in the distribution curves.

INTRODUCTION

ALTHOUGH diffraction yields much more detailed knowledge of the structure of crystals than it does for liquids, this technique has nevertheless provided valuable information as to the arrangement of atoms in liquids. It has been used extensively for the examination of the elements, as well as a number of compounds, but relatively little work has been done on binary metallic systems.[1] Since it is frequently possible to interpret physical properties in terms of structure it seemed desirable to investigate a series of liquid alloys through the whole range of composition, especially with the hope that various conjectures regarding alloys might be examined and that a correlation might be made between structural trends and trends found in the physical behavior of the system with changing composition.

For example, the existence of inhomogeneities together with superposition of independent atomic distributions near the eutectic composition has been suggested,[2] as well as the possibility of compound formation,[3] and of the persistence of competing residual

* This work was supported by the U. S. Atomic Energy Commission.
† Neutron work carried out at Oak Ridge National Laboratory.
‡ Taken in part from thesis submitted for degree of Master of Science, 1959.

[1] Diffraction studies of liquid alloys previously reported include: (a) Al-Sn, Al-In, Bi-Sn: A. I. Bublik and A. G. Buntar, Kristallografiya **3**, 32–42 (1958). Data for several compositions. (b) Hg-Zn: D. M. Karlikov, Ukrain. Fiz. Zhur. **3**, 370–4 (1958). Density functions given for three alloys. (c) Bi-Pb, Bi-Sn, Sn-Zn, Al-Hg: O. S. Lashko and O. V. Romanova, Ukrain. Fiz. Zhur. **3**, 375–84 (1958). Density functions given for eutectics. (d) In-Sb, Sn-Sb: Krebs, Haucke, and Weygand, Angew. Chem. **70**, 468–9 and 474 (1958). Density functions given for InSb and SnSb. (e) In-Sb: R. C. Buschert, Thesis, Purdue University, 1957. Density function given for InSb. (f) Tl-Hg: R. E. Smallman and B. R. T. Frost, Acta Met. **4**, 611–18 (1956). Intensity data for four alloys. (g) Na-K: N. S. Gingrich and R. E. Henderson, J. Chem. Phys. **20**, 117–20 (1952). Density functions given for five alloys and pure components. (h) Au-Sn: H. Hendus, Z. Naturforsch. **2**, 505–21 (1947). Intensity given for liquid AuSn. (i) Sn-Bi, Sn-Pb, Pb-Bi: H. Richter, Physik. Z. **44**, 406 (1943). Intensities by electron diffraction for selected compositions. (j) K-Hg, Tl-Hg: F. Sauerwald and W. Teske, Z. anorg. u. allgem. Chem. **210**, 247 (1933). Intensity data for several alloys. (k) Na-K: K. Banerjee, Indian J. Phys. **3**, 399 (1929). Intensity data for several alloys.

[2] Reference 1(h).

[3] A discussion of various possibilities as to degree of binding is given by F. Sauerwald, Z. Metallk. **41**, 97–104 (1950).

crystal forces.[4] Unfortunately, judgments as to the worth of such suggestions are difficult to make if based on diffraction data alone, as one suffers from the handicap of having to extract three-dimensional conclusions from one-dimensional descriptions. As to the hope of correlating properties with structure in this particular case, the findings are able to contribute little, but rather raise additional issues in the fascinating question as to the disposition of atoms in the system.

The present work, however, does yield atomic distribution functions over the entire composition range, and permits results to be compared with earlier findings[5–8] for the pure phases and for the eutectic. The system lead-bismuth was chosen for study since it is relatively low melting[9]; and, since the crystals are of widely separate types, it was thought that novel behavior might be revealed. Moreover, the fact that the elements are adajcent makes the x-ray form factor relatively simple to treat. Data were obtained both by neutron and x-ray diffraction, and in the case of the x-ray determinations a new instrumental arrangement was used which offers a number of advantages not available with conventional film methods.

EXPERIMENTAL

The experimental arrangement and the preparation of sample holders used for the neutron determinations followed closely the techniques previously described.[5]

Samples for both x-ray and neutron determinations were prepared from weighed quantities of reagent grade metals and were thoroughly mixed by bubbling hydrogen through the molten solutions. The design of the purification apparatus, due to Cathcart,[10] permitted inclusion of the sample holder for filling in the hydrogen atmosphere. Samples were allowed to cool and then transferred to the diffraction apparatus.

The equipment used for the x-ray work was a diffraction spectrometer especially designed for the determination by counting techniques of the x-ray intensity scattered from liquids. The main features are similar to those of the spectrometer in use at the Oak Ridge National Laboratory.[11] It employs the familiar Bragg-Brentano focusing geometry, but the synchronous counter-rotation of both detector and x-ray source about a horizontal axis permits viewing the diffraction from the free, level surface of the sample. This arrangement eliminates correcting for sample-holder absorption and renders the sample absorption correction negligible. The stationary sample also makes convenient the adjustment of sample position, interchange of various sample mounts, and the making of vacuum and electrical connections needed for high-temperature studies.

Monochromatization of the diffracted beam is by a sodium chloride crystal bent and ground to focus the incident divergent radiation on a scintillation detector. This makes it unnecessary to consider fluorescent radiation either as a correction to observed intensity or as a limitation in selecting systems for study. The amplified signal from the detector is fed to a pulse height analyzer which rejects pulses due to higher order reflections from wavelengths shorter than that of the molybdenum $K\alpha$ radiation which the crystal was adjusted to reflect.

The apparatus is arranged automatically to advance the x-ray source (a North American Philips diffraction tube) and detector through a sequence of equally spaced angular positions and to print the time needed to accumulate a preset number of counts at each position. For the range of s from 0.3 to 4.5, 1600 counts were taken with an angular increment of 0.6° (in 2θ); from 4.5 to 10, 2560 with an angular increment of 1.2°; and from 10 to 14.5, 3200 with an angular increment of 2.4°. Each determination lasted from 25 to 30 hours and the x-ray output was continuously monitored and found to vary insignificantly.

The sample, mounted in a shallow stainless steel tray (1.25 in. long by 0.75 in. wide), lay in a slotted nickel bar whose ends were wound with Nichrome heating coils and which was supported at one end by a thin-walled, steel cylinder. A thermocouple well in the sample holder gave the sample temperature, and auxiliary thermocouples provided signals for temperature control, which was by means of a saturable core reactor device. Thermal gradients were minimized by independent adjustment of the two heating coils, and sample temperature was found to change by not more than 0.2° after equilibrium had been reached.

The heater was enclosed in a water-cooled, cylindrical brass shield which could be aligned to make the instrument's axis of rotation lie in the sample surface. The shield was fitted with 0.010-in. beryllium windows for passage of the x-ray beam, and a small diffusion pump backed with a mechanical pump was used to maintain a vacuum ($<0.01\ \mu$ Hg) in the system. Shiny metal surfaces were preserved for the duration of the experiments.

TREATMENT OF DATA

The treatment of the neutron data followed the method outlined previously,[5] with the independent scattering being taken from the limiting value of intensity at large s. The intensity was corrected for the

---

[4] V. I. Danilov and I. V. Radchenko, Physik. Z. Sowjetunion **12**, 745–55 (1937).

[5] P. C. Sharrah and G. P. Smith, J. Chem. Phys. **21**, 228–32 (1953). Data for lead and bismuth.

[6] Danilova, Danilov, and Spektor, Doklady Akad. Nauk SSSR **82**, 561–4 (1952). Data for lead and bismuth.

[7] O. Chamberlain, Phys. Rev. **77**, 305–13 (1950). Data for lead and bismuth.

[8] References 1(a) (gives data for bismuth), 1(h) (gives data for lead and bismuth), and 1(c) (gives data for eutectic).

[9] Phase diagrams for the system lead-bismuth are given by: W. E. Barlow, J. Am. Chem. Soc. **32**, 1390 (1910); H. S. Strickler and H. Seltz, *ibid.* **58**, 2084–93 (1936); T. Takase, Nippon Kinzoku Gakkaishi **1**, 143 (1937).

[10] J. V. Cathcart and W. D. Manley, Corrosion **10**, 432 (1954).

[11] Agron, Danford, Bredig, Levy, and Sharrah, Acta Cryst. **10**, 739 (1957).

scattering of the quartz sample holder, but an absorption correction was felt unnecessary because of the small size of the sample and the small absorption cross sections. The intensities are shown in Fig. 1.

The x-ray intensity data were corrected for background and for polarization and were scaled to electron units by the method of Hultgren, Gingrich, and Warren,[12] which requires that the area under the curve of $f^2si(s)$[13] be zero. Numerical integrations necessary for these determinations were carried out on an IBM 650 digital computer and utilized data up to s of 13.

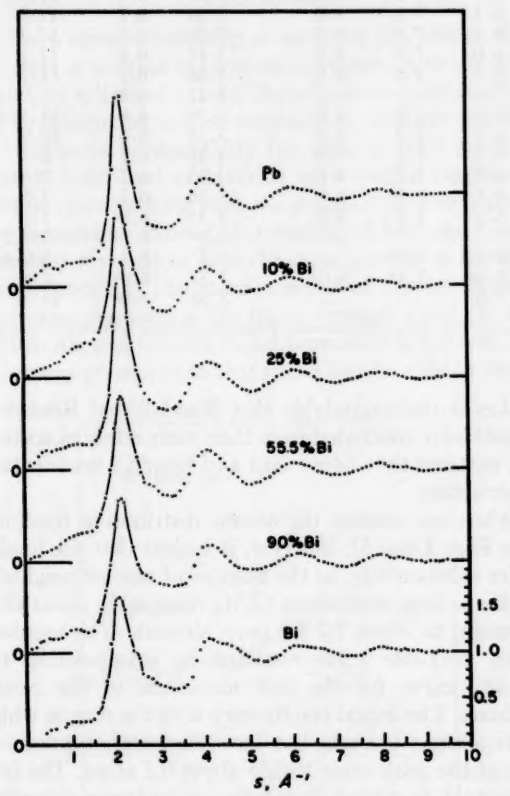

FIG. 1. Relative intensities of neutrons scattered by lead, bismuth, and four alloys. Composition is in wt %.

An average form factor corrected for dispersion was used for each solution and was obtained by taking the sum of atomic form factors[14] weighted by the appropriate mole fractions. No incoherent correction was included, because the ratio of incoherent to total intensity is small at low angle and because the monochromator

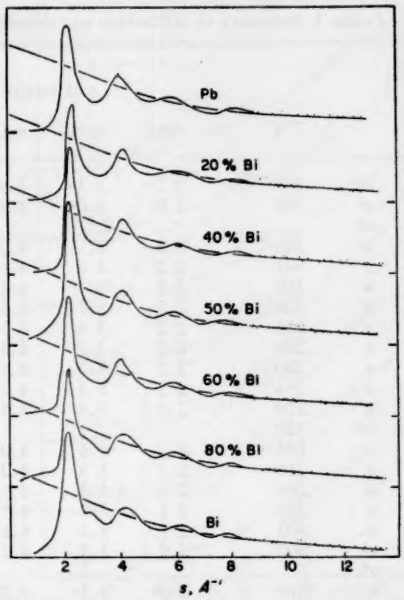

FIG. 2. Relative intensities of x-ray scattering from lead, bismuth, and five alloys. Composition is in wt %. The monotonic curves represent the calculated independent scattering.

was found to discriminate against the incoherent radiation at sufficiently high angle. The corrected, normalized intensities are shown in Fig. 2.

In evaluating the Fourier sine transforms of $si(s)$ necessary to yield the distribution functions, the upper limit in s was taken as approximately 9.5 since, beyond this value, the fluctuations of intensity about the calculated independently scattered intensity were apparently statistical and $i(s)$ was therefore assumed to be zero. The numerical integrations were carried out on

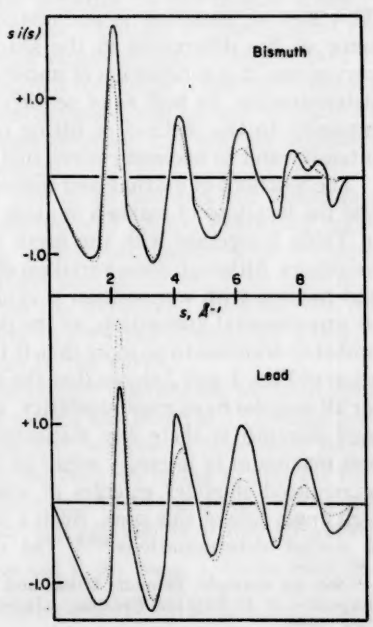

FIG. 3. Comparison of $si(s)$ obtained from neutron and x-ray data, represented by dotted and solid curves, respectively.

[12] Hultgren, Gingrich, and Warren, J. Chem. Phys. **3**, 351 (1935).

[13] The symbols and formulas in this paper are those customarily used and are given, for example, by N. S. Gingrich, Revs. Modern Phys. **15**, 90–110 (1943).

[14] Thomas-Fermi form factors are tabulated in *Internationale Tabellen zur Bestimmung von Kristallstrukturen, Vol. II* (Gebrueder Borntraeger, Berlin, 1935). Dispersion corrections were those of C. H. Dauben and D. H. Templeton, Acta Cryst. **8**, 841 (1955).

TABLE I. Summary of diffraction and density results. (References to previous determinations are from text.)

			s at intensity maxima and minima, A^{-1}							r at density maxima, A		Mean number of nearest neighbors
		T°C	max.	min.	max.	min.	max.	min.	max.	1st	2nd	
Pb	x[1h]	375	2.2[a]	3.1[a]	3.9[a]	5.0[a]	5.9[a]	6.8[a]	...	3.40	6.4[a]	8+4
Pb	n[7]	390	2.0[a]	3.0[a]	4.1[a]	...	...	...	...	3.4	6.4	12±1
Pb	x[6]	...	...	...	...	...	...	...	...	3.4[a]	6.2[a]	11
Pb	n[5]	350	2.3	3.1	4.2	5.2	6.1	7.0	8.2	3.40	6.6	9.4
Pb	x	331	2.2	3.2	4.1	5.2	6.0	7.4	8.2	3.39	6.8	12.1
Pb	n	350	2.2	3.3	4.1	5.2	6.1	7.1	8.1	3.38	6.7	11.7
10% Bi	n	330	2.2	3.2	4.1	5.0	6.0	7.0	8.0	3.40	6.7	11.0
20% Bi	x	266	2.2	3.4	4.1	5.1	6.1	7.5	8.2	3.39	6.4	12.5
25% Bi	n	260	2.2	3.2	4.1	5.1	6.1	7.0	8.0	3.39	6.7	11.8
40% Bi	x	200	2.2	3.4	4.1	5.4	6.1	7.5	8.2	3.36	6.5	12.2
50% Bi	x	154	2.2	3.4	4.1	5.3	6.0	7.0	8.0	3.41	6.8	12.1
55.5% Bi	n	170	2.2	3.3	4.1	5.0	6.1	7.0	8.0	3.38	6.7	11.7
55.5% Bi	x[1c]	130	...	...	...	...	...	...	...	3.45	6.8[a]	...
60% Bi	x	154	2.1	3.4	4.0	5.2	6.0	7.2	8.0	3.39	6.8	11.5
80% Bi	x	216	2.1	3.5	4.2	5.3	6.0	7.2	8.0	3.35	6.6	10.9
90% Bi	n	260	2.1	3.3	4.1	5.1	6.2	7.3	8.0	3.37	6.7	8.3
Bi	x	285	2.1	3.4	4.1	5.5	6.2	7.2	8.0	3.35	6.7	7.6
Bi	n	300	2.1	3.4	4.1	5.3	6.1	7.3	8.0	3.36	6.7	7.8
Bi	n[5]	300	2.2	3.3	4.2	5.3	6.2	7.2	8.2	3.35	6.8	7.7
Bi	x[6]	...	...	...	...	...	...	...	...	3.2[a]	6.5[a]	7–7.5
Bi	n[7]	310	2.0[a]	3.3[a]	4.2[a]	5.2[a]	6.4[a]	7.6[a]	...	3.2	6.7	8 to 4A
Bi	x[1h]	340	2.1[a]	3.5[a]	4.1[a]	5.4[a]	5.9[a]	7.1[a]	8.0[a]	3.32	6.6[a]	7–8
Bi	x[1a]	280	2.1	3.1	3.9	4.8	5.6	...	...	3.55	5.9[a]	10.5

[a] Estimated from graphs given in reference.

a Bendix G–15D digital computer. Weddle's[15] rule with an increment in s of 0.1 was used, and the transform was evaluated in steps of $\pi/30$ in r.

RESULTS

It is interesting to compare the reduced intensity data for lead and bismuth obtained by the two diffraction techniques. Although there is relatively good agreement in peak positions for lead, it can be seen in Fig. 3 that a marked disagreement occurs at about $s=8$ for bismuth. This sort of variation is undoubtedly responsible for some of the differences in the shapes of the density curves, and it is a reflection of uncertainties in intensity determination, as well as of sensitivity of the reduced intensity to the method of fitting of the independent intensity and to necessary correction factors.

The locations of maxima and minima in the intensity, and the locations of maxima in atom density are shown in Table I together with the mean number of nearest neighbors. Although some variation of intensity maxima and minima with composition is evident, this seems to be experimental fluctuation, as the positions shown are probably accurate to no more than 0.1 unit in s. Examination of Figs. 1 and 2 shows that the scattering patterns for all samples have great similarity, and only for nearly pure bismuth is there any distinctive shift. Here the first maximum in intensity seems to be in closer, and a pronounced shoulder emerges at about $s=2.9$ on the high angle side of this peak. Such a shoulder is evident in earlier determinations.[5,7,8] The over-all similarity makes it understandable that Randall and Rooksby[16] should have concluded from their early study of scattering patterns that liquid lead and bismuth are identical in structure.

When one obtains the atomic distribution functions (see Figs. 4 and 5), however, it is clear that the liquids differ substantially, as the number of nearest neighbors begins to drop from about 12, its value up to about 60% bismuth, to about 7.7 for pure bismuth. The numbers given in Table I are obtained by extrapolating the density curve for the first maximum to the zeroth ordinate. The actual results vary with the way in which extrapolation is made, but those shown are representative of the peak areas within about 0.5 atom. The first main peak is skewed, in most cases, to larger distances, and if one were to assume a Gaussian distribution of distances whose half-widths were taken from the left half of the peak, the appropriate area would correspond to about two less atoms than given in Table I. In the absence of any indication that there is a superposition of distributions represented in the first peak, the *total* area is the one that is viewed as physically significant.

Besides the shift in number of nearest neighbors, the bismuth specimens are distinguished by the appearance of a second small maximum in the density function at about $r=4.5$ A. The appearance of this peak has been referred to earlier[5] but it was believed due to a peak shape modification[17] effected by the high-angle

[15] See, for example, Bennett, Milne, and Bateman, *Numerical Integration of Differential Equations* (Dover Publications, New York, 1956).

[16] J. T. Randall and H. P. Rooksby, Trans. Faraday Soc. **33**, 109–10 (1937).

[17] A comprehensive discussion of factors affecting peak shapes is given by J. Waser and V. Schomaker, Revs. Modern Phys. **25**, 671 (1953).

cutoff in the intensity determination. Consideration of the present work leads to belief that the peak may indeed be real, since it appears beyond the expected position ($\Delta r = 0.85$) for cutoff ripple and is not matched by a similar maximum on the other side of the main peak. This peak is well resolved (at 4.8A) in the transform of electron diffraction intensity obtained by Bublik and Buntar.[18] Its significance is not clear in terms of structure, but its area in this work corresponds to about 10 additional atoms up to a distance of 5A.

DISCUSSION

It is always tempting to interpret the atomic distribution in a liquid in terms of the structure of the solid,[18] and, to a limited extent, there is some correspondence. The number of nearest neighbors in the lead-rich alloys is found to be essentially the same in both liquid and solid. Solid lead crystallizes with twelve neighbors in cubic close packing, and the β phase (in which there is presumably a random distribution of lead and bismuth atoms) crystallizes with the same number in hexagonal close-packing. The mean number of nearest neighbors remains constant in the liquid through about 60 wt % bismuth, and for pure liquid bismuth it is between 1 and 2 atoms greater than that found for the solid, namely 6.

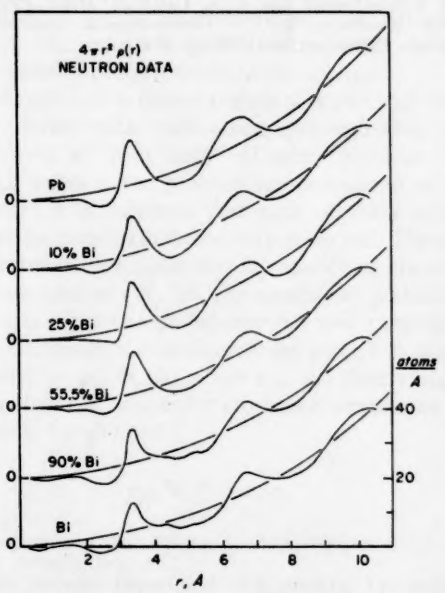

FIG. 4. Atomic density functions obtained from neutron data. The parabolic curves are those that would be obtained for a liquid of uniform density equal to the macroscopic density of the liquid. Macroscopic densities used in this figure and Fig. 5 are interpolated from data in American Smelting and Refining Company Reports Nos. N1, N3, N4, N5, N6, N8onr-644 (1948–50).

[18] Structural information for metallic solids is conveniently tabulated by W. B. Pearson, *Metal Physics and Physical Metallurgy*, Vol. 4: *Handbook of Lattice Spacings and Structures of Metals and Alloys* (Pergamon Press, London, 1958), pp. 459, 466, 803.

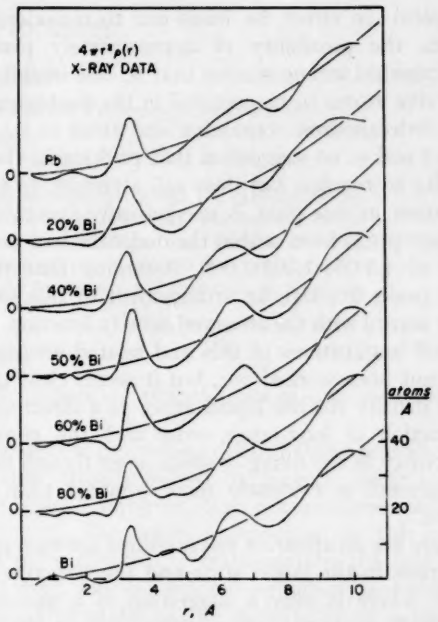

FIG. 5. Atomic density functions obtained from x-ray data. The parabolic curves are those that would be obtained for a liquid of uniform density equal to the macroscopic density of the liquid.

Of the 6 neighbors in the solid, 3 are found at 3.105 and 3 at 3.474 A, and it is seen that for the liquid the first maximum in density lies between these values.

On the other hand, the mean distance of nearest neighbors in the lead-rich liquids is smaller than the corresponding distance in the crystals at room temperature, namely, 3.49A for lead and 3.50A for the β phase. This comparison of distances, taken together with the coordination number of 12 for both liquid and solid, makes the smaller densities for the liquids appear inconsistent. In fact, the retention of coordination number and the smaller observed density might have suggested that the liquid is formed by a dilation of the solid. But that this is unreasonable can be seen not only from the smaller contact distance, but also by considering the distance spectrum.

Taking liquid lead as an example, one would expect to find, for a face-centered lattice, important maxima at $n^{\frac{1}{3}} \times$(distance of first maximum) with n=integer. The most important near peaks would be expected for $n=3$, 5, and 7, yet the second and third maxima correspond more nearly to $n=4$ and 8, while for 5 there is a distinct minimum in the curve.

The Kirkwood-Boggs[19] distribution for hard spheres would place the second maximum at 1.71 times greater distance than the first, whereas it is actually found at almost twice the distance. In trying to account for the large coordination number and the spacing of the second peak in particular, the suggestions of Bernal[20] appear to

[19] J. G. Kirkwood and E. M. Boggs, J. Chem. Phys. **10**, 394 (1942).

[20] J. D. Bernal, Nature **183**, 141–7 (1959).

be useful. In effect, he leads one to consider, among others, the possibility of approximately pentagonal dodecahedral arrangements; that is, one imagines each of twelve atoms to be centered in the pentagonal faces of a dodecahedron containing one atom at its center. Bernal makes no suggestion that packing in the liquid is quite so regular, but does call attention to the configuration as one that is energetically favorable. The first few peaks from within the dodecahedron are in the ratio of 1:1.051:1.203:2.000. Assuming that the first three peaks overlap, an arrangement of this sort is in closer accord with the observed density function. As yet, the full implications of this and related arrangements have not been worked out, but it seems clear that the lower density for the liquid arises as a direct result of destruction of long-range order and the consequent inefficiency in the filling of space, even though the local arrangement is evidently more compact than in the crystal.

There are no apparent relationships between physical properties in the liquid state and the structure of the liquid. There is only a suggestion of a minimum in viscosity[21] near the composition (about 60 wt % bismuth) where the coordination number begins to diminish, but there are no such coincidences evident for thermodynamic data. For example, there is a small positive departure from linearity in the concentration dependence of liquid alloy volumes, and this reaches a maximum between 20 and 30 wt % bismuth.[22]

Both the entropy and enthalpy changes for mixing[23] are nearly symmetrical about mole fraction 0.5 (nearly 50 wt % in this system). Explanations of this symmetry are frequently based on a lattice or similar model with constant coordination number, but this postulate is not reasonable in light of the present work, and even though a concentration dependence may be taken into account, it appears that the structural description in this and similar systems is far more complicated than that afforded by a simple lattice.

ACKNOWLEDGMENTS

The authors wish to acknowledge the kind assistance of Professor James Scroggs, University of Arkansas, and Mr. Thomas McNamara of International Business Machines in planning and carrying out certain parts of the numerical work.

The assistance given by Dr. J. V. Cathcart, Dr. H. A. Levy, and Dr. G. P. Smith during the early stages of the neutron studies, as well as the opportunity to use the neutron spectrometer at the Oak Ridge National Laboratory, is also gratefully acknowledged.

[21] R. Arpi, Z. Metallographie **5**, 142 (1914).

[22] These observations are made from plots of density data given in reference 21.

[23] O. Kubaschewski and J. A. Catterall, *Metal Physics and Physical Metallurgy*, Vol. 3: *Thermochemical Data of Alloys* (Pergamon Press, London, 1956), p. 124.

First-Order Stochastic Processes

IRVIN M. KRIEGER* AND PAUL J. GANS†

Department of Chemistry and Chemical Engineering, Case Institute of Technology, Cleveland, Ohio

(Received August 5, 1959)

A general class of "first-order" stochastic processes is defined as those for which the probability per unit time of a transition out of a state is proportional to the occupancy of that state. The solution to the differential-difference equation for the process, obtained earlier by Siegert [Phys. Rev. **76**, 1708 (1949)], is obtained here using more elementary mathematics. The resultant solution is used to demonstrate that a system relaxing by first-order processes from one equilibrium state to another will maintain, at all times, a multinomial distribution.

INTRODUCTION

THE term "stochastic process" is defined in Doob's[1] monograph as "any process running along in time and controlled by probabilistic laws." If it is possible to demonstrate or to postulate that a system of physicochemical interest is governed by probability considerations, then the determination of its time-dependent behavior is reduced to the solution of a stochastic problem. This approach has been utilized to obtain useful results in particular systems by Siegert,[2] Klein,[3] and by Shuler[4–8] and co-authors. The purpose of the present paper is to define a general class of "first-order" stochastic problems which includes the problems investigated in the papers referred to above, to set up and solve the resultant stochastic problem, and to indicate some of the properties of the solution.

We will consider a closed system of n particles which do not interact with each other, although they may interact with a "heat bath" of other particles. The accessible states of the particles are considered as cells in a space; it is assumed that each of the r cells is accessible by some path from every other cell. The state of the system is described then by specifying the set of occupation numbers $\mathbf{N}$, i.e., the number of particles n_i in each cell i. Let the probability per unit time that a particle undergoes a transition from state i to state j be denoted by $p_{ij}(\mathbf{N}, t)$, where t is the time variable. We now define a first-order stochastic process as one in $\mathbf{N}$ which, for all i and j,

$$p_{ij}(\mathbf{N}, t)=\alpha_{ij}n_i, \tag{1}$$

where the transition probabilities α_{ij} are independent of $\mathbf{N}$ and t.

The first-order problem as defined above actually was set up and formally solved by Siegert, using matrix methods. (Note, however, that our α_{ij} corresponds to Siegert's α_{ji}.) The solution presented in this paper employs more elementary mathematics; the fact that Siegert's work was not utilized by subsequent authors seems to us to establish the desirability of a simpler approach. An original result of the present paper is a theorem which states that a first-order system which has attained equilibrium will, upon introduction of a disturbance which changes the transition probabilities, relax to a new equilibrium through a set of multinomial distributions. This theorem is of interest because the multinomial form characterizes the canonical distribution.

THE DIFFERENCE EQUATION

We will postulate a time interval δt which is so small that at most only one transition can take place in δt. The probability $p_{ii}\delta t$ that a particle in state i undergoes no change in the interval is thus

$$p_{ii}\delta t=1-\sum_{j\neq i}p_{ij}\delta t. \tag{2}$$

We can now write the customary difference equation relating the probability $P(n_1, \cdots n_i, \cdots n_j, \cdots n_r, t+\delta t)$ that the system is described by the set of occupation numbers $(n_1, \cdots n_i, \cdots n_j, \cdots n_r)$ at time $t+\delta t$ to the probability $P(n_1, \cdots n_i+1, \cdots n_j-1, \cdots n_r, t)$ that it was described at time t by occupation numbers $(n_1, \cdots n_i+1, \cdots n_j-1, \cdots n_r)$ as

$$\begin{aligned}P(n_1, \cdots n_i, \cdots n_j, \cdots n_r, t+\delta t)&=\sum_i\sum_{j\neq i}P(n_1, \cdots n_i+1, \cdots n_j-1, \cdots n_r, t)p_{ij}\delta t\\&\quad+P(n_1, \cdots n_i, \cdots n_j, \cdots n_r, t)\prod_i p_{ii}\delta t.\end{aligned} \tag{3}$$

From the normalization relation [Eq. (2)] we have

$$\prod_i p_{ii}\delta t=\sum_{j\neq i}\sum_i p_{ij}\delta t+\mathcal{O}(\delta t)^2, \tag{4}$$

where $\mathcal{O}(\delta t)^2$ indicates terms of second or higher order in δt. Recalling now the definition, Eq. (1), of the

* Present address: Faculté des Sciences, Université Libre de Bruxelles, Brussels, Belgium.

† Present address: Department of Chemistry, University of Illinois, Urbana, Illinois.

[1] J. L. Doob, *Stochastic Processes* (John Wiley & Sons, Inc., New York, 1953).

[2] A. J. F. Siegert, Phys. Rev. **76**, 1708 (1949).

[3] M. J. Klein, Phys. Rev. **103**, 17 (1956).

[4] E. W. Montroll and K. E. Shuler, J. Chem. Phys. **26**, 454 (1957).

[5] K. E. Shuler, J. Phys. Chem. **61**, 849 (1957).

[6] Bazley, Montroll, Rubin, and Shuler, J. Chem. Phys. **28**, 700 (1958).

[7] R. Herman and K. E. Shuler, J. Chem. Phys. **29**, 366 (1958).

[8] E. W. Montroll and K. E. Shuler, *Advances in Chemical Physics* (Interscience Publishers, Inc., New York, 1958), Vol. I, p. 361.

first-order process, we obtain

$$P(\mathbf{N}, t+\delta t)-P(\mathbf{N}, t)$$
$$=\sum_{j\neq i}\sum_{i}P(n_1, \cdots n_i+1, \cdots n_j-1, \cdots n_r, t)\alpha_{ij}(n_i+1)\delta t$$
$$-\sum_{j\neq i}\sum_{i}P(n_1, \cdots n_i, \cdots n_j, \cdots n_r, t)\alpha_{ij}n_i\delta t+\mathcal{O}(\delta t).^2 \quad (5)$$

If we divide both sides by δt and let δt approach 0, we have, invoking the definition of the partial derivative, our differential-difference equation,

$$\partial P(\mathbf{N}, t)/\partial t=\sum_{j\neq i}\sum_{i}\alpha_{ij}[(n_i+1)$$
$$\cdot P(n_1, \cdots n_i+1, \cdots n_j-1, \cdots n_r, t)-n_iP(\mathbf{N}, t)]. \quad (6)$$

SOLUTION OF DIFFERENCE EQUATION

The method of generating functions is suitable to transform the differential-difference equation [Eq. (6)] to a partial differential equation. We define the generating function $G(x_1, \cdots x_r, t)$ by the relation

$$G(x_1, \cdots x_r, t)=\sum_{n}P(n_1, \cdots n_r, t)\prod_{i}x_i^{n_i}, \quad (7)$$

where the subscript n on the summation is used to indicate that the summation takes place over all values of n_1, n_2, etc., subject to the restriction that

$$\sum_{k}n_k=n. \quad (8)$$

Several important and useful properties of the generating function are reviewed in the Appendix. If the differential-difference equation is multiplied on both sides by $\prod_k x_k^{n_k}$ and then both sides are summed over all n_i subject to the restriction [Eq. (8)], we obtain the partial differential equation

$$\partial G/\partial t=\sum_{j\neq i}\sum_{i}\alpha_{ij}(x_j-x_i)(\partial G/\partial x_i)$$
$$=\sum_{j}\sum_{i}\alpha_{ij}(x_j-x_i)(\partial G/\partial x_i). \quad (9)$$

The set of transition probabilities forms a matrix with undefined diagonal elements α_{ii}. We may define arbitrarily the missing elements by the relationship

$$\alpha_{ii}=-\sum_{j\neq i}\alpha_{ij}, \quad (10)$$

so that $\sum_j\alpha_{ij}=0$. We can then simplify the expression [Eq. (9)] to

$$\partial G/\partial t=\sum_{j}\sum_{i}\alpha_{ij}x_j(\partial G/\partial x_i). \quad (11)$$

The general solution of Eq. (11) is obtained by the method of characteristics.[9] We consider the set of ordinary differential equations subsidiary to Eq. (11),

$$(dt/1)=\{dx_i/\sum_{j}\alpha_{ij}x_j\}; \qquad dG=0. \quad (12)$$

[There are r differential terms typified by the bracketed expression in Eq. (12).] If we select a set of r arbitrary multipliers b_{ki}, then it can be shown from Eq. (12) that

$$\sum_{i}b_{ki}dx_i/\sum_{i}b_{ki}\sum_{j}\alpha_{ij}x_j=dt, \quad (13)$$

since

$$dx_i=dt\sum_{j}\alpha_{ij}x_j. \quad (14)$$

If we select r such sets of multipliers, Eq. (12) can be transformed to

$$dt=\{\sum_{i}b_{ki}dx_i/\sum_{i}b_{ki}\sum_{j}\alpha_{ij}x_j\}; \qquad dG=0. \quad (15)$$

We impose now upon the previously arbitrary coefficients the requirement that they satisfy the relation,

$$\sum_{i}b_{ki}\alpha_{ij}=b_{kj}\lambda_k. \quad (16)$$

This requirement is equivalent to setting the multipliers, b_{ki}, equal to the components of the left eigenvector of the α matrix corresponding to the kth eigenvalue, λ_k, since Eq. (16) can be rewritten

$$\sum_{i}b_{ki}(\alpha_{ij}-\lambda_k\delta_{ij})=0, \quad (17)$$

where δ_{ij} is the Kronecker delta. The condition for the existence of a solution to Eq. (17) is that the secular determinant $\det(\alpha_{ij}-\lambda_k\delta_{ij})$ be zero. Siegert has shown that the α matrix has one, and only one, zero eigenvalue if all states are accessible, and that the remaining eigenvalues have negative real parts. (See also the Appendix.)

By reversing the order of the summations in Eq. (13) and introducing the relationship [Eq. (16)], we obtain

$$\sum_{i}b_{ij}dx_i/\sum_{i}b_{ki}\sum_{j}\alpha_{ij}x_j=(1/\lambda_k)d\ln(\sum_{j}b_{kj}x_j), \quad (18)$$

and hence the transformed subsidiary equations are

$$dt=\{(1/\lambda_k)d\ln(\sum_{j}b_{kj}x_j)\}; \qquad dG=0. \quad (19)$$

The general solution of Eq. (19) is

$$G=\phi(I_1, \cdots I_k, \cdots I_r), \quad (20)$$

where

$$I_k=\sum_{j}b_{kj}x_j\exp(\lambda_k t). \quad (21)$$

The exact form of the arbitrary function ϕ in Eq. (20) is determined by the boundary conditions.

SOLUTION FOR KNOWN INITIAL POPULATIONS

Let m_i be the value of n_i at zero time, and G^0 and I_k^0 be the corresponding initial values of G and I_k,

[9] F. H. Miller, *Partial Differential Equations* (John Wiley & Sons, Inc., New York, 1941).

respectively. We have then

$$G^0=\phi(I_1^0, \cdots I_k^0, \cdots I_r^0), \tag{22}$$

$$I_k^0=\sum_j b_{kj}x_j, \tag{23}$$

and

$$G^0=\prod_i x_i^{m_i}. \tag{24}$$

We can solve the r simultaneous equations [Eq. (23)] by the method of determinants, obtaining

$$x_j=B^{-1}\sum_k I_k^0 B^{kj}, \tag{25}$$

where $B=\det(b_{kj})$ is the determinant of the multipliers and B^{kj} is the cofactor of b_{kj}. Thus

$$G^0=\prod_i (B^{-1}\sum_k I_k^0 B^{ki})^{m_i}. \tag{26}$$

Since the functional relationship among G and the integrals I_k is time independent, we may write:

$$G=\prod_i [B^{-1}\sum_k B^{ki}\sum_j b_{kj}x_j \exp(\lambda_k t)]^{m_i}. \tag{27}$$

In the infinite time limit, all the terms of the form $\exp(\lambda_k t)$ vanish except the one corresponding to the zero eigenvalue, which we will call λ_r. The generating function G_∞ in this limit thus becomes

$$G_\infty=\prod_i [B^{-1}B^{ri}\sum_j b_{rj}x_j]^{m_i}. \tag{28}$$

It is proved in the Appendix that

$$\sum_j b_{rj}B^{ri}=B, \tag{29}$$

and hence G_∞ reduces to

$$G_\infty=\prod_i [\sum_j b_{rj}x_j/\sum_j b_{rj}]^{m_i}=[\sum_j b_{rj}x_j/\sum_j b_{rj}]^n. \tag{30}$$

Thus the infinite time limit is independent of the initial population. This expression [Eq. (30)] is the generating function for the multinomial distribution:

$$P(n_1, \cdots n_r, \infty)=(n!/\prod_i n_i!)\prod_i [b_{ri}/\sum_j b_{rj}]^{n_i}. \tag{31}$$

It is instructive to examine the moments of the distribution. The average value $\langle n_i\rangle_\infty$ of n_i at equilibrium is

$$\langle n_i\rangle_\infty=[(\partial \ln G_\infty)/(\partial \ln x_i)]\,|_{\text{all } x_j=1}=(nb_{ri}/\sum_j b_{rj}). \tag{32}$$

If we introduce the Boltzmann relation

$$\langle n_i\rangle_\infty/n=[\exp(-\beta\epsilon_i)]/[\sum_i \exp(-\beta\epsilon_i)], \tag{33}$$

where $\beta=(kT)^{-1}$, we see that $b_{ri}=A\exp(-\beta\epsilon_i)$, where A is a constant depending on the choice of the zero of energy. Thus Eq. (31) becomes the distribution function for the canonical ensemble,

$$P(N, \infty)=Z^{-1}\exp[-\beta E(N)], \tag{34}$$

where

$$E(N)=\sum_i n_i\epsilon_i \tag{35}$$

is the total energy for the distribution, and

$$Z=(\prod_i n_i!/n!)[\sum_j \exp(-\beta\epsilon_j)]^n \tag{36}$$

is the partition function for the system.

RELAXATION FROM AN EQUILIBRIUM STATE

It is of interest to investigate the time-dependent behavior of a system, initially at equilibrium, which is disturbed so as to alter the transition probabilities from initial values α_{ij}^0 to new values α_{ij}. Equations (22) and (23) still apply, but the zero-time generating function for this case is

$$G^0=[\sum_i A_i^0 x_i]^n, \tag{37}$$

where $A_i^0=b_{ri}^0/\sum_j b_{rj}^0$, the quantities b_{ij}^0 being the multipliers corresponding to the initial transition probabilities. We thus obtain, using the substitution [Eq. (25)] and the time-invariance of the function [Eq. (20)],

$$G=[\sum_i A_i^0 B^{-1}\sum_k B^{ki}\sum_j b_{kj}x_j \exp(\lambda_k t)]^n. \tag{38}$$

Interchanging orders of summation, we can rearrange Eq. (38) to the form:

$$G=[\sum_j A_j(t)x_j]^n, \tag{39}$$

with

$$A_j(t)=\sum_i A_i^0\sum_k b_{kj}B^{-1}B^{ki}\exp(\lambda_k t). \tag{40}$$

We see then that equilibrium is characterized by a multinomial distribution, and that a system relaxing by first-order processes from one equilibrium distribution to another maintains at all times a multinomial distribution. This theorem is the generalization of the theorem of the Montroll and Shuler on the relaxation of a system of harmonic oscillators. For their system, however, Montroll and Shuler were able to isolate the temperature variable, and hence to show that the intermediate distributions were identical with true equilibrium distributions at an intermediate temperature.

ACKNOWLEDGMENT

The authors wish to acknowledge the contribution of Dr. Thomas J. Dougherty in offering valuable suggestions and stimulating discussion during the course of this work. One of us (PJG) wishes to acknowledge the financial support of the Dow Chemical Company through the William R. Veazey Fellowship.

APPENDIX I. PROPERTIES OF THE GENERATING FUNCTION

Since

$$G(x_1, \cdots x_r, t) = \sum_n P(n_1, \cdots n_r, t) \prod_i x_i^{n_i},$$

then

$$\partial G/\partial t = \sum_n (\partial P/\partial t) \prod_i x_i^{n_i};$$

$$\partial G/\partial x_j = \sum_n (n_j+1)\, P(n_1, \cdots n_j+1, \cdots n_r, t) \prod_i x_i^{n_i};$$

$$x_j G = \sum_n P(n_1, \cdots n_j-1, \cdots n_r, t) \prod_i x_i^{n_i};$$

$$x_j(\partial G/\partial x_j) = \sum_n n_j P(n_1, \cdots n_r, t) \prod_i x_i^{n_i};$$

$$G(1, 1, \cdots 1, t) = \sum_n P(n_1, \cdots n_r, t) = 1;$$

$$x_j(\partial G/\partial x_j) \mid_{\text{all } x_i=1} = (\partial \ln G)/(\partial \ln x_j) \mid_{\text{all } x_j=1} = \langle n_j \rangle;$$

$$(\partial^\nu \ln G)/(\partial (\ln x_j)^\nu) \mid_{\text{all } x_i=1} = \langle n_j{}^\nu \rangle.$$

APPENDIX II. PROPERTIES OF THE EIGENVALUES

The product of the eigenvalues of the α matrix is $\det(\alpha_{ij})$, the value of the α determinant. We can prove that $\det(\alpha_{ij})=0$ by adding all other columns to the first column, thus obtaining a column of zeros, since $\sum_j \alpha_{ij}=0$. Therefore, at least one eigenvalue is zero.

To prove that the real parts of the eigenvalues are nonpositive, we note that

$$\lambda_k = b_{kj}{}^{-1} \sum_i b_{ki} \alpha_{ij} = b_{kj}{}^{-1} \sum_i \alpha_{ij} (b_{ki} - b_{kj}).$$

Multiplying by $b_{kj}{}^*(b_{kj}{}^*)^{-1}$, where $b_{kj}{}^*$ is the complex conjugate of b_{kj}, we obtain, for all j,

$$\lambda_k = (b_{kj} b_{kj}{}^*)^{-1} \sum_i \alpha_{ij} (b_{ki} b_{kj}{}^* - b_{kj} b_{kj}{}^*).$$

Let b_{kl} be the largest of the multipliers b_{kj}, so that $|b_{kl}| \geq |b_{kj}|$ for all j. Hence

$$Re(b_{ki} b_{kl}{}^*) \leq b_{kl} b_{kl}{}^*.$$

If we set $j=l$ in the expression for λ_k, we see that

$$Re(\lambda_k) = (b_{kl} b_{kl}{}^*)^{-1} \sum_i \alpha_{il} [Re(b_{ki} b_{kl}{}^*) - b_{kl} b_{kl}{}^*],$$

and hence that $Re(\lambda_k) \leqslant 0$.

APPENDIX III. PROPERTIES OF THE EIGENVECTORS

Since $\sum_i b_{ki} \alpha_{ij} = b_{kj} \lambda_k$, we have by summation over j,

$$\sum_j \sum_i b_{ki} \alpha_{ij} = \sum_j b_{kj} \lambda_k.$$

On interchanging orders of summation,

$$\sum_i b_{ki} \sum_j \alpha_{ij} = \lambda_k \sum_j b_{kj}.$$

Since $\sum_j \alpha_{ij}=0$ for all i, then either $\lambda_k=0$ or $\sum_j b_{kj}=0$.

A basic property of determinants[10] is

$$\sum_k b_{kj} B^{kl} = B \delta_{jl},$$

where δ_{jl} is the Kronecker delta. By summing over j, we obtain

$$\sum_j \sum_k b_{kj} B^{kl} = B.$$

On interchanging order of summation,

$$\sum_k B^{kl} \sum_j b_{kj} = B.$$

Since $\sum_j b_{kj}=0$ for $k \neq r$, we obtain

$$B^{rl} \sum_j b_{rj} = B.$$

[10] H. Margenau and G. M. Murphy, *The Mathematics of Physics and Chemistry* (D. Van Nostrand Company, Inc., Princeton, New Jersey, 1943), Chap. 10.

Potential Energy Constants, Rotational Distortion Constants, and Thermodynamic Properties for NH_3, ND_3; PH_3, PD_3; AsH_3, and AsD_3

S. SUNDARAM, FRANK SUSZEK, AND FORREST F. CLEVELAND

Spectroscopy Laboratory, Department of Physics, Illinois Institute of Technology, Chicago 16, Illinois*

(Received August 13, 1959)

Normal coordinate analyses have been made for ammonia (NH_3), phosphine (PH_3), and arsine (AsH_3) by the Wilson **FG** matrix method. Using the data on anharmonicities, and the corresponding completely deuterated molecules, the constants of the most general quadratic potential energy function have been obtained for all these molecules. Based on the technique of Kivelson and Wilson, the rotational distortion constants of all the 6 molecules have been determined and compared with the results obtained from previous rotational spectral data. The molar thermodynamic properties, heat content, free energy, entropy, and heat capacity also have been calculated for temperatures from 100 to 1000°K for the ideal gaseous state at 1 atmos pressure and for a rigid-rotor, harmonic-oscillator approximation.

INTRODUCTION

THE normal vibrations of the pyramidal XY_3 molecules have been studied by several authors,[1-3] using various types of potential energy functions. Wilson[4] and Howard and Wilson[5] have discussed their symmetry properties. Certain of the effects of Coriolis interactions on the energies have been studied by Teller and Tisza,[6] Teller,[7] and Johnston and Dennison.[8] The effects of changes in the internuclear distances on the rotational energies have been considered by Slawsky and Dennison.[9] Shaffer[10] and Nielsen[11] have derived the complete expressions for the vibrational-rotational energies of this type of molecule so as to include all effects arising from Coriolis interactions, anharmonicities, and the like.

Recently, Wilson and Polo,[12] McKean and Schatz,[13] and Venkateswarlu and Sundaram[14] have made potential energy constant calculations for some molecules of this type, using the Wilson **FG** matrix method.[15,16] However, these groups of investigators either had neglected, or made some assumptions with respect to, the interaction constants. One of the aims of the present investigation therefore is to obtain the complete quadratic force field in the molecules of the XY_3 type (X=N, P, As and Y=H, D) studied here. This has been possible in these cases because data are available on isotopic molecules.

Further, as a check on the validity of the potential energy constants obtained, calculations of the rotational distortion constants for these molecules have been made using the technique of Kivelson and Wilson.[17] The calculated values are compared with values available in the literature.

POTENTIAL ENERGY CONSTANTS

The pyramidal XY_3 type molecules studied here have the symmetry C_{3v}. According to the selection rules, they therefore have 2 nondegenerate a_1 and 2 doubly degenerate e modes of vibration. If one considers the data from a pair of molecules like XH_3 and XD_3 (X=N or P or As), the 8 fundamental vibrational wave numbers can be used to set up 8 equations involving the 6 constants of the most general quadratic potential energy function. However, if harmonic wave numbers have been used, because of the product rule,[18] only 6 out of the above 8 equations will be distinct and therefore the 6 potential energy constants can be determined unambiguously.

The above considerations, therefore, lead to the problem of first finding the anharmonic constants, x_{ik}, to correct the observed fundamentals (σ), to obtain the zero-order frequencies and, therefore, the harmonic wave numbers (ω). McKean and Schatz[13] have given the values of these anharmonic constants for NH_3, PH_3, and AsH_3 based on the method of Dennison.[19] In this study, the anharmonic constants (x_{ik}) for ND_3, PD_3, and AsD_3 have been obtained using the relation[19]

$$\omega_i^* = \sigma_i^* (1 + x_{ik} \sigma_i^* / \sigma_i),$$

* Publication No. 131.

[1] D. M. Dennison, Phil. Mag. **1**, 195 (1926).

[2] F. Lechner, Sitzber. Akad. Wiss. Wien, Math.-naturw. Kl., Abt. IIa **141**, 291, 633 (1932).

[3] J. E. Rosenthal, Phys. Rev. **47**, 235 (1935).

[4] E. B. Wilson, Jr., J. Chem. Phys. **2**, 432 (1934).

[5] J. B. Howard and E. B. Wilson, Jr., J. Chem. Phys. **2**, 630 (1934).

[6] E. Teller and L. Tisza, Z. Physik **73**, 791 (1932).

[7] E. Teller, *Hand- und Jahrbuch der Chemischen Physik* (1934), Vol. 9, p. 125.

[8] M. Johnston and D. M. Dennison, Phys. Rev. **48**, 868 (1935).

[9] Z. I. Slawsky and D. M. Dennison, J. Chem. Phys. **7**, 509 (1939).

[10] W. H. Shaffer, J. Chem. Phys. **9**, 607 (1939).

[11] H. H. Nielsen, Revs. Modern Phys. **23**, 90 (1951).

[12] M. K. Wilson and S. R. Polo, J. Chem. Phys. **20**, 1716 (1952).

[13] D. C. McKean and P. N. Schatz, J. Chem. Phys. **24**, 316 (1956).

[14] K. Venkateswarlu and S. Sundaram, Proc. Phys. Soc. (London) **A69**, 180 (1956).

[15] E. B. Wilson, Jr., J. Chem. Phys. **7**, 1047 (1939); **9**, 76 (1941).

[16] A. G. Meister, and F. F. Cleveland, Am. J. Phys. **14**, 13 (1946).

[17] D. Kivelson and E. B. Wilson, Jr., J. Chem. Phys. **20**, 1575 (1952); **21**, 1229 (1953).

[18] O. Redlich, Z. physik. Chem. **B28**, 371 (1935).

[19] D. M. Dennison, Revs. Modern Phys. **12**, 175 (1940).

TABLE I. Harmonic wave numbers (in c/cm) for the gaseous state and the structural parameters for the XY_3 type molecules.

Species	Designation	NH_3	ND_3	PH_3	PD_3	AsH_3	AsD_3
a_1	ω_1	3540	2527	2448	1760	2209	1571
a_1	ω_2	1055	812	1045	759	972	695
e	ω_3	3547	2621	2390	1720[a]	2225	1580
e	ω_4	1676	1217	1153	822	1012	718
Y—X—Y angle		106° 40′		93° 50′		91° 34′	
X—Y distance (A)		1.012		1.424		1.523	

[a] Calculated by use of the product rule.

where σ_i^*, ω_i^* are for the deuterated molecule, and σ_i, x_{ik} are for the hydride. The x_{ik} values given by McKean and Schatz[13] have been used here. As a check, the product rule was verified with the calculated ω values for all cases. The check was nearly perfect in each case.

The elements of the **G** matrices were obtained by the Wilson s_{kt} vector method as described by Meister and Cleveland.[16] The observed fundamentals used in these calculations, are those from Benedict and Plyler[20] for NH_3 and ND_3, and from Herzberg and Herzberg,[21] and Herzberg[22] for the other molecules. The harmonic wave numbers obtained, together with the molecular parameters used, are listed in Table I. For PD_3, the product rule was used to evaluate one of the fundamentals not reported in the literature.[22]

By the method outlined above the 6 symmetry force constants, and, therefore, the 6 constants of the harmonic potential energy function have been determined. The results are given in Table II. The notation is the same as that of Davis, Cleveland, and Meister.[23] The constants in Table II are transferable to partially deuterated molecules of the type XH_2D and XHD_2, the results for which will be reported elsewhere.

TABLE II. Potential energy constants for XY_3 type molecues.[a,b]

Constant	NH_3 and ND_3	PH_3 and PD_3	AsH_3 and AsD_3
f_h	6.94020	3.32847	2.68937
$f_h{}^h$	0.15970	0.05482	0.08280
$f_h{}^{hh}$	0.10303	−0.07341	0.35655
$f_h{}^{hh}$	0.23640	−0.00758	−0.49674
f_{hh}	0.62042	0.73330	0.92251
$f_{hh}{}^{hh}$	−0.05752	−0.02874	−0.12596

[a] Constants for bond stretchings, and interactions between stretchings, are in md/A; interactions between stretching and bending constants are in md/rad; and bendings, and interactions between bendings, are in md A/rad².

[b] The number of significant figures is necessary to obtain internal consistency in calculations.

ROTATIONAL DISTORTION CONSTANTS

Kivelson and Wilson,[17] and Wilson,[24] have given the methods of calculating the rotational distortion constants from the vibrational force constants for symmetric rotor molecules. Dowling, Gold, and Meister[25] have applied this method to some ZX_3Y type molecules of symmetry C_{3v}. In the present study, the derivatives $[J_{xx}{}^i]_0$, $[J_{zz}{}^i]_0$, and $[J_{xz}{}^i]_0$ of the moment of inertia tensor have been obtained with respect to the symmetry coordinates used. These expressions are in agreement with those given by Schatz.[26] The constants D_J, D_{JK}, and D_K for the molecules have been obtained using the relations given by Wilson.[24]

TABLE III. Rotational distortion constants for the XY_3 type molecules (Mcps).[a]

Molecule	D_J Calc.	D_J Obs.	$-D_{JK}$ Calc.	$-D_{JK}$ Obs.	D_K Calc.
NH_3	22.68	24.27[b]	41.19	43.65[b]	23.91
ND_3	5.67	5.85[b]	10.68	10.98[b]	6.36
PH_3	3.27	3.15[c]	3.76	...	3.55
PD_3	0.81	0.81[c]	0.90	−1.3[d]	0.86
AsH_3	2.24	2.13[c]	2.22	...	2.15
AsD_3	0.57	0.53[c]	0.20	...	0.17

[a] Calc. = calculated. Obs. = observed.
[b] Reference 20.
[c] Reference 27.
[d] Reference 28.

Table III compares the rotational distortion constants, calculated in the present investigation for the 6 molecules, with those of previous investigators. In the case of NH_3 and ND_3, the present values agree very closely with those given by Benedict and Plyler[20] from a rotational spectral analysis. For PH_3 and PD_3, the D_J values are in very good agreement with the results of Stroup, Oetjen, and Bell[27] and of Burrus *et al.*[28] For PD_3, the value of 1.3 Mcps for D_{JK} obtained by Burrus[29] from the microwave experiments does not seem reasonable, and it differs greatly from the present value which is negative. The values for D_J and D_{JK} for PH_3 reported by Slawsky and Dennison[9] seem rather high. For AsH_3 and AsD_3, the D_J values agree with those of Stroup *et al.*[27] No values have been reported in the literature for D_K and therefore no comparison is possible.

THERMODYNAMIC PROPERTIES

By using the molecular parameters and the harmonic vibrational wave numbers for the gaseous state given

[20] W. S. Benedict and E. K. Plyler, Can. J. Phys. **35**, 1235 (1957).
[21] G. Herzberg and L. Herzberg, *American Institute of Physics Handbook* (McGraw-Hill Book Company, Inc., New York, 1957), p. 7–148.
[22] G. Herzberg, *Raman and Infrared Spectra* (D. Van Nostrand Company, Inc., Princeton, New Jersey, 1945), p. 164.
[23] Davis, Cleveland, and Meister, J. Chem. Phys. **20**, 454 (1952).
[24] E. B. Wilson, Jr., J. Chem. Phys. **27**, 986 (1957).
[25] Dowling, Gold, and Meister, J. Mol. Spectroscopy **1**, 265 (1957).
[26] P. N. Schatz, J. Chem. Phys. **29**, 481 (1958).
[27] Stroup, Oetjen, and Bell, J. Opt. Soc. Am. **43**, 1096 (1953).
[28] Burrus, Jache, and Gordy, Phys. Rev. **95**, 706 (1954).
[29] C. A. Burrus, J. Chem. Phys. **28**, 427 (1958).

TABLE IV. Heat content $H°$, free energy $F°$, entropy $S°$, and heat capacity $C_p°$, for NH_3 and ND_3 for the ideal gaseous state at 1 atmos pressure.[a]

T (°K)	$(H°-E_0°)/T$		$-(F°-E_0°)/T$		$S°$		$C_p°$	
	NH_3	ND_3	NH_3	ND_3	NH_3	ND_3	NH_3	ND_3
100	7.95	7.95	29.23	31.71	37.18	39.66	7.95	7.95
200	7.95	7.99	34.74	37.22	42.69	45.21	8.01	8.19
273.16	7.99	8.11	37.22	39.73	45.21	47.84	8.23	8.74
298.16	8.02	8.17	37.92	40.44	45.94	48.61	8.35	8.97
300	8.02	8.18	37.97	40.49	45.99	48.67	8.36	8.99
400	8.18	8.50	40.30	42.88	48.48	51.38	8.97	9.99
500	8.41	8.90	42.15	44.82	50.56	53.72	9.70	10.99
600	8.69	9.33	43.71	46.48	52.40	55.81	10.43	11.92
700	8.98	9.76	45.07	47.95	54.05	57.71	11.13	12.78
800	9.30	10.19	46.29	49.28	55.58	59.47	11.81	13.57
900	9.61	10.61	47.40	50.51	57.01	61.12	12.45	14.28
1000	9.92	11.01	48.43	51.65	58.35	62.66	13.05	14.91

[a] T is the temperature in degrees Kelvin; the other quantities are in cal deg^{-1} $mole^{-1}$; and $E_0°$ is the energy of one mole of perfect gas at absolute zero temperature.

TABLE V. Heat content $H°$, free energy $F°$, entropy $S°$, and heat capacity $C_p°$, for PH_3 and PD_3 for the ideal gaseous state at 1 atmos pressure.[a]

T (°K)	$(H°-E_0°)/T$		$-(F°-E_0°)/T$		$S°$		$C_p°$	
	PH_3	PD_3	PH_3	PD_3	PH_3	PD_3	PH_3	PD_3
100	7.95	7.95	33.39	35.67	41.34	43.62	7.95	7.95
200	7.96	8.06	38.90	41.20	46.86	49.26	8.08	8.58
273.16	8.05	8.33	41.39	44.04	49.44	52.37	8.54	9.62
298.16	8.10	8.46	42.10	44.48	50.20	52.94	8.76	10.00
300	8.10	8.47	42.15	44.53	50.25	53.00	8.78	10.03
400	8.40	9.05	44.51	47.05	52.91	56.10	9.83	11.53
500	8.79	9.68	46.43	49.13	55.22	58.81	10.92	12.89
600	9.23	10.32	48.07	50.95	57.30	61.27	11.95	14.06
700	9.69	10.92	49.53	52.59	59.22	63.51	12.91	15.02
800	10.15	11.49	50.85	54.09	61.00	65.58	13.76	15.81
900	10.59	12.00	52.07	55.47	62.66	67.47	14.51	16.44
1000	11.02	12.47	53.21	56.76	64.23	69.23	15.16	16.95

[a] T is the temperature in degrees Kelvin; the other quantities are in cal deg^{-1} $mole^{-1}$; and $E_0°$ is the energy of one mole of perfect gas at absolute zero temperature.

TABLE VI. Heat content $H°$, free energy $F°$, entropy $S°$, and heat capacity $C_p°$, for AsH_3 and AsD_3 for the ideal gaseous state at 1 atmos pressure.[a]

T (°K)	$(H°-E_0°)/T$		$-(F°-E_0°)/T$		$S°$		$C_p°$	
	AsH_3	AsD_3	AsH_3	AsD_3	AsH_3	AsD_3	AsH_3	AsD_3
100	7.95	7.95	36.31	38.45	44.26	46.40	7.95	7.97
200	7.98	8.13	41.82	43.99	49.80	52.12	8.18	8.91
273.16	8.11	8.50	44.32	46.58	52.43	55.08	8.82	10.13
298.16	8.18	8.66	45.03	47.33	53.22	55.99	9.10	10.55
300	8.19	8.67	45.08	47.38	53.27	56.05	9.12	10.58
400	8.57	9.35	47.49	49.97	56.06	59.32	10.32	12.17
500	9.04	10.05	49.45	52.13	58.49	62.18	11.48	13.55
600	9.54	10.73	51.14	54.02	60.68	64.75	12.55	14.69
700	10.04	11.37	52.65	55.72	62.69	67.09	13.51	15.60
800	10.53	11.94	54.02	57.28	64.55	69.22	14.36	16.33
900	10.99	12.46	55.29	58.72	66.28	71.18	15.08	16.91
1000	11.43	12.93	56.47	60.05	67.90	72.98	15.69	17.36

[a] T is the temperature in degrees Kelvin; the other quantities are in cal deg^{-1} $mole^{-1}$; and $E_0°$ is the energy of one mole of perfect gas at absolute zero temperature.

in Table I, the molar thermodynamic properties, heat content, free energy, entropy, and heat capacity, have been calculated. The values are listed in Tables IV to VI for the various molecules. The calculations are for the ideal gaseous state at 1 atmos pressure for a rigid-rotor, harmonic-oscillator approximation.

Overstreet and Giauque[30] obtained 45.94±0.1 cal deg^{-1} mole^{-1} from thermal data and 45.91 cal deg^{-1} mole^{-1} from spectroscopic data for the entropy of NH_3 at 1 atmos pressure and 298.16°K. These agree well with the present value of 45.94 cal deg^{-1} mole^{-1}. Danze[31] obtained a slightly larger value of 46.44 cal deg^{-1} mole^{-1}.

Masi[32] has listed values of the heat capacity of NH_3 at 1 atmos pressure for temperatures between 300 and 600°K. These values average 0.36 cal deg^{-1} mole^{-1} higher than the present values.

For PH_3, Stevenson and Yost[33] had computed the heat content and free energies from 298.1°K to 1500°K and the entropy at 298°K only. The value of the entropy at 298°K is 50.20 cal deg^{-1} mole^{-1} (present value, 50.20 at 298.16°K) while the heat content and the free energy average 0.11 and 0.08 cal deg^{-1} mole^{-1}, respectively, higher than the present values. Altshuller[34] has given calculated values of the thermodynamic functions for PH_3. These values have been obtained by using the observed anharmonic wave numbers, and are slightly higher than the present values. The average of the differences are 0.12 cal deg^{-1} mole^{-1} for heat content, 0.03 for free energy, 0.15 for entropy, and 0.18 for heat capacity.

For AsH_3, Sherman and Giauque[35] have reported values of the thermodynamic properties, using the anharmonic wave numbers, between 100° and 500°K. These average higher than the present values by 0.02 cal deg^{-1} mole^{-1} for the heat content, 0.01 for the free energy, 0.03 for the entropy, and 0.09 for the heat capacity.

ACKNOWLEDGMENT

This work was aided by a grant from the National Science Foundation. The authors are thankful for this assistance.

[30] R. Overstreet and W. F. Giauque, J. Am. Chem. Soc. **59**, 254 (1937).
[31] J. Danze, Rev. universelle mines **13**, 3 (1937).
[32] J. F. Masi, Trans. Am. Soc. Mech. Engrs. **76**, 1067 (1954).
[33] D. D. Stevenson and D. M. Yost, J. Chem. Phys. **9**, 403 (1941).
[34] A. P. Altshuller, J. Am. Chem. Soc. **77**, 4220 (1955).
[35] R. H. Sherman and W. F. Giauque, J. Am. Chem. Soc. **77**, 2154 (1955).

Electron Spin Resonance of an Irradiated Single Crystal of Alanine: Second-Order Effects in Free Radical Resonances*

ICHIRO MIYAGAWA AND WALTER GORDY

Department of Physics, Duke University, Durham, North Carolina

(Received August 10, 1959)

The electron spin resonance of single crystals of *l*- and *d*-alanine has been observed at $T=300°K$ and analyzed for different orientations of the crystal in the magnetic field and at several microwave frequencies ranging from 9 kMc/sec to 34 kMc/sec. The stable free radical produced by the irradiation is proved to be of the form $CH_3\dot{C}HR$, where R is a group which has no nuclei with detectable coupling. The hydrogens of the CH_3 group of the radical are shown to have equivalent, isotropic coupling of 26 gauss each, essentially independent of the frequency of observation. This CH_3 group coupling is interpreted as arising from *s* orbital spin density of the hydrogens, via hyperconjugation. The hydrogen of the CH group has both an isotropic, Fermi term, $A_f=20$ gauss, arising from *s* orbital density on the hydrogen, and an anisotropic term $A_\mu=7$ gauss arising from dipole-dipole interaction of the proton moment with the electron spin density, ρ_C, on the carbon. Although the signs of A_f and A_μ could not be learned, they are shown to be of opposite sign. Hence the spin density is negative on either H or C. Principal values of the CH coupling are $A_1=7$ gauss, $A_2=A_3=27$ gauss. The value of ρ_C is shown to be 0.80 approximately. For certain orientations of the crystal the CH coupling becomes equal to the CH_3 coupling, and a quintet pattern is observed. Interesting second-order transitions are observed which for the [001] orientation become in the region of 24 kMc/sec as strong as the normal first-order transitions. A general theory is developed which accounts satisfactorily for these second-order effects which are probably of consequence in the electron spin resonance patterns of numerous other free radicals trapped within solids.

INTRODUCTION

NUMEROUS studies[1] have now been made of the x- and γ-irradiated organic and biochemical solids in the powdered or polycrystalline form. Although much useful information has been obtained and a few free radicals, including the important free ethyl and free methyl radicals,[2,3] have been identified with reasonable certainty from their resonance patterns, in most instances it has not been possible to identify the free radicals involved nor to explain their incompletely resolved resonance patterns. The difficulties of interpretation arise mostly from small anisotropies in the *g* factor and in the nuclear coupling terms which tend to scramble the structural patterns in the polycrystalline solids, also from second-order transitions, as will be shown in the present work, which produce confusing new components in the nuclear hyperfine structure.

Considerably more information can be obtained from the study of irradiated single crystals of organic solids provided that these can be prepared and their spin resonance analyzed. Because of the complexity of most organic crystals it seems unlikely that such analysis will be possible for many single crystals. We hope, however, that a complete analysis of a few of the simpler organic single crystals will improve the understanding and interpretation of the data obtained upon the more complex and often more important substances which can be studied only in the amorphous or powdered form.

Already we have made an analysis of the electron spin resonance of an irradiated single crystal of dimethylglyoxime,[4] which has only one molecule in the unit cell and in which the electron spin density of the free radical was found to be concentrated on a single nitrogen. For several reasons the spin resonance of a single crystal of alanine proved much more difficult to analyze than that of dimethylglyoxime. In alanine there are four molecules in unit cell, and the free radicals produced by the irradiation generally have four different orientations for a given orientation of the crystal in the magnetic field; there are four coupling hydrogens, one of which has different coupling from the other three; there are second-order transitions which give rise to confusing components at certain frequencies.

In this laboratory a single crystal of *l*-alanine was prepared, and an incomplete study made of its x-ray induced spin resonance.[5] An analysis of that incomplete preliminary data did not prove possible primarily because of the unrecognized second-order transitions which happen to be pronounced at the frequencies of the observation. Nevertheless, this study revealed the complicated nature of the superficially simple resonance pattern of the powdered form. It was the

* This research was supported by the U. S. Air Force through the Air Force Office of Scientific Research and Development Command and by the Office of Ordnance Research, Department of the Army. Reproduction in whole or in part is permitted for any purpose of the United States Government. A report of this work was given at the Washington Meeting of the American Physical Society, May, 1959.

[1] (a) Gordy, Ard, and Shields, Proc. Natl. Acad. Sci. U. S. **41**, 983 (1955); 996 (1955); see also the following reviews: (b) P. B. Sogo and B. M. Tolbert, Advances Biol. Med. Phys. **5**, 1 (1957); (c) D. J. E. Ingram, *Free Radicals as Studied by Electron Spin Resonance* (Butterworth's Scientific Publications, Ltd., London, 1958); (d) M. S. Matheson, "Radiation chemistry in rigid organic materials: the detection of intermediates," *Proceedings of the Second United Nations International Conference on the Peaceful Uses of Atomic Energy* (United Nations, Geneva, 1958), Vol. 29, p. 217.

[2] W. Gordy and C. G. McCormick, J. Am. Chem. Soc. **78**, 3243 (1956).

[3] B. Smaller and M. S. Matheson, J. Chem. Phys. **28**, 1169 (1958).

[4] I. Miyagawa and W. Gordy, J. Chem. Phys. **30**, 1590 (1959).

[5] van Roggen, van Roggen, and Gordy, Bull. Am. Phys. Soc. II **1**, 266 (1956).

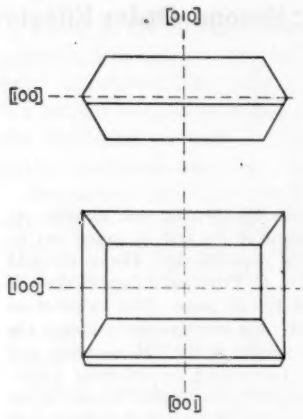

FIG. 1. The crystalline form and the crystallographic axes of *l*-alanine.

stimulus for the present, more comprehensive study which has cleared up most of the confusing details of the resonance and which has provided, we think, information useful to the understanding of the nature of other organic free radicals such as C_2H_5 produced by irradiation in powdered organic solids.

EXPERIMENTAL METHOD

The present measurements were made at various frequencies ranging from 9 kMc/sec (*X* band) to 34 kMc/sec (*J* band). Klystron sources and bolometer detectors were used for all frequencies. In all measurements a low-frequency magnetic modulation of the resonance was employed with a phase-lock-in detector and amplifier tuned to the second harmonic of the modulation frequency. This resulted in a detected signal which for the low-amplitude modulation employed was essentially the second derivative of the actual resonance contour. The signals were automatically recorded on curved coordinate graph paper with an Esterline-Angus recorder synchronized with the gradual variation of the magnetic field through the resonance. The patterns shown in the figures thus represent the second derivative of the absorption intensity as a function of the magnetic field at a fixed microwave frequency. For all curves shown, the magnetic field increases from left to right, and the arrows pointing downward indicate the field strength where the DPPH resonance with $g=2.0036$ would occur.

All resonances shown and those for which analysis was made were both irradiated and observed at room temperature. Some unpublished observations by H. Shields in this laboratory show that the resonance pattern of irradiated alanine is changed in a complex manner by the cooling of the irradiated sample to liquid air temperature. In the present study we made no attempt to analyze the lower temperature patterns. Air has no noticeable effect on the spin resonance of irradiated alanine. Hence, for convenience, we made our studies under normal atmospheric conditions.

Single crystals of both *d*- and *l*-alanine were prepared and, as was expected, were found to have the same spin resonance pattern when irradiated. The crystals were grown from aqueous solutions of alanine by slow evaporation of the water.

The irradiation was accomplished with a kilocurie cobalt-60 gamma ray source. The dosages ranges from 1 to 5 million *r*.

FIRST-ORDER ANALYSIS OF RESULTS

The single crystal of *d*- or *l*-alanine is orthorhombic. Figure 1 shows its crystalline form and indicates its crystal axes as described in the Baker Index of Crystals.[6] The symmetry of *d*-alanine, and certainly also *l*-alanine, is D_{2A}^4 $2_12_12_1$, and the unit cell contains four molecules.[7]

If the assumption is made that the free radicals formed by the irradiation have their magnetic axes fixed in space, the four molecules in unit cell should give rise to free radicals of four different orientations. This is found to be true. When, however, the magnetic field is parallel to one of the crystallographic axes (see Fig. 1), the four orientations are found to be magnetically equivalent. For other orientations they are generally unequivalent.

At *X* band (9 kMc/sec) and at *J* band (34 kMc/sec) where the second-order effects treated in the next section are not pronounced, the resonance patterns for the orientations of the magnetic field along the three

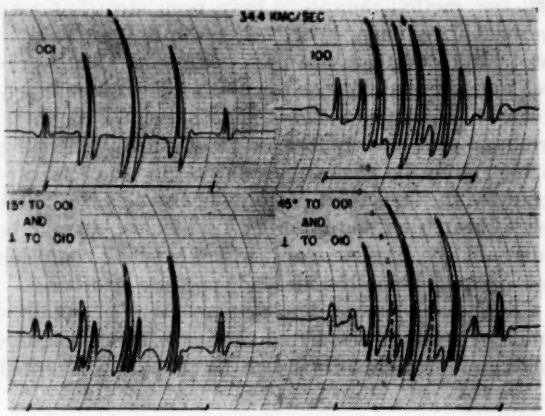

FIG. 2. Electron spin resonance curves for a gamma-irradiated single crystal of *l*-alanine at 34.4 kMc/sec for various orientations of the crystal in the magnetic field. The curved bars show the theoretical patterns to the first-order approximation. The theoretical patterns are based on the assumption that the four hydrogens have equivalent coupling with the imposed field along [001], that one of the hydrogens has different coupling from the other three for the [100] orientations, and that for the intermediate orientations, 15° and 45°, both these combinations are present, one of which is indicated by broken lines. The orientations of 15° and 45° are in the plane perpendicular to the [010] axis and are measured relative to the [001] axis. The arrows pointing downward indicate the position for $g=2.0036$. The horizontal straight line under each spectrum is the scale of 100 gauss.

[6] M. W. Porter and R. C. Spiller, *The Baker Index of Crystals* (W. Heffer and Sons, Cambridge, England, 1951), Vol. I, Pt. 2, 0.730.

[7] J. D. Bernal, Z. Krist **A78**, 363 (1931).

crystallographic axes are relatively simple and can be used to ascertain the form of the free radical. This fortunate simplification arises from the magnetic equivalence of the four radicals in unit cell for these three orientations.

Figures 2 and 3 show the resonance patterns obtained at 34 kMc/sec with the magnetic field imposed along each of the three crystallographic axes. They also show other patterns with orientations as indicated. The pattern for the [001] axis is, within the resolution obtainable, a quintet, as is expected for an electron spin with four equally coupling protons of 26 gauss per proton. The relative intensities are close to those expected for such a quintet, 1:4:6:4:1. For the orientations, [100] and [010], the resonance pattern is a quartet with a doublet substructure with intensity ratios of approximately 1:1:3:3:3:3:1:1. The observed patterns for these orientations can arise from three equivalently coupling hydrogen nuclei with coupling, ΔH, of 26 gauss and a fourth with coupling of 20 gauss. Figures 2 and 3 also give, for comparison, theoretical patterns calculated from first-order theory for the cases of four equivalently coupling hydrogens and for that of three equivalent and one different. The correspondence with the observed patterns is evident. Table I gives the component spacing for different orientations of the crystal and for different observation frequencies. Table II gives the g factor for the different orientations of H along the crystallographic axes measured by comparison with the DPPH powder with $g=2.0036$. The probable error is ± 0.0001. Thus the g factor is near that for the free electron spin, 2.0023, and almost, but not completely, isotropic. In the succeeding analysis we shall neglect the small anisotropy in g.

Figure 2 shows how the pattern changes from the quintet for the [001] orientation to the eight-line pattern for the [100] orientation with the rotation of the magnetic field. The absorption at an intermediate direction is of a superposition of two different patterns. This is expected because in those directions the four

TABLE I. The component spacings for the methyl group and the C—H group observed at different frequencies and in different orientations.

Direction	Microwave frequency (kMc/sec)	Spacing (gauss) Methyl	C—H
[001]	34.4	27.0	27.0
	24.3	25.5	25.5
	9.03	26.1	26.1
[100]	34.4	24.6	14.7
	24.3	23.5	14.1
	9.03	24.5	18.7
[010]	34.4	26.0	18.7
	24.3	24.9	16.7
	9.03	25.4	19.7

TABLE II. The g factor in different directions.

Direction	g factor[a]
[001]	2.0040
[100]	2.0047
[010]	2.0033

[a] The g factor of DPPH is assumed as 2.0036.

orientations in unit cell are grouped into two pairs, to each of which two magnetically equivalent configurations belong. One of the two patterns is practically a quintet at a direction as far as 60° from the [001] axis. This is amazing but is justified by the calculation with the matrix elements which will be given later (Table IV). The spectrum for the [110] direction likewise contains both these patterns (Fig. 3).

From the observed patterns for the [100] and [001] orientations and from a consideration of the structure of the alanine molecule, we are justified in assuming that the free radical observed in irradiated alanine is of the form

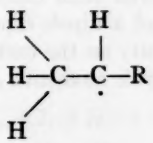

where R is the group which has no noticeable coupling. Thus we must conclude that the close equivalence of the coupling of the four proton spins with the electron spin for the [001] orientation is an accident. This interesting accident, combined with the scrambling of the substructure by slight anisotropy in the g factor and by anisotropy in the coupling for the CH hydrogen, makes the pattern observed for the powder appear to be a quintet arising from four equivalent protons. This led to an incorrect surmise[1(a)] that the radical might be the symmetrical one $(C_2H_4)^+$. Later, however, it was concluded from measurements on alanyl peptides[8] in powdered form that the apparent equivalence must be an accident and that the free radical is probably of the form given above.

It was earlier pointed out that the nuclear coupling of the end or CH_3 hydrogens must arise from hyperconjugation[8] which in valence bond language is described by contributing structures of the form

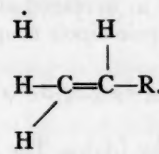

No mechanism was proposed for the —CH group

[8] C. G. McCormick and W. Gordy, J. Phys. Chem. **62**, 783 (1958); see also H. Shields and W. Gordy, *ibid.* **62**, 789 (1958).

coupling, but it was assumed to be equivalent to that for each CH of the free methyl radical, for which the coupling mechanisms have been discussed by Karplus.[9] Since the coupling per H in the free methyl radical is observed[2,3] to be 25 gauss, this assumption agrees with the apparently equal couplings observed for the CH_3 and CH hydrogens in the above radical and also for the CH_3 and CH_2 in the free ethyl radical. Nevertheless, it seems probable that the coupling of 25 gauss per proton observed in the free methyl radical is mostly isotropic since the radicals are likely tumbling under the conditions of observation. The present experiment, on the other hand, shows that the $CH_3\dot{C}HR$ radical is not tumbling freely and that the CH group has a significant anisotropic dipole-dipole coupling term.

Since the couplings of the CH_3 protons in the CH_3CHR radical are equivalent and isotropic and must occur via a Fermi type interaction from spin density in the s orbitals of the hydrogens, these interactions can be represented in the spin Hamiltonian by $\Sigma(A_{zz}I_z)_{CH_3}$, where the summation is taken over the three equivalent hydrogens. The CH hydrogen has both an isotropic Fermi term caused by a slight spin density on the H and a dipole-dipole term caused by appreciable spin density on the carbon. Classically, the interaction of two dipole moments, μ_1 and μ_2, separated by a distance r is

$$\frac{\mu_1\cdot\mu_2}{r^3}-\frac{3(\mu_1\cdot\mathbf{r})(\mu_2\cdot\mathbf{r})}{r^5}.$$

In this first-order treatment we assume quantization of both S and I along the field, or z axis. The effective electron spin and nuclear moments along z are $-g_s\beta S_z$ and $g_I\beta_I I_z$ where g_s is the g factor of the electron spin, β is the Bohr magneton, g_I is the nuclear g factor of hydrogen, β_I is the nuclear magneton, and I is the nuclear spin. For simplicity we assume that the effective spin density on the CH carbon can be represented by a density ρ_C located on the CH bond axis. We can then express the above dipole-dipole term as

$$\frac{\rho_C g_s\beta g_I\beta_I}{\langle r^3\rangle_{Av}}(3\cos^2\theta-1)S_zI_z,$$

where θ is the angle between the CH bond axis and the applied magnetic field H, and $\langle r^3\rangle_{Av}$ is the effective separation of ρ_C and μ_I averaged along the bond axis. We designate this dipole-dipole coupling constant as

$$(A_\mu)_{CH}=\rho_C g_s\beta g_I\beta_I/\langle r^3\rangle_{Av}, \quad (1)$$

and the Fermi part by $(A_f)_{CH}$. The Fermi term is

$$(A_f)_{CH}=16\pi\beta\beta_I g_I(\phi_0^*\phi_0)\rho_{CH}/3. \quad (2)$$

[9] M. Karplus, J. Chem. Phys. **30**, 15 (1959).

where ρ_{CH} is the s electron spin density on the hydrogen of the CH. Likewise, we designate the Fermi coupling constant of the CH_3 protons by $(A_f)_{CH_3}$. With these simplifications the spin Hamiltonian can be written

$$\mathcal{H}=\{g_s\beta H+\Sigma(A_fI_z)_{CH_3}+[A_fI_z+A_\mu(3\cos^2\theta-1)I_z]_{CH}\}S_z. \quad (3)$$

The energy eigenvalues are thus

$$W=\{g_s\beta H+\Sigma(A_fM_I)_{CH_3}+[A_fM_I+A_\mu(3\cos^2\theta-1)M_I]_{CH}\}M_s. \quad (4)$$

With the observation frequency held constant, the resonant values of the magnetic field are

$$H=H_0-(A_f)_{CH_3}(\pm\tfrac{1}{2}\pm\tfrac{1}{2}\pm\tfrac{1}{2})\mp\tfrac{1}{2}\{(A_f)_{CH}+(A_\mu)_{CH}(3\cos^2\theta-1)\}, \quad (5)$$

where $H_0=h\nu_0/g_s\beta$ and the coupling constants are measured in magnetic field units, in gauss. In this expression all possible combinations of the plus and minus signs are taken.

SECOND-ORDER EFFECTS

The first-order treatment in the previous section which gives approximate agreement in the J- or X-band region is completely inadequate to explain the spectrum observed in the intermediate K-band region. In the K-band region second-order transitions of intensity comparable to the normal first-order ones are observed. These first-order forbidden transitions also give rise to detectable components in the X- or J-band regions, but they are of much lower intensity there than in the K-band region.

Although these second-order transitions, so far as we know, are detected and analyzed here for the first time in hydrocarbon free radicals, they are probably of general occurrence in free radicals within solids, particularly in the aliphatic-type radicals produced by irradiation of solids. They are unquestionably important in determining the structure of the electron spin resonance of the free ethyl radical, $\cdot CH_2CH_3$, in rigid lattices where it is not free to tumble and of the $-CH_2-\dot{C}H-CH_2-$ radical believed to be observed in irradiated polyethylene and other polymers.[1(a)] The effects arise from the anisotropic dipole-dipole coupling of the CH group, which gives rise to off-diagonal elements, combined with the comparable magnitude of the nuclear paramagnetic term $-g_I\beta_I\mathbf{I}\cdot\mathbf{H}$. A somewhat related phenomenon has been observed by Zeldes and Livingston[10] in the spin resonance of trapped atomic hydrogen and has been treated theoretically by Trammell, Zeldes, and Livingston.[11]

[10] H. Zeldes and R. Livingston, Phys. Rev. **96**, 1702 (1954).
[11] Trammell, Zeldes, and Livingston, Phys. Rev. **110**, 630 (1958).

As discussed in the first-order treatment, only the CH group of the CH_3—CH—R radical has a significant anisotropic coupling. Thus we can for simplicity ignore the CH_3 (which simply can be added to the result, as in the above treatment) and can treat here only the CH coupling.

The spin Hamiltonian which described the CH interaction is expressed adequately by

$$\mathcal{H}=g_s\beta HS_z+(A_{zz}I_z+A_{zz}I_x+A_{zy}I_y)S_z-g_I\beta_I HI_z, \quad (6)$$

in which the last term represents the direct interaction of the CH hydrogen nucleus with the field, and the elements $(A_{zz}I_z+A_{zy}I_y)S_z$ represent the important off-diagonal elements. The contribution of such terms as $A_{xy}I_yS_x$ are negligibly small, and to this approximation the Hamiltonian commutes with S_z

$$[\mathcal{H}, S_z]=0.$$

The expectation values of $\mathcal{H}$ for the electronic spin state are therefore

$$\mathcal{H}(\pm)=\pm\tfrac{1}{2}\{g_s\beta H+(A_{zz}\mp 2g_I\beta_I H)I_z+A_{zz}I_x+A_{zy}I_y\},$$

where the plus sign corresponds to the upper state with $M_s=\frac{1}{2}$ and the minus sign to the ground state with $M_s=-\frac{1}{2}$. The $\mathcal{H}(+)$ and $\mathcal{H}(-)$ are still operators with regard to nuclear spin. The nonvanishing matrix elements of $\mathcal{H}(+)$ with $I=\frac{1}{2}$ and $M_I=\pm\frac{1}{2}$ for hydrogen are:

$$\langle\tfrac{1}{2}\,|\,\mathcal{H}(+)\,|\,\tfrac{1}{2}\rangle=\tfrac{1}{2}(g_s\beta H)+\tfrac{1}{4}A_{zz}-\tfrac{1}{2}(g_I\beta_I H)$$

$$\langle-\tfrac{1}{2}\,|\,\mathcal{H}(+)\,|\,-\tfrac{1}{2}\rangle=\tfrac{1}{2}(g_s\beta H)-\tfrac{1}{4}A_{zz}+\tfrac{1}{2}(g_I\beta_I H)$$

$$\langle\tfrac{1}{2}\,|\,\mathcal{H}(+)\,|\,-\tfrac{1}{2}\rangle=\tfrac{1}{4}(A_{zz}-iA_{zy})$$

$$\langle-\tfrac{1}{2}\,|\,\mathcal{H}(+)\,|\,\tfrac{1}{2}\rangle=\tfrac{1}{4}(A_{zz}+iA_{zy}).$$

The secular equation which gives the energy eigenvalues of $\mathcal{H}(+)$ for the upper state $(M_s=\frac{1}{2})$ is

M_1	$\frac{1}{2}$	$-\frac{1}{2}$
$\frac{1}{2}$	$\frac{1}{2}(g_s\beta H)+\frac{1}{4}A_{zz}$ $-\frac{1}{2}(g_I\beta_I H)-W$	$\frac{1}{4}(A_{zz}-iA_{zy})$
$-\frac{1}{2}$	$\frac{1}{4}(A_{zy}+iA_{zy})$	$\frac{1}{2}(g_s\beta H)-\frac{1}{4}A_{zz}$ $+\frac{1}{2}(g_I\beta_I H)-W$

or

$$[W-\tfrac{1}{2}(g_s\beta H)-\tfrac{1}{4}A_{zz}+\tfrac{1}{2}(g_I\beta_I H)]$$

$$\cdot[W-\tfrac{1}{2}(g_s\beta H)+\tfrac{1}{4}A_{zz}-\tfrac{1}{2}(g_I\beta_I H)]=(A_{zz}^2+A_{zy}^2)/16.$$

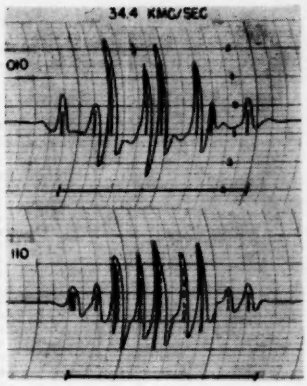

FIG. 3. Absorption curves similar to Fig. 2 at 34.4 kMc/sec but for the imposed magnetic field along the [010] and the [110] directions. The [110] direction is perpendicular to the [001] axis and 45° from the [010] and the [100] axes.

The levels are

$$W_{\frac{1}{2}}(\pm)=\tfrac{1}{2}(g_s\beta H)\pm\tfrac{1}{4}\{(A_{zz}-2g_I\beta_I H)^2+(A_{zz}^2+A_{zy}^2)\}^{\frac{1}{2}}. \quad (8)$$

Similarly it is shown that the lower levels $(M_s=-\frac{1}{2}$ state) are given by

$$W_{-\frac{1}{2}}(\pm)=\tfrac{1}{2}(g_s\beta H)$$

$$\pm\tfrac{1}{4}\{(A_{zz}+2g_I\beta_I H)^2+(A_{zz}^2+A_{zy}^2)\}^{\frac{1}{2}}. \quad (9)$$

We label the bracketed term by

$$A_\pm=\{(A_{zz}\pm 2g_I\beta_I H)^2+c^2\}^{\frac{1}{2}}, \quad (10)$$

$$c^2=(A_{zz}^2+A_{zy}^2). \quad (11)$$

The four levels are then more conveniently expressed by

$$W_{\frac{1}{2}}(\pm)=\tfrac{1}{2}(g_s\beta H)\pm\tfrac{1}{4}A_-, \quad (12)$$

$$W_{-\frac{1}{2}}(\pm)=-\tfrac{1}{2}(g_s\beta H)\pm\tfrac{1}{4}A_+. \quad (13)$$

The energy levels are shown, but not to scale, with the possible transitions indicated in Fig. 4. Transitions indicated by the solid arrows give rise to frequencies

$$h\nu_1=g\beta H+\tfrac{1}{4}(A_++A_-),$$

$$h\nu_2=g\beta H-\tfrac{1}{4}(A_++A_-),$$

or to a doublet of spacing in magnetic field units

$$d_+=(A_++A_-)/2g\beta. \quad (14)$$

Similarly, the transitions indicated by the broken arrows give rise to a doublet of spacing

$$d_-=(A_+-A_-)/2g\beta. \quad (15)$$

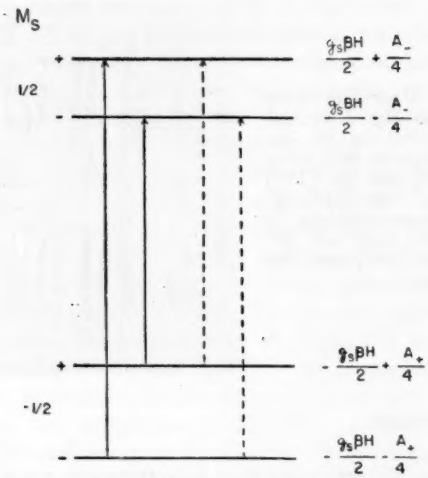

FIG. 4. The energy diagram for the system with $S=1/2$ and $I=1/2$, the Hamiltonian of which includes nondiagonal, nuclear hyperfine terms and the nuclear paramagnetic term. The vertical lines show the possible transitions in the microwave region. The transitions shown by solid lines give a doublet with spacing d_+, and the transition shown by broken lines gives another doublet with spacing d_-.

The foregoing treatment shows that the $M_I=+\frac{1}{2}$ and $M_I=-\frac{1}{2}$ states are intermixed. Thus the normal selection rules restricting changes in M_I do not apply. The actual nuclear substates can be represented as a linear combination of $M_I=\pm\frac{1}{2}$ states with wave functions,

$$\left.\begin{aligned}
&\psi_{\frac{1}{2}}(+)=l_{\frac{1}{2}}I(+\tfrac{1}{2})+m_{\frac{1}{2}}I(-\tfrac{1}{2}) \quad \text{for} \quad \tfrac{1}{2}(g_s\beta H)+\tfrac{1}{4}A_-\\
&\psi_{\frac{1}{2}}(-)=m_{\frac{1}{2}}{}^*I(+\tfrac{1}{2})-l_{\frac{1}{2}}{}^*I(-\tfrac{1}{2}) \quad \text{for} \quad \tfrac{1}{2}(g_s\beta H)-\tfrac{1}{4}A_-\\
&\psi_{-\frac{1}{2}}(+)=l_{-\frac{1}{2}}I(+\tfrac{1}{2})+m_{-\frac{1}{2}}I(-\tfrac{1}{2}) \quad \text{for} \quad \tfrac{1}{2}(-g_s\beta H)+\tfrac{1}{4}A_+\\
&\psi_{-\frac{1}{2}}(-)=m_{-\frac{1}{2}}{}^*I(+\tfrac{1}{2})-l_{-\frac{1}{2}}{}^*I(-\tfrac{1}{2}) \quad \text{for} \quad \tfrac{1}{2}(-g_s\beta H)-\tfrac{1}{4}A_+
\end{aligned}\right\}, \tag{16}$$

where

$$\left.\begin{aligned}
l_{\frac{1}{2}}/m_{\frac{1}{2}}&=(A_{zz}+A_--2g_I\beta_IH)/(A_{xz}+iA_{zy})\\
l_{-\frac{1}{2}}/m_{-\frac{1}{2}}&=(A_{zz}-iA_{zy})/(A_{zz}+A_++2g_I\beta_IH)
\end{aligned}\right\}. \tag{17}$$

The transition probability is proportional to

$$\langle\tfrac{1}{2}\,|\,S_x+iS_y\,|\,-\tfrac{1}{2}\rangle|^2\,|\,\psi_{\frac{1}{2}}{}^*(\pm)\psi_{-\frac{1}{2}}(\pm)\,|^2.$$

The intensity ratio of the two doublets, the d_- and the d_+, is given by

$$a=\frac{(\text{Int.})_-}{(\text{Int.})_+}=\frac{|\psi_{\frac{1}{2}}{}^*(+)\psi_{-\frac{1}{2}}(+)\,|^2}{|\psi_{\frac{1}{2}}{}^*(+)\psi_{-\frac{1}{2}}(-)\,|^2}=\frac{|\psi_{\frac{1}{2}}{}^*(-)\psi_{-\frac{1}{2}}(-)\,|^2}{|\psi_{\frac{1}{2}}{}^*(-)\psi_{-\frac{1}{2}}(+)\,|^2}$$

$$=\frac{c^2(A_+-A_-+4g_I\beta_IH)^2}{\{(A_{zz}+A_--2g_I\beta_IH)(A_{zz}+A_++2g_I\beta_IH)+c^2\}^2}. \tag{18}$$

We define normalized intensities of the d_+ and d_- doublets by:

$$\left.\begin{aligned}
I_{d+}&=1/(1+a)\\
I_{d-}&=1-I_{d+}
\end{aligned}\right\}. \tag{19}$$

Figure 5 shows the doublet spacings (or d_+/A_{zz} and d_-/A_{zz}) plotted as a function of $\log(2g_I\beta_IH/A_{zz})$ for various values of $c^2/A_{zz}{}^2$. Figure 6 gives similar plots of the relative intensities I_{d+} and I_{d-}. They give a general impression of what to expect of second-order effects of this kind, and they will be useful in the analysis of other cases. It is interesting in Fig. 6 that the intensity of the second-order transition is the same as that of the first-order transition at a certain magnetic field which is approximately $A_{zz}/(2g_I\beta_I)$. Table III shows the spacings and the intensities for extreme cases, $H=0$, $H\to\infty$ and $c^2=0$. For all the listed cases, only the first-order transition ($\Delta M_I=0$) is allowed, and the second-order transition ($\Delta M_I=\pm1$) is completely forbidden. The second-order transition is detectable only if both of the two conditions, $c^2=A_{xz}{}^2+A_{zy}{}^2\neq0$ and $H\simeq A_{zz}/(2g_I\beta_I)$, are realized.

With the assumption that the CH_3 group gives rise to a symmetrical quartet upon which the CH effects are superimposed, the d_- and d_+ for the CH group can be obtained directly from the resonance curves. The values of A_- and A_+ can then be computed from equations (14) and (15). With A_- and A_+ and the known value of $2g_I\beta_IH$ for the applied H, A_{zz} and c^2 can be

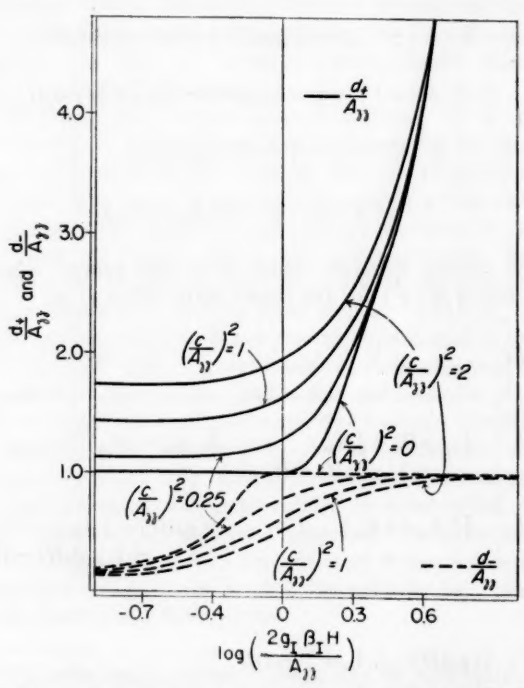

FIG. 5. The values of d_+/A_{zz} and d_-/A_{zz} plotted as a function of $\log(2g_I\beta_IH/A_{zz})$ for different values of $(c/A_{zz})^2$.

TABLE III. The spacings of the doublet, d_+ and d_-, for extreme cases. The numbers in brackets show relative intensities.[a]

Magnetic field (H)	$c^2=A_{xz}^2+A_{xy}^2$	Transition $\Delta M_I=0$[b]	Transition $\Delta M_I=\pm1$[b]
0	$\neq0$	$d_+=(A_{zz}^2+A_{xz}^2+A_{xy}^2)^{\frac{1}{2}}$, (1)	$d_-=0$, (0)
∞	$\neq0$	$d_-=A_{zz}$, (1)	$d_+\to\infty$, (0)
$<A_{zz}/(2g_I\beta_I)$	0	$d_+=A_{zz}$, (1)	$d_-=2g_I\beta_IH$, (0)
$>A_{zz}/(2g_I\beta_I)$	0	$d_-=A_{zz}$, (1)	$d_+=2g_I\beta_IH$, (0)

[a] They are the same as Id_+ and Id_-.
[b] Those notations are correct for the extreme cases in this table.

obtained from Eq. (10). The values thus obtained for A_{zz} and c^2 for the three crystallographic axes [001], [100], and [010] give the values and the directions of the principal elements of the (A) tensor which are listed in Table IV. Table V shows d_+ and d_- and their relative intensities, I_{d+} and I_{d-}, calculated with the above principal elements at various directions and at various frequencies. It is seen from Table V that for the [001] axis the d_+ doublet predominates in intensity in the X-band region, 9 kMc/sec, and the d_- doublet predominates in the J-band region, 34 kMc/sec. In the K-band region, near 24 kMc/sec, the intensities of the two become equal.

Figures 7–9 show a comparison of the calculated and observed patterns for the three frequencies and for the imposed magnetic field along the [001], the [100], and the [010] axes. The agreement is seen to be good. However, to make the interpretation more convincing, we give the sequence of curves in Fig. 10 in the K-band region, where the intensity reversal of the d_+ and d_- doublets occurs and where the relative intensity varies rapidly with frequency.

The signs of the principal values of (A) in Table IV could not be determined in the present experiment, but the three of them must have the same sign. If this were not true, the spacing of the CH doublet would be zero in certain directions, in disagreement with our observations.

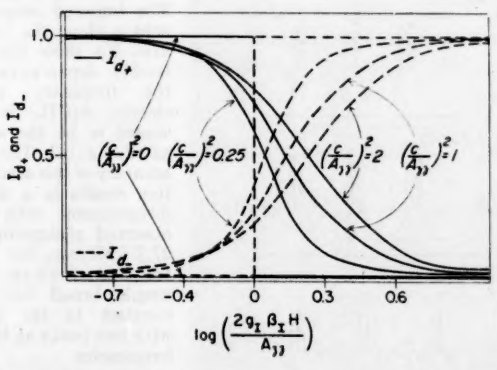

FIG. 6. The relative intensities, I_{d+} and I_{d-}, of the doublets d_+ and d_- plotted as a function of $\log(2g_I\beta_IH/A_{zz})$ for different values of $(c/A_{zz})^2$.

Since two of the principal values listed for A are equal, an axially symmetric coupling is indicated. Presumably this axis of symmetry is the CH bond. Strictly, however, A is probably not axially symmetric.

From the principal values of A one can obtain the values of the Fermi (A_f) and dipole-dipole (A_μ) coupling constants. Assuming an axis of symmetry in the coupling as indicated, one can write (see first-order treatment)

$$A=A_f+A_\mu(3\cos^2\theta-1),$$

where θ is the angle between the axis of symmetry (axis of A_1) and the applied field. Thus with $\theta=0$ and 90° we obtain

$$A_1=A_f+2A_\mu=\pm7 \text{ gauss},$$

$$A_2=A_3=A_f-A_\mu=\pm27 \text{ gauss}.$$

For reasons already given, we must take the signs both plus or both minus. Thus we obtain

$$A_f=\pm20 \text{ gauss},$$

$$A_\mu=\mp7 \text{ gauss},$$

where the plus and minus signs must be taken together. Although we cannot obtain the signs of A_f and A_μ individually, we find that they must be of opposite sign.

The origin of A_μ is the classical interaction between the proton magnetic moment and the electron spin

TABLE IV. The values and the directions of the principal elements of the nuclear coupling constant (A) for the C—H group.

Principal element	Value (gauss)	Direction[a] l	m	n
A_1	7	0.141	0.748	0.648
A_2	27		$\perp A_1$	
A_3	27		$\perp A_1$	

[a] The l, m, and n show the direction cosines in regard to [001], [100], and [010] axes, respectively. Actually, the A_1 axis can sssume the four different directions, (l, m, n), ($-l$, m, n), (l, $-m$, n), and (l, m, $-n$) because the crystal is orthorhombic and the unit cell contains four molecules.

TABLE V. The spacings of the doublets, d_+ and d_-, and their intensities, I_{d+} and I_{d-}, for the C—H group, calculated with the constants listed in Table IV. The number in the bracket shows observed value.

Direction	Microwave frequency (kMc/sec)	d_+ (gauss)	I_{d+}	d_- (gauss)	I_{d-}
[001]	34.4	37.5	0.027	26.5	0.973
	24.3	28.0	0.562	25.2	0.438
	9.03	26.8	0.998	9.7	0.002
[100]	34.4	38.8	0.094	15.2(14.7)[a]	0.906
	24.3	29.0	0.222	14.5(14.1)[a]	0.778
	9.03	19.6(18.7)[a]	0.897	8.0	0.103
[010]	34.4	38.9	0.108	17.8(18.7)[a]	0.892
	24.3	29.4	0.282	16.8(16.7)[a]	0.718
	9.03	21.7(19.7)[a]	0.937	8.4	0.063

[a] Those vlaues are the same as the component spacings for the C—H group listed in Table I.

density on the adjacent carbon atom. Possible contributions of hydrogen $2p$ electron spin density on the H would be too small to account for any significant part of A_μ, since the $2p$ orbital density would give an A_μ of only 3.2 gauss. Hence, the unlike signs of A_μ and A_f show that the electron spin density must be negative either on the carbon or on the hydrogen. The existence of negative spin density has been theoretically predicted by McConnell and Chesnut.[12] They also proposed that the Fermi coupling of a proton is proportional to the electron spin density on the carbon to which it is bonded, as

$$A_f = \rho_C Q,$$

where ρ_C is the spin density on the adjacent carbon and Q is the proportionality constant, which obviously is the Fermi coupling for $\rho_C = 1$. The Q is evaluated from

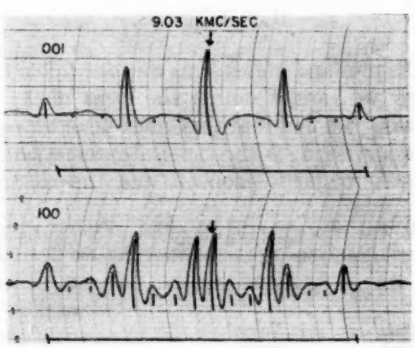

FIG. 7. The calculated and observed spectra at 9.03 kMc/sec for the imposed magnetic field along the [001] axis and the [100] axis. The calculations include the second-order effects and were done with the principal elements listed in Table IV. The horizontal line under each spectrum is the scale for 100 gauss.

[12] H. M. McConnell and D. B. Chesnut, J. Chem. Phys. **27**, 984 (1957); *ibid.* **28**, 107 (1958).

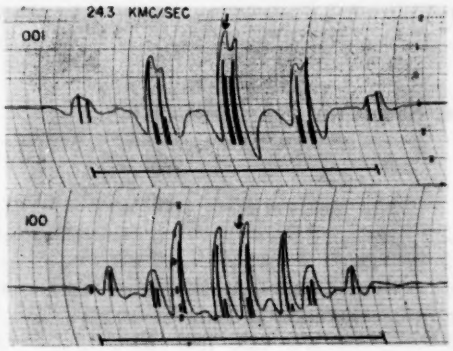

FIG. 8. The calculated and observed spectra similar to Fig. 7, but at 24.3 kMc/sec. The second-order effects are pronounced for the [001] orientation at this frequency.

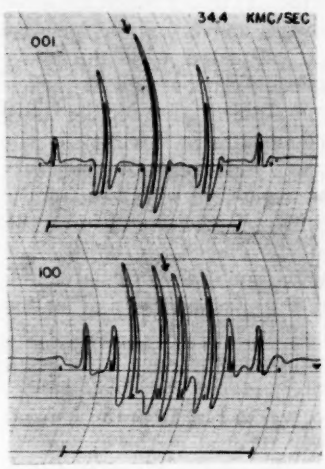

FIG. 9. The calculated and observed spectra similar to Fig. 7, but at 34.4 kMc/sec. The second-order transitions indicated by the short bars are extremely weak at this frequency.

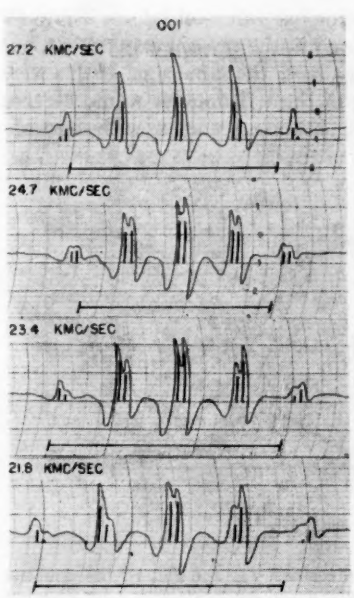

FIG. 10. The calculated and observed spectra for different frequencies in the K-band region where the second-order effects are strong and frequency-sensitive. The imposed magnetic field is along the [001] axis. To show the intensity dependence on the frequency more clearly, $A(CH_3)$ is assumed to be the same as $(d_+ + d_-)/2$. The inaccuracy of this assumption results in a slight disagreement with the observed absorption at 27.2 kMc/sec, the central line of which is a simple broad line, in contrast to the lines with two peaks at lower frequencies.

the coupling of the free methyl radical which has $\rho_C \approx 1$ and which is thought to be tumbling sufficiently in solids to average out the contribution from A_μ and to leave the observed coupling as due only to A_f. The value for the coupling in the free methyl radical as observed in this laboratory in various solids is near 25 gauss. We choose 25 gauss for Q, and with $A_f = 20$ gauss we obtain

$$|\rho_C| = |A_f/Q| = 0.80$$

for the spin density on the CH carbon of the present radical. This value is in satisfactory agreement with the interpretation that there must be a spin density of 0.05 on each of the CH_3 hydrogens, or a total of 0.15, to account for the CH_3 coupling of 26 gauss per proton through hyperconjugation and to leave a residual spin density of 0.85 for the CH and R groups combined. Consistency in the two results would require that the spin density on the R group be small.

We can also estimate, but in a much more questionable manner, a value of ρ_C from A_μ. If we assume the total spin density to be at the center of the carbon atom and hence 1.10 Angstroms from the hydrogen nucleus, we obtain a value of only 0.33 for ρ_C from the $A_\mu = 7$ gauss. This, however, is certainly not a realistic assumption. The electron spin density on the carbon must be in a nearly pure p orbital which projects out at right angles to the bond with the lobes centered approximately at a distance of the carbon covalent radius from the carbon nucleus. If we assume an effective ρ_C at a distance of 0.60 A from the carbon and on a line at right angles to the CH bond, a value of $\rho_C = 0.75$ is obtained from A_μ, in good agreement with the values obtained from A_f or form the CH_3 coupling. The reasonable assumption that the ρ_C is concentrated off the CH bond axis increases the value of ρ_C both because of the larger $\langle r^3 \rangle$ and because of the angular dependence of the coupling. To obtain the correct ρ_C from A_μ one must average over the electronic orbital which ρ_C occupies.[13] However, the accuracy of the value of A_μ and our knowledge of the orbital do not justify this procedure.

We wish to thank Arend von Roggen, C. G. McCormick, and Howard Shields for making some preliminary observations on the alanine crystal.

[13] H. M. McConnell and John Strathdee, Mol. Phys. **2**, 129 (1959).

Paramagnetic Resonance in Charred Dextrose*

R. C. PASTOR AND R. H. HOSKINS

Research Laboratories, Hughes Aircraft Company, Culver City, California

(Received July 24, 1959)

The magnetic-resonance properties of charred dextrose outgassed in high vacuum were studied. Line-width measurements in conjunction with elementary analyses for two series of chars provide some evidence of the effect of cyclization on the observed widths. Low-temperature measurements of T_1 (*c-w* and direct pulse) have provided a better understanding of the nature of the distribution and saturation behavior of the spin systems.

I. INTRODUCTION

THE magnetic properties of chars, especially of sugar chars, and of other carbonaceous solids have been studied in order to understand the pyrolytic processes and the gradual transition of the carbon-rich material to graphite. It should be noted that these systems are unique in that, under controlled pyrolysis, wide ranges of relaxation times T_1, T_2 and of spin density N are available. However, it is found that these parameters are not completely independent of one another. We submit here the results of studies (at X band) of the magnetic properties of high-vacuum chars which, it is felt, may be of use to other workers in the field in understanding further the pyrolytic processes.†

II. PREPARATION OF SAMPLES

The char samples were prepared from anhydrous dextrose (Mallinckrodt, analytical grade). The first stage (initial charring) in the pyrolysis consisted in gradually heating the dextrose; a minimum of two days was required in order to reach 200°C. The sample was kept at this temperature for about two or three days after which tarry materials ceased to distill over. Throughout the initial charring, the batch was constantly flushed with 99% pure N_2 (Series 1 chars), or with O_2 (Series 2 chars).

In the second stage of the pyrolysis, N_2 was the flush gas used. The batch was gradually heated in increments of about 10°C hr^{-1} to a higher temperature and was left at such temperature for at least 12 hours.[1] Under a steady flow of N_2, the batch was then cooled to room temperature. The material was removed from the furnace, ground in the open, and a portion bottled. The remaining material was returned to the furnace, flushed with N_2 for some time, gradually heated to the next higher temperature, and maintained at such temperature for 12 hours. The second-stage cycle was repeated until a series of bottled chars was obtained whose heat treatment spanned the temperature range of 250 to 590°C.

Each char sample was carefully funneled into a thin-walled, spherical bulb (Corning 707) formed at the end of a sample tube (see Fig. 1). The sample tubes were then connected to a vacuum manifold, the bulbs kept under liquid N_2, and the pressure reduced gradually. A two-day period of slow pumping, combined with the gradual recession of the coolant level, made it possible to obtain a pressure of 10^{-4} mm without causing any vigorous outgassing of the fine powder. This procedure left the capillary stem free of char particles, a condition necessary to ensure a vacuum-tight seal when the sample was sealed off the line. When the sample had warmed to room temperature and the line pressure was 10^{-6} mm, it was gradually outgassed at higher temperatures until a temperature was reached which was about 50°C less than that of the heat treatment used on the char in the second stage of the pyrolysis. Samples were processed in vacuum in the increasing order of heat-treatment temperature. About a week of degassing was needed before the pressure was less than or equal to 10^{-7} mm with the sample either hot or cold. This condition was taken to be the point of minimum outgassing, and the sample was sealed off the line.

Series 1 chars were used to study the effect of O_2 after the final heat treatment. Before sealing off the samples from the line, O_2 was admitted. Five minutes was allowed for equilibration at room temperature at a given pressure of O_2 before sealing.

III. RESULTS AND DISCUSSION

A. Line Width

The observed line widths of dextrose pyrolyzed and heat treated in a controlled atmosphere (or in a vacuum) have been shown to be a useful magnetic-resonance parameter for characterizing the resultant chars.[1] The study of line widths *vs* temperatures of heat treatment has provided a basis for classifying the stages of transition leading to the end product (graphite crystallites). The sensitive dependence of line widths on the concentration of adsorbed paramagnetic gases

* This work was supported in part by the U. S. Army Signal Corps.

† Magnetic resonance studies of chars for the past five years have been carried out by independent groups of investigators (J. Uebersfeld *et al.*, in France; D. J. E. Ingram *et al.*, in England; L. S. Singer *et al.*, in the United States; etc.). The authors would like to thank the referee for calling their attention to a recent book, *Free Radicals*, by D. J. E. Ingram (Academic Press, Inc., New York, 1958), which reviews the experimental and theoretical aspects of pyrolysis.

[1] Pastor, Weil, Brown, and Turkevich, Phys. Rev. **102**, 918 (1956).

for certain chars has opened up a new application of magnetic resonance to surface chemistry.

Line-width studies in polycrystalline materials involving polynuclear hydrocarbanions (negatively charged free radicals) show a correlation with the extent of delocalization of the π electrons in the parent hydrocarbon.[2] The extent of delocalization may be measured, roughly, in terms of the extent of cyclization. In Part 1 an attempt is made to show this correlation by employing oxygen to block the progress of cyclization in the course of char formation.

In Part 2, the use of high-vacuum chars has made it possible to obtain preliminary evidence on the effect of physically and chemically sorbed oxygen on line widths. This study also leads one to deduce a gross feature of the nature of distribution of the spins. This deduction is supported by the result of measurements of relaxation times (see Sec. III B).

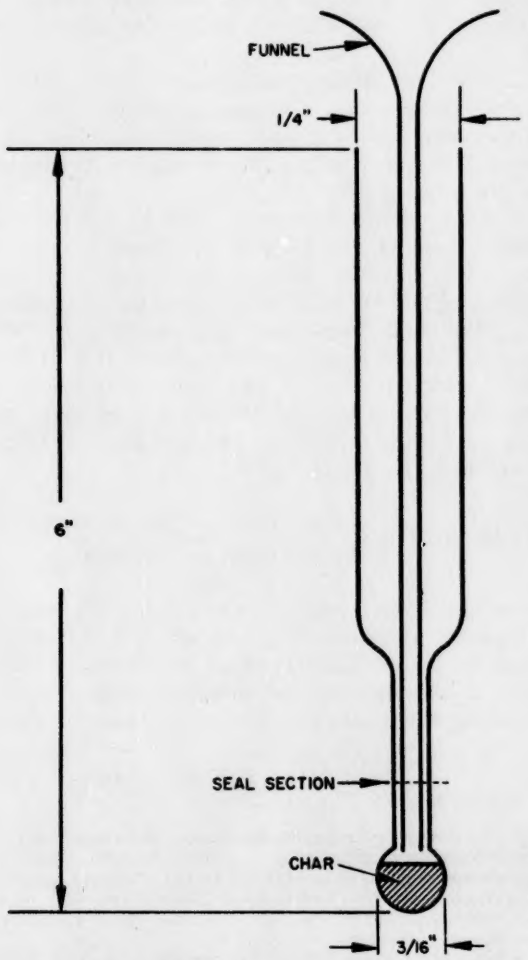

FIG. 1. Sample tube and funnel for introducing char.

[2] R. C. Pastor and J. Turkevich, J. Chem. Phys. **23**, 1731 (1955).

TABLE I. Line width measured at room temperature *vs* the temperature at which char was heat treated.

Pyrolytic temperature, °C	ΔH_{ms}, oersteds Series 1	Series 2	Region
250	6.4	...	
300	6.6	6.7	A
350	6.6	...	
400	6.6	5.8	
450	3.9	4.6	
500	2.5	2.9	
550	0.76	1.06	B
555	0.58	0.83	
560	0.41	0.73	
565	0.49	0.71	
575	0.55	0.67	C
590	0.63	0.66	

1. *Effect of* O_2 *before Final Heat Treatment*

The results of line-width (between maxima in the derivative display of resonance) measurements at room temperature are summarized in Table I.

The line widths (Series 1) observed at room temperature show three distinct regions in the pyrolysis:[3]

Region A:—$250°C \leq t_A \lesssim 400°$; the width is essentially constant.

Region B:—$400°C < t_B \lesssim 565°C$; the width decreases with increasing temperature, and at the upper temperature limit the observed width is about 20 times sharper than that in Region A.

Region C:—$t_C > 565°C$; the width increases with increasing temperature.

In Regions A and B, the spin density increases from about 5×10^{17} to 5×10^{20} cm^{-3}, while in Region C it is found that the integrated absorption steadily diminishes with increasing temperature, the electrons being paired in bonds during the process of extensive growth of the graphite crystallites. Although x-ray measurements indicate the presence of small, isolated, graphite-like structures in Region A, this stage of pyrolysis is characterized by the copious elimination of volatile matter. Considerable aromatization seems to be more characteristic of Region B.[4] It is also in this region that a marked decrease of resistivity[5] and an increase in adsorptive capacity[6] with increase in temperature are noticed.[7]

In Region A, Series 1 and 2 have about the same widths. Region B seems to start at a slightly lower py-

[3] Our results for the behavior of the normal char (Series 1) are in agreement with similar work reported earlier; see Reference 1.

[4] Gibson, Holohan, and Riley, J. Chem. Soc. **1946**, 456.

[5] Winslow, Baker, and Yager, J. Am. Chem. Soc. **77**, 4751 (1955).

[6] Pastor, Weil, Brown, and Turkevich, *Advances in Catalysis* **9**, 107–113 (1957).

[7] At the upper temperature limit of Region B, the char is known to manifest an optimum value of thermally activated adsorption (see reference 6). Thus, magnetic resonance lends support to the view that a mechanism of sorption makes use of free valencies, i.e., unpaired electrons.

TABLE II. Results of elementary analyses of chars.

Weight, %	Series 1 Chars 300°C	450°C	550°C	Series 2 Chars 300°C	450°C	550°C
Ash	0.13	0.00	0.00	0.09	0.02	0.07
C	80.63	86.57	93.38	71.47	75.43	92.33
H	3.35	3.10	2.79	3.27	4.19	2.54
N	0.09	0.04	0.12	0.18	0.19	0.30
O (By difference)	(15.8)	(10.3)	(3.7)	(25.0)	(20.2)	(4.8)
(mol C+mol O)/100g	7.71	7.86	8.01	7.52	7.55	7.99
(mol C)/(mol O)	6.8	11.2	33.7	3.8	5.0	25.6

rolytic temperature for Series 2. However, the decrease in width with increasing temperature is slower. It is seen that Series 2 gives absorptions which are broader than the corresponding ones in Series 1. The pyrolytic temperature at which the line width is a minimum is less defined in Series 2, and it would seem that in Region C this minimum is displaced toward higher temperatures. In Series 1, the temperature at which the line width is a minimum lies within 560±5°C.[8]

Comparison of the samples pyrolyzed at 300, 450, and 550°C shows that spin density is approximately the same in Series 1 and 2. This indicates that spin density depends mainly on pyrolytic temperature and that it is unaffected by the two conditions of preliminary charring.[9] It should be noted that in Region B, where width varies sensitively with temperature (by a factor of ten over a 100°C interval), there is almost a constant difference of 0.3 oersted between Series 1 and 2. As remarked previously, this is the region where aromatization in structure proceeds with a net increase in spin density with increase in temperature. (In Region C, extensive cyclization proceeds with a net decrease in spin density with increase in temperature.) In spin systems in which exchange is considerable, a correlation has been demonstrated between the decrease in width and the extent of ring condensation.[2] Thus, in comparing the two series at constant widths, one sees that Series 2 is displaced from Series 1 by about 25°C. It would seem then that the effect of the preliminary treatment with O_2 resulted in a less-pronounced aromatization. This blocking effect on cyclization suggests that preoxidation led to the appreciable incorporation of oxygen into the char; the oxygen most likely assumed positions which carbon would occupy in the normal chars (Series 1).[10] This view is supported by the results of elementary analysis[11] on the char samples, which is shown in Table II.

The following features of Table II should be noted:

1. In both series, the carbon content increases and the oxygen content decreases with increasing temperature of heat treatment. This is a known and expected feature.[12]

2. It is seen that preoxidation exerts a slight influence on the incorporation of nitrogen (flush gas), the relative amount increasing with temperature of heat treatment. This is of no interest, at present, since the amount in mol N is negligible.

3. From the last two rows in Table II, it is seen that (mol C+mol O) per 100 g is approximately equal for the 300°C char in Series 1 and 2, although their (mol C)/(mol O) ratio differs by a factor of almost two. The main effect, then, of preoxidation at 200°C may be *ideally* formulated as follows: If $C_iH_jO_k$ is the empirical formula of the normal char (Series 1) and $C_{i'}H_{j'}O_{k'}$ is that for the preoxidized char, then $j=j'$, and $i+k=i'+k'$, with $i>i'$ and $k<k'$. It follows from these conditions that

$$(\%H)_1/(\%H)_2=\frac{[(\%C/12.01)+(\%O/16.00)]_1}{[(\%C/12.01)+(\%O/16.00)]_2}. \quad (1)$$

Subscripts 1 and 2 refer to Series 1 and 2, respectively. This relation cannot hold at temperatures much higher than 200°C since Table II shows that there is a difference in the spectrum of molecular fragmentation.[13] Applying this relation to the 300°C char, we obtain

$$(\%H)_1/(\%H)_2=3.35/3.27=1.025$$

[8] The char having minimum width possesses many unique characteristics that make it appear attractive as a magnetometric material [see Hoskins and Pastor, J. Appl. Phys. (to be published)]. Its properties may be summarized as follows: $g=2.0023\pm0.0003$, spin density $=5\times10^{20}$ cm^{-3}, line width $=0.36$ oersted (maximum deflections of derivative curve), all properties independent of temperature from 500 to 1.4°K.

[9] This does not seem surprising when it is realized that the types of bonds ruptured in both cases are about the same. For instance, in the pyrolysis of free cellulose at about the same temperature, the main volatile products given off are CO_2 and CO. See K. Tamaru, Bull. Fac. Eng. (Yokohama National University) **2**, 83 (1953).

[10] This was unexpected as it was thought that the role of O_2 in the preliminary charring would be mainly to form volatile decomposition products, such as H_2O, CO, CO_2, etc., leading to low-temperature chars with high ratios of (mol C)/(mol H).

[11] Analysis performed by Elek Microanalytical Laboratory, Los Angeles, California.

[12] The (mol C+mol O+mol H) per 100 g is 11.0±0.2 for Series 1 and 11.0±0.5 for Series 2. The value for pure carbon is 8.33 and (mol C)/(mol O) approaches infinity.

[13] Note that the removal of fragments rich in C and O in the case of the 450°C char in Series 2 has resulted in a high percent of H, which is not the normal trend in Series 1.

and

$$\frac{[(\%C/12.01)+(\%O/16.00)]_1}{[(\%C/12.01)+(\%O/16.00)]_2}$$

$$=\frac{(80.63/12.01)+(15.8/16.00)}{(71.47/12.01)+(25.0/16.00)}=1.025.$$

The good agreement is somewhat fortuitous since the conditions supporting Eq. (1) probably do not hold in a rigorous stoichiometric fashion. However, the analytical and magnetic-resonance results are in accord in the interpretation of the effect of O_2 before the final heat treatment of charred dextrose.[14]

2. *Effect of* O_2 *after Final Heat Treatment*

A summary of the results of magnetic-resonance measurements on line widths is shown in Table III. In each case, the width was normalized to unity for zero pressure of O_2 over the char.

It is seen that samples belonging to Region A (300°C) and the first part of Region B (450°C) were hardly affected by oxygen. The results in Columns b, c, and d for the 560°C char may be explained on the basis of the known adsorption and chemisorption behavior of oxygen on charcoal.

In Column b, one attributes the behavior primarily to absorbed oxygen. In this stage, oxygen is able to go from the charcoal surface to the gas phase and back, there being a time lag in its evaporation from the charcoal surface. It is conceivable that in this stage, oxygen is able to provide an additional relaxation mechanism involving the walls of the container.[15]

At room temperature the chemisorption rate is slow, and Column c is indicative of a small residual background of oxygen. Attempts to desorb by heating lead to the cleavage of carbon oxides.[16] Heating also accelerates the chemisorption of the residual oxygen. Hence, the net effect of heating is to convert oxygen to carbon oxides, which, unlike oxygen, are unable to provide an efficient relaxation mechanism. Since bonds are again ruptured in the process of liberating carbon oxides, the spin density tends to its initial value. This explains Column d. The results in Table III demonstrate two distinct roles played by oxygen.

In the adsorbed stage, it is known that the effect of oxygen is readily reversed, without heating, by mere evacuation.[17] One deals here with essentially van der Waals binding rather than with a bond which involves electron pairing. This is in agreement with Singer's observation that the integrated absorption is independent of the pressure of oxygen.[18] Of many adsorbates tried, only two gases, both paramagnetic, *viz.*, O_2 and NO, are known to accomplish this "poisoning effect." This indicates that the additional relaxation mechanism proceeds via a magnetic interaction (spin flips).

In the chemisorbed stage, the situation is different. Since the unpaired electrons are the source of partial valencies, it is not surprising that this stage leads to a decrease in the integrated absorption. Such cases have been observed and reported.[18] In the present experiment, it was not possible to determine this feature. The small bulbs used contained oxygen in small amounts so that the effect on the integrated absorption was on the order of 0.1%.[19] Unfortunately, there are no data available on the time dependence of line widths between Columns b and c since the chemisorption effect was not detected earlier. However, the present results indicate that measurements such as those in Column b may be misleading unless one distinguishes the effect of physical equilibrium from that of chemical equilibrium.

Samples belonging to Region A and the early part of Region B are subject to the same action of adsorbed oxygen. However, adsorption is much less efficient than it is for the 560°C char. Up to a pressure of 60 mm of oxygen, no appreciable change in line width is noticed, while for the 560°C char, the effect on T_1 would have been such that the resultant width would have been about five times broader than that for the lower-

TABLE III. Line width measured at room temperature *vs* initial pressure of oxygen over the char.

	Normalized widths in Series 1 chars				
Pressure,[a] mm	350°C	450°C	560°C		
0	(1.00)[b]	(1.00)[b]	(1.00)[b]	(1.00)[c]	(1.00)[d]
6	1.03	1.00	2.6	1.25	1.00
15	...	...	4.4	1.30	1.00
25	1.00	1.00	...	...	...
30	...	...	12.5	1.35	1.00
45	...	...	22.4	1.35	1.00
61	0.99	1.01	...	...	...

[a] This is the initial pressure of O_2 over the sealed sample.
[b] In this column, the widths were measured a few hours after the samples were prepared.
[c] In this column, widths were measured after 80 days of storage at room temperature.
[d] After measurements in Column c, samples were heated for one-half hour at 430°C, cooled to room temperature, and the widths were again measured.

[14] The blocking effect of preoxidation on aromatization or cyclization would also be reflected in the *d-c* resistivity behavior with thermal treatment. This is seen in the work of Winslow *et al.* (reference 5). The effect of oxygen content of char (or parent material) on cyclization seems sufficiently pronounced for magnetic-resonance measurements with high-vacuum chars to establish differences arising from the starting material.

[15] L. S. Singer and W. J. Spry, Bull. Am. Phys. Soc., II **1**, 214 (1956). This mechanism may be checked further by cooling char to low temperatures, where the adsorbate has very little mobility.

[16] H. S. Taylor and H. A. Taylor, *Elementary Physical Chemistry* (D. Van Nostrand Company, Inc., Princeton, New Jersey, 1942), third edition, p. 442.

[17] See references 1 and 6 and the references cited in them.

[18] Singer, Spry, and Smith, Paper presented at the Third Biennial Carbon Conference, University of Buffalo (June, 1957). See also references cited.

[19] The proportion of char to oxygen may be altered to measure this effect and the heat of activation. One sees here another possible application of magnetic resonance.

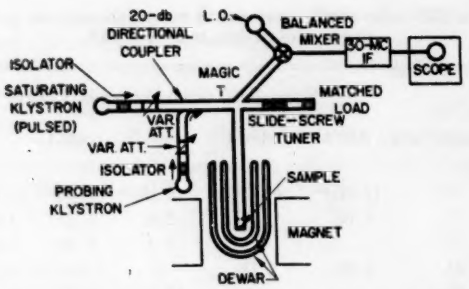

FIG. 2. Apparatus for the direct observation of relaxation times.

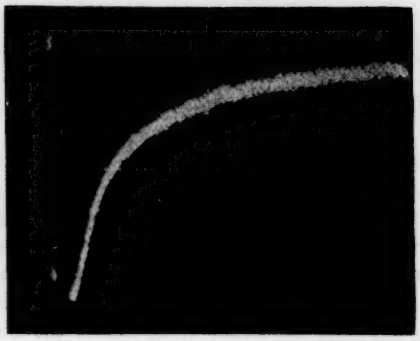

FIG. 3. Recovery curve of χ'' after saturation for a Series 1, 400°C char at 1.4°K. The time scale is 50 μsec per large division.

temperature chars.[20] Since the latter chars do not possess large specific adsorptive surfaces, the free radical species are, in effect, distributed in volume rather than on the surface and thus are less accessible to oxygen. This picture finds further support from the results of relaxation measurements discussed below. Chars in the high-temperature part of Region B have large specific adsorptive surfaces and would more likely approximate more closely to the case where the free radical species are largely localized on the surface and are therefore sensitive to the action of adsorbed oxygen.

B. Relaxation Times

The spin-lattice relaxation time T_1 is generally measured by a *c-w* saturation method.[21] The quantity determined in these measurements is the product T_1T_2, and provided that the line is homogeneously[22] broadened, T_2, the spin-spin relaxation time, may be obtained from the line width. Singer *et al.*[18] have determined T_1 in this manner at room temperature in a series of charred-sucrose samples.[23] For charring temperatures below about 450°C, however, the saturation behavior of the resonance is no longer homogeneous, and the line-broadening mechanism appears to be of the inhomogeneous type.[22] That is, the over-all line width does not result from spin-spin interaction. For charring temperatures below 300°C, the saturation behavior has the characteristics of an inhomogeneously broadened line, and a measurement of T_1T_2 can again be used to determine T_1, provided that T_2 is determined not from the over-all line width but from the dipolar-broadened line width calculated from the spin density. In the charring temperature region between 300 and 450°C, the saturation behavior lies between the inhomogeneous and the homogeneous case, and T_1 is best determined by a direct-pulse method. In this method, a pulse of microwave power sufficiently intense to saturate the resonance is applied with the static magnetic field fixed at the resonant value, so that $\chi''(H_1)$ is zero at the termination of the saturating pulse; then, a small microwave probing signal is used to monitor the growth of χ'' to $\chi''(H_1=0)$. Thus T_1 is measured directly on a time scale. The apparatus used in determining T_1 in this manner is shown in Fig. 2.

The recovery from saturation in the samples measured followed a simple exponential curve to a good

TABLE IV. Values of T_1 at low temperatures obtained by direct-pulse method.

	T_1, msec					
	Series 1			Series 2		
Pyrolytic temperature, °C	77°K	4.2°K	1.4°K	77°K	4.2°K	1.4°K
250	2.0	40.	40.	...	...	...
300	0.50	1.6	2.0	0.25	1.0	2.0
350	0.07	0.12	0.28	...	...	...
400	...	0.04	0.08	...	<0.03	<0.03
450	...	...	<0.03	...	...	...

TABLE V. Values of T_2 derived from *c-w* saturation and direct-pulse methods for 300°C char, Series 2.

Temperature, °K	T_1T_2, sec^2 (*c-w* saturation meas.)	T_1, sec (direct-pulse meas.)	T_2, sec (calc.)
77	2×10^{-11}	0.25×10^{-3}	8×10^{-8}
4.2	1×10^{-10}	1.0×10^{-3}	10×10^{-8}

[20] Singer *et al.* (see reference 18) have measured a two-orders-of-magnitude decrease in T_1 at a 60-mm pressure of oxygen on a 450°C char obtained from sucrose. We assume in our case that chemisorption, being slow, had not progressed appreciably in the time that transpired before the first resonance measurements were made.

[21] Bloembergen, Purcell, and Pound, Phys. Rev. **73**, 679 (1948).

[22] A. M. Portis, Phys. Rev. **91**, 1071 (1953).

[23] *Note added in proof.* We have extended *c-w* saturation measurements on the 560°C char to the low temperature range. At 77°K and at 4.2°K the saturation behavior is homogeneous and the product T_1T_2 in the usual saturation parameter equals $[(\sqrt{3}/2)\gamma\Delta H]^{-2}$ where ΔH is full width at half maximum of the resonance. The short apparent spin lattice relaxation time is due to the draining off of energy by the exchange interactions. See N. Bloembergen and S. Wang, Phys. Rev. **93**, 72 (1954).

approximation. The results of these measurements are given in Table IV. A typical recovery curve is shown in Fig. 3.

C-w saturation measurements were also undertaken on the Series 2, 300°C char at 77 and 4.2°K. The saturation behavior was of the inhomogeneous type. From the measured values of T_1T_2, T_2 may be calculated by using the values for T_1 in Table IV. The results are given in Table V.

As one would expect, the calculated value of T_2 is seen to be independent of temperature. We may estimate the expected line width of the individual spin packets due to dipolar broadening on the basis of a uniform distribution of spins in the sample; taking[24] $N\sim10^{19}$ cm^{-3}, we find $\Delta H\sim1$ oersted. This value may be compared with that obtained from the calculated value of T_2 above: 0.85 oersted. Thus, a uniform distribution of unpaired spins seems likely in the low-temperature chars, as suggested in Section III A.

[24] Singer *et al.* (See reference 18) have determined spin density as a function of charring temperature down to 350°C. The value of 10^{19} cm^{-3} is an extrapolation of their data to 300°C.

THE JOURNAL OF CHEMICAL PHYSICS VOLUME 32, NUMBER 1 JANUARY, 1960

Conditions Imposed by Gross Properties on the Intermolecular Potential

H. L. FRISCH AND E. HELFAND

Bell Telephone Laboratories, Murray Hill, New Jersey

(Received July 20, 1959)

The conditions for, and implications of, the existence of a maximum in the second virial coefficient as a function of temperature are investigated. Brief comment is made on the use of the inversion of Laplace transforms, with respect to the reciprocal temperature, to obtain information about intermolecular potentials and cross sections from second virial coefficients and dilute gas transport coefficients.

IN a recent paper Keller and Zumino[1] have considered the question of the amount of information about the form of the intermolecular potential which is available from thermodynamic data. This problem undoubtedly would be as important to the chemist as the interpretation of nucleon scattering is to the physicist if we did not know the force law of the fundamental constituents of molecules or if we had not developed quantum mechanics. Still, the difficulties of making theoretical calculations of intermolecular potentials, especially in the repulsive region, are such that it is surprising that the chemical question had not been raised long ago. Therefore we would like to make several further observations along these lines.

The fact that one experimentally observes a maximum in a plot of the second virial coefficient versus temperature has in the past been used in a qualitative way to rule out certain general potential forms.[2] We now prove that a necessary and sufficient condition for such a maximum to exist is

$$\int_a^\infty \varphi(r)r^2dr>0, \tag{1}$$

where $\phi<0$ for some value of r, $\varphi(r)$ is the intermolecular potential function, and a is the range of any hard sphere cutoff.*

The proof follows from an examination of the second virial coefficient and its first two derivatives which are

$$B(\beta)=-2\pi\int_a^\infty(e^{-\beta\varphi}-1)r^2dr+(2\pi/3)a^3, \tag{2}$$

$$B'(\beta)=2\pi\int_a^\infty\varphi e^{-\beta\varphi}r^2dr=F(\beta), \tag{3}$$

and

$$B''(\beta)=-2\pi\int_a^\infty\varphi^2e^{-\beta\varphi}r^2dr<0, \tag{4}$$

where β is the monotone function of T, $\beta=1/kT$. By virtue of Eq. (4), $F(\beta)$ is monotone decreasing. Hence, $B(\beta)$ can have at most a single maximum at the value of β which satisfies

$$F(\beta)=0. \tag{5}$$

First let φ assume negative values for some region in $0\leq r<\infty$. Then it follows from Eq. (3) that for sufficiently large $\beta(0\leq\beta<\infty)$, $F(\beta)<0$; in particular

$$\lim_{\beta\to\infty}F(\beta)\to-\infty.$$

[1] J. B. Keller and B. Zumino, J. Chem. Phys. **30**, 1351 (1959).
[2] R. H. Fowler, *Statistical Mechanics* (Cambridge University Press, New York, 1955), p. 302.

* Physically, such a cutoff indicates that at some degree of penetration, the potential rapidly rises to values much greater than the thermal energies under consideration.

Consider now a plot of the monotone decreasing function $F(\beta)$ versus β. A necessary and sufficient condition that $F(\beta)$ intersect the abscissa is (by continuity) that

$$[F(0)/2\pi]=\int_a^\infty \varphi r^2 dr>0. \tag{6}$$

A similar argument shows that when $\varphi\geq 0$ for all $0\leq r<\infty$, no maximum in $B(\beta)$ as a function of T can occur.

Certain physical consequencies of the above are: (1) $B(\beta)$ can have at most one maximum (and no minimum) as a function of temperature. (2) Intermolecular potentials which are purely repulsive or of the Sutherland type (including the square well) lead to second virial coefficients without a maximum. (3) The observed maximum of $B(\beta)$ for H_2 and He suggests that the repulsive part of φ is sufficiently "soft" for Eq. (6) to apply. These results remain valid for angle-dependent potentials if the condition expressed by Eq. (6) is replaced by[3]

$$\int_a^\infty\int_0^{2\pi}\int_0^\pi\int_0^\pi \phi\ \sin\theta_1 d\theta_1\ \sin\theta_2 d\theta_2 d(\psi_2-\psi_1) r^2 dr>0. \tag{6'}$$

More information is derivable by using Laplace transforms. Another form of Keller and Zumino's results is obtained by beginning with the second virial coefficient in the form

$$\beta^{-1}B(\beta)=-(2\pi/3)\int_0^\infty r^3(d\phi/dr)\ \exp(-\beta\phi)dr. \tag{7}$$

If, as usual, ϕ has one repulsive portion $\phi_+(r)$ and one attractive portion $\phi_-(r)$, then single-valued inverses $r_+(\phi)$ and $r_-(\phi)$ are determined. The zero of energy is taken as the minimum of the potential well so that the potential at infinite separation is ϵ. Equation (7) can be written in the form

$$(3/2\pi)\beta^{-1}B(\beta)=-\int_\infty^0 r_+^3(\varphi)e^{-\beta\varphi}d\varphi-\int_0^\epsilon r_-^3(\varphi)e^{-\beta\varphi}d\varphi. \tag{8}$$

It has been assumed that the potential is infinite at zero separation. The second integral can be extended to infinity by defining $r_-(\varphi)=0$ for $\varphi\geq\epsilon$. The second virial coefficient then takes the form of the Laplace transform

$$(3/2\pi)\beta^{-1}B(\beta)=\int_0^\infty [r_+^3(\varphi)-r_-^3(\varphi)]e^{-\beta\varphi}d\varphi. \tag{9}$$

An inversion gives the volume contained between the points of equal potential on the attractive and repulsive branch, and gives the complete potential for values greater than ϵ. This is the same information Keller and Zumino obtained.[1]

The Laplace inversion, in principle, also can be used to determine the cross sections, $Q^{(l)}(\epsilon)$ (functions of impact energy ϵ) which arise in gas transport theory.[4] From the transport coefficients one can obtain† the integrals

$$2(\pi m)^{\frac{1}{2}}\beta^{-(s+3/2)}\Omega^{(l,s)}(\beta)=\int_0^\infty e^{-\beta\epsilon}\epsilon^{s+1}Q^{(l)}(\epsilon)d\epsilon \tag{10}$$

which we note have the form of Laplace transforms with respect to β.

[3] Hirschfelder, Curtiss, and Bird, *Molecular Theory of Gases and Liquids* (John Wiley and Sons, Inc., New York, 1954), p. 153.

[4] Reference 3, Ch. 8.

† $\Omega^{(1,1)}$ and $\Omega^{(2,2)}$ are related to the self-diffusion coefficient and the viscosity (or thermal conductivity), respectively, only in first approximation. Corrections for the small higher-order terms can be made with any reasonable potential model.

THE JOURNAL OF CHEMICAL PHYSICS VOLUME 32, NUMBER 1 JANUARY, 1960

Infrared Absorption Spectrum of the Silicate Ion in the Garnet Structure

K. A. WICKERSHEIM, R. A. LEFEVER, AND B. M. HANKING

Hughes Research Laboratories, Culver City, California

(Received July 20, 1959)

Infrared absorption bands at 912 and 861 cm^{-1} exhibited by some crystals of yttrium iron garnet and similar bands exhibited by some rare earth iron garnet crystals have been identified as vibrational fundamentals of a silicate ion impurity. The bands are assigned to split components of a triply degenerate vibration (ν_3) of the tetrahedral SiO_4 ion. The splitting of this vibration into a nondegenerate and a doubly degenerate vibration is attributed to distortion of the silicate ion along an S_4 axis by the garnet structure. Integrated absorption measurements identify the 912 cm^{-1} band as the nondegenerate component.

Information obtained from the isolated silicate ion in yttrium iron garnet is used to interpret the spectra of the silicate garnets. Complete removal of the degeneracy of vibrations arising from ν_3 is observed in the silicate garnets, suggesting that the majority of the silicate ions possess a local symmetry lower than that predicted by the assigned space group Ia3d–O_h^{10}.

INTRODUCTION

IN recent years a number of "silicon-free" garnets (for example $Y_3Al_5O_{12}$, $Y_3Ga_5O_{12}$, and $Y_3Fe_5O_{12}$)[1–4] have been synthesized. Yttrium iron garnet (YIG) and the rare earth iron garnets have proven to be of special interest since they are ferrimagnetic.

We have found that two infrared absorption bands previously reported for YIG,[5] and presumed to be part of its lattice vibration spectrum are in reality vibration bands of the silicate ion. Since these bands have been observed by us in all flux-grown iron garnets produced in these laboratories and in all iron garnets obtained from four other sources, it would appear that silicon occurs commonly as an impurity in YIG and the rare earth iron garnets.

In contrast to the silicate garnets, (e.g., grossularite, $Ca_3Al_2Si_3O_{12}$), the synthetic garnets mentioned above should contain only trivalent cations. The introduction of tetravalent silicon into the synthetic garnets as an impurity, however, should allow incorporation of a corresponding concentration of divalent cations. In the synthetic iron garnets the divalent impurity could be ferrous iron[6] (present as a significant equilibrium constituent in the melt and accepted by the silicate garnets), divalent lead (present in abundance during growth from lead oxide flux but probably too large to be accepted by the garnets), or any of a number of other metal ions which may be present as impurities during the growth process.

While the infrared spectra of the silicate garnets have been reported before,[7–9] little interpretation of the bands observed appears in print. The purpose of this paper is to present the spectrum of the silicate ion in YIG and in several rare earth iron garnets, and to correlate this spectrum with that of the silicate garnets. It will be shown that the spectrum of the isolated silicate ion can be understood in terms of its configuration in the garnet structure, and that this in turn assists in the interpretation of the silicate garnet spectrum.

STRUCTURAL CONSIDERATIONS

The natural garnets are orthosilicates. That is, the SiO_4 groups are discrete, each oxygen being bonded to only one silicon. The space group has been assigned as Ia3d–O_h^{10}.[10,11] The cubic unit cell has sides whose length varies for the various garnets from about 11.5 to 12.1A. There are eight formula units per unit cell.

In the assigned garnet structure, the cations are on special positions at the centers of oxygen polyhedra. The silicon ion is centered in a distorted oxygen tetrahedron, the trivalent ion (Al, Cr, or Fe^{3+}) is at the center of a distorted octahedron, and the divalent ion (Ca, Mg, Mn^{2+}, or Fe^{2+}) is at the center of a very irregular dodecahedron. The oxygens require three positional parameters. Menzer[10] determined the oxygen parmeters for most of the natural garnets using powder techniques. Abrahams and Geller[11] have carried out a more precise determination of the oxygen parameters for grossularite.

Yttrium iron garnet and the rare earth iron garnets are reported to be isomorphic with the natural garnets.*

[1] H. S. Yoder and M. L. Keith, Am. Min. **36**, 519 (1951).
[2] M. L. Keith and R. Roy, Am. Min. **39**, 1 (1954).
[3] F. Bertaut and F. Forrat, Compt. rend. **242**, 382 (1956).
[4] S. Geller and M. A. Gilleo, Acta Cryst. **10**, 239 (1957).
[5] Porter, Spencer, and LeCraw, J. Appl. Phys. **29**, 495 (1958).
[6] The replacement of yttrium or ferric iron by ferrous iron would be expected to alter the saturation magnetization and Curie temperature of YIG over and above any changes produced by preferential replacement of tetrahedral ion by silicon. In addition, ferrous iron may produce broadened ferromagnetic resonance lines. [R. L. White, Phys. Rev. Letters **2**, 465 (1959).] We are investigating the possibility of a ferrous iron to silicon correlation and its magnetic consequences.
[7] H. H. Adler, American Petroleum Institute Project 49, Preliminary Report No. 8, Section I (1950).
[8] Hunt, Wisherd, and Bonham, Anal. Chem. **22**, 1478 (1950).
[9] D. L. Wood, Paper presented at the Symposium on Molecular Structure and Spectroscopy, Ohio State University, June, 1958.
[10] G. Menzer, Z. Krist **69**, 300 (1928).
[11] S. C. Abrahams and S. Geller, Acta Cryst. **11**, 437 (1958).
* As noted in reference 13 the existence in YIG and the rare earth iron garnets of a net magnetic moment in each unit cell below the Curie temperature implies that the symmetry of these crystals is *not* cubic, but the deviations from cubic symmetry are not detected by x-ray diffraction.

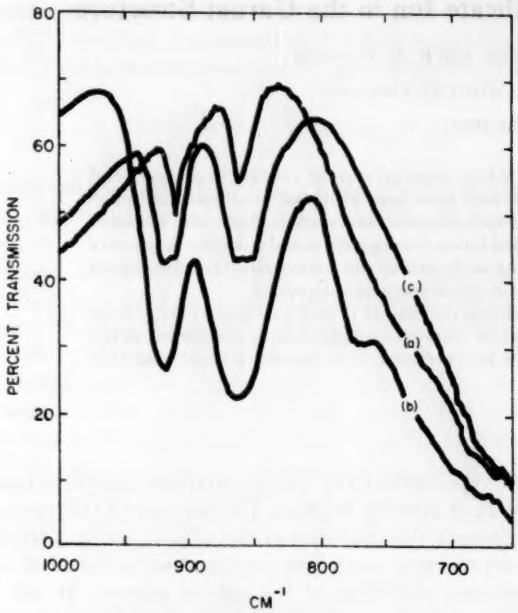

FIG. 1. Spectrum of the silicate ion in yttrium iron garnet (1.0% by weight in KBr pellet).

The lattice constants are somewhat larger, running from about 12.2 to 12.6A.[12] Geller and Gilleo[13] have carried out a detailed single crystal X-ray study of yttrium iron garnet and have computed the oxygen parameters, but similar information is lacking for the rare earth iron garnets.

In YIG and the rare earth iron garnets, Fe^{3+} occupies both the tetrahedral site (replacing the silicon of the natural garnet) and the octahedral or normal trivalent ion site, while yttrium or one of the rare earth ions replaces the divalent ion of the silicate garnets.

CRYSTAL GROWTH

The majority of the synthetic garnets used in this study, including YIG, yttrium gallium garnet, and several rare earth iron garnets, were grown by one of us (R.A.L.) from lead oxide flux[14] and/or by the flame fusion (Verneuil) process. Flux-grown garnets were also obtained from another source within the company,† and from three outside laboratories. In addition, a flame fusion YIG was purchased from the Linde Company. The silicate garnets were selected from the U.C.L.A. Department of Geology mineral collection.

The silicon contents of the raw materials and synthetic garnets were determined spectrochemically. The Fe_2O_3 and PbO employed for flux growth contained 0.027 and 0.024 wt % silicon, respectively. Silicon contents of the yttrium oxide (99.9% pure) and rare earth oxides (99.8% pure) were not determined. Garnets prepared by the flux technique using these materials contained 0.05 to 0.06 wt % silicon, which is sufficient to produce prominent SiO_4 vibration bands in the infrared spectrum. If we convert these figures to percent replacement of tetrahedral iron in the garnet structure by silicon, we obtain 0.4 to 0.7% replacement. Infrared absorption spectra and spectrochemical analyses of flux-grown garnets from outside sources indicate 0.2 to 11.3% replacement of tetrahedral iron by silicon.

Flame-fusion garnets were grown from powders containing the Fe_2O_3 and yttrium oxide described above and identical powders containing additional silicon in the form of SiO_2. The most silicon-free YIG (SiO_4 bands not observable with the technique used in this study) was produced by flame fusion, using carbonyl iron powder (0.0053 wt % silicon) in place of Fe_2O_3.

SAMPLE PREPARATION AND INSTRUMENTAL TECHNIQUE

The infrared spectrum of YIG previously reported[5] was obtained from a thin polished single crystal slab. The spectra of the silicate garnets previously published were obtained either from mulls[7] or from very fine powder deposited on sodium chloride windows.[8] We employed the KBr pellet technique, which reduced sample preparation problems and allowed reasonably quantitative measurements to be made. Small percentages by weight of garnet powder, prepared by hand grinding in an agate mortar, were mixed with 300 mg of KBr powder. Pellets were then pressed using a Perkin-Elmer KBr die. Typical percentages by weight of both the silicate and non-silicate garnets used in the pellets are indicated with their spectra.

Because of the poor match between the refractive indices of the garnets and the KBr, scattering losses are significant at short wavelengths. Scattering is a strong function of the ratio of wavelength to average particle size. Scattering losses, particularly for the iron garnets, increase sharply at frequencies above 1000 cm^{-1}, but the region of greatest interest to us lies between 800 and 1000 cm^{-1}. In this region pellet transmission was relatively high and there was no need to resort to special techniques for producing small particle size samples.

All spectra were obtained with a Perkin-Elmer Model[21] spectrometer using sodium chloride optics. The instrument calibration was checked against atmospheric absorption bands. Band minima reported (except for very diffuse bands) are thought to be accurate to better than two wave numbers.

SPECTRA

The spectra of three samples of YIG are shown in Fig. 1. The decrease in transmission at the high frequency end of each spectrum is the result of scattering losses already mentioned, while the decrease in transmission at the low frequency end is characteristic of all

[12] R. Pauthenet, Doctoral Thesis, University of Grenoble (1958).
[13] S. Geller and M. A. Gilleo, J. Phys. Chem. Solids **3**, 30 (1957).
[14] J. W. Nielsen, J. Appl. Phys. **29**, 390 (1958).
† M. K. Jack, Microwave Laboratory.

iron garnet samples regardless of silicon content, and seems to represent the edge of the lattice fundamental region.

The two bands near 915 and 860 cm^{-1} will be shown to be characteristic of the silicate ion. Curve (a) is the spectrum of one of our standard flux-grown YIG crystals. The spectra of the flux-grown rare earth iron garnets resemble curve (a) but the frequencies of the two bands decrease linearly with increasing lattice constant of the host garnet. Their shift is illustrated in Fig. 2 where the lattice constants used are those determined by Pauthenet.[12] The separation of the two bands increases very slightly in going from ytterbium iron garnet to europium iron garnet.

Curve (b) of Fig. 1 is the spectrum of a YIG sample in which approximately 11% of the tetrahedral iron has been replaced by silicon (1.28% silicon impurity by weight). The two silicate bands are broadened and shifted slightly towards higher frequencies in addition to being much more intense.

Curve (c) is the spectrum of a YIG crystal grown by the flame-fusion process using a powder containing Y_2O_3, analytical reagent grade Fe_2O_3 and an additional 1% by weight of SiO_2. The illustrated broadening and doubling of the silicate bands is typical of the flame fusion garnets studied by us.

All of the spectra of Fig. 1 have one feature in common. The lower frequency band is both slightly more intense and somewhat broader than the higher frequency band. It is possible to estimate the integrated absorption of the two bands by using samples containing enough silicon to provide moderately intense bands but not so much that resolution becomes incomplete. If the integrated absorption coefficient for each band is divided by the band frequency, a number proportional to the net transition moment for the band is obtained. The ratio of the net transition moment of the lower frequency band to that of the higher frequency band is 2 to 1 to the accuracy of the calculation.

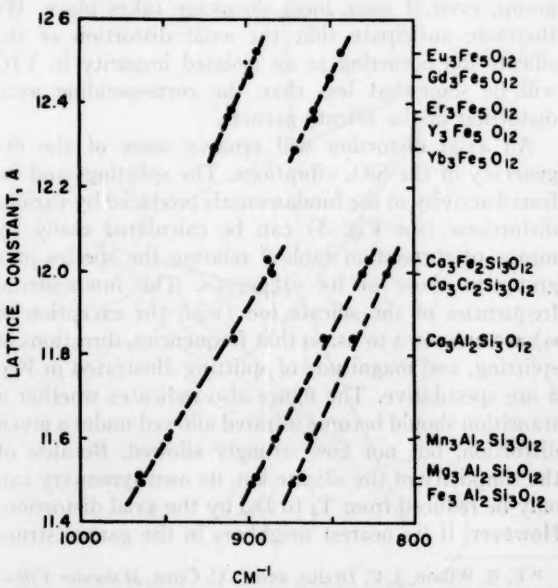

FIG. 2. Shift of silicate frequencies with garnet lattice constant.

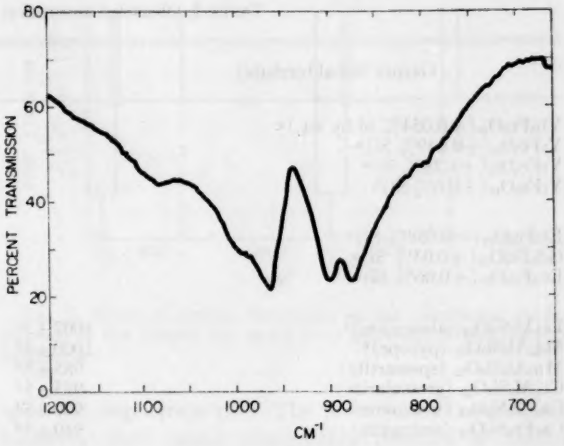

FIG. 3. Spectrum of almandite (0.2% by weight in KBr pellet).

A typical spectrum of the natural garnets, that of a sample of almandite, is shown in Fig. 3. There are three strong, sharp bands of almost equal intensity. The two of lowest frequency are only slightly separated from each other, while the high frequency band is more widely split from the first two. There is also a weak, diffuse band just above the three strong bands in frequency. Other still weaker bands appear as shoulders. We have run KBr pellet spectra of samples of the various natural garnets. All the spectra are qualitatively similar to the one shown. Band frequencies (listed in Table I) decrease with increasing lattice constant in a nearly linear fashion.‡ The shift of the three sharp bands with lattice constant is also illustrated in Fig. 2. The lattice constants used are those given by Menzer.[10]

INTERPRETATION OF THE SPECTRA

The fact that the 861 and 912 cm^{-1} bands exhibited by YIG are the result of an impurity was suggested by the observation that the bands varied in intensity from sample to sample, and in fact were missing altogether in a sample of synthetic yttrium gallium garnet. A positive correlation between the intensities of the two bands and the silicon content of the YIG was established by adding known amounts of silica to a powder used for flame-fusion growth studies. This nearly quantitative correlation was confirmed by spectrochemical analysis of several of the garnets studied.

When the spectra of the natural garnets were obtained, it became apparent that there were strong similarities between the silicate garnet spectra and the unidentified bands of the nonsilicate garnets. The sili-

‡ Adler[7] also noted the frequency shift with lattice constant and suggested that it might be of "diagnostic" value.

TABLE I. Observed absorption bands between 800 and 1050 cm^{-1}.

Garnet (ideal formula)	Band minima in cm^{-1}			
$Yb_3Fe_5O_{12}$(+0.054% Si by wt.)[a]		920±1	871±1	
$Y_3Fe_5O_{12}$(+0.049% Si)[a]		912±1	861±1	
$Y_3Fe_5O_{12}$(+1.28% Si)[a]		917±1	862±2	
$Y_3Fe_5O_{12}$(+0.6% Si)[b]	918±2	911±2	862±2	850±2
$Er_3Fe_5O_{12}$(+0.058% Si)[a]		911±1	861±1	
$Gd_3Fe_5O_{12}$(+0.03% Si)[a]		900±1	850±1	
$Eu_3Fe_5O_{12}$(+0.06% Si)[a]		897±1	845±3	
$Fe_3Al_2Si_3O_{12}$ (almandite)[c]	1002±5[d]	965±2	898±2	874±2
$Mg_3Al_2Si_3O_{12}$ (pyrope)[c]	1000±5[d]	965±2	896±2	868±2
$Mn_3Al_2Si_3O_{12}$ (spessartite)	985±5[d]	950±2	884±2	864±2
$Ca_3Al_2Si_3O_{12}$ (grossularite)	955±5[d]	909±2	854±2	835±2
$Ca_3Cr_2Si_3O_{12}$ (uvarovite)	940±5[d]	887±2	832±2	817±2
$Ca_3Fe_2Si_3O_{12}$ (andradite)	940±5[d]	889±2	828±2	815±2

[a] Flux-grown.
[b] Flame fusion grown.
[c] Average of four samples.
[d] Diffuse, weak band.
[e] Average of two samples.

cate minerals in general exhibit intense absorption bands in the region from 800 to 1100 cm^{-1}. The spectra of the orthosilicates in particular possess remarkably similar bands between 800 and 1000 cm^{-1}. Launer[15] has pointed out that since the orthosilicates embrace a variety of positive ions and crystal structures, it is reasonable to assign these bands to vibrations of the independent SiO_4 group which all the orthosilicates have in common.

If we assume that the 861 and 912 cm^{-1} bands of YIG as well as the three sharp bands of the natural garnets arise from vibrations of the SiO_4 ion, it is still necessary to decide which vibrational modes of the ion are involved. There are four vibrational frequencies for the isolated tetrahedral XY_4 molecule (point group T_d).[16] One vibration of frequency ν_1 is nondegenerate (species A_1); the second, of frequency ν_2, is doubly degenerate (species E); the remaining two vibrations, of frequency ν_3 and ν_4, are triply degenerate (species F_2). ν_1 corresponds to the totally symmetric stretching mode. ν_3 also involves stretching of the Si—O bonds with the silicon atom moving against the oxygen atoms. ν_2 and ν_4 are deformation modes. Only ν_3 and ν_4 are infrared active.

We can get some idea of the relative frequencies of the various modes of the SiO_4 ion from the frequencies known[17] for similar molecules and ions (e.g., SiF_4, SO_4^{2-}, PO_4^{3-}). We conclude that only the stretching fundamental, ν_3, should appear in the infrared in the vicinity of 900 cm^{-1} while the other infrared active fundamental, ν_4, should fall between 400 and 600 cm^{-1}.

In the silicate garnets, the SiO_4 ion does not form a perfect tetrahedron. According to x-ray studies the SiO_4 ion lies on an S_4 axis of the garnet and is distorted along one of its own S_4 axes so that two oxygen to oxygen distances are considerably shorter than the remaining four[11] (see Fig. 4). The same is true of the FeO_4 tetrahedron in YIG and the rare earth iron garnets.[12] Although the FeO_4 tetrahedron in YIG is more distorted than the SiO_4 tetrahedron in the silicate garnets, the silicate ion is considerably smaller than the FeO_4 group. If an FeO_4 group is removed from a crystal of YIG, the hole which remains will no doubt be somewhat larger than that required by a substituting SiO_4 group, even if some local shrinkage takes place. We therefore anticipate that the axial distortion of the silicate ion occurring as an isolated impurity in YIG will be somewhat less than the corresponding axial distortion in the silicate garnets.

An axial distortion will remove some of the degeneracy of the SiO_4 vibrations. The splittings and infrared activity of the fundamentals produced by various distortions (see Fig. 5) can be calculated easily by means of correlation tables[18] relating the species of a group to those of its subgroups. The fundamental frequencies of the silicate ion (with the exception of ν_3) are unknown to us, so that frequencies, directions of splitting, and magnitude of splitting illustrated in Fig. 5 are speculative. The figure also indicates whether a transition should become infrared allowed under a given distortion, but not how strongly allowed. Because of the simplicity of the silicate ion, its own symmetry can only be reduced from T_d to D_{2d} by the axial distortion. However, if its nearest neighbors in the garnet struc-

[15] P. J. Launer, Am. Min. **37**, 764 (1952).
[16] G. Herzberg, *Infrared and Raman Spectra* (D. Van Nostrand Company, Inc., New York, 1945), p. 100.
[17] J. Le Compte, *Handbuch der Physik* (Springer, Berlin, 1958), Volume XXVI, p. 629 and p. 825.
[18] E. B. Wilson, J. C. Decius, and P. C. Cross, *Molecular Vibrations* (McGraw-Hill Book Company, Inc., New York, 1955), p. 340.

ture play any direct role in the actual SiO_4 vibrations, the appropriate symmetry should be S_4. Either D_{2d} or S_4 symmetry will produce splitting of each of the triply degenerate vibrations into a nondegenerate vibration and a doubly degenerate vibration. Any further reduction of symmetry will result in a complete removal of degeneracy.

We identify the two bands at 861 and 912 cm^{-1} in YIG as the two components of ν_3 produced by the axial distortion. The space group Ia3d—O_h^{10} contains three sets of mutually perpendicular, non-intersecting S_4 axes. If we assume that SiO_4 ions are equally distributed on these axes, we should have a 2 to 1 integrated intensity ratio (corrected for frequency) between the doubly degenerate and nondegenerate components of ν_3 (assuming that transition moments are not altered significantly by the distortion). The measured intensity ratio identifies the 912 cm^{-1} band in YIG as the nondegenerate component of ν_3 and the 861 cm^{-1} band as the doubly degenerate component. This is reasonable since the distortion in the garnets forces the Si—O bonds more nearly parallel to the locally unique (S_4) axis. Therefore a stretching mode along the axis should be of higher frequency than the same type of mode perpendicular to the axis.

The lower frequency band is approximately half again as broad as the higher frequency band. This suggests that the residual twofold degeneracy is being lifted slightly. There are at least two mechanisms by which the residual degeneracy of the silicate ion vibrations could be lifted in YIG. The substitution of a single charge-compensating divalent ion on any one of the 14 metal ion sites adjacent to the silicate ion would remove locally the fourfold rotary reflection axis and thereby split the degenerate pair. The presence of the internal magnetic field could conceivably produce a similar effect.

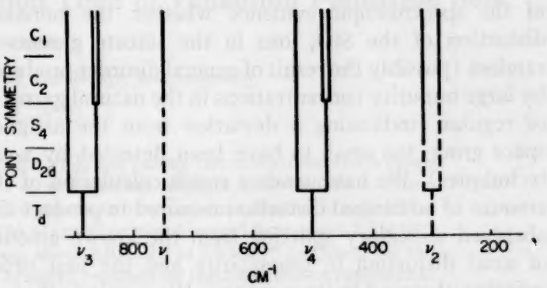

FIG. 5. Effect of certain distortions on the vibrational fundamentals of the silicate ion (solid lines represent infrared active frequencies).

The situation in the silicate garnets is quite different from that in the nonsilicate garnets. The silicate ions are no longer isolated from one another but are part of a coupled framework of silicate ions. The coupling of silicate ions will produce many extensive vibrational modes for each local molecular mode of the SiO_4 ion. No new infrared active fundamentals should be produced however, since all 12 SiO_4 ions in the primitive cell are symmetrically equivalent. Hornig[19] has shown that the site group approximation is valid in such a case. Therefore, no degenerate vibrational mode of the SiO_4 ion obtained by the local symmetry approach should be split when the whole crystal is considered.

On the other hand, a comparison of the spectra of the natural garnets with the spectrum of the silicate ion in the nonsilicate garnets (see Fig. 2) leads us to believe that the three strong sharp bands in the silicate garnet spectra arise from the three components of ν_3 completely resolved. The lower frequency pair of bands appears to correspond to the broadened lower frequency component of ν_3 of the silicate ion in YIG, while the higher frequency band agrees well with the nondegenerate component of ν_3. The separation of the lower frequency pair of bands from the higher frequency band in the natural garnets is somewhat greater than the related splitting in YIG, which supports our hypothesis that the axial distortion of the silicate ion should be greater in the silicate garnets than when the silicate ion occurs as an isolated impurity in YIG. The weak, diffuse bands and shoulders in the spectra of the silicate garnets are presumed to be produced by combinations of lower-frequency vibrations.

The principal feature of the silicate garnet spectra to be explained is the apparent complete removal of degeneracy of the silicate vibrations. If our interpretation of the spectrum is correct, the implication is that a large number (if not all) of the silicate ions possess C_2 or C_1 symmetry instead of the S_4 symmetry predicted by the assigned space group. It is difficult to decide on the basis

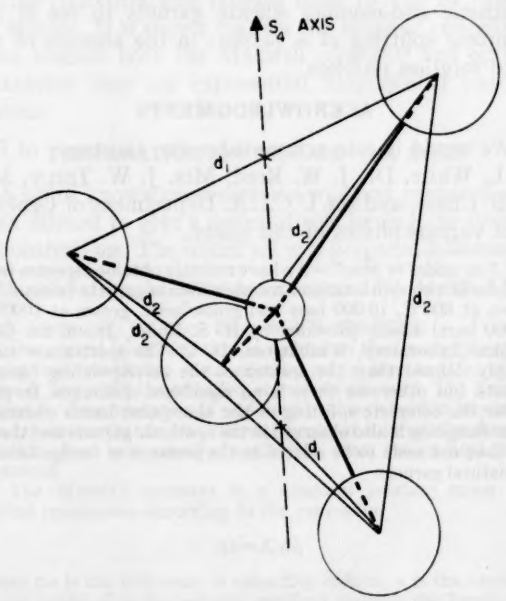

FIG. 4. Silicate ion in the garnet lattice ($d_1 < d_2$).

[19] D. F. Hornig, J. Chem. Phys. **16**, 1063 (1948).

of the spectroscopic evidence whether the nonaxial distortion of the SiO_4 ions in the silicate garnets is random (possibly the result of general disorder produced by large impurity concentrations in the natural garnets) or regular (indicating a deviation from the assigned space group too small to have been detected by x-ray techniques). We have made a rough calculation of the amount of additional distortion required to produce the observed secondary splitting from the known amount of axial distortion in grossularite and the first order splitting observed in its spectrum. We conclude that an error of only 0.04 A in oxygen to oxygen distances would be sufficient to produce the secondary splitting observed, and this estimate may be high, since the conditions for Fermi resonance between the first excited states of the two lower frequency components of ν_3 will be met if they are split even slightly. The two resultant modes will belong to the same species (whether the appropriate symmetry is C_2 or C_1) and the corresponding vibrational energy levels will be very close to one another. Thus the observed splitting could be caused by a smaller distortion than that obtained from our rough calculation.

It is our opinion that the secondary spectral splitting in the silicate garnets is too well defined, too reproducible from sample to sample, and too regular in its variation from one garnet type to the next to be the result of a disorder of the solid solution type. Still we cannot eliminate the disorder possibility. A study of pure synthetic silicate garnets would probably be helpful in this connection. If, on the other hand, the distortion is a regular feature of the garnet structure, it might be most observable by x-ray techniques in pyrope or almandite, where the secondary spectral splittings are most pronounced.

The broadening and apparent splitting of the absorption bands in the spectra of the flame fusion garnets is not yet understood. We have performed annealing experiments (1400°C for 24 hr followed by slow cooling) on several flame fusion garnets to see if a correctable local disordering were involved. After annealing, the flame-fusion garnets containing low silicon concentrations exhibited spectra which resembled more strongly the spectra of the flux-grown garnets. But flame fusion garnets with a high silicon concentration (e.g., 0.6 wt %) exhibited very complex spectra after annealing. The spectra of silicon-containing flux-grown crystals used as control samples did not alter on annealing. The SiO_4 spectra of the flame-fusion garnets before annealing suggest a high degree of localized lattice imperfection, and this may lead to precipitation of silicate phases on annealing in silicon rich samples.

CONCLUSIONS

This study has identified silicon in the form of the silicate ion as an impurity in the nonsilicate garnets. It is estimated that as little as 0.005% silicon by weight can be detected by infrared spectroscopy using the KBr pellet technique. This limit of detection could be lowered still further if single crystal samples were used.

The sensitivity of the silicate ion spectrum to lattice constant provides a "labeling" of the various rare earth iron garnets as well as the silicate garnets. The possibility of using the lattice constant shift in the natural ganrets for analytic purposes has already been suggested.[7]

The absorption bands observed near 900 cm^{-1} in both yttrium iron garnet and in the silicate garnets have been assigned to vibrational fundamentals arising from the triply degenerate fundamental, ν_3, of the undistorted tetrahedral SiO_4 ion. The degree of removal of the degeneracy of ν_3 is a measure of the distortion of the SiO_4 tetrahedron. Whereas a simple splitting of ν_3 into nondegenerate and doubly degenerate components is anticipated on the basis of the assigned garnet space group, partial splitting of the doubly degenerate component as well is observed in YIG, and complete splitting is observed in the silicate garnets. The additional splitting suggests that a net nonaxial distortion, either regular or random, is experienced by a large fraction of the silicate ions.

Additional work, including an investigation of the second triply degenerate infrared active fundamental (ν_4) of the silicate ion in the garnets, is planned.¶ It may also prove worthwhile to examine the spectra of synthetic end-member silicate garnets to see if the complete splitting of ν_3 persists in the absence of the solid solution problem.

ACKNOWLEDGMENTS

We would like to acknowledge the assistance of Dr. R. L. White, Dr. J. W. Reed, Mrs. J. W. Torpy, Mr. A. B. Chase, and the U.C.L.A. Department of Geology with various phases of this study.

¶ *Note added in proof*:—We have recently obtained spectra from samples of two synthetic end-member silicate garnets (almandite, grown at 800°C, 10 000 bars and grossularite, grown at 1000°C, 10 000 bars) kindly provided by H. S. Yoder, Jr., of the Geophysical Laboratory, Washington, D. C. The spectra are more sharply defined than the spectra of the corresponding natural garnets, but otherwise there is no significant difference. In particular the complete splitting of the absorption bands discussed in the foregoing is also observed in the synthetic garnets and therefore does not seem to be related to the presence of foreign ions in the natural garnets.

Streaming Birefringence and Optical Relaxation Time of Vanadium Pentoxide Sols*

WILLIAM T. FOREMAN

Baird-Atomic, Inc., 33 University Road, Cambridge, Massachusetts

(Received April 21, 1959)

Maxwell constant and optical relaxation time is studied for V_2O_5 sols having concentrations which range from 0.01 to 0.1 volume percent using mercury green, 5461 A, and mercury red light, 6000 to 6800 A. These quantities were measured in a device which sheared the sols between two coaxial discs, that is, in a direction which corresponds to the radial one in a Couette device. The Maxwell constant ranged from about 1.5×10^{-2} to about 4.5×10^{-6} cm²/dyne for freshly made sols and from about 8.0×10^{-2} to 2.9×10^{-6} cm²/dyne for the same sols when they were 29 days old. It is shown that the Maxwell constant for these sols was an exponential function of concentration and that the optical relaxation time and Maxwell constant could be related for them. Because the Maxwell constant is an exponential function of sol concentration, it is suggested that the expression for the rotary diffusion constant of an infinitely dilute sol of rod-shaped particles can be made applicable to more concentrated sols by multiplying it by the term $(e^{sC}-1)/sC$, where C is concentration and s is the slope of the curve relating sol concentration to Maxwell constant, to account for the change in particle interaction with change in sol concentration.

The viscosity and spectral transmission of these sols were also checked. It was found that the viscosity ranged from 1.0 cp for the most dilute sol to about 1.25 cp for the sol of concentration 0.1 volume percent. These sols were found to have a transmission which peaked at about 6800 A and dropped rapidly on either side of this value.

INTRODUCTION

THE discovery of streaming birefringence is generally attributed to James Clerk Maxwell, who noticed that a viscous liquid, such as Canada balsam, exhibits optical anisotropy when agitated. Since his initial discovery, the effect has been found in many pure liquids and sols; it is quite large in vanadium pentoxide or bentonite sols.

The related effect, rotary diffusion, has been referred to in the literature, but with the exception of Langmuir[1] no one has studied its reciprocal quantity, optical relaxation time.[2] In this paper the Maxwell constant[3] and optical relaxation time are studied for V_2O_5 sols having concentrations ranging from 10^{-3} to 10^{-4} parts by volume. It is shown that for the range of concentrations studied both the Maxwell constant[3] and optical relaxation time are exponential functions of concentration.

PREPARATION OF GRADED V_2O_5 SOLS

A sol of known concentration was first prepared and then diluted to give a series of sols having the desired concentrations. The initial sol was prepared following a modified method of Hauser.[4] Thirty g of ammonium metavanadate and 150 cc dilute nitric acid (1 part dilute nitric acid of 1.4 specific gravity to 5 parts water) were ground together. The mixture was then placed on a filter and washed with distilled water until the filtrate began to come through the filter distinctly colored. The precipitate was then washed off the filter into a beaker and 550 cc distilled water in which was dissolved 0.30 g gelatin[5] was added (roughly 1 g gelatin for each 100 g V_2O_5, exclusive of water). After dispersion, about 24 hours, the sol was filtered through glass wool to remove any solid matter which remained.

Although Hauser[4] did not mention the sol's sensitivity to impurities, it was found that to prepare a good sol one must use distilled water and freshly cleaned glassware, otherwise the sol will agglomerate immediately. However, if it has been properly prepared the sol will disperse almost entirely within 24 hours. When dispersion is complete the sol will look like a reddish-brown liquid having uniform viscosity and exhibiting no scattering.

Microscopic examination of a filtered disperse sol exhibits a structure which appears "matt-like" in texture. Dark field illumination shows no light scattering and examination of the sample between crossed polaroids gives no evidence of optical birefringence. It would thus appear that the "matt" is really composed of much finer particles, presumably V_2O_5 crystals. This fact would suggest that the V_2O_5 sol is a collection of micellular structures each of which is composed

* Supported by the Army under contract DA-44-009-ENG-3119.

[1] I. Langmuir, J. Chem. Phys. 6, 873–896 (1938).

[2] The optical relaxation time is defined as the time required for the optical retardation of an oriented sol to drop to $(1/e)$ of the value it had when the orienting stress was removed. The time required for flow relaxation is neglected in this definition because it can be shown that in the measurements of interest the flow relaxation time was usually much less than the optical times measured.

[3] The Maxwell constant is a constant relating stress and optical retardation according to the expression

$$\Delta n = K\eta G,$$

where Δn is the difference in refractive indices, n is the viscosity of the liquid, G is the velocity gradient through the liquid, and K is the Maxwell constant.

[4] Hauser's notes in care of Alan Michaels at Massachusetts Institute of Technology, Cambridge, Massachusetts, Expt. 39, p. 33, gives information on V_2O_5 sols.

[5] The gelatin acts as a preservative. Sols prepared without gelatin deteriorate within a week, while those prepared with gelatin may last for months or even years, with gradually increasing Maxwell constant.

of V_2O_5 crystals. Langmuir[1] suggests that such a situation exists in bentonite sols.

Although one would expect to determine the sol concentration directly from calculation, the losses inherent in the preparation of a small quantity of sol made such an approach impossible. It was then necessary to analyze this sol to determine its concentration. Analysis was performed, by the dry weight technique, on a known quantity of sol which had been precipitated by dilute nitric acid. For five analyses the greatest difference between the average concentration, 0.5 volume percent, and any one determination was no more than 24%. By comparison the calculated value of sol concentration was 1.26% by volume.

This original sol was so concentrated that it had very little optical transmission, hence it was diluted in steps by mixing a certain portion of it with a certain quantity of distilled water. The resulting concentrations ranged from 0.1 to 0.01% by volume.

VISCOSITY AND SPECTRAL TRANSMISSION OF SOLS

It is known that sufficiently concentrated V_2O_5 sols will be thixotropic but, since there were no data available on how the viscosity of these sols varied with concentration, it was decided to measure the viscosity of each one. The measurements were made by means of a capillary viscosimeter. They showed that the viscosity was nearly a linear function of concentration for sols up to 0.1 volume percent, at which the viscosity was about 0.0125 poise. Measurements for more concentrated sols, however, showed the viscosity to be an exponential function of concentration. This behavior agrees with that determined by Peterlin[6] and Yang[7] for polymer solutions.

The spectral transmission of these sols was measured for a one-cm pathlength in a Beckman spectrophotometer. These measurements showed that the sols have a peak transmission at about 680 mμ and that their transmission decreases rapidly toward either the red or blue. Although none of these sols showed any transmission at 5461 A in the Beckman spectrophotometer, visual observation showed that in layers 1/16-inch thick they would transmit sufficiently for the birefringence measurements.

STREAMING BIREFRINGENCE AS A FUNCTION OF SOL CONCENTRATION

It has long been known that V_2O_5 sols exhibit large values of streaming birefringence, but there are no data in the literature relating concentration and streaming birefringence. For this reason it appeared quite desirable to see how the streaming birefringence varied with sol concentration, and whether or not any relation existed between a sol's optical relaxation time and its streaming birefringence. One might expect the streaming birefringence to increase with sol concentration and Langmuir[1] also suggests that in concentrated V_2O_5 sols the relaxation time is longer than for dilute sols. We are thus led to suspect that some relation might exist between sol concentration, streaming birefringence, and relaxation time.

Before describing the measurements of streaming birefringence it is convenient to give some of the relations between streaming birefringence, shear, and viscosity.

In 1939 Peterlin and Stuart[8] presented a theory relating changes in refractive index (Δn) of a dispersion to its composition and the stress applied to it. Later Edsall, Gadd, and Sheraga[9] performed some calculations, based on the theory of Peterlin and Stuart,[8] to find numerical relations between the angle of isocline, change in refractive index, particle size and shape, and fluid viscosity for a dispersion subjected to shear in a Couette device.[10] Whereas Edsall, Gadd, and Sheraga were interested in the relations between the angle of isocline χ, the orientation factor $f(\alpha, R)$, and shear for sols sheared at high rates in a Couette device, we are interested in comparing similar quantities for sols subjected to low rates of shear. Although most other investigations of streaming birefringence were made with a Couette device which shears the sol or liquid between two cylinders the present study of birefringence was made in a device that shears the sol between two discs. With this device, described presently, the liquid is viewed along an axis that is parallel to the velocity gradient and normal to the streamlines of flow. As shown by Stewartson[11] the velocity gradient between discs is linear for zero Reynolds number and very nearly linear for a Reynolds number of ten. For the fastest flow obtainable in this study the Reynolds number was only slightly greater than two. For the few measurements taken at this rate one might expect a very slight nonlinearity, but for most of the measurements taken at far smaller gradients the assumption of a linear gradient certainly holds. The change in viewing direction in this device may change some constants in the equations relating birefringence, viscosity, and stress, but it should not change the form of these equations. With this thought in mind let us note the pertinent relations.

The first relation of interest is one that is analogous to an expression given by Alcock and Sadron.[12] This equation which relates the birefringence to shear for liquid sheared between two discs is given by

$$\Delta n_z = K_z \eta (dU_x/dZ) = K_z \eta G_z, \qquad (1a)$$

[6] A. Peterlin, Proc. Intern. Congr. Rheol. 2nd Congr. Oxford, 1953, p. 343; J. Polymer Sci. **12**, 45 (1954).
[7] Jen Tsi Yang, J. Am. Chem. Soc. **80**, Eq. (5b), p. 5140, or Eq. (13b), p. 5145 (1958).
[8] A. Peterlin and H. A. Stuart, Z. Physik. **112**, 1, 129 (1939).
[9] Edsall, Gadd, and Sheraga, J. Chem. Phys. **19**, 1101–1108 (1951).
[10] Edsall, Rich, and Goldstein, Rev. Sci. Instr. **23**, 695–701 (1952).
[11] K. Stewartson, Proc. Camb. Phil. Soc. **49**, 333–341 (1953).
[12] E. D. Alcock and C. Sadron, Physics **6**, 92–95 (1935).

where Δn_z is the difference of the indices $n(x)$ in the plane of flow and $n(y)$ measured normal to the flow plane, K_z is the z component of Maxwell constant (cm²/dyne) defined for the present viewing coordinates, η is the viscosity,[13] and G_z is the gradient dU_x/dZ.

As shown by Edsall and Muralt[14] the optical ellipsoid for slow rates of flow lies at an angle of 45 degrees to the streamline of flow. Thus any value of K_z given in this paper should be multiplied by $\sqrt{2}$ to get the value of Maxwell constant seen if one were to look normal to the optical ellipsoid in the xz plane. This latter value of Maxwell constant (not K_z) might correspond to that which one would see with a Couette device, but there is no assurance that this is true. Edsall, Gadd, and Sheraga[9] give the relation

$$\Delta n_z = (2\pi/n_a)C(g_1-g_2)f(\alpha, R) \qquad (1b)$$

which when combined with Eq. (1a) results in

$$K_z\eta G_z = (1/2n_a)CLf(\alpha, R), \qquad (2)$$

where C is the volume fraction of the particles in the sol, n_a is the average refractive index of the mixture, and $L=4\pi(g_1-g_2)$ and $f(\alpha, R)$, respectively, are optical and orientation factors which are described in the next paragraph.

The optical factor relates refractive indices and shape, while the orientation factor relates shear and rotary diffusion for the particles concerned. Peterlin and Stuart[8] give the orientation factor as a series

$$f(\alpha, R) = (\alpha R/15)\{1-(\alpha^2/72)[1+(6R^2/35)]+\cdots\}, \qquad (3a)$$

in which $\alpha=G/\theta$, and $R=(p^2-1)/(p^2+1)$, where $G_z=dU_x/dZ$ is the velocity gradient, $\theta=1/2\tau_z$ is the rotary diffusion constant, and $p=a/b$ is the axial ratio of the particles in question. If the flow is sufficiently slow[15] Eq. (3a) can be approximated giving

$$f_z(\alpha, R) = \alpha/M = 2\tau_a G_z/M \qquad (3b)$$

where the constant M depends upon the direction of viewing. On substituting Eq. (3b) into Eq. (2) there results

$$K_z = (1/M)(C/\eta n_a)L\tau_z, \qquad (4)$$

where the constant $1/M$ is to be evaluated from experiment. According to Eq. (4) the Maxwell constant should vary linearly with concentration and relaxation time τ_z. However, one should note two significant facts with regard to τ_z: (1) The relaxation time (τ_z) is also found to vary with concentration and, (2) The particles in question will have rotational freedom around three mutually perpendicular axes, hence the relaxation time for the "measured" optical retardation might not correspond to the τ_z in Eq. (4) even though the two could have some functional relation.

In order to check the validity of Eq. (4) it was necessary to measure K_z and τ_z as a function of concentration and to evaluate L from theory for the various sols. The measurements of streaming birefringence and optical relaxation time are given in the next section and the calculation of the optical factor is given in the one following it.

Most, if not all, previous information about streaming birefringence has been obtained by shearing a liquid in a Couette concentric cylinder arrangement. In all cases known to the author, the direction of viewing the birefringence was along the axis of rotation of the cylinder. Because the axial distance along which the birefringence is viewed in the Couette arrangement

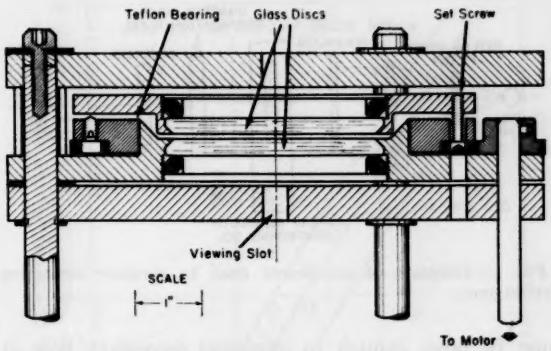

FIG. 1. Cross section of shear generator drawn normal to the viewing slot.

[13] For infinitely dilute sols η is the viscosity of the solvent. Peterlin,[6] however, indicates that in moderately concentrated solutions the viscosity acting on the solute molecule, termed effective viscosity, is intermediate between that of the pure solvent and that for the solution. According to Peterlin the effective viscosity, solvent viscosity, and solution viscosity are related by the expression: $\eta_s=\eta_l+ck\eta^*$ where η_s is the solution viscosity, η_l is the liquid viscosity, η^* is the effective viscosity, and the product ck is given by $\ln(\eta_s/\eta_l)$. Both Peterlin[6] and Yang[7] demonstrate that these relations hold for polymer solutions over a wide range of concentrations with the exception of low ones.

Because the V_2O_5 sols discussed in this paper exhibited a viscosity that varied exponentially with concentration as the polymer solutions did, it is tempting to apply these relations to them. However, the demonstration of their validity for polymer solutions does not prove that they apply in a sol made up of submicroscopic particles dispersed in water, even though it strongly suggests that they do. Furthermore, even if we assumed this relation to apply, the effective viscosity determined from it for the most viscous sol would only be about 10% larger than that for pure water. On the other hand, scatter in values of Maxwell constant or relaxation time is greater than 10%, hence for these data it is not possible to demonstrate the applicability of these relations. For these reasons we shall, throughout this paper, use only the viscosity of pure water, which is about 0.01 poise.

[14] A. L. Muralt and J. T. Edsall, J. Biol. Chem. **89**, 315 (1930).

[15] Because of the range of concentrations studied it was not practical to set the same upper velocity gradient for all sols. Instead optical retardation as a function of gradient was determined for flows ranging from zero velocity up to some arbitrary maximum. The linear portion of each curve, starting at its origin, would then correspond to the region in which α was less than about 5 for which the approximation Eq. (3b) holds. If a suitable curve could not be obtained for a particular disc separation the distance between plates was increased making it possible to get the same retardation for a lower gradient.

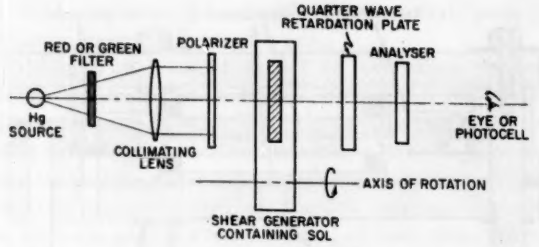

FIG. 2. Diagram of equipment used to measure streaming birefringence.

must be large enough to minimize secondary flow at the ends of the cylinders, the length of the liquid column viewed cannot be indefinitely shortened, and is limited in practical cases to distances larger than a few millimeters.

The present device, of which a cross section taken normal to the long axis of the viewing slot as shown in Fig. 1, was made in such a way that the direction of viewing is normal to the streamline of flow and parallel to the flow gradient. Further, the path length can be freely adjusted down to zero, and liquids with very large streaming birefringence in thin layers thus become accessible for study.

The thick aluminum plates at the extreme top and bottom have corresponding slots through which the sample can be viewed. The sample remains between the upper and lower bevelled glass discs by capillarity, and is free to run into the annular recess between the stainless steel mounting discs. The upper mounting disc is free to revolve, and is driven by a gear at its periphery, pivoting on bearing surfaces of Teflon sheet which function well at room temperature.

To determine the shear on the sample the optical measurements were made at a certain distance from the center. Then the liquid under the top disc would move with a velocity given by

$$v_s = r\omega, \tag{5}$$

where v_s is in cm/sec, r is in centimeters, and ω is in radians per second. For low rates of shear the gradient is uniform, giving

$$G_x = dU_x/dZ = v_s/Z, \tag{6}$$

in which v_s is given by Eq. (5) and Z is the length of gap between discs.

Before performing any measurements of streaming birefringence, it was first necessary to separate the glass discs in the shear generator by 1/16 inch and to align the optics. The disc separation was effected by three adjusting screws which permitted a setting accuracy of about 10%. It can be shown, however, that the distance between discs is not critical except insofar as it will determine the rotational velocity of the top plate for which "saturation effects"[15] could become important.

Before aligning the optics (Fig. 2) it was necessary to allow a five minute warmup for the mercury arc bulb. After this time, the V_2O_5 sample was placed in the shear generator (through a hole in the top plate) and the optics were aligned so that collimated light would pass up through a viewing slit in the generator. This slit was arranged to coincide with a radius of the discs, hence the slit was perpendicular to the flow field and the optic axis of the sheared liquid. The polarizer was oriented at $-45°$ to the viewing slit; thus when the liquid was sheared, its optic axis would be oriented at $-45°$ with respect to the polarizer axis. The quarter-wave plate was oriented with its optic axis parallel to the polarizer's axis. With this setting and no shear, complete extinction should have been achieved. If it was not achieved then the analyzer and quarter-wave plate were reset to give complete extinction for zero shear.

Having completed this initial adjustment, the motor used to drive the shear generator was started and a check was made to determine whether or not it was possible, for any rate of shear, to get extinction by rotating only the analyzer. However, if it was also necessary to rotate the quarter-wave plate and polarizer, then it was presumed that the original angular setting between the polarizer and the viewing slit had not been properly set. In this case the angle was reset and rechecked to see whether or not extinction could be achieved by rotating only the analyzer.

When rotating only the analyzer to obtain complete extinction, the angle between the polarizer axis and the viewing slit was particularly sensitive for an old sol having a large Maxwell constant, but not so sensitive for a young sol having a small Maxwell constant. Besides the sensitivity to angular setting, it was found initially that the two following factors also contributed to difficulties in getting complete extinction: (1) At first the presence of yellow and red radiation in the green light passing from the V_2O_5 made it impossible to get complete extinction with even the youngest sol. This difficulty was eliminated by the use of two green filters, which definitely improved the monochromatic nature of the emergent green light. No such difficulty was encountered for the red light. (2) Initially, the light was allowed to come up through a wide slit. Thus, there was considerable light whose optic axis was oriented at an angle other than the required angle of $-45°$ with respect to the polarizer axis. This light could not be extinguished. This difficulty was eliminated by use of a narrow slit which passed light whose optic axis had an angular spread of only a few degrees.

With all adjustments properly made, it was possible to get extinction for any rate of shear by rotating only the analyzer. The retardation could then be calculated from a relation derived from an equation given by Hsü, Richartz, and Liang.[16] This relation as derived

[16] Hsu, Richartz, and Liang, J. Opt. Soc. Am. **37**, 104 (1947) Eq. (12). In their equation set $\gamma_3 = 0$ to derive Eq. (7).

from their expression is given by

$$\delta = 2(\phi_0 - \phi_s), \qquad (7)$$

where ϕ_0 is the angular setting of the analyzer to give extinction with no shear and ϕ_s is the angular setting of the analyzer to give extinction with shear.

The optical retardation and Maxwell constant are related by the equation

$$\delta(\text{degrees}) = (360/\lambda)\int K_s \eta (dv/dZ)\, dZ \qquad (8a)$$

which for a linear gradient becomes

$$K_s = \delta\lambda/360\eta v_s, \qquad (8b)$$

where δ is the retardation in degrees, λ is 5461×10^{-8} cm (mercury green light) or 6400×10^{-8} cm (mercury red light), η is about 0.01 poise for water at room temperature, and v_s is the velocity of the top of the liquid.

By using Eq. (8b) the Maxwell constant was calculated from values of (δ) at different rates of shear for each of the 10 sols (0.1% through 0.01%). The light sources were the mercury green, 5461 A, and mercury red, 6400±400 A. These Maxwell constants are plotted as a function of concentration in Figs. (3) and (4). It will be noticed that the Maxwell constant varies exponentially with concentration for the sols studied and also that for each sol it increases with the sol's age.

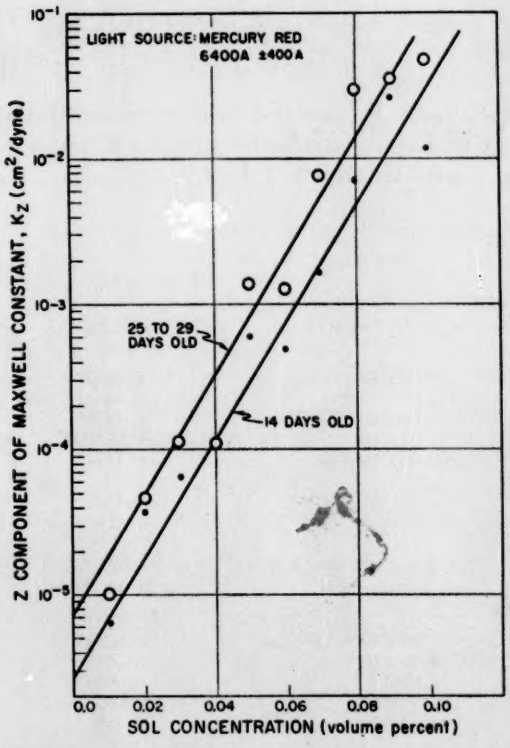

FIG. 3. Maxwell constant as a function of sol concentration for mercury red light.

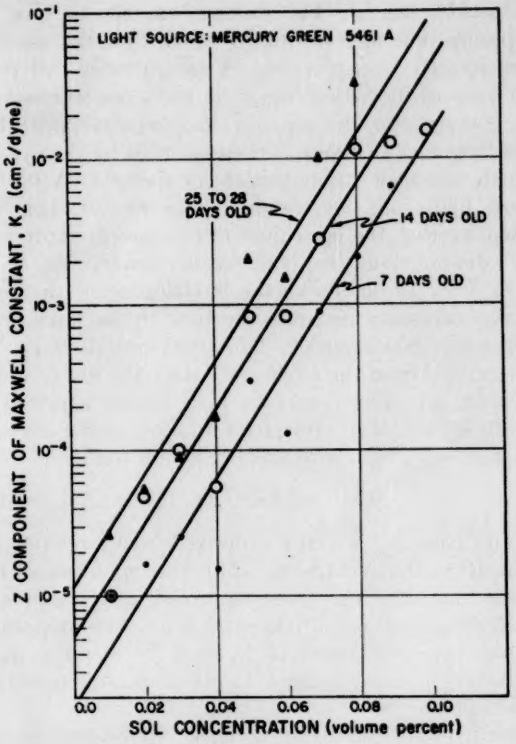

FIG. 4. Maxwell constant as a function of sol concentration for mercury green light.

Simultaneous with the increase of Maxwell constant, an increase of birefringence decay time was also observed. The method of observing the change in decay time with sol concentration and some of the implications of this change which were discussed by Langmuir,[1] are described in the following section.

OPTICAL RELAXATION TIME AS A FUNCTION OF SOL CONCENTRATIONS

The birefringence decay time was measured by means of the previous apparatus employed along with a 1P21 photomultiplier, a power supply to run the photomultiplier and an oscilloscope to record its output. As in the previous measurements the optics were set so as to give complete extinction for zero shear (and zero birefringence). The oscilloscope had a driven sweep which was triggered by a stop mounted on top of the shear generator.

To obtain the data, a sample was placed in the shear generator and, with the arc source running, the optics were aligned as described in the previous section. The motor was then disconnected from the shear generator and a stop was fastened onto the generator's top disc (the one which normally rotates).

With the room lights off, the voltage input to the photomultiplier was adjusted so as to give a scope trace

of useable height. The camera was set to give an exposure time of 5 sec during which time the top disc was rotated against a stop. A switch connected from the stop to the sweep-trigger on the scope would start the sweep after the top disc had been stopped. The resulting decay curve was then recorded by the camera which was open during this entire operation. With the room lights out, the residual light was of such low intensity that the open time of the camera shutter (5 sec) did not result in any noticeable film fogging.

In order to determine the birefringence decay time it was necessary to relate the time to the amount of remaining birefringence. The time could easily be determined from the scope trace since the source was a mercury arc lamp that gave light having a period of 1/120 second. The optical retardation at the time of interest was then calculated from the equation

$$\delta(t)=2\sin^{-1}(A_t/A_m)^{\frac{1}{2}}. \tag{9}$$

In this equation, which was derived from a relation by Hsü, Richartz, and Liang,[16] A_t is the amplitude of the scope trace for the time concerned and A_m is the maximum signal amplitude of the trace. This amplitude would correspond to $\sin(\delta/2)$ for $\delta/2=90°$. The trace preceding it would be for $\delta/2>90$, whose sine would be less than one.

Two sets of photographic traces were obtained for each sol from 0.05% through 0.09% with the mercury red and the mercury green source. To find the relaxation time for each of these traces it was first necessary to calculate δ as a function of time. This was done by using Eq. (9), taking the peak of each trace as A_m for $\delta/2=90°$, and plotting the results on semilog paper. The optical relaxation time was then calculated from the tail portion of the resulting curve. These values are given in Table I.

At this point it would be instructive to determine whether or not any relation existed between the Maxwell constant K and the relaxation time in the sols studied. Before doing this, however, it is first necessary to calculate the optical factor L for a V_2O_5 dispersion in water. This factor can be calculated from an equation given by Peterlin and Stuart[8] after making two simplifying assumptions. First let us assume that the axial ratio of V_2O_5 is greater than 5. Second, we shall assume that the V_2O_5 crystals are optically isotropic. This second assumption may be contrary to the facts as indicated by Edsall and Muralt.[14] Nevertheless, as shown in the following, this assumption does not appear to introduce severe error into the result.

Subject to these assumptions the equation of optical factor given by Peterlin and Stuart reduces to

$$L=(n^2-n_l^2)^2/(n^2+n_l^2), \tag{10}$$

where n is the refractive index of the V_2O_5 particles and n_l is the index for water.

The refractive index of V_2O_5 could not be found in the literature, hence an estimate of its value was made from molecular and atomic refractivities. The value of refractive index so calculated was 1.95, for which the optical factor L from Eq. (10) is 0.75. By using this value for the optical factor, setting $\eta=0.01$ poise, and setting $n_0=1.40$, Eq. (4) reduces to

$$K_s=(1/M)(.75/1.4\times0.01)C\tau_s \tag{11a}$$

$$=(1/M)53.57C\tau_s. \tag{11b}$$

Values of $1/M$ calculated from the measured relaxation time and the interpolated values of K_s taken from Figs. 3 and 4 are given in Table I.

TABLE I. Relaxation time and $1/M$ for V_2O_5 sols of different concentrations.

Concentration in parts by volume	τ_s (seconds) Sols 20–21 days old Hg Red, 6400±400 A	$C\tau_s$ 20 days old sol	K_s interpolated from Fig. 3 (red light)	$(1/M)=(K_s/53.57C\tau_s)$ (red light)
0.0005	0.287	0.000143	5.00×10^{-4} cm²/dyne	0.065269
0.0006	0.272	0.000163	12.50×10^{-4} "	0.14315
0.0007	0.70	0.000490	32.00×10^{-4} "	0.12191
0.0008	2.78	0.00240	81.00×10^{-4} "	0.0630007
0.0009	2.47	0.00223	200.00×10^{-4} "	0.16742
				Av 0.112
Concentration in parts by volume	τ_s (seconds) Sols 8–9 days old Hg Green, 5461 A	$C\tau_s$ 8 days old sol	K_s interpolated from Fig. 4 (green light)	$(1/M)=(K_s/53.57C\tau_s)$ (green light)
0.0005	0.254	0.000127	1.80×10^{-4} cm²/dyne	0.02647
0.0006	0.304	0.000182	4.30×10^{-4} "	0.0441
0.0007	0.2875	0.000201	10.6×10^{-4} "	0.09844
0.0008	0.701	0.000561	26.00×10^{-4} "	0.08651
0.0009	2.20	0.00198	63.50×10^{-4} "	0.05987
				Av 0.06308

TABLE II. Values of the length of semimajor axis for ellipsoidal particles having an axial ratio (p) of five. The Maxwell constants used were taken from the curves of Figs. 3 and 4 for sols of maximum concentration. Eq. (14) was used to calculate a_z from K_z and Eq. (13) was used to calculate a_0 from a_z.

Maxwell constant	Light source	Sol age	$a_z=7.21\times10^{-4}(K_z)^{1/3}$ (microns)	Product of slope and concentration $=sC$	$a_0=a_z[sC/(e^{sC}-1)]^{1/3}$ (microns)
0.013 cm²/dyne	Hg green	7 days	1.69	8.92	0.179
0.039 "	5461 A	14 days	2.44		0.258
0.084 "		25 to 28 days	3.16		0.335
0.030 "	Hg Red	14 days	2.24	9.40	0.208
0.088 "	6400 ±400 A	25 to 29 days	3.20		0.297

DISCUSSION OF RESULTS

Although the values of $(1/M)$ in Table I are found to exhibit considerable spread, their mean value, 0.0875, (by averaging 0.112 and 0.0631) is only slightly larger than the value of 1/15 given by Peterlin and Stuart.[8] No check was made to determine the cause or causes of the variation in the calculated ratio $(1/M)$ because of the scatter in and scarcity of the data, but two possible causes for it will be mentioned.

First we should note that the optical factor given by Peterlin and Stuart[8] makes no allowance for absorption, yet these sols exhibit very large absorption on either side of the peak at 6800 A. Conceivably, use of relations such as those given by Snellman and Björnstahl[17] would reduce this variation somewhat, but it is doubtful that much improvement would result from their use as a comparison of Figs. 3 and 4 will show. Within the limits set by the data the two curves of Maxwell constant for the 25 to 29 day old sols can be made to coincide simultaneously with the coincidence of the curves at 14 days. While this does not prove the Maxwell constant to be invariant with wavelength it does suggest that the variation is small.

A second explanation of this variation, that some evaporation occurred during the course of measurements, is suggested by the fact that with two exceptions the relaxation times for the 20 day old sols are larger than those for 8 day old sols. Because of the manner in which these times were measured it is unlikely that their values could have been affected by a change in wavelength, but they would certainly have been affected by evaporation. Since the ratio $(1/M)$ varies as $K_z/C\tau_z$, an unaccounted increase in concentration through evaporation, would increase K_z making $(1/M)$ appear larger than it ought to be.

Because the average value of M is in agreement with that given by Peterlin and Stuart,[8] whose value is 15, and because it was observed that the Maxwell constant and optical relaxation time were both larger in more concentrated sols, it is in order to say something more about the relation between relaxation time and sol concentration.

Various authors,[9,18] suggest that for infinitely dilute sols the relaxation time is given by Perrin's equation[19]

$$\tau_z=(1/2\theta)=\tfrac{8}{3}(\pi\eta a_0^3/kT)(2\ln 2p-1)^{-1}, \quad (12)$$

where η is the solvent viscosity in poise, a_0 is the length of the particle's semimajor axis, k is Boltzmann's constant, T is the temperature in degrees Kelvin, and $p=a/b$ is the axial ratio for needle-shaped particles.

According to this equation, the relaxation time should be independent of sol concentration. This is contrary to the present findings and those of Langmuir.[1] His studies showed that the relaxation time of bentonite (not V_2O_5) sols was definitely related to the sol concentration, and if a sol was sufficiently concentrated, it would have an infinite relaxation time (e.g. birefringence would exist in the absence of shear). In order to reconcile these seemingly divergent points of view, it is suggested that Perrin's equation[19] giving relaxation time for infinitely dilute sols be multiplied by the quantity

$$e^{sC}-1/sC, \quad (13)$$

where C would be the concentration expressed as a volume fraction, s would be the slope of the curve relating the Z component of Maxwell constant and concentration, and the other constants would be as previously described.

By expanding the exponential e^{sC} it can be seen that as the sol becomes dilute the equation for τ_z asymptotically approaches Perrin's equation, while for more concentrated sols $C\tau_z$ would vary as $(A/s)e^{sC}$. The former behavior fits the findings of Edsall[9] and others for dilute sols, while the latter one is in agreement with the curves of Figs. 3 and 4 relating Maxwell constant and sol concentration. It is interesting to note that for intermediate concentrations, Eq. (13) has a form similar to that of some equations given by Yang.[7]

If one assumes that Eq. (12) should be rewritten so as to include Eq. (13) it is then instructive to speculate about the significance of this correction term. This term could account for changes of particle size with sol concentration or it could account for particle interac-

[17] Von O. Snellman and Y. Björnstahl, Kolloid-Beihefte **52**, 403–465 (1941), Eqs. 6.29, 6.30, 6.31, p. 432.

[18] M. Goldstein, J. Chem. Phys. **20**, 677–682 (1952).

[19] F. Perrin, J. phys. radium [7] **5**, 497–511 (1934).

tion. The latter possibility is suggested by Langmuir[1] for bentonite sols.

In order to decide whether or not the correction term, Eq. (13), accounts for changes in particle size with change in concentration we shall give the length of the semimajor axis for the most concentrated sol determined with and without the correction term and also note the implication of changes in particle size with concentration. The values of semimajor axis which are considered to depend on sol concentration are calculated from the relation

$$a_z = (K_z)^{\frac{1}{3}}\left[\frac{3}{8}\frac{kT}{\pi\eta}\frac{(2\ln 2p-1)}{53.57(1/M)C}\right]^{1/3}$$
$$= 7.21\times10^{-4}(K_z)^{1/3} \qquad (14)$$

for the values $k=1.38\times10^{-16}$ ergs/degree, $T=295°$K, $\eta=0.01$ poise, $p=5$, $1/M=0.0875$, $C=0.001$ cm^3 V_2O_5 per cm^3 H_2O, and K_z given in Table II. The corresponding values of a_0, the value considered to be independent of concentration, were calculated from a_z using Eq. (13) and the values of (sC) given Table II. The corresponding values of a_z and a_0 differ by factors of about ten.

Not only is a_z larger than a_0 for the 0.1% sol, its value will vary quite noticeably with changes in sol concentration. Thus for a_z one would expect sols of different concentration to exhibit markedly different values of scattering. However, visual observation indicates that, while absorption varies strongly with sol concentration, little, if any, variation in scattering can be detected for good sols of different concentration. Thus it would appear that particle size depends less strongly than particle number on sol concentration, that is, the particle size varies as a_0 and hence increase of τ_0 with concentration depends more upon change of particle number and particle interaction than change of particle size. This is also in agreement with a statement made by Hauser[4]:

"The original sol particles are extremely fine, well below 100 mμ, and of anisometric configuration."

CONCLUSIONS

Spectral measurements of V_2O_5 sols show that they are quite transparent in the red portions of the spectrum and very opaque in the green and blue portions. Sols containing 0.001 cm^3 V_2O_5 per cm^3 H_2O exhibit very little scattering.

It has been found that sufficiently dilute sols are not thixotropic although they are more viscous than pure water. The sols studied had viscosities ranging from about 0.01 poise up to 0.0125 poise.

It is shown that for the range of sols studied the Maxwell constant is an exponential function of the sol concentration. It is also shown that a relation exists between optical relaxation time and Maxwell constant.

It is suggested that Perrin's equation[19] for the relaxation time of a dilute dispersion of rod-shaped particles be modified by an exponential multiplier to account for particle interaction in more concentrated sols. It appears that in concentrated sols, the average particle size differs little from that of dilute sols, but, as the sol concentration increases, the number of particles rises almost linearly with concentration and the particle interaction rises exponentially with sol concentration.

ACKNOWLEDGMENT

The author wishes to acknowledge Stephen J. Sullivan, Jr., who measured the transmission of the V_2O_5 sols reported and Myron C. Block and Dr. D. Z. Robinson for many helpful discussions which contributed greatly to the studies made.

Negative Ion Formation in NO_2 by Electron Attachment

R. E. Fox

Westinghouse Research Laboratories, Pittsburgh 35, Pennsylvania

(Received August 14, 1959)

Negative ion formation in NO_2 by electron attachment is studied at low pressures as a function of electron energy in a mass spectrometer. The principle ion formed is found to be O^- which onsets at 1.35 ± 0.05 ev and whose apparent maximum occurs at 1.90 ev. Comparison of the peak shape with the electron energy distribution indicates the maximum cross section occurs within 0.1 ev of threshold. The NO_2^- ion whose maximum cross section is only about one-hundredth that for O^- appears to have the same energy dependence. Crude estimates of the cross section for attachment yield order of magnitude values of 10^{-18} cm^2 for O^- and 10^{-20} cm^2 for NO_2^-.

IN view of the large negative ion of mass 46 found in the upper atmosphere by rocket-borne mass spectrometers,[1] considerable interest has been raised as to the negative ion formation in NO_2. Appreciable amounts of NO_2^- are observed by Branscomb[2] in a high pressure discharge of O_2 when small contaminants of N_2 are present.

The negative ions formed by electron capture in NO_2 have been studied in the low pressure ion source of a mass spectrometer. The mass spectrometer is a 90° sectional magnetic field type employing the retarding potential difference method[3] for obtaining ionization due to electrons with a narrow energy spread. The energy scale is determined by a simultaneous measurement[4] of the negative ions formed and the electrons passing through the collision chamber as a function of the electron accelerating voltage.

In order to obtain appreciable signals, the pulsing techniques[3] normally employed on the electron beam and ion beam are abandoned and a dc voltage on the ion repeller plate is employed. This would be necessary if the ions were formed with appreciable kinetic energy, or if there is a contact potential between the ion repeller plate and the ionization chamber ion slit.

The electron collector is biased 10 v positively with respect to the ionization chamber such that the electrons are accelerated to the collector upon leaving the ionization chamber. This precaution is found to be necessary when operating at low electron energies in order to prevent reflection of low energy electrons at the surface of the electron collector. After suitable baking procedures, the background pressure is reduced to about 10^{-9} mm Hg.

EXPERIMENTAL RESULTS

NO_2 gas is admitted until the pressure in the ion source is of the order of 10^{-4} mm Hg. The only ion of appreciable quantity is O^-. The NO_2^- ion current which appears to have the same energy dependence for formation is only 1/100 that of the O^- ion and is too small to make an energy dependence measurement with any appreciable accuracy.

In Fig. 1, curve 2 shows the O^- formation from NO_2 as a function of the electron acceleration voltage. Curve 1 shows the electron current passing through the ionization chamber as a function of the same electron accelerating voltage. This curve then is a retarding potential curve for the electrons and the differential of this curve shown by the dotted curve gives the electron energy distribution. It should be noted that contrary to the way energy distributions are normally shown, this distribution is reversed energy-wise, the higher energy electrons being to the left. The voltage difference between the onsets of the two curves is then the energy in electron volts above zero at which the O^- ion appears.

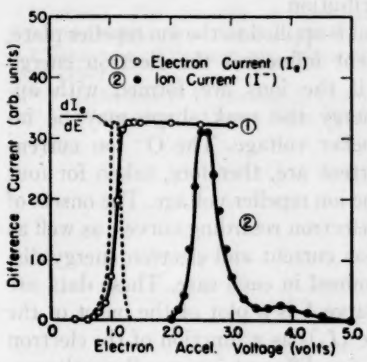

FIG. 1. Curve 1. The electron current passing through the ionizing chamber as a function of the electron accelerating voltage. Curve 2. The negative ion current O^- from NO_2 as a function of the electron accelerating voltage. The dashed curve is the differential of the electron retard curve (1) indicating the electron energy distribution.

From this figure it is seen that the energy difference between the maximum of the electron energy distribution and the maximum of the negative ion peak agrees very closely with that between the two onsets. This indicates that the value of the energy for the maximum cross section occurs very nearly at the value for the onset. If the cross section for attachment as a function of energy is a delta function whose energy width is comparable or smaller than the width of the electron energy distribution then one could determine the

[1] Johnson, Heppner, Holmes, and Meadows, "Results obtained with rocket-borne ion spectrometers," I.G.Y. Rocket Report Series No. 1, July (1958) National Academy of Science, p. 123.

[2] L. M. Branscomb, Advances in Electronics and Electron Phys. 9, 91 (1957).

[3] Fox, Hickam, Grove, and Kjeldaas, Rev. Sci. Instr. 26, 1101 (1955).

[4] W. M. Hickam and R. E. Fox, J. Chem. Phys. 25, 642 (1956).

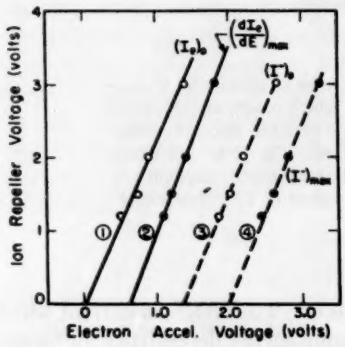

FIG. 2. Ion repeller voltage effects on the electron energy. Curve 1 shows the energy shifts in the onsets of the electron retard curves as measured by the electron accelerating voltage for different values of the ion repeller voltage. Curve 2 is a similar plot of the shift in the maximum of the electron energy distributions. Curve 3 is a plot of the shift in the O^- onset for different ion repeller voltages, and Curve 4 is a similar plot of the O^- maximum current.

energy more precisely by comparing the energy difference between the maxima. However, if the capture cross section obeys some other function with energy then there will be an energy displacement of the measured maximum value of the cross section with respect to the true value due to the finite width of the electron energy distribution.

Since a dc potential is applied to the ion repeller plate, this potential gradient influences the electron energy distribution. Also, if the ions are formed with appreciable kinetic energy the peak shape may be influenced by the repeller voltage. The O^- ion current and the electron current are, therefore, taken for four different values of the ion repeller voltage. The onsets of the ion current and electron retarding curves, as well as the maxima of the ion current and electron energy distributions are determined in each case. These data are plotted in Fig. 2. Curve 1 is a plot of the onset of the electron retard curve $(I_e)_0$ as a function of the electron accelerating voltage for different ion repeller voltages. Curve 3 gives the corresponding onsets of the negative ion current $(I^-)_0$ for the different ion repeller voltages. Within experimental error these curves are parallel and are separated by 1.35 ev. Curve 2 is a plot of the maximum of the electron energy distribution (dI_e/dE) max while curve 4 is a plot of the maximum of the ion current (I^-) max. These two curves are likewise parallel and are separated by 1.35 ev. It is seen, therefore, that the repeller voltage influence on the electron energy distribution as determined by a retardation of the electron beam is equally reflected in the electron energy as determined by electron capture to form a negative ion. It is clear that this situation holds only for negative ions where the applied repeller voltage forms a retarding field for the electron beam.

The fact that the observed maximum capture cross section appears at the same energy as the onset for capture indicates the true cross section must rise very steeply and must decrease very rapidly from the maximum value in an energy range small compared to the width of the electron energy distribution.

A more direct comparison of the peak shape with the electron distribution is shown in Fig. 3. Here is plotted the ion current as a function of the electron energy. Also shown by the dashed curve is the electron distribution. Note that here the distribution is shown in the normal manner with the high energy electrons to the right. It is, therefore, to be remembered that the low energy side of the ion peak is first produced by the high-energy side of the electron distribution. A comparison shows that these portions of the two curves are essentially identical. The high energy side of the ion peak decreases somewhat more slowly than the electron distribution, therefore, the true cross section is not a sharp delta function as found[4] for the case of SF_6^-. It is not a "broad delta" function since the top of the peak is not broader than that of the electron distribution. It would appear that the shape of the capture cross section would be more closely approximated by a right triangle with a very small apex angle. The O^- peak width at half maximum is 0.45 ev compared to 0.2 ev for that of the electron beam.

A second maximum is found at about 3.0 ev or 1.1 ev above the first maximum. Because the two peaks are not resolved it is not possible to determine the onset but it is estimated at about 2.5 ev. It is not possible to assign this second peak to any known impurity and hence, it is believed that this represents a second mechanism for the formation of this ion. It can possibly arise from an excited state of the NO_2^- molecule

$$NO_2+e\rightarrow(NO_2^-)^*\rightarrow NO+O^-.$$

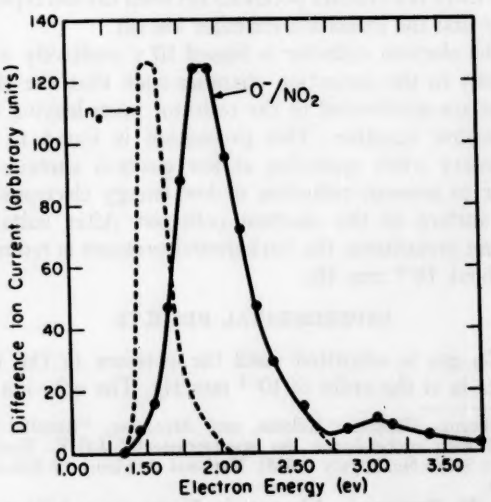

FIG. 3. O^- from NO_2 as a function of electron energy. The dashed curve shows the electron energy distribution used in obtaining the data. The onset of the electron retard curve was assumed to be zero energy.

A third O^- peak about equal in magnitude to the small peak at 3-ev onsets at about 7.5±0.3 ev and maximizes at about 8.75 ev. This peak may be due to an impurity. Hagstrum and Tate[5] report the appearance potential of O^- from NO at 7.0+0.3 ev. Another alternative is O^- from H_2O[6] at 7.5±0.3 ev.

Measurements of the pressure were very unreliable due to a considerable interaction of NO_2 on the filament. Attempts were made with pure tungsten and with thoriated iridium filaments. It appears that the O^- ion current is linear with pressure whereas the NO_2^- is proportional to the square of the pressure. However, since the NO_2^- peak is so small this could not be determined with certainty. The reaction with the filament is such that the filament is destroyed, after only about 10 hours of operation.

From a crude estimate of the pressure in the ion source at between 10^{-4} and 10^{-5} mm Hg and using only those electrons in an 0.1-ev energy band, then a maximum cross section for formation of O^- is estimated to be of the order of 10^{-18} cm^2. On the same basis the cross section of the NO_2^- ion is estimated at 10^{-20} cm^2.

If the dissociated fragments have zero kinetic energy and are in unexcited states then one has a value of 1.35 ev for the difference of the dissociation energy and the electron affinity of oxygen. Since the electron affinity of O^- is well established[7] at 1.47 ev, one obtains the maximum value of the dissociation energy as 2.82 ev. If any of the 1.35 ev results in kinetic energy of the fragments then the dissociation energy would be even smaller than 2.82 ev. The value obtained from thermochemical data[8] is 3.12 ev.

In a recent study of the ionization of NO_2, Nakayama *et al.*[9] used the 3.12-ev value of the dissociation energy to arrive at a value of 10.89 ev for the ion pair production of NO^+ and O^-. They observed a strong adsorption at 10.83±0.02 ev in close agreement with this value. The calculation, however, assumes that the ions have zero kinetic energy. If the ions have kinetic energy then the 10.83 value would necessitate a smaller dissociation energy in closer agreement with 2.82 ev. Collin and Lossing,[10] however, in a direct measurement of the appearance potential of NO^+ from NO_2 obtain a value of 10.1 ev. They offer no explanation as to why the observed value is so low other than a possibility of pyrolysis of the NO_2 on the filament producing NO. Since the ionization potential of NO is 9.25[11] this would produce a lowering of the appearance potential of NO^+ from NO_2 depending on the amount of pyrolysis and the sensitivity of the detector.

[5] H. D. Hagstrum and J. T. Tate, Phys. Rev. **59**, 354 (1941).
[6] Mann, Hustrulid, and Tate, Phys. Rev. **58**, 340 (1940).
[7] S. J. Smith and L. M. Branscomb, J. Research Natl. Bur. Standards **55**, 165 (1955).
[8] Cottrell, *The Strength of Chemical Bonds* (Butterworths Scientific Publications, London, 1954).
[9] Nakayama, Kitamura and Watanabe, J. Chem. Phys. **30**, 1180 (1959).
[10] J. Collin and F. P. Lossing, J. Chem. Phys. **28**, 900 (1957).
[11] K. Watanabe, J. Chem. Phys. **26**, 542 (1957).

NMR Study of Bonding in Some Solid Boron Compounds*†

A. H. SILVER‡ AND P. J. BRAY

Brown University, Providence, Rhode Island

(Received August 3, 1959)

Nuclear magnetic resonance studies of B^{11} have been performed in powder samples of some metal borides, boron-nitrogen compounds, borofluorides and borohydrides, and borates. The B^{11} nuclear electrical quadrupole interactions have been measured and used in the Townes and Dailey approach to estimate the probable bonding electron configurations.

1. INTRODUCTION

A RECORDING spectrometer of the Pound-Watkins type was used to study the B^{11} nuclear magnetic resonance spectrum in a number of boron compounds.[1] The nuclear electrical quadrupole interaction of B^{11} was measured in each compound from spectra obtained with powdered samples. The experimental results are used in combination with the Townes and Dailey method[2] of predicting quadrupole interactions to estimate the bonding electron configurations in these materials.

In all cases studied the quadrupole interaction is treated as a perturbation on the Zeeman energy levels. First- and second-order perturbation theory as previously applied to powder spectra of nuclei with half-integral spin is employed.[1,3,4] The quadrupole coupling constant of B^{11} for one excess p electron, $(eqQ)_p$, is taken as 5.39 Mcps.[2,5]

2. METAL BORIDES

In 1950, Kiessling[6] published the results of a study of the structure of various borides. Several of these have been investigated during this research.

One series with the formula MB_2 has the structure of AlB_2. The crystal structure is planar with the boron atoms lying in a hexagonal arrangement similar to carbon in graphite. The metal atoms are placed between the boron layers. Each metal atom has twelve equidistant boron neighbors and each boron has three planar boron neighbors while residing in a triangular prism formed by the metal atoms.

Two materials of this group, TiB_2 and ZrB_2, were obtained.[7] The powders appear metallic and load the oscillator slightly. The nuclear magnetic resonance of the B^{11} isotope was observed in TiB_2 and ZrB_2 at a Larmor frequency of 7.177 Mcps. Both resonances have the form predicted[3] for a first-order quadrupole perturbation of the $m=\pm\frac{1}{2}\leftrightarrow\pm\frac{3}{2}$ satellites in a powder sample. The derivative curves are shown in Fig. 1. It may be noted that the satellites in the TiB_2 are well separated

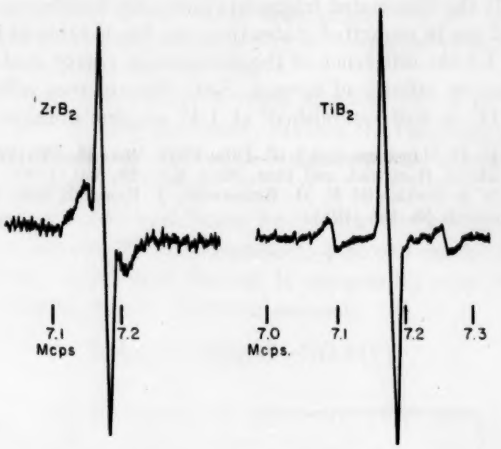

FIG. 1. B^{11} nuclear magnetic resonance in polycrystalline TiB_2 and ZrB_2. $\nu_0=7.177$ Mcps.

from the central line and the derivative of each satellite goes through zero. On the other hand, in ZrB_2 the splitting is much smaller and the satellites are nearly submerged in the central line.

Since the boron atoms in TiB_2 and ZrB_2 have threefold symmetry, the asymmetry parameter, η, is zero. The magnitude of the quadrupole coupling constant, $|(eqQ)|$, is then simply twice the separation in frequency of the satellite lines. For TiB_2, $|(eqQ)|$ is 360 ± 20 kcps and for ZrB_2 it is 118 ± 10 kcps.

The B—B single bond length is generally taken[2] as 1.76 A. The B—B nearest neighbor distance is 1.75 A in TiB_2 and 1.83 A in ZrB_2. One is inclined to assume

* Research supported by the U. S. Atomic Energy Commission under Contract AT(30-1)-1880.

† Submitted by A. H. Silver in partial fulfillment of the requirements for the degree of Doctor of Philosophy at Rensselaer Polytechnic Institute, Troy, New York.

‡ Present address: Scientific Laboratory, Ford Motor Company, Dearborn, Michigan.

[1] A. H. Silver, Ph.D. thesis, Rensselaer Polytechnic Institute (1958); A. H. Silver and P. J. Bray, J. Chem. Phys. **29**, 984 (1958); **31**, 247 (1959).

[2] C. H. Townes and A. L. Schawlow, *Microwave Spectroscopy* (McGraw-Hill Book Company, Inc., New York, 1955).

[3] M. H. Cohen and F. Reif, *Solid State Physics*, edited by F. Seitz and D. Turnbull (Academic Press, Inc., New York, 1957), Vol. 5.

[4] J. F. Hon and P. J. Bray, Phys. Rev. **110**, 624 (1958).

[5] G. Wessel, Phys. Rev. **92**, 158 (1953).

[6] R. Kiessling, Acta Chem. Scand. **4**, 209 (1950).

[7] TiB_2 was obtained from both the Norton Company and the National Carbon Corporation. ZrB_2 was obtained from the Norton Company.

that the planar B—B bonds are trigonal, sp^2, σ bonds. This would use all three valence electrons of a neutral boron atom and, based on a Townes and Dailey approximation, should give $(eqQ) = -(eqQ)_p = -5.39$ Mcps. This is more than an order of magnitude larger than the observed value. Further, the sp^2 configuration does not account for the bonding of the metal atoms or for interplanar bonding. It is conceivable that "metallic bonding" plays a major role. However, the tendency of boron to resemble silicon rather than Group III metals tends to discount this. Taking a hint from the electron characterization of graphite, one may postulate that the boron layers attract electrons from the metal layers. The electrons would go into boron p_π orbitals bringing about resonating double bonds between the adjacent borons in a layer. If each metal atom were to contribute two electrons, each boron would be a B^- ion. Electrostatic attraction would exist between the boron and metal ions and bonding between boron layers could arise from π-orbital overlap. The resulting electronic at configuration the boron ion would be spherically symmetric and the contribution to eqQ would be zero. It appears that the latter configuration is dominant. The weighting of the charged configuration, equal to the boron π-electron density, is 0.933 for TiB_2 and 0.978 for ZrB_2. The difference in the coupling constants may be due to a difference in ionic contribution associated with the difference in lattice parameters. The change in lattice parameter is in the proper direction.

3. BORON-NITROGEN COMPOUNDS

Powdered samples of boron nitride and *B*-trichloroborazole were obtained and studied.[8] Both materials have boron and nitrogen bonded to each other in six-membered rings similar to carbon in graphite and benzene.

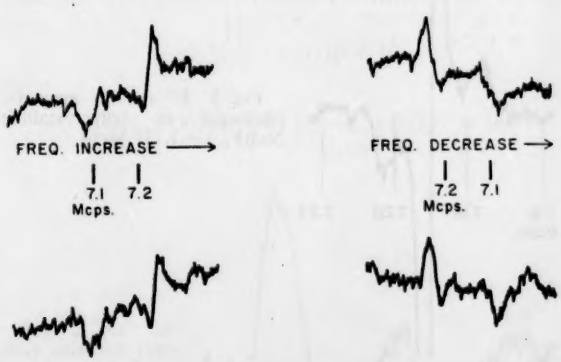

FIG. 2. B^{11} nuclear magnetic resonance in polycrystalline boron nitride, BN. $\nu_0 = 7.177$ Mcps. Drive speed = 200 kcps/hr.

[8] Polycrystalline *B*-trichloroborazole was supplied by Dr. A. W. Laubengayer of Cornell University. Crystalline samples of boron nitride were provided by Dr. R. S. Pease, Atomic Energy Research Establishment, Harwell, England, Dr. G. R. Finlay, Norton Company and J. Bowman, National Carbon Research Laboratory.

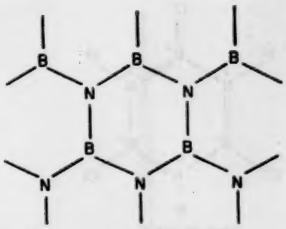

FIG. 3. Proposed resonating structures for boron nitride.

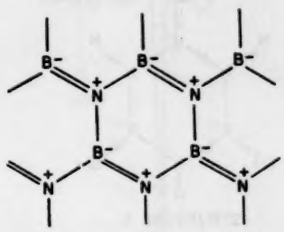

Boron nitride is a fine, light powder which has the constituency of graphite or talc. With high temperatures and pressure *in vacuo*, the powder can be crystallized into a hexagonal, graphite-like layer structure.[9] Each boron atom has three nitrogen neighbors in a plane and conversely. The atoms directly above and below each boron atom in the adjacent planes are nitrogens.

The B^{11} resonance was observed at 7.177 Mcps with considerable difficulty. Both cold and hot-pressed slugs were used in order to improve the filling factor. A very broad weak resonance was observed only with high gain, maximum modulation and long integration times. Figure 2 presents four of the recorder curves for BN. The resonance is the derivative of the central, $m = \frac{1}{2} \leftrightarrow -\frac{1}{2}$, transition broadened by second-order quadrupole perturbation.[3,10] The separation of the two derivative peaks is 160 ± 5 kcps. From second-order theory the magnitude of the quadrupole coupling constant of B^{11} in BN is 2.96 ± 0.10 Mcps.

The distortion in the line shape arises from several effects. The diminishing of the low-frequency peak relative to the high-frequency peak can be explained on the basis of imperfections in the structure which cause variation in (eqQ) and η.[1,10] Annealing of the samples should remove this effect. Another distortion is due to the long integrating time constant. This is noticed in the difference in line shape when changing the direction of the sweep.

The measured magnitude of the coupling constant, 2.96 Mcps, is equal to 55% of $(eqQ)_p$. From the structure of BN, $\eta = 0$. If the boron electrons formed three planar trigonal bonds to the neighboring nitrogen atoms as shown in Fig. 3(a), the coupling constant would be $-(eqQ)_p = -5.39$ Mcps. It has generally been believed that each nitrogen atom donates an electron

[9] R. S. Pease, Acta Cryst. **5**, 356 (1952).
[10] A. H. Silver and P. J. Bray, J. Chem. Phys. **29**, 984 (1958).

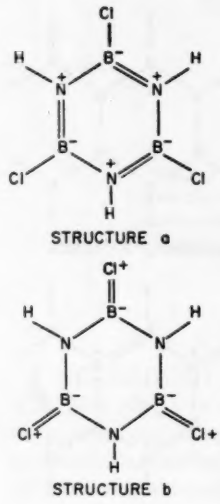

FIG. 4. Resonating structures in *B*-trichloroborazole.

to the boron allowing resonating double bonds to be formed as shown in Fig. 3(b). The double bond structures have zero coupling constant. Based only on the structures in Fig. 3, the measured quadrupole coupling implies 55% single bond and 45% double bond configurations. The possible resonating structure involving a positively charged boron atom, B^+, bonded to two nitrogens (the third neighboring nitrogen being N^-) has a coupling constant equal[11] to that of the structure in Fig. 3(a). Consequently, the figure of 45% double bond configuration is valid and boron has a net charge of $-0.45e$.

B-Trichloroborazole, $Cl_3H_3B_3N_3$ is similar in structure to a substituted benzene compound.[12] The B^{11} resonance was observed at 7.177 Mcps. Only the central transition was observed and the experimental signal-to-noise ratio is less than 10. There was no second-order broadening of this line. From the observed line width, it is estimated that $|(eqQ)|$ is less than 0.80 Mcps.

Resonating structures as shown in Fig. 4 have been suggested for *B*-trichloroborazole.[12] Based on these structures the quadrupole coupling of boron is small compared to $(eqQ)_p$. If one observed the pure quadrupole resonance of the chlorine the weights of the structures could be estimated. Attempts to observe the chlorine quadrupole resonance have been unsuccessful.

4. BOROFLUORIDES AND BOROHYDRIDES

The borofluorides (MBF_4) and borohydrides (MBH_4) are ionic compounds in which the boron is believed to reside at the center of a tetrahedron of either fluorine or hydrogen atoms.[13] While the complete structures and positions have not been precisely determined, the materials are similar to many of the sulfates (MSO_4) and perchlorates ($MClO_4$). Most borofluorides and borohydrides are difficult to obtain in pure form and they also tend to absorb water. Similar to the perchlorates, these compounds have both high- and low-temperature forms. The high-temperature phase is cubic while the low-temperature phase is orthorhombic.

Above 20°C sodium borohydride ($NaBH_4$) is believed to be two interpenetrating face-centered cubic lattices composed of Na^+ and $(BH_4)^-$ ions.[14] X-ray techniques could not locate the positions of the H atoms and a tetrahedral configuration was assumed. If the $(BH_4)^-$ is a perfect tetrahedron, the boron is in a position of tetrahedral symmetry and $(eqQ)_{B^{11}}$ should be zero. Similarly, the sodium atoms should have cubic symmetry and no quadrupole coupling constant.

Both the B^{11} and Na^{23} resonances were observed in powdered $NaBH_4$ at 23°C. The boron resonance at 7.177 Mcps and the sodium resonance at 5.92 Mcps are both narrow symmetric lines with no observable satellites. This result is in agreement with a $(BH_4)^-$ tetrahedron and zero coupling constant.

Sodium borofluroide $NaBF_4$ is orthorhombic at room temperatures and reported to be isomorphous with $CaSO_4$.[15] Several structure determinations do not agree on the exact atomic positions.[16] The $(BF_4)^-$ are believed to be tetrahedral groups.

The B^{11} and Na^{23} resonances were observed at 7.177 and 5.92 Mcps, respectively. Figure 5 shows the B^{11} resonance. The symmetric pair of satellite lines are

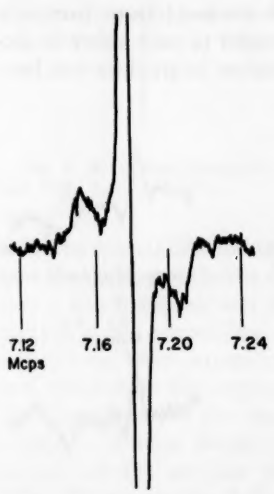

FIG. 5. B^{11} nuclear magnetic resonance in polycrystalline $NaBF_4$. $\nu_0 = 7.177$ Mcps.

[11] The value $-\frac{3}{2}(eqQ)_p$ is calculated from the wave functions for three sp^2 trigonal bonds employed two at a time. For a positively charged atom, the Townes and Dailey approximation requires multiplication of the coupling constant by $(1+\epsilon)$ where ϵ is a correction factor tabulated by Townes and Schawlow (see reference 2). For B^{11}, ϵ is 0.5. Hence, $eqQ = -(eqQ)_p$ as for the structure of Fig. 3(a).

[12] D. L. Coursen and J. L. Hoard, J. Am. Chem. Soc. **74**, 1742 (1952).

[13] A. F. Wells, *Structural Inorganic Chemistry* (Clarendon Press, Oxford, 1950).

[14] A. M. Soldate, J. Am. Chem. Soc. **69**, 987 (1947).

[15] R. W. G. Wyckoff, *Crystal Structures* (Interscience Publishers, Inc., New York, 1951), Vol. II.

[16] *Structure Reports*, A. J. C. Wilson, editor (N. V. A. Oosthoek's Uitgevers Mij, Utrecht, Netherlands, 1952), Vol. 12, p. 190.

separated by 52±6 kcps. From the powder line shape observed, it is assumed that the separation of the derivative maxima occurs at $(1-\eta)\ eqQ/2$[3,4], where η is the asymmetry parameter. Wyckoff[15] describes $NaBF_4$ as nearly tetragonal from which it appears that η is small. Under this assumption $(eqQ) \doteq 104$ kcps.

The Na^{23} resonance line is displayed in Fig. 6. Since the spin of Na^{23} is $\frac{3}{2}$, the line shape is recognized as the derivative of the central, $m=\frac{1}{2}\leftrightarrow-\frac{1}{2}$, transition broadened by a uniform second-order quadrupole interaction.[3,10] The over-all peak-to-peak separation is 26.2 kcps from which the quadrupole coupling constant is calculated as 1.09±0.20 Mcps assuming η is negligible.

If one considers the $(BF_4)^-$ group as a point charge, the sodium and boron positions are equivalent and the magnitude of the field gradients, q, would be the same for each position. Further, if the $(BF_4)^-$ group is a perfect tetrahedron with charge $+pe$ assigned to the boron at the center and charge $-(1+p)e/4$ to the fluorines at each corner, there is no contrbution from those fluorines to the field gradient at the boron position. The charge distribution over neighboring $(BF_4)^-$ groups will, of course, contribute something to the boron field gradient. Sodium ions, however, have the fluorines as nearest nieghbors and the sodium field gradient will be more strongly influenced by the charge distribution over the $(BF_4)^-$ units. For the same field gradient q at the B^{11} and Na^{23} nuclei the ratio of the quadrupole coupling constants is

$$(eqQ)\mathrm{Na}^{23}/(eqQ)\mathrm{B}^{11}=(\beta Q)\mathrm{Na}^{23}/(\beta Q)\mathrm{B}^{11},$$

where the β's are the appropriate antishielding factors for the atoms in a solid.[3] It is understood that q does not include contributions from polarization of the core electrons. The observed coupling constants are in the ratio

$$(eqQ)\mathrm{Na}^{23}/(eqQ)\mathrm{B}^{11} \doteq 10,$$

while

$$[(\,|\,1-\gamma_\infty\,|\,Q)\mathrm{Na}^{23}]/[(\,|\,1-\gamma_\infty\,|\,Q)\mathrm{B}^{11}] \doteq 18,$$

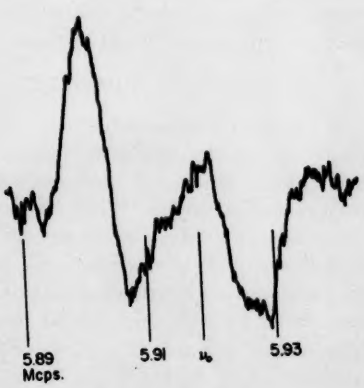

FIG. 6. Na^{23} nuclear magnetic resonance in polycrystalline $NaBF_4$. ν_0= 5.918 Mcps.

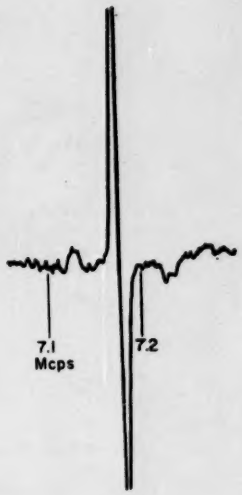

FIG. 7. B^{11} magnetic resonance in polycrystalline NH_4BF_4. ν_0= 7.177 Mcps.

where the $|\,1-\gamma_\infty\,|$ are the calculated values[17] of β for atomic states. Discrepancy in the two ratios is due to the difference in values of β and $|\,1-\gamma_\infty\,|$ for the same ion and to the distribution of charge over the tetrahedral units. If the atomic positions were known precisely, a calculation of the values of $q(Na^{23})$ and $q(B^{11})$ as a function of the parameter p would be useful in establishing the charge distribution over the $(BF_4)^-$ units.

The two compounds KBF_4 and NH_4BF_4 are isomorphous with the $BaSO_4$ structure at room temperature.[15] The B^{11} resonances were observed at 7.177 Mcps. One pair of symmetrically placed satellites were observed in each sample. The separation of the satellite derivative peaks is 110 kcps in each case. From the line shape as shown in Fig. 7 it is assumed that the separation of the derivative peaks is $(1+\eta)\,(eqQ/2)$[3,4] from which

$$[(1+\eta)eqQ]_{\mathrm{KBF_4,NH_4BF_4}}=220\pm20 \text{ kcps}.$$

Since $0\leq\eta\leq1$,

$$110 \text{ kcps}\leq(eqQ)_{\mathrm{KBF_4,NH_4BF_4}}\leq220 \text{ kcps}.$$

5. BORATES

Boron forms an extensive system of borates analogous to the silicates. No complete systematic study of the borates has been made and the correct structural formulas for many compounds have not been assigned. The possibility of forming three planar bonds as in TiB_2, ZrB_2, and BN or four tetrahedral bonds as in $(BF_4)^-$

[17] The values given below were used in this calculation.

$Q_{Na^{23}}=0.100\times10^{-24}$ cm^2	See reference 3, Sec. 28.
$Q_{B^{11}}=3.55\times10^{-26}$ cm^2	G. Wessel, Phys. Rev. **92**, 158 (1953).
$\gamma_\infty(Na^+)=-4.53$	T. P. Das and R. Bersohn, Phys. Rev. **102**, 733 (1956).
$\gamma_\infty(B^{+++})=0.145$	

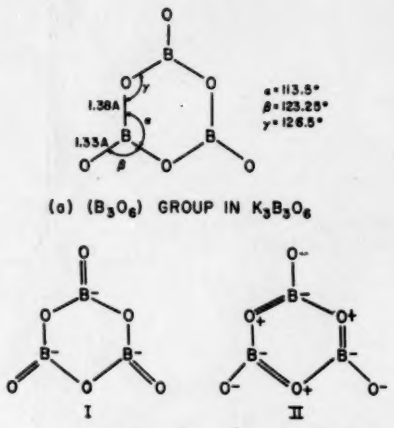

FIG. 8. Configuration of $(B_3O)^{3-}$ in $K_3B_3O_6$.

increases the difficulty of the problem. A small number of boron-oxygen compounds have been investigated as part of this research. The results on boron oxide glasses have previously been reported[10] and the results on the hydrated boron oxide system will be reported separately.[18]

Wells[13] has presented a general structural plan for the simpler borates where each boron bonds to three oxygens in a planar (BO_3) configuration. The oxygen atoms may have one or two bonds and the various (BO_3) groups may bond to each other by "sharing" one or more oxygens. The structural formulas are written as $(M)_n^{n+}$ $(BO_2)_n^{n-}$ where M is a monovalent cation. Two metaborates $K_3B_3O_6$ and CaB_2O_4 have been studied by nuclear resonance. The structures of both materials have been determined by Zachariasen[19,20] by x-ray methods. In each compound two oxygen atoms are shared between adjacent (BO_3) groups.

The borate units $(B_3O_6)^{3-}$ in potassium metaborate are arranged as shown in Fig. 8(a).[19] The whole group is planar. A symmetric B^{11} nuclear resonance was observed at 7.177 Mcps in a pressed powder sample. The line width measured between points of maximum slope on the derivative trace is 15 kcps. An upper limit of 0.95 Mcps on the quadrupole coupling constant can be estimated from the absence of second-order effects on this central transition. The absence of observable satellites shifted in first order from the Larmor frequency may be due to the poor signal-to-noise ratio available.

Zachariasen[19] has proposed the bonding in the $(B_3O_6)^{3-}$ groups as a resonance between the covalent structures shown in Fig. 8(b). He states that structure I is somewhat more important because of the interatomic

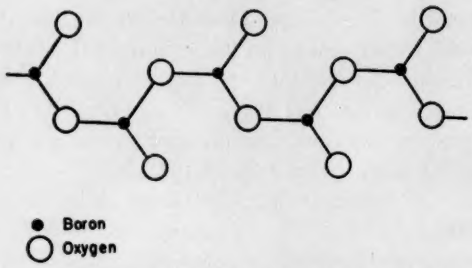

FIG. 9. Configuration of $(BO_2)_n^{n-}$ chains in CaB_2O_4.

distances. Based on a Townes and Dailey model the predicted quadrupole interaction is nearly zero for either structure. However, since all O—B—O angles are not equal, there may be a small quadrupole interaction. An investigation of single crystals of $K_3B_3O_6$ or the isomorphous $Na_3B_3O_6$ would be useful in determining the proper bonding.

In calcium metaborate the borate groups are infinite chains of $(BO_2)_n^{n-}$ oriented parallel to the c axis of the orthorhombic crystal structure.[20] The oxygen atoms are shared as shown in Fig. 9. The boron resonance at 7.177 Mcps in a powdered sample is a narrow symmetric line with no second-order quadrupole effects and no observable satellite lines. Here again the signal-to-noise ratio indicates that satellites would not be observable. The line width is 12 kcps from which an upper limit of 0.81 Mcps is estimated for the quadrupole interaction. Each boron atom in the $(BO_2)_n^{n-}$ chains can have resonating double bonds to its oxygen neighbors similar to those occurring in the potassium metaborate structures, Fig. 8. It appears that the boron will have a double bond character of at least 85% since three single bonds give a quadrupole interaction of 5.39 Mcps.

The small quadrupole interaction in these metaborates, where two oxygen atoms in each (BO_3) group are shared, should be contrasted with the large quadrupole interactions reported in B_2O_3 glass[10] and in orthoboric acid,[18] H_3BO_3. In the B_2O_3 glass all oxygens are shared while in the orthoboric acid no oxygens are shared directly. The reduction in the quadrupole interaction for three coordinated boron atoms apparently depends on the availability of extra electrons for the formation of double bonds.

SUMMARY

It has been demonstrated that information about the electronic bonding in boron compounds can be derived from measurement of the quadrupole interaction in polycrystalline solids. When the complex containing boron acquires excess electrons the boron tends to fill its valence shell by forming four bonds. This can be accomplished by fourfold coordination as in the borofluorides and borohydrides or by threefold coordination with a double bond as in TiB_2, ZrB_2, and the metaborates.

[18] A. H. Silver, Bull. Am. Phys. Soc. Ser. II, 4, 11 (1959). More complete results will be published.
[19] W. H. Zachariasen, J. Chem. Phys. 5, 919 (1937).
[20] W. H. Zachariasen and G. E. Zeigler, Z. Krist. 83, 354 (1932).

Role of Thermal Diffusion in the Electrolytic Separation of Isotopes in Liquid Metals

PAUL C. MANGELSDORF, JR.

Institute for the Study of Metals, University of Chicago, Chicago 37, Illinois

(Received April 13, 1959)

From the principles of irreversible thermodynamics and the known properties of metals it is inferred that there is a contribution to the Haeffner effect isotope separations arising from the isothermal heat flux accompanying the current flow. The magnitude of this contribution is estimated to be a significant fraction of the observed effect, but of opposite sign.

THE existence of an isotope separation in liquid metals due to the passage of electric currents was first discovered in mercury by Haeffner[1] and is now generally known as the "Haeffner effect." It has since been found in a number of liquid metals: cadmium,[2] gallium,[3,4] indium,[5] lithium,[6] potassium,[7,8] rubidium,[8,9] tin,[2] and zinc[2]; and has been re-investigated in mercury.[10,11] In every one of these cases the lighter isotope was found to be enriched at the anode.

The separation effect has been found to increase with temperature in gallium,[4] indium,[5] mercury,[11] potassium,[8] rubidium,[8,9] and tin,[2] contrary to theoretical expectations based on considerations of isotopic differences in electronic momentum transfer.[12] A part of this temperature dependence can be attributed to increases in ionic mobilities with temperature which would give a more rapid approach to a steady state.[13] However, it appears that in all these cases except tin the amount of the separation to be expected when the steady state is ultimately achieved also increases with temperature. In potassium and rubidium Lodding has found distinct temperature maxima, well above the melting points, beyond which the steady state separations decline quite sharply.

Since the motion of electrons is so much more rapid than that of the ions, it is conventional to assume that the scattering of the electrons depends only on the instantaneous configuration of the ions and not on their instantaneous motions. At elevated temperatures any isotopic differences in configuration should tend to vanish as the system approaches the classical limit in which kinetic and potential energies are independently distributed. On this account it is difficult to invoke any straightforward difference in "electronic friction" to explain the effect.

Klemm[14] managed to overcome this difficulty by postulating the existence of both mobile and immobile ions in the liquid metal, the mobile ions having much higher scattering cross sections for the electrons. The mobile ions are thus driven toward the anode, the lighter ions moving more rapidly, while the immobile ions move *en masse* toward the cathode. At first sight this "self-transference" hypothesis does not appear to be consistent with the more familiar notion of a liquid as a fluid in which there is no sharp *qualitative* distinction between the Brownian motion of a large suspended particle and the random thermal motion of the molecules, or ions, themselves. It may be shown, however, that the effects of Klemm's "self-transference" will result whenever the instantaneous mobility of an ion with respect to surrounding ions is correlated with the instaneous electron scattering power of the ion, or with the instantaneous charge of the ion. Such correlations seem quite probable and should lead to isotope separations of the kind observed.

While the observed separations can probably be largely explained by "self-transference," they are also of a magnitude which might easily arise from thermal diffusion. And because of the quite substantial *isothermal heat flux* which must necessarily exist whenever a strong electric field is applied to a metal, it is entirely probable that thermal diffusion does occur in these systems and does influence the isotopic separations.

Putting aside the question of mass transport for the moment, we may use the formalism of irreversible thermodynamics to relate the current density $\mathbf{I}$ and the heat flux $\mathbf{J}$ to the potential gradient ∇V and the thermal gradient ∇T[15]:

$$\mathbf{I}=-\sigma\nabla V-(L_{12}/T^2)\nabla T, \quad (1)$$

$$\mathbf{J}=-(L_{21}/T)\nabla V-K\nabla T, \quad (2)$$

where σ is the electrical conductivity, K the thermal

[1] E. Haeffner, Nature **172**, 775 (1953).
[2] A. Lodding, Z. Naturforsch. **12a**, 569 (1957).
[3] Golman, Nief, and Roth, Compt. Rend. **243**, 1414 (1956).
[4] G. Nief and E. Roth, Compt. Rend. **239**, 162 (1954).
[5] Lodding, Lunden, and Ubisch, Z. Naturforsch. **11a**, 139 (1956).
[6] Lunden, Lodding, and Fischer, Z. Naturforsch. **12a**, 268 (1957).
[7] Lunden, Reuterswärd, and Lodding, Z. Naturforsch. **10a**, 924 (1955).
[8] A. Lodding (to appear in Z. Naturforsch.).
[9] A. Lodding, Z. Naturforsch. **14a**, 7 (1959).
[10] Haeffner, Sjöborg, and Lindhe, Z. Naturforsch. **11a**, 71 (1956).
[11] Bogoiavlenskii, Grigorev, Rudenko, and Dolgopolov, J. Exp. Theoret. Phys. (U.S.S.R.) **33**, 581 (1957).
[12] P. G. de Gennes, J. Phys. Radium **17**, 343 (1956).
[13] C. E. Bresler and G. E. Pikus, J. Tech. Phys. (U.S.S.R.) **26**, 109 (1956).
[14] A. Klemm, Z. Naturforsch. **8a**, 397 (1953); **9a**, 1031 (1954).
[15] S. R. de Groot, *Thermodynamics of Irreversible Processes* (North-Holland Publishing Company, Amsterdam, 1952), Eq. (6), p. 143.

conductivity, and $L_{12}=L_{21}$ by the Onsager reciprocity relation. Quite clearly the electric field alone gives rise to an *isothermal heat flux*:

$$\mathbf{J}_{\text{isothermal}}=-(L_{21}/T)\nabla\mathbf{V}. \quad (3)$$

If we reverse the usual procedure of irreversible thermodynamics and consider the forces to be linear functions of all the fluxes, as was done by Klemm,[14] we see that formally, at least, this isothermal heat flux will contribute to the isotope separation. According to the principles of irreversible thermodynamics the amount of this contribution should be the same for a given heat flux, regardless of how it is produced, or of whether there also exists an additional separation due directly to the flow of electric current.

Now if we were to maintain a liquid metal in a given thermal gradient while preventing the flow of electric current we should expect an amount of isotope separation, arising from the thermal motions of the ions, comparable with that in nonmetallic liquids. There would, of course, be a static thermoelectric field set up, but it seems unlikely that this field would affect the separation one way or another since the isotopes would have equal charges and the electrons would have no net motion.

Under these conditions the total heat flux in the metal would be enormously greater than in other liquids because of the greater thermal conductivity. Consequently the effectiveness of a given heat flux in producing isotopic separation will be correspondingly less in the metal. However, this reduced effectiveness is taken account of if we use our equations to define an *apparent thermal gradient* to be used in the usual equations of thermal diffusion. This apparent gradient "$\nabla\mathbf{T}$" is that which would give rise to the given heat flux in the absence of an electric field,

$$\text{“}\nabla\mathbf{T}\text{”}=-\mathbf{J}/K=(L_{21}/KT)\nabla\mathbf{V}. \quad (4)$$

In order to evaluate the coefficient L_{21}, or L_{12}, we make use of the absolute thermoelectric power S, which is defined as the open-circuit ($\mathbf{I}=0$) potential gradient produced in a metal by a thermal gradient

$$\nabla\mathbf{V}=-S\nabla\mathbf{T}(\text{no current flux}), \quad (5)$$

whence

$$L_{12}=\sigma T^2 S \quad (6)$$

and

$$\text{“}\nabla\mathbf{T}\text{”}=(\sigma T/K)S\nabla\mathbf{V}. \quad (7)$$

Now the ratio $(K/\sigma T)$ is the well-known "Lorenz number" having a value of very nearly 2.5×10^{-8} (v/degree)^2 in all metals at all temperatures.[16] The absolute thermoelectric power is usually of the order of one to ten μv per degree, and may be either positive or negative depending on the metal and the temperature.

[16] N. F. Mott and H. Jones, *The Theory of the Properties of Metals and Alloys* (Oxford University Press, London, 1936), p. 307.

TABLE I.

Metal	T°K	S[a] (μv/degree)	A_{TD} (calc.)[b] (degrees/v)	A (obs.)[c] (degrees/v)
Hg	318	−4.0	−150	850[d]
	323	−4.0	−150	1120
	388	−5.2	−200	1000[d]
Li	561	24	1000	1460
K	352	−13.5	−550	910
	366	−14	−550	1310, 1170
	431	−16.5	−650	1450
	451	−17	−700	1630
	553	−21	−850	1670
	608	−23	−900	270
Rb	321	−7.5	−300	1720
	371	−11.5	−450	1960
	415	−14	−550	3360
	447	−17.5	−700	2580
	479	−20	−800	2500, 2060
	505	−22	−900	750
	538	−24.5	−1000	510

[a] Reference 18.
[b] The values of A_{TD} are calculated from Eq. (11), assuming $(\alpha m/\Delta m)$ to be approximately +1.0.
[c] The observed values of A were obtained by multiplying the values of κ, as estimated by Lodding,[2,3] by the factor $e/k=1.16\times10^4$ (degrees/v).
[d] Values of β, found by Bogoiavlenskii *et al.*,[11] multiplied by e/k.

Combining these figures we see that the apparent thermal gradient will most certainly be 40 degrees/v and might easily be 400 degrees/v.

In the theory of ordinary thermal diffusion the steady-state concentration gradient is related to the thermal gradient which produces it by the equation

$$\nabla\mathbf{X}_1=(\alpha X_1X_2/T)\nabla\mathbf{T}, \quad (8)$$

where x_1 and x_2 are the mole fractions.[17]

On substituting the apparent thermal gradient into this expression, and integrating, we find

$$\ln(X_1/X_2)-\ln(X_1/X_2)_0=\alpha(\sigma T/K)S(V-V_0)/T. \quad (9)$$

This may be compared with the empirical expressions for the observed isotope separation[3,11]

$$\ln(X_1/X_2)-\ln(X_1/X_2)_0 =A[(m_2-m_1)/\langle m\rangle](V-V_0)/T, \quad (10)$$

and we see that the expected contribution to the separation factor A due to thermal diffusion should be

$$A_{TD}=(\alpha m/\Delta m)(\sigma T/K)S. \quad (11)$$

Unfortunately the subject of isotopic separation by thermal diffusion in liquids has not been explored to any appreciable extent, either experimentally or theoretically. We have no way of calculating what $(\alpha m/\Delta m)$ ought to be in liquid metals. According to the theory of thermal diffusion in gases and in fluids of hard spheres $(\alpha m/\Delta m)$ should be positive, causing the lighter species

[17] W. Jost, *Diffusion in Solids, Liquids, and Gases* (Academic Press, Inc., New York, 1952), p. 494, Eq. 12.27).

to be enriched at the hotter end of the diffusion column. If this rule is obeyed in liquid metals we should expect the isothermal heat flux to cause the lighter isotope to move to the cathode, contrary to what is observed, whenever the thermoelectric power is negative, as is theoretically predicted for free electron systems.

The magnitude of $(\alpha m/\Delta m)$ in gases is usually about 0.2. Thermal diffusion separations appear in general to be greater in liquids than in gases so that a value of $+1.0$ for $(\alpha m/\Delta m)$ in liquid metals might be a reasonable guess.

Of the nine liquid metals in which the Haeffner effect has been studied, only lithium, mercury, potassium, and rubidium appear to have values of S reported in the literature.[18] For these we have calculated the values of A_{TD} shown in the accompanying table, assuming $(\alpha m/\Delta m)$ to be unity. The observed values of the separation factor A are also shown.

We see that, taking all the available experimental information at its face value, the estimated thermal diffusion effect plays a significant, but not determining, role in the observed separations. This is not in itself a particularly useful result since it appears to increase the amount of the Haeffner effect to be accounted for by "self-transference," and it does not shed any light on the distinctive temperature dependence found by Lodding in potassium and rubidium. However, if the sharp decline in the Haeffner effect in these metals at higher temperatures is due to a rapid extinction of "self-transference" we might well expect that at still higher temperatures the Haeffner effect would be negative and would be determined solely by thermal diffusion. Such a negative effect would be very awkward to explain on the basis of "self-transference" alone.

It is also just barely possible that the entire Haeffner effect can be explained by thermal diffusion. In the theory of gaseous thermal diffusion for the case of point particles repelling each other with a force given by $f=b/R^n$ the theoretical expression for $(\alpha m/\Delta m)$ is proportional to the quantity $(N-5)/(N-1)$ and is otherwise nearly independent of N (cf. reference 17, p. 519, Eq. 12.109). If one were to assume that the coulomb repulsion with $N=2$ played an important part in the ionic interactions leading to thermal diffusion in liquid metals one would anticipate a value of $(\alpha m/\Delta m)$ which would be negative and greater by a factor of about three. This would probably be sufficient to account for all the observed separations, except in lithium. The distinctive temperature dependences might be related to an increase in the effective N with temperature as collisions become more energetic and the distance of closest approach diminishes.

Although this latter conjecture does not seem very likely, it does emphasize the need for investigation of isotopic separation by thermal diffusion in liquid metals. We hope to be able to devise a method by which we can measure such separations.

The author wishes to thank Professor O. J. Kleppa, Professor R. M. Mazo, Professor H. B. Huntington, and Professor A. Klemm for helpful comment and discussion; special thanks are due to Professor A. Lodding for making his data on the temperature dependence in the alkali metals available to the author before publication, and to Professor S. A. Rice for other assistance.

[18] G. Borelius, *Handbuch der Metallphysik* (Akademische Verlag, Leipzig, 1935), Band I, Teil I, pp. 399–400.

Letters to the Editor

THE Letters to the Editor section is subdivided into three parts entitled Communications, Comments and Errata, and Notes. These three sections are all subject to the same limitations on length. The textual material of each Letter is limited to a number of words equal to 950 minus the following: (a) 200 words for each average-sized figure; (b) 50 words for each displayed equation; (c) 7 words for each line of table including headings and horizontal rulings. No proof will be sent to the authors of "Communications" and "Comments and Errata." Proof will be sent to the authors of "Notes." The publication charge for Letters is $30 per page, with a minimum of $30 per Letter. If honored, the Institution will be entitled to 100 reprints without covers. See issues of May–September, 1957, for descriptions of categories.

Communications

Pressure-Induced Shifts of HCl Lines Due to Foreign Gases*

D. H. RANK, W. B. BIRTLEY, D. P. EASTMAN, AND T. A. WIGGINS

Department of Physics, The Pennsylvania State University, University Park, Pennsylvania

(Received November 13, 1959)

A PAPER by Kimel, Hirshfeld, and Jaffe[1] has appeared recently in which they have demonstrated the shifting of the band lines of the 2-0 band of HCl as the result of self-broadening and foreign gas broadening. The results given in this paper[1] show a strong dependence of the pressure shifting on the rotational quantum numbers of the band lines. The general features of these curves $d\nu$ *vs* J is that the pressure shifts appear to approach an asymptotic value at high J values.

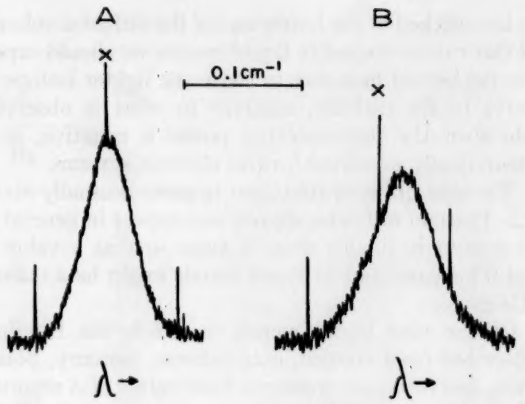

FIG. 1. Display of absorption line $R(10)$ of HCl band 2-0: (A) with 2.5 cm Hg pressure HCl; (B) $R(10)$ with the addition of 1 atmos of argon. The markers denoted by an X represent identical wavelengths. The red shift and line broadening is readily apparent.

Dr. Jaffe (in private communication with D. H. R.) has requested us to spot check some of his measurements since the effects observed are small and might be questioned or ignored until verified by another laboratory. The 5-meter double-passed vacuum grating spectrograph in our laboratory is similar to the instrument used by Jaffe. Our instrument has been rebuilt during the past summer and gives somewhat higher resolving power and wavelength sensitivity than the instrument used by Jaffe.

We have measured the pressure shifting of the $R(10)$ and $R(0)$ lines of the 2-0 band of HCl^{35} making use of He, Ne, H_2, Ar, O_2, N_2, CO, CO_2, and N_2O as the foreign

TABLE I. Data on the shifting of the $R(10)$ and $R(0)$ lines of the 2-0 band of HCl^{35}. The HCl pressure was ≤ 2.5 cm Hg in all cases. The optical polarizabilities α have been obtained from Landolt-Bornstein.[2] The fifth and sixth columns are calculated under S.T.P. conditions. The last column is the calculated increase in line breadth of the HCl line for 1 atmos pressure of foreign gas assuming linearity of broadening with pressure of the foreign gas.

	Foreign gas	Optical polarizability α cm³	Shift $\Delta\nu$ cm⁻¹	Standard deviation δ cm⁻¹	$(\Delta\nu/P)\times$ (cm⁻¹/cm Hg)	$(\Delta\nu/\nu)\times$ $(1/P$ cm Hg)	Half-width increase in cm⁻¹
$R(10)$	He	0.20×10^{-24}	$+5.9\times10^{-3}$	$\pm1.7\times10^{-3}$	$+0.9\times10^{-4}$	$+1.6\times10^{-6}$	0.023
	Ne	0.39	+1.0	±1.4	+0.2	+0.3	0.017
	H_2	0.79	−13.7	±2.9	−2.1	−3.7	0.046
	O_2	1.60	−18.7	±1.7	−2.9	−5.0	0.029
	Ar	1.63	−20.9	±1.7	−3.3	−5.6	0.020
	N_2	1.76	−19.9	±1.9	−3.1	−5.4	0.029
	CO	1.95	−24.7	±2.9	−3.9	−6.7	0.043
	CO_2	2.65	−31.7	±4.6	−5.0	−8.6	0.086
	N_2O	3.00	−31.2	±2.2	−4.9	−8.4	0.072
$R(0)$	He	0.20	+1.5	±2.1	+0.2	+0.4	0.037
	Ar	1.63	+7.3	±1.0	+1.2	+2.0	0.082
	N_2	1.76	−3.1	±3.3	−0.5	−0.9	0.172
	CO	1.95	−3.3	±2.7	−0.5	−0.9	0.177
	CO_2	2.65	+3.8[a]	±2.3	+1.2	+2.1	0.209

[a] This shift was measured with 32 cm Hg pressure of foreign gas.

gases. The measured pressure shifts are given in Table I. A one-meter absorption tube was used to make these measurements. The HCl pressure employed was 2.5 cm Hg or less. After scanning the line contour an appropriate pressure of foreign gas was added and the line scanned again. Reference markers were introduced onto the recordings at identical wavelength positions by means of a mechanical and electrical system which coupled the scanner to the recorder. In Fig. 1(A) and (B) we have displayed a typical recording. Figure 1(A) shows the $R(10)$ line of HCl along with its reference wavelength markers. Figure 1(B) shows a similar scan of the $R(10)$ line with 64-cm pressure of argon added to the HCl. Positions of identical wavelength are indicated by means of X's placed over the wavelength markers. Inspection of the figure shows that the wavelength shift to the red produced by the foreign gas is easily observable and measurable with considerable accuracy.

In Table I we have given the pressure coefficients $\Delta\nu/P$ resulting from our measurements. We have also calculated $\Delta\nu/P/\nu$ (the pressure shift in cm^{-1} per cm of Hg pressure per cm^{-1}). The optical polarizabilities of the various foreign gases obtained from Landolt-Bornstein[2] are given. The standard deviations δ of the measurements are given to illustrate the precision obtained. The comparison of our experimental results with those of Jaffe *et al.*[1] and other further results communicated to D. H. R. by Dr. Jaffe are eminently satisfactory.

We have measured the increase of the half-intensity breadth of the HCl lines for some of the foreign gases. The results of these measurements appear in the last column of Table I.

* This research was assisted by support from Contract Nonr-656(12) NR 019-401 of the Office of Naval Research.

[1] Kimel, Hirshfeld, and Jaffe, J. Chem. Phys. **31**, 81 (1959).

[2] *Landolt-Bornstein Tables* (Springer-Verlag, Berlin, 1950), sixth edition, Vol. 1, Part 3/2, p. 510; and Vol. 1, Part 1, p. 401.

TABLE I. Pressure-induced shifts of lines in the 2-0 band of HCl^{35} due to polar gases. Units: $cm^{-1}\times10^{-4}$ per cm Hg foreign gas pressure at 24° C.

Line	CO	SO_2	CH_3Cl	DCl
$P(6)$	1.82	0.43	1.96	...
$P(5)$	2.00[a]	...	1.69[a]	...
$P(4)$	1.45	0.50	1.68	0.55
$P(3)$	1.26	0.45	1.30	0.55
$P(2)$	0.96	[b]	1.21	0.86b[c]
$P(1)$	1.02	[b]	1.37	1.73b
$R(0)$	0.14	[b]	0.21	2.80
$R(1)$	0.56	[b]	0.54	1.40
$R(2)$	0.67	[b]	0.51	0.72b
$R(3)$	1.11	1.39	0.96	1.20b
$R(4)$	1.84	1.50	1.38	0.09
$R(5)$	2.34	1.68	2.06	0.85
$R(6)$	2.93	2.02	3.12	1.34
$R(7)$	3.18	2.36	2.79	1.81
$R(8)$	3.42	2.74	4.17	...
$R(9)$	3.65	...	4.50	...

[a] Measured on the HCl^{37} line.
[b] Too broad for measurement.
[c] Values marked b are blue shifts. All others are red shifts.

Pressure-Induced Shifts of HCl Lines Due to Foreign Gases*

M. A. HIRSHFELD, J. H. JAFFE, AND S. KIMEL

The Weizmann Institute of Science, Rehovoth, Israel

(Received November 12, 1959)

INFRARED absorption lines are shifted as the pressure of the sample is changed. It has been pointed out that in spite of the smallness of the effect ($\sim$0.01 cm^{-1} per atmos) there are advantages in studying it at low pressures ($\sim$1 atmos). Shifts have been reported using a pressure difference of 50 cm Hg for the 2-0 band of HCl, both in the case of self-shifts (due to HCl gas only) and foreign gas shifts (due to dry air). They were determined for each individual line of the band and it was found that there is a very strong dependence of the effect on the rotational quantum number.[1] With the same experimental technique, shifts of lines in the HCl 2–0 band have now been determined for a wide range of foreign gases.† Results are listed in Table I for four polar gases. With CO, SO_2, and CH_3Cl, in spite of different dipole mo-

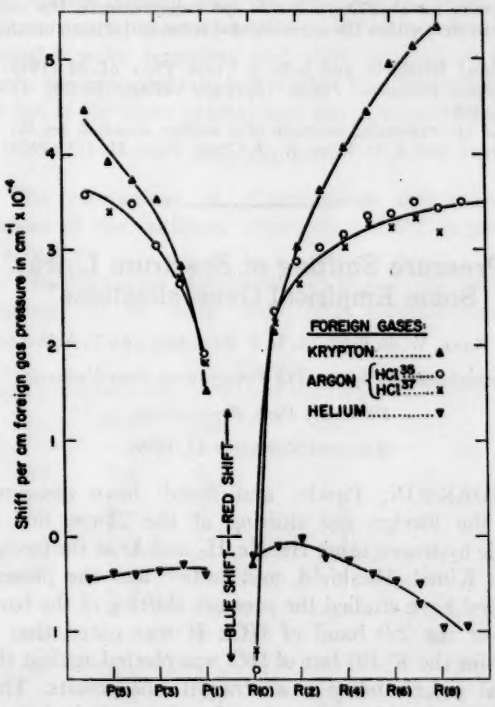

FIG. 1. Pressure-induced shifts of lines in the 2-0 band of HCl due to noble gases (24°C).

ments the effects are similar and of about the same magnitude. The shifts are all toward the red and increase steadily with J number. With DCl, some of the lines are shifted toward the blue.

Figure 1 shows results for helium, argon, and krypton. For high J numbers the ratio of the shifts for krypton and argon [1.55 for $R(8)$] is found to be approximately equal to the ratio of the respective polarizabilities[2] ($\alpha_{Kr}=2.48\times10^{-24}$ cc; $\alpha_{Ar}=1.63\times10^{-24}$ cc). This suggests that the perturbation of the vibrational and rotational energy levels (which results in the line shifts) is mainly due to dipole-induced dipole interactions. The potential at the HCl molecule due to an induced atomic dipole, situated at a distance R from it, is given by

$$V=-(\alpha\mu^2/2R^6)(1+3\cos^2\theta),$$

where μ is the dipole moment of HCl and θ is the angle between the HCl molecular axis and the line joining the molecules. The potential is symmetrical about this line and the case is relatively simple to treat theoretically.

The shifts with helium do not fit into this picture[3] and it may be concluded that the dipole-induced dipole interaction is not dominant and repulsive forces, which are relatively less important with Kr and Ar, must be taken into account in this case.

* This work was supported in part by the Geophysics Research Directorate, U. S. Air Force Cambridge Research Center under Contract AF 61(052)-57, through the European Office, ARDC.

† We are grateful to Dr. D. H. Rank of the Pennsylvania State University for checking a few of our measurements. His values agree to well within the experimental error (private communication).

[1] Kimel, Hirshfeld, and Jaffe, J. Chem. Phys. **31**, 81 (1959).

[2] *Landolt-Bornstein Tables* (Springer-Verlag, Berlin, 1950), I/1, p. 401.

[3] For an interesting example of a similar situation see W. W. Robertson and A. D. King, Jr., J. Chem. Phys. **31**, 473 (1959).

Pressure Shifting of Spectrum Lines: Some Empirical Generalizations*

D. H. RANK, W. B. BIRTLEY, D. P. EASTMAN, AND T. A. WIGGINS

Department of Physics, The Pennsylvania State University, University Park, Pennsylvania

(Received November 13, 1959)

ANDERSON, Pipkin, and Baird[1] have measured the foreign gas shifting of the 21-cm line of atomic hydrogen using He, Ne, H_2, and Ar as the foreign gases. Kimel, Hirshfeld, and Jaffe[2,3] and the present authors[4] have studied the pressure shifting of the band lines of the 2-0 band of HCl. It was noted that if $\Delta\nu/P$ for the $R(10)$ line of HCl was plotted against the optical polarizability α a straight line results. This same relationship exists for the data of Anderson, Pipkin, and Baird.[1] (Actually a somewhat better fit of the data may be obtained by plotting $\Delta\nu/P$ *vs* $\alpha^{\frac{1}{2}}$. The necessary power of α can be decided by measurements using xenon as the foreign gas. Intuitively and theoretically the first power of α is preferable.) Furthermore it was noted that if the $\Delta\nu/P$ values mentioned in the foregoing were divided by the frequency of the line itself and plotted against α, parallel and almost coincident straight lines result.

We have displayed the foregoing data in Fig. 1. Curve A represents the data of Anderson, Pipkin, and Baird[1] on the 21-cm line of atomic hydrogen. Curve B represents the data on the $R(10)$ line of HCl which is obtained from reference 4. The errors quoted by A.P.B. and the standard deviations of the $R(10)$ lines shifts are indicated in the figure in the usual manner. We have treated the data obtained by Füchtbauer, Joos, and Dinkelacker[5] on the foreign gas shifting of the mercury resonance line λ2536 in a similar manner and these results are displayed in Fig. 1 on both curves by means of the triangular points.

The results displayed in Fig. 1 show that the magnitude of the foreign gas shifts observed for the 21-cm line of atomic hydrogen, the $R(10)$ line of the 2–0 band of HCl and the resonance line of mercury are proportional to the frequency over a frequency range of 10^6 and probably proportional to the optical polarizability of the foreign gas.

The theoretical treatments of pressure broadening and pressure shifting of spectral lines available in the literature are extensive, conflicting, and generally unsatisfactory particularly with respect to band

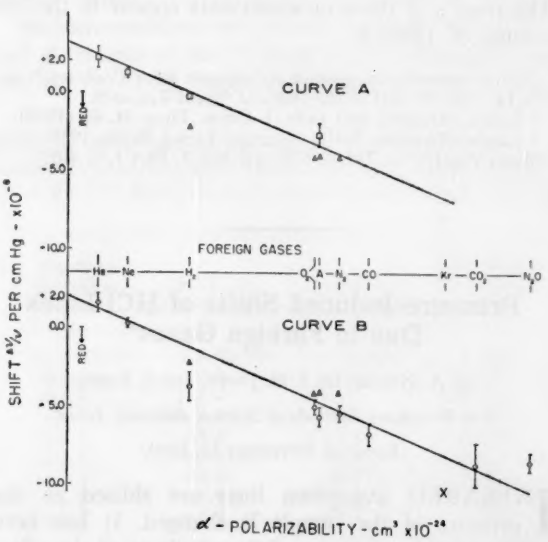

FIG. 1. Plot of $(\Delta\nu/\nu)(1/P)$ *vs* the polarizability α for various foreign gases. Curve A is calculated from Anderson, Pipkin, and Baird.[1] Curve B is calculated from our present measurements. The point marked X results from the measurement on krypton by Jaffe *et al.* (private communication). The triangular points in both curves are calculated from the Füchtbauer, Joos, and Dinkelacker[5] measurements of λ2536 Hg.

spectra. It is well known that the pressure shifts of the resonance lines and lines involving higher electronic states of alkali atoms are of a different order of magnitude than the shifts under discussion here.

The J dependence of pressure shifting observed by Jaffe *et al.*[2] must be caused by essentially two processes. (1) A fundamental pressure shift proportional to the frequency of the transition and dependent on the polarizability of the foreign gas. (2) A J-dependent contribution of opposite sign for lower J's.

The existence of J-dependent pressure shifting in infrared band spectra coupled with the fact of the availability of suitable experimental tools for quantitative measurements of these small displacements should furnish powerful methods for exploring pressure broadening and shifting of spectrum lines.

We have noticed that the broadening of the HCl lines we have observed is quite different for the different foreign gases used. These results are given in the last column of Table I of our previous communication.[4] It is obvious by inspection of this table that when the polarizability of the foreign gas is anisotropic the broadening is much greater than for foreign gases whose polarizability is isotropic. However, the large breadths cannot be explained by the application of a simple linear additivity theorem.

* This research was assisted by support from Contract Nonr-656(12) NR 019-401 of the Office of Naval Research.

[1] Anderson, Pipkin, and Baird, Bull. Am. Phys. Soc. Ser. II, **4**, 418 (1959).

[2] Kimel, Hirshfeld, and Jaffe, J. Chem. Phys. **31**, 81 (1959).

[3] Hirshfeld, Jaffe, and Kimel, J. Chem. Phys. **32**, 297 (1960), this issue.

[4] Rank, Birtley, Eastman, and Wiggins, J. Chem. Phys. **32**, 296 (1960), this issue.

[5] Füchtbauer, Joos, and Dinkelacker, Ann. Phys. **71**, 204 (1923).

Mechanism for the Optical Absorption in Some Paramagnetic Salts

ROBERT ENGLMAN

Department of Physics, Israel Institute of Technology, Haifa, Israel

(Received November 2, 1959)

THERE exists a wide set of experimental results for absorption in the optical frequency range by octahedrally hydrated paramagnetic ions. The theoretical explanation of these results aims at the prediction of the frequency of absorption as well as its intensity. For the former the ligand field theory and its refinements provide the answer, whereas for the intensity one needs to find the mechanism which enables the "forbidden" (even-even) transitions to occur. In a few recent papers[1] the intensities for a number of specific ions have been calculated on the assumption, essentially, that the high-energy odd parity states of the free ion retain sufficiently their character even in the hydrous complex to be regarded as contaminants of the low-energy even states.

In a new, alternative theory we dispense with this assumption. Instead, we regard as the contaminants the charge transfer states of the complex, whose absorption bands are often observed in the near ultraviolet. The mixing-in is effected, just as before, by the odd-type vibration of the complex, but now the high-frequency modes are predominantly effective. (This gives for the intensity the temperature variation which agrees with observation.)

The theory gives for the oscillator strength of the band the general expression

$$\text{O.S.}=B[(E_f-E_i)/(E_f-E_e)^2]N.$$

The energies of the final, initial, and charge transfer states appear in the expression; they are known empirically. N is an integer which depends on the symmetry type of the states. Thus for the transitions

	$A_2\rightarrow T_2$,	$A_2\rightarrow T_1$;	$T_1\rightarrow T_2$,	$T_1\rightarrow T_1$;	$T_2\rightarrow E$;	$E\rightarrow T_2$;
$N=$	18	6	10	6	8	12

B depends only on the ion (i.e., not on the particular transition). It is not possible to determine B without further assumptions, since it depends, apart from the temperature, on the ionic mass and the vibrational frequency (300–350 cm^{-1}), and on overlap integrals of the charge transfer and $3d$ ionic states. With some drastic assumptions we used a model to find the charge transfer wave functions and thus determined B. In fact, we supposed that B varies but little from ion to ion of the same valency and found accordingly that

$$B_{2+}/B_{3+}\simeq 10.$$

The comparison of experimental and calculated values of the oscillator strengths ($\times 10^4$) is given in Table I.

The calculated values for each ion are probably accurate to no more than 50%. Nevertheless, the

TABLE I.

Ion	Obs.[a]	Calc.	Ion	Obs.[a]	Calc.
Ti^{3+}	0.8	0.72	Cr^{2+}	1.8	2.2
V^{3+}	0.6	0.5	Fe^{2+}	0.4	0.6
	1.1	1.1			
			Co^{2+}	0.3	0.3
Cr^{3+}	1.6	1.2		0.9	0.7
	2.2	1.5			
			Ni^{2+}	0.45	0.5
Mn^{3+}	1.1	0.73		0.35	0.2
				0.6	0.6
V^{2+}	0.1	2.4			
	0.2	1.9	Cu^{2+}	1.4	2.2

[a] O. G. Holmes and D. S. McClure, J. Chem. Phys. **26**, 1686 (1957).

tendency for agreement (V^{2+} excepted) is gratifying. Agreement within any one ion is even more significant.

A detailed account of the calculations will be published elsewhere.

The value of advice by Professor M. H. L. Pryce and Dr. S. Tanabe on the idea contained in this note is acknowledged.

[1] A. D. Liehr and C. J. Ballhausen, Phys. Rev. **106**, 1161 (1957); S. Koide and M. H. L. Pryce, Phil. Mag. **3**, 607 (1958); C. J. Ballhausen and A. D. Liehr, Mol. Phys. **2**, 123 (1959); S. Koide, Phil. Mag. **4**, 243 (1959); R. Englman and M. H. L. Pryce, (unpublished calculations).

Positive Hole Injection into Organic Crystals*

H. KALLMANN AND M. POPE

Department of Physics, New York University, Washington Square, New York

(Received November 2, 1959)

IT has been shown[1] that the variation of bulk and surface photoconductivity in anthracene with the wavelength of the incident light is similar to the optical absorption dependence on wavelength. It is also known[2] that the surface conductivity of anthracene is markedly affected by the presence of certain gases, and is also sensitized to light of longer wavelengths than are usually effective in producing photoconductivity.

We have now observed large changes in bulk conductivity in anthracene which can be attributed in one case to the interaction between an optically excited electrode layer and the unexcited adjacent anthracene, and, in another case, to a dark interaction between the anthracene and the adjacent electrode.

The experimental techniques used have been described in detail elsewhere.[3,4] The general procedure was to use an electrolyte as the electrodes for thin (10 μ) single crystals of anthracene. An electrolyte consisting of a saturated solution of I_2 in 1M NaI was placed against one surface of the crystal and a solution containing 1M NaI without iodine was placed in contact with the opposite surface. Light of wavelength 4360 A was then passed through the NaI solution, on through the anthracene crystal, into the I_2 solution where it was absorbed. This was repeated using 3650 A, which was absorbed however by the anthracene crystal, producing photoconductivity in the crystal.

The results of these experiments were compared with those obtained when both surfaces of the crystal were in contact with 1M NaI solution which contained no iodine. All the results are given in Table I. The adjective "sensitized" was used to describe experiments in which iodine played a role.

The following points will be noted. The dark conductivity was independent of the polarity of the applied voltage when both electrodes were identical. When one electrode contained I_2, the dark current was increased by a factor of 82 when the voltage of the iodine compartment was made 50 v positive, while the current was increased by a factor of 3.7 when a negative voltage was applied to the iodine solution.

Using 3650-A light and identical electrodes, the ratio of i_+/i_- at 50 v was 68. The addition of I_2 increased i_- by a factor of 143 while i_+ changed very little.

Using 4360-A light, to which the anthracene is practically transparent, and identical electrodes, the ratio of i_+/i_- at 50 v is 1. This current is 4×10^{-4} that of i_+ at 3650 A. With iodine added to one compartment, i_- increased by a factor of 2400, becoming as large as the maximum forward current using 3650-A light, which the anthracene absorbed. The current i_+ changed very little; so the ratio i_-/i_+ was 2400.

These experiments were repeated on other crystals, with similar results. The magnitude of the sensitization

TABLE I. Hole injection into anthracene.

Applied voltage Volts	Dark current $i_+{}^a=i_-{}^a$ $\times10^{12}$ amp	Sensitized dark current i_+	Sensitized dark current i_-	3650 A Photocurrent i_+	3650 A Photocurrent i_-	Sensitized 3650 A Photocurrent i_+	Sensitized 3650 A Photocurrent i_-	4360 A Photocurrent i_+	4360 A Photocurrent i_-	Sensitized 4360 A Photocurrent i_+	Sensitized 4360 A Photocurrent i_-
		$\times10^{12}$ amp		$\times10^{9}$ amp[b]		$\times10^{9}$ amp[b]		$\times10^{12}$ amp		$\times10^{9}$ amp[b]	
2	...	1	4	10	0.33	13	2.7	4.5	3.5	0.0045	0.16
4	0.3	1.5	8	21	0.40	23	8.8	6.0	4.5	0.0065	0.84
8	0.5	2.5	60	29	0.46	34	27	8.0	6.0	0.0085	5.2
15	0.9	3.5	165	36	0.52	39	55	10	8.0	0.012	19.5
30	1.7	8.5	225	40	0.58	43	80	14	13	0.016	40
50	3.0	11	245	42	0.62	47	89	19	18	0.020	48

Area of crystal: 0.1 cm²
Intensity of 3650 A light: 320 μw/cm²
Intensity of 4360 A light: 920 μw/cm²

[a] i_+ and i_- refer to currents measured when the polarity of the face of the crystal not in contact with the iodine was made positive and negative, respectively; they are also the currents measured when the polarity of the side through which the light entered was positive and negative, respectively.
[b] Note change in scale.

effect increases as the concentration of I_2 in the iodide increases. Light of wavelength 5360 A did not induce any photoconductivity at all in anthracene, using identical NaI electrodes. However, there was a distinct increase in i_- with this light even when I_2 was added in small concentration to the positive compartment, although the absorption of 5360-A light by I_2 solution is about 1/20 of that of 4360-A light.

The quantum efficiency for the photocurrent at 3650 A was 230 quanta absorbed per carrier liberated in the anthracene. When I_2 was added to the 1*M* iodide solution, the efficiency of the 4360-A light was 340 quanta absorbed in the I_2 solution per carrier produced in the anthracene. In all cases, the currents were almost saturated at 50 v or lower.

Upon removal of the I_2 solution, and its replacement with iodide solution, the dark resistance of the crystal returned immediately to a value close to the starting resistance, indicating little if any reaction with the iodine. The results we have observed are consistent with the assumption that the iodine extracts an electron from the anthracene crystal, injecting a positive hole inside the anthracene which will travel under the action of the field through the crystal to the negative electrode. This reaction takes place both in the dark, and with much greater magnitude when the iodine is illuminated with energetic radiation within its absorption band.

A more complete discussion of these results will be given shortly in another paper.

The efforts of Mr. Peter Gordon, who made most of these measurements, are greatly appreciated.

* Grateful acknowledgment is made of the assistance of the Office of Naval Research [NONR 285(41)] in this work and of the Air Force Cambridge Research Center, Contract AF 19(604)-3888.

[1] Compton, Schneider, and Waddington, J. Chem. Phys. **27**, 160 (1957).
[2] D. M. J. Compton and T. C. Waddington, J. Chem. Phys. **25**, 1075 (1956).
[3] H. Kallmann and M. Pope, Rev. Sci. Instr. **29**, 993 (1958).
[4] H. Kallmann and M. Pope, Rev. Sci. Instr. **30**, 44–6 (1959).

Catalytic Effects in the Dissociation of Oxygen in Microwave Discharges*

F. KAUFMAN AND J. R. KELSO
Ballistic Research Laboratories, Aberdeen Proving Ground, Maryland

(Received November 5, 1959)

IT has long been known that small amounts of certain added species increase the extent of dissociation of simple, diatomic molecules (O_2, N_2, H_2) in electric discharges. Thus, H_2O increases the dissociation of H_2[1,2] as well as that of O_2,[3,4] while O_2 or H_2O increase the dissociation of N_2.[5,6] Such catalytic activity has often been ascribed to wall effects, i.e., the more efficient poisoning of the surface towards atom recombination processes, though recent investigators have realized increasingly that it may be due to homogeneous reactions in the discharge.

We are studying these effects systematically and have started with oxygen dissociation because of our recent work with atomic oxygen[7,8] and because of its importance in upper atmosphere physics. A flow system was used, the pressure range was 0.4 to 1.3 mm Hg and the flow rates 0.5 to 3.3 cc/sec NTP of O_2, though most experiments were run at 0.8 mm Hg and 1.6 cc/sec. The discharge was excited by a C.W. magnetron (Raytheon QK 390, 2450 Mc, up to 800 w of microwave power) in a quartz tube (i.d. 10 mm, 5 mm, or 2 mm). Downstream from it a larger glass tube (19 mm i.d., 100 cm long) with two sealed-in glass jets 60 cm apart, and two photomultiplier stations 8 cm downstream from each of the two jets served to measure the intensity of the air afterglow and to titrate the atomic oxygen with added NO_2.[7,8] The NO_2 titration was simplified by installing a ball-type flowmeter and by keeping the reservoir of pure NO_2 at one of three temperatures, −12°C, 0°C, or +18°C in suitable constant temperature baths. Thus, the absolute concentration of atomic oxygen (O) could be measured instantaneously at either of two positions. Relative values of (O) were measured independently by the intensity of the air afterglow in the presence of known amounts of NO added at the upstream jet.

The gases investigated for their possible catalytic effect on O-atom production were N_2, NO, H_2, Ar, He, CO_2, and N_2O. They were added to the low-pressure oxygen flow before the discharge and their flow rate was measured directly or by the pressure drop in a small closed system as indicated on a Wallace and Tiernan dial pressure gauge.

The measured intensity of the air afterglow could also be used to determine the amount of NO made in the discharge by adding known amounts of NO downstream and extrapolating from the measured increase of emission intensity under constant discharge conditions.

The purity of the oxygen proved to be of critical importance. O_2 was obtained from specially selected cylinders with or without condensation at 77°K, or from $KClO_3$ or $KMnO_4$ by careful thermal decomposition and condensation.

The results are as follows: A powerful catalytic effect for O-atom production was found in the presence of added N_2, NO, or N_2O as well as in the presence of H_2. No effect was found for added He, Ar, or CO_2. The dissociation of O_2 in microwave discharges which normally ranges around 10 to 20% $[\equiv(O)/(O_2)_0]$ is almost entirely due to nitrogeneous or hydrogenous impurities (primarily N_2 and H_2O). Our "purest" O_2 so far has given 0.9%. Small amounts of added N_2 (0.01 to 0.05%) increase the O-atom yield at a rate equivalent to the formation of 80–90 O atoms for one N_2 molecule. For H_2 the corresponding yield is 160–200. For NO and N_2O it is 40–45 and 80–90, and the nitrogeneous discharge product is, in each case, NO in about 90% yield. This strongly suggests that nitrogen-

containing compounds are rapidly converted to NO and points up the positive importance of NO^+ in the dissociation scheme.

In no case was there an appreciable change in the slow decay of O atoms downstream for small additions of N_2 or H_2. The catalytic effects were rapidly and completely reversible. These facts together with the large "chain lengths" at the short residence time and low pressure rule out any explanation which would ascribe the phenomena to surface effects in or out of the discharge.

The many OI emission lines (e.g., 3947, 4368, 5329–30 A) from the discharge were recorded with a Leeds and Northrup Photoelectric Recording Spectrometer. Their intensities were unchanged for additions of N_2 which increased (O) about sixfold and rose by less than a factor of two for large N_2 additions which raised (O) about 20-fold. It appears that the highly excited upper states of these transitions are not populated by excitation of ground-state atoms, but arise perhaps by dissociative recombination of O_2^+ with electrons of 3 to 5 ev.

It is clear that neither this dissociative recombination nor the frequently invoked excitation of a repulsive molecular study by electron collision followed by dissociation are major mechanisms for the dissociation of oxygen. The striking efficiency of N_2 or H_2 rather suggests chainlike sequences consisting of very fast ion-electron or ion-molecule reactions, e.g., $NO^+ + e \rightarrow N + O$; $N + O_2^+ \rightarrow NO^+ + O$. Initial, semiquantitative measurements of the concentration of free electrons in the discharge region by a microwave attenuation method have shown n_e to be unchanged for a N_2 addition which raised (O) 40-fold. These will be refined and repeated.

The even greater catalytic effect of H_2 is surprising. In the short time of residence in the discharge (1 to 5 msec) it does not seem possible that H_2O could be formed and regenerated about 100 times as a major link in the chain. Possibly, the dissociative recombination of OH^+ could be of importance, though the corresponding regeneration step $H + O_2^+ \rightarrow OH^+ + O$ is endothermic and cannot occur.

The work will now be extended to other dissociations, to radio frequency discharges, and to a more direct experimental examination of the nature and concentrations of ions present in the discharge.

* Work supported by the Advanced Research Projects Administration under contract ARPA 67–59. Presented in part at the 12th Annual Gaseous Electronics Conference, Washington, D.C., October 14–16, 1959.

[1] R. W. Wood, Phil. Mag. **44**, 538 (1922).
[2] T. M. Shaw, J. Chem. Phys. (to be published).
[3] P. D. Copeland, Phys. Rev. **36**, 1221 (1930).
[4] J. C. Greaves and J. W. Linnett, Trans. Faraday Soc. **55**, 1346 (1959).
[5] B. J. Fontana, J. Chem. Phys. **31**, 148 (1959).
[6] F. Kaufman and J. R. Kelso (unpublished work).
[7] F. Kaufman, Proc. Roy. Soc. (London) **A246**, 123 (1958).
[8] F. Kaufman and J. R. Kelso, Symposium on Combustion, 7th Symposium, London, 1958, p. 53.

Comments and Errata

Note on the Paramagnetic Resonance Spectrum of Fluoroferrate Ion FeF_6^{---}

L. Helmholz and A. V. Guzzo

Department of Chemistry, Washington University, St. Louis, Missouri

(Received November 10, 1959)

In a previous communication[1] we have discussed the paramagnetic resonance spectrum of the fluoroferrate ion FeF_6^{---} in terms of the molecular orbitals occupied by the five unpaired electrons. A number of weak lines were unexplained in this treatment and suggestions were offered concerning their origin. Professor N. Bloembergen of Harvard University has directed our attention to the correct origin of these lines and, following his suggestion, we have revised our interpretation of the spectra.

The weak lines and a relatively small displacement of the positions of the strong lines arise because the magnetic fields at the fluorine nuclei have components perpendicular to the external field due to the field of the unpaired electrons. The magnitude of these components depends on the orientation of the external field relative to the FeF_6^{---} octahedra.

The calculation of the position of the absorption lines proceeds through the inclusion in the Hamiltonian* of the terms

$$H' = A_p \sum_1^6 f_i(\alpha)\, S_z (I_{xi} + I_{yi}) + B \sum_1^6 I_z$$

in addition to the terms employed in the earlier incomplete treatment. Here $f(\alpha)$ is the function of the angle α (defined in reference 1) giving the orientation of the FeF_6^{---} octahedra relative to the external magnetic field and is the same only for pairs of fluorine nuclei related by the center of symmetry. It is, for example, zero for $\alpha = 0$, i.e., for the magnetic field directed along one of the cubic axes. This fact considerably simplifies the interpretation. In the following, A_p and A_s have the same significance as in reference 1, and B is the constant giving the Zeeman energy of a fluorine nucleus.

For the magnetic field perpendicular to one octahedron face the displacements of the absorption maxima from the field $H_0 (= h\nu/g\beta)$ for the transitions with electronic spin component $M_s = +\frac{1}{2}$, $M_s = -\frac{1}{2}$ are given by the expression

$$H - H_0 = n\{[(A_s/2) + B]^2 + (A_p^2/2)\}^{\frac{1}{2}} + m\{[(-A_s/2) + B]^2 + A_p^2/2\}^{\frac{1}{2}}$$

where

$$n, m = 0, \pm 1, 2, \text{ or } 3.$$

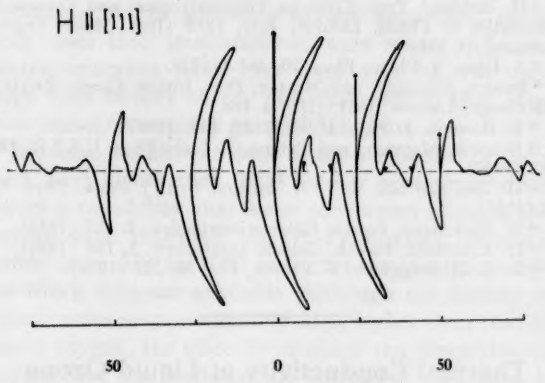

FIG. 1.

Since these are the only two states involved in the well-resolved spectra, they are the only two which concern us. The mixing of the electronic spin-states is negligible and the transitions $M_s=\frac{3}{2}$ to $M_s=\frac{1}{2}$ fall in a different region of magnetic field for H parallel to [111]. The fluorine nuclear spin functions corresponding to these energies become linear combinations of the functions with differing values of ΣI_z and corresponding transitions become allowed between levels of different ΣI_z. The relative intensities of these lines are given by the relative values of the sums of the overlaps of the nuclear spin functions over the states involved.

The results are given in Fig. 1, where a spectrum for H parallel to [111] observed at liquid nitrogen temperature is shown. The calculated positions of the absorption maxima, shown by the vertical lines of length proportional to intensity, do not fall precisely at positions of zero slope of the derivation curve. If allowance is made for the displacement of the maxima of the weak lines because of the proximity of the strong lines good agreement is obtained.

The parameters A_s and A_p are very nearly the same as obtained previously: $A_s=24.0\pm0.5$ gauss, $A_p=7.0\pm0.5$ gauss. The molecular orbital coefficients consequently remain unaffected.

In the [110] direction the resolution is not sufficiently good to permit identification of the "forbidden" lines but the qualitative features of the derivative curve are in agreement with calculations.

The spectra of MnF_6^{--} and CrF_6^{---} ions show hyperfine structure which is so strongly influenced by the terms of H', that the interpretation in terms of a simplified (reference 1) scheme is impossible. A discussion of the spectra and electronic structure of these ions is in preparation at present.

[1] L. Helmholz, J. Chem. Phys. **31**, 172 (1959).

* The necessity of this addition has been pointed out to us also in a communication by Clogston, Gordon, Jaccarino, Peter, and Walker of the Bell Telephone Laboratories.

Some Remarks on the Paper "Thermal Conductivity of Liquid Ozone" by T. E. Waterman, D. P. Kirsh, and R. I. Brabets

H. ZIEBLAND

Ministry of Supply, Explosives Research and Development Establishment, Waltham Abbey, Essex, England

(Received May 27, 1959)

IN a recent paper [J. Chem. Phys. **29**, 905 (1958)] Waterman, Kirsh, and Brabets reported on their measurements of the thermal conductivity of liquid ozone.

In contrast with the trend exhibited by normal nonassociating liquids whose thermal conductivity falls with increasing temperature, the thermal conductivity of liquid ozone was found to increase with rising temperature. No explanation of this anomalous behavior was attempted by the authors, and because of lack of adequate physical data on ozone it proved impossible to analyze their results on this substance.

The authors, however, measured at one temperature the thermal conductivity of liquid oxygen, a substance for which extensive measurements by other observers are available. With the aid of these, and the one point determined by Waterman *et al.*, an indirect assessment of their work on ozone has been attempted here. In their Fig. 4 they showed, together with their own value on oxygen, one point due to Hammann,[1] one due to Prosad,[2] and two points from a paper by Burton and Ziebland.[3] In this presentation the value found by Waterman *et al.* is almost identical with the arithmetic mean formed from the four points mentioned in the foregoing. The authors then state that their values on oxygen were in agreement with those presently assumed to be the most accurate ones. Considering the large differences between the data by Hammann and by Prosad on one hand, and those by Burton and Ziebland on the other, it is not at all clear to which of those data this statement refers.

The question "Which data should be regarded as reliable?" can be answered at once. The authors have unfortunately overlooked two further investigations on the thermal conductivity of liquid oxygen, *viz.*, one rather extensive study by Tsederberg and Timrot,[4] and some individual points by Keyes.[5] The results of these two observers agree within 2 to 3 percent with those of Ziebland and Burton.[3,6] Particularly noteworthy is the excellent agreement of the latter authors with the data by Tsederberg and Timrot, as it is maintained over the entire range of pressure and temperature common to both investigations. A brief comparison of all available information on the thermal conductivity of liquid oxygen was made by Ziebland.[7]

In view of this evidence some doubts must be expressed as to the reliability of Hammann's data, the more so as his simultaneously published results on nitrogen have also been criticized by a number of ob-

servers[8–12] and have been found as much as 65% too high.

The value attributed to Prosad was evaluated from heat transfer experiments on condensing oxygen vapor, and, with the various assumptions made, can at best be regarded as an estimate only.

To avoid misunderstandings it ought to be pointed out that the two points attributed to Burton and Ziebland in their Fig. 4 are in fact points on their 1 atmos isobar and, for the sake of clarity, should have been joined by a line. The difference in the trend with temperature of ozone and oxygen would thus have been much emphasized.

From the foregoing it can be concluded with reasonable certainty that the thermal conductivity of liquid oxygen at −195.8°C is 3.95×10^{-4} cal/cm sec deg C±2% and that in consequence the value by Waterman *et al.* seems to be about 12% too high. From the following analysis of this discrepancy it seems likely that their results on ozone are also in error.

While several plausible explanations of the anomalous trend of the thermal conductivity of ozone could be put forward, such as association, slow decomposition, or exothermic reaction of ozone with certain parts of the apparatus, none of these arguments would be valid for oxygen. There remains to discuss one of the most common causes of substantial error in measurements of the thermal conductivity of fluids, *viz.*, the occurrence of convection in the layer of fluid through which the measured amount of heat is being passed. There are several investigations on natural convection in *horizontal* annuli,[13,14] and it has been conclusively established that natural convection cannot occur if the product of Grashoff and Prandtl numbers is below 1000. For vertical annuli Beckmann,[13] from a few of his own experiments, tentatively suggested the same upper limit of this criterion, while Briggs[15] recommended a value lower than 600 to prevent the onset of convection. From the characteristic dimensions of the apparatus used in Waterman's experiments and the known physical properties of oxygen, the Gr.-Pr. product was computed for Waterman's value on oxygen and was found to be about 18 000. This is much in excess of the previously mentioned critical limits for convection-free operation of the conductivity cell and it must be concluded that certainly the value on oxygen, but probably even more so the data on ozone, on account of its larger density, were seriously affected by convection. It seems very doubtful indeed whether the authors' claim that an error greater than 5% is inconceivable in their experiments, can be upheld.

[1] G. Hammann, Ann. phys. **32**, 593 (1938).
[2] S. Prosad, Brit. J. Appl. Phys. **3**, 58 (1952).
[3] J. T. A. Burton and H. Ziebland, unpublished Ministry of Supply report, 1956.
[4] N. V. Tsederberg and D. L. Timrot, Zhur. Tekh. Fiz. **26**, 1894 (1956).
[5] F. G. Keyes, Trans. Am. Soc. Mech. Engrs. **77**, 1395 (1955).
[6] H. Ziebland and J. T. A. Burton, Brit. J. Appl. Phys. **6**, 416 (1955).
[7] H. Ziebland, Proc. Conf. on Thermodynamic and Transport Properties of Fluids, London, July, 1957 (Inst. Mech. Engrs. London), p. 211.
[8] A. Uhlir, J. Chem. Phys. **20**, 463 (1952).
[9] Powers, Johnston, and Mattox, Proc. Intern. Congr. Refrig., 8th Congr.; London, 1951, (III) p. 186.
[10] E. Borovik, J. Phys. U.S.S.R. **11**, 149, (1947).
[11] Borovik, Matveev, and Panina, J. Tech. Phys. U.S.S.R. **10**, 988 (1940).
[12] H. Ziebland and J. T. A. Burton, Brit. J. Appl. Phys. **9**, 52 (1957).
[13] W. Beckmann, Forsch. Gebiete Ingenieurw. **2**, 165 (1931).
[14] H. Kraussold, Forsch. Gebiete Ingenieurw. **5**, 186 (1934).
[15] D. K. H. Briggs and F. Popper, Fuel **33**, 222 (1954).

Thermal Conductivity of Liquid Ozone

[J. Chem. Phys. **29**, 905, (1958)]

T. E. Waterman, D. P. Kirsh, and R. I. Brabets

Armour Research Foundation, Chicago, Illinois

(Received September 3, 1959)

In reply to the remarks by Mr. Ziebland concerning our work on liquid ozone, we did not attempt to explain the apparent rise in thermal conductivity of liquid ozone with temperature, since the pressure of each determination was the vapor pressure of the ozone. Across the experimental range, this value increased from 0.2 mm at −195.8°C to 212 mm at −128°C. The reason we did not assess the reliability of the available oxygen data was that our measurements of the thermal conductivity of carbon tetrachloride and water were within 2% of the values recommended by Challoner and Powell[1] in their comprehensive evaluation of the room temperature data on these liquids. Thus, we noted the general agreement with the information at hand, and then directed our efforts toward the ozone determinations.

We did not investigate the effects of convection on the oxygen data further, because we noted a gradual curvature in the k *vs* Δt plot, apparently starting at a Δt of 0.6°C, which we believed to indicate the onset of convection (convection was visually observed at a Δt of about 8°C).

Mr. Ziebland cites the Grashoff-Prandtl (Gr.-Pr.) product[2] as a criterion for the onset of convection, and he suggests the experiments of Beckmann[3] (Gr.-Pr.= 1000) and Briggs[4] (Gr.-Pr.=600) to indicate an upper limit below which convection does not occur. Their method of indicating this limit essentially was to note the point which heat input q ceases to be proportional to temperature difference Δt. Although the portion of experimental points on the oxygen data which lie in this region are insufficient to eliminate absolutely the possibility of slight curvature below the Δt of 0.6°C indicated in the foregoing, we re-examined the data obtained for carbon tetrachloride in this respect, and we found no evidence for convection below a Δt of 1.3°C or a Gr-Pr. product of 4900. Thus, we believe that the limits suggested by Beckmann and Briggs are not

applicable to the geometry of our apparatus, as in both cases their measurements were made with concentric cylinders where the inner cylinder was very large with respect to the film thickness so that they more closely resembled parallel flat plates.

We have insufficient data to set a new Gr.-Pr. product limit higher than 4900 for our geometry, which leaves a possibility that some convection affected the oxygen data. However, the Gr.-Pr. product for ozone varies from 550 to 2000 over the temperature range for which data are available. Although the density of liquid ozone is approximately 33% higher than that of liquid oxygen, the viscosity is about ten times that of oxygen and the coefficient of volumetric expansion is roughly one-half that of oxygen, thus the lower Gr.-Pr. product. Therefore, we still believe that our data on liquid ozone are accurate to within 5%.

[1] A. R. Challoner and R. W. Powell, Proc. Roy. Soc. (London) **A238**, 90 (1956).
[2] For purposes of calculating the Gr.-Pr. product, the dimensions given in our original paper as radii are actually diameters. Mr. Ziebland's paper incorporates the correct values.
[3] W. Beckmann, Forsch. Gebiete Ingenieurw. **2**, 165 (1931).
[4] D. K. H. Briggs and F. Popper, Fuel **33**, 222 (1954).

Notes

Free Radicals from the Flash Photolysis of Phenol*

L. I. Grossweiner and E. F. Zwicker

Department of Physics, Illinois Institute of Technology, Technology Center, Chicago 16, Illinois

(Received August 27, 1959)

Porter and Strachan[1] have shown that the benzyl free radical has two systems of absorption bands in M.P. glass at −197°C, with long-wavelength peak maxima at 317.8 and 463.5 mμ. Because of its similar electronic structure, the phenoxy free radical would be expected to show analogous absorption systems, but Porter and Wright[2] found only a single diffuse band at 292.0 mμ in the gas phase. Grossweiner[3] reported that the photolysis of both aqueous phenol at *p*H 7 and the phenolate ion at *p*H 12 produces a short-lived absorption system with bands below 400 mμ. Grossweiner and Mulac[4] obtained this spectrum from the photolysis of phenol in ethanol, cyclohexane, and carbon tetrachloride, and also from anisole in ethanol. They assigned these spectra to the phenol radical cation and the anisole radical cation, respectively. The production of the radical cation from the photolysis of the phenolate ion was explained by assuming that the initial product is the phenoxy free radical, and that a rapid association with hydrogen ion occurs at *p*H 12.

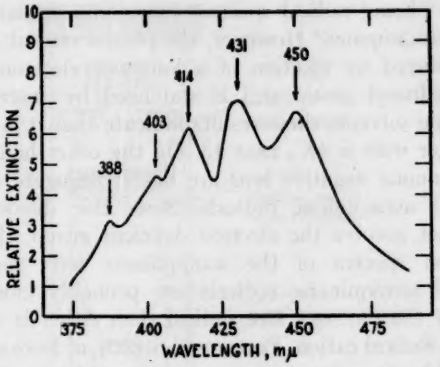

Fig. 1. The absorption spectrum of the phenoxy free radical, produced by flash photolysis of phenol in 1.0 *M* NaOH.

This work has been extended by flash photolysis of aqueous, oxygen-free phenol solutions at various acidities. The samples were contained in a 30 cm fused silica cell and irradiated with a 1000-joule, 25-μsec flash lamp. Spectra were taken on Kodak 103-F plates with the Hilger "medium" quartz prism spectrograph. Between *p*H 3 and 12, the spectrum assigned to the phenol radical cation is produced. The maxima of the resolved bands, as re-measured at higher dispersion, are 398.9±0.4, 382.1±0.4, and 368.1±1.0 mμ. The durations of the transient spectra are approximately constant at 200 μsec over the *p*H range, indicating that hydrogen or hydroxyl ions are not primary reactants in the disappearance of the transient substance. However, when 0.01 wt. % phenol is photolyzed in 1.0 *M* sodium hydroxide, a quite different transient spectrum is produced; see Fig. 1. Blank runs with the sodium hydroxide solutions show the occurrence of a very broad transient spectrum through the visible region, possibly due to the photolysis of carbonate ion, and this was subtracted from the spectra obtained with phenol, to give the result shown. This spectrum is now assigned to the longer wavelength system of the phenoxy free radical, for the following reasons: (a) Although the initial reactant at *p*H 12 and *p*H 14 is the phenolate ion, different transient spectra are produced at these acidities. This is explained if the transient products are acid-base conjugates. The phenol radical cation should be a weaker acid than aqueous phenol,[4] so that the displacement of the equilibrium near *p*H 13 is consistent with the assignment of the acid and base to the phenol radical cation and phenoxy free radical, respectively; (b) the spectrum assigned to the phenoxy free radical strongly resembles the longer wavelength system of the benzyl free radical. Both show three prominent bands followed by a series of weaker bands into the ultraviolet. Further, the hypsochromic shift of the longer wavelength phenoxy radical system is 14 mμ, which is very close to the difference between the maxima of the shorter wavelength gas phase phenoxy and benzyl radical spectra.[2]

The phenol radical spectra show some similarity to the semiquinones.[5] However, the phenol radical cation is produced by ejection of a lone-pair electron from the hydroxyl group and is stabilized by interaction with the solvent; these results indicate that it is acidic in water with a pK_a near 13. On the other hand, the semiquinone negative ions are bases conjugate to the neutral semiquinone radicals. Since this dissociation does not involve the electron deficient group, the absorption spectra of the semiquinone ions and the neutral semiquinone radicals are probably closer to that of the phenoxy free radical than either is to the phenol radical cation. Porter and Strachan[6] have shown that side-chain bond fission is the predominant primary photochemical step in the photolysis of many aromatic molecules. Possible factors promoting electron-ejection are the occurrence of atoms with lone-pair electrons near the head of the side-chain and relatively small molecular size.

* Supported by the U. S. Atomic Energy Commission.

[1] G. Porter and E. Strachan, Spectrochim. Acta **12**, 299 (1958).
[2] G. Porter and F. J. Wright, Trans. Faraday Soc. **51**, 1469 (1955).
[3] L. I. Grossweiner, J. Chem. Phys. **24**, 1255 (1956).
[4] L. I. Grossweiner and W. A. Mulac, Radiation Research **10**, 515 (1959).
[5] N. K. Bridge and G. Porter, Proc. Roy. Soc. (London) **A244**, 259 (1958).
[6] G. Porter and E. Strachan, Trans. Faraday Soc. **54**, 1595 (1958).

Structure of Water

GEORGE W. BRADY AND W. J. ROMANOW

Bell Telephone Laboratories, Inc., Murray Hill, New Jersey

(Received September 21, 1959)

THE determination of the structure of water by x-ray diffraction was first made by Morgan and Warren.[1] Their results indicated that at room temperature there were ~4.6 nearest neighbors at a distance of 2.92 A, and they concluded that water possessed a quasi-tetrahedral structure in which H_2O molecule endeavored to surround itself with 4 neighbors. Recently, van Panthaleon van Eck, Mendel, and Boog,[2] using essentially the same technique as Morgan and Warren, have obtained different results which indicate that the nearest neighbor distance is 3.1 A. They do not give a figure for the number of nearest neighbors but instead use a density argument in conjunction with their measured spacing to postulate an octahedral structure for water. The structure of water is of great interest to us in our work on ionic solutions.[3] Accordingly, we decided to determine the radial distribution curve of water in an attempt to resolve the conflicting views.

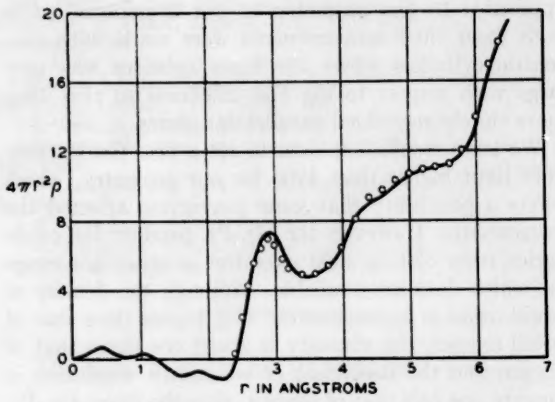

FIG. 1. Radial distribution curve for water at 28.0°C. Full line, our data; circles, data of Morgan and Warren.[1]

The technique of measurement has been described previously.[3] A large proportion of the scattering from H_2O at large angle is incoherent (because of the two H's) and the data in this range are consequently not as precise as we would wish. Accordingly, the distribution function was determined first by using only the data up to values of $s=6.5$ ($s=4\pi/\lambda \sin\theta$); then the data from $s=6.5$ to $s=10.0$ were added to this. There was no significant difference in results obtained with the two sets of data, except of course, the expected one, that the use of a larger range of s values produced a better peak resolution. This satisfied us that no spurious detail was introduced by inclusion of the large angle data.

In Fig. 1 our results are shown as the full line. The data of Morgan and Warren are plotted as circles. It is seen that there is nearly perfect agreement between the two curves. We do not agree at all with the results of van Panthaleon van Eck *et al.* The experimental details in their paper make mention of two facts which may have bearing on the discrepancy. First of all they quote their upper limits for s as 5–8. This is rather a short range on which to base their calculations, and is presumably the result of using only Cu$K\alpha$ radiation for their measurements. Secondly, they apply a temperature factor to the data, a procedure which really has little theoretical justification. It would have been easier to evaluate their data if they had determined a nearest neighbor number to support their contention of a hexagonal structure. We feel that their procedure of using a rigid model to interpret a density is not strictly valid in the liquid state.

It is, of course, a pleasure that our results agree so well with the pioneer work of Warren in this field, done in 1938 when instrumentation was not nearly as advanced as it is today.

[1] J. Morgan and B. E. Warren, J. Chem. Phys. **6**, 666 (1938).
[2] van Panthaleon van Eck, Mendel, and Boog, Discussions Faraday Soc. **24**, 200 (1957).
[3] G. W. Brady and J. T. Krause, J. Chem. Phys. **27**, 304 (1957): G. W. Brady, J. Chem. Phys. **28**, 464 (1958); J. Chem. Phys. **29**, 1371 (1958).

Isotope Exchange Processes in Solid Nitrogen under Electron Bombardment*

RALPH KLEIN† AND ERWIN M. HÖRL

National Bureau of Standards, Washington, D. C.

(Received September 24, 1959)

IT is well established that part of the glow from solid nitrogen irradiated with electrons involves atomic transitions.[1,2] Ground state ^4S atoms have been observed in irradiated solid nitrogen at 4.2 K with electron paramagnetic resonance and ^2D and ^2P atoms by their emission spectra. Additional information on some of the processes occurring in irradiated solid nitrogen can be obtained by a study of the isotope exchange in mixtures of $N^{14}N^{14}$—$N^{15}N^{15}$.

The investigations were carried out by means of a glass cryostat shown in Fig. 1. A known amount of the $N^{14}N^{14}$—$N^{15}N^{15}$ mixture was admitted to the central chamber by means of the gas inlet tubing and condensed on the glass surface (target) cooled by liquid helium or liquid hydrogen. The solid nitrogen layer was then irradiated with electrons of 15 or 20 kev for times up to 60 min. Electron beam currents between 5 and 10 μA were used. The electron gun was that of a slightly modified Steigerwald design. A fluorescent screen was mounted for checking the beam alignment and a wire screen cylinder inserted for avoiding charge effects on the glass walls. The beam could be centered on the target by observations of the green glow of the irradiated solid nitrogen.

After electron bombardment, the deposit was evaporated and the gas collected. Analyses were made with a Mass Spectrometer (Consolidated Model No. 21–620) to obtain the increase in $N^{14}N^{15}$ over that of the original sample. Blank runs showed that no exchange occurred in the absence of irradiation.

The experimental results were measured in terms of G values. These are shown in Table I. G is the yield per 100 ev in terms of the number of $N^{14}N^{15}$ molecules produced multiplied by a factor of two to account for recombination of like atoms if all the atoms produced recombined in a random manner. $G \leqq 10$ since $D(N-N) \approx 10$ ev.

TABLE I. Isotope exchange in solid nitrogen under electron bombardment.

Temp. °K	Time (min)	kv	μA	G	Diluent argon (%)
4.2	9.3	20	6	0.3	
4.2	30	20	4	0.2	
4.2	10	20	4	0.1	
4.2	60	20	4	0.2	
20	60	20	6	0.04	
4.2	45	15	6	0.06	90
4.2	30	15	6	0.03	50

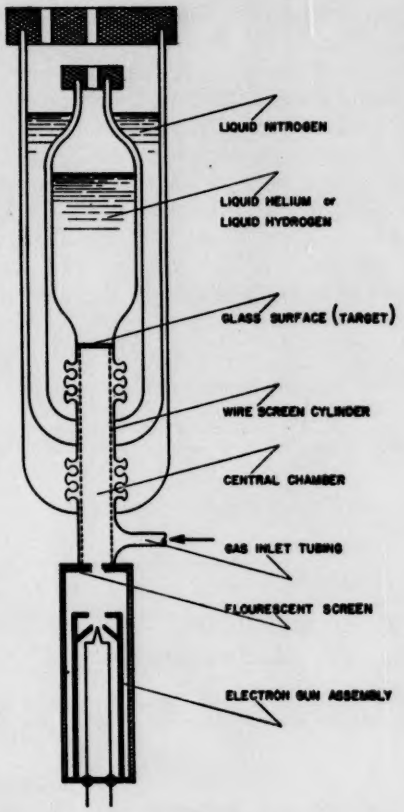

FIG. 1. Cryostat for electron bombardment of solid nitrogen.

The data show that the G value for the exchange process at 4.2 K is about 0.2. The value of 0.04 at 20°K is unexpected since the "cage" effect should be considerably less at the higher temperature. The detailed process by which exchange occurs is, at present, a matter of speculation. The primary processes causing the electron energy losses must involve electronic excitation and ionization of molecules. Energy loss measurements in gaseous nitrogen with 35-kev electrons[3] show as major losses 12.78, 14.01, 15.86, 8.5, and 17.40 ev in order of decreasing intensity. These losses can be interpreted on the basis of well-known electronic transitions of the N_2 molecule. Similar behavior may be expected with solid nitrogen. The excited molecular and ionic states may decay to lower ones or dissociate to atoms. Atom recombination can lead to isotope exchange. The reaction

$$N(^4S)+N_2(X^1\Sigma_g^+)\rightarrow N_2+N$$

cannot occur at low temperatures because of an activation energy requirement probably in excess of 0.5 ev. This does not exclude processes involving excited atoms such as

$$N(^2D)+N_2(X^1\Sigma_g^+)\rightarrow N_2+N.$$

Excited molecule-molecule, excited ion-molecule, or

ion-excited molecule reactions may also lead to exchange.

The lower G value at 20°K compared to 4.2°K appears to be reflected in the lower glow intensity. Both these facts might be explained qualitatively if a nonradiative transition for excited molecules is sufficiently temperature dependent. With added argon there is also a decrease in the G factor although the indicated difference between the 50 and 90% argon samples may not be experimentally significant. The possibility exists that energy transfer through the solid can occur by an exciton mechanism.

* This research was performed under the National Bureau of Standards Free Radicals Research Program, supported by the Department of the Army.

† Guest scientist, Olin Mathieson Chemical Corporation.

[1] C. M. Herzfeld and H. P. Broida, Phys. Rev. **101**, 606 (1956).
[2] Peyron, Hörl, Brown, and Broida, J. Chem. Phys. **30**, 1304 (1959).
[3] W. Dietrich, Z. Phys. **152**, 87 (1958).

Study of Rhombohedral V_2O_3 by Neutron Diffraction*

A. Paoletti, *Comitato Nazionale Ricerche Nucleari, Rome, Italy, and Brookhaven National Laboratory, Upton, New York*

AND

S. J. Pickart, *U. S. Naval Ordnance Laboratory, White Oak, Silver Spring, Maryland, and Brookhaven National Laboratory, Upton, New York*

(Received August 31, 1959)

NUMEROUS investigations have shown anomalies in the behavior of V_2O_3 at 168°K and in the region between 370 and 500°K. At 168°K the magnetic susceptibility has a maximum, and in the higher temperature region the susceptibility is independent of temperature.[1–3] V_2O_3 also shows at 168 and 533°K anomalies in the specific heat,[4,5] electrical conductivity, and thermal expansion.[6] From all these data, by analogy with $\alpha-Fe_2O_3$ and Cr_2O_3, it has been concluded that V_2O_3 has an antiferromagnetic spin arrangement at low temperatures with $T_N=168°K$[1,2,4,6,7]; some authors[2,7] also interpret the irregularities at 533°K as an antiferromagnetic transition.

A neutron diffraction investigation was undertaken to observe any antiferromagnetic spin arrangement and to obtain some knowledge of the oxygen parameter. Like $\alpha-Fe_2O_3$, V_2O_3 has the rhombohedral corundum structure (space group $R\bar{3}C$), with two parameters specifying the positions of the oxygen and vanadium atoms. Powder x-ray measurements[8] have shown the metal parameter to be 0.10 ± 0.01 but yield little information concerning the oxygen parameter. Because of the low scattering amplitude of vanadium for neutrons, the nuclear coherent scattering in the present case is almost entirely from oxygen and will be relatively insensitive to the metal parameter.

The sample, prepared by hydrogen reduction of V_2O_5 at red heat, contained 99% of the specified composition by analysis, and its x-ray powder pattern showed only the rhombohedral phase. Magnetic susceptibility measurements between 77°K and room temperature exhibited the anomaly near 170°K that was previously observed.[1,2]

The powder neutron diffraction patterns taken with a cylindrical sample at room temperature and 4.2°K are reproduced in Fig. 1. Analysis of the patterns at different temperatures shows that, first of all, the intensities observed at room temperature are in fair agreement with the calculated ones for an oxygen parameter of 0.30 ± 0.01, which is very close to that of $\alpha-Fe_2O_3$. Next, at 4.2°K the pattern shows a small new reflection at $2\theta=12°$ [displaced about 0.9° from the (111) position]. The half width of the (210) reflection increases by a factor of two, but without a change of the integrated intensity, and no superlattice reflections are observed. Finally, at 77°K the pattern was observed to be the same as at 4.2°K. The intensity of the peak at $2\theta=12°$ and the broadening of (210) remain the same.

Unless the V^{3+} moment is much smaller than the two Bohr magnetons indicated by the slope of the high-temperature susceptibility,[3] there is no evidence in these observations of an antiferromagnetic spin arrangement below 168°K. This follows because coherent magnetic reflections should be observable for any choice of the three possible sequences of spin sign along the rhombohedral axis: (a) (++−−), (b) (+−+−), or (c) (+−−+). For model (a) (found[9] in $\alpha-Fe_2O_3$), observable magnetic reflections should appear at the (111), (100), and (210) positions; for model (b) (found[10] in Cr_2O_3), at (110), (211), and (200); and for model (c) (not yet observed in an antiferromagnet), at (100), (221), and ($\bar{1}$11). If the extra peak appearing at 4.2°K were a (111) magnetic reflection, there should be a (100) reflection with at least half the intensity, no matter what the inclination of the spin axis (assumed single) relative to [111]. Comparison of the observable limit of the data with the magnetic structure factors indicates that any ordered moment must be less than one-half Bohr magneton per V^{3+} ion.

While it is thus difficult to explain the data on the basis of an antiferromagnetic transition at 168°K, the changes in the neutron diffraction pattern can be accounted for by a structural transition. Prior evidence of such a transition has been found by a low-temperature x-ray study.[11] The absence of any scattering from the vanadium atoms makes identification of this new crystal phase from the neutron data extremely difficult.

It may be pointed out that also in Ti_2O_3 powder neutron diffraction measurements[12] show no evidence of the antiferromagnetism suggested by susceptibility and lattice parameter data.[13] These apparent inconsistencies between different experimental approaches to the problem might conceivably be reconciled by

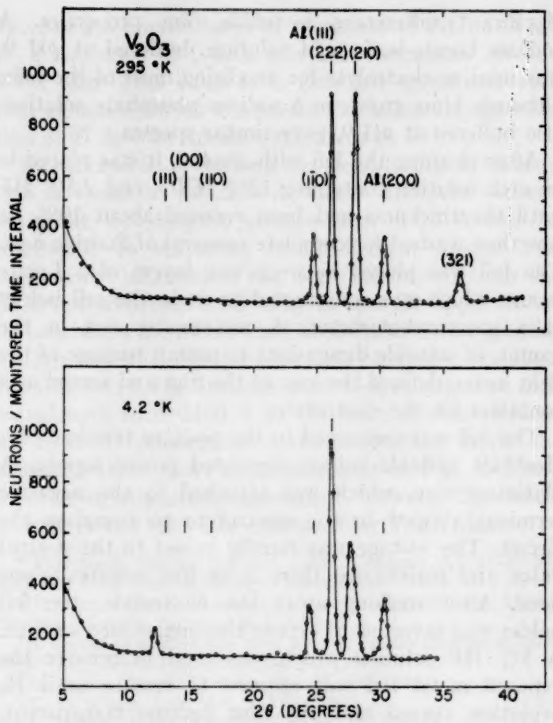

FIG. 1. Neutron diffraction patterns obtained from a cylindrical V_2O_3 powder sample enclosed in an aluminum cryostat. Data were taken at room temperature and 4.2°K.

assuming changes in the effective moment of the ions upon ordering, or by a state of short range order in the arrangement of the antiferromagnetically coupled spins. With regard to the first alternative, a careful measurement of the small angle scattering at room temperature and at 4.2°K, above and below the supposed Néel temperature, shows no decrease attributable to the disappearance of a paramagnetic diffuse scattering.

The authors are indebted to Dr. T. R. McGuire for making the susceptibility measurements.

* Work carried out under the auspices of the U. S. Atomic Energy Commission and the National Security Agency.

[1] E. Hoschek and W. Klemm, Z. anorg. u. allgem. Chem. **242**, 63 (1939).
[2] J. Wucher, J. Recherches centre natl. recherche sci. Labs Bellevue (Paris) **21**, 254 (1952).
[3] S. Teranishi and K. Tarawa, J. Chem. Phys. **27**, 1217 (1957).
[4] J. Jaffray and R. Lyand, J. Recherches centre natl. recherche sci. Labs Bellevue (Paris) **21**, 249 (1952).
[5] C. T. Anderson, J. Amer. Chem. Soc. **58**, 564 (1936).
[6] M. Foex, J. Recherches centre natl. recherche sci. Labs Bellevue (Paris) **21**, 238 (1952).
[7] T. Morin, Bell System Tech. J. **37**, 1047 (1958); Nagamiya, Yosida, and Kubo, Advances in Physics (Taylor and Francis, London, England, 1955), Vol. 4, p. 1.
[8] W. Zachariasen, Skrifter Norske Videnskaps-Akad. Oslo I. Mat. Naturv. Kl. No. 4, **1928**.
[9] Shull, Strauser, and Wollan, Phys. Rev. **83**, 333 (1951).
[10] B. N. Brockhouse, J. Chem. Phys. **21**, 961 (1953).
[11] S. Goldsztaub and R. Wey, J. Recherches centre natl. recherche sci. Labs Bellevue (Paris) **21**, 247 (1952).
[12] G. Shirane and S. J. Pickart (to be published).
[13] A. D. Pearson, J. Phys. Chem. Solids **5**, 316 (1958).

Possible Symptom of the Jahn-Teller Effect in the Negative Ions of Coronene and Triphenylene*

M. G. TOWNSEND AND S. I. WEISSMAN
Washington University, St. Louis, Missouri

(Received September 28, 1959)

THE electron spin resonance absorption lines of the anions of coronene and triphenylene are broader than those of the anions of most other aromatic hydrocarbons. While spectra of typical anions may have of the order of one hundred resolved lines in a span of twenty or thirty oersteds, the thirteen evenly spaced lines of coronene negative ion are but poorly resolved. Representative spectra are shown in the accompanying figure.

The anions were produced by reduction with either lithium, sodium, or potassium. Measurements were made at various concentrations, including the lowest ones at which any signal was discernible. Temperature was varied between 210 and 300°K. Modulation amplitude, microwave power level, and field homogeneity for the measurement of the spectra of coronene and triphenylene negative ions were identical to those which produced narrow lines from other ions. Under no conditions could narrower lines than those displayed in the figure be achieved.

Saturation measurements revealed that the spin lattice relaxation time in the most dilute solution of coronene ion is shorter than in biphenyl negative ion. Increase of the microwave power by a factor of ten produced a threefold decrease in signal for the latter, but only a fifteen percent decrease for the former.

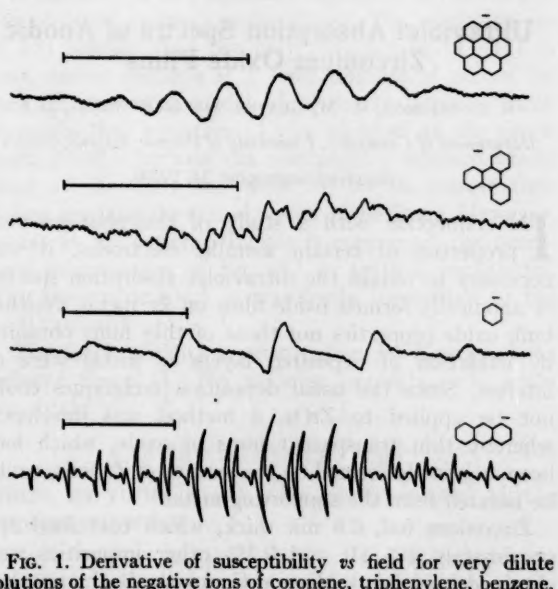

FIG. 1. Derivative of susceptibility *vs* field for very dilute solutions of the negative ions of coronene, triphenylene, benzene, and anthracene.

We suggest that the unusually broad lines of the coronene and triphenylene ions may be associated with Jahn-Teller distortions. The normal states of these ions would be orbitally degenerate if the full symmetries of the parent molecules were retained. While we have been unable to make any estimate worth mentioning of the contributions of Jahn-Teller distortions it is conceivable that they could provide a path for relaxation. As the free radical molecule carries out the complex motions associated with the Jahn-Teller distortion[1,2] the electronic distribution varies. The variations in electronic distribution modulate the hyperfine interactions and may thereby produce relaxation.

We should note that the lines in benzene negative ion are also broader than those of most aromatic negative ions, and it is possible that here also the Jahn-Teller effect contributes to the line breadth. However, solutions of benzene negative ion necessarily contain unreduced benzene and we have not yet determined the contribution to the line breadth of the exchange reaction between the ion and the parent molecule. The latter effect was eliminated with coronene and triphenylene through complete reduction.

* This work has been supported by the U. S. Air Force through the Air Force Office of Scientific Research and Development Command under Contract AP 49-638-464. Reproduction in whole or in part is permitted for any purpose of the U. S. Government.

[1] W. Moffitt and A. Liehr, Phys. Rev. **106**, 1195 (1957).

[2] Longuet-Higgins, Öpik, Pryce, and Sack, Proc. Roy. Soc. (London) **A244**, 1 (1958).

Uitraviolet Absorption Spectra of Anodic Zirconium Oxide Films*

R. E. Salomon, W. M. Graven, and G. B. Adams, Jr.†

Department of Chemistry, University of Oregon, Eugene, Oregon

(Received September 24, 1959)

In connection with a study of the photogalvanic properties of certain metallic electrodes, it was necessary to obtain the ultraviolet absorption spectra of anodically formed oxide films on Zr metal. Neither bulk oxide properties nor those of thin films obtained by oxidation of deposited layers of metal were of interest. Since the usual deposition techniques could not be applied to ZrO_2, a method was developed whereby thin transparent films of oxide, which had been anodically formed on the surface of Zr foils, could be isolated from the supporting metal.[1]

Zirconium foil, 0.8 mil thick, which contained approximately 2% Hf and 0.2% other impurities was obtained from Foote Mineral Company. Both annealed and unannealed foils were used without observing significant differences in oxide film properties. A sodium borate-boric acid solution, buffered at *p*H 9, was used as electrolyte for anodizing most of the foils, although films grown in a sodium phosphate solution, also buffered at *p*H 9, gave similar spectra.

After cleaning the foil with alcohol, it was placed in an etch solution containing 12% HNO_3 and 2.5% HF until the thickness had been reduced about 10%. It was then washed for complete removal of fluoride ions. The foil was placed between two layers of a Lucite mount which was constructed to fit in the cell holder of a spectrophotometer. A rectangular slot in the mount, of suitable dimensions to permit passage of the light beam, defined the area of the film and served as a container for the electrolyte.

The foil was connected to the positive terminal of a Heathkit variable voltage regulated power supply. A platinum wire, which was attached to the negative terminal, dipped in the electrolyte to complete the circuit. The voltage was rapidly raised to the desired value and maintained there from five minutes to one hour. After washing away the electrolyte, the foil holder was inverted to expose the unanodized surface. A 1% HF solution which was used to remove the exposed metal foil was allowed to remain until H_2 evolution ceased and the film became transparent, after which the film was thoroughly washed.

The dry films had a corrugated appearance and exhibited characteristic interference colors, although each appeared to be completely transparent when viewed perpendicularly to the surface. Numerous films were produced with formation voltages ranging from 30 to 200 v. Absorbance measurements were made with a Cary, Model 11, recording spectrophotometer.

The absorption spectrum of a typical film which was obtained with a 150-v formation voltage is shown in Fig. 1. Interference produces the pattern of alternating maxima and minima, the separation of which may be used to obtain the film thickness. Using Young's

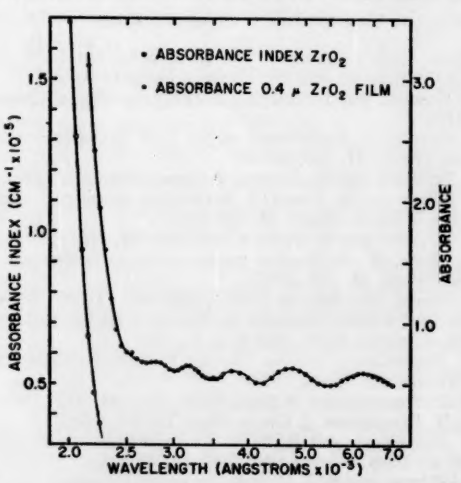

Fig. 1. Absorption spectra of thin zirconium oxide films.

value of 2.4 for the index of refraction of ZrO_2 at 3000 A[2] a thickness of 0.405μ has been computed for the 150-v film. This value is in excellent agreement with that calculated from a reported thickness-voltage relation of 27 A/v for anodic oxide films on Zr.[3]

By extrapolation the long wavelength limit of absorption is found to be 2500 A, since "apparent" absorbance at wavelengths greater than 3000 A can be attributed to scattering and reflection losses. This "apparent" absorbance has been subtracted from the observed absorbances in order to test the applicability of Lambert's law. Corrected absorbances were plotted against film thickness for nine films ranging in thickness from 0.08 to 0.5 μ. Straight lines were obtained at each wavelength from 2400 A to the limit of measurement at 2000 A. Absorbance indices obtained from the slopes of these plots are also shown in Fig. 1. There is order-of-magnitude agreement between the result at 2000 A and the value estimated for Ta_2O_5 films.[4]

* This work was carried out under Contract AT(45-1)-535 with the U. S. Atomic Energy Commission.

† Present address: Lockheed Aircraft Corporation, Missile Systems Division, Sunnyvale, California.

[1] A similar procedure has been used to obtain aluminum oxide films. See: Chem. Eng. News **36**, 141 (1958).
[2] L. Young, Trans. Faraday Soc. **55**, 632 (1959).
[3] R. D. Misch, Acta Met. **5**, 179 (1957).
[4] L. Young, Trans. Faraday Soc. **50**, 153 (1954).

Generalization of the Laminar Flame Action Principle for Arrhenius-Type Rate Functions*

GERALD ROSEN†
Guggenheim Jet Propulsion Center, Princeton, New Jersey

(Received July 7, 1959)

IN a previous paper[1] the author set up a variational principle which could be used to obtain reliable estimates of the burning velocity and temperature distribution for a laminar flame. The previous work was partially in support of the investigations of Spalding[2] and retained a tacit assumption made by Spalding, namely, that the reaction rate expression vanishes at the cold boundary, $\Phi(0)=0$. The work which follows generalizes the variational principle for reaction rate expressions with $\Phi(0)\neq 0$. Our results apply to any physically interesting rate function, in particular the Arrhenius-type, without ever evoking a somewhat questionable "cutoff" procedure.

The basic system for the laminar flame,[1]

$$(d^2\tau/d\xi^2)+(\lambda\Phi(\tau)/\xi^2)=0, \tag{1}$$

$$\tau(0)=0, \qquad \tau(\infty)=1, \tag{2}$$

admits equivalent solutions if ξ is replaced everywhere by $C\xi$, with C a positive constant. Since the physics gives $(d\tau/d\xi)_{\xi=0}\neq 0$, the scale of any solution is conveniently fixed by requiring $(d\tau/d\xi)_{\xi=0}=1$.

Once again we consider the functional (I−14)‡

$$\Lambda=\Lambda[\tau]\equiv\frac{\int_0^\infty \tfrac{1}{2}(d\tau/d\xi)^2 d\xi}{\int_0^\infty V d\xi} \tag{3}$$

but with (I−15) generalized to read

$$V=(1/\xi^2)\int_0^\tau \Phi(\tau)d\tau-(1/\xi)\Phi(0). \tag{4}$$

Then the action principle asserts:

The dimensionless temperature distribution $\tau(\xi)$ must be such that the functional (3) assumes its smallest possible value; this number is the eigenvalue proportional to the inverse square of the burning velocity. Admissible $\tau(\xi)$'s are continuously differentiable and satisfy the boundary conditions (2) and the scale condition $(d\tau/d\xi)_{\xi=0}=1$.

Proof: First notice that for any admissible $\tau(\xi)$

$$(1/\xi)\int_0^\tau \Phi(\tau)d\tau=\Phi(0)+0(\xi^\epsilon) \tag{5}$$

with $\epsilon>0$, for as $\xi\to 0$ the left side of (5) defines a derivative. Substituting (5) into (4), we find $V=0(\xi^{-1+\epsilon})$, which is sufficient to guarantee the existence of the denominator in (3), if taken with the normalization (I−13). Finally observe that under a variation of $\tau(\xi)$ to a neighboring member of the class of admissible functions, the change induced in (3) is still given by (I−17), since the new term in (4) does not involve $\tau(\xi)$. Consequently, Eq. (1) follows from $\delta\Lambda=0$ with $\Lambda=\lambda$, the unique eigenvalue.

A subtlety in this standard argument is relevant to the physical problem under study. The minimization of (3) implies that the curly bracket in (I−17) is zero, except perhaps at a *finite* number of points. In fact, the physical model of a steady laminar flame demands that equation (1) be violated at the single point $\xi=0$; otherwise the combustible mixture would react at the finite rate $\Phi(0)\neq 0$ for an infinite time before reaching the actual region of the flame. However, as far as the action principle is concerned, the necessary modification of Eq. (1) at $\xi=0$ is immaterial. The eigenvalue $\lambda=\Lambda$ is manifestly insensitive to the $\xi=0$ "cutoff."

The Rayleigh-Ritz approximation for λ proceeds as before.[1] Since (I−26) satisfies $(d\tau/d\xi)_{\xi=0}=1$, again we obtain

$$\lambda=\tfrac{1}{6}+\tfrac{1}{3}[(1-q+q^2)^{\frac{1}{2}}-q] \tag{6}$$

where, by virtue of (4), (I−28) is replaced by the stronger expression

$$q\equiv\int_1^\infty\left\{\int_0^{1/\eta}(\Phi(\tau)-\Phi(0))d\tau\right\}d\eta. \tag{7}$$

The solution is completed with the formula for the burning velocity[2]

$$S_u=(1/\rho_u)\left[\frac{1}{H\lambda}\int_{T_u}^{T_b}k(T)f(T)dT\right]^{\frac{1}{2}} \qquad (8)$$

in which $f(T)$ is the volumetric production of the product species. It should be remarked that this method of calculating the eigenvalue burning velocity transcends the *centroid rule*,[2] inasmuch as the Klein iteration procedure breaks down if $\Phi(0)\neq 0$, and if the derivative of $\Phi(\tau)$ at $\tau=0$ is not less than a certain bound.

* This work was sponsored by Project SQUID which is supported by the Office of Naval Research, Department of the Navy, under contract Nonr 1858(25) NR-098-038.

† Research Associate, Department of Aeronautical Engineering, Princeton University. Present address, Institutet För Teoretisk Fysik, Vanadisvägen 9, Stockholm Sweden.

[1] G. Rosen, *Symposium on Combustion*, 7th Symposium, London, 1958, pp. 339, 412.

[2] D. B. Spalding, Combustion and Flame **1**, 287 (1957).

‡ Equation numbers preceded by a **I** refer to the previous work.[1]

Isotope Effects in the Chromic Acid Oxidation of Benzyl-α-*t* Alcohol*

ERNEST M. HODNETT† AND LOUIS KAPLAN

Argonne National Laboratory, Lemont, Illinois

(Received September 21, 1959)

THE observation of large deuterium[1] and tritium[2] isotope effects in the oxidation of 2-propanol by aqueous chromic acid has demonstrated that fission of the carbon-hydrogen bond of the alcohol occurs in the rate-determining step of the oxidation. The mechanism of the oxidation of primary alcohols by chromic acid might differ from that suggested for secondary alcohols. This communication presents the results of a study of the isotope effect in the oxidation of benzyl alcohol labeled with tritium on the methylene carbon atom.

Benzyl-α-*t* alcohol was prepared by reduction of benzaldehyde with lithium aluminum hydride-*t*, and freed from benzaldehyde by washing its solution in benzene with sodium bisulfite. The distilled product contained less than 0.05 mole percent of aldehyde. The benzoic acid obtained by oxidation with alkaline permanganate was tritium-free.

Aqueous solutions 0.025 *M* in the alcohol, 0.3 *M* in perchloric acid, and containing varying amounts of potassium dichromate were maintained at 37.5° in a nitrogen atmosphere until the chromium (VI) was completely reduced. Aliquots were assayed for unreacted benzyl alcohol by phthalation, for benzaldehyde by precipitation of the 2,4-dinitrophenylhydrazone, and for benzoic acid by extraction and titration. Benzyl alcohol and benzaldehyde were assayed[4] for tritium as the 3,5-dinitrobenzoate and as the 2,4-dinitrophenylhydrazone, respectively. (Under the conditions used, benzaldehyde was the principal product of the oxidation. Benzoic acid was formed to the extent of less than one percent at 50% oxidation, increasing to about 8% at 82% reaction.)

TABLE I. Chromic acid oxidation of benzyl-α-*t* alcohol in 0.3 *M* $HClO_4$.

Alcohol Oxidized, %	Specific activity, μc/mmole		$\frac{k_{PhCHTOH}}{k_{PhCH_2OH}}$	$\frac{N_{Ald}^0}{N_{Alc}^0}$
	Alcohol	Aldehyde		
0	10.66			
5.6	10.76	6.18		0.581
10.7	10.89	6.24		0.583
49.0	13.09	6.79	0.681	
51.0	13.09	6.79	0.698	
64.8	14.48	7.19	0.698	
79.6	17.51	7.65	0.681	
		Mean	0.69	0.58

The results, summarized in Table I, indicate that the tritiated alcohol is oxidized more slowly than the normal compound. The ratio of the rate constants is calculated from the equation[5]

$$k_{PhCHTOH}/k_{PhCH_2OH}=1+\log(N_A/N_A^0)/\log(A/A_0),$$

where N_A and N_A^0 represent the specific activities of the residual and initial alcohol, respectively, and A/A_0 is the fraction of the alcohol remaining unoxidized. The average value of this ratio, 0.69, agrees reasonably well with a less certain value of 0.66 calculated[6] from the increase in specific activity of the aldehyde. If all of the alcohol is assumed to be oxidized by a single process, represented by the equations

$$C_6H_5CH_2OH+[O]\xrightarrow{2k_1}C_6H_5CHO,$$

$$C_6H_5CHTOH+[O]\xrightarrow{k_2,\ k_3}C_6H_5CTO,$$

then $k_{PhCHTOH}/k_{PhCH_2OH}=(k_3+k_2)/2k_1$. For such a case, the value of k_3/k_1, the secondary isotope effect, can be shown[7] to be equal to $2N_{Ald}^0/N_{Alc}^0$ where N_{Ald}^0 and N_{Alc}^0 are the molar activities of the aldehyde and of the alcohol at infinitesimal extent of reaction. Combining the value $k_3/k_1=1.16$ with $(k_3+k_2)/2k_1=0.69$ leads to a value of the intermolecular isotope effect $k_2/k_1=0.22$, and of the intramolecular isotope effect $k_2/k_3=0.19$.

The observed value of the secondary isotope effect, $k_3/k_1=1.16$, is somewhat surprising. There is no obvious reason why a protium atom should be removed 16% more rapidly from a molecule of the tritiated alcohol than from the normal alcohol, although

somewhat similar results have been reported for some other reactions.[7] (The high value of N_{A1d}^0/N_{A1e}^0 cannot be attributed to tritium enrichment of the aldehyde by further oxidation, since the amount of benzoic acid formed in the early stages of the oxidation is too small to affect the results significantly.)

There is a possible alternative explanation for a value of N_{A1d}^0/N_{A1e}^0 greater than one-half which does not require that k_2/k_1 be greater than unity. If some process occurred without C—H bond rupture in the rate-determining step, there would be little or no difference in reaction rate between $PhCH_2OH$ and PhCHTOH, but there might still be a large intramolecular isotope effect (k_T/k_H) for a molecule of PhCHTOH in a subsequent fast step. For such a process, N_{A1d}^0/N_{A1e}^0 would be equal to $1/(1+k_T/k_H)$ with a value between 0.5 and 1. If 23% of the alcohol were oxidized by a process with no intermolecular isotope effect and an intramolecular isotope effect, k_T/k_H, of 0.19, and the balance of the alcohol were oxidized by a process with an intermolecular isotope effect k_2/k_1 and an intramolecular isotope effect k_2/k_3 both equal to 0.19, the calculated values of "$k_{PhCHTOH}/k_{PhCH_2OH}$" and of N_{A1d}^0/N_{A1e}^0 would be 0.69 and 0.58, respectively, as observed.

* Based on work performed under the auspices of the U. S. Atomic Energy Commission. Presented at the 125th meeting of the American Chemical Society, Kansas City, Missouri, April, 1954.

† Present address: Department of Chemistry, Oklahoma State University, Stillwater, Oklahoma.

[1] F. H. Westheimer and N. Nicolaides, J. Am. Chem. Soc. **71**, 25 (1949).
[2] L. Kaplan, J. Am. Chem. Soc. **77**, 5469 (1955).
[3] F. H. Westheimer, Chem. Revs. **45**, 419 (1949) and later papers.
[4] Wilzbach, Kaplan, and Brown, Science **118**, 522 (1953).
[5] L. Kaplan, J. Am. Chem. Soc. **76**, 4645 (1954).
[6] J. Bigeleisen, Science **110**, 14 (1949).
[7] D. W. Coillet and G. M. Harris, J. Am. Chem. Soc. **75**, 1486 (1953); G. M. Harris, J. Phys. Chem. **56**, 891 (1952).

Note on the Infrared Dichroism of Axially Oriented Polymers

S. KRIMM

Harrison M. Randall Laboratory of Physics, University of Michigan, Ann Arbor, Michigan

(Received August 24, 1959)

IT has been pointed out[1] that, in cases where it is permissible[2] to consider a polymer as being constituted of a fraction f of chains aligned exactly parallel to the fiber axis, the remainder, $1-f$, being completely randomly oriented, it is possible to place significant limits on the angle θ which a transition moment makes with the molecular chain axis. This does not depend upon prior knowledge of f or of $R_0=2\cot^2\theta$, the dichroic ratio of a perfectly aligned set of chains. It may be of interest to note that in certain special cases, which are, however, of frequent occurrence in polymers, the angle θ can be uniquely determined, and therefore also the quantity f. This occurs under certain circumstances when two transition moments associated with a portion of the molecule are perpendicular to each other, such as those of $\nu_s(CH_2)$ and $\nu_a(CH_2)$, and the amide I and amide V bands of the peptide group.[3]

Suppose that two transition moments $\mathbf{M}_1$ and $\mathbf{M}_2$ are perpendicular to each other, $\mathbf{M}_1$ making an angle of θ_1 with the molecular chain axis. If $\mathbf{M}_2$ makes an angle ω with the plane defined by $\mathbf{M}_1$ and the chain axis, then the angle between $\mathbf{M}_2$ and the chain axis is given by $\cos\theta_2=\cos\omega\sin\theta_1$. Thus, if

$$R_{01}=2\cot^2\theta_1, \tag{1}$$

then

$$R_{02}=4\cos^2\omega/(R_{01}+2\sin^2\omega). \tag{2}$$

By using the relationship[4]

$$f=[(R-1)(R_0+2)]/[(R_0-1)(R+2)], \tag{3}$$

where R is the observed dichroic ratio, and equating the right hand side of Eq. (3) for the two bands, we find that

$$\cot^2\theta_1=\{[A-B(1-3\cos^2\omega)]/2A+B\}, \tag{4}$$

where

$$A=(R_1+2)(R_2-1),$$
$$B=(R_2+2)(R_1-1). \tag{5}$$

Since A and B are experimentally determined quantities, θ_1 can be obtained if ω is known (except for the case $\omega=\pi/4$).

Two interesting special cases of Eq. (4) are often found in polymers, viz., $\omega=0$ and $\omega=\pi/2$. These correspond to $\mathbf{M}_2$ being in the plane formed by $\mathbf{M}_1$ and the chain axis direction, and $\mathbf{M}_2$ perpendicular to this plane, respectively. For these cases

$$\cot^2\theta_1=(A+2B)/(2A+B), \quad \text{for } \omega=0, \tag{6}$$

$$\cot^2\theta_1=(A-B)/(2A+B), \quad \text{for } \omega=\pi/2. \tag{7}$$

Thus, no assumptions as to the chain orientation distribution or fraction of disordered material are required. In fact, after θ_1 is determined f can be found from Eq. (3), and using this f the θ values for other modes can immediately be obtained from the observed dichroic ratios of their bands. It is pertinent to note that observations on three mutually perpendicular moments will not permit determination of ω in general, since in this case R_{03} is not independent of R_{01} and R_{02}.

[1] R. D. B. Fraser, J. Chem. Phys. **29**, 1428 (1958).
[2] M. Beer, Proc. Roy. Soc. (London) **A236**, 136 (1956).
[3] Miyazawa, Shimanouchi, and Mizushima, J. Chem. Phys. **24**, 408 (1956).
[4] R. D. B. Fraser, J. Chem. Phys. **24**, 89 (1956).

N^{14} Pure Quadrupole Resonances of Acetonitrile and Hydrocyanic Acid*

HISAO NEGITA, P. A. CASABELLA, AND P. J. BRAY

Department of Physics, Brown University, Providence, Rhode Island

(Received September 14, 1959)

THE N^{14} pure quadrupole resonances of solid acetonitrile CH_3CN were reported previously.[1] However a different set of resonances has been found in this compound, at the same temperature, in a sample which was frozen more quickly than the sample used in the previous experiments. In addition the resonances of hydrocyanic acid HCN have been observed at both dry ice and liquid nitrogen temperatures. The results are in good agreement with those of x-ray analysis,[2] which show that the crystal form changes at 170.37°K.[3]

The pure quadrupole resonances of N^{14} which has a spin of unity occur at

$$\nu_1=(3+\eta)eQq/4,$$
$$\nu_2=(3-\eta)eQq/4, \qquad (1)$$

where η is the electric field gradient asymmetry parameter, and eQq is the quadrupole coupling constant. From these equations η can be calculated as precisely as the frequency itself for a polycrystalline sample. On this point, nitrogen has an obvious advantage over chlorine or bromine for which a single crystal must be used in a Zeeman splitting experiment in order to determine η.

N^{14} pure quadrupole resonances have been found in the two compounds mentioned above, using a Pound-Watkins type spectrometer.[4] Their frequencies were measured with a BC–221 frequency meter. The samples of acetonitrile and hydrocyanic acid were provided by Eastman Kodak Company and Eltex Chemical Corporation, respectively.

Table I shows the results for acetonitrile. The α form was obtained by hanging the sample above the surface of liquid nitrogen for about thirty minutes to an hour and then lowering it into the liquid nitrogen. The β form, on the other hand, was obtained by immersing the sample in liquid nitrogen directly with no pre-cooling. The data for the α form were reported previously, but they were checked again and are listed for comparison. According to the cooling procedures, the samples of α form should be more stable at lower temperature.

TABLE I. N^{14} pure quadrupole resonances of acetonitrile at 77°K.

	α form	β form
ν_1 (Mcps)	2.8078±0.0002	2.8108±0.0002
ν_2 (Mcps)	2.7992±0.0002	2.7954±0.0002
eQq (Mcps)	3.7380±0.0003	3.7375±0.0003
η (%)	0.46±0.02	0.82±0.02

TABLE II. N^{14} pure quadrupole resonances of hydrocyanic acid.

	77°K	195°K
ν_1 (Mcps)	3.0223±0.0002	2.9178±0.0002
ν_2 (Mcps)	3.0052±0.0002	
eQq (Mcps)	4.0183±0.0003	3.8904±0.0003
η (%)	0.85±0.02	0

As seen from the table, the coupling constants of both forms are almost the same, while the asymmetry parameter of the β form is about twice as large as that of the α form. This may be caused by a slight change of molecular arrangement from the α to the β form. However, no further information about the crystal structures can be obtained from these data.

The intensity of the absorption line is much stronger, and the line width is much narrower in the β form. The latter effect may be caused partly by the larger asymmetry parameter of the β form, as predicted by the previous paper.[1]

Table II shows the results for hydrocyanic acid. There is a pair of resonances at 77°K but only one at 195°K. The latter resonance is as strong as that of hexamethylenetetramine, although the former are very weak.

According to the x-ray analysis of this compound, it crystallizes in tetragonal form above the transition point 170.37°K. The unit cell of dimensions $a=b=4.63$ A, $c=4.34$ A contains two molecules. Below the transition point the crystal changes to orthorhombic form with unit cell dimensions of $a=4.13$ A, $b=4.35$ A, and $c=4.34$ A. In both cases the linear molecules of hydrocyanic acid are oriented in the same direction as the c axis. Thus, in the high-temperature form, the electric field gradient at the nitrogen nucleus is symmetric about the molecular axis, and the asymmetry parameter η becomes zero which results in only one resonance. In the low-temperature form, however, this is not the case.

The coupling constants of both acetonitrile and hydrocyanic acid are known for the gaseous state from microwave spectroscopy.[5,6] These data are listed in Table III in comparison with the solid data. The coupling constants of acetonitrile are lower than those of hydrocyanic acid in both states. This fact may be attributed to the contribution of the structure $^+HCH_2{=}C{=}N^-$ by hyperconjugation[7] in acetonitrile. The

TABLE III. Comparison of the coupling constants in gaseous and solid states.

Compound	Gas	Solid (77°K)	Solid/Gas
Acetonitrile	4.35 Mcps	3.738 Mcps	85.9%
Hydrocyanic acid	4.58	4.108	89.7

coupling constant of ethyl cyanide[1] C_2H_5CN, in which hyperconjugation is less effective than acetonitrile is 3.7756 Mcps at 77°K. This value is a little higher than that of acetonitrile but still much lower than that of hydrocyanic acid.

The authors wish to thank Mr. H. O. Hooper for his suggestions in the course of this work.

* Research supported by a grant from the National Science Foundation.

[1] P. A. Casabella and P. J. Bray, J. Chem. Phys. **29**, 1105 (1958).
[2] W. G. Dulmage and W. N. Lipscomb, Acta Cryst. **4**, 330 (1951).
[3] W. F. Giauque and R. A. Ruehrwein, J. Am. Chem. Soc. **61**, 2626 (1939).
[4] G. D. Watkins, thesis, Harvard University (1952).
[5] Kesslar, Ring, Trambarulo, and Gordy, Phys. Rev. **79**, 54 (1950).
[6] Simmons, Anderson, and Gordy, Phys. Rev. **77**, 77 (1950).
[7] J. W. Baker, *Hyperconjugation* (Oxford University Press, New York, 1952), p. 27.

Measurement of Dipole Moments at Microwave Frequencies*

JAMES E. BOGGS AND A. P. DEAM

Department of Chemistry and Electrical Engineering Research Laboratory, The University of Texas, Austin 12, Texas

(Received September 8, 1959)

THE ease and accuracy with which the dielectric constant of a gas can be measured using resonant cavity techniques in the microwave region suggest that such methods would be ideally suited to the determination of the dipole moments of gases. Such determinations have been made by Magnuson[1] for 1,2-dichlorotetrafluoroethane, 2,2,3-trichloroheptafluorobutane, and chlorine trifluoride.

In order to calculate the dipole moment, the static or low-frequency value of the dielectric constant is needed. It has been shown[2–5] that for many gases the dielectric constant varies with frequency in the microwave region so that the static value is often not determined directly. The dispersion, when it occurs, is always of the nonresonant type, the dielectric constant falling below the static value. The dispersion curve is fitted approximately by the Debye equation, but more exactly by the Cole-Cole equation which makes allowance for a distribution of line-broadening constants.[5]

Asymmetric top molecules with *a*- or *c*-type selection rules can undergo transitions between the asymmetry doublet levels which in many cases are nearly degenerate and therefore occur at nearly zero frequency.[6] The effect of such transitions, broadened by pressure, accounts for the nonresonant dispersion observed in such molecules. Symmetric-top molecules also show nonresonant dispersion which has been attributed either to transitions between levels which are symmetric and antisymmetric with respect to inversion[5,6] or to an "Umklapp effect" on collision.[7] Linear molecules and asymmetric top molecules with *b*-type selection rules present no difficulties.

It would be expected that the three substances for which Magnuson has determined the value of the dipole moment would exhibit dispersion. At 9300 Mc, the dielectric constant should be below the static value and the calculated dipole moment should be below the true value. We have measured the dielectric constant of 1,2-dichlorotetrafluoroethane at 400 Mc and 40.0° over a range of pressures. From these measurements the parameters in the dielectric dispersion curve can be obtained as discussed previously.[5]

The apparatus and method used were the same as previously described.[5] The 1,2-dichlorotetrafluoroethane, obtained from The Matheson Company, was analyzed mass spectrometrically and found to be free of significant quantities of any impurity except for traces of the asymmetrical isomer. Since this was the same material used by Magnuson, it was not purified further.

As accurate low-pressure nonideality corrections for 1,2-dichlorotetrafluoroethane are not available, Magnuson used a value determined from his measurements to make the molar polarization independent of pressure. From the data presented below it can be shown that the molar polarization should not be completely independent of pressure even at Magnuson's measuring frequency of 9300 Mc, the molar polarization rising by 0.14 cc above the zero-pressure value at a pressure of 1500 mm. Thus it would appear that the nonideality correction used by Magnuson was too large. For the present experiments, the molar volume was taken as $RT/p-0.66$ liters, the correction term being obtained by correcting Magnuson's value (which would be 0.713) for the expected dispersion at his measuring frequency.

The results obtained are shown in Fig. 1. The solid line is a plot of the Debye equation $(P-P_\infty)/(P_0-P_\infty)=1/[1+(p_M/p)^2]$, where P_0 is the molar polarization at

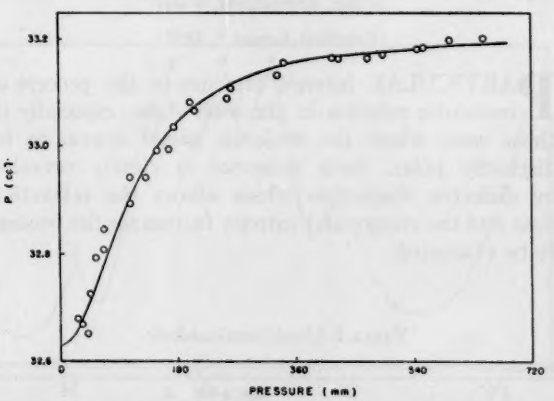

FIG. 1. The molar polarization of 1,2-dichlorotetrafluoroethane as a function of pressure, measured at 402 Mc and 40.0°.

low frequency (or at high pressure), P_∞ is the molar polarization at frequencies above the dispersive region (or at low pressure), and p_M is the pressure at the midpoint of the dispersion curve. The curve is plotted for the values $P_0=33.21$ cc, $P_\infty=32.63$ cc, and $p_M=114$ mm. This corresponds to a line-broadening constant of 3.5 Mc/mm. No attempt has been made to evaluate the Cole-Cole parameter since the accuracy of the data when the entire dispersion covers a range of only 0.58 cc is inadequate.

Our low-pressure value of 32.63 cc means that the molar polarization measured at 9300 Mc should range from 32.63 to 32.77 cc as the pressure is varied between zero and 1500 mm. Magnuson's value[1] of 32.97 cc is somewhat higher than this, but the difference is within the experimental error in the absolute value. Magnuson obtained a value of the distortion polarization of 27.45 cc. If we assume that his value for the total polarization should have been higher by about 0.58 cc, the dipole moment of 1,2-dichlorotetrafluoroethane becomes 0.56 rather than the 0.53 reported by Magnuson. For other gases the error caused by ignoring the dispersion can be very much greater.

* This work has been supported by Air Force Contract AF 33(616)-5581.

[1] D. W. Magnuson, J. Chem. Phys. **24**, 344 (1956).
[2] Boggs, Crain, and Whiteford, J. Phys. Chem. **61**, 482 (1957).
[3] J. E. Boggs, J. Am. Chem. Soc. **80**, 4235 (1958).
[4] Boggs, Whiteford, and Thompson, J. Phys. Chem. **63**, 713 (1959).
[5] J. E. Boggs and A. P. Deam, J. Phys. Chem. (to be published).
[6] E. B. Wilson, Jr., J. Chem. Phys. **63**, 1339 (1959).
[7] W. Maier and H. K. Wimmel, Z. Physik **153**, 297 (1958); *ibid.* **154**, 133 (1959).

Molecular Rotation and Dielectric Relaxation in a Crystal Lattice

COLIN CLEMETT AND MANSEL DAVIES

The Edward Davies Chemical Laboratories, University College of Wales, Aberystwyth, Wales

(Received August 5, 1959)

PARTICULAR interest attaches to the process of molecular rotation in the solid state, especially in those cases where the molecule would appear to be distinctly polar. Such behavior is clearly revealed by dielectric dispersion which allows the relaxation time and the energy and entropy factors for the process to be evaluated.

TABLE I. Liquid succinonitrile.

t°C	59	65	74
$(\epsilon_0-\epsilon_\infty)$	51.8	50.5	48.4
$10^{12}\tau$ sec	18.6	16.4	14.3

TABLE II. Solid succinotrile

t°C	25.5	39.8	50.0
$(\epsilon_0-\epsilon_\infty)$	62.1	57.8	55.0
$10^{12}\tau$ sec.	61±4	49±3	43±2

We wish to report the findings for succinonitrile ($NC\cdot CH_2\cdot CH_2\cdot CN$, m.p. 56.8°C) whose dielectric properties we have studied in both liquid and solid states up to frequencies of 900 Mcps. Low-frequency measurements were made in the Hartshorn-Ward apparatus and coaxial line measurements (from 250 to 910 Mcps) with the system already described.[1]

The liquid was examined at 59, 65, and 74°C, each ±0.5°C: ϵ' values were ±1 percent, tanδ±2 percent. Within the accuracy of the data they fitted the simple (Debye) dispersion relations with the parameters given in Table I and $\epsilon_\infty=4.0$. A previous precise value of ϵ_0 is 56.5 at 57°C and ϵ_∞ is coincident with ϵ' for the solid below the rotational m.p.[2] By writing

$$\tau=A\exp(\Delta H/RT),$$

these data give $\Delta H=3.9$ kcal/g mole and $A=4.8\times10^{-14}$ sec. This value of ΔH is precisely that deduced[3] from the expression for the viscosity, $\eta=A'\exp(\Delta H\eta/RT)$. If one uses the expression

$$\tau=(h/kT)\exp[\Delta H^*/RT-\Delta S^*/R], \qquad (1)$$

one finds $\Delta H^*=3.2$ kcal/g mole and $\Delta S^*=0.0$ cal/g mole°K.

Somewhat larger uncertainty pertains to the data for the solid: ϵ' values were ±2% and tanδ±3% at 50° and these increased as the specimens were cooled in the line owing to the tendency for the homogeneous glass-like specimens to develop internal crystal faces and the possible formation of fissures. However, repeated determinations at 50.0, 39.8, and 25.5 (±0.5)°C produced consistent results, the scatter in tanδ at 25° (where it is a maximum) being ±6%. Again, the data fit a single relaxation time at each temperature: the dispersion factors are summarized in Table II. Here ϵ_∞ was taken as 4.4, partly on the basis of a measured value near −50°C and 8.5 kMcps. Morgan and White found 62.6 for ϵ_0 in the solid at 37°C. The rotational freezing-point at which the molecular freedom is lost in the solid is defined by infrared observations as −43.7°C.[4]

In $\tau=A\exp(\Delta H/RT)$ the solid data give $A=60\times10^{-14}$ sec. $\Delta H=2.7$ kcal/g mole: the values corresponding to Eq. (1) are $\Delta H^*=2.0_8$ kcal/g mole; $\Delta S^*=-4.8$ cal/g mole°K.

It is particularly interesting to find that ΔH is certainly less than for the relaxation in the liquid. The dielectric data make it clear that the rotation in the solid involves the whole molecule as the ϵ' values lead to a dipole moment (3.5D) essentially the same as in the vapour (3.5D) or in dilute solution (3.8D).[5]

The apparent negative entropy of activation in the solid recalls similar values where low ΔH terms obtain.[6] Its significance is presumably that the rotation in the solid requires cooperation between adjacent molecules to the extent of increasing the local order.

[1] Williams, J. Phys. Chem. **63**, 534 (1959).
[2] Morgan and White, J. Chem. Phys. **5**, 655 (1937).
[3] Timmermans, *Physico-Chemical Constants of Pure Organic Compounds* (Elsevier Publishing Company, Inc., Amsterdam, 1950).
[4] Janz and Fitzgerald, J. Chem. Phys. **23**, 1973 (1955).
[5] Bloom and Sutton, J. Chem. Soc. **1941**, 727.
[6] Davies, Quart. Revs. (London) **8**, 267 (1954).

NMR Studies on 1-Methoxyvinyl Esters*

MARTIN SAUNDERS, JANIS PLOSTNIEKS, PETER S. WHARTON, AND HARRY H. WASSERMAN

Sterling Chemistry Laboratory, Yale University, New Haven, Connecticut

(Received August 3, 1959)

WE have examined the NMR spectra of compounds of type I

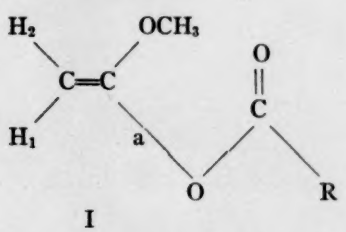

I

Ia, R=CH₃
Ib, R=C₆H₅
Ic, R=CF₃

which have recently been prepared for the first time by the reactions of methoxyacetylene with carboxylic acids.[1] By determining the shifts of the methylene hydrogens we have obtained information concerning the relative spatial influences of the acyloxy groups, $-CH_3CO_2-$, $C_6H_5CO_2-$, and CF_3CO_2- on these methylene hydrogens.

In Table I are listed the chemical shifts and coupling constants of the two methylene hydrogens (obtained from the typical *AB* quadruplet) as well as the chemical shifts of the methoxyl hydrogens for the three cases studied.

Substitution of a benzoyl group for an acetyl group shifted the methylene hydrogens 0.155 and 0.111 ppm downfield. This shift is probably largely the result of the magnetic anisotropy of the benzene ring, and is in the expected direction and roughly of the expected magnitude assuming that the benzene ring, ester group, and double bond are coplanar and using the theoretical curve of Johnson and Bovey.[2]

In the case of Ic, measurement of bond distances in the planar model indicates methylene hydrogen distances of approximately 5 and 6 A from the trifluoromethyl group, the observed chemical shifts being 0.285 and 0.200 ppm downfield relative to Ia. The trifluoromethyl group thus appears to have a large antishielding effect compared to methyl.

TABLE I. NMR spectra of 1-methoxyvinyl esters in dilute CCl_4 solution referred to benzene capillary, 40 Mc (all upfield).

R	δ_1 (ppm)	δ_2 (ppm)	J_{12} (cps)	δ_{OCH_3} (ppm)
CH_3	2.810±0.01	2.855±0.01	3.3 ±0.3	2.924±0.005
C_6H_5	2.655±0.005	2.744±0.005	3.65±0.1	2.866±0.005
CF_3	2.525±0.005	2.655±0.005	4.55±0.1	2.804±0.005

The effect of benzoyl group is at least partly accounted for by its magnetic anisotropy. In the case of the trifluoromethyl group in addition to the magnetic anisotropy a strong polar effect would be expected to operate on the electrons of the intervening bonds so that they in turn would affect the chemical shift of the methylene hydrogens.

In exploring mechanistic aspects of the reaction of carboxylic acids with methoxyacetylene we studied the reaction of *O*-deutero benzoic acid ($C_6H_5CO_2D$) with excess methoxyacetylene in the presence of mercuric ion.[1] The result was a mixture containing four species: Ia, both monodeutero adducts, and the dideutero ester.† This mixture most probably resulted from exchange of the acetylenic hydrogen with the deutero acid, as shown by recovery of unreacted methoxyacetylene containing deuterium. The amount of deuterium found by mass spectral analysis of the recovered acetylene was that expected from statistical mixing.

The spectrum of this mixture (Fig. 1) contains six peaks in the olefinic hydrogen region (measured in cps from center of peaks 3 and 4)

1, −4.54	2, −1.66	3, −1.00
4, 1.00	5, 2.68	6, 4.79.

The two peaks (Nos. 2 and 5) which are present in addition to those found in Ib are assigned to the two

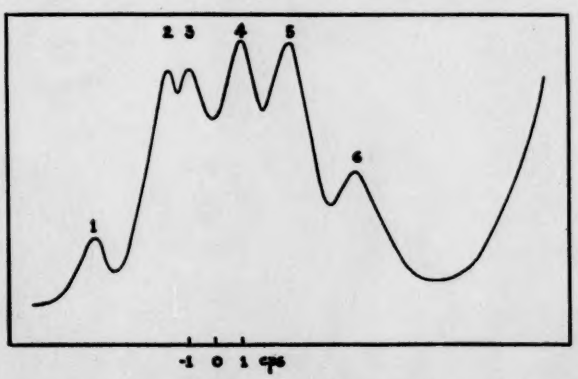

FIG. 1. NMR Spectrum of reaction product of C_6H_5COOD with $H-C\equiv C-OCH_3$ (neat).

isomeric monodeutero vinyl esters. It is noteworthy that the monodeutero peaks are asymmetrically placed with respect to the dihydro spectrum Fig. 1, and are displaced upfield 0.50 and 0.52±0.05 cps from the positions calculated for these peaks (neat spectrum).

Substitution of deuterium for hydrogen thus causes an upfield shift of a second proton attached to the same carbon atom. Tiers[4] observed a similar deuterium isotope effect, in the case of α-deuterotoluene, which he ascribed to a difference in electron donating power for deuterium compared to hydrogen. However, this phenomenon can also be explained by a nonlinear dependence of the effect of a protonic charge on a neighboring proton, with distance, which could cause an isotope shift due to the difference in zero point vibrational amplitudes of C—H and C—D bonds.[5]

* Contribution No. 1558 from the Department of Chemistry, Yale University.

† The presence of the dideutero ester was inferred from the carbon-carbon double bond stretching frequencies in the infrared spectrum.

[1] H. H. Wasserman and P. S. Wharton, Tetrahedron **3**, 321 (1958).

[2] C. E. Johnson and F. A. Bovey, J. Chem. Phys. **29**, 1012 (1958).

[3] G. E. Wheland, *Resonance in Organic Chemistry* (John Wiley & Sons, Inc., New York, 1955).

[4] G. V. D. Tiers, J. Chem. Phys. **29**, 963 (1958).

[5] H. S. Gutowsky, J. Chem. Phys. **31**, 1683 (1959).